THE JOURNAL OF

PHYSICAL CHEMISTRY

Volume 74, Number 2 January 22, 1970

NOTES

AUTHOR INDEX

THE JOURNAL OF
PHYSICAL CHEMISTRY

VOLUME 74, NUMBER 2 JANUARY 22, 1970

Chlorophyll–Poly(vinylpyridine) Complexes. II. Depolarization of Fluorescence[1a]

by G. R. Seely

Charles F. Kettering Research Laboratory, Yellow Springs, Ohio 45387 *(Received June 20, 1969)*

Intermolecular energy transfer was studied by the depolarization of fluorescence of pyrochlorophyll bound to poly(4-vinylpyridine) in nitromethane solution. An advantage of this system is that the average distance between pyrochlorophyll molecules can be varied over a wide range without changing the molar concentration of pigment significantly. The procedure for correcting the fluorescence data for the effects of reabsorption and secondary fluorescence is described. The decrease in the emission anisotropy with increase in pigment density on the polymer is better described by Ore's theory than by Jablonski's and is not noticeably dependent on the molecular weight of the polymer in the range 140,000 to >2,000,000. The distribution of polymer segments, to which the acceptor pyrochlorophyll molecules are bound, was calculated for the statistically equivalent random chain of Kuhn. The relative emission anisotropy was calculated from this distribution for chains of various lengths by application of Ore's equation with trial values of R_0 (Förster's critical distance for energy transfer). Best fit to experimental data was obtained for $R_0 = 42$ Å. The calculation of emission anisotropy from polymer configuration theory describes its behavior at all pigment densities within experimental precision and correctly accounts for the lack of dependence on the molecular weight of the polymer.

Introduction

In the first paper of this series,[1b] we described the preparation and spectral properties of a new kind of aggregate of chlorophyll or its derivatives, prepared by complexing the pigment with poly(4-vinylpyridine) in nitromethane solution. These aggregates are versatile and convenient model systems for the study of energy transfer and trapping processes, such as are presumed to occur in the natural chlorophyll aggregate, the photosynthetic unit of the green plant.[2,3] We now present a study of energy transfer in these synthetic aggregates, based on the dependence of polarization of fluorescence on pigment density.

When the fluorescence of a molecule in a solution of low viscosity (such as nitromethane) is excited with plane polarized light, the fluorescence is almost entirely unpolarized, owing to rotational diffusion of the excited molecule within the lifetime of the excited state. If the molecule is in a solution of high viscosity, or if it is attached to a polymer, some degree of polarization may be retained in the fluorescence because of restriction of the rotational motion of the molecule. However, if the concentration of fluorescent molecules is large enough, excitation energy may pass one to another by the resonance transfer mechanism of Förster,[4] with rapid loss of the original direction of polarization. The degree of polarization of fluorescence under these conditions is therefore closely related to the probability that excitation energy is transferred. A great advantage of the study of depolarization of fluorescence in the chlorophyll–polymer system over the more usual studies of concentration depolarization is that the density of chlorophyll in an aggregate can be varied easily and arbitrarily with relatively little change in the

(1) (a) Contribution No. 356; (b) G. R. Seely, *J. Phys. Chem.*, 71, 2091 (1967).

(2) R. Emerson and W. Arnold, *J. Gen. Physiol.*, 16, 191 (1932).

(3) R. K. Clayton, "Molecular Physics in Photosynthesis," Blaisdell Publishing Co., New York, N. Y., 1965, pp 14–18, 119–124, 164–167.

(4) T. Förster, *Ann. Phys.* (Leipzig), 2, 55 (1948).

molar concentration or light absorption properties of the solution.

In the present work we used pyrochlorophyll *a* (10-decarbomethoxychlorophyll) instead of chlorophyll, because it binds somewhat more firmly to the polymer and is not subject to allomerization.[1b] However, we have obtained quantitatively similar results with chlorophyll *a*,[1b] chlorophyll *b*, and Zn pyropheophytin *a*.

The solution properties of poly(4-vinylpyridine) in nitromethane are those of a randomly coiled polymer. Since the spatial density of polymer segments increases with the molecular weight of such a polymer, it seemed likely that energy transfer would be the more extensive, the greater the molecular weight. Therefore, we examined depolarization of fluorescence with a series of polymer fractions covering a wide range of molecular weight.

The experimental results have been interpreted successfully with the aid of theories describing the rate of energy transfer and the distribution of polymer segments in solution.

Experimental Section

The preparation of pyrochlorophyll has been described.[1b]

Nitromethane was fractionally distilled under N_2 twice, each time with benzene added to drive off water as an azeotrope. The middle cut of the second distillation was collected in a flask with a side arm. The flask was sealed; the contents were frozen three times with discard of small supernatants and were stored frozen by Dry Ice under N_2. The water content was around 0.01%, satisfactory for our purpose. To draw a sample, some of the nitromethane was thawed, poured into the side arm, and partially frozen; the supernatant was poured into a second side arm and drained. The sample was then thawed and withdrawn by syringe through a stopcock under cover of N_2. Thus the nitromethane was further purified as it was used.

Preparation of Poly(4-vinylpyridine) Fractions. Three 22-ml samples of freshly distilled 4-vinylpyridine were each diluted with 25 ml of ethanol and heated at the reflux temperature under N_2 for 3–4.5 hr with 10, 3, and 1 mg of 2,2′azobis[2-methylpropionitrile], respectively, as initiator. The solutions were cooled and diluted with ethanol, and the polymer was precipitated with heptane. The polymer was redissolved in isopropyl alcohol and reprecipitated with heptane to free it from unreacted vinylpyridine.

The polymers (A, B, and C) were fractionated by successive precipitation with 1:1 heptane–ethyl acetate from isopropyl alcohol solution. Three or four fractions of each polymer were collected, reprecipitated one or more times to remove low-molecular-weight material, and dried under vacuum. We also used a polymer fraction (D1) of high intrinsic viscosity prepared earlier by a similar method.

Fractions that were large enough were characterized by the intrinsic viscosity in ethanol ($[\eta]_{et}$) and in nitromethane ($[\eta]_{nm}$), and by the weight-average molecular weight (M_w), the radius of gyration $\langle S^2\rangle_{et}^{1/2}$, and the second virial coefficient (B) from light-scattering measurements in absolute ethanol. Light scattering in nitromethane failed to yield characteristics of the polymer in that solvent for reasons alluded to earlier[1b] and explicated elsewhere.[5] Properties of the fractions are listed in Table I.

The intrinsic viscosities of the lower molecular weight fractions in ethanol approach those expected from the equations of Berkowitz, *et al.*,[6] and Boyes and Strauss,[7] but the intrinsic viscosities of the higher molecular weight fractions are low, suggesting that these fractions are more highly branched than those on which the equations were based. If all the fractions are considered, the ratio $[\eta]_{nm}/M_w^{1/2}$ has no discernible dependence on molecular weight.

For the analysis of the results, the length b of a segment of the statistically equivalent random coil in the model of Kuhn[8] is required and is calculated from the equations[9]

$$b^2 = 6\langle S^2\rangle_{nm}/Z \quad (1)$$

$$Zb = M_w a/m \quad (2)$$

$$[\eta]_{nm} = \Phi'\langle S^2\rangle_{nm}^{3/2}/M_w \quad (3)$$

In these equations, Z is the number of segments in the statistically equivalent chain, m is the monomer molecular weight (105.13), a is the contribution of a monomer unit to the extension of the polymer chain, taken as 2.53 Å, and Φ' is a constant, the value of which according to recent determinations[10] is 3.94×10^{22} per mole ($[\eta]$ in deciliters per gram).

Apparatus and Procedure. An aliquot of a solution of pyrochlorophyll in benzene, and 0.010 ml of α-methylnaphthalene,[1b] were introduced into a cuvette, of 30-mm inside diameter and 5 mm thick. The benzene was evaporated by a stream of N_2, and the residue was diluted with nitromethane to a volume of 3.5 ml and a pyrochlorophyll concentration of about 1.7×10^{-5} M. A solution of 1.5% poly(vinylpyridine) in nitromethane was filtered through a "very fine" filter and was added in portions of 0.025 ml or more to the cuvette, to a total of 0.4–0.7 ml. The contents were flushed with N_2 after each addition. Fluorescence was excited by the collimated light of a projector lamp

(5) G. R. Seely, *Macromolecules*, **2**, 302 (1969).

(6) J. B. Berkowitz, M. Yamin, and R. M. Fuoss, *J. Polym. Sci.*, **28**, 69 (1958).

(7) A. G. Boyes and U. P. Strauss, *ibid.*, **22**, 463 (1956).

(8) W. Kuhn, *Kolloid-Z.*, **68**, 2 (1934).

(9) H. Morawetz, "Macromolecules in Solution," Interscience Publishers, New York, N. Y., 1965, pp 112–121, 305.

(10) G. C. Berry, *J. Chem. Phys.*, **46**, 1338 (1967); C. W. Pyun and M. Fixman, *ibid.*, **42**, 3838 (1965).

Table I: Characteristics of Poly(4-vinylpyridine) Fractions in Ethanol and Nitromethane Solution at 25°

Fraction no.	$[\eta]_{et}$, dl/g	$[\eta]_{mn}$, dl/g	$10^{-6} M_w$	$\langle S^2 \rangle_{et}^{1/2}$, Å	$10^4 B$, ml/g	$10^3[\eta]_{nm}/M_w^{1/2}$	b, Å
A2	1.43	0.75	0.44	400	5.9	1.12	23.3
A3	1.12	0.56	0.32	260	6.0	0.98	21.2
A4	0.67	0.31	0.14	240	5.6	0.83	19.0
B1	2.75	1.42	2.50	950	5.6	0.90	20.1
B2	1.85	0.98	0.87	470	7.0	1.05	22.2
B3	1.60	0.71	0.50	410	6.2	1.00	21.6
C1	2.70	1.58	~5	...	6.0	...	...
C2	2.02	1.19	1.08	640	5.1	1.14	23.6
D1	3.54	...	...	...	...	...	...
				Av	5.9	1.00	21.4

and passed through a 660-nm interference filter (Baird-Atomic), a polarizing plate (Polacoat, Inc.), and an aperture limiting the beam to a diameter of 8 mm. The voltage of the projector lamp was stabilized by a Sola transformer.

Fluorescent light emanating from the front face of the cuvette at an angle of 45° to the normal was passed through a 680-nm interference filter (Baird-Atomic) and a polarizing plate and was detected by an EMI 9558B photomultiplier with 10^6-ohm input resistance. The photomultiplier current was measured with a Keithley 610B electrometer. The fluorescence intensity was determined with the excitation light polarized in the vertical and in the horizontal position; the polarizer in front of the photomultiplier was kept in the vertical orientation.

For quantum yield determinations, an Osram Cd spectral lamp replaced the projector lamp, and appropriate changes were made in the filters.

The relative spectral sensitivity $S(\lambda)$ of the photomultiplier was determined by the quantum counter method,[11] using rhodamine B for the 400–600-nm region and methylene blue for the 550–700-nm region.[12] Comparison was made with the light scattered from a filtered solution of colloidal silica (Ludox, a gift of E. I. du Pont de Nemours and Co.).[13]

The fluorescence intensity readings were immediately subjected to three corrections. Intensity of light scattered from the cuvette with nitromethane but without pyrochlorophyll, amounting to 1–2% of the maximum fluorescence intensity, was subtracted. The intensity of exciting light depended on the orientation of the polarizer; an asymmetry factor of about 0.87 was determined from the fluorescence of pyrochlorophyll in acetone and applied to fluorescence with vertical polarization. This factor was redetermined with each set of measurements. The visible output of the projector lamp was monitored by an Eppley thermopile covered by a blue filter, and correction was made for small variations during the run. The fluorescence intensity readings so corrected are designated M_v and M_h for polarizer orientation vertical and horizontal. An example of the variation of M_v and M_h with the ratio of polymer pyridine unit concentration to pyrochlorophyll concentration, (py)/(Chl), is shown in Figure 1.

Certain calculations in the third part of Results and Discussion were performed on the Mark I computer *via* the General Electric time-sharing service, programmed in BASIC language.

Results and Discussion

Our goal is to be able to interpret results such as those of Figure 1 so as to construct a mathematical model for the transfer of energy in the pigment–polymer aggregate. For this we need suitable theories for energy transfer as a function of pigment concentration and for the distribution of polymer segments (*i.e.*, of attached pigment molecules) in space.

But first it is necessary to correct the fluorescence intensities for the effects of reabsorption of fluorescent light and the consequent secondary fluorescence. Pyrochlorophyll reabsorbs its fluorescence appreciably at the lowest concentrations which are practicable in this study. The usual expedient of working at very low concentrations is limited in this system by dissociation of the aggregate.[1b] The procedure for making this correction is rather complicated, and it seems best to describe it in detail.

The results are therefore presented and analyzed in three stages: (1) a photometric stage, in which the yield and polarization of the primary fluorescence are calculated from M_v and M_h; (2) a mechanistic stage, in which the variation of polarization with pigment density is explained in terms of Förster's theory of energy transfer, but with an unknown scale factor for distance; and (3) a configurational stage, in which the introduction of a model for the polymer segment distribution makes possible the determination of the

(11) W. H. Melhuish, *N. Z. J. Sci.*, 37.2B, 142 (1955); *J. Opt. Soc. Amer.*, 52, 1256 (1962).

(12) G. R. Seely, *J. Phys. Chem.*, 73, 125 (1969).

(13) J. P. Kratohvil, G. Deželic, M. Kerker, and E. Matijevic, *J. Polym. Sci.*, 57, 59 (1962).

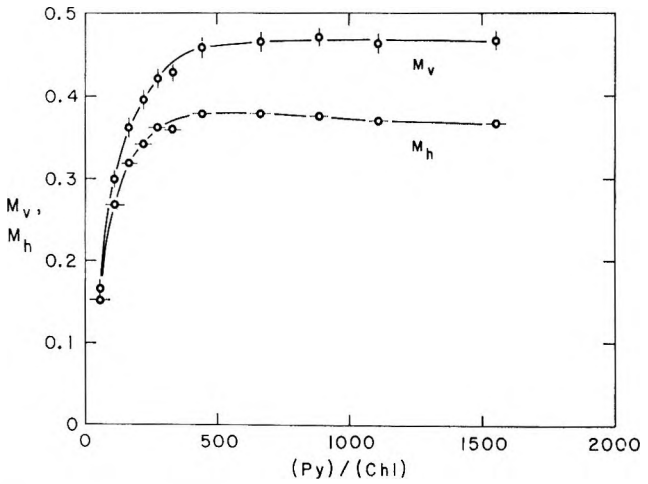

Figure 1. Relative intensities of vertically polarized fluorescence excited with vertically (M_v) and horizontally (M_h) polarized light (660 nm), as functions of the polymer pyridine unit to pyrochlorophyll ratio. Ordinate scale in arbitrary units. Data for polymer fraction Cl.

distance parameter R_0 of Förster's theory, over which excitation energy has a 50% chance of being transferred during the lifetime of the excited state.

Photometric Stage. The rate of absorption (I_a) of incident light (I_0) is proportional to $I_0\rho_{max}T_F$, where ρ_{max} is the absorbance (ρ) at the peak of the band near 666 nm, and T_F is the integral over the product of the transmittance $T(\lambda)$ of the 660-nm interference

$$T_F = \int_0^\infty \frac{T(\lambda)(1 - 10^{-\rho(\lambda)})d\lambda}{\rho_{max}} \quad (4)$$

and the fraction of light absorbed at each wavelength λ. The integral in (4) was evaluated graphically, normalized to 1 at $\rho_{max} = 0$, and plotted as a function of ρ_{max}.

The rate of primary fluorescence is $I^{(1)} = \phi I_a$, where ϕ is the quantum yield, whether energy is transferred or not. The rate of absorption of primary fluorescence is $I_r^{(1)} = \phi I_a R$, where R, the fraction reabsorbed, is formally given by the integral

$$R = \int_0^\infty F(\lambda)(1 - 10^{-\beta\rho})d\lambda \quad (5)$$

$F(\lambda)$ is the normalized fluorescence spectrum and β is, in general, a function of geometry, wavelength, and concentration. The rate of secondary fluorescence is then $\phi^2 I_a R$, and of this, $\phi^2 I_a R^2$ is reabsorbed, etc.[14] Summed over all orders, the fluorescence that escapes the cell is $\phi I_a(1 - R)/(1 - \phi R)$.

Polarization of the incident light introduces a factor T_p into the expression for light absorbed, and the fluorescence becomes more anisotropic. The intensities $I_v^{(1)}$ and $I_h^{(1)}$ of vertically and horizontally polarized primary fluorescence, excited by vertically polarized light, are in general different, but

$$I_v^{(1)} + 2I_h^{(1)} = \phi I_a \quad (6)$$

Second and higher orders of fluorescence are nearly unpolarized, so $I_v^{(2)} = I_h^{(2)} = {}^1/_3 I^{(2)}$, etc. The total vertically and horizontally polarized fluorescence components that escape the cuvette in the direction of the photomultiplier are therefore proportional to

$$I_v = I_v^{(1)}(1 - R) + {}^1/_3\phi I_a R(1 - R) + {}^1/_3\phi^2 I_a R^2(1 - R) + \ldots \quad (7)$$

$$I_h = I_h^{(1)}(1 - R) + {}^1/_3\phi I_a(1 + R) + \ldots \quad (8)$$

The photomultiplier readings are related to fluorescence intensities by eq 9

$$M_v = \Omega T_p' \int_0^\infty I_v(\lambda)D(\rho,\lambda)S(\lambda)T'(\lambda)d\lambda \quad (9)$$

and a similar expression for M_h. The instrument constant Ω includes the solid angle intercepted by the photomultiplier but also the effects of refraction and reflection in the apparatus; T_p' and $T'(\lambda)$ are the transmittances of the polarizing plate and the 680-nm interference filter in front of the photomultiplier; $S(\lambda)$ is the sensitivity of the photomultiplier (amperes/einstein), and $D(\rho,\lambda)$ is a dissymmetry factor that compensates for the circumstance that as more light is absorbed near the front of the cuvette, more fluorescence escapes from the front than from the back. To proceed further, factors in the integral must be replaced by average values over the wavelength interval of fluorescence

$$M_{v(h)} = \Omega T_p' D(\rho)\bar{S}\bar{T}' I_{v(h)} \quad (10)$$

The quantum yield is found by combining eq 7, 8, and 10

$$\phi = \frac{M_v + 2M_h}{\Omega T_p T_p' T_F \bar{T}' \bar{S} D(\rho)(1 - R)\rho_{max} I_0 + (M_v + 2M_h)R} \quad (11)$$

To express the extent of polarization, we follow Jablonski[15] in using the emission anisotropy r

$$r = (I_v^{(1)} - I_h^{(1)})/(I_v^{(1)} + 2I_h^{(1)}) \quad (12)$$

rather than the degree of polarization $p = (I_v^{(1)} - I_h^{(1)})/(I_v^{(1)} + I_h^{(1)})$, because the denominator of the former is proportional to the quantum yield of fluorescence. When eq 6, 7, 8, and 10 are combined with eq 12

$$r = (M_v - M_h)/\Omega T_p T_p' T_F \bar{T}' \bar{S} D(\rho)(1 - R)\rho_{max} I_0 \phi \quad (13)$$

From Figure 1 and from previously published data[1b] it is evident that fluorescence is partly quenched at the

(14) The approximations are made that fluorescence of all orders has the same geometric distribution and that the spectrum of the fluorescence that escapes the cell is sensibly independent of concentration.

(15) A. Jablonski, *Z. Naturforsch.*, *A*, **16**, 1 (1961).

lower (py)/(Chl) values. The quenching mechanism proposed in the first article of this series was transfer of excitation energy to a relatively small number of "quenching centers," probably consisting of two pigment molecules adjacent on the chain. If this is correct, then fluorescence quenched is fluorescence transferred, and its yield should be included in the denominator of eq 13. For the calculation of r we have therefore replaced the observed quantum yield ϕ by the maximum value ϕ_0 obtaining at high (py)/(Chl) ratios.

Equation 13 is therefore modified to read

$$r = (M_v - M_h)/\Omega' D(\rho)(1 - R)\rho_{max} T_F \phi_0 \quad (14)$$

where $\Omega' = \Omega T_p T_p' \bar{T}' \bar{S} I_0$ contains all factors not strongly dependent on pigment concentration.

Although the reabsorption can, in principle, be calculated,[16] it is more reliable to determine Ω', R, and $D(\rho)(1 - R)$ experimentally as functions of ρ_{max}. The usual method of determining R from a plot of apparent quantum yield of fluorescence against ρ_{max} is impracticable for the pyrochlorophyll–polymer aggregate because of dissociation at very low concentrations[1b] and variation of the degree of polarization with variation of (py)/(Chl). However, the red absorption band of pyrochlorophyll in dimethyl sulfoxide is in nearly the same position and has nearly the same half-width as in sparse aggregates on polymer in nitromethane.[1b,17] The three quantities were therefore calculated from fluorescence of pyrochlorophyll at series of concentrations in dimethyl sulfoxide and assumed to be valid for the pyrochlorophyll–polymer complex.

First, the quantum yield ϕ_{ms} of fluorescence in dimethyl sulfoxide was determined, with excitation by Cd 6438-Å light. For these measurements, the polarizing plates and the 680-nm interference filter were omitted, and the 660-nm filter over the incident light was replaced by a 640-nm filter. As 6438-Å light is not strongly absorbed by pyrochlorophyll, $D(\rho) \cong 1$, and the expression for the photomultiplier reading becomes

$$M_f = \Omega I_0 S(\lambda_f)(1 - 10^{-\rho}) \times (1 - R)\phi_{ms}/(1 - \phi_{ms}R) \quad (15)$$

where ρ is now the absorbance at 6438 Å.

The proportionality factor Ω was eliminated by measuring the intensity (M_s) of light scattered from a solution of colloidal silica (Ludox) of turbidity ν at 6438 Å[12,18]

$$M_s = (3/4)\Omega \left(\frac{n_f \sqrt{2n_f^2 - 1}}{n_s \sqrt{2n_s^2 - 1}} \right) (1 + \cos^2 \theta_s) I_0 \times (1 - 10^{-\tau}) S(\lambda_s) \quad (16)$$

In these equations, $\lambda_f \cong 670$ nm, $\lambda_s = 644$ nm, and θ_s is determined by the law of refraction $\sin 45°/\sin \theta_s = n_s$. The factor containing the refractive indices n_f and n_s of the fluorescence and scattering media is a correction to Ω.[19]

Extrapolation of values of $M_f/(1 - 10^{-\rho})$ to zero concentration of pyrochlorophyll gave $\phi_{ms} = 0.297$ and, in the process, a curve for R as a function of ρ_{max} for Cd light.

Next, values of $D(\rho)(1 - R)/(1 - \phi_{ms}R)$ were calculated over a range of pyrochlorophyll concentration from fluorescence intensities excited by the projector lamp with the 660-nm filter. Although R for 660-nm excitation is not the same function of ρ_{max} as R for 6438-Å excitation, there should be little error in the use of the latter function in the quantity $(1 - \phi_{ms}R)$, which then makes possible the calculation of $D(\rho)(1 - R)$ required in eq 11 and 14.

Finally, the value of Ω' was calculated from eq 11, as a function of ρ_{max} for pyrochlorophyll in dimethyl sulfoxide, with interferences filters and polarizers in place. With the established values of T_F, R, $D(\rho)(1 - R)$, and ϕ_{ms}, the calculated value of Ω' at fixed incident light intensity was constant from $\rho_{max} = 0.1$ to 1.0.

Values of ϕ and r were calculated from M_v and M_h by eq 11 and 14. In Figure 2 are plotted curves for ϕ and r, obtained from the data of Figure 1. The value of ϕ becomes quite constant at higher (py)/(Chl) ratios and provides the value of ϕ_0 used in eq 14. Application of the correction for secondary fluorescence increases r as much as 10% over the value of $(M_v - M_h)/(M_v + 2M_h)$.

Mechanistic Stage. Förster's mechanism,[4] in which the rate of energy transfer depends on the inverse sixth power of the distance between donor and acceptor, appears quite well established[20] for the kind of transfer we are dealing with. The main difficulty in applying the theory to depolarization of fluorescence in real systems is the proper reckoning of the probability of return transfer to the initially excited (donor) molecule when there is more than one possible energy acceptor molecule. Förster's original calculations were for systems with very little or very much transfer; the intermediate case was left unsolved.[4]

Ore approached the problem by calculating the probability that even though an acceptor molecule is the nearest neighbor of a donor molecule, the donor is not the nearest neighbor of the acceptor.[21] If it is not, the energy is assumed never to return to the initially excited molecule, and the relative emission anisotropy r/r_0 is given by

(16) A. Budó and I. Ketskeméty, *J. Chem. Phys.*, **25**, 595 (1956); W. H. Melhuish, *J. Phys. Chem.*, **65**, 229 (1961).

(17) G. R. Seely and R. G. Jensen, *Spectrochim. Acta*, **21**, 1835 (1965).

(18) G. Weber and F. W. J. Teale, *Trans. Faraday Soc.*, **53**, 646 (1957).

(19) E. H. Gilmore, G. E. Gibson, and D. S. McClure, *J. Chem. Phys.*, **23**, 399 (1955).

(20) L. Stryer and R. P. Haugland, *Proc. Nat. Acad. Sci., U. S.*, **58**, 719 (1967); G. Gabor, *Biopolymers*, **67**, 809 (1968).

(21) A. Ore, *J. Chem. Phys.*, **31**, 442 (1959).

$$\frac{r}{r_0} = \int_0^\infty \frac{\xi^2(\xi^2 + \gamma^2)e^{-\xi}d\xi}{(\xi^2 + \gamma^2)^2 - \gamma^4 \exp(-11\xi/16)} \quad (17)$$

In eq 17, r_0 is the value of r in the absence of energy transfer, $\gamma = c/c_0$, ξ is the average number of molecules in a sphere of radius R, c is the concentration, and c_0 is the critical concentration, defined by Förster as $3000/4\pi N_a R_0^3$, where N_a is Avogadro's number.

In Jablonski's theory each initially excited molecule belongs to a cluster of one or more molecules, all of which have the same probability of emitting fluorescence.[22] If light emitted by any molecule but the initially excited one is polarized randomly, his result can be simplified to

$$\frac{r}{r_0} = 2(\nu - 1 + e^{-\nu})/\nu^2 \quad (18)$$

The parameter ν is proportional to c/c_0.

In a recent paper,[23] Knox has critically compared these and other theories of fluorescence depolarization and has presented a new, modified cluster calculation, the results of which are somewhat closer to Jablonski's than to Ore's.

Kawski tested the equations of Ore and Jablonski with fluorescence depolarization of solutions of several dyes and found good agreement with both.[24] We attempted to fit our experimental data to both equations, and with one exception, found better agreement with Ore's than with Jablonski's.

The emission anisotropy values from Figure 2 are plotted logarithmically in Figure 3, and to them is matched a segment of a logarithmic plot of eq 17. Comparison of the ordinate and abscissa scales gives the value of r_0 and the value of $[(\text{Chl})/(\text{py})]_0$, at which $c = c_0$. The curve for Jablonski's equation is also shown, fitted to the experimental points at $r = r_0/2$; it deviates imperceptibly from the curve for Ore's equation at lesser depolarizations.

Table II lists the values of ϕ_0 calculated from eq 11, r_0, and $[(\text{Chl})/(\text{py})]_0$ obtained by comparison with

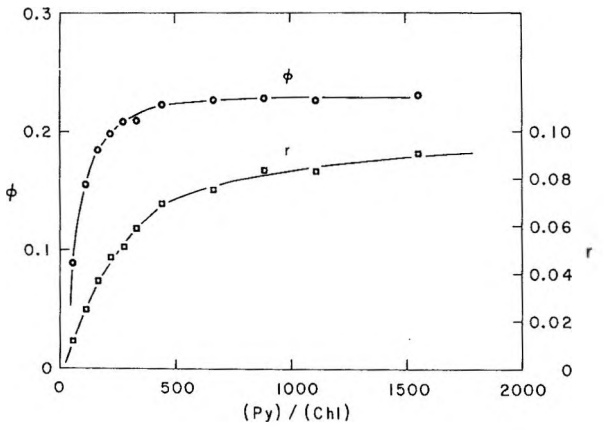

Figure 2. Quantum yield ϕ of fluorescence and emission anisotropy r calculated from the data of Figure 1 by eq 11 and 14.

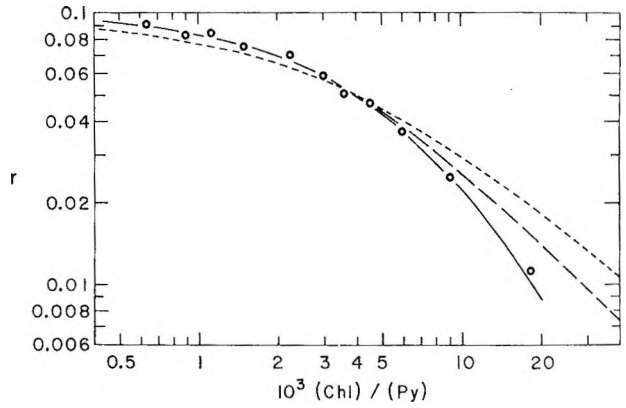

Figure 3. Emission anisotropy data of Figure 2 fitted to master curve of Ore's eq 17, the solid line. The long-dashed curve is Jablonski's eq 18, which can be made nearly coincident with Ore's equation when $(\text{Chl})/(\text{py}) < 0.005$. The short-dashed curve is Ore's equation integrated over a Gaussian distribution of concentration and placed so as to intersect the solid curve at $r = 0.05$.

eq 17 as in Figure 3, for each of the polymer fractions of Table I. In all cases but one (fraction A2), the points fit the theoretical curve within experimental precision until 90% of the initial polarization is lost. There is spectral evidence that solutions of fraction A2 were so contaminated with water that the pigment may not have been entirely bound to the polymer at low polymer concentrations.

Table II: Parameters Derived from Application of Ore's Eq 14 to Depolarization of Fluorescence of Pyrochlorophyll on Poly(vinylpyridine)[a]

Fraction no.	$10^{-6} M_w$	ϕ_0	r_0	$10^3[(\text{Chl})/(\text{py})]_0$
A2	0.44	0.211	0.113	7.65
A3	0.32	0.234	0.105	3.63
A4	1.14	0.227	0.109	4.70
B1	2.50	0.212	0.110	3.90
B2	0.87	0.212	0.102	4.46
B3	0.50	0.242	0.101	3.45
C1	~5	0.228	0.102	4.13
C2	1.08	0.212	0.104	4.61
D1	...	0.255	0.106	3.85
	Av[b]	0.228	0.105	4.09

[a] ϕ_0 = maximum quantum yield of fluorescence, r_0 = maximum emission anisotropy, $[(\text{Chl})/(\text{py})]_0$ = concentration ratio at which $c = c_0$ of Förster's theory. [b] Fraction A2 omitted.

The experimental values of ϕ_0 and r_0 average 0.228 and 0.105 and show an approximately 10% variation. With the omission of fraction A2, the average value of

(22) A. Jablonski, *Acta Phys. Pol.*, **14**, 295 (1955); **17**, 481 (1958).
(23) R. S. Knox, *Physica*, **39**, 361 (1968).
(24) A. Kawski, *Z. Naturforsch., A*, **18**, 961 (1963).

$[(\text{Chl})/(\text{py})]_0$ is 4.09×10^{-3} with only a $\pm 15\%$ variation. There is no consistent dependence of the value of $[(\text{Chl})/(\text{py})]_0$ on molecular weight or any of the other configurational properties of the polymer listed in or inferable from Table I.

The average value of $[(\text{Chl})/(\text{py})]_0$ implies that energy transfer is 50% efficient when there is one pigment molecule to about 250 pyridine units. If the polymer chain were straight, this would correspond to an average separation between pyrochlorophyll molecules of more than 600 Å, which would be an entirely unacceptable value for R_0. However, the polymer chain is not straight but coiled, so that transfer is generally over a much shorter distance, to a pigment molecule which is not necessarily the nearest neighbor as measured along the chain. Transfer from a pigment on one polymer molecule to a pigment on another molecule would be a very rare event at the pyrochlorophyll concentration used.

One might have supposed that the higher the molecular weight, the denser would be the distribution of polymer segments, and the larger the value of $[(\text{py})/(\text{Chl})]_c$. Since experimentally there is no apparent effect of molecular weight, its influence on the segment distribution at distances of the order of R_0 must be small.

Configurational Stage. Although the form of the concentration dependence of depolarization is satisfactorily accounted for by Ore's equation, it is not possible to relate $[(\text{Chl})/(\text{py})]_0$ to c_0 and R_0 without an appropriate function for the spatial distribution of polymer segments, to which the spatial distribution of pigment molecules is assumed proportional.

It is a common practice to represent the segment distribution of a random coil polymer by a Gaussian function about the center of gravity of the coil. However, if Ore's equation as a function of γ is integrated over a Gaussian distribution of γ, the predicted polarization declines much too slowly with pigment concentration (short-dashed curve of Figure 3) to account for the experimental results. The reason, of course, is that the Gaussian distribution, by ignoring the connectivity of the chain segments, predicts polarizations that are much too large for pigment molecules at long distances from the center of gravity.

Although a Gaussian distribution cannot be assumed for the segments of the polymer molecule as a whole, it is nevertheless valid to retain it as an approximation to the link-to-link distance distribution of the equivalent random coil. In the model presented below for the calculation of emission anisotropy, the initially excited pyrochlorophyll is located half-way along a random coil, which is equivalent in Kuhn's sense to a polymer of $2Mb/a$ monomer units, where $2M = Z$. End effects are thus assumed to be negligible, which is justified experimentally and *a posteriori* by the results of the calculation. The density distribution function for a chain element N segments removed from the center is

$$\left(\frac{3}{2\pi Nb^2}\right)^{3/2} e^{-3R^2/2Nb^2}$$

and the average segment density at a distance R is twice the sum $W(R)$

$$W(R) = \left(\frac{3}{2\pi b^2}\right)^{3/2} \sum_{N=1}^{M} N^{-3/2} e^{-3R^2/2Nb^2} \tag{19}$$

This summation was performed by computer for values of R/b in units from 1 to 20, and for M from 50 to 1050 in steps of 100.

To calculate the emission anisotropy, the polymer segments, and consequently the acceptor pigment molecules, are considered to be concentrated on spherical shells at distances (R) from the initially excited molecule which are integral multiples of b.[25] An initially excited molecule is said to be of class j is the smallest shell which contains an acceptor has radius jb. The probability that an initially excited molecule belongs to class j is $P(j)$. If the relative emission anisotropy (r/r_0) for a molecule of class j, calculated by Ore's equation, is X_j, then the observed relative emission anisotropy of the whole sample is

$$r/r_0 = \sum_{j=1}^{\infty} P(j)X_j \tag{20}$$

If this quantity is calculated as a function of (Chl)/(py) for various values of R_0/b, comparison with experiment and the known value of b give the value of R_0 which best describes the results.

Since the attachment of one pyrochlorophyll to the polymer blocks several pyridine units,[1b] and probabilities $P(j)$ were calculated by a site model which better provides for attrition of pyridine units available for binding. The total number of sites on the polymer is $S = 2Mb/sa$, where s is the number of pyridine units per site. The value of s is approximately 6 according to past experience.[1b] Variation of s from 4 to 9 was found to make very little difference in the final result.

The average number of sites on and within the jth shell is

$$S_j = \left(\frac{8\pi b^3}{s}\right) \sum_{j'=1}^{j} j'^2 W(j'b) \tag{21}$$

If $F = 2Mb(\text{Chl})/a(\text{py})$ is the number of acceptor pigment molecules on the polymer, the probabilities that the initially excited molecule belongs to classes j are

$$P(1) = 1 - \frac{(S - S_1)!(S - F)!}{(S - S_1 - F)S!} \tag{22}$$

$$P(j) = \frac{(S - F)!}{S!}\left\{\frac{(S - S_{j-1})!}{(S - S_{j-1} - F)!} - \frac{(S - S_j)!}{(S - S_j - F)!}\right\} \tag{23}$$

(25) The division of space made here turns out to be undesirably coarse; however, a finer division does not seem to be warranted in the context of Kuhn's theory.

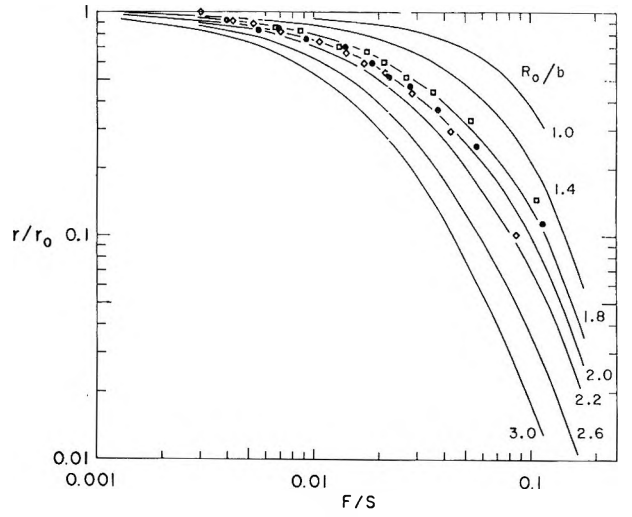

Figure 4. Emission anisotropy data for pyrochlorophyll on polymer fractions C1 (●), A4 (□), and B3 (◇) superposed on a family of curves of relative emission anisotropy (r/r_0) *vs.* pyrochlorophyll/site ratio F/S, calculated by eq 25 with $M = 1050$ and s = 6.22.

On application of Stirling's approximation, these become

$$P(j) = (1 - F/S)^{S-F} \times \left\{ \frac{(1 - S_{j-1}/S)^{S-S_{j-1}}}{(1 - S_{j-1}/S - F/S)^{S-S_{j-1}-F}} - \frac{(1 - S_j/S)^{S-S_j}}{(1 - S_j/S - F/S)^{S-S_j-F}} \right\} \quad (24)$$

To get proper convergence of the results at high pigment concentration and small values of R_0/b, it was found necessary to consider the consequences of multiple occupancy by pigment of the first occupied shell. The probability that there are just n acceptors in the jth shell is $P^n(j)(1 - P(j))$, neglecting attrition of sites. Considering up to $n = 5$ acceptors in the first occupied shell, emission anisotropies were calculated by computer from the properly modified Ore's eq 25, for various values of R_0/b, s, F/S, and M

$$\frac{r}{r_0} = \sum_{j=1}^{20} \sum_{n=1}^{5} \times \frac{P^n(j)(1 - P(j))(1 + (R_0/jb)^6)}{[(1 + (R_0/jb)^6)(1 + n(R_0/jb)^6) - n(R_0/jb)^{12} \exp(-11S_jF/16S)]} \quad (25)$$

Figure 4 shows part of a family of curves calculated for $M = 1050$ and experimental points for three polymer samples superimposed on them. The curves are all similar in shape to the curve for Ore's equation (Figure 3), but not identical. Similar families were calculated for other values of M, but only for $M < 250$ was there appreciable deviation from the curves shown.

The relationship of the abscissa F/S of Figure 4 to the abscissa of an experimental plot of r against (Chl)/(py) is fixed by the value of s, which for these calculations was 6.22. A larger or smaller value of s affects the shape of the curves very little, though of course it alters the relationship between the abscissas. There is, therefore, no latitude in the horizontal placement of the experimental points, though they may be adjusted vertically to give the best fitting value of r_0.

In Table III are listed the values of r_0 and R_0/b obtained by comparisons such as shown in Figure 4, together with the value of M for the family of curves with which comparison was made. This value was chosen to correspond most nearly to the molecular weight of the polymer. The best fitting value of R_0/b does not depend strongly on the value of M. As an extreme example, experimental points for the lowest molecular weight fraction A4, which in Figure 4 fit best to the curve for $R_0/b = 1.8$ of the family for $M = 1050$, fit best to $R_0/b = 2.0$ when $M = 50$.

Table III: Values of r_0 and R_0/b from Curves like Those of Figure 4 Which Best Fit Experimental Data

Fraction no.	M[a]	r_0	R_0/b
A2	250	0.108	1.4
A3	150	0.102	2.2
A4	50	0.098	2.0
B1	1050	0.102	2.0
B2	1050	0.094	1.8
B3	250	0.089	2.0
C1	1050	0.101	2.0
C2	1050	0.097	1.8
D1	1050	0.091	2.0
	Av[b]	0.097	1.975

[a] Value of M for set of curves from which best fitting values of r_0 and R_0/b were taken. Sets of curves for $M > 250$ are very nearly coincident. [b] Fraction A2 omitted.

The average value of r_0 is about 10% lower than the average determined by fitting to eq 17.

The average value of R_0/b corresponds, with b = 21.4 Å, to a value of 42 Å for Förster's critical transfer distance R_0. This value appears reasonable, as it is less than that for some strongly fluorescent dyes.[24] However, higher values of R_0 for chlorophyll *a* have been defended on theoretical and experimental grounds.[23,26] Correction of Förster's estimate[4] of 80 Å to our conditions along lines suggested by Duysens[27] gives an estimate of 56 Å for R_0. Weber[28] found a value of 36 Å for R_0, but this value has been questioned on theoretical grounds.[23]

There is little room for variation of R_0 in the theory presented in this paper, and if a larger value of R_0 is indeed correct, the source of the discrepancy must be

(26) R. S. Knox, personal communication; it should be noted that our R_0 is his $\bar{R}_0$.[23]

(27) L. N. M. Duysens, *Progr. Biophys.*, **14**, 1 (1964).

(28) G. Weber in "Comparative Biochemistry of Photoreactive Systems," M. B. Allen, Ed., Academic Press, New York, N. Y., 1960, p 395.

sought first, in failure of the Kuhn statistically equivalent random coil to describe the short-range polymer segment distribution correctly, and second, in failure of Ore's equation to evaluate correctly back transfer to the initially excited molecule.[23]

Acknowledgments. This work was supported in part by National Science Foundation Grants No. GB-5098 and GB-7893. We are grateful to Dr. R. S. Knox for a stimulating discussion and to Mr. T. Meyer for his technical assistance.

Application of the Magnetophotoselection Method to the Assignment of a Preferred Rotamer Structure in Bicarbazole

by Gary Paul Rabold

The Dow Chemical Company, Radiochemistry Research Laboratory, Midland, Michigan 48640

and James M. Gaidis

The Dow Chemical Company, Eastern Research Laboratory, Wayland, Massachusetts 01778 *(Received May 19, 1969)*

The magnetophotoselection method has been used to determine the geometry of bicarbazole in a frozen solvent glass at 77° K. The geometry of bicarbazole is such that the two ring systems are mutually perpendicular and the two short in-plane axes are collinear. This arrangement requires that the hybridization of the nitrogen atoms be sp^2. The zero field splitting parameters for bicarbazole are $D = 0.1056\ cm^{-1}$ and $E = 0.0075\ cm^{-1}$, and the triplet half-life is 5.53 sec. These are quite close to the carbazole values of $D = 0.1024\ cm^{-1}$, $E = 0.0066\ cm^{-1}$, and $t_{1/2} = 5.63$ sec. The results require that there be intramolecular energy transfer in bicarbazole from one ring system to the other, but the data do not differentiate between singlet–singlet or triplet–triplet energy transfer mechanisms.

Introduction

Studies of the triplet states of aromatic hydrocarbons and heterocycles have been considerably advanced by the application of electron spin resonance (esr) spectroscopy.[1,2] More recently the magnetophotoselection (mps) method has further increased the range of questions one may ask about triplet states.[3-8] The principal applications of the mps method to date have been in three areas. First, the unambiguous assignment of the correct stationary resonance field (srf) peaks to the $N \| H$ orientations has aided in the correct determination of zero field splitting (zfs) parameters.[4,7a,8] Here N is the molecular axis which is perpendicular to the molecular plane and H is the external magnetic field. Second, the mps method has been used as a corroborative tool in studies of the polarization of optical transitions.[6] Finally, it has been successfully applied to the study of intermolecular energy transfer.[5]

We report herein the results of a unique application of the mps method to the question of the molecular geometry of bicarbazole and the hybridization of its two nitrogen atoms. The results provide strong evidence for intramolecular energy transfer from one carbazole moiety to the other, although it is not possible to distinguish unambiguously between singlet–singlet or triplet–triplet energy transfer mechanisms in the absence of data on the polarization of luminescence. The overall pathway for population of the triplet state can be given as

$$S_0 \xrightarrow{h\nu} S^* \longrightarrow T \qquad (1)$$

where S_0 is the ground singlet state, S^* is an excited singlet state, and T is the lowest triplet state. Results

(1) E. Wasserman, L. Snyder, and W. A. Yager, *J. Chem. Phys.*, **41**, 1763 (1964).

(2) J. H. van der Waals and M. S. de Groot, *Mol. Phys.*, **2**, 333 (1959); *ibid.*, **3**, 190 (1960).

(3) J. M. Lhoste, A. Haug, and M. Ptak, *J. Chem. Phys.*, **44**, 648 (1966); *ibid.*, **44**, 654 (1966).

(4) M. A. El-Sayed and S. Siegel, *ibid.*, **44**, 1416 (1966).

(5) S. Siegel and L. Goldstein, *ibid.*, **44**, 2780 (1966).

(6) S. Siegel and H. S. Judeikis, *J. Phys. Chem.*, **70**, 2205 (1966).

(7) (a) G. P. Rabold and L. H. Piette, *Photochem. Photobiol.*, **5**, 733 (1966); (b) G. P. Rabold and L. H. Piette, *Spectrosc. Lett.*, **1**, 211 (1968).

(8) Y. Gondo and A. H. Maki, *J. Phys. Chem.*, **72**, 3215 (1968).

are also presented for carbazole which are in excellent agreement with those reported earlier by Siegel and Judeikis,[6] who excited with light having a broader wavelength distribution. In this study, carbazole serves as a model for bicarbazole.

Experimental Section

Materials. Carbazole was obtained commercially. Its esr spectrum and triplet state lifetime were in agreement with the corresponding values reported in the literature.[9] There were no peaks in the esr spectrum which did not arise from carbazole. Bicarbazole (mp 221–222°) was prepared according to a published procedure.[10] As with carbazole there were no peaks in the bicarbazole esr spectrum which were attributable to impurities. The solvents were shown to be free of interfering impurities.

Methods. The esr spectra were measured with a Varian V-4502 esr spectrometer operating at a modulation frequency of 100 kHz. A Varian V-4531 rectangular cavity, which operates in the TE 102 mode, was employed. Samples were made up to *ca.* 3×10^{-3} *M* or less in a 1:1 mixture of ethanol–methanol in 4-mm o.d. quartz tubes which were stoppered with rubber serum caps, but not degassed. It was established by visual observation of the phosphorescence that the concentrations were such that essentially all of the light was absorbed by the sample. The standard quartz Dewar was employed to obtain the low temperature. No spectra were recorded of samples which had "cracked" glasses, and the Dewar was kept free of ice particles. Otherwise, no precautions were taken to avoid depolarization of the incident light. The optical arrangement, which uses an Osram 200-W super pressure mercury lamp in conjunction with a Bausch and Lomb high intensity grating monochromator, has been described elsewhere.[7a] A polaroid plate, PL 105 UV, made by Polacoat Inc., was used in place of the Glan-Thompson polarizing prism. Throughout this paper the terms parallel and perpendicular refer to the orientation of the electric vector, *E*, of the polarized light with respect to the external magnetic field, *H*. The band width of the exciting light, according to Bausch and Lomb specifications, is about 42 nm under our experimental conditions. Figure 1 shows the spectral output of the light source at several monochromator settings. The microdensitometer traces of the photographic plate are plotted as $100 - \%\ T$ *vs.* wavelength, where *T* is the transmitted light. Thus, in the context of this paper, the term excitation wavelength actually refers to a fairly broad band at the designated monochromator setting.

In this system there was no significant problem with signal-to-noise optimization, as can be seen from the relatively low noise levels in the spectra presented. In the mps experiments only the srf regions of the spectra were recorded in order to minimize photodecomposition, which might otherwise introduce inaccuracies into the intensity measurements.

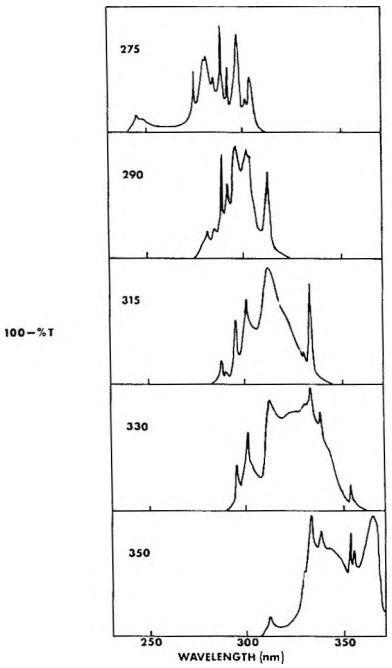

Figure 1. Densitometer traces of the spectral output of the light source at several monochromator settings. The ordinate values are one hundred minus percent transmission. The monochromator settings are given at the left of each box.

The magnetic field was measured directly from the spectrometer fieldial after initially calibrating it with a Rawson Lush Type 920 rotating coil gauss meter. A short program was written to calculate the zfs parameters using the method of Wasserman, Snyder, and Yager.[1] Based on the assumption of a nearly isotropic *g* tensor, $\mathbf{H}_0$ was varied by iteration until the differences between the *g* values were minimized. Zfs parameters obtained by this method agreed with literature values to within 0.3 mK.

Decay times for the triplet states were obtained by observing the disappearance of the $\Delta m = 2$ peaks in the esr spectra. The decays adhered strictly to first-order kinetics over more than three half-lives.

Esr Spectra

The esr spectra of triplets in a frozen solvent glass consist of peaks arising from two classes of transitions. These are the $\Delta m = 2$ and the $\Delta m = 1$ transitions, where *m* is the strong-field quantum number of the electron. We concern ourselves here only with the $\Delta m = 1$ transitions. These give rise to three pairs of peaks in the esr spectrum, where each pair arises from a set of molecules having one of the three molecular axes parallel to the laboratory magnetic field. A detailed line shape analysis for triplet states in a frozen solvent glass has been given in the literature by Wasser-

(9) S. Siegel and H. S. Judeikis, *J. Phys. Chem.*, **70**, 2201 (1966).
(10) W. H. Perkin, Jr., and S. H. Tucker, *J. Chem. Soc.*, 216 (1921).

man, Snyder, and Yager.[1] The Hamiltonian for the zero field dipolar spin–spin interaction is expressed as

$$\mathcal{H} = D(S_z^2 - {}^1/_3S^2) + E(S_x^2 - S_y^2) \qquad (2)$$

where D and E are the zfs parameters and S_i^2 is the projection of the spin angular momentum along the ith molecular axis. The magnitudes of D and E afford a measure of the spatial distribution of the two electrons over the molecular framework.

Photoselection Studies

The principles underlying photoselection experiments have been discussed in detail in a review by Albrecht.[11] We present here only the essential features of this method and refer the reader to the review for more detail. For π,π^* singlet excitation only those molecules will be excited which have an appropriate transition moment closely parallel to the direction of polarization of the exciting light. For an idealized aromatic molecule of suitable symmetry we may assume that two transition moments lie along the two mutually perpendicular in-plane molecular axes and that the transition moment perpendicular to the molecular plane is vanishingly small. Thus, under the proper conditions, it is possible to obtain a nearly uniaxially oriented collection of excited molecules from a randomly oriented ground-state population. In the cases of broad band excitation or of overlapping of absorption bands one may obtain two sets of uniaxially oriented excited states. The relative population of each set will depend on the spectral region of excitation and on the spectral distribution of the exciting light. The combination of polarized excitation with esr detection has been called magnetophotoselection.[4,12]

Results

The esr spectra of the carbazole and bicarbazole triplet states generated with unpolarized 315-nm light are shown in Figure 2. The centers of the spectra are not included, since the signals arise only from free-radical intermediates resulting from photochemical reactions. The molecular axes are assigned as L, M, and N for the long in-plane, short in-plane, and perpendicular axes, in conformity with the notation of Siegel and Judeikis.[6] The peaks in the esr spectra are labeled to correspond to the alignment of the designated molecular axes parallel to the external magnetic field. The values of the zfs parameters are $D = 0.1024$, $E = 0.0066$ cm^{-1} for carbazole and $D = 0.1056$, $E = 0.0075$ cm^{-1} for bicarbazole.

Some esr spectra of carbazole, taken under photoselection conditions are shown in Figure 3. Only the low-field peaks are shown since the corresponding high-field peaks respond to polarized excitation in the same way. The continuous background between peaks was not recorded so that the total time of exposure of the sample to irradiation would be kept as short as possible. In this manner any effects of photochemical reactions are minimized. The ratio of the L to the M peak amplitudes is 0.92 and 1.10 for excitation with 315 full and 280 full (wavelength and polarization) light, respectively, whereas the ratios are 1.1 and 2 with 315 parallel and 280 parallel excitation, and 0.58 and 0.31 with 315 perpendicular and 280 perpendicular light. This points out that the relative amplitudes of the srf peaks[8] depend both on the wavelength and the direction of polarization of the exciting light. A complete summary of the results of the mps experiments on carbazole is given in Table I. The half-life of the carbazole triplet state in the 1:1 MeOH/EtOH frozen glass at 77° K, as measured from the decay of the $\Delta m = 2$ esr signal, is 5.63 sec.

In Figure 4 are presented the results of some mps experiments on bicarbazole at three different exciting wavelengths. It is fairly obvious that the ratios of the L to the M peak amplitudes are quite low with 315 parallel excitation and are fairly high with 280 parallel

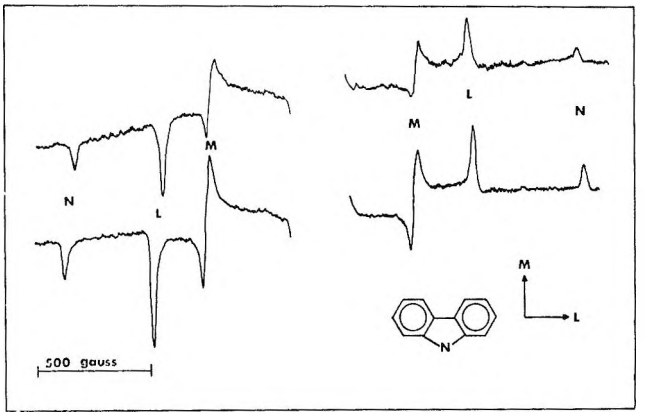

Figure 2. $\Delta M = 1$ esr spectra of carbazole (upper) and bicarbazole (lower) and axis assignments.

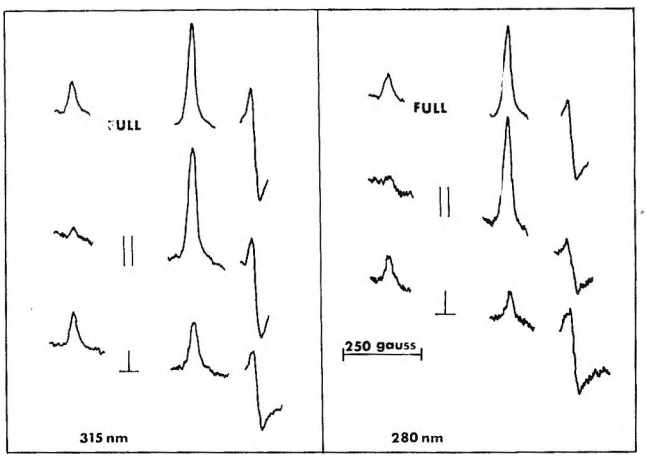

Figure 3. Esr spectra of carbazole under magnetophotoselection conditions.

(11) A. C. Albrecht, *J. Mol. Spectrosc.*, **6**, 84 (1961).
(12) P. Kottis and R. Lefebvre, *J. Chem. Phys.*, **41**, 3660 (1964).

Table I: Summary of the Magnetophotoselection Results for Carbazole and Bicarbazole[a]

Excitation wavelength, nm	Peak intensity (∥) M	(∥) L	(∥) N	(⊥) M	(⊥) L	(⊥) N
350	36.2	10.3	1.5	9.5	12.8	5.5
340	48	23.6	3.5	22.2	20.8	11
332	48	36.3	4.3	25.8	22.2	12.3
315	48	54.5	6.8	35	21.8	15.8
280	16.5	35	2.5	25	9.5	9
350	58	9.6	3	11	25.8	8.2
335	50	18.5	6	19.5	28.8	9
315	64.5	37.3	12.7	35.5	42	13.4
300	45	32.2	9.8	32	30.8	9.8
290	32	25.4	7.9	24.2	21.3	7.2
280	24	34.6	10.1	34.8	26.3	9.4

[a] The top set of data is for carbazole, the lower set for bicarbazole.

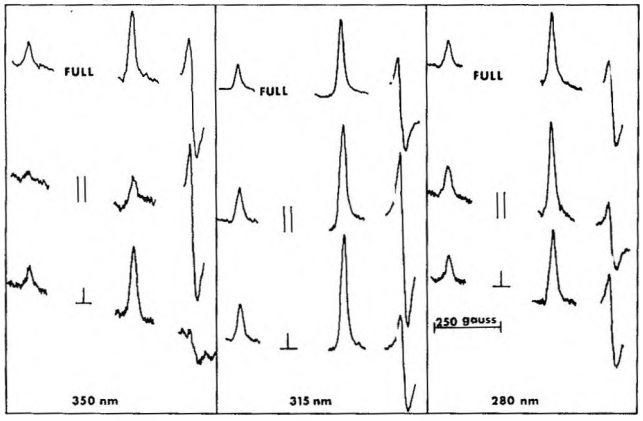

Figure 4. Esr spectra of bicarbazole under magnetophotoselection conditions.

excitation, and that the relative ratios are reversed with perpendicular excitation. What is more interesting for this molecule, however, is that the ratio of $N\|/N\perp$ is the same as $L\|/L\perp$ at all wavelengths. Thus there is observed an equivalence between the N and L molecular axes in their responses to excitation with polarized light. The complete results for the mps experiments with bicarbazole are summarized in Table I along with those for carbazole. The half-life of the bicarbazole triplet state is 5.53 sec.

The uv absorption spectrum of bicarbazole is similar to that for carbazole in the number, relative intensity, and spacing of the bands, but is shifted approximately 10 nm to shorter wavelength. The carbazole spectrum is in complete agreement with that presented by Siegel and Judeikis.[6]

Discussion

We first show how one may predict the features of the esr spectra for carbazole under photoselection conditions. The rectangles in Figure 5 represent carbazole

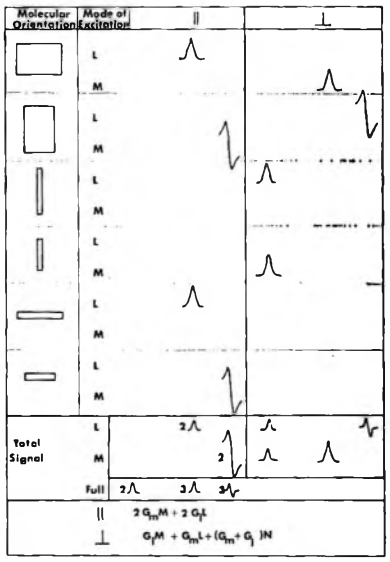

Figure 5. Predicted esr spectra for carbazole under magnetophotoselection conditions.

molecules, with L and M being the long and short in-plane molecular axes. The six unique orientations of the molecule with respect to the external magnetic field are shown, where the magnetic field is in the plane of the paper and parallel to the L axis of the uppermost molecules. To a first approximation only these six orientations need be considered since they have the highest probability of esr observation regardless of which molecules are excited. The mode of excitation is given as either parallel (direction of polarization of the exciting light parallel to the external field) or perpendicular, and as L (the excitation wavelength is suitable for absorption along the long molecular axis) or M. Within each box the abscissa is the laboratory magnetic field with a range of values sufficiently broad to encompass the three low-field peaks of the $\Delta m = 1$ transitions. For the first orientation, only L peaks will be observed in the esr spectrum, and these will arise from parallel excitation along the L axis and perpendicular excitation along the M axis. The notation we use is that parallel excitation gives G_lL and perpendicular excitation affords G_mL, where G_i is the probability of excitation along the ith axis and L is the peak designation. Using this same notation the second orientation will give G_mM under parallel excitation and G_lM under perpendicular excitation. For the third and fourth orientations parallel light will not be absorbed since the requirement that there be a nonvanishing transition moment parallel to the direction of the polarization of the light is not fulfilled. The assumption is made here that the transition moment along the molecular N axis is negligible. With perpendicular excitation, orientations three and four give rise to G_lN and G_mN. The last two orientations give rise to G_lL and G_mM with parallel excitation and no peaks with perpendicular irradiation. We can now sum up over all six molecular orientations to obtain

the total predicted spectrum. If light of a wavelength suitable only for excitation along the L axis is used, the photoselected esr spectrum will have an L peak with a statistical weight of 2 under parallel excitation, and an N and an M peak with statistical weights of 1 under perpendicular excitation. If excitation is only along the M molecular axis, then the photoselected esr spectrum will have an M peak with a weight of 2 with parallel excitation and an N and an L peak with weights of 1 with perpendicular excitation. If, either because of overlap of absorption bands or because of broad band excitation, there is excitation involving components of both molecular axes then the predicted peak intensities can be expressed as $2G_mM + 2G_lL$ for parallel excitation and $G_lM + G_mL + (G_m + G_l)N$ for perpendicular excitation. From the above considerations one would predict the ratio $M||/M\perp$ to vary as $2G_m/G_l$ and the ratio $L||/L\perp$ to vary as $2G_l/G_m$. Further, given an experimental value of $M||/M\perp$ under a given set of experimental conditions this treatment predicts a unique value for $L||/L\perp$. The agreement between these predictions and the experimental results is quite good. It will be noticed that no N peaks are predicted during parallel excitation, whereas there clearly are N peaks in the actual parallel spectra of Figure 3. These are quite small and could arise from the depolarization of the exciting light, from a small nonvanishing transition moment along the N axis, or from the noncoincidence of the molecular, optical, and magnetic axes.[6] This simple case has been treated in detail since the same reasoning is used below for the more complex models of bicarbazole. If satisfactory agreement between the predictions and the experimental results could not be obtained for carbazole itself, it would be of little value to extend the treatment to bicarbazole.[13,14]

The usual expression for the polarization ratio, P_i, is given as

$$P_i = (||_i - \perp_i)/(||_i + \perp_i) \qquad (3)$$

where the subscript i refers to a molecular axis assignment (L, M, or N), and $||$ and $\perp$ are the ith peak intensities under conditions of parallel and perpendicular excitation. Siegel and Judeikis[6] have derived an expression for r_i, the component of polarization along the ith axis, which is given as

$$r_i = (1 + (1 + 4k/3)P_i)/(3 - P_i) \qquad (4)$$

where k is a depolarization factor. We have used a value of $k = 0.1$. The trends presented in Figure 6 are relatively unaffected by a value of k up to 0.5.

In Figure 6 we present plots of r_i *vs.* wavelength for carbazole and bicarbazole. For carbazole r_M decreases from 0.7 at 350 nm to about 0.25 at 280 nm, r_L increases from *ca.* 0.30 at 350 nm to 0.7 at 280 nm, and r_N is small and nearly constant over the entire wavelength range. Although r_M for bicarbazole is quite like that for carbazole, both r_L and r_N respond in distinctly different ways in the different molecules. In fact r_N and r_L are the same in bicarbazole within experimental error, indicating that the N and L molecular axes are apparently equivalent. It remains for us therefore to propose a structure which will enable us to predict this result.

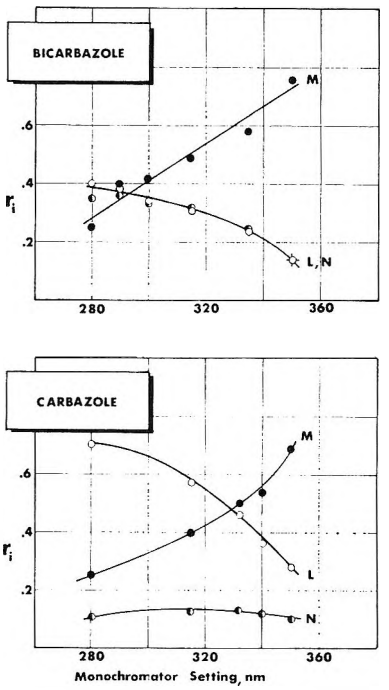

Figure 6. Plots of the polarization components *vs.* monochromator setting for carbazole and bicarbazole.

In the ensuing discussion several assumptions are made. (1) We assume that the carbazole moieties in bicarbazole absorb light independently. Thus each carbazole moiety has the same selection rules for absorption as does carbazole itself. This is reasonable in view of the great similarity of the uv absorption spectra. If the chromophores did interact significantly, one might expect a bathochromic shift (*cf.* $\Delta^{9,9'}$-bifluorenylidene) rather than the slight blue shift which is experimentally obtained. (2) There is intramolecular energy transfer such that although the light is absorbed by a single carbazole moiety, there is an equal probability that the triplet state will reside on either half of the molecule.[15a,b] While this is stated here as

(13) We are grateful to a referee for bringing to our attention the importance of considering depopulation of the ground state.[11,14] In the limit of very high intensity, the triplet-state molecules lose their orientation and the polarization phenomenon is not observed.[14] In our experiments, the highest light intensity is achieved with 315-nm light. At this wavelength a threefold variation of the intensity leads to no significant change in the observed polarization ratios, and we therefore conclude that ground-state depletion is not occurring to a significant extent.

(14) B. I. Stepanov and V. P. Gribkovskii, *Opt. Spectrosc.*, 8, 114 (1960) (translated from *Opt. Spectrosk.*, 8, 224 (1960)).

(15) (a) P. J. Wagner and G. S. Hammond, "Advances in Photochemistry," Vol. 5, Interscience Publishers, New York, N. Y., 1968, p 49; R. A. Keller and L. J. Dolby, *J. Amer. Chem. Soc.*, 91, 1293 (1969). (b) The orientation dependence for triplet–triplet energy transfer is of widespread current interest.[5] Our understanding of such systems should be substantially aided by additional studies planned on systems similar to bicarbazole.

an assumption it in fact results logically from the data. The energy transfer could be either singlet–singlet or triplet–triplet, a question which could be readily resolved by measurements on the polarization of fluorescence. If it is triplet–triplet energy transfer, its rate must be significantly faster than the measured triplet lifetime and slower than T_1, the lifetime of the magnetic spin state, which has been estimated as 10^{-7} sec for the naphthalene triplet state.[5] If the rate of triplet–triplet energy transfer were faster than T_1, the zfs parameters D and E would not be so nearly equal for carbazole and bicarbazole. (3) It is assumed that there is no depolarization due to intermolecular energy transfer. This is entirely reasonable for the concentration range used in this study.[5] (4) It is assumed that there is a close coincidence of the molecular, optical, and magnetic axes. The molecular symmetry is sufficiently high that this assumption is quite reasonable. (5) The assumption which has the most bearing on the results is that the long wavelength transition is predominantly short axis polarized and the short wavelength transition is predominantly long axis polarized. We can make this assumption with confidence on the basis of Hückel molecular orbital (MO) calculations.[16] The transition of an electron from the highest filled to the lowest empty molecular orbital requires the **E** vector to be parallel to the short axis of carbazole. The theory behind the predictions has been well tested in the case of naphthalene,[17–19] anthracene,[18,20,21] phenanthrene,[18,19,22] chrysene,[19] perylene,[23] and dibenzofuran, dibenzothiophene, and carbazole.[6] The agreement between theory and experiment represents a substantial achievement for MO theory.[24]

The four proposed structures are shown in Figure 7. Structures I and II are a pair of rotamers with sp^2 hybridization at nitrogen. Structures III and IV are also a pair of rotamers, but with sp^3 hybridization at the nitrogen atoms. Both rotamers II and III should respond in mps experiments like carbazole itself, whether there is intramolecular energy transfer or not, since the L, M, and N axes of one carbazole moiety are parallel to the same axes on the other carbazole moiety. Since the experimental results clearly show that the esr spectra of carbazole and bicarbazole respond differently to polarized excitation, both rotamers II and III can be eliminated as serious possibilities.[25,26]

Let us turn now to Figure 8 to see what mps results are predicted for rotamer I. As was done earlier for carbazole, we consider what peaks will be observed in the esr spectrum for each of the six molecular orientations along the external magnetic field as the direction of polarization of the exciting light is changed. Again, the magnetic field is in the plane of the paper and parallel to the M axes of the uppermost molecule. Since there are two chromophores, absorption by each chromophore is considered separately. For the first orientation parallel light will be absorbed by the

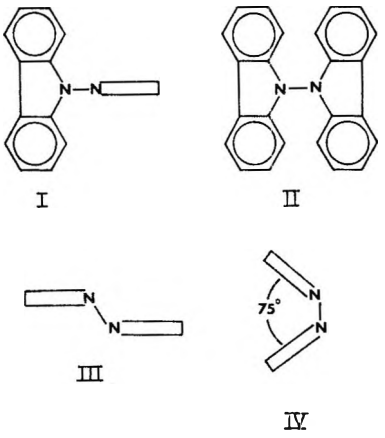

Figure 7. Rotamer structures for bicarbazole.

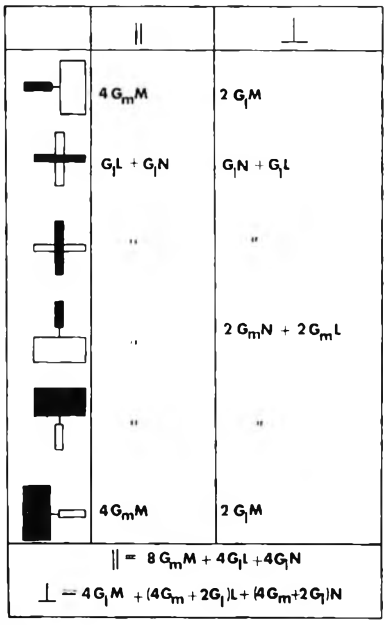

Figure 8. Predicted esr spectra for bicarbazole rotamer I under magnetophotoselection conditions.

(16) h_N = 1.0, k_{CN} = 0.9. These values may vary over the range h_N = 0–1.8 and k_{CN} = 1.0–0.5 without affecting the ordering of the levels. See ref 24, p 117.

(17) D. S. McClure, *J. Chem. Phys.*, **22**, 1256 (1954).

(18) D. S. McClure, *ibid.*, **22**, 1668 (1954).

(19) M. A. El-Sayed and T. Pavlopoulos, *ibid.*, **39**, 834 (1963).

(20) J. W. Sidman, *ibid.*, **25**, 115 (1956).

(21) J. W. Sidman, *ibid.*, **25**, 122 (1956).

(22) R. M. Hochstrasser and G. J. Small, *ibid.*, **45**, 2270 (1966).

(23) R. M. Hochstrasser, *ibid.*, **40**, 2559 (1964); J. Tanaka, *Bull. Chem. Soc. Jap.*, **36**, 1237 (1963).

(24) A. Streitwieser, Jr., "Molecular Orbital Theory for Organic Chemists," John Wiley & Sons, New York, N. Y., 1961, p 217.

(25) The nmr spectrum of bicarbazole (6% in THF, 60 and 100 MHz) shows well-separated multiplets at 6.75 δ (1,8,1′,8′), 7.18 δ (2,3,6,7,2′,3′,6′,7′), and 8.10 δ (4,5,4′,5′). The set at 8.10 δ is shifted downfield by the ring current in the central ring of carbazole,[26] and the set at 6.75 δ is shifted upfield by the magnetic anisotropy of an aromatic ring. Only in rotamers I and III would the proton set (1,8,1′,8′) be shielded. Rotamers II and IV may be eliminated from consideration since they predict a downfield shift for the (1,8,1′,8′) set.

(26) J. M. Gaidis and R. West, to be published.

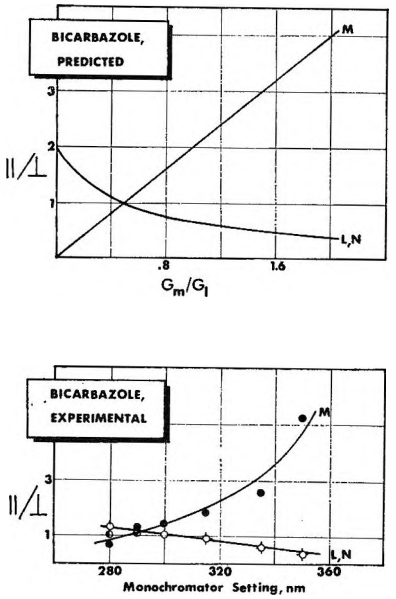

Figure 9. Comparison of the predicted *vs.* the experimental values for the ratios of the parallel and perpendicular components of the esr spectra.

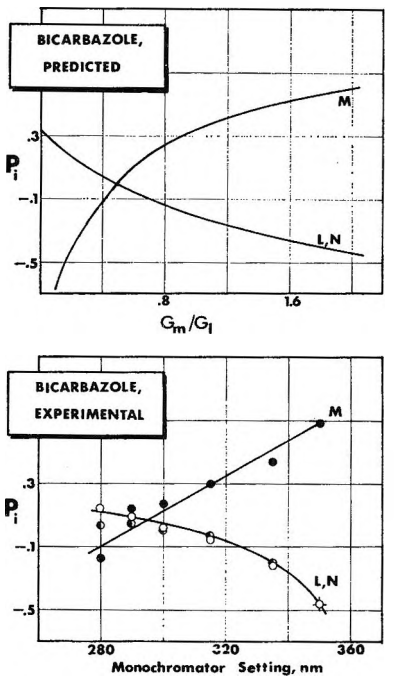

Figure 10. Comparison of the predicted *vs.* the experimental values for P_i.

shaded chromophore with a probability G_m. Because of energy transfer esr peaks will be observed for both the shaded and the open carbazole moieties, each of which gives rise to an M peak. Thus what actually appears in the esr spectrum from this orientation from excitation of the shaded chromophore is $^1/_2G_mM + {}^1/_2 \cdot G_mM$, where the weighting factor $^1/_2$ is a consequence of the intramolecular energy transfer. Since there is an equal probability that the light will be absorbed by the unshaded half of the molecules, the total esr transition

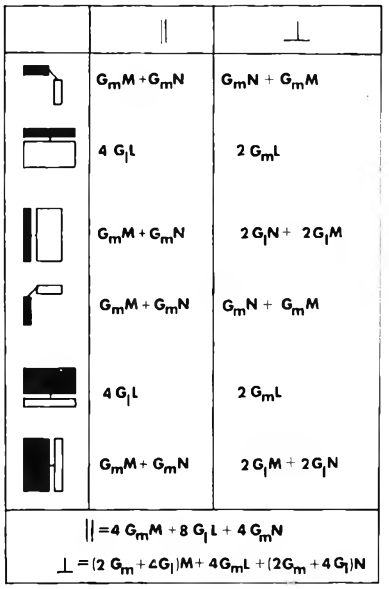

Figure 11. Predicted esr spectra for bicarbazole rotamer IV under magnetophotoselection conditions.

will be, for parallel excitation, $G_mM + G_mM = 2G_mM$. For convenience every entry in the figure has been multiplied by a factor of 2. For this same orientation, perpendicular light will be absorbed only along the L axis of the unshaded chromophore with a probability G_l. With intramolecular energy transfer there will be observed the peaks $^1/_2G_lM + {}^1/_2G_lM$. Turning to the second orientation, parallel light will be absorbed only along the L axis of the shaded chromophore with a probability G_l and will give, after energy transfer, $^1/_2G_lL + {}^1/_2G_lN$. Perpendicular light will be absorbed only along the L axis of the unshaded chromophore and will also give $^1/_2G_lL + {}^1/_2G_lN$. The only remaining unique orientations are the fourth and fifth under perpendicular excitation. Similar reasoning leads to the peaks $G_mN + G_mL$ for these orientations. Summing up over all six molecular orientations we obtain the peak amplitudes $8G_mM + 4G_lL + 4G_lN$ for parallel excitation and $4G_lM + (4G_m + 2G_l)L + (4G_m + 2G_l)N$ for perpendicular excitation. From this we can calculate the predicted ratios of the peaks obtained from each excitation mode. These are

$$\begin{aligned} M||/M\perp &= 2G_m/G_l \\ L||/L\perp &= 2G_l/(2G_m + G_l) \\ N||/N\perp &= 2G_l/(2G_m + G_l) \end{aligned} \tag{5}$$

This model thus predicts that the L and N peaks will appear to be equivalent in mps experiments.

In Figures 9 and 10 the predictions from eq 4 are compared with the experimental results. The relation between the abscissas of the two curves is not known, and therefore the differences in the curvatures are not of consequence. We are concerned only with the ordinate values, and it can be seen that the agreement between

the experimental and the predicted results is excellent. Thus in Figure 9 we see that the L and N axes are predicted to be equivalent, and the results agree. The model predicts the curves will intersect at an ordinate value of 1, and again the results agree. At a given ratio of $M||/M\perp$ it can be seen that the corresponding values of $L||/L\perp$ or $N||/N\perp$ are in good agreement with the predicted ones. The experimental results are thus in complete accord with the predictions based on rotamer I. However, it remains to show that rotamer IV is inconsistent with the experimental results.

The results predicted for an mps experiment on rotamer IV can be obtained by reference to Figure 11. The simplifying approximation is made that the dihedral angle is 90° rather than the actual angle of about 75°. After going through the same reasoning as was used with rotamer I, one finds predicted intensities of $4G_mM + 8G_lL + 4G_mN$ for parallel excitation and $(2G_m + 4G_l)M + 4G_mL + (2G_m + 4G_l)N$ for perpendicular excitation. From this one predicts the following peak ratios

$$\begin{aligned} M||/M\perp &= 2G_m/(G_m + 2G_l) \\ L||/L\perp &= 2G_l/G_m \\ N||/N\perp &= 2G_m/(G_m + 2G_l) \end{aligned} \tag{6}$$

This model predicts the same type of curves as are shown in Figures 9 and 10 with G_m and G_l interchanged. More importantly, it predicts that the M and the N axes will be equivalent. Based on the validity of the above-mentioned optical selection rules, this last prediction is inconsistent with the experimental data, and therefore rotamer IV is rejected as a possible structure.[27]

Conclusions

A consideration of the several possible structures of 9,9′-bicarbazole has shown that each one would have a distinct and identifiable response in mps experiments. Esr spectra were calculated for the several rotamers with the aid of well-founded selection rules for determining the polarization of optical transitions. The excellent agreement between the experimental results and those predicted for the twisted structure with sp^2 nitrogen (rotamer I) leads to its selection as the favored conformer.

(27) NOTE ADDED IN PROOF. It has come to our attention that the low-energy electronic transition in carbazole has been experimentally demonstrated to be short axis polarized [A. Bree and R. Zwarich, *J. Chem. Phys.*, **49**, 3355 (1968)]. We had assumed this in the Discussion section.

Nuclear Spin–Lattice Relaxation and Chemical Shift Studies of Fluorocarbon–Hydrocarbon Mixtures

by Charles L. Watkins and Wallace S. Brey, Jr.

Department of Chemistry, University of Florida, Gainesville, Florida 32601
(Received May 19, 1969)

The concentration dependence of the ^{19}F spin–lattice relaxation times and the proton chemical shifts has been studied for four hexafluorobenzene–hydrocarbon mixtures. These physical measurements provide no indication of the existence of specific fluorocarbon–hydrocarbon interactions in the hexafluorobenzene–cyclohexane and hexafluorobenzene–benzene systems. The results confirm the existence of a weak interaction in the hexafluorobenzene–mesitylene system. Complex formation is detected in the hexafluorobenzene–dimethylformamide system. The experimental results do not offer any evidence for charge-transfer interactions. A discontinuity is observed in the viscosity-corrected T_1 plot as a function of fluorocarbon concentration in the 2,2,2-trifluoroethanol–ethanol system indicating strong mixed hydrogen bonding involving the hydroxyl groups.

Introduction

The properties of perfluorocarbon–hydrocarbon mixtures have generated a considerable amount of interest in the past few years.[1] Various thermodynamic and spectroscopic studies have been conducted, chiefly to explain the unusual solubility relations encountered. The chief approach to the analysis of the thermodynamic properties of these systems has been the solubility parameter theory[2] first proposed by Scatchard and Hildebrand. Experimental data accumulated after the first attempt by Scott[3] to apply the regular solution theory to fluorocarbon–hydrocarbon mixtures were in disagreement with that theory.[4–11]

Various attempts have been made to explain this unusual solution behavior. One proposal was that the hydrocarbon molecules interpenetrated in a special way,[5,12] and Hildebrand suggested that the solubility parameters for the hydrocarbons should be taken from the solubility behavior rather than from the heats of vaporization.[13] Attempts have been made to apply the "corresponding states" treatment of Scott,[14] but the geometric mean law fails to predict the correct magnitude of unlike interactions. Reid[15] proposed a correction based on the estimated ionization potentials of the solution constituents, but the most nearly successful treatment seems to be that of Munn[16] who used an equation involving directly the interaction energies as predicted from molecular polarizabilities of the components.

Recent studies of hexafluorobenzene with various hydrocarbon solvents indicate the possibility of charge-transfer complex formation in aromatic perfluorocarbon–aromatic hydrocarbon systems.[17–19] Most of the systems form a 1:1 solid complex. X-Ray and wide-line nuclear magnetic resonance studies indicate that the solid complexes exist in alternate stacked planes.[20,21] This stacking arrangement is also thought to prevail to some extent in the liquid state. Strong n-electron donors give rise to a new absorption band in the ultraviolet spectrum when mixed with hexafluorobenzene. However, no absorption attributed to charge-transfer complex formation has been reported for π-electron donors.[22–24] A slight shift in the absorption tail of the π-electron donor was noted by Hammond for some

(1) R. L. Scott, *J. Phys. Chem.*, **62**, 136 (1958).

(2) J. H. Hildebrand and R. L. Scott, "Solubility of Nonelectrolytes," 3rd ed, Reinhold Publishing Corp., New York, N. Y., 1950.

(3) R. L. Scott, *J. Amer. Chem. Soc.*, **70**, 4090 (1948).

(4) J. H. Simons and J. W. Mausteller, *J. Chem. Phys.*, **20**, 1516 (1952).

(5) J. H. Simons and R. D. Dunlap, *ibid.*, **18**, 335 (1950).

(6) J. H. Hildebrand, B. B. Fisher, and H. A. Benesi, *J. Amer. Chem. Soc.*, **72**, 4348 (1950).

(7) G. J. Rotariu, R. J. Hanrahan, and R. E. Fruin, *ibid.*, **76**, 3752 (1954).

(8) N. Thorp and R. L. Scott, *J. Phys. Chem.*, **60**, 670 (1956).

(9) N. Thorp and R. L. Scott, *ibid.*, **60**, 1441 (1956).

(10) I. M. Croll and R. L. Scott, *ibid.*, **62**, 954 (1958).

(11) I. M. Croll and R. L. Scott, *ibid.*, **68**, 3853 (1964).

(12) R. D. Dunlap, *J. Chem. Phys.*, **21**, 1293 (1953).

(13) J. H. Hildebrand, *ibid.*, **18**, 1337 (1950).

(14) R. L. Scott, *ibid.*, **25**, 193 (1956).

(15) T. M. Reid, III, *J. Phys. Chem.*, **59**, 425 (1955).

(16) R. J. Munn, *Trans. Faraday Soc.*, **57**, 187 (1961).

(17) D. V. Fenby, I. A. McLure, and R. L. Scott, *J. Phys. Chem.*, **70**, 602 (1966).

(18) G. S. Prosser and C. P. Patrick, *Nature*, **187**, 1021 (1960).

(19) W. A. Duncan and F. L. Swinton, *Trans. Faraday Soc.*, **62**, 1082 (1966).

(20) J. C. A. Boeyens and F. H. Herbstein, *J. Phys. Chem.*, **69**, 2153 (1965).

(21) D. F. R. Gilson and C. A. McDowell, *Can. J. Chem.*, **44**, 945 (1966).

(22) R. Foster and C. A. Fyfe, *Chem. Commun.*, 642 (1965).

(23) P. R. Hammond, *J. Chem. Soc., A*, 145 (1968).

(24) T. G. Beaumont and K. M. C. Davis, *ibid., B*, 1131 (1967).

hexafluorobenzene–aromatic hydrocarbon systems.[23] However, the donor absorption prevents any observation of a charge-transfer maximum. The lack of observation of a charge-transfer absorption may be attributed to the small overlap of the π-donor orbitals with the weak acceptor orbitals of hexafluorobenzene. Preliminary nuclear magnetic resonance investigations of the hexafluorobenzene–hexamethylbenzene–carbon tetrachloride system showed a concentration-independent fluorine chemical shift.[22] Phase diagrams, volume changes on mixing, and dipole moments have been reported by Swinton[19,25] for six hexafluorobenzene–hydrocarbon systems. He concludes that the existence of a compound in the solid state does not necessarily imply any specific interaction in the liquid state. Scott[26] divides any interactions which might occur in a system composed of an aromatic fluorocarbon and a hydrocarbon into three categories: physical interactions such as dispersion forces, specific chemical interactions such as charge transfer, and specific interactions between aromatic rings such as quadrupolar–quadrupolar and bond dipolar interactions.

A fluorocarbon–hydrocarbon system in which there is a known specific chemical interaction is the 2,2,2-trifluoroethanol–ethanol system. Ethanol and 2,2,2-trifluoroethanol (TFE) resemble each other in molecular structure, boiling point, and dielectric constant, but differ considerably in acidity, basicity, and solvating ability.[27] Since the two liquids are miscible in all proportions, the TFE–ethanol system is of interest in studying hydrogen bonding and relative solvating ability between the two components and in comparing with the hexafluorobenzene–hydrocarbon systems.

The above hydrocarbon–fluorocarbon mixtures have been examined by measurement of the concentration dependence of the ^{19}F spin–lattice relaxation time and of the proton chemical shift to determine what types of solute–solvent interactions are occurring. The Bloembergen, Purcell, and Pound theory[28] gives the dependence of T_1 on the temperature and viscosity for liquids. $1/T_1$, the inverse of the spin–lattice time, is proportional to the ratio of the viscosity to the absolute temperature, η/T, provided the correlation time describing the motion is much less than the Larmor frequency. For solutions in which molecular association occurs, the BPP theory does not hold since the correlation time for the motion considered is usually much longer than for unassociated liquids, and T_1 usually possesses a minimum. Giulotto[29] and Murthy[30] have both observed minima in T_1 where strong association occurs. Brownstein[31] has studied by spin–lattice relaxation various weakly interacting systems which do not show a chemical shift change with change in concentration.

Experimental Section

The ^{19}F spin–lattice relaxation times were measured by the method of adiabatic fast passage at 56.4 MHz. The linear sweep unit of a Varian DP-60 spectrometer was replaced by a Wavetek function generator which provided a triangular sweep which was fed directly to the sweep coils. The sweep was displayed on a Hewlett-Packard Model 120B oscilloscope. The field position and period were adjusted until there was a null point on the return trace. At least five independent measurements were made on each solution. For most of the measurements, the average deviation was 0.10–0.15 sec.

The temperature was regulated by the flow rate of dry nitrogen through a Varian V4340 variable temperature probe assembly. The temperature was determined by a copper–constantan thermocouple placed within the Dewar insert, accurate to 1°. All of the T_1 measurements were taken at 30° except for the hexafluorobenzene–mesitylene mixtures which were taken at 40°.

The removal of molecular oxygen is very important since paramagnetic species can provide a dominant relaxation mechanism.[28,32] The pump–freeze–thaw method was used to remove any oxygen present. The cycle was repeated at least ten times for each sample.

The relative viscosity measurements were made using an Ostwald viscometer; 4 ml of solution were used in each case. Each measurement was repeated five times, using a water bath in which the temperature could be regulated to 0.1°. Results of the viscosity measurements are given in Table I.

Table I: Relative Viscosities of Mixtures at 30°

X_f[a]	C_6F_6–C_6H_{12}	C_6F_6–C_6H_6	C_6F_6–$C_6H_2(CH_3)_3$[b]	C_6F_6–HCON–$(CH_3)_2$	CF_3CH_2–OH–C_6H_6	CF_3CH_2–OH–C_2H_5OH
0.90	0.95	0.97	0.99	0.99	0.80	0.87
0.80	0.89	0.93	1.04	1.00	0.67	0.79
0.70	0.84	0.86	1.07	1.00	0.58	0.73
0.60	0.80	0.82	1.10	1.00	0.50	0.70
0.50	0.78	0.80	1.08	1.00	0.46	0.64
0.40	0.78	0.74	1.04	1.00	0.41	0.61
0.30	0.80	0.70	0.96	0.99	0.39	0.60
0.20	0.82	0.66	0.89	0.96	0.36	0.60
0.10	0.88	0.65	0.83	0.93	0.36	0.59

[a] X_f is the mole fraction of the fluorine-containing component. [b] Measured at 40°.

(25) W. A. Duncan, J. P. Sheridan, and F. L. Swinton, *Trans. Faraday Soc.*, **62**, 1090 (1966).

(26) D. V. Fenby and R. L. Scott, *J. Phys. Chem.*, **71**, 4103 (1967).

(27) L. M. Mukherjee and E. Grunwald, *ibid.*, **62**, 1311 (1958).

(28) N. Bloembergen, E. M. Purcell, and R. V. Pound, *Phys. Rev.*, **73**, 679 (1948).

(29) L. Giulotto, G. Lanzi, and L. Tosca, *J. Chem. Phys.*, **24**, 632 (1956).

(30) C. R. K. Murthy and R. D. Spence, *ibid.*, **33**, 945 (1960).

(31) S. Brownstein, private communication.

(32) A. Abragam, "The Principles of Nuclear Magnetism," Oxford University Press, London, 1961.

The proton nmr chemical shifts were obtained with a Varian A-60 spectrometer. Tetramethylsilane was used as the internal reference.

The fluorocarbons were obtained from Peninsular ChemResearch, Inc. The best available grades of hydrocarbons were obtained from various vendors. All the compounds except ethanol and 2,2,2-trifluoroethanol were dried and distilled just before using. Ethanol and 2,2,2-trifluoroethanol were used as obtained. The purity of the compounds was also checked by nmr spectroscopy.

Results and Discussion

Hexafluorobenzene–cyclohexane mixtures were studied to provide a reference system. Swinton[33] argues that only physical interactions such as dispersion forces should be present. The phase diagram of this system[19] does not show a congruent melting point but several barely noticeable incongruent melting points, which may be attributed to solid-state packing rather than to specific interactions. In the hexafluorobenzene–cyclohexane system the unlike interactions are about 5% weaker than the value predicted by the geometric mean combining rule.[33]

A plot of the viscosity-corrected ^{19}F spin–lattice relaxation time as a function of hexafluorobenzene mole fraction is shown in Figure 1. The value of $(\eta/\eta_0)T_1$, where η is the solution viscosity and η_0 is the viscosity of pure hexafluorobenzene, decreases with decreasing fluorocarbon concentration, leveling off at about 0.5 mole fraction. This behavior may be interpreted as the initial breakup, with addition of cyclohexane, of large, loose fluorocarbon clusters into smaller, more rigid clusters.[29,31] Further addition of cyclohexane beyond 0.5 mole fraction provides a continuous hydrocarbon phase for the segregated fluorocarbon clusters. The proton chemical shift of cyclohexane does not change over the investigated concentration range.

The hexafluorobenzene–benzene system has a congruent melting point at 24° and 1:1 mole ratio.[19] A plot of the viscosity-corrected ^{19}F spin–lattice relaxation time as a function of fluorocarbon concentration is also shown in Figure 1 for the hexafluorobenzene–benzene system. Initially, with addition of benzene, $(\eta/\eta_0)T_1$ decreases as the fluorocarbon clusters are broken up, and then at 0.5 mole fraction the plot levels off. The experimental results show fairly large scatter but do not appear to justify drawing other than a smooth curve. The proton chemical shift of benzene is invariant over the investigated concentration range. Thus the behavior of the benzene system is similar to that of the cyclohexane system, and any specific hydrocarbon–fluorocarbon interaction must be extremely weak.

The hexafluorobenzene–mesitylene system has a congruent melting point at 36° and 1:1 mole ratio. The excess volumes of mixing have been measured for

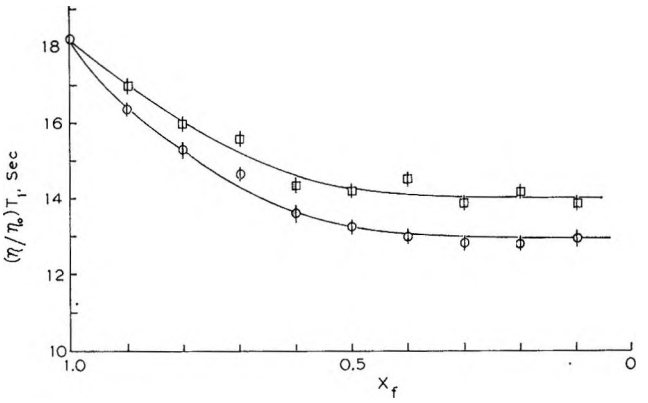

Figure 1. The concentration dependence of the viscosity-adjusted relaxation time in the hexafluorobenzene–cyclohexane (○) and hexafluorobenzene–benzene (□) systems where X_f represents the hexafluorobenzene mole fraction. The lengths of the vertical lines represent the ranges of values observed in replicate measurements.

the benzene–, cyclohexane–, and mesitylene–hexafluorobenzene systems.[25] Also, the excess free energies[33,35] and enthalpies[17,26] of mixing have been measured for the benzene and cyclohexane–hexafluorobenzene systems. The presence of a specific interaction, such as formation of a charge-transfer complex, would have the effect of reducing the magnitude of all the thermodynamic excess functions from the large, positive values that are characteristic of perfluorocarbon–hydrocarbon systems. For example, in the hexafluorobenzene–cyclohexane system where there is little possibility of charge-transfer interaction, the excess free energy, enthalpy, entropy, and volume change of mixing are all large and positive. The values for the hexafluorobenzene–benzene system are somewhat lower. Although only the volume of mixing has been reported in the literature, Swinton[34] states that all the thermodynamic excess functions for the hexafluorobenzene–mesitylene system are negative. A comparison of the excess free energies of mixing for the hexafluorobenzene–benzene, –toluene, and –*p*-xylene systems indicates that as methyl groups are added to the ring, the excess free energy of mixing becomes more negative.[35]

It is also possible that molecular complexes in these systems may be stabilized by electrostatic interactions.[35] The most probable interactions of this type are dipole–quadrupole or dipole–dipole interactions. Such an interaction should be at a maximum when the two molecules are lined up face-to-face. This type of interaction can explain the thermodynamic evidence. Since methyl groups have a negative inductive effect and would lower the ionization potential, mesitylene

(33) W. J. Gaw and F. L. Swinton, *Trans. Faraday Soc.*, **64**, 637 (1968).

(34) W. J. Gaw and F. L. Swinton, *Nature*, **212**, 283 (1966).

(35) W. J. Gaw and F. L. Swinton, *Trans. Faraday Soc.*, **64**, 2023 (1968).

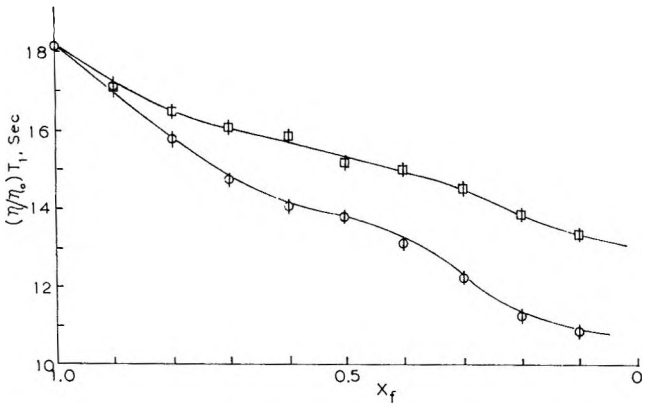

Figure 2. The concentration dependence of $(\eta/\eta_0)T_1$ in the hexafluorobenzene–mesitylene (○) and hexafluorobenzene–dimethylformamide (□) systems where X_f represents the hexafluorobenzene mole fraction.

should possess a somewhat larger π-quadrupole moment than benzene.

Figure 2 shows a plot of $(\eta/\eta_0)T_1$ as a function of fluorocarbon mole fraction for the hexafluorobenzene–mesitylene system. All measurements were taken at 40°. Initially, the viscosity-corrected relaxation time decreases with addition of mesitylene due to the breakup of fluorocarbon clustering. This trend is interrupted near 0.5 mole fraction, indicative of a weak fluorocarbon–hydrocarbon interaction. Finally, as more mesitylene is added, the curve falls and begins to level off.

The proton chemical shifts were measured also for hexafluorobenzene–mesitylene mixtures, and the results are given in Table II. The methyl chemical shift changes with concentration, the peak being farthest upfield near 0.5 mole fraction. The aromatic hydrogens are farthest downfield in pure mesitylene. Upon addition of hexafluorobenzene, the aromatic resonance moves upfield to about 0.5 mole fraction and then does not change with further addition of fluorocarbon. Although it is not entirely clear how the chemical shifts are to be interpreted, the downfield value in pure mesitylene would appear to result from the combination of dispersion forces and molecular geometry which permits pairs of molecules to assume a face-to-face orientation in which their methyl groups alternate. Dilution with fluorobenzene leads to replacement of such clusters by π complexes of a different geometry, in which both methyl and ring hydrogens are more shielded, probably because of a lateral displacement of the face-to-face rings of unlike molecules. Finally, as the fluorobenzene is in excess, edgewise approach of the fluorobenzene molecules to the mesitylene unit of the complex is more likely, and the anisotropy of the fluorobenzene aromatic system leads to unshielding of the projecting methyl hydrogens.

Whether or not these π-molecular complexes are held together primarily by charge-transfer or electrostatic interactions is not known. The negative inductive

Table II: Concentration Dependence of Proton Chemical Shifts and Viscosity-Adjusted Relaxation Time in the Hexafluorobenzene–Mesitylene System

Mole fraction of hexafluorobenzene	Aromatic shift, Hz[a]	Methyl shift, Hz[a]	$(\eta/\eta_0)T_1$, sec
0.90	390.3	129.0	17.2
0.80	389.7	127.6	15.8
0.70	390.0	127.0	14.8
0.60	390.7	127.0	14.1
0.50	389.6	126.0	13.8
0.40	390.7	126.0	13.1
0.30	392.5	126.5	12.3
0.20	394.1	127.3	11.3
0.10	396.0	128.0	10.9
0.00	397.8	129.0	...

[a] The chemical shifts are measured downfield from tetramethylsilane at an operating frequency of 60 MHz. The uncertainty of the values is estimated to be ±0.3 Hz.

effect of the methyl groups in mesitylene would increase the possibility of both charge-transfer and electrostatic stabilization. Chemical shift data have been used to argue for charge-transfer complexes in such systems as 7,7,8,8-tetracyanoquinodimethane with benzene.[36] In such complexes the shielding of the electron acceptor increases with increasing electron donor concentration. However, the fluorine resonance in hexafluorobenzene moves to lower field in going from 0.9 mole fraction hexafluorobenzene in mesitylene to 0.1 mole fraction hexafluorobenzene in mesitylene by 2.0 Hz at 56.4-MHz operating frequency. In the absence of any spectroscopic evidence, electrostatic forces are the most probable source of interaction.

Beaumont and Davis[24] have investigated the ultraviolet spectra of several hexafluorobenzene systems with various π- and n-electron donors. No charge-transfer absorption bands could be obtained for π-electron donors, but several n-electron donor systems indicate charge-transfer absorption. Symmetry arguments forbid the direct overlap of the π-molecular orbitals of the rings in π-electron donor–acceptor systems such as benzene–hexafluorobenzene. The rings must be displaced relative to each other for charge transfer to occur. However, superposition of the ring systems, as in the solid state, provides the most attractive orientation for dispersion and polarization forces.

The hexafluorobenzene–dimethylformamide (DMF) system was studied to investigate further any possible charge-transfer effects. There is a possibility that the lone pair of electrons on the oxygen or nitrogen atom could be an n-electron donor with hexafluorobenzene being the electron acceptor. A plot of the viscosity-corrected T_1 as a function of hexafluorobenzene con-

(36) M. W. Hanna and A. L. Ashbaugh, *J. Phys. Chem.*, 68, 811 (1964).

centration is shown in Figure 2. The trend of the curve is much like that for hexafluorobenzene–mesitylene, with an initial breakup of hexafluorobenzene clusters followed by a region in the middle range of concentration indicating specific interaction with DMF.

The proton chemical shifts of DMF are given in Table III. The carbonyl proton shift moves upfield with increasing fluorocarbon concentration, consistent with increasing dissociation of DMF. The change of about 13 Hz from pure DMF to 0.10 mole fraction in hexafluorobenzene may be compared to a change of about 8 Hz observed in these laboratories as DMF is diluted with carbon tetrachloride over the same concentration range. The resonances of the α-methyl and β-methyl groups move about 2 Hz downfield and 2 Hz upfield, respectively, on dilution of pure DMF to 0.10 mole fraction in hexafluorobenzene, whereas both move about 1 Hz downfield when the diluent is carbon tetrachloride. In DMF–benzene, Hatton and Richards[37] pointed out that the DMF molecule is situated such that the carbonyl group is as far away as possible from the benzene ring. The α-methyl shift changes appreciably with concentration while the β-methyl shift is unchanged. They interpreted these results to mean that the α-methyl group was positioned over the center of the ring to retain the planar configuration of the amide. In the present case, since hexafluorobenzene is a better electron acceptor than benzene, the carbonyl group is not repelled as greatly. The carbonyl group may complex slightly with the hexafluorobenzene, which would explain the chemical shift results. The upfield chemical shift of the carbonyl group with increasing hexafluorobenzene concentration could be explained as a combination of the self-dissociation of DMF and interaction with the hexafluorobenzene. The fact that the methyl shifts change very slightly in hexafluorobenzene and carbon tetrachloride indicates that the geometry involved in any complex formation is considerably different from that in the DMF–benzene system.

Table III: Concentration Dependence of Proton Chemical Shifts and Viscosity-Adjusted Relaxation Time in the Hexafluorobenzene–Dimethylformamide System

Mole fraction of hexafluorobenzene	Carbonyl shift, Hz[a]	α-Methyl shift, Hz[a]	β-Methyl shift, Hz[a]	$(\eta/\eta_0)T_1$, sec
0.90	466.0	178.0	165.0	16.9
0.80	467.2	178.4	164.9	16.5
0.70	468.8	179.0	165.8	16.2
0.60	470.1	177.3	165.2	15.9
0.50	471.5	176.5	165.0	15.2
0.40	473.6	176.5	164.0	15.0
0.30	475.5	177.0	166.0	14.6
0.20	477.2	176.3	166.2	13.9
0.10	478.7	176.2	166.4	13.4
0.00	480.9	176.2	166.7	...

[a] The chemical shifts are measured downfield from tetramethylsilane at an operating frequency of 60 MHz.

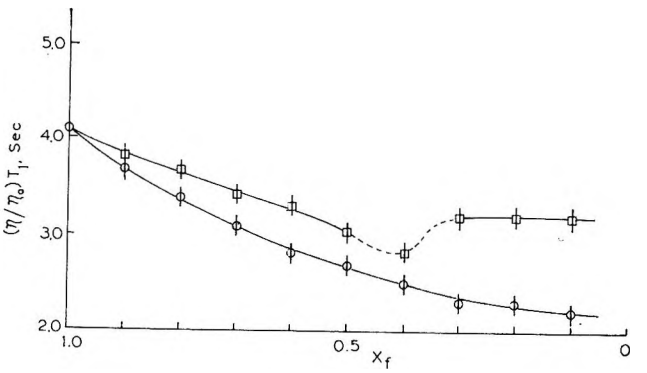

Figure 3. The concentration dependence of $(\eta/\eta_0)T_1$ in the 2,2,2-trifluoroethanol–benzene (○) and 2,2,2-trifluoroethanol–ethanol (□) systems where X_f represents the 2,2,2-trifluoroethanol mole fraction. The dashed section of the curve is drawn in the region of the minimum values, where results are not sufficiently precise to define the detailed nature of the variation.

Preliminary uv studies of the hexafluorobenzene–DMF system were carried out. Beaumont and Davis reported a range of 265–353 mμ for the charge-transfer band maximum for several amines with hexafluorobenzene. No new band or shoulder on the parent bands was noted in this region although both hexafluorobenzene and DMF absorb at about 255 mμ, and these absorptions might obscure the new band.

Infrared bands in the TFE–ethanol system, corresponding to monomer, dimer, and higher complexes, were assigned by Mukherjee and Grunwald.[27] Also, they found TFE to be a better hydrogen-bonding donor in an inert solvent than ethanol. Rao, *et al.*,[38] showed, using nmr spectroscopy, that TFE is less associated than is ethanol in an inert solvent.

In mixtures of TFE and ethanol, a new infrared band appears with a maximum at 3400 cm^{-1}. This is attributed to formation of mixed hydrogen-bonded species, the most important being the TFE–ethanol dimer. The calculated equilibrium constant for mixed dimer formation is about ten times greater than for ethanol dimer formation.[27]

A plot of the concentration dependence of $(\eta/\eta_0)T_1$ for TFE in benzene is given in Figure 3. The value of $(\eta/\eta_0)T_1$ decreases with decreasing TFE concentration indicating the breakup of large complexes. This breakup is still incomplete, even at 0.1 mole fraction. TFE shows self-association over the concentration range studied. Figure 3 also shows a plot of the concentration dependence of $(\eta/\eta_0)T_1$ in the TFE–

(37) J. V. Hatton and R. E. Richards, *Mol. Phys.*, 5, 139 (1962).

(38) B. D. N Rao, P. Venkateswarlu, A. S. N. Murthy, and C. N. R. Rao, *Can. J. Chem.*, 40, 387 (1962).

ethanol system without solvent. As ethanol is added, there is a decrease in $(\eta/\eta_0)T_1$. This decrease, however, is not as great as in benzene, because the formation of mixed complexes lowers the degree of self-association. Instead of the TFE breaking into smaller units as it does in an inert solvent, it is tied up in large hydrogen-bonded clusters or chains. Mukherjee and Grunwald[27] postulate that when TFE is in excess, there are hydrogen-bonded chains with ethanol being the terminal acceptor. Also, when TFE is added to ethanol, there are hydrogen-bonded chains formed with TFE being the terminal donor. The motion of the perfluoromethyl group in TFE seems unaffected from 0.1 to 0.4 mole fraction TFE. This fact indicates that any chains formed are breaking and re-forming faster than can be detected on the nmr time scale. Also, there is probably little hydrogen–fluorine hydrogen bonding present. However, at about 0.42 mole fraction TFE there is a discontinuity indicating very strong hydrogen bonding involving the hydroxyl groups.[29,30] Probably the chief species is the mixed dimer, with higher complexes also present. Mixed hydrogen bonding seems to be a much stronger interaction than the self-association of either ethanol or TFE.

Acknowledgment. The authors gratefully acknowledge the financial support of this research by NASA, in the form of a traineeship held by C. L. Watkins.

Phosphorescence Yields and Radical Yields from Photolysis of Tetramethyl-*p*-phenylenediamine in 3-Methylpentane Glass Containing Alkyl Halides[1a]

by William G. French[1b] and John E. Willard

Department of Chemistry, University of Wisconsin, Madison, Wisconsin
(Received June 16, 1969)

The yields of alkyl radicals produced from alkyl halide solutes by dissociative electron capture ($RX + e^- \rightarrow R + X^-$) during photoionization of tetramethyl-*p*-phenylenediamine (TMPD) in 3-methylpentane (3MP) glass at 77°K decrease in the order RCl > RBr > RI. The analogous radical yields from radiolysis of RX in 3MP are not dependent on the halogen. Phosphorescence yields and lifetimes indicate that the reductions in radical yields from the iodides and bromides in the TMPD system result from the formation of TMPD–RX complexes in which the lifetime of the TMPD triplet state is reduced. Shortening of the triplet state lifetime lowers the probability of the two-photon photoionization process. The phosphorescence yields with and without CH_3I present indicate a $[TMPD\text{–}CH_3I]/[TMPD][CH_3I]$ ratio in the glass at 77°K of 760. These data help to explain earlier observations on the effect of methyl iodide on the electrical conductivity of solutions of photoionized TMPD in 3MP glass during warmup from 77°K. Additional observations include (1) the rate of production of free radicals in the TMPD system is proportional to the second power of the light intensity, as expected; (2) CH_3F undergoes dissociative electron capture in 3MP at 77°K, although such dissociation with thermal electrons is endothermic in the gas phase; and (3) the ratio of yields of CH_3, C_2H_5, and i-C_3H_7 from dissociative electron capture by the corresponding chlorides, using electrons from the photoionization of TMPD, is 1.00:1.25:1.75, rather than decreasing with increasing carbon number as reported earlier.

Introduction

The quantum yields of trapped CH_3 radicals produced by dissociative electron capture when N,N,N′N′-tetramethyl-*p*-phenylenediamine (TMPD) is photoionized at 77°K in 3-methylpentane (3MP) glass containing 1 mol % CH_3Cl, CH_3Br, or CH_3I are in the ratio of 10:3:1.[2] The yields of ethyl radicals from the ethyl halides show a similar decrease from the chloride to the iodide.[2] It has been suggested[2] that these differences, which are opposite in trend to that observed for electron capture

(1) (a) This work has been supported in part by U. S. Atomic Energy Commission Contract AT(11-1)-1715, by the W. F. Vilas Trust of the University of Wisconsin, and by a Public Health Service Fellowship (F1-GM-28,853) from the National Institute of General Medical Sciences; (b) Bell Telephone Laboratories, Murray Hill, N. J. 07974.

(2) R. F. C. Claridge and J. E. Willard, *J. Amer. Chem. Soc.*, **87**, 4992 (1965).

in liquid aqueous systems[3] and for dissociative electron capture in a liquid hydrocarbon,[4] may be caused by differences in complexing of the halides with TMPD. Consistent with this suggestion, it has subsequently been shown that $G(RX + e^- \rightarrow R + X^-)$ in the radiolysis of 3MP glass containing an alkyl halide (but no TMPD) is independent of whether the halide is a chloride, bromide, or iodide.[5] Evidence from studies of radical yields as a function of TMPD and alkyl chloride concentrations are ambiguous with respect to the role of complexing.[6] The optical spectra of unirradiated solutions of methyl halides and TMPD in 3MP at 77°K show only the normal spectrum of TMPD (with peaks at 325 and 265 nm). Following illumination in the 325-nm absorption band of TMPD, the $TMPD^+$ signal (with peaks at 632 and 575 nm) is completely obscured if 10^{-2} mole fraction of CH_3I is present; CH_3Br causes a broad absorption in the 360-nm region; and CH_3Cl produces very little change. These effects have been observed in both earlier work[6] and the present work.

Photoionization of TMPD is believed to occur by a two-photon process in which the second photon is adsorbed by the triplet state.[7] Any effect which shortens the lifetime of this state must decrease the quantum yield of photoionization, and hence of free-radical formation by dissociative capture. If TMPD is complexed with an alkyl halide, this might be expected to quench or change the lifetime of the triplet state. We have therefore investigated the effects of CH_3Cl, CH_3Br, and CH_3I on the yield and lifetime of TMPD phosphorescence in 3MP at 77°K.

We have also (1) determined the effect of light intensity on the rate of radical production by dissociative electron capture during photoionization of TMPD; (2) correlated the effects of methyl halides on the phosphorescence intensity from TMPD in 3MP glass with their effects on the warmup electrical conductivity[8] of the system; and (3) revised earlier estimates[2] of the relative yields of methyl, ethyl, propyl, and butyl radicals formed by dissociative electron capture of the corresponding halides by electrons from TMPD.

Experimental Section[9a]

All samples were prepared from purified degassed reagents. Solute concentrations are given in units of mole fraction (mf).

Phillips Pure grade 3-methylpentane was purified by passing through a 0.5-m column of silica gel, freshly activated at 400°. Eastman White Label CH_3I, C_2H_5I, C_2H_5Br, and n-C_3H_7I were used as received. Matheson USP grade C_2H_5Cl, High Purity grade CH_3Cl, and 99.5% minimum purity CH_3Br and CH_3F were used as received.

Measurements of the decay of TMPD phosphorescence were made by recording the output of an IP21 photomultiplier tube which monitored the sample after flash photolysis at 77°K.[9b] The sample consisted of 4 ml of 10^{-5} mf TMPD in 3MP in a 1 cm × 1 cm fused silica cell. It was mounted under liquid nitrogen in a dewar with flat Pyrex windows. The dewar was positioned midway between, and about 5 cm from, the photomultiplier tube and a Xe-filled fused silica flash lamp 10 cm long and 1 cm in diameter. The flash energies were about 700 J, the flash intensity decayed to 1% of its maximum value in about 100 μsec, and the perturbation of the photomultiplier as a result of the flash was over in less than 0.1 sec after the flash. The output of the photomultiplier was recorded on a Hewlett-Packard 680M strip chart recorder which had a full-scale response time of 0.1 sec.

A high-intensity Bausch and Lomb monochromator with a 200-W high pressure mercury lamp was used in determining the effect of light intensity on the rate of radical production. It was set at 315 nm with a 10-nm band width and focused on the sample held in a Varian liquid nitrogen dewar in the esr cavity. Cary wire mesh neutral density filters were used to vary the intensity.

Electrical conductivity measurements during warmup of illuminated 3MP–TMPD–RX glasses were made as described earlier.[8]

Determination of absolute yields of trapped radicals by double integration of the first derivative esr spectrum and comparison with a standard was not feasible in the presence of an unknown yield of $TMPD^+$. The relative yields of methyl radicals from different methyl halides, or the relative yields of ethyl radicals from ethyl halides, could be determined to *ca.* ±20% by comparing esr peak heights from different samples exposed to identical illumination in identical sample tubes. This is possible because the $TMPD^+$ esr signal is sufficiently broad so that its contribution to the signal height in these samples is less than 10%, and the contribution of the 3MP radical signal is likewise small. In order to determine the yield of ethyl and propyl radicals, from ethyl and propyl chloride, relative to the yield of methyl radicals from methyl chloride, the ratio of the line heights of the different kinds of radicals at equal concentration was determined with samples of the various alkyl chlorides in 3MP which were γ-irradiated to identical doses. G values for both the

(3) A. Szutka, J. K. Thomas, S. Gordon, and E. J. Hart, *J. Phys. Chem.*, **69**, 289 (1965).

(4) P. R. Geissler and J. E. Willard, *ibid.*, **67**, 1675 (1963).

(5) M. Shirom and J. E. Willard, *ibid.*, **72**, 1702 (1968).

(6) R. F. C. Claridge and J. E. Willard, unpublished.

(7) (a) G. E. Johnson and A. C. Albrecht, *J. Chem. Phys.*, **44**, 3162 (1966); (b) G. E. Johnson and A. C. Albrecht, *ibid.*, **44**, 3179 (1966); (c) K. D. Cadogan and A. C. Albrecht, *J. Phys. Chem.*, **72**, 929 (1968).

(8) B. Wiseall and J. E. Willard, *J. Chem. Phys.*, **46**, 4387 (1967).

(9) (a) Further details are given in the Ph.D. thesis of W. G. French, University of Wisconsin, 1969; (b) we are indebted to John R. Miller of our laboratory for assistance with these measurements.

3MP radicals (which are independent of the presence of solute) and for the alkyl radicals from alkyl halide solutes are known for 3MP glass at 77°K.[5] Therefore, by subtracting the height of the 3MP radical signal in the absence of solute from the apparent line height due to the solute radical when solute was present, values for the concentration of each radical in terms of the height of one of its prominent lines were obtained and could be used in comparing yields of different radical species resulting from photoionization of TMPD in the presence of alkyl halides. This method of comparing the yields of different radicals has yielded corrected values for the relative yields of methyl, ethyl, and propyl radicals reported earlier.[2]

Results

Relative Radical Yields from Different Alkyl Halides. Table I lists the relative yields of alkyl radicals produced by dissociative electron capture by seven alkyl halides following the photoionization of TMPD in 3MP glass at 77°K. All determinations were made with 1.1×10^{-2} mf of the halide and 0.9×10^{-4} mf TMPD, with a photolysis time of 5.0 min, using an AH4 lamp with a Pyrex filter. A 5-min irradiation produced a strong enough signal for easy measurement but was short enough so that the growth rate was approximately constant (*i.e.*, TMPD depletion and adsorption by $TMPD^+$ were both small), and only a small correction was needed for radical decay during the photolysis period. Each of the values of Table I for relative yield from TMPD photolysis is based on at least three determinations, with the maximum deviation from the mean being 10%. The absolute concentration of methyl radicals following the 5-min irradiation of CH_3Cl solutions was about 10^{-5} mf. The relative yields of CH_3, C_2H_5, and C_3H_7 from the corresponding chlorides (1.00 : 1.25 : 1.75) are to be noted since the trend is in the opposite direction to that reported earlier[2] on the basis of a less valid method for comparing such concentrations.

Table I: Yields of Alkyl Radicals Produced by Dissociative Electron Capture in 3MP at 77°K[a]

Alkyl halide	Relative yields from TMPD photolysis	G(R) from γ irradiation[b]
CH_3Cl	1.00	0.8
CH_3Br	0.30	0.8
CH_3I	0.10	0.8
C_2H_5Cl	1.25	1.1
C_2H_5Br	0.75	1.1
C_2H_5I	<0.20	1.1
C_3H_7Cl	1.75	1.1

[a] 9×10^{-5} mf TMPD, 1.1×10^{-2} mf RX. [b] Reference 5.

Since the gas phase dissociative electron capture reaction has been reported for alkyl chlorides, bromides, and iodides, but dissociative electron capture by thermal electrons is forbidden by energetic considerations for alkyl fluorides,[10] it is especially interesting that the methyl radical was observed following the radiolysis of $<10^{-2}$ mf CH_3F in 3MP at 77°K and following the photoionization of TMPD in 3MP glass containing $<10^{-2}$ mf CH_3F. Quantitative comparison of the CH_3 yields from CH_3F to those of Table I for the other methyl halides was not possible because the solubility of CH_3F in 3MP is not known. When 0.2 ml of 3MP was frozen in an esr tube of 2-ml volume containing 1.0×10^{-2} mf CH_3F relative to the 3MP, two layers of solid were observed, indicating phase separation. In TMPD photoionization experiments the yield of CH_3 radicals from such a glass was less than 5% of the yield from 1.0×10^{-2} mf CH_3Cl in 3MP at 77°K.

Light Intensity Dependence of Quantum Yields of Radicals. The initial rate of production of electrons by photoionization of TMPD in 3MP at 77°K is proportional to the square of the light intensity.[7] Figure 1 shows that the rate of production of radicals when an alkyl halide is present in the system also varies as the square of the light intensity, as is to be expected if they result from dissociative electron capture.

Phosphorescence of TMPD in the Presence of Alkyl Halides. When 3MP containing 10^{-5} mf TMPD was exposed to a flash from the flash lamp, the initial intensity of phosphorescence and its rate of decay were unaffected by the presence of CH_3Cl at concentrations at least as high as 8.5×10^{-3} mf (Figure 2). The half-life of 2.5 sec is consistent with that reported earlier.[7] The presence of 1.5×10^{-3} mf CH_3I decreased the initial intensity by 60% without changing the decay rate of the remainder (Figure 2). The presence of 6.5×10^{-3} mf CH_3Br decreased the integrated intensity observed by about 30% and increased the initial decay rate (Figure 3). The effect of the concentration of CH_3I on the ratio of initial phosphorescence intensity in the presence of CH_3I to that in its absence is illustrated in Table II. The effects of C_2H_5Br and C_3H_7Br were identical with that illustrated for CH_3Br in Figure 3, at the same concentrations of solutes.

Discussion

TMPD–RX Complexing Indicated by Phosphorescence Yields. We interpret the reduction of the phosphorescence yield caused by CH_3I (Figure 2) to indicate that a portion of the TMPD is complexed by the CH_3I and that the phosphorescence lifetime of the TMPD triplet in the complex is so short that it is not observed in our measurements which start a few tenths of a second after the end of the exciting flash. CH_3Br appears to produce similar complexing, with the phos-

(10) (a) V. H. Diebeler and R. M. Reese, *J. Res. Nat. Bur. Stand.*, **54**, 127 (1955); (b) J. A. Kerr, *Chem. Rev.*, **66**, 464 (1966).

Table II: Relative Initial Phosphorescence Following Flash Photolysis of Solutions of TMPD and CH_3I in 3MP at 77°K

TMPD, mf × 10^5	CH_3I, mf × 10^3	I/I_0 (obsd)[a]	I/I_0 (calcd)[b]
0.95	1.5	0.50	0.47
2.3	1.5	0.47	0.47
2.3	7.5	0.14	0.22
2.3	0.15	0.9	0.91
1.0	8.5	0.10	0.17

[a] Ratio of initial intensity of phosphorescence with the CH_3I present to that without it present. [b] Calculated assuming $[TMPD\text{-}CH_3I]/[TMPD][CH_3I] = 760$.

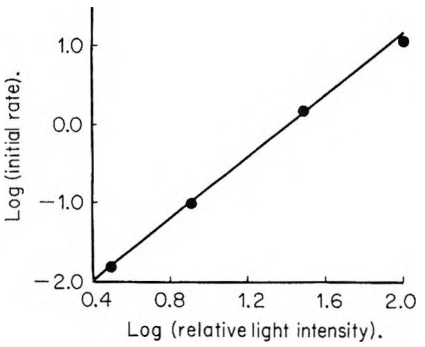

Figure 1. Effect of light intensity on the initial rate of C_2H_5 formation (arbitrary units) during the photolysis of TMPD–C_2H_5Cl solutions in 3MP at 77°K: 1×10^{-2} mf C_2H_5Cl, 5×10^{-3} mf TMPD, 315-nm radiation.

phorescence lifetime being reduced but still being in the marginally measurable range, while CH_3Cl either is not complexed, or if complexed, does not affect the phosphorescence lifetime.

Reduction of triplet state lifetimes by spin–orbit coupling with halogen atoms has been reported for naphthalene in propyl halides at 77°K.[11] In these experiments the lifetime of the phosphorescence was 0.52 sec in C_3H_7Cl, 0.14 sec in C_3H_7Br, and 0.076 sec in C_3H_7I. Such data raise the question as to whether the differences in phosphorescence lifetimes which we have observed may be due only to the fact that spin–orbit coupling of the triplet state with the halogens decreases from iodine to chlorine and may not involve complexing. However, the data of Figure 2 and Table II seem to require complexing, since CH_3I causes a concentration-dependent decrease in the yield of phosphorescence, without changing the half-life of that which remains. At 5×10^{-3} mf CH_3I the average distance of a TMPD molecule from a CH_3I molecule is two or three molecular diameters. If randomly distributed CH_3I were interacting with triplet TMPD to reduce the lifetime, a plot of the logarithm of the phosphorescence *vs.* time would be expected to show a decreasing slope with time as a result of the various proximities of CH_3I molecules to TMPD molecules.

If I is the phosphorescence intensity in the presence of

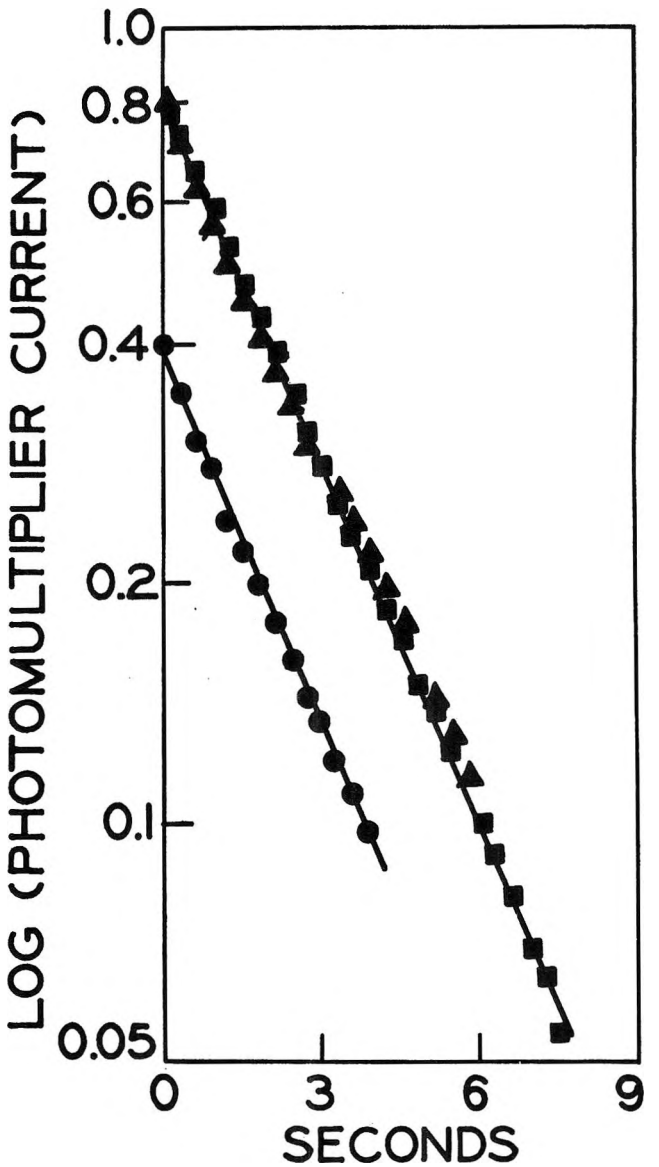

Figure 2. Semilog plot of phosphorescence decay after flash photolysis of: ■, 10^{-5} mf TMPD; ▲, 10^{-5} mf TMPD + 1.5 10^{-3} mf CH_3Cl; and ●, 10^{-5} mf TMPD + 1.5×10^{-3} mf CH_3I.

CH_3I and I_0 that with no additive, I/I_0 should represent the fraction of the TMPD which is not complexed. Using the I/I_0 values of Table II, an average value of the equilibrium constant for complexing ($K = [TMPD\text{-}CH_3I]/[TMPD][CH_3I]$) of 760 ± 90 may be calculated. The values of I/I_0 calculated from this are given in the last column of Table II. The equilibrium constant determined in this way is expected to be representative of some temperature, higher than 77°K, at which the equilibrium is frozen in, and to show some variation from experiment to experiment, dependent on the rate of cooling.

If it is assumed that the phosphorescence decay for

(11) S. P. McGlynn, M. J. Reynolds, G. W. Daigre, and N. D. Christodyleas, *J. Phys. Chem.*, 66, 2499 (1962).

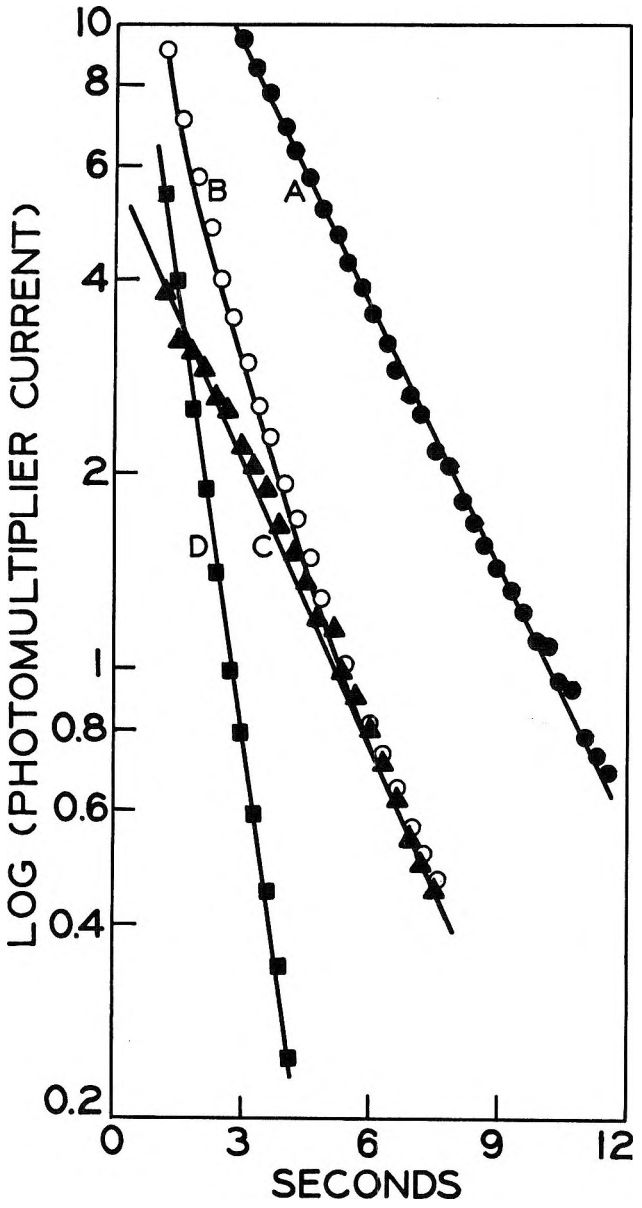

Figure 3. Semilog plot of phosphorescence decay after flash photolysis of: ●, 10^{-5} mf TMPD; and ○, 10^{-5} mf TMPD + 6.5×10^{-3} mf CH_3Br. Plots C, ▲, and D, ■, are the resolution of plot B into two linear plots.

the sample containing CH_3Br can be resolved into two first-order decays, one of uncomplexed TMPD with the half-life of 2.5 sec, and the other of a TMPD-CH_3Br complex, as shown in Figure 3, the half-life of the latter is less than 1.0 sec. Assuming the intercept of the 2.5-sec decay with the zero ordinate represents the initial phosphorescence from uncomplexed TMPD, the equilibrium constant, calculated in the same manner as above for CH_3I, is *ca.* 400. If the assumption that the curve is resolvable into two well-defined decays is not correct, the only alternative to explain the change in phosphorescence decay characteristics caused by CH_3Br is that the decay rate decreases continuously with time because of the random proximity of the TMPD molecules to CH_3Br molecules able to shorten the lifetime of the triplet state by spin–orbit coupling. This explanation appears improbable when it is noted that the phosphorescence decay rate in the presence of CH_3I was identical with that in its absence, at concentrations equivalent to those of Figure 3 for CH_3Br. A third explanation for the effect of CH_3Br, *i.e.*, that all the TMPD molecules are complexed, is ruled out by the fact that the phosphorescence decay shown by curve B of Figure 3 is not linear.

Cadogan and Albrecht[7c] observed that 5×10^{-3} *M* oxygen quenched 50% of the TMPD phosphorescence in 3MP at 77°K but had no effect on the lifetime. They attributed this effect to the formation of a complex between O_2 and TMPD.[7c]

Influence of TMPD–RX Complexing on Radical Yields. The yields of free radicals formed from different alkyl halides by the $RX + e^- \rightarrow R + X^-$ process are strongly dependent on whether X is Cl, Br, or I when the electrons are produced by photoionization of TMPD, but not when the electrons are produced by γ irradiation (Table I). It has been suggested[2] that this effect might result from different equilibrium constants for complexing of the different alkyl halides with TMPD, coupled with a higher probability for dissociative capture on the part of molecules so complexed. This model favored the conclusion that complexing of alkyl halides with TMPD in 3MP at 77°K decreases in the order RCl > RBr > RI, because the quantum yields of radicals formed by the photoionization of TMPD fall in this order.

From the phosphorescence data of Table II and Figures 2 and 3 we now conclude that the differences in radical yields from the iodides, bromides, and chlorides are due at least in part to differences in the yields of photoionization of the TMPD, these differences resulting from reduction of the triplet state lifetime of the TMPD when it is complexed. Photoionization of TMPD occurs through a two-photon process.[7,12] The excited singlet state formed by the first photon populates a triplet state by radiationless transfer, and the second photon causes ionization from the triplet state in competition with decay by phosphorescence. For a fixed incident light intensity, the rate of photoionization is proportional to the steady-state concentration of the triplet state, which is proportional to the average lifetime of this state. Thus the yield of electrons and of radicals produced by dissociative electron capture would be expected to be decreased by additives which decrease the phosphorescence yield or lifetime, as observed. These considerations suggest that the complexing of alkyl halides with TMPD in 3MP at 77°K decreases in the order RI > RBr > RCl.

The conclusion that TMPD is less complexed by CH_3Cl than CH_3I and CH_3Br is based on extrapolation

(12) B. Brocklehurst, W. A. Gibbons, F. T. Land, G. Porter, and M. I. Savadatti, *Trans. Faraday Soc.*, **62**, 1793 (1966).

the phosphorescence results for CH_3I and CH_3Br. possibility that TMPD is highly complexed by Cl but that the phosphorescence is not affected ause spin–orbit coupling of Cl with the triplet state gligible) cannot be excluded. Thus it is not possi- to say whether the high yield of trapped radicals CH_3Cl relative to CH_3Br and CH_3I is due solely to act that it does not alter the triplet state lifetime— lso to some other factor. Similarly the data leave the possibility that the increase in radical yields CH_3Cl to C_2H_5Cl to C_3H_7Cl may not depend on the ation of triplet state lifetimes, but is due to dif- ices in electron capture probability.

able III summarizes the available data on relative ls of alkane formation by hot radical attack on the matrix and of trapped radicals when TMPD is oionized in the presence of three different alkyl ides. The decrease in the yield of alkanes by hot al reaction as the number of carbon atoms in the al increases is plausibly related to the increasing ber of degrees of freedom in the radical.

III: Relative Yields of Alkanes and Trapped Radicals Different Alkyl Halides Activated by Photolysis of D in 3MP Glass

	CH_3Cl	C_2H_5Cl	C_3H_7Cl
RH/R	3.8	1.7	0.28
R[a]	1.0	1.25	1.75
RH[a,b]	3.8	2.12	0.56
R + RH[a]	4.8	3.37	2.31

elative quantum yields, the yield of CH_3 being arbitrarily n as 1. [b] Derived from the data of the first two rows: = R(RH/R).

Interpretation of Electrical Conductivity Results. When either γ-irradiated 3MP glass, or 3MP glass in which TMPD has been photoionized, is warmed from 77°K with an applied potential, an electrical conductivity peak appears with a maximum at *ca.* 108°K.[8] It is ascribed to the movement of positive and negative ions. The presence of 10^{-2} mf of the electron scavenger CH_3I does not alter the peak in γ-irradiated samples, indicating that the ions formed from CH_3I must have about the same mobility and move the same distance under the influence of the field as those present in the absence of CH_3I. In contrast to the γ-irradiated system, 10^{-2} mf CH_3I greatly reduces the 108°K conductivity peak from the photolysis of 10^{-5} mf TMPD in 3MP. From the phosphorescence studies of the present paper it may be concluded that at least part of this reduction results from a reduction in the quantum yield of photoionization, by reduction in the triplet state lifetime. In a further test of these relationships, it has been observed by Bruce Dietrich of our laboratory that the ratio of areas of the conductivity peaks for solutions of 10^{-4} mf TMPD in 3MP glass at 77°K and identical solutions with 10^{-2} mf of alkyl halide additive is: TMPD in 3MP only, 1; CH_3I, 0.01; CH_3Br, 0.07; CH_3Cl, 0.16; C_2H_5Cl, 0.23; C_3H_7Cl, 0.30. The qualitative trend is consistent with the phosphorescence yields in the presence of methyl iodide, bromide, and chloride. The cause of the increase in areas of the conductivity peaks in the sequence from methyl to ethyl to propyl chloride in parallel with a decrease in the total yield of RH + R from dissociative capture and an increase in the yield of R is not apparent. It may possibly be related to differences in the average distance of charge movement in the direction of the applied field prior to neutralization.

The Effect of Electron, Positive Ion, and Hydrogen Atom Scavengers on the Yields of Atomic and Molecular Hydrogen in the Radiolysis of Liquid Cyclohexane[1a]

by K.-D. Asmus,[1b] John M. Warman,[1c] and Robert H. Schuler

Radiation Research Laboratories, Mellon Institute, Carnegie-Mellon University, Pittsburgh, Pennsylvania 15213
(Received June 26, 1969)

Electron scavengers are found to depress the hydrogen yield from the γ irradiation of cyclohexane by an amount approximately equivalent to the yield of scavenged electrons. It is concluded that in pure cyclohexane neutralization of the positive ions by electrons yields hydrogen with near unit efficiency but that little hydrogen is produced when neutralization occurs with secondary negative ions. A somewhat lower efficiency is noted for hydrogen production from positive-ion electron neutralization in other hydrocarbons, particularly the more highly branched ones. Cyclopropane solutions also show a decrease in hydrogen production which is equivalent to the yield of products from secondary positive-ion reactions. Little hydrogen is produced from the solute. In the case of ethylene as a solute both positive-ion reactions and hydrogen atom scavenging appear to be responsible for decreases observed in the hydrogen yield. Production of ethyl radicals has been studied in considerable detail and from effects of cyclopropane and electron scavengers on their yield it is concluded that the hydrogen atom yield from pure cyclohexane is ~1.5. This hydrogen atom yield is, however, depressed by the presence of either electron or positive-ion scavengers so that a somewhat lower value is appropriate to cases where solutes are present. Equations are given which are based on the empirically observed concentration dependence for ion-scavenging processes and which quantitatively describe the atomic and molecular yields of hydrogen from the various solutions.

Introduction

During recent years several important discoveries[2-4] have made it quite evident that certain solutes can interfere with the ion-recombination processes which occur in the radiolysis of pure saturated hydrocarbons and alter the subsequent chemistry. Because hydrogen is a major radiolysis product, its yield might well be expected to be affected by any change in the neutralization process. Consideration of this subject is, of course, not new. Since the early 1950's[5] radiation chemists have been concerned that ionic reactions, particularly those involving electron capture, might come into play when solutes are added to hydrocarbons. The first experimental attempt to examine the possible effects of electron capture in some detail was that of Williams and Hamill[6] in their study of the radicals produced in the radiolysis of solutions of alkyl halides in hydrocarbons. They found that at solute concentrations of the order of 1 mol % appreciable yields of alkyl radicals ($G \sim 2$–3) were produced from the solute and suggested that these alkyl radicals resulted, for the most part, from processes involving dissociative capture of electrons. Following this it was found by one of the present authors that a number of substances which seemed likely to be scavengers of electrons depressed the hydrogen yield from cyclohexane by several units when present at concentrations of only ~0.1 M.[7] It was suggested that a large part of the observed reduction might be due to changes in the neutralization reactions. The effect of electron capture on the neutralization processes leading to hydrogen formation was later explored more fully by Dyne.[8] In these earlier studies it was not completely obvious how one could easily distinguish between the effects produced by reactions of hydrogen atoms and those produced by

(1) (a) Supported in part by the U. S. Atomic Energy Commission; (b) Hahn–Meitner Institute, Berlin, Germany; (c) Argonne National Laboratory, Argonne, Ill.

(2) G. Scholes and M. Simic, *Nature*, **202**, 895 (1964), found high yields of nitrogen from solutions of N_2O in cyclohexane, *e.g.*, at 0.1 M N_2O, $G(N_2)$ ~4. Since N_2O was known to be a good electron scavenger in aqueous systems, they suggested that the nitrogen was produced by electron capture processes.

(3) F. Williams, *J. Amer. Chem. Soc.*, **86**, 3954 (1964), found G(HD) ~0.4 for a 0.07 M ND_3 solution in cyclohexane. It was presumed that this HD resulted from proton transfer from the solvent ion to ND_3 which was followed by production of D atoms upon neutralization of the product ND_3H^+ ion. The D atoms would then, of course, abstract hydrogen from the solvent to form HD.

(4) P. Ausloos, A. A. Scala, and S. G. Lias, *ibid.*, **88**, 1583 (1966); P. Ausloos, A. A. Scala, and S. G. Lias, *ibid.*, **88**, 5701 (1966), showed that irradiation of solutions of perdeuteriocyclopropane in pentane, isopentane, and other hydrocarbons gave appreciable yields of 1,1,2,2,-3,3-hexadeuteriopropane. This propane was presumed to be produced by H_2 transfer from the solvent ion to the solute by analogy with reactions observed in the gas phase.

(5) See, for example, J. L. Magee and M. Burton, *J. Amer. Chem. Soc.*, **73**, 523 (1951).

(6) R. R. Williams, Jr., and W. H. Hamill, *Radiat. Res.*, **1**, 158 (1954).

(7) R. H. Schuler, *J. Phys. Chem.*, **61**, 1472 (1957).

(8) P. J. Dyne, *Can. J. Chem.*, **43**, 1080 (1965).

reaction of electrons. Certain facts, such as an increased hydrogen yield from HI solutions[7] (which would not occur if hydrogen atom scavenging alone was involved) made it quite clear that solutes could be involved in reactions over and above those of thermal hydrogen atoms. It was, however, not possible to give a quantitative treatment of the data because a kinetic model was not available from which one could derive a description of the concentration dependence of electron scavenging. The more recent observations mentioned above[2-4] and also the work of Hamill and coworkers[9] on the production of ionic species in organic glasses have again focused attention on the importance of processes involving ionic species. In the interim period, radio-chromatographic experiments have been developed which allow examination of details of the radiation chemistry of dilute solutions for a number of the solutes of interest. In particular, it has been possible to reinvestigate the dissociation of alkyl halides in experiments of the type originally carried out by Williams and Hamill. Such studies have yielded a quantitative description for the concentration dependence of the electron capture process.[10] In related work a similar description has also been found to be applicable to reactions involving positive-ion scavengers.[11] It is the purpose of the present contribution to attempt to integrate this description with observations of the effects of solutes on the production of molecular and atomic hydrogen.

Experimental Section

Phillips Research Grade cyclohexane was chromatographed on silica gel prior to use and outgassed on a vacuum line by conventional freeze–pump–thaw methods. In early experiments CO_2 was found to be quite effective in reducing the hydrogen yield and subsequently considerable care was used to remove dissolved CO_2 by additional pumping at room temperature. Solutes (N_2O, SF_6, CO_2, CH_3Br, CH_3Cl, C_2H_5Br, C_2H_4, C_2D_4, c-C_3H_6, c-C_3D_6, and ND_3) were outgassed and distilled on the vacuum line. Mass spectrometer analysis showed no significant impurity levels. Solutes were metered on the vacuum line and added to the solvent prior to the final distillation procedure. Hydrocarbon samples were 5 or 10 cc and filled all but a small portion of the irradiation vessel so that essentially all of the solute (>95%) was in solution.

Irradiations were made in a ^{60}Co γ irradiator at a dose rate of 6×10^{18} eV g^{-1} hr^{-1}. Doses were 0.6–2 $\times$ 10^{19} eV/g for cases where measurements of hydrogen production were involved and $\sim 5 \times 10^{17}$ eV/g where ethyl radicals were determined. Absolute yields were obtained by comparison of the rate of product formation with that for oxidation of ferrous ion in the Fricke dosimeter in the standard way. Gas analysis was carried out by toepling the product volatile at liquid nitrogen temperature to a measuring McLeod gauge and subsequently analyzing an aliquot mass spectrometrically. Ethyl radical yields from ethylene solutions were determined using radioiodine as a scavenger. The radioethyl iodide product was separated chromatographically in experiments essentially identical with those previously described.[10,12,13] The concentration of iodine used in these experiments was $\sim 5 \times 10^{-4}$ M and should have been sufficient to quantitatively (*i.e.* >99%) scavenge the ethyl radicals.[12]

Results and Discussion

Hydrogen Yield from Pure Cyclohexane. The initial experiments on cyclohexane degassed in the normal way at liquid nitrogen temperature gave a hydrogen yield of 5.4. Because of the pronounced effect of CO_2 on the hydrogen yield indicated below, it was soon realized that there was probably enough (*i.e.* $\sim 10^{-4}$ M) CO_2 dissolved in the solutions to reduce the hydrogen yield by a significant amount. For three experiments in which CO_2 was carefully eliminated from the cyclohexane, yields of 5.60, 5.55, and 5.65 were observed at doses, respectively, of 0.6, 0.6, and 1.8×10^{19} eV/g. At these doses, olefin sufficient to reduce the initial hydrogen yield by ~0.1 unit will have already been built up. According to the treatment of the dose dependence given in the Appendix, the initial yield, $G(H_2)_0$, should be higher in these three experiments by, respectively, 0.05, 0.05, and 0.10 unit. Accordingly, $G(H_2)_0$ for the pure hydrocarbon is taken as 5.67 (the average of 5.65, 5.60, and 5.75) and is believed to be accurate to ~0.1. To the extent that the hydrogen produced by reactions of free ions might not be included in the observed initial yields, the value of $G(H_2)_0$ may be even slightly higher. Numerous other investigators have reported initial hydrogen yields from cyclohexane of ~5.6.[14]

Effect of Electron Scavengers on the Hydrogen Yield from Cyclohexane. Addition of CH_3Cl, CH_3Br, or C_2H_5Br to cyclohexane results in a pronounced decrease in the yield of hydrogen as is indicated in Figure 1. For solutes other than CH_3Br the yields are plotted at an effective concentration $[S]_{eff}$ where the actual concentration has been multiplied by a factor α_s/α_{CH_3Br} as described below. The present results from the CH_3Br solutions are in agreement with those obtained in the earlier study mentioned in the Introduction.[7] The results from N_2O, SF_6, and CO_2 solutions obtained in these

(9) For a summary of this work see Chapter 9 by W. H. Hamill in "Radical Ions," E. T. Kaiser and L. Kevan, Ed., Interscience Publishers, New York, N. Y., 1968.

(10) J. M. Warman, K.-D. Asmus, and R. H. Schuler, *J. Phys. Chem.*, 73, 931 (1969).

(11) S. J. Rzad, R. H. Schuler, and A. Hummel, *J. Chem. Phys.*, 51, 1369 (1969).

(12) R. H. Schuler and R. R. Kuntz, *J. Phys. Chem.*, 67, 1004 (1963).

(13) J. L. McCrumb and R. H. Schuler, *ibid.*, 71, 1953 (1967).

(14) See, for example, the summary by W. A. Cramer in "Aspects of Hydrocarbon Radiolysis," T. Gaümann and J. Hoigne, Ed., Academic Press, London, 1968, p 154 ff.

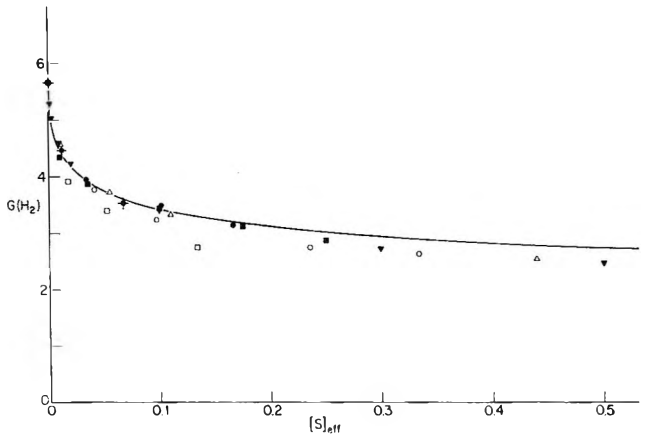

Figure 1. Effect of electron scavengers on H_2 production from cyclohexane. ✱, pure cyclohexane. Solutes: ●, CH_3Cl; ◆ CH_3Cl (Ref. 7); ○, CH_3Br; ⊡, C_2H_5Br; △, SF_6; ▽, N_2O; ■, CO_2. Points plotted at effective solute concentration which is taken as actual concentration times α_s/α_{CH_3Br} (as described in text). Curve calculated from eq III with $\epsilon = 1$ and $\alpha_s = \alpha_{CH_3Br} = 16.2\ M^{-1}$.

laboratories, which are also given in Figure 1, show a form for the concentration dependence which is very similar to that given by the halides. These latter results are, in general, similar to those reported by other workers[2,15-21] though in certain cases slight differences exist in the values given for a particular solute concentration. In fact the literature values are not always internally consistent (*e.g.*, hydrogen yields from 2.8[2] to 3.6[16] have been reported for 0.1 M N_2O solutions in cyclohexane). For many purposes such variations in the reported values would be of little consequence. A correlation of the type being attempted here, however, depends very sensitively on the absolute values of the yields and on relatively minor details of observed differences so that it is necessary to have an internally consistent set of data. The measurements of the present study were carried out with this in mind.

Many solutes in addition to the ones studied here have been found to depress the hydrogen yield from cyclohexane to approximately 3 when present at a concentration ~0.1 M.[7,22-28] Certain of these (*e.g.*, the alkyl iodides, CCl_4, and benzyl chloride) are, however, also expected to react with hydrogen atoms so that their effect on hydrogen production is certainly complex. Accordingly, results from these solutes are not considered in the present discussion though it is noted that at ~0.1 M the yields tend to be about one unit lower than those observed at the same concentration of CH_3Br, N_2O, or SF_6. This difference is reasonable in view of the estimate of ~0.95 given below for the yield of hydrogen atoms at electron scavenger concentrations of ~0.1 M. Other solutes such as SO_2, the perfluoroalkanes, N_2O, SF_6, and CO_2 appear likely to react only with electrons. In most of these latter cases products from electron capture have not, as yet, been measured and a direct correlation between electron capture and the effect on hydrogen production is not possible. One exception is a study of perfluorocyclohexane solutions in cyclohexane where Sagert[19] found the yield of $C_6F_{11}H$ to be about equal to that for reduction of hydrogen. Since it is not possible to state on *a priori* grounds that each electron captured by a solute will result in an equivalent decrease in the hydrogen yield (and in fact in certain cases it is quite obvious that this is not so; see below), further detailed experimental information is necessary.

Studies in which ethylene was added to the methyl halide solutions make it clear that hydrogen atoms do not readily attack the chloride and probably do not attack the bromide to any significant extent.[10] With these solutes, forms of energy transfer other than electron capture do not seem to come into play,[29] so that the observed reduction in the yield of hydrogen appears to result entirely from changes in the neutralization processes. From the data of Table I it is seen that for methyl chloride solutions the reduction in the yield of hydrogen is equal to the yield of methyl radicals. In the case of methyl bromide the reduction is slightly greater though the difference is small (0.1–0.3 unit). The data of this table imply that there is, very nearly at least, a 1:1 correspondence between electron capture as measured by methyl radical production and the decrease in the yield of hydrogen. That this should be so would appear to be fortuitous since it effectively involves unit efficiency for hydrogen production from electron positive ion recombination and, in fact, the work of Robinson and Freeman[28] which will be commented on later shows that there can be a wide variation in this efficiency.

(15) S. Sato, R. Yugeta, K. Shinsaka, and T. Terao, *Bull. Chem. Soc. Jap.*, **39**, 156 (1966).

(16) W. V. Sherman, *J. Chem. Soc.*, A599 (1966).

(17) S. Sato, T. Terao, M. Kono, and S. Shida, *Bull. Chem. Soc. Jap.*, **40**, 1818 (1967).

(18) N. H. Sagert and A. S. Blair, *Can. J. Chem.*, **45**, 1351 (1967).

(19) N. H. Sagert, *ibid.*, **46**, 95 (1968).

(20) N. H. Sagert, *ibid.*, **46**, 336 (1968).

(21) C. S. Munday, J. T. Richards, G. Scholes, and M. Simic, "The Chemistry of Ionization and Excitation," G. R. A. Johnson and G. Scholes, Ed., Taylor and Francis, London, 1967, p 151.

(22) M. Burton, J. Chang, S. Lipsky, and M. P. Reddy, *Radiat. Res.*, **8**, 203 (1958).

(23) J. A. Stone and P. J. Dyne, *Can. J. Chem.*, **42**, 669 (1963).

(24) C. E. Klots, Y. Raef, and R. H. Johnsen, *J. Phys. Chem.*, **68**, 2040 (1964).

(25) L. A. Rajbenbach, *J. Amer. Chem. Soc.*, **88**, 4275 (1966); L. A. Rajbenbach and U. Kaldor, *J. Chem. Phys.*, **47**, 242 (1967).

(26) R. J. Hagemann and H. A. Schwarz, *J. Phys. Chem.*, **71**, 2694 (1967).

(27) L. S. Polak, N. Ya. Chernyak, and A. S. Shcherbakova, *Khim. Vys. Energ.*, **1**, 220 (1967); L. S. Polak, N. Ya. Chernyak, and A. S. Shcherbakova, *ibid.*, **2**, 317 (1968).

(28) M. G. Robinson and G. R. Freeman, *J. Chem. Phys.*, **48**, 983 (1968).

(29) J. M. Warman, K.-D. Asmus, and R. H. Schuler, Advances in Chemistry Series, No. 82, American Chemical Society, Washington, D. C., 1968, p 25.

The stoichiometry involved in hydrogen production can be described, in a general sense, by the scheme

$$RH^+ + e^- \longrightarrow (RH)^* \longrightarrow \epsilon' \cdot H_2 \quad (1)$$

$$e^- + S \longrightarrow S^- \quad (2)$$

$$RH^+ + S^- \longrightarrow (RH + S)^* \longrightarrow \epsilon'' \cdot H_2 \quad (3)$$

where ϵ' and ϵ'' are the efficiencies for production of hydrogen from reactions 1 and 3. The difference between these efficiencies is

$$\epsilon = \epsilon' - \epsilon'' = \frac{G(H_2)_0 - G(H_2)}{G(e)_s} \quad (I)$$

where $G(e)_s$ is the yield of electrons scavenged in reaction 2. The efficiency difference indicated by the experiments is given in the final column of Table I. In general one expects that neutralization will not lead to the formation of multiple additional carbon–carbon bonds in more than a small fraction of the cases so that ϵ' cannot be greatly in excess of unity. The results show, therefore, that the efficiency of hydrogen production from reaction 3 is zero or nearly so. This fact does not seem to be completely unreasonable since electron capture reduces the recombination energy by an amount equal to the electron affinity of the negative ion and also distributes the remaining available energy between two product molecules.

Table I: Hydrogen and Methyl Radical Yields from CH_3Cl and CH_3Br Solutions in Cyclohexane

	[CH_3X]	$G(H_2)$	$G(CH_3)^a$	$G(H_2 + CH_3)$	$\frac{G(H_2)_0 - G(H_2)}{G(CH_3)}$
...	0	5.67[b]	...	5.67	...
CH_3Cl	0.099	3.90	1.71	5.61	1.02
	0.101	3.95	1.72	5.67	0.99
	0.106	4.00	1.74	5.74	0.95
	0.302	3.49	2.23	5.76	0.98
	0.503	3.13	2.47	5.60	1.02
CH_3Br	0.041	3.77	1.81	5.58	1.04
	0.097	3.24	2.21	5.45	1.09
	0.236	2.74	2.61	5.35	1.11
	0.334	2.63	2.76	5.40	1.09

[a] Radical yields from solute interpolated from data of ref 10. [b] Extrapolated to zero dose; see Appendix.

The yields of alkyl radicals from alkyl chloride and bromide solutions can be described over a wide range of concentrations by

$$G(P) = G(e)_s = G_{fi} + G_{gi}\frac{(\alpha_s S)^{1/2}}{1 + (\alpha_s S)^{1/2}} \quad (II)[10]$$

In eq II, G_{fi} is interpreted as the yield of electrons which are homogeneously distributed throughout the solution and which react as free ions at all reasonable solute concentrations. G_{gi} represents the yield of electrons which do not escape from the coulombic force field of their geminate partners and therefore react with solutes appreciably only when the latter are present at relatively high concentrations. The term α_s is an empirical parameter which describes the competition between electron capture by the solute and the ion-recombination process. It is found to have a value of 16.2 M^{-1} in the case of methyl bromide and 5.41 M^{-1} in the case of methyl chloride.[10] For cyclohexane both physical[30-33] and chemical[34,35] measurements give $G_{fi} \sim 0.1$ and extrapolation of the radical yields from the alkyl halide solutions to infinite solute concentration indicates that $G_{gi} \sim 3.8$.[10] Combining eq I and II and taking $G(H_2)_0 = 5.67$ allows one to write

$$G(H_2) = 5.67 - \epsilon\left[0.1 + 3.8\frac{(\alpha_s S)^{1/2}}{1 + (\alpha_s S)^{1/2}}\right] \quad (III)$$

The solid curve in Figure 1 was computed using this equation with $\epsilon = 1$ and $\alpha_s = 16.2\ M^{-1}$ (*i.e.*, the value of α for CH_3Br). The data for solutes other than CH_3Br are normalized by multiplying their concentration by the relative values α_s/α_{CH_3Br} (0.33 for CH_3Cl and 0.48 for C_2H_5Br being taken from scavenging studies with these solutes[10]). This curve fits the CH_3Cl data very well (as can be inferred from Table I). It also fits the CH_3Br data reasonably well though at high concentrations the observed yields tend to be slightly low. For SF_6, α_s/α_{CH_3Br} is taken as 1.1 from competitive studies of its effect on the yield of electrons scavenged by CH_3Br.[36] For N_2O and CO_2 values of 1.00 and 0.50 were chosen to give a fit of the data at 0.05 M (in view of the lack of other definitive measurements of α_s on these two solutes). The ratios for SF_6, N_2O, and CO_2 correspond to values for α_s of 18, 16, and 8 M^{-1}, respectively.

If one is certain that a particular solute does not react with hydrogen atoms then one should be able to determine α_s by comparing the hydrogen yield for a given solution with the curve of Figure 1, as is illustrated by the treatment of the data for N_2O and CO_2. While this approach is valuable where other measurements of α_s are not available or cannot be regarded as reliable, it must be recognized that small uncertainties in the yield are magnified greatly. Thus the two literature values for $G(H_2)$ from 0.1 M N_2O solutions mentioned earlier (2.8 and 3.6) lead to values of α which differ by a factor of 4. In another example, Sato, *et al.*,[5] superimpose their data from CO_2, SF_6, and N_2O solu-

(30) A. O. Allen and A. Hummel, *Discussions Faraday Soc.*, **36**, 95 (1963); A. Hummel, A. O. Allen, and F. H. Watson, Jr., *J. Chem. Phys.*, **44**, 3431 (1966).

(31) G. R. Freeman, *ibid.*, **38**, 1022 (1963); G. R. Freeman and J. M. Fayadh, *ibid.*, **43**, 86 (1965).

(32) W. F. Schmidt, *Z. Naturforsch.*, **23b**, 126 (1968).

(33) W. F. Schmidt and A. O. Allen, *Science*, **160**, 301 (1968); *J. Phys. Chem.*, **72**, 3730 (1968).

(34) S. J. Rzad and R. H. Schuler, *ibid.*, **72**, 228 (1968).

(35) S. J. Rzad and J. M. Warman, *J. Chem. Phys.*, **49**, 2861 (1968).

(36) P. P. Infelta and R. H. Schuler, to be published.

tions on the same curve. From this it would seem that the three solutes scavenge electrons with the efficiency. However, the present results show that it takes approximately twice the concentration of CO_2 to produce the same effect as CH_3Br, N_2O, and SF_6. According to the present results CO_2 appears to be only about 50% as reactive as these other solutes. This conclusion of a lower reactivity for CO_2 corresponds to a difference of only $\sim$0.2 in the comparisons of the hydrogen yields at concentrations of $\sim$0.1 M so that considerable error is possible.

In the initial studies on nitrous oxide solutions it was assumed that the nitrogen yield gave a true measure of the number of electrons captured by the solute and that the somewhat smaller decrease in the hydrogen yield represented only a fractional decrease in the efficiency of hydrogen production from the recombination process. More recently it has been generally recognized that secondary reactions are in part responsible for the high nitrogen yields. Sato and coworkers[15] pointed out that the yield for formation of nitrogen is approximately twice that for reduction in hydrogen and suggested that the latter can be taken as a measure of the electron scavenging process. This suggestion is essentially justified by the results of the present work on cyclohexane. Their numerical conclusion that 2 molecules of nitrogen are produced for each electron which reacts with N_2O is, however, not similarly borne out. The hydrogen yields which they reported for the N_2O containing solutions are comparable to those given in Figure 1. The yield for the solute-free system given by them is, however, only 5.1. Dose effects, which will be of a considerably lesser importance for the N_2O solutions than for the pure hydrocarbon, appear to come into play since an initial yield of 5.6 is reported elsewhere in work from the same laboratories. The decreases in $G(H_2)$ are, therefore, considerably greater than those indicated by Sato, *et al.*, and the multiplication factor is dependent on the N_2O concentration and seems to vary between 1 and 2 as has already been commented on by the present authors.[29]

In cases where other effects contribute to the reduction in hydrogen (*e.g.*, the alkyl iodides) interpretation of the results in terms of eq III is, of course, completely inappropriate and would lead to erroneous values of α. Thus, if one ascribes the reduction in H_2 produced by ethyl bromide solely to electron scavenging, then one concludes that ethyl and methyl bromides have about the same reactivities toward electrons. Both direct measurements on these two solutes and competitive studies between them indicate that ethyl bromide is only about one-half as reactive as methyl bromide.[10] Some other effect must come into play to explain the low yields of hydrogen from the ethyl bromide solutions.

Effect of Electron Scavengers on the Hydrogen Yield from Other Hydrocarbons. According to eq II the reciprocal of α_s represents the scavenger concentration at which half of the geminately recombining electrons are scavenged. For N_2O in cyclohexane this concentration is 0.06 M. In the absence of a large free ion yield the decrease in $G(H_2)$ at a solute concentration of $1/\alpha_s$ should represent one-half of the total hydrogen yield resulting from ion recombination provided, of course, that neutralization by the secondary negative ions produced in the N_2O containing systems yields no hydrogen. Robinson and Freeman[28] have studied the effect of nitrous oxide on the hydrogen yield from a number of saturated hydrocarbons. If the reactivity of N_2O is similar in all hydrocarbons, as is indicated by the similarity of the observed nitrogen yields in the N_2O concentration range of 0.02—0.1 M, then it is possible to estimate the contribution of ion recombination to the hydrogen production for each of these hydrocarbons. These estimates, taken as twice the decrease observed at 0.06 M N_2O, are given in Table II. The efficiencies of H_2 formation from ion recombination calculated on the assumption that the ion-pair yield is 4.0 in all hydrocarbons are also given. From this it appears that the formation of H_2 occurs with less than unit efficiency for the majority of hydrocarbons and that cyclohexane is a pronounced exception in that the efficiency is nearly equal to (but not necessarily identical with) 1. One interesting aspect of the values in Table II is that the considerable differences observed in the hydrogen yields for the pure hydrocarbons appear to result mainly from a low efficiency for formation of hydrogen from the ion-recombination process, particularly when a highly branched hydrocarbon is involved. The hydrogen yield remaining after subtraction of the above estimate of the contribution from ion recombination is relatively constant at a value within a few tenths of 1.6. The production of hydrogen from nonionic processes, therefore, seems to be relatively independent of struc-

Table II: Hydrogen Yields from Hydrocarbon–N_2O Solutions

	$G(H_2)_0$	$2\Delta G(H_2)^a$	$G(H_2)_0 - 2\Delta G(H_2)$	ϵ'^b
3-Methylpentane	3.9[c]	2.3[c]	1.6	0.6
n-Hexane	5.1[c]	3.4[c]	1.7	0.9
n-Heptane	4.7[c]	3.4[c]	1.3	0.9
Cyclopentane	4.9[c]	3.2[c]	1.7	0.8
Methylcyclopentane	4.2[d]	2.4[d]	1.8	0.6
Cyclohexane	5.6[c]	4.0[c]	1.6	1.0
Methylcyclohexane	4.7[c]	3.2[c]	1.5	0.8
2,2,4-Trimethylpentane	2.4[e]	1.2[e]	1.2	0.3

[a] Twice the reduction observed at 0.06 M N_2O. [b] Calculated assuming an ion-pair yield of 4.0. [c] From M. G. Robinson and G. R. Freeman, *J. Chem. Phys.*, **48**, 983 (1968). [d] From E. D. Stover and G. R. Freeman, *ibid.*, **48**, 3902 (1968). [e] S. J. Rzad and J. M. Warman, unpublished results.

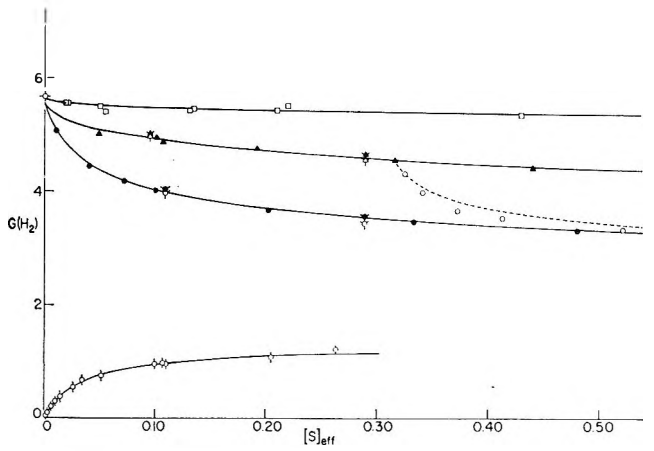

Figure 2. Effect of ammonia (□), cyclopropane (▲), and ethylene (●) on hydrogen production from cyclopropane. Points plotted at effective solute concentration 2.16, 0.93 and 1 times the actual concentrations. Solid flagged points are for total hydrogen and open flagged points for H_2 produced from deuteriocyclopropane and deuterioethylene solutions. Open circles (○) are for addition of ethylene to 0.34 M cyclopropane solutions. Data of lower curves ϕ are for ethyl radical produced from ethylene solutions. Curves are calculated as described in text.

ture while that from ionic processes is strongly dependent on structure.

Effect of Positive Ion Scavengers on the Hydrogen Yield. With the knowledge that ~1 molecule of H_2 is formed upon neutralization of each positive ion produced in the radiolysis of pure cyclohexane, one can readily examine the effect of changes in the identity of the ions when positive ion scavengers are added to the system. The work of Williams on ND_3 solutions[3] shows that the yield of H_2 drops but that of total hydrogen remains very nearly constant. From this latter observation it would seem that neutralization of the secondary ions produced in the cyclohexane–ammonia system results in hydrogen formation with near unit efficiency. Results from similar studies in these laboratories,[37] while again differing slightly in detail with the published values, confirm the general ideas and conclusions of his work. The total hydrogen yields (which are slightly higher than those given by Williams) are reported in Figure 2 at an effective concentration 2.16 times the actual concentration ($\alpha_{ND_3} = 0.93\ M^{-1}$).[37] At ammonia concentrations ~0.1 M the yields are about 0.2 unit less than the value for $G(H_2)_0$ given above (5.67). The hydrogen yields from the ammonia system are strongly affected by electron scavengers[37] so that the slight reduction observed here could result from trace impurities in the ammonia. If the decrease is real, the efficiency of production of hydrogen by neutralization of the secondary ion formed from the NH_3 is ~20% less than for the initial ion. In any event the two efficiencies do not differ greatly and since the former seems likely to be close to unity, so also does the latter (as has already been concluded from the studies with electron scavengers). It is noted that in the case of methylcyclopentane, Stover and Freeman[38] have shown that the total hydrogen increases with added ammonia. This increase is as expected since the value of ϵ of 0.6 given in Table II for this hydrocarbon would indicate that neutralization of the secondary ion in the ammonia system should give more hydrogen than neutralization of the original ion.

Change in the identity of the positive ion to another organic ion might not be expected to have any pronounced effect on hydrogen production. However, it is known that addition of cyclopropane, which is a good positive ion scavenger,[4,11,34,39] results in an appreciable reduction in the hydrogen yield from cyclohexane.[28] There is no evidence from competitive studies with methyl chloride and with ethylene that this solute reacts either with electrons or with hydrogen atoms and so it seems likely that the reduction in $G(H_2)$ accompanies the change in the positive ion. The principal products formed from cyclopropane are propane and propyl cyclohexane[34] with the sum of their yields being describable by eq II with $\alpha_\Delta = 0.40\ M^{-1}$.[11] A direct comparison of this sum with the depression in hydrogen production observed in the present study shows that the two quantities are essentially equal. This is illustrated in Figure 2 where the solid curve through the cyclopropane points was calculated from eq III with $\epsilon = 1$ and $\alpha_\Delta = 0.40\ M^{-1}$. The good agreement implies, of course, that neutralization of the secondary positive ions formed from the cyclopropane does not yield hydrogen. That this is so has already been indicated by the work of Ausloos, *et al.*,[39] where experiments with deuteriocyclopropane (which were, however, from studies carried out in the solid at −196°) showed that the hydrogen had little deuterium content. Experiments at room temperature carried out during the course of the present work gave a similar result and are reported in Table III. It is seen that the yield of H_2 is only slightly lower than that of total hydrogen. Robinson and Freeman[28] in their treatment of the data from cyclopropane solutions assumed that the reduction was a correct measure of the yield for the positive ion reactions. This assumption seems to be justified by the present study in the case of cyclohexane but would be incorrect for other hydrocarbons where the efficiency of H_2 production from the original ions is less than unity.

Ethylene as a Positive Ion and Hydrogen Atom Scavenger and Its Effect on Hydrogen Production. Ethylene is, of course, expected to act as a scavenger for hydrogen atoms to give ethyl radicals.

$$H\cdot + C_2H_4 \xrightarrow{k_1} C_2H_5\cdot \qquad (4)$$

(37) K.-D. Asmus, to be published.

(38) E. D. Stover and G. R. Freeman, *J. Chem. Phys.*, **48**, 983 (1968).

(39) P. Ausloos, A. A. Scala, and S. G. Lias, *J. Amer. Chem. Soc.*, **89**, 3677 (1967).

Table III: Hydrogen Yields from Deuteriocyclopropane and Deuterioethylene Solutions

Solute	Concn, M	G Total hydrogen	G H_2	G HD	G D_2	G H_2(calcd)[a]
c-C_3D_6[b]	0.102	4.99	4.96	0.033	0.002	4.93
	0.311	4.63	4.54	0.082	0.005	4.58
C_2D_4[c]	0.109	4.04	3.97	0.032	0.041	3.98
	0.289	3.54	3.43	0.049	0.057	3.53

[a] For cyclopropane calculated from eq III and for ethylene from eq XIII with ϵ taken as 1 and the other parameters as described in the text. [b] Protium content, 0.74 atom %. [c] Protium content, 0.61 atom %.

The yield of ethyl radicals has been measured both by titration with iodine[13] and by sampling with $^{14}CH_3\cdot$ radicals.[40] The values obtained by the former method are shown in Figure 2. Though complications are now apparent and will be discussed below, both sets of results indicate that at accessible ethylene concentrations a competition occurs between reaction 4 and abstraction of hydrogen from the solvent.

$$H\cdot + RH \xrightarrow{k_2} H_2 + R\cdot \qquad (5)$$

In these earlier studies estimates of 0.0034[13] and 0.0037[40] were given for k_2/k_1 on the assumption that a simple competition existed for a constant yield of hydrogen atoms. Measurements of the hydrogen yield from ethylene solutions, which are reported in Figure 2, clearly show that the reduction in $G(H_2)$ is considerably in excess of the measured ethyl radical yield. The difference, which is $\sim$1 at 10^{-1} M C_2H_4, could conceivably result from abstraction of hydrogen from the solvent by "hot" ethyl radicals formed in reaction 4. Recent studies with $^{14}C_2H_4$ in cyclohexane containing scavenger iodine show that this is not the case.[41]

Since ethylene is known to be a scavenger of positive ions, from competitive studies with cyclopropane[42] it might be expected to affect the hydrogen production in much the same manner as does the cyclopropane. The competition experiments show that ethylene is $\sim$10% more reactive than cyclopropane (*i.e.*, $\alpha_{C_2H_4} = 0.43$ M^{-1})[42] so that ionic reactions should occur to an important extent at the concentrations under discussion here. Experiments with deuterioethylene reported in Table III show only a very small deuterium content in the hydrogen produced, though in contrast to the results with deuteriocyclopropane a small yield of D_2 is observed. These experiments show that little hydrogen is derived from neutralization of the solute ion and accordingly $G(H_2)$ should be calculable from eq III if, in addition, one subtracts the yield attributable to reaction 4. The observed hydrogen yields are, in fact, reproduced quite well if the ethyl radical yields given by the lower curve of Figure 2 are taken as a measure of reaction 4. However, since ionic reactions are likely to contribute to ethyl radical formation such an interpretation seems to be somewhat of an oversimplification. It is quite clear though, that the hydrogen yield from the solutions containing ethylene is depressed from that of the pure hydrocarbon both as a result of hydrogen atom scavenging and also as a result of changes in the neutralization process. This latter effect vitiates any attempt to use measurements of hydrogen depression in determinations of hydrogen atom yields from pure hydrocarbons and makes it difficult to determine addition–abstraction rate constant ratios.

To a large extent one can avoid the problems indicated in the above paragraph if one adds small amounts of ethylene to a solution already containing an appreciable concentration of a positive-ion scavenger that does not react with hydrogen atoms. Then the effect of ethylene on the ionic processes can be treated as an incremental situation and will be far less pronounced than for the pure hydrocarbon. Results from experiments in which ethylene was added to a 0.34 M cyclopropane solution are reported in Figure 2. Over the range studied (0–0.2 M C_2H_4) the hydrogen atom yield should be essentially constant and the molecular hydrogen is expected to decrease by only 0.2 unit. If the decrease in hydrogen produced upon adding ethylene to the cyclopropane containing system is corrected for the latter effect it should be possible to treat the resultant decrease as a simple competitive situation. When this is done the hydrogen atom yield for 0.3–0.5 M ethylene solutions is estimated to be 1.3 and the ratio of rate constants for abstraction and scavenging 0.004. The values of the yields predicted by the slightly higher rate constant ratio given below are given by the dashed curve in Figure 2.

The Ethyl Radical Yield from Ethylene Solutions. Unfortunately, since neither the hydrogen atom yield nor k_2/k_1 is known with confidence, one cannot calculate the contribution of reaction 4 to the ethyl radical yield, and while previous investigations have attempted to use measurements of $G(C_2H_5)$ to determine these quantities, it seems evident from the above observations on hydrogen production that $G(H)$ is not constant but dependent on the ethylene concentration. From the fact that propyl radicals are produced from cyclopropane *via* ionic intermediates, it also seems likely that ionic reactions may very well contribute to ethyl radical formation. Experiments in which cyclopropane has been added to the ethylene solutions have been carried out in an attempt to sort out contributions from these possible complicating effects and the results

(40) R. A. Holroyd, *J. Phys. Chem.*, **70**, 1341 (1966).

(41) G. W. Klein, private communication. An ethane-^{14}C yield of 0.2 was observed from a 0.1 M $^{14}C_2H_4$ solution in cyclohexane containing 10^{-3} M I_2. This yield increased to 0.4 upon the addition of 0.1 M CCl_4 as expected if the ethane was produced mostly from reactions of positive ions (see ref 11). In any event the ethane produced is not sufficient to account for the difference observed in $G(H_2)$.

(42) S. J. Rzad, to be published.

Table IV: Ethyl Radical Yields from Ethylene–Cyclopropane Solutions in Cyclohexane

$[C_2H_4]$	$[C_3H_6]$	$G(H)_S$[a]	$G(C_2H_5)_{ion}$[b]	Q	G_{obs}	G_{calcd}[c]
0.263	0	1.22	0.095	0.905	1.21[d]	1.14
0.205	0	1.24	0.087	0.922	1.08	1.11
0.108	0	1.28	0.070	0.947	0.96[d]	0.98
0.107	0	1.28	0.069	0.946	0.98	0.98
0.100	0	1.29	1.068	0.948	0.96	0.96
0.0506	0	1.33	0.053	0.976	0.75	0.76
0.0338	0	1.34	0.046	0.986	0.68[d]	0.63
0.0252	0	1.36	0.041	1.004	0.55	0.53
0.0139	0	1.37	0.034	1.033	0.38[d]	0.36
0.0092	0	1.39	0.029	1.052	0.30	0.27
0.0061	0	1.39	0.026	1.090	0.21[d]	0.20
0.0024	0	1.41	0.020	1.232	0.09[d]	0.09
0.0012	0	1.42	0.017	1.439	0.05[d]	0.05
0.104	0.213	1.21	0.034	0.860	0.86	0.88
0.304	0.305	1.15	0.064	0.832	1.10	1.06
0.205	0.301	1.16	0.049	0.837	1.01	1.01
0.102	0.303	1.18	0.029	0.841	0.81	0.86
0.100	0.301	1.19	0.028	0.840	0.85	0.85
0.075	0.307	1.19	0.022	0.840	0.76	0.77
0.0506	0.301	1.20	0.016	0.841	0.64	0.66
0.0290	0.307	1.20	0.009	0.839	0.51	0.49
0.0252	0.301	1.21	0.008	0.841	0.44	0.45
0.0104	0.306	1.21	0.003	0.838	0.26	0.23

[a] Hydrogen atom yield for cyclohexane containing ethylene and cyclopropane at the indicated concentrations as calculated from eq IV. [b] Yield of ethyl radicals from secondary ionic reactions, calculated from eq VI. [c] Total yield of ethyl radicals calculated from eq VII. [d] Data from ref 13. [a,b,c] Parameters used in calculations: $G(H)_0 = 1.46, f(H)_{neut} = 0.23, f(C_2H_5)_{sec} = 0.09$, $\alpha_{S_1} = 0.43\ M^{-1}$, $\alpha_{S_2} = 0.40\ M^{-1}$, $G_{fi} = 0.1$, $G_{gi} = 3.8$, $k_2/k_1 = 0.00475$, [RH] = 9.3 M.

are reported in Table IV. It is found that the addition of 0.3 M cyclopropane causes a reduction of ~10% in the ethyl radical yield at both 0.1 and 0.01 M ethylene concentrations. This reduction apparently does not result from a simple chemical competition between the two solutes. Complications due to intervention of ionic processes seem clearly to be involved. It is also noted in Figure 3 that there is a considerable difference in both the intercepts and slopes for the usual competition plots of the data with and without added cyclopropane. The data can be treated quantitatively if one introduces two terms into the detailed scheme: $f(H)_{neut}$, the fraction of neutralization processes involving the initial ions which give rise to hydrogen atom production, and $f(C_2H_5)_{sec}$, the fraction of secondary positive ion reactions which ultimately result in ethyl radical formation. As a result of the first term the hydrogen atom yield from the pure solvent, $G(H)_0$, should be reduced to

$$G(H)_{S_1,S_2} = G(H)_0 - f(H)_{neut}\left[G_{fi} + G_{gi}\frac{\sqrt{\alpha_1 S_1 + \alpha_2 S_2}}{1 + \sqrt{\alpha_1 S_1 + \alpha_2 S_2}}\right] \quad \text{(IV)}$$

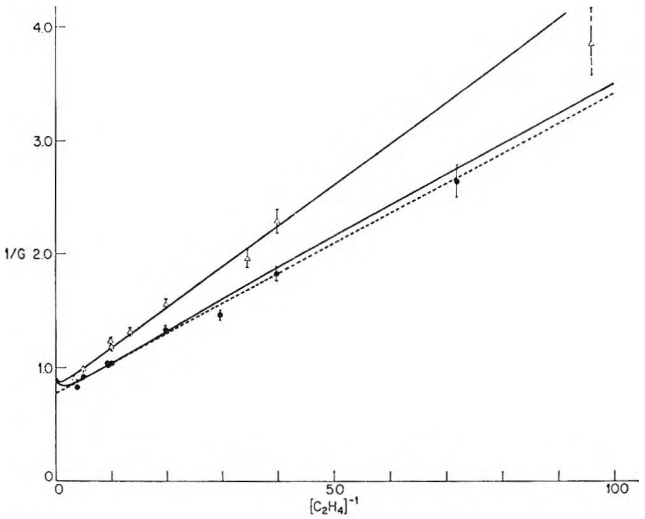

Figure 3. Plot of $1/G(C_2H_5)$ *vs.* $1/[C_2H_4]$: ●, ethylene solutions; ▲, ethylene solutions containing 0.3 M cyclopropane. Error limits reflect differences of ±0.02 in G. Dashed line through the ethylene points corresponds to dependence expected for simple competition between reactions 4 and 5 if $G(H)$ were 1.28 and $k_2/k_1 = 0.0036$ and is used for interpolation in the comparisons of Table V. The difference between the two curves, however, demonstrates that complexities over and above a simple competitive situation are present. The solid curves are calculated from Equation VII on the assumption that 23% of the neutralization processes involving the initial ions give hydrogen atoms and that 9% of the positive ion reactions with ethylene give ethyl radicals (see text).

when ethylene and cyclopropane are added at concentrations S_1 and S_2. The ethyl radical yield produced by reaction of these H atoms with the ethylene will be given by

$$G(C_2H_5)_{H\ atom} = G(H)_{S_1,S_2}\frac{1}{1 + \frac{k_2}{k_1}\frac{[RH]}{S_1}} \quad \text{(V)}$$

The ethyl radical yield produced by positive ion reactions with the ethylene will be given by

$$G(C_2H_5)_{ion} = f(C_2H_5)_{sec} \times \left[G_{fi} + G_{gi}\frac{\sqrt{\alpha_1 S_1 + \alpha_2 S_2}}{1 + \sqrt{\alpha_1 S_1 + \alpha_2 S_2}}\right]\frac{\alpha_1 S_1}{\alpha_1 S_1 + \alpha_2 S_2} \quad \text{(VI)}$$

If these are the sole sources of ethyl radicals then the total yield will be

$$G(C_2H_5) = \left\{G(H)_0 - f(H)_{neut}\left[G_{fi} + G_{gi}\frac{\sqrt{\alpha_1 S_1 + \alpha_2 S_2}}{1 + \sqrt{\alpha_1 S_1 + \alpha_2 S_2}}\right]\right\}\frac{1}{1 + \frac{k_2}{k_1}\frac{[RH]}{S_1}} + f(C_2H_5)_{sec} \times \left[G_{fi} + G_{gi}\frac{\sqrt{\alpha_1 S_1 + \alpha_2 S_2}}{1 + \sqrt{\alpha_1 S_1 + \alpha_2 S_2}}\right]\frac{\alpha_1 S_1}{\alpha_1 S_1 + \alpha_2 S_2} \quad \text{(VII)}$$

The values of the parameters G_{fi}, G_{gi}, α_1, and α_2 arei ndependently available from other experiments and S_1, S_2, and [RH] are, of course, experimental quantities. The numerical values of the four parameters $G(H)_0$, k_2/k_1, $f(H)_{neut}$, and $f(C_2H_5)_{sec}$ remain to be defined by the available experimental information.

If we look only at the decrease of the ethyl radicals produced by adding cyclopropane at a given ethylene concentration then the parameter $G(H)_0$ can be eliminated, *i.e.*

$$G(C_2H_5)_{S_1} - G(C_2H_5)_{S_1,S_2} = f(C_2H_5)_{sec}\left\{\left(G_{fi} + G_{gi}\frac{\sqrt{\alpha_1 S_1}}{1+\sqrt{\alpha_1 S_1}}\right) - \left(G_{fi} + G_{gi}\frac{\sqrt{\alpha_1 S_1 + \alpha_2 S_2}}{1+\sqrt{\alpha_1 S_1 + \alpha_2 S_2}}\right)\times \frac{\alpha_1 S_1}{\alpha_1 S_1 + \alpha_2 S_2}\right\} + f(H)_{neut}\cdot G_{gi}\times \left(\frac{\sqrt{\alpha_1 S_1 + \alpha_2 S_2}}{1+\sqrt{\alpha_1 S_1 + \alpha_2 S_2}}\right) - \left(\frac{\sqrt{\alpha_1 S_1}}{1+\sqrt{\alpha_1 S_1}}\right)\left(\frac{1}{1+\frac{k_2}{k_1}\frac{[RH]}{S_1}}\right) \quad \text{(VIII)}$$

The experimentally observed differences are given in column 6 of Table V. As it turns out, for any given set of values of $f(H)_{neut}$ and $f(C_2H_5)_{sec}$ the right-hand side of eq VIII is only mildly dependent on the choice of k_2/k_1 which from the overall studies is certainly very near to 0.004. This leaves only $f(H)_{neut}$ and $f(C_2H_5)_{sec}$ to be determined to describe the observed differences. By fixing the value of either of these quantities and then varying the other in order to minimize the deviations between the calculated and observed differences one finds optimum agreement when the values are interrelated by

$$f(H)_{neut} + 1.3f(C_2H_5)_{sec} \simeq 0.35 \quad \text{(IX)}$$

Within this relationship examination of the deviations between the observed and calculated differences gives little preference to the choice of any one set of values over any other. The difference measurements, however, do place upper limits of 0.35 on the fraction of positive ion–electron recombination processes which can give H atoms and of 0.26 on the fraction of the ionic processes involving ethylene which can give ethyl radicals. The actual fractions are complementary.

If one rearranges eq VII into the form

$$\frac{1}{G(C_2H_5)}\frac{\left[1 - \frac{f(H)_{neut}}{G(H)_0}(G(\text{ion}))\right]}{\left[1 - \frac{f(C_2H_5)_{sec}}{G(C_2H_5)}(G(\text{ion}))\cdot\frac{\alpha_1 S_1}{\alpha_1 S_1 + \alpha_2 S_2}\right]} = \frac{1}{G(H)_0}\left[1 + \frac{k_2}{k_1}\frac{[RH]}{[C_2H_4]}\right] \quad \text{(X)}$$

where $G(\text{ion}) = G_{fi} + G_{gi}\dfrac{\sqrt{\alpha_1 S_1 + \alpha_2 S_2}}{1+\sqrt{\alpha_1 S_1 + \alpha_2 S_2}}$

and sets

$$Q = \frac{1 - \frac{f(H)_{neut}}{G(H)_0}(G(\text{ion}))}{1 - \frac{f(C_2H_5)_{sec}}{G(C_2H_5)}(G(\text{ion}))\frac{\alpha_1 S_1}{\alpha_1 S_1 + \alpha_2 S_2}} \quad \text{(XI)}$$

then a simple linear relationship of the normal competition type between $Q/G(C_2H_5)$ and $1/C_2H_4$ is expected. The quantity Q can be considered to be a correction factor which both allows the data to be presented as a competition relationship and also serves to superimpose the curves obtained with and without added cyclopropane. While Q contains the quantity $G(H)_0$ it is not grossly sensitive to it and one can approach the problem of obtaining values for $G(H)_0$ and k_2/k_1 as one of successive approximations. In fact, with any reasonable initial choice of $G(H)_0$ only a single iteration is required. For any given choice of $f(H)_{neut}$ and $f(C_2H_5)_{sec}$ the appropriate values of $G(H)_0$ and k_2/k_1 are readily determined from the intercept and slope of a plot of Q/C_2H_5 *vs.* $1/C_2H_4$. The linearity of such a relationship is indicated in Figure 4 for $f(H)_{neut} = 0.23$ and $f(C_2H_5)_{sec} = 0.09$ where $G(H)_0 = 1.46$ and $k_2/k_1 = 0.00475$. A comparison of the results from the various experiments with the values calculated from eq VII using these parameters (and $G_{fi} = 0.1$, $G_{gi} = 3.8$, [RH] = 9.3 M, $\alpha_1 = 0.43$, $\alpha_2 = 0.40$) is given in Table IV. Except for the experiment at 0.263 M C_2H_4, the agreement is seen to be excellent. Similar agreement is, however, obtained with other choices of the parameters consistent with eq IX and one must rely on further arguments (as discussed below) for the particular set of parameters used in compiling Table IV. Unfortunately, the value of the hydrogen atom yield determined by the above ap-

Table V: Comparison of Ethyl Radical Yields from Ethylene and Ethylene–Cyclopropane Solutions

$[C_2H_4]$	$[C_3H_6]$	$G(C_2H_5)_\Delta$	$G(C_2H_5)_0$[a]	Difference: Calcd[b]	Difference: Obsd
0.104	0.213	0.855	(0.968)	0.090	0.113
0.304	0.305	1.100	(1.154)	0.089	0.054
0.205	0.301	1.011	1.079	0.099	0.068
0.102	0.303	0.810	(0.965)	0.110	0.155
0.100	0.301	0.846	0.960	0.110	0.114
0.075	0.307	0.760	(0.886)	0.111	0.126
0.0506	0.301	0.642	0.760	0.105	0.118
0.0290	0.307	0.510	(0.598)	0.093	0.088
0.0252	0.301	0.436	0.547	0.087	0.111
0.0104	0.306	0.260	(0.303)	0.060	0.043

[a] Ethyl radical yield in the absence of cyclopropane. Quantities in parentheses interpolated using dashed line of Figure 3. [b] Calcd from eq VIII.

proach depends very sensitively on the choice of $f(H)_{neut}$ and $f(C_2H_5)_{sec}$. With $f(C_2H_5)_{sec} = 0$ and $f(H)_{neut} = 0.35$, $G(H)_0$ is 1.67. With $f(H)_{neut} = 0$ and $f(C_2H_5)_{sec} = 0.26$, it is 1.01. These values represent the upper and lower limits for the possible yield of hydrogen atoms consonant with these experiments.

Data on the effect of electron scavengers on the ethyl radical yield should provide the information necessary to fix the parameters $f(H)_{neut}$ and $f(C_2H_5)_{sec}$ because electron scavengers are expected to increase the importance of positive-ion reactions[11] while decreasing the contribution from reactions of atomic hydrogen. Carbon tetrachloride has, in fact, been found to increase the ethane and ethylcyclohexane yields from iodine scavenged solutions of ethylene in cyclohexane.[41] Data on the effect of SF_6, N_2O, and CH_3Cl on the ethyl radical yield are given in Figure 5 where it is seen that these solutes depress the yield slightly.[43] A quantitative description of the expected dependence on electron scavenger concentration can be given by reference to the treatment of the effects observed with cyclopropane solutions.[11] In that case the data can be explained if one assumes that the lifetime of the positive entity increases by a factor r_D when the electron is converted into a large negative ion. By analogy the ethyl radical yield should be given in the present case by

$$G(C_2H_5)_{S_1,S_2} = \left\{G(H)_0 - f(H)_{neut}\left[G_{fi} + G_{gi}\frac{\sqrt{\alpha_1 S_1 + \alpha_2 S_2}}{1 + \sqrt{\alpha_1 S_1 + \alpha_2 S_2}}\right]\right\}\frac{1}{1 + \frac{k_2}{k_1}\frac{[RH]}{S_1}} + f(C_2H_5)_{sec}\left\{G_{fi} + G_{gi}\left\{1 - \frac{1}{1 + \sqrt{\alpha_1 S_1 + \alpha_2 S_2}} - \left[\frac{1}{1 + \sqrt{\alpha_1 S_1 r_D}} - \frac{1}{1 + \sqrt{\alpha_1 S_1 + \alpha_2 S_2}}\right]\times \frac{\alpha_2 [S_2]}{\alpha_2 S_2 + \alpha_1 S_1 (1 - r_D)}\right\}\right\} \quad \text{(XII)}$$

where S_1 and S_2 are, respectively, the concentrations of ethylene and electron scavenger. The first term on the right side of eq XII accounts for the decrease in the yield of ethyl radicals which results from the decreased hydrogen atom yield upon addition of an electron scavenger and the second term accounts for the increase in the ionic contribution to ethyl radical which results from the increased ion-pair lifetime. For various solutes in cyclohexane this increased lifetime has been found to be of the order of a factor of 20.[11] This second term is always positive so that if $f(H)_{neut}$ is 0, the ethyl radical yield should increase upon the addition of electron scavenger. If $f(C_2H_5)_{sec}$ is 0 then the yield should decrease in a very pronounced fashion. The limiting behaviors of the ethyl radical yield corresponding to these two conditions are given by the dashed curves in the figure. If the results from the N_2O and SF_6 containing solutions are taken as typical as those for electron scavengers then the data can be fit very well if $f(C_2H_5)_{sec} = 0.09$ and $f(H)_{neut} = 0.23$ as indicated by the solid curve. This treatment is particularly sensitive to the choice of $f(C_2H_5)_{sec}$ and the data cannot be fit by a value of $f(C_2H_5)_{sec}$ which deviates significantly from 0.09. If we accept these parameters then $G(H)_0 = 1.46$ and $k_2/k_1 = 0.00475$.[44] These values are, respectively, 10 and 40% higher than those obtained by considering the concentration dependence for ethyl radical formation solely in terms of a competition between reactions 4 and 5. As pointed out previously,[13] the magnitude of the rate constant ratio leads to an estimate of the absolute rate constant for the addition of hydrogen atoms in liquid cyclohexane which is quite comparable to that measured in gas-phase experiments.

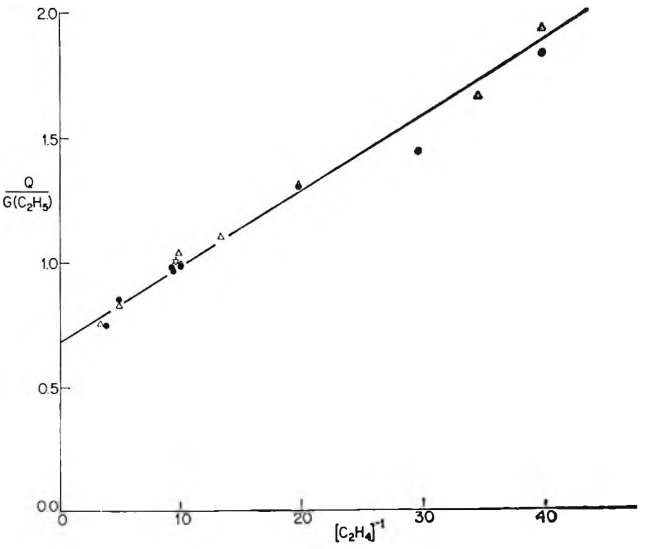

Figure 4. Competition plot of $Q/G(C_2H_5)$ *vs.* $1/[C_2H_4]$: ●, ethylene only; △, ethylene plus 0.3 M cyclopropane; ☆, ethylene plus 0.2 M cyclopropane. Linear relationship corresponds to $G(H)_0 = 1.46$ and $k_2/k_1 = 0.00475$.

An overall comparison of the available data can now be made with a common set of the various parameters.

(43) The addition of methyl bromide to 0.1 *M* solutions of C_2H_4 in cyclohexane depresses the ethyl radical yield considerably more than does that of other electron scavengers. The mixed system C_2H_4–CH_3Br is at the moment considered to be anomalous since the methyl radical yield is greater than from solutions containing only methyl bromide (see ref 10). It may be that at the higher methyl bromide concentrations some hydrogen atom attack on the bromide does occur. However, if this is so some additional complication must also be present to cause an increase in the methyl radical yield upon the addition of ethylene.

(44) It is interesting to note in Table IV that the values of Q for the solutions containing 0.3 *M* cyclopropane are nearly independent of ethylene concentration. If Q is, in fact, constant it follows that a plot of $1/G(C_2H_5)$ *vs.* $1/(C_2H_4)$ should be linear and have an intercept $1/QG(H)_0$ and a slope $(1/QG(H)_0)(k_2/k_1)$. That such a plot is linear is seen in Figure 3 where the data for the cyclopropane-containing solutions appear to obey a simple competition relation but where, according to the present treatment, the intercept cannot be interpreted simply in terms of a hydrogen atom yield. The ratio of slope to intercept, however, does give the ratio of rate constants which should be reasonably accurate. From the data of the figure this ratio is 0.0045.

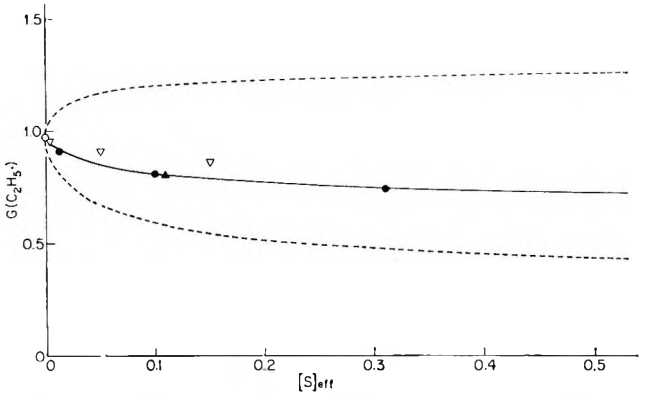

Figure 5. Effect of electron scavengers on the ethyl radical yield from 0.1 M ethylene solutions: ○, ethylene only; ●, added SF_6; ▲, added N_2O; ▽, added CH_3Cl. Solid curve calculated from eq XII with the parameters given in the text. Limiting situations for $f(H)_{neut} = 0$ and $f(C_2H_5) = 0$ are given respectively by the upper and lower dashed curves (with the other parameters determined for best overall fit of data from ethylene and ethylene–cyclopropane solutions).

For ethyl radical formation such has been done in Tables IV and V, in Figure 3 where the solid curves are those calculated from eq VII and in Figure 5 where the calculation is from eq XII with $r_D = 17$. The minima in the curves of Figure 3 perhaps seem peculiar. In fact they correspond to maxima in the ethyl radical yield curves which result from an increase in the efficiency of scavenging which is superimposed on a decrease in yield of hydrogen atom production as the ethylene concentration is increased. For solutions containing ethylene in the range 0.3–0.5 *M* a hydrogen atom yield ~1.2 is calculated from eq IV (see Table IV). This value may be compared with the value ~1.3 inferred from the experiments mentioned above in which ethylene was added to a 0.34 *M* cyclopropane solution.[45] Some additional measure of check on the overall details is obtained from the solid curve through the ethylene points of Figure 2. This curve is calculated assuming that the reduction in hydrogen is equal to the sum of the yields for ionic reactions and for addition of hydrogen atoms to ethylene, *i.e.*

$$G(H_2)_{[C_2H_4]} = 5.67 - \epsilon\left[G_{fi} + G_{gi}\frac{\sqrt{\alpha_1[C_2H_4]}}{1+\sqrt{\alpha_1[C_2H_4]}}\right] - \left[G(H)_0 - f(H)_{neut}\left(G_{fi} + G_{gi}\frac{\sqrt{\alpha_1[C_2H_4]}}{1+\sqrt{\alpha_1[C_2H_4]}}\right)\right]\cdot\frac{1}{1+\frac{k_2}{k_1}\frac{[RH]}{[C_2H_4]}} \quad \text{(XIII)}$$

with ϵ taken as 1.0. It is seen that the observed hydrogen yields are predicted very well by the proposed scheme with the values of the parameters independently determined in other experiments.

With $f(H)_{neut} = 0.23$ and $f(C_2H_5)_{sec} = 0.09$, for pure cyclohexane the total hydrogen atom yield is 1.46 and that from the neutralization process is (0.23)(3.9) = 0.89 leaving a difference of 0.57 to come from processes which are not affected by changes in the neutralization reactions and which seem likely not to involve ionic intermediates.[46] This split leads to the estimates given in Table VI for the various sources of H_2.

Table VI: Estimates of the Source of the H_2 Yield from Pure Cyclohexane

	Molecular[a]	Atomic	Total
Ionic	3.01	0.89	3.90
Nonionic	1.20	0.57	1.77
Total	4.21	1.46	5.67

[a] Includes any H_2 produced by hot hydrogen atom abstraction of hydrogen from the solvent.

Appendix

Dependence of H_2 Yield on Dose. In the irradiation of hydrocarbons, the reduction in the H_2 yield which results from the buildup of olefin at the finite doses required for hydrogen measurements makes it difficult to determine the correct initial yield. This problem has been generally recognized and in many cases doses have been limited to levels where the expected effect is not great. Dyne and Stone,[47] for example, show that the hydrogen yield from cyclohexane is decreased by about 1 unit at a dose of ~10^7 rads but that at doses of several 100,000 rads it is not appreciably different from the apparent initial yield. The present work, however, points to small effects which because of the square root relationship between the depression of the yield of H_2 and olefin concentration (eq III) can still be present at doses ~10^5 rads where the levels of radiolysis products are 10^{-4} to 10^{-3} *M*. This fact makes determination of $G(H_2)_0$ from "initial" slopes difficult. A better approach would seem to involve an estimation of the correction to the observed yields for the depression due to ionic reactions and for scavenging of the hydrogen atoms by the products of the radiolysis. In cyclohexane, for example, cyclohexene initially builds up with a *G* of 3.27.[47] At a dose of 100,000 rads this corresponds to a terminal concentration of 2.7×10^{-4} *M*. At this level the depression due to ionic reactions is expected to be directly proportional to the square root

(45) The hydrogen atom yield should be considerably lower at comparable concentrations of electron scavengers; for example, with the parameters given here according to eq IV for 0.1 *M* CH_3Br $G(H)$ will be reduced to 0.95.

(46) The upper limit to the number of hydrogen atoms which can come from ion neutralization is 35% of 3.9 or 1.36. This would occur if $f(C_2H_5)_{sec}$ were 0 and $f(H)_{neut} = 0.35$. Under this assumption the data indicate $G(H)_0$ to be 1.67. By difference the minimum yield of hydrogen atoms which can come from nonionic processes is 0.31 (and the maximum if 1.01 as indicated in the text). At least some hydrogen atoms must come from a nonionic source and the intermediate values indicated in Table VI seem very reasonable.

(47) P. J. Dyne and J. A. Stone, *Can. J. Chem.*, **39**, 2381 (1961).

Table VII: Estimated Corrections for Dose Dependence of the Hydrogen Yield from Cyclohexane

Dose, rads	Correction for ionic reaction	Correction[a] for H atom addition	Total estimated depression	$G(H_2)_{obs}$[b]	$G(H_2)_0$[c]
10,000	0.016	0.0004	0.01	...	...
30,000	0.029	0.0012	0.03	...	...
100,000	0.050	0.004	0.05	5.50	5.55
300,000	0.087	0.012	0.10	5.45	5.55
1,000,000	0.16	0.041	0.20	5.32	5.52
3,000,000	0.25	0.12	0.37	5.13	5.50
10,000,000	0.49	0.27	0.76	4.80	5.56

[a] k_2/k_1 is assumed to be 0.005. [b] From the data of Dyne and Stone, *Can. J. Chem.*, **39**, 2381 (1961). [c] From the sum of columns 4 and 5. The yields reported by Dyne and Stone are about 2% lower than those given in the present study.

of the dose and that due to hydrogen atom addition reactions to be directly proportional to the dose. Averaged over the experiment, the first correction is given by $^2/_3(3.8)\epsilon\sqrt{\alpha[\text{olefin}]_f}$, where $[\text{olefin}]_f$ is the olefin concentration at the end of the irradiation and α is the appropriate parameter for the olefin. Similarly, the correction for H atom addition to the olefin is approximately given by $[\text{olefin}]_f \cdot G(H)_0/(2k_2/k_1[RH])$. In cyclohexane $\alpha[\text{olefin}]_f$ for the cyclohexene produced is estimated as 3.9×10^{-9} per rad from the latter's competitive effect on the cyclopropane reaction.[34] The corrections estimated for various dose levels are given in Table VII and added to the yields reported by Dyne and Stone[47] to correct their values to zero dose. This sum can be compared to their reported initial yield of 5.55. From the constancy of the values in the final column the form for the total correction seems to be good and the values of the corrections reasonable at doses $\sim 10^6$ rads. At lower doses the corrections should be quite accurate.

Two comments should be made on the dose effect. First, the depression of hydrogen production by interference with the ionic reactions appears to be more important than effects involving H atom scavenging. From this it follows that dose effects should be much less important in solutions containing ion scavengers than for the pure solvent. Secondly, the interpretation of $G(H_2)_0$ is ambiguous to the extent that the "free ions" are a potential source of hydrogen which is not realizable in any real experiment.

Kinetics of the Dimerization of the $C_6H_6^+$ Ion in Gaseous Benzene[1]

by S. Wexler and L. G. Pobo

Chemistry Division, Argonne National Laboratory, Argonne, Illinois 60439 *(Received June 27, 1969)*

A kinetic study of the reaction of the $C_6H_6^+$ ion in gaseous benzene to form $C_{12}H_{12}^+$ has been made by the technique of high-pressure mass spectrometry. Within the range of source conditions studied, the dimeric species is formed by an over-all fourth-order process, third order in benzene concentration and first order in primary $C_6H_6^+$ abundance. A negative activation energy of approximately 10 kcal/mol has been measured for the over-all sequence of reactions leading to the dimer. These observations support a proposed mechanism of three consecutive ionic reactions for the formation of the $C_{12}H_{12}^+$ ion: charge exchange between primary $C_6H_6^+$ and a benzene molecule, dimerization of the excited $C_6H_6^+$ secondary ion, and collisional stabilization of the $C_{12}H_{12}^+$ product.

A. Introduction

Within a recent short period of time, three publications have appeared describing almost simultaneous studies, with "high-pressure" mass spectrometers, of the dimerization of the $C_6H_6^+$ ion with a benzene molecule to form a $C_{12}H_{12}^+$ species.[2-4] There was agreement between Wexler and Clow and Giardini-Guidoni and Zocchi that dimerization of the $C_6H_6^+$ ion was a prominent and efficient ionic reaction in gaseous benzene, and consequently this process was of great importance in the radiation chemistry of gaseous and possibly liquid benzene. These conclusions were at variance with those of Field, Hamlet, and Libby, who found in their

(1) Based on work performed under the auspices of the U. S. Atomic Energy Commission.

(2) F. H. Field, P. Hamlet, and W. F. Libby, *J. Amer. Chem. Soc.*, **89**, 6035 (1967).

(3) S. Wexler and R. P. Clow, *ibid.*, **90**, 3940 (1968).

(4) A. Giardini-Guidoni and F. Zocchi, *Trans. Faraday Soc.*, **64**, 2342 (1968).

mass spectrometer only low and pressure-independent yields of $C_{12}H_{12}^+$ in benzene. Although a plausible explanation of the cause of the difference could not be offered in our original paper,[3] it has since occurred to us that perhaps the temperatures of the gases in the source chambers of the respective instruments may have been quite different, and if the stability of the dimeric ion were very temperature sensitive, great fluctuations in the yield of this species might be expected. The source temperature in our experiment was measured as 122 ± 2°, and the ion source of Giardini-Guidoni and Zocchi was presumably at room temperature (~23°). Though the temperature in the spectrometer used by Field, *et al.*, was given as 210°, a later publication[5] of results with the same source gave 236° for this parameter.

Obviously, a detailed kinetic study of the ionic dimerization in benzene is required to resolve the discrepancy, and such an investigation is reported in this paper. Moreover, it is desirable to study this phenomenon in greater detail, because dimerization appears to be a general characteristic of the ions of aromatic molecules,[6] and as a consequence the process should be of great importance in the radiolysis of these compounds. The idea for this type of study has apparently occurred simultaneously to Field, Hamlet, and Libby[5,7] and to Tiernan and Bhattacharya[8] in addition to us, and a comparison of the observations of these related but not identical mass spectrometric investigations is certainly worthwhile.

B. Experimental Section

A detailed description of the proton-beam high-pressure mass spectrometer, in which the primary ionization is provoked by a well collimated beam of 2-MeV protons from a Van de Graaff electrostatic generator, and of the novel source chamber that is heated by circulating mineral oil has been given in earlier communications from this laboratory.[6,9] Zone-refined benzene of very high purity (99.999%; James Hinton Co., Valparaiso, Fla.) was used without further purification but after thorough outgassing.

The yields of the $C_6H_6^+$ ion and its dimer $C_{12}H_{12}^+$ were measured in benzene vapor at several pressures in the range from 0.025 to 1.00 Torr, at several temperatures in the range from 22 to 96°, and at several repeller field strengths from 10.8 to 54.0 V/cm. All the data have been corrected for naturally occurring C^{13}.

C. Results and Discussion

1. Kinetic Order of Dependence of $C_{12}H_{12}^+/C_6H_6^+$ Abundance Ratio on Benzene Concentration. Graphs of ratios of $C_{12}H_{12}^+/C_6H_6^+$ abundances as functions of the pressure of benzene in the source chamber of our mass spectrometer are presented on log–log scales in Figures 1–5. Each figure contains the array of curves for a fixed repeller field, an individual curve

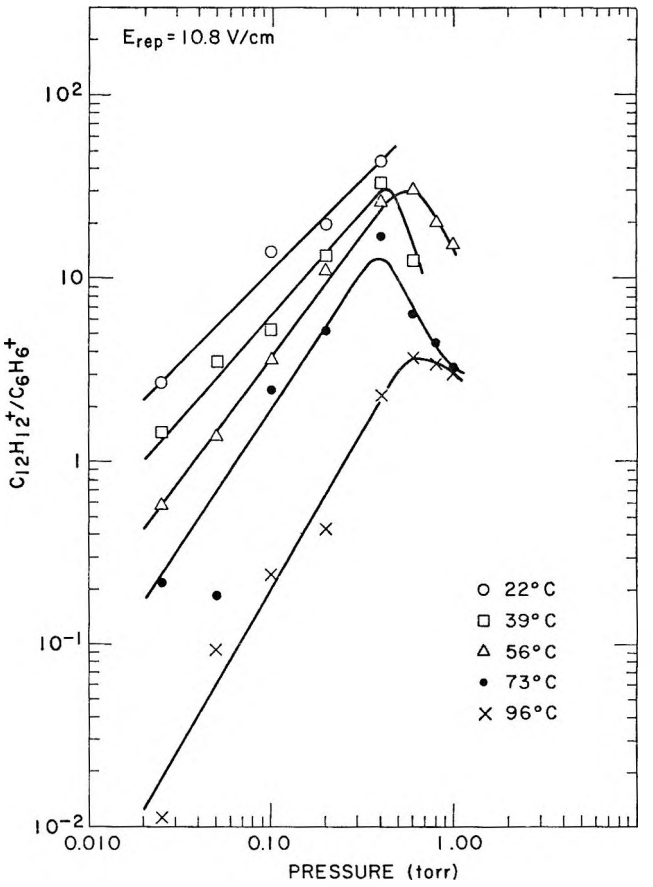

Figure 1. Dependence of $C_{12}H_{12}^+/C_6H_6^+$ abundance ratio on benzene pressure in the source chamber of the high-pressure mass spectrometer; E_{rep} = 10.8 V/cm.

representing the data for the indicated temperature. Study of the figures reveals that, in general, the curves remain linear over variations of the abundance ratios amounting to three to four orders of magnitude. The linearity usually extends from the lowest benzene pressure (0.025 Torr) up to approximately 0.40 Torr, before the ratio reaches a maximum and then often decreases. Note that for each repeller field the linear portions of the curves extend to progressively higher source pressures with rising temperature, and at 96° the curves are mostly straight even at 1.00 Torr. A comparison of the plots of data taken at the same temperature shows that often the linearity reaches to higher source pressures as the repeller field is increased. Thus, the

(5) F. H. Field, P. Hamlet, and W. F. Libby, *J. Amer. Chem. Soc.*, 91, 2839 (1969).

(6) S. Wexler and L. G. Pobo, *ibid.*, 91, 7233 (1969).

(7) F. H. Field, P. Hamlet, and W. F. Libby, Abstracts, 157th National Meeting, of the American Chemical Society Minneapolis, Minn., April 13–18, 1969.

(8) T. O. Tiernan and A. K. Bhattacharya, Abstracts, 157th National Meeting, of the American Chemical Society Minneapolis, Minn., April 13–18, 1969.

(9) S. Wexler, A. Lifshitz, and A. Quattrochi in "Ion-Molecule Reactions in the Gas Phase," P. Ausloos, Ed., Advances in Chemistry Series, No. 58, American Chemical Society, Washington, D. C., 1966, p 193.

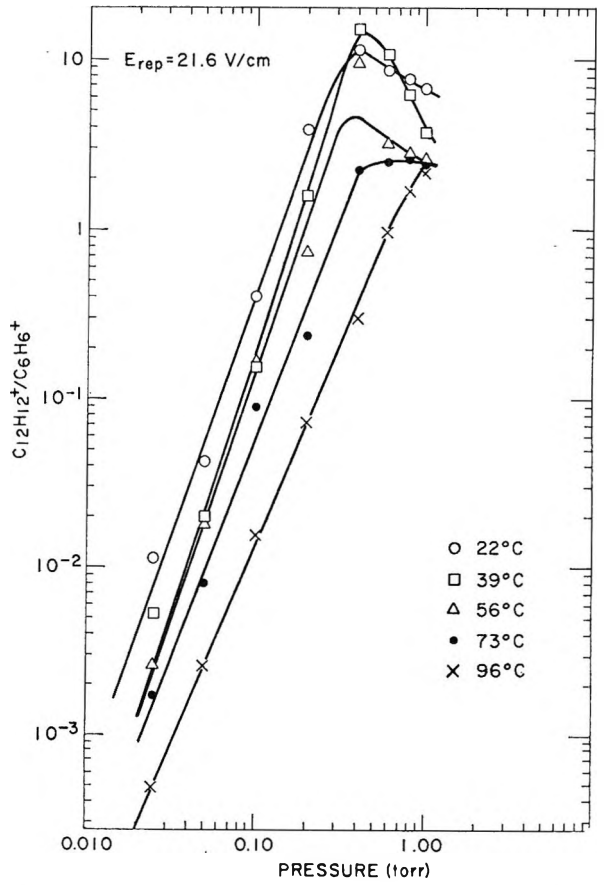

Figure 2. Dependence of $C_{12}H_{12}^+/C_6H_6^+$ abundance ratio on benzene pressure in the source chamber of the high-pressure mass spectrometer; E_{rep} = 21.6 V/cm.

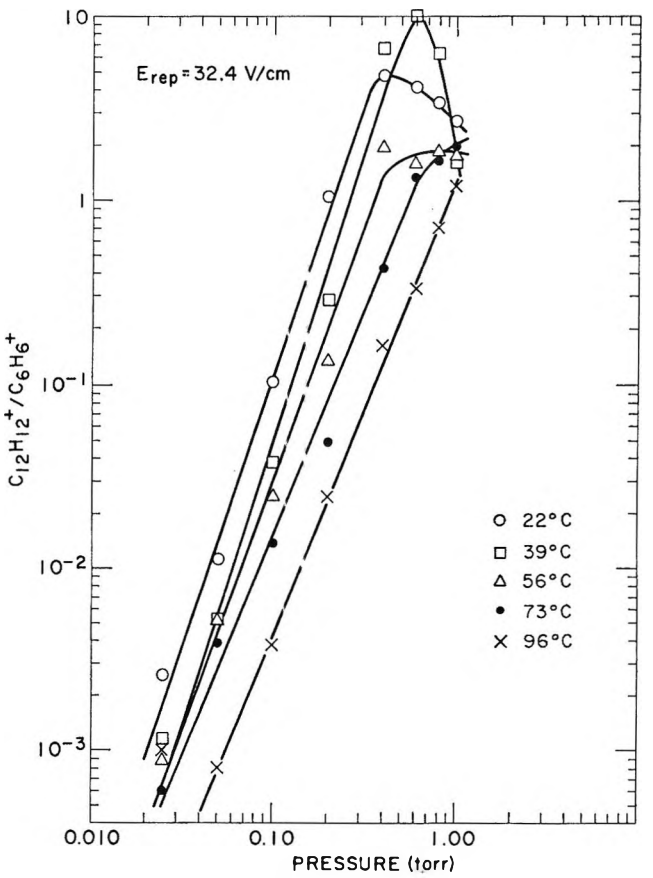

Figure 3. Dependence of $C_{12}H_{12}^+/C_6H_6^+$ abundance ratio on benzene pressure in the source chamber of the high-pressure mass spectrometer; E_{rep} = 32.4 V/cm.

plots are still linear at 1.00 Torr when the field strengths are equal to or greater than 43.2 V/cm and the temperature is 73°, but exceptions to this behavior are observed (*e.g.*, the contrary behavior of the curves for 43.2 and 54.0 V/cm at 56°).

From the slope of the linear portion of each curve the kinetic order dependence of the ionic ratio on benzene concentration may be determined. These are collected in Table I. Though the slopes of the log–log plots increase from 1.0 to 1.7 as the source temperature is raised when the repeller field is 10.8 V/cm, the dependence of the intensity ratio on benzene concentration becomes invariant with both field strength and temperature at and above 21.6 V/cm. The kinetic order determined for the latter field strengths is 2.8 ± 0.2.

The third-order dependence of the ionic ratio on gas concentration may be accounted for by the following mechanism for the dimerization

$$(C_6H_6^+)^{\ddagger} + C_6H_6 \xrightarrow{k_1} (C_6H_6^+)^* + C_6H_6^* \quad (1)$$

$$(C_6H_6^+)^* + C_6H_6 \underset{k_{-2}}{\overset{k_2}{\rightleftharpoons}} (C_{12}H_{12}^+)^* \quad (2)$$

$$(C_{12}H_{12}^+)^* + C_6H_6 \xrightarrow{k_3} C_{12}H_{12}^+ + C_6H_6^* \quad (3)$$

The ionic parent species $(C_6H_6^+)^{\ddagger}$ produced by proton ionization is considered to exchange charge with a benzene molecule to give a $(C_6H_6^+)^*$ ion in a lower state of excitation and/or lower kinetic energy than the primary ion, and the former then condenses with another benzene to give the excited dimer $(C_{12}H_{12}^+)^*$. The dimer may either dissociate to the monomer or be stabilized by collision with a third benzene molecule. Strong evidence that the charge exchange of the first step (eq 1) is a prominent reaction in benzene vapor has already been presented by several workers,[2-4,8] but the mechanismt hen presupposes a preequilibrium (reaction 2) followed by a rate-determining step (reaction 3). For such a sequence of events, one may show that

Table I: Kinetic Order Dependence of $C_{12}H_{12}^+/C_6H_6^+$ Yield Ratio on Benzene Concentration

Source temp., °C	Repeller field strength, V/cm				
	10.8	21.3	32.4	43.2	54.0
22	1.0	2.9	3.0	2.6	2.8
39	1.2	3.1	3.1	3.1	3.1
56	1.3	2.9	2.8	2.5	2.5
73	1.5	2.7	2.5	2.7	2.9
96	1.7	2.4	2.5	2.7	2.8

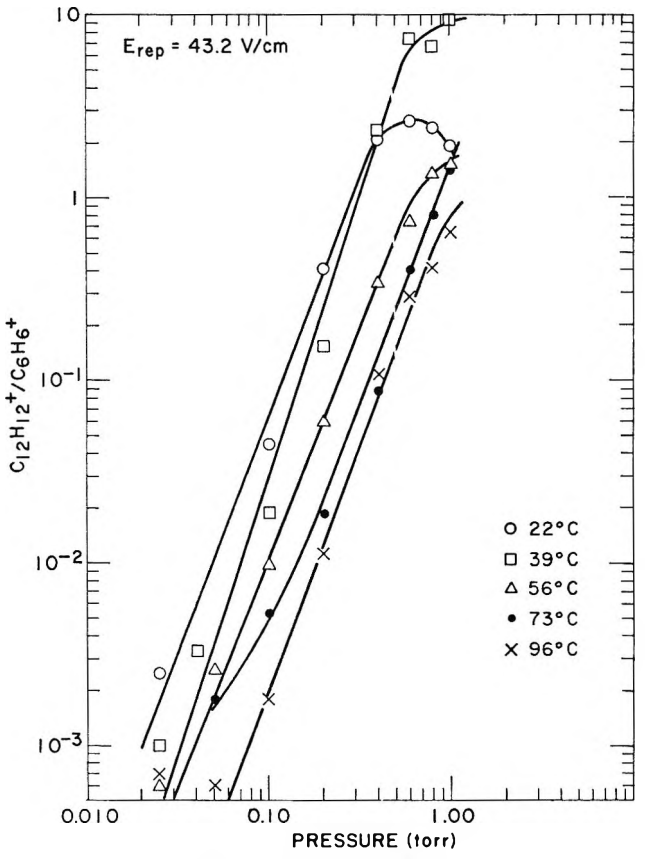

Figure 4. Dependence of $C_{12}H_{12}^+/C_6H_6^+$ abundance ratio on benzene pressure in the source chamber of the high-pressure mass spectrometer; E_{rep} = 43.2 V/cm.

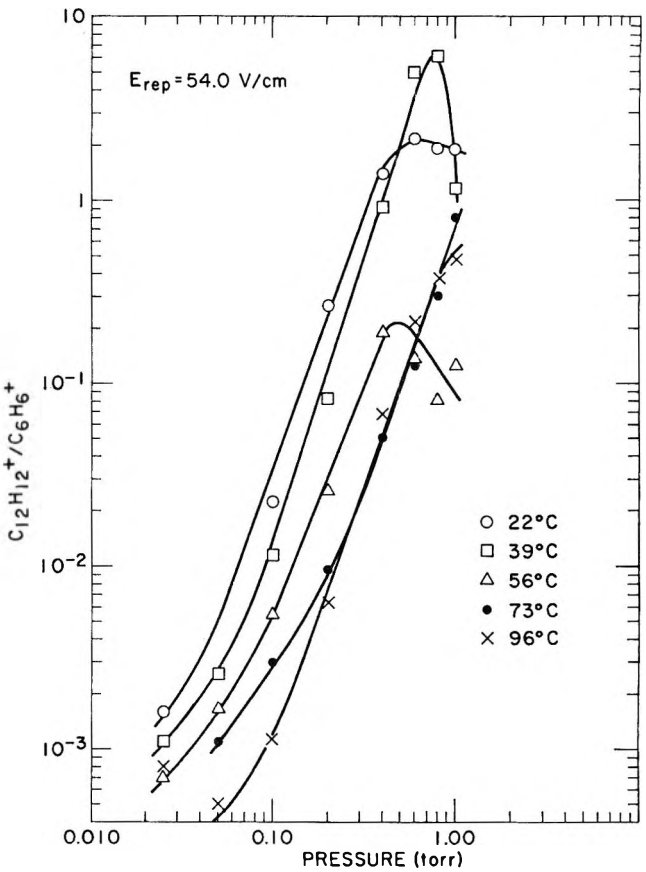

Figure 5. Dependence of $C_{12}H_{12}^+/C_6H_6^+$ abundance ratio on benzene pressure in the source chamber of the high-pressure mass spectrometer; E_{rep} = 54.0 V/cm.

the dimer ion current $I(C_{12}H_{12}^+)$ should be approximately given by

$$I(C_{12}H_{12}^+) \approx \frac{k_1k_2k_3I(C_6H_6^+)^{\mp}(C_6H_6)^3t^2}{2(k_{-2} + k_3(C_6H_6))} \quad (4)$$

This equation is derived when one begins with the appropriate rate equations for reactions 3 and 2

$$\frac{d(C_{12}H_{12}^+)}{dt} = k_3(C_{12}H_{12}^+)^*(C_6H_6) \quad (5)$$

and

$$\frac{d(C_{12}H_{12}^+)^*}{dt} = 0 = k_2(C_6H_6^+)^*(C_6H_6) - k_{-2}(C_{12}H_{12}^+)^* - k_3(C_{12}H_{12}^+)^*(C_6H_6) \quad (6)$$

Combination of eq 5 and 6 gives

$$\frac{d(C_{12}H_{12}^+)}{dt} = \frac{k_2k_3(C_6H_6^+)^*(C_6H_6)^2}{k_{-2} + k_3(C_6H_6)} \quad (7)$$

If we now make the reasonable assumption that the rate of charge exchange is faster than the rate of dimerization

$$\frac{d(C_6H_6^+)^*}{dt} \approx k_1(C_6H_6^+)^{\mp}(C_6H_6) \quad (8)$$

and thus taking the average concentration of primary ions

$$\frac{d(C_{12}H_{12}^+)}{dt} \approx \frac{k_1k_2k_3\overline{(C_6H_6^+)^{\mp}}(C_6H_6)^3t}{k_{-2} + k_3(C_6H_6)} \quad (9)$$

where t is the drift time for an ion from the plane of ionization in the source chamber (the position of the proton beam) to the exit slit. Integration gives the approximate expression

$$(C_{12}H_{12}^+) \approx \frac{k_1k_2k_3\overline{(C_6H_6^+)^{\mp}}(C_6H_6)^3t^2}{2(k_{-2} + k_3(C_6H_6))} \quad (10)$$

Under the conditions of the experiment, $I(C_{12}H_{12}^+)$ is proportional to the integrated concentration of dimer, while $I(C_6H_6^+)^{\mp}$ is proportional to the average concentration of primary ions. Equation 4 then follows directly.

Since $k_{-2} \gg k_3(C_6H_6)$ and $K_2 = k_2/k_{-2}$

$$\frac{I(C_{12}H_{12}^+)}{I(C_6H_6^+)^{\mp}} \approx k_1K_2k_3(C_6H_6)^3t^2 \simeq k_{app}(C_6H_6)^3t^2 \quad (11)$$

where the k's are the respective rate constants for the reactions cited above and K_2 is the equilibrium constant for the formation of the excited intermediate bimolecular complex.

Note that the mechanism and rate equations proposed take into account the steady-state conditions in the source chamber, where gradients of ion concentrations exist between the plane of primary ionization and the ion exit. It should also be noted that we have assumed that the intensities of the transients $(C_6H_6^+)^*$ and $(C_{12}H_{12}^+)^*$ actually measured at the detector of the mass spectrometer will be small relative to the intensities of the primary and collision stabilized product species, respectively. It is probable that these excited ionic species will dissociate in flight after leaving the ion source and they therefore will not be detected.

2. *Effect of Temperature on Dimer Formation.* Another outstanding feature of the data presented in Figures 1–5 is the very strong inverse effect of increasing temperature on the ratio of $C_{12}H_{12}^+$ to $C_6H_6^+$ abundances. Note that for fixed repeller field and benzene pressure the ratio may decrease more than a factor of 100 when the temperature is raised from 22 to 96°. Arrhenius plots of the data were made on the basis of the rate expression given in eq 11. In calculating benzene concentrations from the pressure measurements the corresponding source temperature was taken into account. Although the data from most of the experiments gave linear plots over the range of temperatures investigated, several of the curves tended to have a concave downward curvature. An illustrative curve for each form of behavior is shown in Figures 6a and b, respectively. All the curves of log k_{app} *vs.* $1/T$ (T = absolute temperature), it should be noted, exhibited a positive slope, indicating that the over-all process of forming the dimer $C_{12}H_{12}^+$ ion possessed a "negative" activation energy. The values of the apparent activation energies determined from the slopes of these curves are assembled in Table II. One sees that the data are in reasonable agreement in the pressure range from 0.10 to 0.60 Torr and that they suggest that the apparent activation energy for the chain of ionic reactions is approximately −10 kcal/mol. Lower values were measured under conditions of lower pressure and higher field strengths, and at higher pressures. Quite probably, the mechanism of the dimerization is then altered from that of eq 1–3. When the pressure is too low and the field strength too high, equilibrium (eq 2) may not be established, and when the benzene concentration is too high, side reactions may alter the observed temperature characteristics of the dimerization. An indication that equilibrium is being approached is the extended linearity of the log ratio–log pressure curves (Figures 1–5) as the temperature is raised. As the temperature of the gas increases, the preequilibrium of eq 2 is facilitated and thus becomes more influential in the mechanism. Curvature of the Arrhenius plots, which often occurs for the data collected under the extreme conditions (see Table II), is further evidence that other reactions may then be complicating the mechanism proposed for the formation of $C_{12}H_{12}^+$.

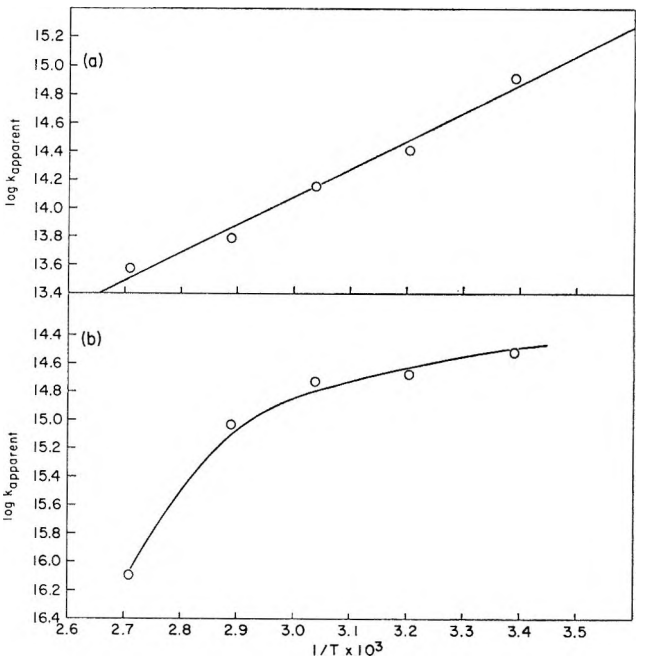

Figure 6. Representative log k_{app} *vs.* $1/T$ plots of data from studies of effect of temperature on formation of dimeric $C_{12}H_{12}^+$ species in gaseous benzene: a, a normal linear Arrhenius plot with negative activation energy, the data taken from an experiment with a repeller field strength of 32.4 V/cm and a benzene pressure of 0.20 Torr; b, an illustrative curve showing the curvature in an Arrhenius plot of data taken under extreme conditions of field and/or pressure (the data are for 10.8 V/cm and 0.20 Torr).

Table II: Apparent Activation Energy[a] for Formation of $C_{12}H_{12}^+$ in Gaseous Benzene

Benzene pressure, Torr	Repeller field strength, V/cm				
	10.8	21.6	32.4	43.2	54.0
0.025	−9.4	−8.2	−4.1	*b*	−2.7
0.050	−15.1	−8.8	*b*	*b*	−4.5
0.10	*b*	−10.5	−7.7	−7.5	−6.3
0.20	*b*	−10.8	−9.0	−9.3	−11.3
0.40	*b*	−10.0	−10.0	−10.1	−10.0
0.60	*b*	−7.3	−6.2	*b*	*b*
0.80		−4.1	−4.3	*b*	*b*
1.00		−2.7	−0.6	*b*	−2.3

[a] Units of kilocalories per mole. [b] Curve exhibits too great a curvature for accurate estimation of its slope.

The formulation of the mode of reaction cited above (eq 1–3) accounts for the negative activation energy found for the dimerization. Since the apparent rate constant for the sequence of ionic reactions is the product of two bimolecular rate constants and an equilibrium constant ($k_{app} = k_1K_2k_3$), the apparent energy of activation E_{app} may be shown to be the sum of the activation energies for reactions 1 and 3 and the heat of reaction 2

$$E_{app} = E_1 + \Delta H_2 + E_3 \qquad (12)$$

The associative equilibrium step will be exothermic, making ΔH_2 negative while reactions 1 and 3 should have positive activation energies. If $\Delta H_2 > E_1 + E_2$, a condition likely to exist in these sequential reactions, the apparent energy of activation should be observed to be negative. It is of interest to recall that, similarly, negative activation energies have been observed for a large number of termolecular reactions. These include the recombination of halogen atoms[10-13] and the reactions of nitric oxide with O_2[14] and with halogen molecules.[15] In all these neutral–neutral reactions a preequilibrium was followed by a rate-determining step, the mechanism considered to apply being analogous to the sequence proposed in eq 1–3.

The apparent activation energy measured in our experiments, *ca.* −10 kcal/mol, should be the lower limit of the binding energy of the $C_{12}H_{12}^+$ dimer ion, and it would be the true value if the activation energies for charge exchange (eq 1) and collisional stabilization (eq 3) were zero. Our value is somewhat lower than the 15 kcal/mol reported by Field, Hamlet, and Libby[5,7] for the association energy of this dimer. They claimed that under the conditions of their high pressure–mass spectrometric studies only the equilibrium conditions of eq 2 prevailed in their source chamber above 0.10 Torr pressure, since their $K_2 = (C_{12}H_{12}^+)/(C_6H_6^+)(C_6H_6)$ then remained constant. Our experience, on the contrary, was that equilibrium, as defined by constancy of the above relation, was not the prevailing condition in the present experiments. Values of K_2 calculated varied by as much as two orders of magnitude over the range of benzene concentrations used in our work. Further, the third-order dependence of the $(C_{12}H_{12}^+)/(C_6H_6^+)$ abundance ratio (Table I) would preclude the occurrence of a simple equilibrium in these studies.

The kinetic order of 3 for the dependence of the dimer to monomer ion ratio on C_6H_6 concentration leads to the conclusion that $C_{12}H_{12}^+$ is formed by an over-all fourth-order process, third order in benzene concentration and first order in primary $C_6H_6^+$ ion abundance. This is one higher than that concluded by Tiernan and Bhattacharya,[8] who proposed that $C_{12}H_{12}^+$ is formed by either reactions 1 and 2 or reactions 2 and 3. But since they found from their experiments with a tandem mass spectrometer that excited $C_6H_6^+$ produced by charge exchange between primary $C_6H_6^+$ ions and benzene molecules is the principal reactant that gives the $C_{12}H_{12}^+$ species, charge exchange followed by dimerization must have been the mode of reaction in their high-pressure experiments. This is in agreement with the mechanism proposed by us, but the higher kinetic order and negative activation energy measured in this study would require a rate-determining step that follows the preequilibria of reaction 2. Collisional stabilization of the excited $C_{12}H_{12}^+$ product is a plausible reaction, for such reactions are quite common in consecutive ion–molecule reactions.[9] However, it is of interest to note that lower kinetic orders are observed (Table I) at the lowest field strength (10.8 V/cm) and that the order appears to be approaching 2 as the temperature of the source is raised. These data appear to be in agreement with the results of Tiernan and Bhattacharya, whose order determination was made at a field strength of 10 V/cm and a temperature of about 200°. It is reasonable to conclude that the efficient conversion of reactant ion translational energy into internal energy of the ion–neutral complex would make the dimer ion more energetic and thus would require that it undergo an additional collisional stabilization to be observed at our higher field strengths.

Acknowledgment. The authors wish to thank Dr. J. C. Sullivan for informative discussions on the theoretical aspects of this kinetic study.

(10) E. Rabinowitch and W. C. Wood, *J. Chem. Phys.*, **4**, 497 (1936).

(11) D. Britton and N. Davidson, *ibid.*, **25**, 810 (1956).

(12) R. Marshall and N. Davidson, *ibid.*, **21**, 659 (1953).

(13) D. L. Bunker and N. Davidson, *J. Amer. Chem. Soc.*, **80**, 5085 (1958).

(14) M. Bodenstein and I. Ramstetter, *Z. Phys. Chem.* (Leipzig), **100**, 106 (1922); M. Bodenstein, *Helv. Chim. Acta*, **18**, 743 (1935).

(15) M. Trautz and V. P. Dalal, *Z. Anorg. Allg. Chem.*, **102**, 149 (1918).

Kinetics of the Reaction $NO_2 + CO \rightarrow NO + CO_2$. Single-Pulse Shock Tube Studies[1a]

by Alexander Burcat and Assa Lifshitz

Department of Inorganic Chemistry, The Hebrew University of Jerusalem, Jerusalem, Israel (*Received May 28, 1969*)

The kinetics of the homogeneous reaction $NO_2 + CO \rightarrow NO + CO_2$ was studied in a single-pulse shock tube over the temperature range 1050–1500°K. Six reaction mixtures, covering the range of 0.743–4.55% NO_2 and 1.25–5.0% CO in argon were used. Product analysis was carried out by vapor phase chromatography. The following rate law was found compatible with the experimental results

$$\text{rate} = k_b[NO_2]^{0.77}[CO]^{1.13}[Ar]^{0.1}$$

where $k_b = 10^{12.1} \exp[-27{,}600/RT]$ cc mol^{-1} sec^{-1}. This value falls slightly above the extrapolated Arrhenius curves of three low-temperature studies. The reaction is assumed to proceed *via* a three-center atomic displacement mechanism.

I. Introduction

The reaction $NO_2 + CO \rightarrow CO_2 + NO$ is a typical atom transfer reaction in which both the reactants and products are stable molecules. Its kinetics can be studied in a shock tube without the need for microsecond resolution techniques. The reaction was studied by conventional techniques by three groups of investigators,[1b-3] covering the temperature ranges 448–563°K,[1b] 540–727°K,[2] and 666–746°K.[3] In one study[2] the carbon-13 isotope effect was reported.

There were two reasons why it was found desirable to extend the kinetic study of this reaction to the shock-tube region. This elementary reaction is expected to obey an Arrhenius type temperature dependence. As the high temperatures prevail in the single pulse shock tube, the dwell times available are of the order of a millisecond. Bimolecular rate constants higher by many orders of magnitude than those obtained at the low-temperature range are therefore expected. A comparison of the low- and high-temperature rate constants by a long Arrhenius plot may provide a check for the reliability of the data obtained by the single-pulse shock-tube technique and at the same time verify the validity of the Arrhenius temperature dependence over a wide temperature range. This type of plot has been so far reported only for unimolecular reactions.[4,5]

Another reason for performing this study is related to the effect of the argon diluent on the reaction rate, observed in a number of bimolecular exchange reactions which were studied in the single-pulse shock tube at high dilution in argon.[6-10] When the rate of exchange was expressed in terms of a power rate law, it was necessary to incorporate the argon concentration in the power rate expression. In terms of a reaction order, the order with respect to argon varied between 0.4 and 1.0 depending on the particular reaction studied.[6,8]

The mechanism which attempted to account for these observations assumed the reactions to occur in two steps. The first one is the vibrational excitation of one of the molecules to a high, critical vibrational state, and the second step is the chemical change. In diatomic molecules such as N_2 and D_2 where the efficiency of translation vibration energy exchange is low, the vibrational excitation step is not necessarily a fast step. Since argon was the main constituent in these studies, its incorporation in the rate equation was attributed to its function in exciting the reacting molecules in a step slower than the chemical change.

In the $CO + NO_2 \rightarrow CO_2 + NO$ reaction it is expected that in order to transfer an oxygen atom to CO, the NO_2 molecule must be preexcited to high vibrational states before it can react. Since as a triatomic molecule the vibrational relaxation time of NO_2 is extremely short,[11] the excitation step is expected to be very fast compared to the atom displacement step. There should be no effect of argon on the reaction rate

(1) (a) In partial fulfillment of the requirements for a Ph.D. thesis, submitted to the Senate of the Hebrew University by A. Burcat. (b) R. H. Crist and F. B. Brown, *J. Chem. Phys.*, **9**, 840 (1941).

(2) H. S. Johnston, W. A. Bonner, and D. J. Wilson, *ibid.*, **26**, 1002 (1957).

(3) J. H. Thomas and G. R. Woodman, *Trans. Faraday Soc.*, **63**, 2728 (1967).

(4) W. Tsang, *J. Chem. Phys.*, **41**, 2487, (1964), and related papers.

(5) A. Lifshitz, S. H. Bauer and E. L. Resler, Jr., *ibid.*, **38**, 2056 (1963); A. Lifshitz, H. F. Carroll, and S. H. Bauer, *ibid.*, **39**, 1661 (1963).

(6) A. Bar-Nun and A. Lifshitz, *ibid.*, **47**, 2878, (1967).

(7) A. Bar-Nun and A. Lifshitz, *ibid.*, **51**, 1826 (1969).

(8) A. Burcat, A. Lifshitz, D. Lewis, and S. H. Bauer, *ibid.*, **49**, 1449, (1969).

(9) A. Burcat and A. Lifshitz *ibid.*, **47**, 3079, (1967).

(10) D. Lewis and S. H. Bauer, *J. Amer. Chem. Soc.*, **90**, 5390, (1968).

(11) S. H. Bauer and M. R. Gustavson, *Discussions Faraday Soc.*, **17**, 69 (1954).

according to the suggested "vibrational excitation mechanism." One of the purposes in studying this reaction is to check the effect of argon on the reaction rate.

II. Experimental Section

A. Apparatus and Technique. The reaction was studied in a 2-in. id single-pulse shock tube. The driven section was 13 ft long, made of double tough Pyrex tubing. The driver was 9 ft long, and its length could be varied in small steps in order to achieve the best tuning conditions. The shock tube and its operation have already been described in detail in earlier publications.[5,6] Before each shock, the tube was pumped down to better than 10^{-4} Torr and had a leak (or degassing) rate of $\sim 1\mu$/min. Incident shock speeds were recorded in order to evaluate the reflected shock temperatures. These could be determined with $\sim \pm 0.7\%$ accuracy, which corresponded to $\sim \pm 25°$K in the reflected shock temperature.

Dwell times could be read from the pressure records to within $\pm 10\%$. These were later corrected (increased) by space averaging and by accounting for the contribution to chemical reaction from the cooling phase. These corrections are similar to the ones already discussed in detail in an earlier publication.[5]

B. Materials and Preparation of the Reaction Mixtures. The materials used in this study were from the Matheson Gas Co. The CO and NO_2 (N_2O_4) were listed as 99.5% pure and the argon as 99.998% pure. Driver gas used was pure grade helium.

The preparation of the reaction mixtures involves some difficulty owing to the $N_2O_4 \rightleftharpoons 2NO_2$ equilibrium. In order to prepare a reaction mixture sufficient for a considerable number of shocks, the partial pressure of the nitrogen dioxide in the argon must be of the order of one-third of an atmosphere. At that pressures the equilibrium quantities of N_2O_4 and NO_2 in the gas are comparable. We have calculated these two quantities from the $NO_2(N_2O_4)$ partial pressure in the storage cylinder and the known equilibrium constant of the reaction at the particular room temperature. We assumed no effect of the total argon density on the degree of dissociation of N_2O_4. When running the shock, the partial pressure of the nitrogen dioxide in the shock tube was never higher than a few Torr. At that pressure close to 100% of the gas is present as NO_2. Since the $N_2O_4 \rightleftharpoons 2NO_2$ equilibrium is reached very rapidly, by the time the reaction mixture is transfered to the shock tube the new equilibrium is reached.

In the following six reaction mixtures prepared, the listed percentage is that of a pure NO_2 gas containing no N_2O_4

$$2.97\%\ NO_2 + 5\%\ CO \quad (1)$$

$$0.473\%\ NO_2 + 1.25\%\ CO \quad (2)$$

$$4.55\%\ NO_2 + 5.1\%\ CO \quad (3)$$

$$1.14\%\ NO_2 + 1.28\%\ CO \quad (4)$$

$$1\%\ NO_2 + 4\%\ CO \quad (5)$$

$$1\%\ NO_2 + 1\%\ CO \quad (6)$$

All mixtures were diluted in argon. Mixture 2 was prepared by a fourfold dilution of mixture 1, and 4 by a fourfold dilution of 3.

This was done in order to obtain an exact 4:1 ratios independent of any $2NO_2 \rightleftharpoons N_2O_4$ equilibrium calculations. Mixtures 5 and 6 were prepared at the same time to ensure exactly the same percentage of nitrogen dioxide in both. The storage stainless steel cylinders were seasoned with NO_2 for a few days before being pumped down to a high vacuum.

C. Analysis. Shocked samples were taken from the end block of the driven section and were injected to a Perkin-Elmer 820 gas chromatograph. The NO_2 peak was very unreproducible and therefore only the CO_2 peak was recorded for the purpose of analysis. The concentration of the CO_2 in the gas was calculated from the area under its peak together with the known quantity of gas injected into the gas chromatograph. To avoid errors resulting from possible variation in the sensitivity of the machine during the day, a sample containing a known percentage of CO_2 in argon ($\sim 0.1\%$) was analyzed after each analysis of a shocked sample. The "calibration analysis" was run at exactly the same pressure as that of the shocked sample. The concentration of the CO_2 due to the chemical reaction was always calculated relative to the calibration sample. We have found this method of analysis very satisfactory. The column used for these analyses was 2-m silica gel column, run at 50°.

Since only one component was analyzed, it was necessary to ensure that there was no mixing of the shocked gas with the driver helium. This might cause a decrease in the CO_2 concentration. To check this phenomenon, we have shocked samples of 0.1% CO_2 in argon, simulating the conditions under which the actual shocks were run. There was no difference in the CO_2 concentration between shocked and unshocked samples, indicating that no mixing took place in the region from which the samples were taken.

Another source of error which needed checking is the possible absorption of NO_2 on the metal parts of the driven section. A calibration curve of OD *vs* NO_2-(N_2O_4) pressure in the mm region was prepared with a Cary 14 spectrophotometer around 4000 Å. The reaction mixture after "sitting" in the shock tube for a few minutes was analyzed in the Cary. Within the limits of experimental error the OD at 4000 Å of the reaction mixture was identical with its value on the calibration curve, indicating that no absorption of the NO_2 took place.

III. Temperature Calculations

The reflected shock temperature was calculated from

Table I: Summary of the Experimental Conditions of the Nine Groups of Shocks

Series	No. of shocks	Composition % NO_2	Composition % CO	Composition % Ar	p_1, mm	T_5, °K
1(A)	11	2.97	5.0	92.03	66	1095–1300
1(B)	11	0.743	1.25	98.01	270	1137–1304
1(C)	10	4.55	5.1	90.35	39	1080–1262
1(D)	17	1.137	1.28	97.59	158	1115–1342
2(A)	16	4.55	5.1	90.35	38	1075–1585
2(B)	10	4.55	5.1	90.35	227	1008–1215
2(C)	8	2.97	5.0	92.03	265	1103–1287
3(A)	17	1.0	4.0	95.	120	1070–1255
3(B)	13	1.0	1.0	98.	120	1095–1262

Table II: Five Representative Shocks of Each Group

Series	Shock no.	Composition % NO_2	Composition % CO	Composition % Ar	P_1, Torr	T_5, °K	$C_5 \times 10^6$ mol cc^{-1}	Dwell time, msec	$\frac{[CO_2]}{[NO_2]_0} \times 10^2$	Rate $\times 10^6$ mol cc^{-1} sec^{-1}	$k_b \times 10^{-6}$ cc mol^{-1} sec^{-1}
1A	1	2.97	5	92.03	64	1172	1.86	2.27	8.9	19.49	21.14
	2				66	1107	1.85	2.27	5.9	11.95	13.19
	4				68	1190	1.99	2.27	10.7	25.55	24.20
	10				70	1100	1.96	2.27	4.2	8.23	8.06
	11				68	1199	2.00	2.27	10.3	24.59	23.01
1B	15	0.743	1.25	98.01	270	1141	6.97	2.14	5.7	11.30	11.26
	16				267	1148	6.91	2.14	7.4	15.36	15.55
	19				276	1175	7.26	2.14	10.0	22.81	20.94
	20				286	1170	7.51	2.14	9.7	22.77	19.54
	21				279	1140	7.18	2.14	8.5	18.59	17.46
1C	23	4.55	5.1	90.35	39	1277	1.22	1.75	7.6	21.20	38.64
	27				40	1141	1.16	2.14	3.4	5.89	11.85
	28				41	1084	1.15	2.14	2.6	3.96	8.19
	29				39	1092	1.10	2.14	2.5	3.41	7.70
	30				37	1113	1.05	2.14	3.0	4.45	10.85
1D	33	1.137	1.28	97.68	160	1282	4.51	1.75	8.8	23.03	39.20
	34				161	1162	4.26	2.14	4.4	7.64	14.63
	35				161	1218	4.39	2.14	7.1	14.22	25.60
	36				159	1116	4.09	2.14	3.6	5.72	11.89
	37				154	1157	4.05	2.14	4.8	8.10	17.09
2A	50	4.55	5.1	90.35	42	1077	1.17	2.08	1.6	2.09	4.11
	51				38	1106	1.08	2.08	1.6	1.97	4.56
	52				39	1124	1.12	2.08	1.9	2.74	5.90
	53				42	1109	1.20	2.08	1.8	2.60	4.90
	54				36	1176	1.07	2.08	3.6	6.51	15.38
2B	66	4.55	5.1	90.35	227	1007	6.00	2.27	2.7	22.75	1.71
	67				228	1082	6.34	2.21	6.2	70.85	4.78
	70				228	1147	6.53	2.21	10.9	138.17	8.80
	71				229	1113	6.45	2.21	8.4	102.59	6.68
	74				219	1149	6.27	2.21	10.9	131.92	9.10
2C	76	2.97	5	92.03	275	1225	8.28	2.01	26.1	318.46	17.45
	78				269	1119	7.49	2.08	13.5	138.26	9.26
	79				257	1211	7.42	2.08	25.4	268.50	18.32
	80				265	1164	7.50	2.08	20.9	220.29	14.74
	81				263	1180	7.48	2.08	22.3	235.35	15.80
3A	84	1	4	95	122	1141	3.24	2.40	15.6	20.01	20.15
	93				119	1167	3.21	2.01	14.1	21.29	21.78
	97				120	1136	3.17	1.95	13.6	20.95	21.95
	98				120	1072	3.26	1.82	5.8	8.99	8.91
	99				120	1135	3.18	1.82	11.5	18.76	19.61
3B	101	1	1	98	116	1212	3.14	2.40	4.4	4.72	24.03
	102				122	1219	3.31	2.40	4.3	4.79	21.96
	103				114	1138	2.96	2.40	2.8	2.43	13.94
	112				120	1253	3.32	2.01	6.6	9.57	43.68
	113				120	1181	3.19	1.95	3.2	3.87	19.07

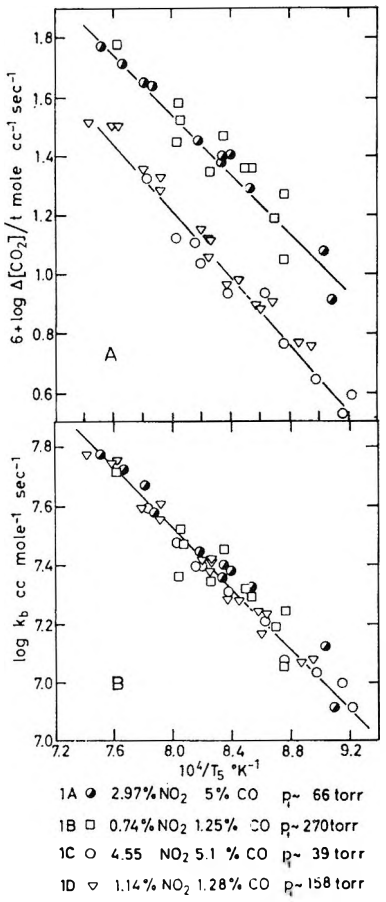

Figure 1. (A) A plot of log $\Delta[CO_2]/t$ *vs.* $1/T$ for the four groups of series 1. Points with equal concentrations of the reactants fall on a single line although there is a 4-fold difference in their argon density, indicating no effect of argon on the reaction rate. (B) A plot of log k_b *vs.* $1/T$ for the four groups appearing in (A). The points coincide to a single line.

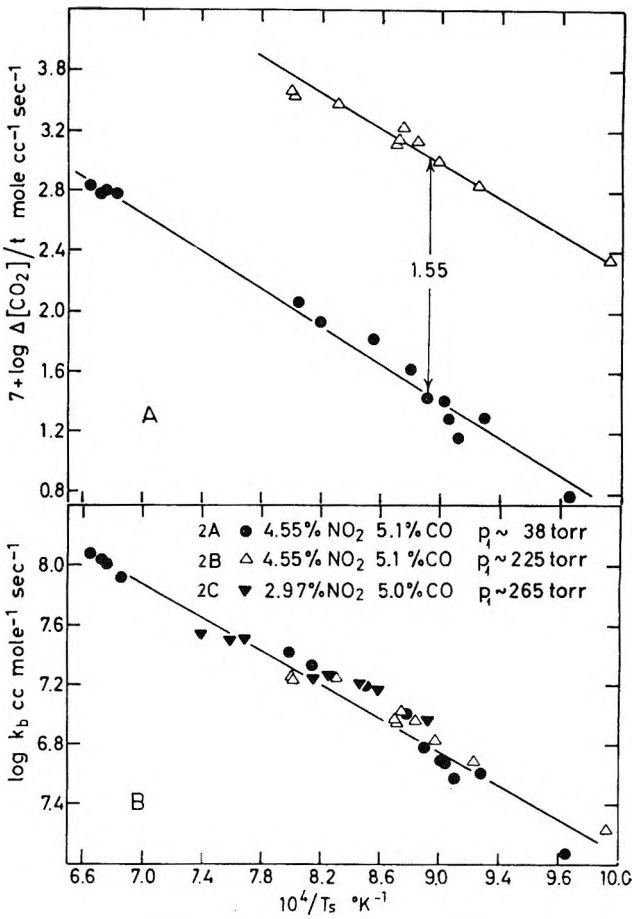

Figure 2. (A) A plot of log $\Delta[CO_2]/t$ *vs.* $1/T$ for two groups of series 2. The distance between the two parallel lines drawn indicates an overall reaction order of 2. (B) A plot of log k_b *vs.* $1/T$ for the three groups in series 2. All points coincide to a single line.

the measured incident shock velocities using the three conservation equations and the ideal gas equation of state, assuming that all the nitrogen dioxide in the reaction mixture was present as NO_2. The temperature increase due to the exothermicity of the reaction (ΔH = 53.56 kcal/mol)[12] was not taken into account at that stage. It was later corrected by adding to the reflected shock temperature half of the temperature increase (ΔT_1) due to the chemical reaction, where

$$\Delta T_1 = \%CO_2 \times \Delta H/(100 \times c_p) \qquad (1)$$

ΔT_1 ranged from a few degrees to several tens depending on the extent of the chemical reaction. This procedure is similiar to the one described in an earlier publication.[5b]

A second, although minor, correction takes into account the fact that only around 97% of nitrogen dioxide is present in the shock tube as NO_2, and a few per cent is still present as N_2O_4. This N_2O_4 dissociates by the incident shock wave resulting in a slight decrease in temperature (ΔT_2), ranging between a fraction of a degree to 5°.

Owing to the exothermicity of the reaction there is also a decrease in density behind the reflected shock during the chemical reaction. The concentration $C_{5(i)}$ of each component was therefore corrected according to the relation

$$C_{5(i)\,(\text{corrected})} = \frac{C_5 \times T_{5(i)}}{T_{5(i)\,(\text{corrected})}} \qquad (2)$$

where

$$T_{5(\text{corrected})} = T_5 - \Delta T_2 + {}^1/_2\Delta T_1 \qquad (3)$$

IV. Results and Discussion

The rate of production of CO_2 can be represented in the general form

$$d[CO_2]/dt = k_b[CO]^a[NO_2]^b[Ar]^c \qquad (4)$$

where a, b, and c are the reaction orders with respect to the CO, NO_2, and argon, respectively. The equilibrium constant of the reaction is very high[12] (1.6 ×

(12) B. J. McBride, S. Heimel, J. G. Ehlers, and S. Gordon, "Thermodynamic Properties to 6000°K for 210 Substances Involving the First 18 Elements," NASA SP-3001 (1963).

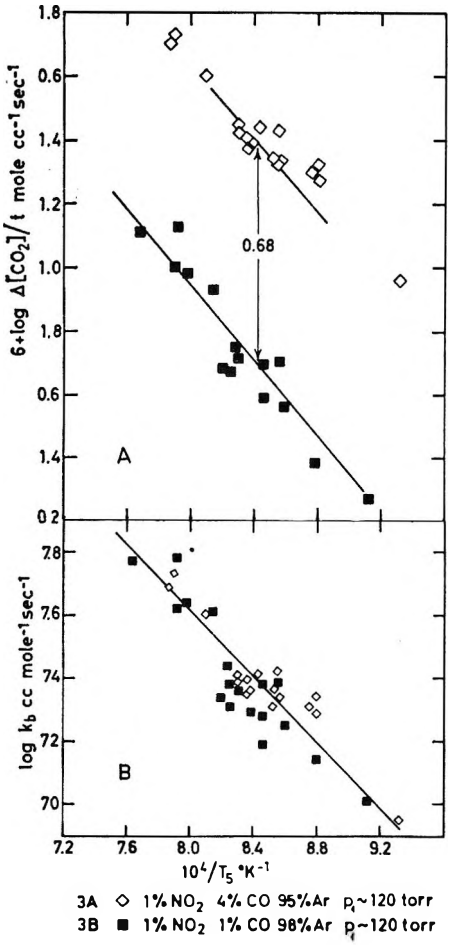

Figure 3. (A) A plot of log $\Delta[CO_2]/t$ *vs.* $1/T$ for the two groups in series 3. The distance between the parallel lines indicates a reaction order of 1.13 with respect to CO. (B) A plot of log k_b *vs.* $1/T$ for the two groups of series 3. The two lines in (A) coincide to a single line.

10^9) so that there is practically no back reaction. To evaluate the parameters a, b, and c, three series of experiments divided into nine groups of runs were carried out. Table I summarized the experimental conditions of the nine groups of runs. In Table II details of five representative shocks from each group are given.

In order to evaluate the effect of argon on the reaction rate in terms of a reaction order, we have compared the rate of production of CO_2 ($\Delta CO_2/t$, where t is the dwell time) in groups 1A and 1B and in groups 1C and 1D. In each of these two pairs the concentrations of the reactants are equal but there is a fourfold difference in the argon density. In Figure 1A the logarithm of $\Delta CO_2/t$ is plotted *vs.* $1/T$ for the four groups 1A–1D. It can readily be seen that the points of each pair fall on a single line indicating very little or no effect of argon on the reaction rate. In Figure 2A we have plotted log $(\Delta CO_2/t)$ *vs.* $1/T$ for groups 2A and 2B in order to obtain the overall reaction order. From the distance between the parallel lines drawn in Figure 2A one can calculate the total reaction order

$$n_{\text{total}} = \frac{\Delta \log (\Delta CO_2/t)}{\log [P(2B)/P(2A)]} = \frac{1.55}{0.77} = 2.0 \quad (5)$$

In Figure 3A, log $\Delta CO_2/t$ is plotted *vs.* $1/T$ for groups 3A and 3B in order to evaluate the reaction order with respect to CO. This is again calculated from the distance between the two parallel lines drawn in Figure 3A. The value obtained for n_{CO} is 1.13.

The power rate expression obtained from these three sets of experiments and which best fits all the data is

$$\text{rate} = k_b[NC_2]^{0.77}[CO]^{1.13}[Ar]^{0.1} \quad (6)$$

In Figures 1B–3B, k_b (cc mol^{-1} sec^{-1}) is plotted *vs.* $1/T$ for the three sets of experiments. The separate lines in Figures 1A–3A coincide to a single line in these figures, confirming the correctness of the values of a, b, and c.

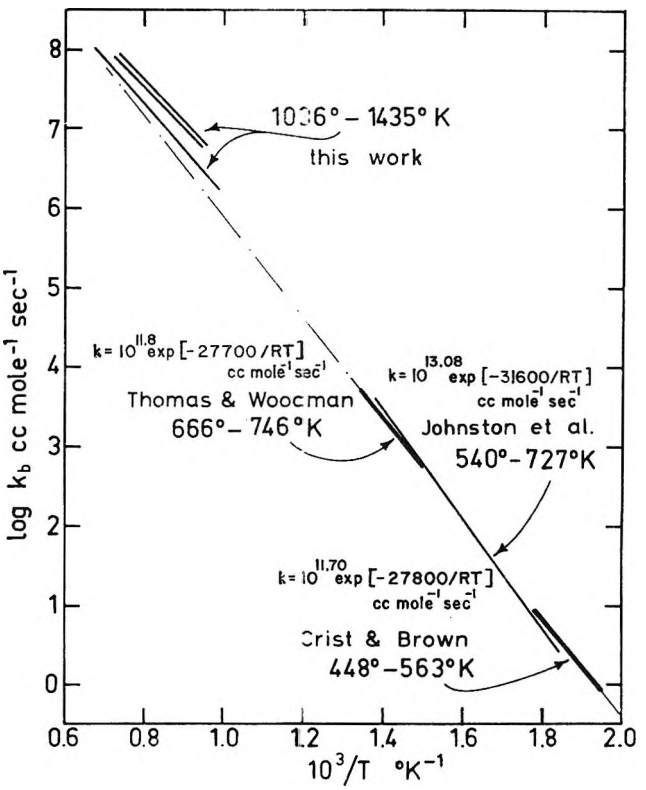

Figure 4. A plot of log k_b *vs.* $1/T$ for three series of experiments as a comparison with the low-temperature rate constants.

There is a slight difference between the values of k_b obtained from the three sets of experiments. This can be seen in Figure 4 where the lines drawn in Figure 1B–3B are given as a comparison to the low-temperature data. These differences are considerably higher than what one may expect owing to uncertainty in the shock speed measurement. As it has been mentioned before, an error of $\pm 0.7\%$ in the shock speed measurement causes a ± 25°K uncertainty in the temperature but a negligible error in the density determination. With an activation energy of ~28 kcal/mol at ~1200°K

this reflects a ±27% uncertainty in the position of the rate constants on a log k_b *vs.* $1/T$ plot. It seems, however, that the differences of the values of k_b of the various series are not due to the experimental inability of determining U_1 more accurately.

We cannot give at the moment a satisfactory explanation for these differences in k_b. We can merely state that this phenomenon was also observed in our recent studies of the $H_2S + D_2$[8] and $NH_3 + D_2$[13] exchange reactions. It clearly indicates that this behavior is typical of the technique rather than the specific reaction studied.

When the high- and the low-temperature rate constants are compared on the basis of an Arrhenius extrapolation, the agreement obtained is very satisfactory considering the long extrapolation.

The most encouraging result obtained from these data is the negligible effect of argon. As mentioned before, no effect of argon on the rate of this reaction is expected according to the "vibrational excitation mechanism." Since translation → vibration energy exchange in NO_2 is very efficient, the atom transfer step should be rate controlling, and this is what is being found.

The 0.1 order with respect to the argon might result from some slight error in the $N_2O_4 \rightleftarrows 2NO_2$ equilibrium calculations, which might cause a slight error in the composition.

Another source for the slight argon dependence may result from some contribution of the reactions

$$Ar + NO_2 \longrightarrow Ar + NO + O$$

$$Ar + CO + O \longrightarrow Ar + CO_2$$

although extrapolation of the dissociation rate of NO_2 to the temperature range covered in this study shows a negligible contribution of the latter to the observed rate.[14]

The reason for obtaining a reaction order higher than unity for CO is unclear. It should be mentioned however that Thomas and Woodman have also reported $n_{CO} = 1.05$ in their low-temperature data.[3]

(13) P. Schechner, A. Burcat, and A. Lifshitz, *J. Chem. Phys.*, in press.
(14) H. Hiroyuki and R. Hardwick, *ibid.*, **39**, 2361 (1963).

Ultrasonic Relaxation of Some Tetraalkylammonium Salts in Acetone at 25°

by G. S. Darbari and S. Petrucci

Department of Chemistry, Polytechnic Institute of Brooklyn, Brooklyn, New York 11201 *(Received April 9, 1969)*

Ultrasonic absorption measurements of 0.1 *M* solutions of Me_4NPi, Et_4NPi, Bu_4NPi, and Bu_4NNO_3 and of solutions of Am_4NBr, Bu_4NBr, and Bu_4NCl in the concentration range 0.05–0.20 *M* at 25° in acetone are reported. (Pi = picrate, Me = methyl, Et = ethyl, Bu = butyl, Am = amyl). After evaluation of possible C–C isomeric relaxation, the results are interpreted by the hypothesis of ionic association. The conclusion is that the forward rate constant is diffusion controlled but the reverse rate constant is not. This conclusion is corroborated by analysis of previous conductance results indicating the presence of two types of ion pairs for similar systems.

Introduction

Classical mass transport experiments and theories like electrical conductance[1] have been extensively applied to alkylammonium salts in aqueous and nonaqueous solvents.[2] These systems were originally chosen so as to have the closest resemblance to the features of the assumed model[1] (ions taken as spheres in a continuum, lack of ion solvent interactions and Stokes hydrodynamics). Surprisingly enough, very often even these systems offered effects that could not be explained by the classical theories. They were rather rationalized in terms of *a posteriori* invoked ion–solvent interactions.[3] The reliability of such effects has been proven by independent tools[4] on the same systems, denying any claims of calculation ambiguities of the conductance theory but rather confirming the presence of real effects. On the other hand, ion–solvent interactions in these systems should represent the weakest form possible out of other comparable interactions that

(1) R. M. Fuoss and F. Accascina, "Electrolytic Conductance," Interscience Publishers, New York, N. Y., 1959.
(2) R. A. Robinson and R. H. Stokes, "Electrolyte Solutions," 2nd ed, rev., Butterworth and Co., Ltd., London, 1959 p, 550.
(3) H. Sadek, E. Hirsch, and R. M. Fuoss in "Electrolytes," B. Pesce, Ed., Pergammon Press Ltd., London, 1962.
(4) S. Petrucci and M. Battistini, *J. Phys. Chem.*, **71**, 1181 (1967); S. Petrucci and F. Fittipaldi, *ibid.*, **71**, 3087 (1967).

Table I[a]: Sound Absorption Coefficients at Different Frequencies for the Various Systems Investigated

Me$_4$NPi, c = 0.10 M

f, MHz	α, cm^{-1}
15	0.0870
21	0.159
25	0.231
27	0.254
33	0.367
35	0.426
45	0.671
55	1.006
65	1.337
75	1.768
85	2.198
105	3.309

Et$_4$NPi, c = 0.10 M

f, MHz	α, cm^{-1}
25	0.225
35	0.449
45	0.702
55	1.11
65	1.39
85	2.44
105	3.57
115	4.20
125	5.24
155	7.83

Bu$_4$NPi, c = 0.10 M

f, MHz	α, cm^{-1}
15	0.072
25	0.213
35	0.403
45	0.670
55	0.969
85	2.37
90	2.63
105	3.61
115	4.34
125	4.99
135	6.19
150	7.55
190	12.25
210	13.63

Bu$_4$NNO$_3$, c = 0.10 M

f, MHz	α, cm^{-1}
15	0.093
25	0.249
35	0.507
45	0.802
55	1.22
65	1.73
90	3.27
95	3.74
110	4.84
115	5.41
125	6.23
130	6.85
150	9.06
170	12.0

Am$_4$NBr,

c = 0.20 M		c = 0.10 M		c = 0.05 M	
f, MHz	α, cm^{-1}	f, MHz	α, cm^{-1}	f, MHz	α, cm^{-1}
10	0.0633	10	0.0480	10	0.0421
30	0.547	30	0.417	30	0.380
50	1.485	50	1.162	50	0.979
70	2.763	70	2.199	70	1.888
90	4.317	85	3.273	90	3.016
110	6.620	95	4.079	110	4.605
130	8.635	105	4.714	130	6.102
150	11.51	110	5.276	150	8.347
170	14.39	130	7.023	170	10.25
190	17.50	170	11.40	190	12.44
210	20.03	190	14.52	210	15.02
		210	17.10	230	17.46
		230	19.57		
		250	23.03		

Bu$_4$NI,

c = 0.20 M		c = 0.10 M		c = 0.05 M	
f, MHz	α, cm^{-1}	f, MHz	α, cm^{-1}	f, MHz	α, cm^{-1}
10	0.0461	10	0.0410	10	0.0353
30	0.403	15	0.0892	30	0.322
50	1.140	25	0.249	50	0.852
70	2.187	30	0.345	70	1.669
90	3.569	35	0.4605	90	2.832
110	5.296	45	0.794	110	4.029

Bu$_4$NI

c = 0.20 M		c = 0.10 M		c = 0.05 M	
f, MHz	α, cm^{-1}	f, MHz	α, cm^{-1}	f, MHz	α, cm^{-1}
130	5.756	50	0.952	130	7.023
150	7.483	55	1.174	150	9.671
170	9.440	65	1.586	170	12.09
190	11.51	70	1.796	190	14.97
210	13.82	75	2.072	210	16.81
		85	2.697	230	20.26
		95	3.399		
		105	4.202		
		110	4.375		
		115	4.778		
		130	5.987		
		150	8.289		
		170	9.556		
		190	12.43		

Bu$_4$NBr,

c = 0.20 M		c = 0.10 M		c = 0.05 M	
f, MHz	α, cm^{-1}	f, MHz	α, cm^{-1}	f, MHz	α, cm^{-1}
15	0.1235	15	0.108	15	0.0892
25	0.328	25	0.282	21	0.176
30	0.4835	35	0.530	27	0.282
35	0.6505	45	0.9095	33	0.4145
50	1.266	50	1.082	39	0.587
55	1.612	70	2.026	45	0.800
65	2.257	75	2.360	57	1.220
70	2.533	85	2.878	69	1.727
75	2.798	95	3.534	75	1.946
85	3.569	105	4.202	81	2.234
95	4.398	115	4.778	87	2.556
105	5.484	125	5.641	95	3.051
115	6.102			99	3.316
125	7.276				
145	9.556				
155	10.36				
185	14.05				
195	14.97				
205	16.58				

Bu$_4$NCl,

c = 0.20 M		c = 0.10 M		c = 0.05 M	
f, MHz	α, cm^{-1}	f, MHz	α, cm^{-1}	f, MHz	α, cm^{-1}
10	0.0691	10	0.0653	10	0.0437
30	0.581	25	0.372	15	0.0921
50	1.589	30	0.535	25	0.265
70	2.878	35	0.698	30	0.368
90	4.835	55	1.700	35	0.501
110	6.965	65	2.266	45	0.840
130	9.786	75	2.856	50	1.013
150	12.43	85	3.626	55	1.186
170	15.43	95	4.433	70	1.957
190	18.305	130	7.555	75	2.164
210	21.41	135	7.977	85	2.648
230	25.10	145	9.337	90	3.051
250	28.21	150	9.745	105	3.851
		155	10.20	110	4.087
		170	11.90	150	7.483
		190	13.94		
		230	19.83		

[a] At least one figure in excess with respect to the sensitivity of the method is reported for the absorption coefficient α. This has been done in order to avoid rounding off errors during possible calculations from these data by others.

are rather well understood for the intermediate cases of transition metals[5] and for the extreme cases of the solution chemistry of square planar Pt(II) and octahedral Co(III) complexes.[6] From a kinetic point of view, (considering the solvent molecules associated with the ions in solution as ligands) the solvent substitution by the associating ionic partner should occur in these systems with a rate comparable to the rate of attack by the incoming ion, namely with rates comparable to diffusion-controlled reactions.

It has been with these preambles in mind and in an effort to understand the mechanism of ionic association in nonaqueous solvents that it was decided in this laboratory to study with a modern kinetic tool a series of systems already investigated by electrical conductance. Kraus, *et al.*,[7] in a series of papers reported the electrical conductance of several alkylammonium halides, nitrates, and picrates in acetone at 25°. These excellent data have recently been reanalyzed[8] by the 1959 version of the Fuoss–Onsager conductance theory for associated electrolytes[1] providing useful parameters such as association constants and minimum approach distance between free ions.

Experimental Section

Materials. Acetone (Baker, reagent grade) was distilled over anhydrous $CuSO_4$ in a 3-ft Vigreux all-Pyrex distillation assembly. Only the middle portion was collected. All the salts were Eastman Kodak reagent grade. They were dried at 40–50° under vacuum at 1 mm up to constancy of weight (±1 mg) before use. This proved to be important especially for Bu_4NCl which is extremely hygroscopic. The solutions were prepared by dissolving weighed amounts of dry salts in freshly purified acetone and diluting to volume in volumetric flasks.

Equipment. A Matec 560 Ultrasonic Pulser-Receiver was used in conjunction with a 531 A oscilloscope and a 608D Hewlett-Packard Standard Signal Generator. The cell assembly and the method of measurements have already been described.[9] Many runs were repeated by changing the piezoelectric crystal from 3 to 5 and to 10 MHz (fundamental frequency) and scanning the sound absorption in all the frequency ranges observable in order to ensure reproducibility after several days with the same solution. The values of the measured frequencies were checked by a crystal calibrated frequency standard. The temperature was maintained within ± 0.05° during the measurements by means of a Forma Junior refrigerated bath.

Results

In Table I the absorption coefficients α (nepers cm^{-1}) and the corresponding frequencies f (MHz) for the various electrolytes investigated are reported. In Figures 1 and 2, representative plots of the quantity (α/f^2) *vs.* f are presented. The data in Figures 1 and 2 are analyzed using a function for a single relaxation[10]

$$\frac{\alpha}{f^2} = \frac{A}{1 + (f/f_r)^2} + B \qquad (1)$$

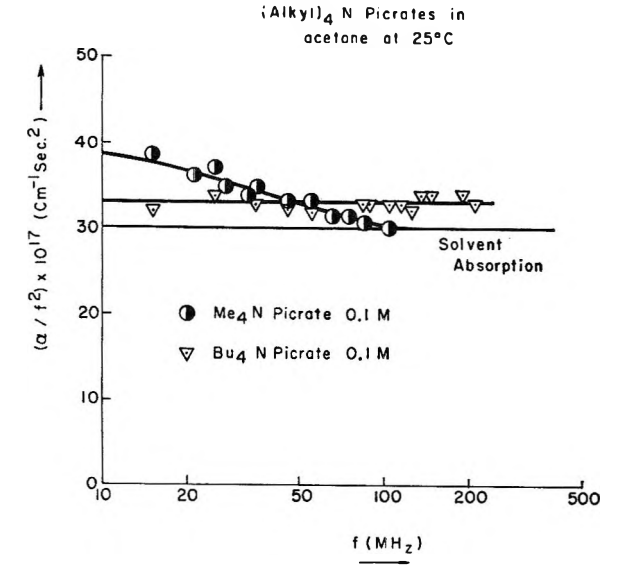

Figure 1. Plot of (α/f^2) *vs.* f for Me_4NPi and Bu_4NPi in acetone at 25°.

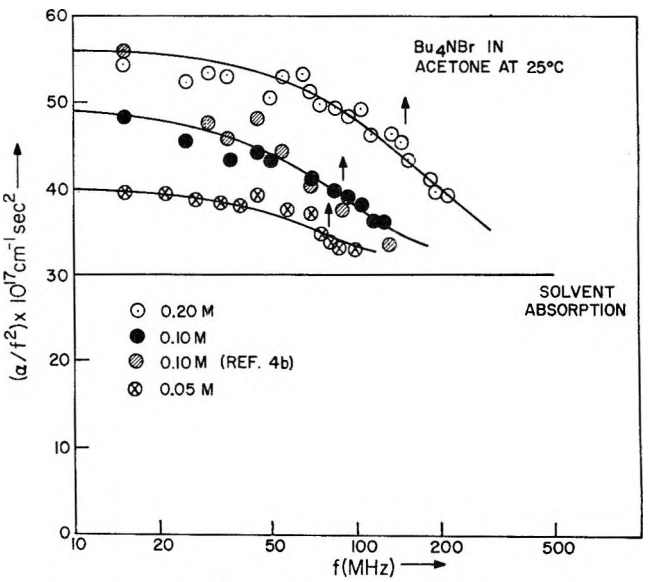

Figure 2. Plot of (α/f^2) *vs.* f for Bu_4NBr in acetone at 25°.

(5) T. R. Stengle and C. H. Langford, *Coordination Chem. Rev.*, **2**, 349 (1967).

(6) C. H. Langford and H. B. Gray, "Ligand Substitution Processes," W. A. Benjamin, New York, N. Y., 1965.

(7) M. B. Reynolds and C. A. Kraus, *J. Amer. Chem. Soc.*, **70**, 1709 (1948); M. J. McDowell and C. A. Kraus, *ibid.*, **73**, 3293 (1951).

(8) D. F. Evans, C. Zawoyski, and R. L. Kay, *J. Phys. Chem.*, **69**, 3878 (1965).

(9) S. Petrucci, *ibid.*, **71**, 1174 (1967).

(10) J. Lamb in "Physical Acoustics," Vol. II, part A, Ed., W. P. Mason, Academic Press, New York, N. Y., 1965.

where A is a constant at each concentration and temperature, f_r is the relaxation frequency, and B is solvent absorption which at 25° was found to be $\alpha_0/f^2 = (30 \pm 2)\ 10^{-17}$ cm^{-1} sec^2 in the range of frequency 10–210 MHz. The individual determinations at the frequencies investigated are reported in Table II. No evidence of solvent relaxation is visible in this frequency range. Additional measurements down to −5° do not show any relaxation in the same frequency range. All the systems showing a relaxation could be interpreted by the single relaxation function (1). The values of A and f_r for the electrolyte solutions investigated are reported in Table III. The parameters A and f_r are precise to about ± 10%. The system 0.1 M Bu_4NBr in acetone already investigated[4b] gave a relaxation frequency of $f_r = 66$ MHz. These data combined with the ones of the present work (Figure 2) give a more reliable value of $f_r = 90 \pm 15$ MHz. The reason of the lower (previously) calculated relaxation frequency is due to a point at 15 MHz (Figure 2) that is clearly too high.

Table II: Sound Absorption Coefficient α and Ratio (α/f^2) for Acetone at 25°

f, MHz	α, cm^{-1}	$(\alpha/f^2) \times 10^{17}$, cm^{-1} sec^2
30	0.273	30.4
50	0.702	28.1
70	1.50	30.6
90	2.39	29.5
110	3.80	31.4
150	7.02	31.2
170	8.23	28.5
190	12.1	33.5
210	12.8	29.0

In this regard one should notice that the overall excess absorptions $(\alpha/f^2 - \alpha_0/f^2)$ with respect to the solvent are rather small. Because of the sensitivity of the method (±2%) and of the small excess absorption, a complete analysis by the excess function $\alpha_{exc}\lambda$ *vs.* f is not feasible with the present data. Indeed the scatter of the individual points is too high especially for the more dilute solutions.

For Me_4NPi, measurements at higher concentration than 0.1 M are not possible because of solubility limitations. (For Me_4NBr the solubility is so low that it is impractical to make any attempt to measure its sound absorption). Therefore, for the picrates this study has been limited to the single concentration 0.1 M in order to allow for a qualitative comparison between different alkylammonium picrates; 0.1 M Bu_4NNO_3 has also been studied to demonstrate the effect of an anion (other than halides or picrate) on the ultrasonic absorption.

Table III: Parameters from Equation 1 for the Various Systems Investigated

Salt	c, M	$A \times 10^{17}$, cm^{-1} sec^2	f_r, MHz
Me_4NPi	0.10	9	35 ± 5
Et_4NPi	0.10	7	85 ± 10
Bu_4NPi	0.10	3	Relaxation frequency above the range of measured frequencies if present
Bu_4NNO_3	0.10	10.5	
Am_4NBr	0.20	32	210 ± 20
	0.10	18	180 ± 20
	0.05	11	160 ± 20
Bu_4NI	0.20	17	240 ± 25
	0.10	9.5	180 ± 20
	0.05	6.0	150 ± 15
Bu_4NBr	0.20	26	150 ± 15
	0.10	19	90 ± 15
	0.05	10	80 ± 10
Bu_4NCl	0.20	38	190 ± 20
	0.10	31	130 ± 15
	0.05	13	95 ± 10

Discussion

The Hypothesis of Isomeric Relaxation. Symons, *et al.*,[11] measured the ultrasonic relaxation of pure 3,3-diethylpentane and of its solutions in *n*-hexane. These authors attributed the observed relaxation to an internal rotation about a C–C bond.

They also suggested that all or part of the ultrasonic absorption of alkylammonium ions in solution[12] is caused by a comparable rotational isomerism. The present authors, although finding this hypothesis very interesting, do not share with this view as applicable to the present data. The following considerations lead to the above conclusion.

Inspection of Figure 1 and Table III shows that a relaxation process is present for Me_4NPi where no internal rotation is possible. Et_4NPi still shows a relaxation at higher frequency than Me_4NPi. For Bu_4NPi if a relaxation is existing (in view of A being statistically larger than B) it is above the range of our measurements. See Figure 1 and Table III. The trend in the ultrasonic absorption going from Me_4NPi to Et_4NPi and to Bu_4NPi might be due to the decreasing association constants the values being K (Λ) = 67 ± 1, 45 ± 2, and 17 ± 5, respectively.[8]

Further, on comparing the observed relaxation effects for Bu_4NNO_3, Bu_4NPi, Bu_4NI, Bu_4NBr, and Bu_4NCl, one may conclude that the relaxation frequency is dependent on the anion for the same cation (Table III and Figure 3).

(11) M. J. Blandamer, M. J. Foster, N. J. Hidden, and M. C. R. Symons, *J. Phys. Chem.*, **72**, 2238 (1968).

(12) S. Petrucci and G. Atkinson, *ibid.*, **70**, 2550 (1966).

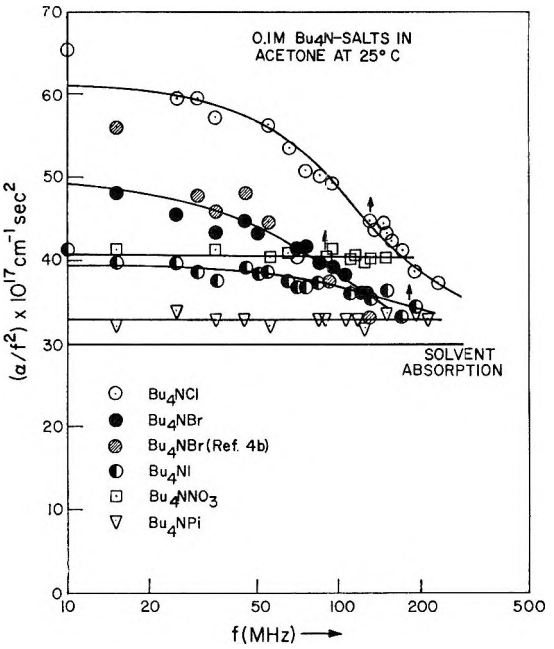

Figure 3. Plot of (α/f^2) *vs.* f for 0.1 M Bu_4NCl, Bu_4NBr, Bu_4NI, Bu_4NNO_3, and Bu_4NPi in acetone at 25°.

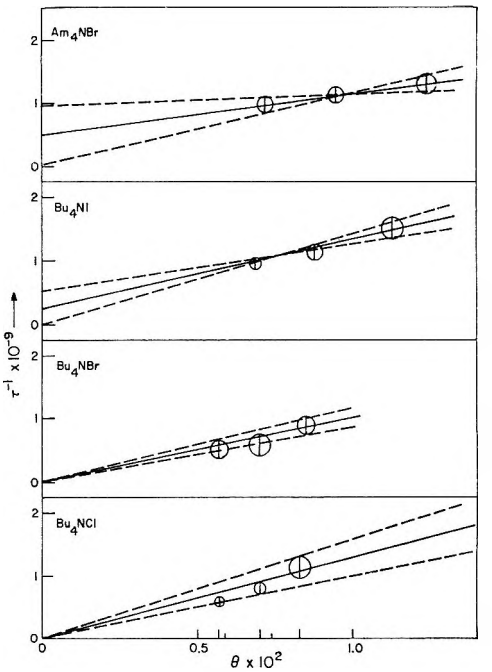

Figure 4. Plot of τ^{-1} *vs.* θ for the tetraalkylammonium halides investigated in acetone at 25°.

Finally, for the same electrolyte, the relaxation frequency is concentration dependent (Table III, Figure 2) indicating a bimolecular (or more complex) process but not a first-order isomeric transformation.

The above rules out rotational isomerism to be the *only* source of excess sound absorption. It remains to discuss the possibility of a *contribution* to the sound absorption due to isomeric relaxation.

This cannot be ruled out in principle; however, our interest is focused on the observed relaxation region and, in particular, on the relaxation frequency of the process observed. Apart from the unlikelihood of having two kinetic processes of different order and nature occurring with the same relaxation time, the data show a single relaxation process varying with the nature of the anion for the same cation. Therefore, even if for a particular electrolyte the overlapping of the two processes exists, the shifting of the frequency with the nature of the anion should reveal the overlapping.

Further, the data can be interpreted with the value of B equal to the sound absorption of the solvent. It means, therefore, that if isomeric relaxation has an observable relaxation, this should show up at frequencies below the investigated region. Finally, it should be remembered that the electrolytes are not heavily associated. Therefore, most of the ions are free. This eliminates the most unlikely possibility, namely of the anion being associated to the cation and influencing with its proximity and nature the internal rotation about C–C bonds.

The Hypothesis of Ionic Association. The hypothesis is advanced, therefore, that the observed relaxation processes are due to ionic association. According to Eigen,[13] the relaxation time $\tau = [2\pi f_r]^{-1}$ is correlated to the forward and reverse rate constants k_f and k_R of the chemical equilibrium by the relation

$$\tau^{-1} = k_f\theta + k_R \tag{2}$$

where the quantity θ is a function of the concentration[13] of the electrolyte of the type

$$\theta = \sigma c\gamma^2_{\pm}\left(2 + \frac{\partial \ln \gamma^2_{\pm})}{\partial \ln \sigma}\right) \tag{3}$$

with σ the degree of ionization, c the stoichiometric concentration, and $\gamma_{\pm}$ the ionic mean activity coefficient. The quantity θ has been estimated by combining the expression for the association constant as determined by electrical conductance and the Debye–Hückel expression for $\gamma_{\pm}$ retaining the quantity a_J from conductance results as the minimum approach distance between the free ions.

$$K(\Lambda) = \frac{1 - \sigma}{\sigma^2 c\gamma_{\pm}{}^2} \tag{4}$$

$$-\log \gamma_{\pm}{}^2 = \frac{2S_f\sqrt{c\sigma}}{1 + Aa_J\sqrt{c\sigma}} \tag{5}$$

Combination of expressions 4 and 5 gives σ and $\gamma_{\pm}{}^2$ and therefore θ from expression 3.

The plots of τ^{-1} *vs.* θ are shown in Figure 4. The results for k_f and k_R are reported in Table IV. In the same table the rates of a diffusion-controlled process

(13) M. Eigen and L. DeMayer in "Investigation of Rates and Mechanisms of Reactions," Vol. VIII, part 2, Ed., A. Weissberger, John Wiley and Sons, New York, N. Y., 1963.

Table IV: Association Constants, a_J Parameters, Fuoss Association Constants, Calculated Forward and Reverse Diffusion-Controlled Rate Constants, and Experimental Forward and Reverse Rates for the Tetraalkylammonium Halides Investigated in Acetone

Electrolyte	$K(\Lambda)$, M^{-1}	$a_J \times 10^8$ cm	K_F[a] M^{-1}	$k_D \times 10^{-10}$ [a], M^{-1} sec^{-1}	$k_{-D} \times 10^{-9}$ [a] sec^{-1}	$k_f \times 10^{-10}$, M^{-1} sec^{-1}	$k_R \times 10^{-9}$, sec^{-1}
Am_4NBr	220 ± 20	7 ± 1	38	8.5	2.2	7 ± 5	0.5 ± 0.5
Bu_4NI	143 ± 6	6.1 ± 0.3	42	9.7	2.3	11 ± 3	0.25 ± 0.25
Bu_4NBr	264 ± 5	5.4 ± 0.2	64	11.1	1.7	10 ± 2	Not
Bu_4NCl	430 ± 5[b]	5.7 ± 0.1[b]	55	10.3	1.9	13 ± 2	measurable

[a] The values of a_J from the conductance calculations have been used for the present calculations. [b] The authors are indebted to Dr. Fennell Evans of Case Western Reserve University, Cleveland, Ohio, for having furnished these data as a private communication.

of ionic recombination k_D and ion pair dissociation k_{-D} are also reported. These quantities have been calculated by means of the relations of Smoluchowski–Debye[14] for k_D and Eigen[15] for k_{-D}, respectively, modified by the use of the Stokes–Einstein equation

$$k_D = \frac{8NkT}{3000\eta}\left(-\frac{b}{e^{-b}-1}\right) \tag{6}$$

$$k_{-D} = \frac{2kT}{\pi\eta a^3}\left(-\frac{b}{1-e^{b}}\right);\ b = \frac{|z_+z_-|e^2}{aDkT} \tag{7}$$

where k is the Boltzmann constant, T the absolute temperature, N Avogadro's number, η the viscosity of the solvent, and b the Bjerrum parameter; a has been set equal to a_J. One can see from Table IV that the experimental k_f and k_D are comparable. Considering the drastic approximations involved (*e.g.*, (1) the use of the Debye–Hückel expression for the activity coefficients at the present concentrations in the calculation of θ, (2) the use of the Debye–Hückel potential in the calculation of the electrostatic factor in eq 6 and 7 $(-b/e^{-b}-1)$, and $(-b/1-e^{b})$, (3) the use of the Stokes–Einstein equation to calculate the diffusion coefficients of the ions through the viscosity of the solvent, and finally (4) the unknown effects of the use of the static activity coefficients for the dynamical process in question where the rate of ionic recombination is comparable to the rate of rearrangement of the ionic atmosphere) the agreement is good enough to conclude that the forward process of ionic recombination to form an ion pair is diffusion controlled or at least close to diffusion controlled. The same cannot be said, however, for the reverse rate constant k_R. Inspection of Table IV shows that k_R is smaller than k_{-D} by about one order of magnitude. For Bu_4NCl and Bu_4NBr, k_R cannot be even read on a τ^{-1} *vs.* θ plot, the intercept being about zero (Figure 4).

Some words must be spent on the reliability of the above conclusions in view of the approximations involved. It is clear from Figure 4 that the intercept of the τ^{-1} *vs.* θ plots cannot ever give a $k_R = k_{-D}$ since this would imply an ordinate larger than the observed τ^{-1} at the highest concentration studied. Therefore, even if the calculated θ values are completely unreliable, the conclusion $k_{-D} > k_R$ remains valid.

In regard to the accuracy of θ, the use of the Debye–Hückel theory to calculate $\gamma_\pm^2$ is one of the major sources of error. In order to try to get an assessment on the reliability of the above conclusions ($k_D \approx k_f$) a calculation has been performed using only the data at the lowest concentration 0.05 M. For these systems, the ionic strength is around 0.02–0.03, that is still in a range where eq 5 may apply with some accuracy.

From eq 2 considering $K(\Lambda) = k_f/k_R$ the following expression for k_f is derived

$$k_f = \tau^{-1}\Big/\left[\theta + \frac{1}{K(\Lambda)}\right] \tag{8}$$

In Table V, the calculated k_f values are reported together with the values of θ used for this concentration. It may be seen that the values of k_f are rather lower than in Table IV (having imposed the condition $(k_f/K(\Lambda) = k_R)$ but still close enough to the calculated diffusion-controlled rates k_D not to invalidate the above conclusions ($k_D \approx k_f$).

Independent Support. The reverse rate constants not being diffusion controlled corresponds to saying that the association process cannot be expressed through a continuum model, or in mathematical terms through the

Table V: Calculated Forward Rate Constant k_f from the Relation

$$k_f = \left[\tau^{-1}\Big/\left(\theta + \frac{1}{K(\Lambda)}\right)\right]$$

Electrolyte	$\theta \times 10^2$, M	$\tau^{-1} \times 10^{-6}$, sec^{-1}	$(\theta + \frac{1}{K(\Lambda)}) \times 10^2$, M	$k_f \times 10^{-10}$, M^{-1} sec^{-1}
Am_4NBr	0.72	10 ± 1	1.17	9 ± 1
Bu_4NI	0.69	9.4 ± 1	1.39	7 ± 1
Bu_4NBr	0.57	5.0 ± 0.7	0.95	5 ± 1
Bu_4NCl	0.57	6.0 ± 0.6	0.80	8 ± 1

(14) M. Von Smoluchowski, *Physik. Z.*, **17**, 557 (1916), P. Debye, *Trans. Electrochem. Soc.*, **82**, 265 (1942).

(15) M. Eigen, *Z. Phys. Chem.*, (Frankfurt am Main), **1**, 176 (1954).

Fuoss expression of ionic association,[16] that is the ratio between eq 6 and 7

$$K_F = \frac{4\pi Na^3}{3000} \exp(b) = \frac{4\pi Na^3}{3000} \exp\left(\frac{|z_+z_-|e^2}{aDkT}\right) \quad (9)$$

This, on the other hand, was self-evident from the conductance results themselves. Indeed in Table IV, the association constants $K(\Lambda)$ obtained through conductance and the parameters a_J are reported. The value of K_F from eq 9 using a_J are also reported. It can be seen that $K_F = 38$–$64\ M^{-1}$ while the experimental data for $K(\Lambda)$ vary between 140 and 430. [Since $k_f \approx k_D$ this corresponds to saying that $k_R < k_{-D}$].

Notice also that in order to force the Fuoss function to reproduce $K(\Lambda)$, one should impose a value of a in formula 9 much smaller than the parameters a_J. One could speculate therefore *from conductance alone* that two minimum approach distances can be calculated from conductance data, a collision diameter between free ions a_J and a minimum distance between the same ions from $K(\Lambda)$ much smaller than a_J. Indeed for Bu_4NI, Sears, *et al.*,[17] have calculated the association constant from conductance data from -55 to 25°. If one plots the log $K(\Lambda)$ *vs.* $(DT)^{-1}$ according to eq 9 one obtains a straight line up to $-30°$ while the last two points at -40 and $-50°$ are somewhat below. From the slope of the straight line one can calculate the parameter $a = 2.2$ Å much smaller again than $a_J = 6.1 \pm 0.3$ Å at 25°. Also, Adams and Laidler[18] in a series of recent papers on association and mass transport of alkylammonium salts in acetone have rationalized the data with the assumption of at least two species of ion pairs, "solvent-separated" and "solvent-shared" ion pairs. The presence of contact ion pairs was postulated at lower dielectric constant than 20. Also, Taylor and Kuntz[19] in a study of ionic association by nmr of $[Me(Bu)_3]$ N–$B(C_6H_5)_4$ in several solvents have concluded from limiting shifts that a large fraction of ion pairs in acetone must be solvent-separated ion pairs.

Conclusions

The systems investigated seem to represent a case where rates of diffusion-controlled approach between ions and rates of desolvation are almost comparable. For the reverse rate constants, however, a substantial difference exists between the diffusion-controlled rates of separation of the less "tight" ion pairs and the rates of separation of the more "tight" ion pairs, having assumed their existence on the basis of independent evidences.[18,19]

Acknowledgments. The authors wish to express their thanks to machinist Richard Parla and his apprentice, Marvin Charles, for having constructed the ultrasonic cell used in this work.

(16) R. M. Fuoss, *J. Amer. Chem. Soc.*, **80**, 5059 (1958).

(17) P. G. Sears, E. D. Wilhoit, and L. R. Dawson, *J. Phys. Chem.*, **60**, 169 (1956).

(18) W. A. Adams and K. J. Laidler, *Can. J. Chem.*, **46**, 1977, 1989, 2006 (1968).

(19) R. P. Taylor and I. D. Kuntz, Jr., *J. Amer. Chem. Soc.*, **91**, 4006 (1969).

Ultrasonic Absorption in Aqueous Salts of the Lanthanides. II. Acetates

by Victor L. Garza[1] and Neil Purdie[2]

Oklahoma State University, Stillwater, Oklahoma 74074 *(Received January 29, 1969)*

The acetate salts of lanthanum, cerium, samarium, and dysprosium have been studied at 25° using the pulse technique of sound absorption over the frequency range 5–75 MHz. For samarium, the sound absorption spectrum was examined as a function of pH, ionic strength, and varying ratios of metal to ligand. Relaxations were observed at 6 ± 0.5 MHz and 35–65 MHz for all salts and for samarium acetate under all conditions. The high-frequency absorption was identified as the acetate desolvation step in the multistep mechanism by comparison with the sound absorption spectra of copper and nickel acetates. Unlike a number of other rare earth systems the low-frequency relaxation was independent of the cation. This relaxation is still associated with the rate-controlling step of substitution into the cation and a kinetic interpretation is introduced to explain the unusual behavior. An explanation is proposed to account for the faster rates of complex formation when sulfate is the ligand, which suggests that the loss of successive water molecules from the coordination sphere of the cation, on chelation, proceeds at a progressively decreasing rate.

Introduction

Relaxation methods have been applied over the last few years to a study of the rates of formation of complexes of the trivalent rare earth cations.[3-9] In the cases where the entering ligand is murexide,[3] sulfate,[4,7,8] anthranilate,[5,6] and oxalate[9] a sufficient number of the metal ions in the series have been studied for an analysis of the dependence of the specific rate constants on cation radius to be made. The dependence is similar in all four cases showing a maximum rate of complex formation for the ions around the middle of the series.

Because of the analogous complex trends with inverse cation radius of such thermodynamic parameters as free energy and enthalpy of complex formation,[10] the same interpretation, that is a change in cation coordination number somewhere around Sm–Eu, has been invoked to account for the nonuniform trend in specific rate constants.

The rates, however, differ in another respect. If the mechanism is dissociative, so that the transition state is formed with a reduced coordination number, and the controlling step in the mechanism is the loss of a water molecule bound to the cation, the rate of complex formation should approximate to the rate of water exchange and be almost independent of the nature of the entering ligand. A comparison of the rates of formation shows that the values for the monosulfate complexes[4,7,8] are, in some cases, an order of magnitude greater. The comparison is not this straightforward, however, because of the experimental conditions used which differ in temperature and ionic strength between sound absorption and temperature jump or pressure jump methods. To remove the possibility that the measured rate constants are related to the experimental conditions or to the method of study, the same system should be studied by more than one technique under similar experimental conditions conducive to that method or not. Such a study is at present in progress with the rare earth anthranilates. Nevertheless different experimental conditions may be insufficient justification for the observed discrepancy in specific rate constants for a particular cation and instead the dissociative mechanism may be oversimplified. Pertinent to this argument is the fact that the ligands, other than sulfate, are chelating ligands in which case the rate-controlling step in the mechanism may be the removal of a water molecule other than the first. For example, as the coordination number of the ligand increases in going from IDA to NTA to EDTA, the rate of formation of the sodium complex was observed to decrease.[11] Marianelli,[12] by using the oxygen-17 nmr line broadening technique has shown that for a coordination number of 9 the rate of water exchange in Gd(III) in perchlorate media ($9 \pm 2 \times 10^8$ sec^{-1}) is approximately equal to the rate of formation of the gadolinium monosulfate (6.7×10^8 sec^{-1})[8] complex. On the other hand,

(1) NSF Summer Research Participant, Pan American College, Edinburg, Texas.

(2) To whom communications should be directed.

(3) G. Geier, *Ber. Bunsenges. Phys. Chem.*, 69, 617 (1965).

(4) N. Purdie and C. A. Vincent, *Trans. Faraday Soc.*, 63, 2745 (1967).

(5) H. B. Silber and J. H. Swinehart, *J. Phys. Chem.*, 71, 4344 (1967).

(6) H. B. Silber, R. D. Farina, and J. H. Swinehart, *Inorg. Chem.*, 8, 819 (1969).

(7) J. J. Grecsek, M.S. Thesis, University of Maryland, 1966.

(8) D. P. Fay, D. Litchinsky, and N. Purdie, *J. Phys. Chem.*, 73, 544 (1969).

(9) A. J. Graffeo and J. L. Bear, *J. Inorg. Nucl. Chem.*, 30, 1577 (1968).

(10) G. H. Nancollas, "Interactions in Electrolyte Solutions," Elsevier Publishing Co. Inc., New York, N. Y., 1966, pp 109, 161.

(11) M. Eigen and G. Maass, *Z. Phys. Chem.* (Frankfurt am Main), 49, 163 (1966).

(12) R. Marianelli, Ph.D. Thesis, University of California, Berkeley, 1966.

from preliminary ^{17}O relaxation studies in acetate media Reuben and Fiat[13] calculated the rate constant of water exchange to be 6.3×10^7 sec^{-1} for Dy(III). This compares favorably with the results for the rates of formation of the murexide,[3] anthranilate,[5,6] and oxalate[9] complexes and may indeed be the value for the exchange of the *second* water molecule from the metal hydration sphere. In other words, the information on water exchange from nmr studies is consistent with observations on complex formation and the dissociative mechanism may be correct with the modification that successive water molecules are exchanged at progressively slower rates.

In this work we have attempted to measure the rates of formation of some of the rare earth acetate complexes and have compared the results with other systems and with the rate of water exchange on Dy(III).

Experimental Section

Measurements of the absorption of ultrasonic energy were made at selected frequencies between 5 and 75 MHz using the pulse method.[14] The system is similar to that described previously[4] for the low-frequency range. The fundamental frequency of the transducer was measured directly and the remaining frequencies checked by calculating the wavelength from the measured velocity of sound in water at 25°. Values were reproducible to ±0.1 MHz over a long period of time. A temperature of 25 ± 0.05° was maintained for all measurements reported.

Solutions

Rare earth acetates and perchlorates with a purity of 99.9% were obtained from the American Potash and Chemical Corporation and used without further purification. Stock solutions of the acetates were prepared with deionized water and analyzed for cation concentration by the titration with standard sodium hydroxide of the acetic acid produced by ion exchange on Dowex 50W-X8, 20–50 mesh resin. The solutions had a pH between 6 and 7. For measurements at pH 4.5, the pH was adjusted in a back titration with standard perchloric acid.

Solutions in which the metal to acetate concentration ratio was changed were prepared by adding the rare earth perchlorate to a standard solution of acetic acid with an appropriate dilution with deionized water. The rare earth perchlorates were previously analyzed for water of crystallization by cation exchange and titration with standard sodium hydroxide. The pH of these solutions was adjusted to 4.5 or 6.5 by titration with standard sodium hydroxide. Precipitation of the rare earth hydroxide was a problem only in cerium solutions and measurements were made only at the lower pH. The supporting electrolyte at high ionic strength was sodium perchlorate.

Results

The attenuation of a plane progressive sound wave traversing a solution is given by the expression

$$I = I_0 \exp(-2\alpha x) \tag{1}$$

where I = sound intensity at distance x, I_0 = sound intensity at distance zero, and α = absorption coefficient for the solution. The assumption is made that the total experimentally measured absorption coefficient is the sum of the contributions from the chemical relaxation and from the classical solvent absorption α_s

$$\alpha = \alpha_{chem} + \alpha_s \tag{2}$$

Solvent absorption becomes critical when the overall absorption is small. In these cases, the vagaries of the instrument must be considered. In making these measurements, the solution and solvent were exchanged in quick succession in the reaction vessel at each frequency without readjusting the parallelism and tuning in the interim, thereby minimizing any contingent variation in α_s.

Before attempting to assign the relaxation due to perturbation of the complex formation equilibria, all other relaxations must be identified and, if possible, eliminated. Two interfering relaxations are possible in this study from (1) the dimerization of acetic acid[15] and (2) the perturbation of the hydrolysis equilibria.

$$Ln^{3+} + yOH^- \rightleftharpoons Ln(OH)_y^{(3-y)+} \tag{3}$$

A small relaxation was observed in dilute solutions of acetic acid around 5–10 kHz but was absent in acetic acid–sodium acetate mixtures at pH 4.5 and 6.5, although a relaxation has previously been reported at lower frequencies[16] around 20 kHz. No relaxation was observed in rare earth perchlorate solutions adjusted to pH 6.5 with standard sodium hydroxide and the possible interference from hydrolysis reactions was assumed to be absent. A further complicating feature in the application of eq 2 stems from the observed fact that the sound absorption in concentrated sodium perchlorate solutions is less than that in pure water.[17] For measurements at 2 M conditions the term α_s in eq 2 was therefore substituted by the measured α_{ClO_4} at all frequencies and the additivity of terms still assumed. A complete listing of experimental data has been deposited as Document No. 00617 with the ASIS National Auxiliary Publications Service.

The relaxation spectra of the aqueous acetates of La(III), Ce(III), Sm(III), and Dy(III) are shown in

(13) J. Reuben and D. Fiat, *Chem. Commun.*, 729 (1967).

(14) M. Eigen and L. DeMaeyer, "Technique of Organic Chemistry," Vol. VIII, Part 2, Interscience Publishers, New York, N. Y., Chapter 18.

(15) R. O. Davies and J. Lamb, *Quart. Rev.* (London), 11, 134 (1957).

(16) T. Yasunaga, H. Inove, and M. Miura, *J. Chem. Phys.*, 43, 2141 (1965).

(17) W. Rüfer, *Ann. Physik.*, 41, 301 (1942).

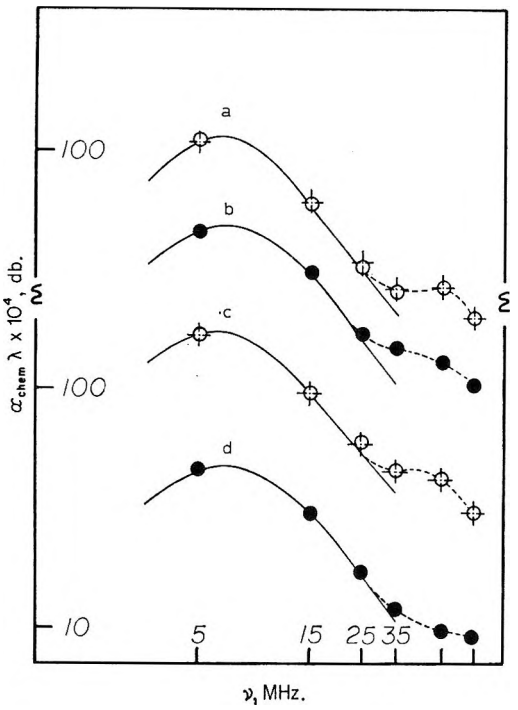

Figure 1. Excess sound absorption *vs.* frequency for (a) 0.03 *F* cerium acetate, pH 4.5, -¦- calculated double relaxation; (b) 0.01 *F* dysprosium acetate, pH 6.5; (c) 0.03 *F* samarium acetate, pH 6.5, -¦- calculated double relaxation; (d) 0.01 *F* lanthanum acetate, pH 6.5.

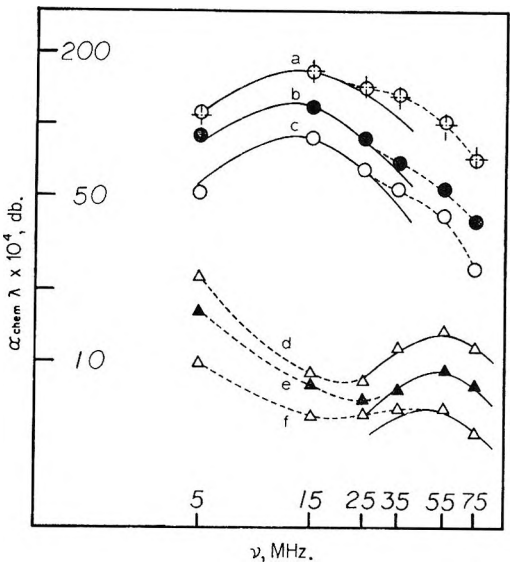

Figure 2. Excess sound absorption *vs.* frequency for (a) 0.035 *F* copper acetate, -¦- calculated double relaxation; ν_{III} = 13.2 MHz, $\alpha\lambda_{III} = 150 \times 10^{-4}$ db; ν_{II} = 55 MHz, $\alpha\lambda_{II} = 60 \times 10^{-4}$ db; (b) 0.35 *F* copper acetate, in 2 *M* $NaClO_4$. (c) 0.015 *F* copper acetate; (d) 0.03 *F* nickel acetate; (e) 0.023 *F* nickel acetate; (*f*) 0.015 *F* nickel acetate.

Figure 1. The solid lines in both figures are calculated single relaxation curves. Unlike the corresponding sulfates,[4] where the relaxation frequency varies with the cation, all of the spectra show a relaxation at 6 ± 0.5 MHz and a second relaxation which in some cases appears only as a shoulder on the low relaxation curve, in the frequency range 35–65 MHz. For the more dilute solutions the data can almost be fitted to a single relaxation within experimental error but for the more concentrated solutions there is real evidence for a double relaxation. In Figure 1, the experimental curve for samarium acetate at 0.03 *F* can be fitted to a theoretical double relaxation with the parameters ν_{III} = 6 MHz, $\alpha\lambda_{III} = 165 \times 10^{-4}$ db and ν_{II} = 65 MHz, $\alpha\lambda_{II} = 30 \times 10^{-4}$ db in the equation

$$\alpha\lambda_{chem} = \frac{2\alpha\lambda_{III}(\nu/\nu_{III})}{1 + (\nu/\nu_{III})^2} + \frac{2\alpha\lambda_{II}(\nu/\nu_{II})}{1 + (\nu/\nu_{II})^2} \qquad (4)$$

where the subscripts III and II refer to the low and high relaxations, respectively. There is apparently little coupling between the relaxations since $\nu_{II} \gg \nu_{III}$ and since the terms in eq 4 are additive. A single relaxation fit for the dilute solutions does not obviate the existence of a high-frequency relaxation; on the contrary, it means that the contribution is within the limits of experimental accuracy. In Figure 2, the double relaxation fit is shown for copper acetate at 0.035 *F*.

Comparing the amplitude and position of the higher relaxation with the corresponding nitrates,[8] this relaxation may safely be associated with acetate desolvation or the combined step of diffusion-controlled encounter and anion desolvation. Further credence is given to this assignment from the analogous relaxations in copper and nickel acetates, Figure 2, and more recently from a similar absorption which has been observed in magnesium and calcium acetates.[18] The disturbing feature of the sound absorption spectra is that the low-frequency relaxation is cation independent. Since a 1:1 complex is not formed exclusively,[19] the possibility exists that the low-frequency maximum is due to desolvation of a second acetate ion in forming a higher outer-sphere complex. However, it is apparent from the copper and nickel acetate systems that the low-frequency relaxation is very definitely dependent upon the cation. We have therefore proceeded on the assumption that the 6-MHz relaxation should be assigned to a cation desolvation step.

From the kinetic derivation[14] the relationship between the relaxation time τ_{ij}, or frequency ν_{ij}, and the rate constants for the slow step, cation desolvation, is

$$\tau_{ij}^{-1} = 2\pi\nu_{ij} = k_{ji} + \mathcal{L}[\Theta(C)]k_{ij} \qquad (5)$$

The function $\Theta(C)$ is introduced because the ion encounter reaction, which includes the equilibrium constants for the preceding steps, is bimolecular, and the form of the function changes depending upon which step

(18) N. Purdie, unpublished results.

(19) A. Sonesson, *Acta Chem. Scand.*, 12, 165, 1937 (1958).

Table I: Analysis of Samarium Acetate Solutions in 2 M $NaClO_4$ Media

$K_1 = 103$;[a] $K_2 = 17.5$[a]

Total metal (10^2 M^{-1})	Total ligand (10^2 M^{-1})	pH	$SmAc^{2+}$, 10^2 M^{-1}	$SmAc_2^+$, 10^2 M^{-1}	Sm^{3+}, 10^2 M^{-1}	Ac^-, 10^2 M^{-1}	$\mathcal{J}\Theta(C)$, M^{-1}	$\alpha\lambda_{III}$, 10^4db
3.0	9.0	6.5	1.67	1.07	0.26	6.22	0.77	173
2.0	6.0	6.5	1.27	0.44	0.29	4.25	0.72	80
1.0	3.0	6.5	0.60	0.14	0.26	2.24	0.49	45
5.4	2.68	4.0	1.61	0.09	3.97	0.35	0.71	48
0.9	2.68	4.5	0.53	0.12	0.25	1.29	0.51	60

[a] Values taken from ref 19.

in the mechanism is the slow step. Rate constants are customarily obtained from the linear plot of $2\pi\nu_{ij}$ *vs.* $\mathcal{J}[\Theta(C)]$ over a range of solution concentrations. The concentration variable was changed in a number of ways: by changing the pH of salt solutions; by adding metal perchlorates to solutions of acetic acid in appropriate proportions to change the ratio of the analytical concentrations of metal to acid, also studied as a function of pH; and by changing the ionic strength of the solution to 2 M in sodium perchlorate.

The systems could not be analyzed for concentrations of complex species in every case since the stability constants in the absence of supporting electrolyte are not known. For those samarium systems[19] at 2 M $NaClO_4$ the results of the analysis are given in Table I. Although $\mathcal{J}[\Theta(C)]$ is changed by almost a factor of 2, the lower relaxation frequency maximum is unchanged at 6 ± 0.5 MHz. This is clearly illustrated by the parallel lines in Figure 3, where the slope is equal to $-1/\nu^2_{III}$ in a plot of α_{chem}/ν^2 *vs.* α_{chem} according to the expression

$$\alpha_{chem}/\nu^2 = -(\alpha_{chem}/\nu^2_{III}) + A \qquad (6)$$

readily obtained by rearranging the equation for a single relaxation.[4] In this equation $A = 2\alpha\lambda_{III}c\nu_{III}$, where c is the velocity of sound, and in every case the intercept on the ordinate gives a value of A consistent with the experimental $\alpha\lambda_{III}$. One would conclude therefore that $k_{ji} \gg \mathcal{J}[\Theta(C)]\ k_{ij}$ and therefore that $k_{ji} = 2\pi\nu_{ij}$ or $3.7 \pm 0.3 \times 10^7$ sec^{-1}. The magnitude of the second term in eq 5 might therefore be decisive in assigning a mechanism to the substitution reaction. In other words, the calculated k_{ij} must not be too large that the relationship $k_{ji} \gg \mathcal{J}[\Theta(C)]\ k_{ij}$ no longer holds.

The results are unusual when compared to the other rare earth systems studied but are precisely what Maass[20] observed for zinc acetate. One might conclude that the role of acetate in complex formation is kinetically unique, except for the fact that in copper and cadmium acetate solutions[20] the relaxation frequency was observed to change with concentration. This dependence, however, was not observed for copper acetate in this work, Figure 2, and a possible explanation

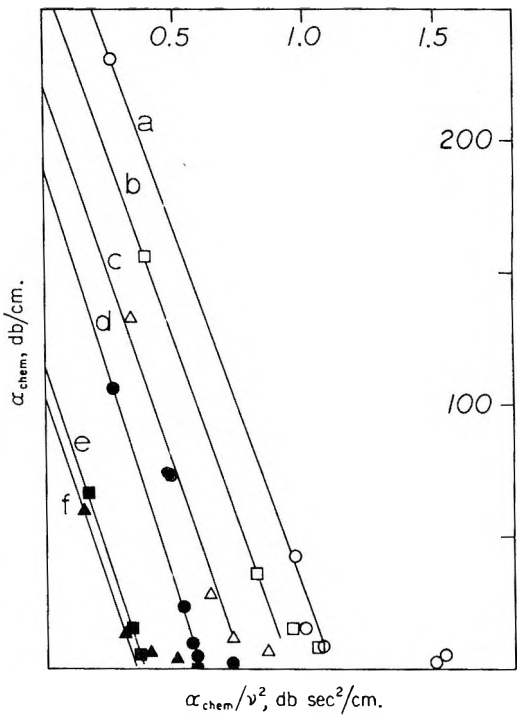

Figure 3. Graphical solution of the equation $\alpha_{chem}/\nu^2 = -(\alpha_{chem}/\nu^2_{III}) + A$ for (a) 0.03 F $SmAc_3$, pH 6.5, ν_{III} = 6 MHz; (b) 1.8×10^{-2} F $Sm(ClO_4)_3$ and 2.7×10^{-2} F acetate, pH 6.5, ν_{III} = 6 MHz; (c) 0.03 F $SmAc_3$ in 2 M $NaClO_4$, pH 6.5, ν_{III} = 5.9 MHz; (d) 0.02 F $SmAc_3$, pH 6.5, ν_{III} = 5.6 MHz. (e) 5.4×10^{-2} F $Sm(ClO_4)_3$ and 2.7×10^{-2} F acetate, pH 4, ν_{III} = 5.8 MHz. (f) 0.01 F $SmAc_3$, pH 6.5, ν_{III} = 5.9 MHz.

is that, as the concentration of salt was increased, the two relaxations converged into one. The relaxation would therefore *appear* to move to higher frequencies. That a similar situation did not occur for the rare earths and for zinc is apparent since the low-frequency maximum is further removed from the anion desolvation relaxation than it is for either copper or cadmium.

Discussion

Acetate in complexing with Nd(III) forms some inner-sphere complex,[21] it is likely that all rare earths

(20) G. Maass, *Z. Phys. Chem.* (Frankfurt am Main), **60**, 138 (1968).

(21) G. Choppin, D. E. Henrie, and K. Buijs, *Inorg. Chem.*, **5**, 1743 (1966).

behave similarly toward acetate, but the bonding is uncertain. A number of possibilities have been described[22] for various cations, including chelation. The ligand has been described as unidentate by Sonesson[19] and Grenthe[23] in thermodynamic studies. However, it must be pointed out that this was conceived prior to the studies and the fact that the acetate complexes are formed with an endothermic heat and a positive entropy which is large compared to the bidentate glycolate ligand[23] still leaves open the possibility that acetate is a bidenate ligand. Manning[24] has argued in favor of a bidentate interaction but in his model he considers the interaction to be that of an ion pair leaving the hydration sphere of the cation intact. Infrared spectroscopy cannot be used to determine the coordination of acetate because of the low symmetry of the anion. Moreover, the complexing process is complicated by the existance of higher complexes[19] with up to three acetates per cation. In our consideration of the origin of this low-frequency relaxation, the function $\mathcal{f}[\Theta(C)]$ in eq 5, which involves the sum of the equilibrium free ion concentrations, is of little consequence, since it does not contribute to a large variation in ν_{III} as the ratio of the concentrations of the complexed species is changed. However, the amplitude of the absorption, which is virtually unchanged when the ratio of $[SmAc^{2+}]$ to $[SmAc_2^+]$ is changed from 4:1 to 18:1, Table I, would suggest that higher complexation equilibria are not involved. This interpretation is not completely convincing principally because of the insensitivity of ν_{III} to $\mathcal{f}[\Theta(C)]$ and Swinehart's[6] suggestion that the formation of the bisacetatolanthanide is observed may be true.

An overall multistep mechanism, which includes chelation, has been discussed by Kustin, Pasternack, and Weinstock[25] and for the present case may be written

$$M^{3+} + Ac^- \underset{k_{21}}{\overset{k_{12}}{\rightleftharpoons}} W_2MW_1Ac^{2+} \qquad (I)$$

$$W_2MW_1Ac^{2+} \underset{k_{32}}{\overset{k_{23}}{\rightleftharpoons}} W_2M - Ac^{2+} \qquad (II)$$

$$W_2M - Ac^{2+} \underset{k_{43}}{\overset{k_{34}}{\rightleftharpoons}} MAc^{2+} \qquad (III)$$

where step I involves diffusion-controlled ion encounter and desolvation of the acetate ion, and W_1 and W_2 are the cation-coordinated water molecules which are successively substituted by the ligand. Either steps II and III are synchronous in which case the 6-MHz relaxation is not representative of a single relaxation, or (a) the first substitution is rate-controlling or (b) ring closure is rate-controlling.

Let us restrict our attention to the last two alternatives; the assumption is made that step I is very rapid compared to subsequent steps. For case (a) since τ_{23} is independent of $\mathcal{f}[\Theta(C)]$,[26] k_{23} is calculated from the relationships $K_T = K_{12}(1 + K_{23})$ and $K_{23} = k_{23}/k_{32}$, where K_T is the overall association constant.[19] The overall second-order forward rate constant $\vec{k} = K_{12}k_{23}$. K_{12}, the equilibrium constant for the first step, is not known from experiment but can be calculated[27] at zero ionic strength. A value of 34 is typical of 1:3 electrolytes but at higher ionic strength the value would be much less than this. A dilemma now arises in the treatment of the results in that K_T values are not known at zero ionic strength and K_{12} values cannot be calculated at high ionic strength. We have chosen the less speculative route and estimated the value of K_{12} at higher ionic strength. The results at 2 M conditions are given in Table II for a K_{12} value of 10. Both

Table II: Rate Constants for the First Substitution Mechanism

$K_{12} = 10$; $k_{32} = 3.7 \times 10^7$ sec^{-1}

Ion	K_T	K_{23}	k_{23}, sec^{-1}	$\vec{k}$, M^{-1} sec^{-1}
La	36	2.6	9.6×10^7	9.6×10^8
Ce	46	3.6	1.3×10^8	1.3×10^9
Sm	103	9.3	3.5×10^8	3.5×10^9
Dy	47	3.7	1.4×10^8	1.4×10^9

forward rate constants from this mechanism are inconsistent with experiment: k_{23} values are too large to satisfy the kinetic requirement that $k_{32} \gg \mathcal{f}[\Theta(C)] \cdot k_{23}$—the range in $\mathcal{f}[\Theta(C)]$ for samarium acetate is 0.5 to 0.8, and $\vec{k}$ for dysprosium acetate is an order of magnitude greater than the preliminary value for the overall rate of 9.2×10^7 M^{-1} sec^{-1} measured by temperature jump[6] at 12.5° and 0.2 M $NaClO_4$. The calculation gives a better correlation with experiment only when K_{12} is chosen to be greater than 10, for example when $K_{12} = 34$, $k_{23} = 1.4 \times 10^7$ sec^{-1}, and $\vec{k} = 4.7 \times 10^8$ M^{-1} sec^{-1}. Such a value for K_{12} is perhaps unrealistic at high ionic strength.

In case (b) an absolute solution cannot be obtained since the unknown parameter K_{23} is introduced. However, for the purposes of a comparison with the first mechanism the same value of $K_{12} = 10$ can be used. This leaves only K_{23} as an adjustable parameter. In the example illustrated in Table III, the three-step mechanism is more consistent with experiment. k_{34} is calculated from $K_T = K_{12}(1 + K_{23} + K_{23}K_{34})$ and $K_{34} = k_{34}/k_{43}$, and $\vec{k}$ from $\vec{k} = K_{12}K_{23}k_{34}$. The variation in k_{34} and $\vec{k}$ with K_{23} is shown in Table III for dysprosium

(22) S. P. Sinha, "Complexes of the Rare Earths," Pergamon Press, New York, N. Y., 1966, p 36.

(23) I. Grenthe, *Acta Chem. Scand.*, **18**, 283 (1964).

(24) P. G. Manning, *Can. J. Chem.*, **43**, 3476 (1965).

(25) K. Kustin, R. F. Pasternack, and E. M. Weinstock, *J. Amer. Chem. Soc.*, **88**, 4610 (1966).

(26) For the expansion of this function see ref 4.

(27) R. A. Robinson and R. H. Stokes, "Electrolyte Solutions," 2nd ed, Butterworth and Co., London, 1959, p 392.

Table III: Variation in k_{34} and $\vec{k}$ with K_{23} for the Second Substitution Mechanism for Dysprosium Acetate at 2 M

$K_T = 47$; $K_{12} = 10$; $k_{43} = 3.7 \times 10^7$ sec^{-1}

K_{23}	K_{34}	k_{34} sec^{-1}	$\vec{k}$, M^{-1} sec^{-1}
1	2.7	1.0×10^8	1.0×10^9
2	0.85	3.1×10^7	6.2×10^8
3	0.23	8.5×10^6	2.5×10^8

acetate. For a K_{23} value of 3, good agreement is obtained with the temperature-jump result[6] considering the temperature difference in the two methods and the kinetic requirement of a relaxation time insensitive to the concentration variable is satisfied. Once again a better correspondence between $\vec{k}$ values results if a value of K_{12} greater than 10 is used. A value of 3 is compatible with $K_{23} = 1$ obtained by Maass[20] for zinc acetate. The results for all of the salts are given in Table IV. Because of the extra stability of the

Table IV: Rate Constants for the Second Substitution Mechanism

$K_{12} = 10$; $k_{32} = 3.7 \times 10^7$ sec^{-1}

Ion	K_T	K_{23}	K_{34}	k_{34}, sec^{-1}	$\vec{k}$, M^{-1} sec^{-1}
La	36	2.3	0.13	4.8×10^6	1.4×10^8
Ce	46	3.0	0.20	7.4×10^6	2.2×10^8
Sm	103	7.5	0.24	8.9×10^6	2.7×10^8
Dy	47	3.0	0.23	8.5×10^6	2.5×10^8

samarium acetate complex, a larger K_{23} has to be used and as such is consistent with the K_{23} values calculated in the first mechanism.

Kinetically, there is good reason to believe that ring closure is the slow step in the formation of the acetate complexes. Apart from dysprosium, the overall rates are in fairly good agreement with those for the murexide and oxalate systems, Table V, where the ligands are indisputably bidentate. Swinehart[6] has already enlarged upon the discrepancy between acetate and anthranilate in complexing with the rare earths, and a possible explanation might lie in the fact that anthranilate is the only ligand of the four which has dissimilar donor atoms. It is evident that a number of other monodentate and chelating ligands should be examined with particular attention being given to the donor

Table V: Rates of Formation of Rare Earth Complexes

$\vec{k}$, M^{-1} sec^{-1}

Ion	Murexide[a]	Anthranilate[b]	Oxalate[c]	Acetate[d]
La	8.6×10^7	5.5×10^7	8.0×10^7	...
Ce	9.5×10^7	...	...	...
Sm	9.6×10^7	6.3×10^7	8.2×10^7	...
Dy	1.7×10^7	1.4×10^7	1.3×10^7	9.2×10^7

[a] $I = 0.1$ M KNO_3, 12°; ref 3. [b] $I = 0.2$ M $NaClO_4$, 12.5°; ref 5 and 6. [c] I not specified, 25°; ref 9. [d] Preliminary result at $I = 0.2$ M $NaClO_4$, 12.5°; ref 6.

atoms. The value of k_{34} for Dy(III) is well within the upper limit for acetate exchange set by the rate constant for water exchange, 6.3×10^7 sec^{-1}, obtained from preliminary ^{17}O relaxation studies,[13] and may indicate some stereospecificity in removing the water from the first hydration sphere. Using the rate constants for samarium acetate, a change in $\mathcal{F}[\Theta(C)]$ of approximately 0.2 produces a change in ν_{III} of 0.4 MHz, which exceeds the resolution capabilities of the method used to calculate ν_{III}, especially when a minimum of experimental points are available, and readily accounts for the fact that a constant ν_{III} is observed experimentally. In spite of the reproducibility of the relaxation frequency from one cation to another, the nonuniform dependence of specific rate constant on the reciprocal cation radius is apparently prevalent on the acetate system, although it should be emphasized that the trend has been imposed on the results by the equivalent trend in stability constant.

In conclusion there appear to be sufficient kinetic grounds to suggest that acetate in rare earth complexes is bidentate. A comparison with the results for zinc sulfate[20] shows the rate of formation of the zinc acetate complex to be considerably slower and there too chelation may occur. Considerably more work is required on unidentate and multidentate systems before this interpretation can be accepted and before it is even conceivable to use kinetic methods to establish a ligand coordination number on a particular metal ion.

Acknowledgment. We wish to acknowledge the financial assistance of the Research Corporation and the Research Foundation, Oklahoma State University. We are also grateful for the support of Victor Garza by the National Science Foundation.

The Thermal Decomposition of Magnesium Perchlorate and of Ammonium Perchlorate and Magnesium Perchlorate Mixtures

by R. J. Acheson and P. W. M. Jacobs

Department of Chemistry, University of Western Ontario, London, Ontario, Canada
(Received June 13, 1969)

The thermal decomposition of magnesium perchlorate (dehydrated prior to decomposition) and of mixtures of magnesium perchlorate with ammonium perchlorate (dehydrated during heating) have been investigated using the techniques of isothermal kinetics, differential thermal analysis (dta) and thermogravimetric analysis (tga). The thermal decomposition of magnesium perchlorate in the temperature range 336–438° yields mainly MgO *in vacuo* but under 740 torr of nitrogen some $MgCl_2$ is formed. The plots of fractional decomposition α against time t for the isothermal decomposition show a sharp break at $\alpha \sim 0.525$ at high temperatures; at low temperatures the break is indistinct. This break is associated with the formation of $Mg(ClO)_2$ in the postulated mechanism. Up to the break, the $\alpha(t)$ curves show that the reaction is at first acceleratory, then mildly decelerator. The activation energies associated with these first two stages are 58 ± 4 and 67 ± 4 kcal/mol, respectively, and these figures are identified in the mechanism with the fissioning of the first and second Cl–O bonds in the ClO_4^- anion. The addition of magnesium perchlorate to ammonium perchlorate accelerates the decomposition of the latter. It is postulated that this is due to the formation of a melt in which the decomposition of ClO_4^- anions leads to O^{2-} which act as proton acceptors, thus facilitating the decomposition of ammonium perchlorate. It is predicted from this mechanism that the Cl_2/HCl ratio in the products from the mixture will be larger than in the products from the decomposition of pure ammonium perchlorate, which is the experimental result.

I. Introduction

The thermal decomposition of magnesium perchlorate has been investigated as part of a continuing program on the decomposition of ammonium perchlorate and of additives which might affect the ammonium perchlorate decomposition rate. The thermal decomposition of barium perchlorate and of mixtures of ammonium perchlorate and barium perchlorate has been described recently.[1] There has been some previous work on the magnesium perchlorate decomposition, but a detailed study so far has been lacking. Dta of magnesium perchlorate hexahydrate and of magnesium perchlorate has been reported.[2,3] The hydrate shows endotherms indicative of partial loss of water followed by a pronounced endotherm at 244° which could be either fusion or hydrate dissolution. Comparison with the data of the dehydrated salt[3] proves it to be the latter (*i.e.*, magnesium perchlorate dissolving in its own water of crystallization) since anhydrous magnesium perchlorate does not melt even when heated to 600°. The bubbling observed by Gordon and Campbell[2] therefore refers either to loss of water or to decomposition of hydrolysis products. Gravimetric studies[4] showed a gradual loss of weight on heating magnesium perchlorate hexahydrate, the final product being MgO. Another study, however, showed[3] $MgO \cdot MgCl_2$ to be the product. This problem of the product distribution was considered by Markowitz,[5] who pointed out that the relative amounts of oxide and chloride in the product could depend on the composition of the gas phase if the equilibration reaction was sufficiently fast.

In a preliminary communication on the decomposition of several metallic perchlorates, Solymosi and Braun[6] described the kinetics as being hard to analyze. This they attributed to the occurrence of an intermediate; nevertheless, an activation energy of 44.4 kcal/mol was reported. Because magnesium oxide is known[7] to react with ammonium perchlorate to form the perchlorate and in view of our interest in the role of magnesium oxide as a catalyst for the ammonium perchlorate decomposition, a thorough investigation of the thermal decomposition of magnesium perchlorate was undertaken. When the experimental work had been completed and the data analyzed, Solymosi[8] published further details of his work on magnesium perchlorate. He, however, employed only pressure measurements whereas, as will emerge later, thermogravimetric techniques are to be preferred for magnesium perchlorate. Because of differences in the character of our $\alpha(t)$ curves (α = fraction decomposed in time

(1) R. J. Acheson and P. W. M. Jacobs, *Can. J. Chem.*, **47**, 3031 (1969).

(2) S. Gordon and C. Campbell, *Anal. Chem.*, **27**, 1102 (1955).

(3) A. A. Zinov'ev and L. J. Cludinova, *Zh. Neorg. Khim.*, **1**, 1722 (1956).

(4) G. G. Marvin and L. B. Woolaver, *Ind. Eng. Chem., Analyt. Ed.*, **17**, 474 (1945).

(5) M. M. Markowitz, *J. Inorg. Nucl. Chem.*, **25**, 407 (1963).

(6) F. Solymosi and Gy. Braun, *Acta Chim. Acad. Sci. Hung.*, **52**, 1 (1967).

(7) F. G. Smith and V. R. Hardy, *Z. Anorg. Allg. Chem.*, **223**, 1 (1935).

(8) F. Solymosi, *Acta Chim. Acad. Sci. Hung.*, **57**, 35 (1968).

t), kinetic analysis, activation energies and discussions of mechanism, we felt it worthwhile to present the data reported in this paper, which also includes consideration of ammonium perchlorate + magnesium perchlorate mixtures.

II. Experimental Procedure

The materials used were magnesium perchlorate hexahydrate (Reagent Grade) and ammonium perchlorate (Certified Reagent) both from Fisher. The magnesium perchlorate hexahydrate was recrystallized twice from distilled water. A Cahn electrobalance was used for thermogravimetric analysis. The kinetics of decomposition at constant temperature were followed by dropping pellets or single crystals of magnesium perchlorate *in vacuo* into a reaction vessel situated in an aluminum block furnace, the temperature of which was controlled electronically to ±0.2°, and following the pressure of gas (volatile at −195°) evolved using McLeod gauges. The salt was dehydrated *in vacuo* at 230° in the same apparatus, using a small auxiliary furnace. This procedure was found to be essential since preliminary experiments in which magnesium perchlorate hexahydrate was dehydrated *in vacuo* on the electrobalance and then exposed to the atmosphere for a few seconds showed that magnesium perchlorate took up approximately 1 mole of water per mole during this brief exposure. In order to follow the kinetics by weight loss, the Cahn balance was modified so that the specimen could be dehydrated *in situ* and then the reaction vessel lowered into the decomposition furnace while a pumping vacuum was maintained. The weight-loss experiments could be performed in various atmospheres, usually 740 Torr of nitrogen (99.999% pure, from Union Carbide).

Both single crystals and pellets made from ground magnesium perchlorate hexahydrate were used. Their mass lay in the range 6–16 mg. Major deformation of samples occurred during dehydration and both pellets and crystals disintegrated into powder prior to thermal decomposition. Melting, however, did not occur.

Mixtures of ammonium perchlorate and magnesium perchlorate hexahydrate were crushed together, well mixed, and stored in a desiccator. These mixtures contained 1.75, 6.6, 20, 50, and 80 mol % magnesium perchlorate. Samples 4–9 mg in mass were outgassed for 1 hr *in vacuo* at room temperature, 740 Torr of nitrogen was introduced to suppress sublimation of ammonium perchlorate, and the samples were then brought rapidly to the decomposition temperature without prior dehydration. (Complete dehydration of magnesium perchlorate at temperatures low enough to prevent decomposition of ammonium perchlorate is not possible.) The kinetics of isothermal decomposition was studied by weight loss. These mixtures were also subjected to tga and dta without further pretreatment.

III. Thermogravimetry of MP

Magnesium perchlorate hexahydrate decomposed *in vacuo* <230° to yield the anhydrous salt which was stable in the range 230–320°. The hydrate could not be dehydrated by pumping alone at room temperature although there was a small loss in weight (1%) which could be associated with the loss of surface moisture, for the hexahydrate proved to be very hygroscopic. The yield of magnesium perchlorate following dehydration was 67.1%, which may be compared with a theoretical yield of 67.4%.

Decomposition of the anhydrous salt occurred >330° (390–440° was range by tga) *in vacuo* or under 740 Torr of N_2. The yield of solid product from tga *in vacuo* was 17.98% of the weight of magnesium perchlorate, which may be compared with a theoretical yield for pure MgO of 18.06%. Thus the solid product was virtually all MgO under these conditions. The yield of solid product from decomposition under 740 Torr was 20.2%, showing that a small percentage of the chloride was formed under a nitrogen atmosphere.

Accurate measurements of the product yield *in vacuo* from isothermal measurements are complicated by concurrent sublimation. Under the conditions of tga (linear rise in T) the effect of this was insignificant. For example, the yield of solid product from three such isothermal runs was 14.7 ± 0.6% (*cf.* 17.98% from tga). As sublimation increased the yield of oxygen decreased but a quantitative correlation between sublimation and the gaseous product yield was not obtained. Sublimation was suppressed effectively completely by 740 Torr nitrogen. In one experiment simultaneous pressure measurements and weight loss measurements were made as the temperature increased at a linear rate. It was found that the weight loss and pressure increase were proportional, showing that under these conditions the product distribution is independent of temperature and of α (for $\alpha < 0.5$).

IV. Kinetics of Thermal Decomposition of Magnesium Perchlorate

Pressure Measurements. Magnesium perchlorate was found to decompose *in vacuo* in the temperature range 418–442° at a conveniently measurable rate to yield an irreproducible amount of oxygen because of concurrent sublimation. The final pressure p_f evolved (after 15 hr) was taken as a measure of complete decomposition and values of α were calculated from p/p_f. $\alpha(t)$ plots showed a brief acceleratory period followed by a deceleratory period up to complete reaction. The power law

$$\alpha = k_1 t^3 \qquad (1)$$

gave an approximate representation of the data in the range $0 < \alpha < \sim 0.1$ though rate constants were irreproducible. Data in the range $0.04 < \alpha < 0.33$ fitted the contracting volume expression

$$R_3(\alpha) \equiv 1 - (1 - \alpha)^{1/3} = k_2 t \qquad (2)$$

though the rate constants k_2 were irreproducible and fell well below the line through the point on the Arrhenius plot for similar rate constants from weight loss measurements. The data for $\alpha > 0.5$ were irreproducible and could not be fitted by any known kinetic equation.

Weight Loss Measurements. The thermal decomposition of MP *in vacuo* showed the same features as indicated above. The reaction was therefore followed under 740 Torr of nitrogen. This suppressed sublimation without apparently altering the rate of decomposition. Typical $\alpha(t)$ curves are shown in Figure 1. The noteworthy features are an initial acceleratory period ($\alpha < \sim 0.1$) followed by a gradual deceleratory period which merges into the final decay period during which the rate is much slower. The transition between the second and third stages is most pronounced at high temperatures (*e. g.*, run 1 in Figure 1) when it appears to take place at $\alpha \simeq 0.56$. The form of these curves suggests that decomposition proceeds *via* an intermediate with the original magnesium perchlorate all consumed by the time the marked change in rate occurs. At lower temperatures the second and third stages merge, with the transition much less well defined.

The power law (1) again fitted the data in the range $0.01 < \alpha < 0.10$ (Figure 2) and the results showed satisfactory reproducibility. Rate constants are given in Table I. The Arrhenius parameters were $E = 58.1$ kcal/mol and log $(A/\text{sec}^{-1}) = 15.6$. This brief acceleratory period was followed by a deceleratory period, stage II, which obeyed eq 2 for $0.04 < \alpha < 0.27$ (Figure 3). These rate constants again showed satisfactory reproducibility and the values of E, 66.7 kcal/mol, and of log (A/sec^{-1}), 17.8, suggest that the chemical processes occurring during the first and second stages are probably rather similar.

Table I: Experimental Rate Constants and Arrhenius Parameters for the Thermal Decomposition of Magnesium Perchlorate

	Stage I		Stage II	
T, °C	$-\log (k_1/\text{min}^{-1})$	α range	$-\log (k_2/\text{min}^{-1})$	α range
407	1.28	0.007–0.167	1.88	0.08–0.25
400	1.38	0.016–0.108	2.04	0.04–0.29
380	2.30	0.020–0.140	Did not obey eq 2	
392	1.58	0.014–0.107	2.33	0.04–0.30
377	2.13	0.004–0.149	2.81	0.04–0.22
377	Did not obey eq 1		3.05	0.02–0.19
377	1.99	0.016–0.079	2.81	0.04–0.32
355	2.65	0.007–0.074	3.61	0.07–0.22
336	3.48	0.003–0.051	Run discontinued	

Arrhenius parameters	log (A/sec^{-1})	E, kcal/mol
Stage I	15.6 ± 1.5	58.1 ± 4.4
Stage II	17.8 ± 1.2	66.7 ± 3.6

The data for stage III were found to be fitted approximately by eq 2 in the range $0.48 < \alpha < 0.75$. The rate constants for stage III were constant, independent of temperature, in the range 377–422°.

V. Kinetics of Thermal Decomposition of Magnesium Perchlorate and Ammonium Perchlorate

Reactant Containing 1.75 Mol % Magnesium Perchlorate. This mixture contained 5% by weight of magnesium perchlorate hexahydrate and therefore 1.6% of water. Dehydration was completed during the warm-up period. Decomposition occurred at a convenient rate in the range 291–343° and was entirely deceleratory. The kinetics obeyed the same equation as was found[9] to fit the thermal decomposition of pure ammonium perchlorate at these temperatures, namely

$$R_2(\alpha) \equiv 1 - (1 - \alpha)^{1/2} = k_3 t \qquad (3)$$

from the time of attainment of temperature equilibrium ($\alpha \sim 0.1$) up to $\alpha = \sim 0.8$. The reaction rate was slightly faster than for pure ammonium perchlorate but the activation energy was 43 kcal/mol compared to 30.6 kcal/mol for pure ammonium perchlorate (Table II).

Table II: Experimental Rate Constants and Arrhenius Parameters for the Thermal Decomposition of Mixtures of Ammonium Perchlorate and Magnesium Perchlorate. k_3 Was Determined by Fitting the Data to Eq 3 and k from the First-Order Equation

1.75 mol % $Mg(ClO_4)_2$		6.6 mol % $Mg(ClO_4)_2$	
T, °C	$-\log (k_3/\text{min}^{-1})$	T, °C	$-\log (k/\text{min}^{-1})$
343.5	1.33	318	1.11
333	1.85	317	1.28
317	2.24	315.5	1.28
310	2.26	292	2.01
300	2.58	287.5	2.03
291	2.89	286.5	2.14

mol % of $Mg(ClO_4)_2$	log (A/sec^{-1})	E, kcal/mol
1.75	12.2 ± 1.5	43.4 ± 4.0
6.6	13.8 ± 1.0	45.2 ± 2.7

Reactant Containing 6.6 Mol % Magnesium Perchlorate. This mixture contained 20% by weight of magnesium perchlorate hexahydrate or 6.6% water. Dehydration was generally complete by the time thermal equilibrium was attained. The temperature range of the reaction was 286–318°; the kinetics were deceleratory and fitted the first-order rate equation in the range $0.27 < \alpha < 0.89$. The activation energy calculated was 45 kcal/mol. The reaction rate was faster by a factor of about 6 than that for mixtures containing 1.75 mol %

(9) P. W. M. Jacobs and A. Russell-Jones, *J. Phys. Chem.*, 72, 202 (1968).

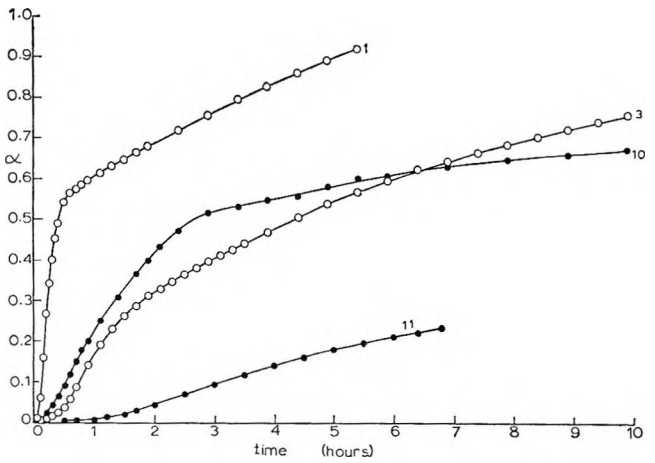

Figure 1. Fractional decomposition of magnesium perchlorate *vs.* time. Run numbers on curves denote: 1, 406.9° *in vacuo;* 3, 377.2° *in vacuo;* 10, 377.2° under 740 Torr of N_2; 11, 354.7° under 740 Torr of N_2.

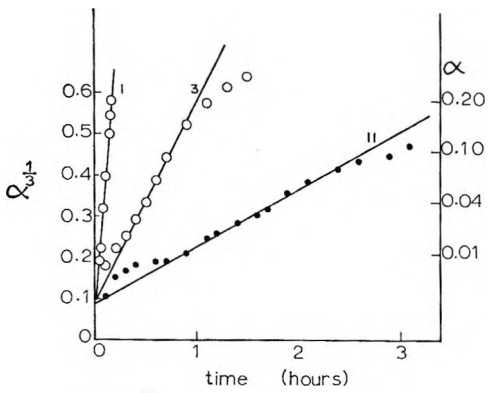

Figure 2. Plots of $\alpha^{1/3}$ *vs.* t for the first stage of the thermal decomposition of magnesium perchlorate for three of the runs shown in Figure 1.

magnesium perchlorate and the kinetics did not obey eq 3. The reaction rate for $\alpha > 0.9$ was slower, and rate constants derived from eq 3 for $\alpha > 0.9$ were comparable with those derived from the same equation from data for pure ammonium perchlorate. The final weight of reactant was 12.5 ± 0.5% of the initial weight taken, suggesting that the residue from thermal decomposition is mostly magnesium perchlorate (calcd 11.2%).

Reactant Containing 20 Mol % Magnesium Perchlorate. This mixture contained 41.1% magnesium perchlorate hexahydrate or 13.4% water. Nevertheless, the hexahydrate was dehydrated before the main reaction occurred at ~273°. The reaction virtually stopped after a loss in weight corresponding to $\alpha \simeq 0.6$. Although the data obeyed first-order kinetics approximately in the range $0.14 < \alpha < 0.44$, the fit was not considered good enough to make the determination of the activation energy a meaningful exercise. The examination of mixtures with a higher magnesium perchlorate hexahydrate content was therefore confined to tga and dta.

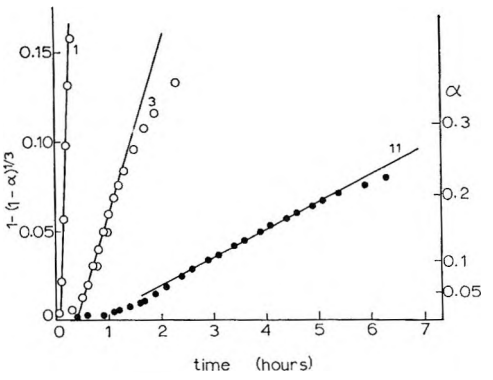

Figure 3. Plots of the function $1 - (1 - \alpha)^{1/3}$ *vs.* t for three of the runs shown in Figure 1.

VI. Tga and Dta of Mixtures of Magnesium Perchlorate Hexahydrate and Ammonium Perchlorate

Dta traces for runs on the five mixtures as well as for pure ammonium perchlorate and magnesium perchlorate are displayed in Figure 4. The shift in the reaction temperature to lower temperatures with increasing magnesium perchlorate hexahydrate concentration, up to 50 mol %, is clearly shown. The sharp exotherm at 331° is superimposed on the general decomposition exotherm and appears to be associated with solidification, but clear evidence for melting is not apparent in the dta curves. The solidification exotherm was not always observed at higher concentrations of magnesium perchlorate either, although it was in some runs: evidently the dta apparatus used was not well adapted to recording rapid temperature changes. Tga of the 6.6 mol % mixture showed the following features. (This sample weighed 8.25 mg and should therefore have contained 0.45 mg of H_2O, 6.87 mg of ammonium perchlorate, 0.92 mg of magnesium perchlorate, and should yield a final residue of ~0.1 mg of MgO.) (i) A weight loss of 0.37 mg occurred in the temperature range 130–274°. This corresponds to dehydration; the following three stages refer to thermal decomposition of ammonium perchlorate. (ii) A slow reaction occurred in the range 278–329°. This accounted for 1.88 mg or 27% of the ammonium perchlorate present and may be interpreted as the normal low-temperature decomposition of ammonium perchlorate.[10] (iii) In the range 332–358° a reaction occurred at a rate $-\mathrm{d}(w/w_0)/\mathrm{d}t = 0.137\ \mathrm{min}^{-1}$, where w_0 = initial weight and w is the weight at time t. This reaction accounted for 3.6 mg or 53% of the ammonium perchlorate and appears to be the catalyzed high-temperature decomposition of ammonium perchlorate, a conclusion which is substantiated by the fact that interpolation of the plot of log $[\mathrm{d}(w/w^0)/\mathrm{d}t]_{max}$ *vs.* T^{-1} for isothermal experiments yields the same rate at 340°. (iv) The reaction slowed down slightly at 363° and this was succeeded by a very rapid

(10) P. W. M. Jacobs and A. Russell-Jones, *AIAA J.*, **5**, 829 (1967).

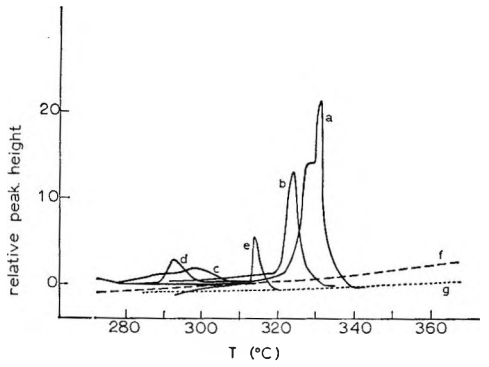

Figure 4. Temperature of decomposition of ammonium perchlorate and magnesium perchlorate mixtures from dta. The temperatures corresponding to the peak heights are, for the given amounts of magnesium perchlorate hexahydrate, (a) 1.75 mol %, 331°; (b) 6.6 mol %, 324°; (c) 20 mol %, 298°; (d) 50 mol %, 293°; (e) 80 mol %, 314°. (f) and (g) are dta traces for pure ammonium perchlorate and pure magnesium perchlorate, respectively.

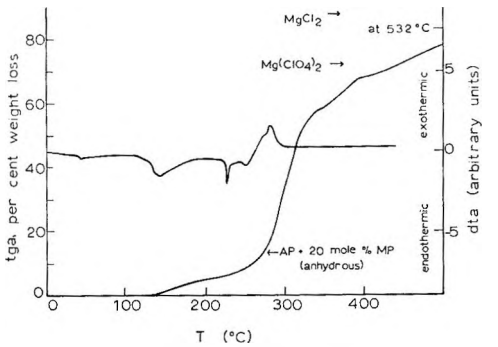

Figure 5. Superimposed dta and tga traces for an ammonium perchlorate and magnesium perchlorate mixture containing 20 mol % magnesium perchlorate. The arrows show the % weight loss which would correspond to the formation of anhydrous magnesium perchlorate and ammonium perchlorate, of magnesium perchlorate alone (with complete decomposition of ammonium perchlorate), and of $MgCl_2$ (MgO is off scale).

reaction at 363° ($-d(w/w_0)/dt = 2.5$ min^{-1}) accounting for 1.24 mg or 12% of the ammonium perchlorate. Thus some 8% of the ammonium perchlorate is not yet accounted for. (v) The residue from (iv) was stable up to 440° when decomposition occurred up to >600°. The final yield was 0.38 mg showing that some reactant (magnesium perchlorate) still remained.

Superimposed tga and dta traces are shown for the mixtures containing 20, 50, and 80 mol % magnesium perchlorate hexahydrate in Figures 5, 6, and 7. The dta trace in Figure 5 shows two stages of dehydration of magnesium perchlorate hexahydrate, the orthorhombic → cubic phase change in ammonium perchlorate, followed by exothermic decomposition of ammonium perchlorate. This interpretation of the thermal events is supported by the evidence from tga. Evidently the catalyzed decomposition commences before dehydration is quite completed (note the arrow corresponding to

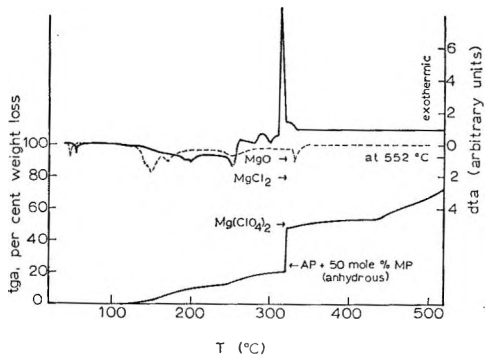

Figure 6. Superimposed dta and tga traces for an ammonium perchlorate and magnesium perchlorate mixture containing 50 mol % magnesium perchlorate. There was no further weight change above 552°, corresponding to formation of MgO. The dashed line shows the dta of pure magnesium perchlorate.

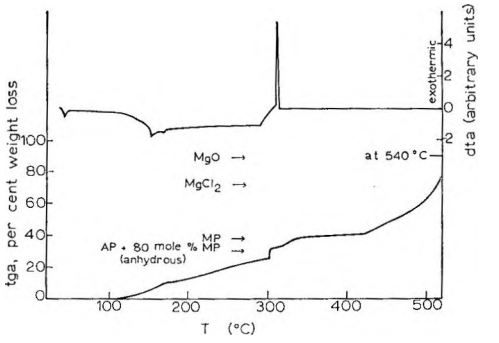

Figure 7. Superimposed dta and tga traces for an ammonium perchlorate and magnesium perchlorate mixture containing 80 mol % magnesium perchlorate.

formation of anhydrous magnesium perchlorate). The decomposition of ammonium perchlorate becomes very rapid following dehydration and then slows down after a temperature of 330° is attained.

The superimposed traces for the mixture containing 50 mol % magnesium perchlorate hexahydrate show broadly similar features. The first two endotherms represent dehydration. The second of these overlaps the ammonium perchlorate phase change which is succeeded by a further dehydration endotherm in the region of 250° (these assignments are being made by comparison with the previously determined dta curves for the pure components; that for magnesium perchlorate hexahydrate is shown in Figure 6 as a dashed line). There is evidence for a very sudden reaction in both the dta and tga traces. The per cent weight loss shows that rapid decomposition commences just before dehydration is complete and that the final product, when all the ammonium perchlorate is consumed, corresponds closely to magnesium perchlorate. Above 430°, decomposition of magnesium perchlorate occurs, a weight loss corresponding to MgO being reached at 552°.

The same features are shown by the 80% mixture except that the weight loss during the rapid reaction is smaller and the phase change is not seen, owing to the

smaller concentration of ammonium perchlorate. Decomposition of magnesium perchlorate starts at ~420° and is complete to MgO at 540°.

VII. Discussion

There are differences of opinion in the literature[3-5] as to what the decomposition products of magnesium perchlorate are, namely MgO, $MgCl_2$, or a mixture. Markowitz[5] has discussed the thermodynamics of perchlorate reactions and has concluded that magnesium perchlorate decomposes to $MgCl_2$ but that O_2 gas then reacts with the $MgCl_2$ to produce MgO. The free energies of formation of MgO and $MgCl_2$ are equal at 427° so that $\Delta G°$ for the reaction

$$MgO(s) + Cl_2(g) = MgCl_2(s) + {}^1/_2O_2(g) \qquad (4)$$

is −0.87 kcal/mol at the O_2 and Cl_2 partial pressures which would result from complete decomposition of magnesium perchlorate to MgO, the observed product from tga *in vacuo*. From Markowitz' data we find that $\Delta G°(MgCl_2) - \Delta G°(MgO)$ varies from −0.7 to +0.1 kcal/mol in the temperature range of interest (600–710°) so that the formation of pure MgO is predicted, if the thermodynamic data are accurate and equilibrium is established, since to form $MgCl_2$ would require a $\Delta G°$ more negative than −0.87 kcal/mol at 700°. *In vacuo* we do find the product to be pure MgO but under conditions hardly favoring the establishment of thermodynamic equilibrium. Under 740 Torr of N_2, the diffusion of product gases away from the solid reactant will be many orders of magnitude slower and there is a better chance of establishing equilibrium. We find approximately 4 mol % of $MgCl_2$ from tga under these conditions, corresponding to a calculated $\Delta G°$ of −0.8 kcal/mol at 600°. Markowitz' value[5] is −0.7 kcal/mol; the agreement is probably within the accuracy of the data, especially as the tga result does not refer to a fixed temperature.

The importance of these considerations is that they tell us that MgO is formed directly as a result of the reaction mechanism and that conversion to a small amount of chloride is a result of equilibration. This is in contrast to barium perchlorate[1] where $BaCl_2$ is formed and is the stable product. If $MgCl_2$ were formed as the decomposition product of magnesium perchlorate and converted to MgO by reaction with O_2, then tga *in vacuo* would give a smaller yield of MgO, and not a larger yield, as found experimentally.

The form of the $\alpha(t)$ curves (Figure 1) suggests that the decomposition of magnesium perchlorate involves at least one intermediate.

The formation of MgO directly implies that the last kinetic step is the bimolecular decomposition of ClO^- ions

$$2ClO^- \longrightarrow Cl_2 + O^{2-} + O \qquad (5)$$

The weight loss accompanying the formation of ClO^- from ClO_4^- corresponds to $\alpha = 0.525$; that corresponding to reaction step 5 is 0.475. Figure 1 shows that the break in the $\alpha(t)$ curves at high temperatures is close to $\alpha = 0.525$. We conclude, then, that the decomposition of magnesium perchlorate occurs in two main stages which are well separated at high temperatures and which comprise, respectively, the formation and subsequent decomposition of hypochlorite.

There are several factors which favor the conclusion that the rate of the last stage (decomposition of ClO^-) is controlled by the rate at which the gaseous products can diffuse away from the reaction centers. The reaction rate is approximately constant over a wide temperature range leading to an apparent activation energy of zero. This is illustrated, for example, by runs 1 and 3 in Figure 1 which show almost the same rate for the final stage and yet the reaction temperatures differ by almost 30°. Furthermore, for at least some runs the kinetics appeared to be of zero order. If Cl_2 can escape only by slow diffusion then a back-reaction will be encouraged. If this is

$$Cl_2 + O^{2-} \longrightarrow 2Cl^- + O \qquad (6)$$

$$O + Cl^- \longrightarrow ClO^- \qquad (7)$$

then the slowness of the final stage will be accounted for.

The formation of ClO^- from ClO_4^- is likely to be itself a multistage process since the splitting off of three O atoms at once from a ClO_4^- ion is unlikely. A possible sequence is

$$ClO_4^- \longrightarrow ClO_3^- + O \qquad (8)$$

$$ClO_3^- \longrightarrow ClO_2^- + O \qquad (9)$$

$$ClO_2^- \longrightarrow ClO^- + O \qquad (10)$$

$$O + O + M \longrightarrow O_2 \qquad (11)$$

The first of these reactions represents a fractional decomposition of $\alpha = 0.175$ and this corresponds reasonably well with the end of the acceleratory period and the onset of the first decay period. A reasonable conclusion that from the acceleratory nature of the first stage is that a mild chain reaction similar to that postulated[1] for the barium perchlorate decomposition operates, so that O atoms liberated in (8) attack perchlorate ions

$$ClO_4^- + O \longrightarrow ClO_3^- + O_2 \qquad (12)$$

being regenerated by further decomposition of ClO_3^-. The power law $\alpha \propto t^3$ would then be an approximate empirical representation of this acceleratory process. It is likely that the next stage of the decomposition, $ClO_3^- \rightarrow ClO_2^- + O$, overlaps the first stage to some extent but the situation is complicated by the possibility of the reverse reaction $ClO_2^- + O \rightarrow ClO_3^-$. Once the decomposition of $ClO_4^- \rightarrow ClO_3^-$ is completed, the next stage of reaction can be envisaged as initiating primarily at the surface of the $Mg(ClO_3)_2$ particles and then

propagating inward, if step 9 is reversible. There is good evidence that $Ba(ClO_2)_2$ disproportionates[11] to the chlorate and chloride and if $Mg(ClO_2)_2$ behaves somewhat similarly, $Mg(ClO_3)_2$ will only decompose readily where the O atoms can escape easily. In the case of the magnesium salts, however, the hypochlorite rather than the chlorate and chloride mixture,[1] appears to be the important intermediate.

Relevant is the fact that magnesium perchlorate hexahydrate contains initially 34% by weight of water and the crystal becomes very broken up during dehydration. Thus O atoms can escape much more readily than in the comparable case of barium perchlorate, and so the back-reactions of ClO_3^- to ClO_4^- can be expected to be less important in magnesium perchlorate than they are in barium perchlorate. However, reaction 9 should be reversible; otherwise the kinetics would be expected to obey a first-order law rather than the contracting volume equation.

The activation energies for the first two stages ($ClO_4^- \rightarrow ClO_3^-$ and $ClO_3^- \rightarrow ClO^-$) are 58 and 67 kcal/mol. These are close to the value expected for the fission of a Cl–O bond, namely[12] 64.3 kcal/mol. The kinetics are thus dominated by the initial steps 8 and 9. The greater stability of barium perchlorate with respect to magnesium perchlorate may be due to the fact that barium perchlorate goes through a phase change[1] at about the temperature at which magnesium perchlorate decomposes: this recrystallization process may help to remove some of the strain and disorder resulting from dehydration and thus make it harder to initiate the reaction.

Magnesium Perchlorate + Ammonium Perchlorate. The decomposition of ammonium perchlorate and magnesium perchlorate mixtures can be understood in terms of a simple hypothesis that magnesium perchlorate is capable of initiating the decomposition of ammonium perchlorate. Relatively small amounts of magnesium perchlorate are effective as shown by the values in Table III. In the detailed description of the 6.6 mol % tga run, it was emphasized that the normal low-temperature decomposition of ammonium perchlorate occurred first: thus it is the high-temperature ammonium perchlorate decomposition which is most susceptible to catalysis. At high magnesium perchlorate concentrations, however, the low-temperature reaction is eliminated (under tga conditions) and the sudden reaction which is shown in Figures 6 and 7 represents decomposition of virtually all the ammonium perchlorate present. At low catalyst concentrations the kinetics obey the same equation as does pure ammonium perchlorate but at higher concentrations the kinetics become first order and then rather ill-defined. The very sharp exotherms shown in the dta traces in Figures 5–7, which are indicative of rapid chemical reaction, are confirmed by tga; although definite evidence of melting is not generally present in the dta traces, the rapidity of the reaction suggests very strongly that the mixtures do melt. If this is indeed so then the following mechanism for the catalyzed reaction can be formulated. The high-temperature decomposition of ammonium perchlorate involves[10] proton transfer from NH_4^+ to ClO_4^- ions giving $HClO_4$ which decomposes and oxidizes the ammonia which is liberated in the proton transfer process. Catalysis implies the substitution of a more efficient process. Present in the melt will be Mg^{2+}, ClO_4^-, and NH_4^+ ions. The known decomposition product of $Mg(ClO_4)_2$ is MgO. Thus if the decomposition of ClO_4^- ions is facilitated in the melt (for example, by the ease with which O atoms can escape) then oxide ions will result by reactions which are stoichiometrically equivalent to

$$2ClO_4^- = Cl_2 + O^{2-} + 3^1/_2O_2 \qquad (13)$$

These oxide ions will form very efficient proton acceptors

$$2NH_4^+ + O^{2-} \longrightarrow H_2O + 2NH_3 \qquad (14)$$

The net result of (13) and (14) is the decomposition of 2 mol of ammonium perchlorate. Since Cl_2 is produced here from the decomposition of ClO_4^- ions rather than from $HClO_4$, it is predicted that, for the catalyzed reaction, the Cl_2/HCl ratio should be much higher than for the uncatalyzed reaction. This is precisely what was found[13] for the products from ammonium perchlorate + ZnO (which, because it also promotes melting, should behave similarly to MgO in this respect). The product when all the ammonium perchlorate has gone will be (resolidified) magnesium perchlorate, as found experimentally (Figures 6 and 7).

Table III: The Dependence of the Maximum Decomposition Rate $[-d(w/w_0)/dt]_{max}$ on the Composition of Ammonium Perchlorate and Magnesium Perchlorate Mixtures at 273°

mol % magnesium perchlorate	$[-d(w/w_0)/dt]_{max}$, min^{-1}
0	1.8×10^{-4}
1.75	5.9×10^{-4}
6.6	1.2×10^{-3}
20.0	7.9×10^{-2}

Furthermore, it is now easy to understand on the basis of this mechanism why MgO and ZnO[14] are such good catalysts for the ammonium perchlorate decomposition. Some surface reaction occurs forming mag-

(11) F. Solymosi and T. Bansagi, *Acta Chim. Acad. Scien. Hung.*, **56**, 251 (1968).

(12) D. D. Wagman, W. H. Evans, I. Halow, V. B. Parker, S. M. Bailey, and R. H. Schumm, "Selected Values of Chemical Thermodynamic Properties," National Bureau of Standards Technical Note 270–1, U. S. Government Printing Office, Washington, D. C., 1965.

(13) L. F. Shmagin and A. A. Shidlovskii, "Research in the Field of Chemistry and Technology of Mineral Salts and Acids," Akad. Nauk SSSR, 1965, pp 112–114.

(14) P. W. M. Jacobs and H. M. Whitehead, *Chem. Rev.*, **69**, 551 (1969).

nesium perchlorate, probably by reaction of the oxide with $HClO_4$ from the ammonium perchlorate, and then a melt of ammonium perchlorate and magnesium perchlorate forms in which the oxide steadily dissolves as O^{2-} ions are removed by (14). This mechanism thus explains the long established use[7] of ammonium perchlorate to form magnesium perchlorate from MgO and the fact that the formation of $Zn(ClO_4)_2$ has been confirmed in the catalysis of the ammonium perchlorate decomposition by ZnO.[15]

It is difficult to assess how essential to the reaction is the formation of a melt. There is, in fact, no real evidence from dta that melting occurs. However, this may be taken to imply that the whole mixture does not form a molten phase; partial melting at the interface between the two materials is not excluded by the dta evidence. The primary evidence would appear to be (i) the fact that the decomposition of ClO_4^- occurs at a much faster rate in the mixture of magnesium perchlorate with ammonium perchlorate than it does in the pure magnesium perchlorate and (ii) the fact that the addition of PbO, ZnO, or CdO to ammonium perchlorate promotes melting.[15] Thus although total melting of the reactants evidently is not a prerequisite for reaction, partial melting at the magnesium perchlorate–ammonium perchlorate interface probably does occur and has the effect of greatly accelerating the decomposition of ammonium perchlorate, as outlined above.

Barium perchlorate is not a catalyst for the ammonium perchlorate decomposition[1] and this is also easily understood in terms of our mechanism, for barium perchlorate decomposes to form the chloride, not the oxide, and so does not form a proton acceptor.

Acknowledgment. We are indebted to the National Research Council of Canada for their support of this work.

(15) A. V. Boldyreva and V. N. Mozzhova, *Kinet. Katal.* **7**, 734 (1966).

Some Electronic Properties of Solutions in Solid Matrices

by O. E. Wagner and W. E. Deeds

The University of Tennessee, Knoxville, Tennessee 37916 *(Received July 8, 1969)*

It has been found that salts together with a little solvent imbedded in an insulating material provide some very interesting electrical characteristics as well as a promising method of obtaining molecular parameters. The slope of the log polarizability *vs.* $1/T$ curve over a limited temperature range was found to be proportional to the ionic dissociation energy of the included molecule. Similarly, the slope of the log resistivity *vs.* $1/T$ curve was found to be proportional to the ionization energy of either the cation or anion plus the ionic dissociation energy. Solving both of the above curves simultaneously gave very good values for the electron affinities of the radicals which became the anion. This provides a method for obtaining electron affinities of radicals which heretofore were considered intractable. With larger amounts of a proper solvent present the dielectric constant was found to be larger than 10^7 at room temperature. Thermoelectric and other measurements on the filled matrix indicated electrons and/or holes as carriers depending on the type of salt used.

Introduction

There is very little literature on the physics of electric conductivity and polarization phenomena manifested by salt-filled porous matrices. The thermodynamic properties of dispersed molecules have been studied quite extensively,[1] but the electrical parameters such as dielectric constant and resistance have not. At present there are many molecules whose parameters are very difficult to study by conventional methods and thus any applicable new methods would be desirable.

It is hypothesized here that if molecules are dispersed in a matrix, the effects of other molecules and the matrix can be combined into an averaged dielectric constant. It will also be assumed here in general that chemical bonding to the matrix has not occurred.

For the purposes of this paper, the matrix is defined to be a porous substance where the pores are of molecular size or larger. The voids or pores are assumed to be interconnecting so that there is a continuous path through the matrix. The latter assumption is made be-

(1) D. H. Everett and F. S. Stone, "The Structure and Properties of Porous Materials," Butterworth and Co., Ltd., London, 1958, pp 1–389.

cause as yet a method has not been found to seal the pores of the matrix on enclosed molecules.

The matrices may be any molecular structure with pores larger than the specific molecule to be put into the pore. The matrices may be ceramics, organics, or combinations of compounds especially designed to achieve or eliminate certain observed effects. A typical matrix might be a metal oxide such as TiO_2, MgO, Al_2O_3, ZrO_2, Nb_2O_5, V_2O_5, or any other oxide that is inert to the included solution's constituents. Matrices can also be made of cellulose or wood (which is mainly a combination of cellulose and lignin). Combinations of types of matrices may be used. In general it is desirable that the matrix provide an environment where the included molecule retains its identity. Further combinations of solids which do not include the above can be imagined.

Wood together with porous ceramic are the chief matrices used in the present work. Wood was found to be most stable as a matrix for most of the molecules tested. Care was taken to remove the volatile substances from the wood by boiling the matrix material for several hours in distilled water. The data obtained from using wood matrices speaks for itself. Wood is very inert to many substances which react with other matrices. Chemical interaction of the matrix and the dispersed molecule was avoided in general, although some interactions were observed in a few cases.

Since very large resistance changes were observed with changes in temperature, it was first assumed that a melting phenomenon was occurring. This was questioned, however, because the resistivity did not change abruptly but varied exponentially over a large temperature range. It was evident that the effect could be used to provide a very sensitive thermistor.

From the start it was assumed that the slope of the resistivity *vs.* temperature curve would be a function of the dielectric constant. To test this hypothesis, the dielectric constant was measured. In measuring the dielectric "constant" it was observed that the dielectric constant was not constant. One of the first molecules studied with respect to dielectric constant was NaCl. It was found that the slope of the log dielectric constant *vs.* $1/T$ curve at the lower temperatures provided almost an exact measure of the known dissociation energy, as did also the slope of the KCl curve. Other molecules also provided very close values. The first molecules studied were diatomic molecules. Since such good dissociation energies were found for diatomic molecules, other polyatomic molecules were tested with good results. The first three molecues studied (NaCl, KCl, and Kl) provided K^2E values that were within 0.1 eV of well known dissociation energies. Because of these results the investigation continued. The K above is the low-temperature dielectric constant while E is the magnitude of the slope of the log dielectric constant *vs.* the reciprocal of the absolute temperature curve.

Using the ionic dissociation energy, one can often obtain the electron affinity of one of the ions. Electron affinities are important parameters in several fields, such as health physics.[2] The excellent agreement between the electron affinities measured by this and other methods was considered as increasing confidence in this technique for obtaining molecular parameters.

Possible Mechanisms

Two phenomena are basically being considered. These phenomena are the resistivity *vs.* temperature characteristics of a salt dispersed in a matrix and the dielectric constant *vs.* temperature of the same system. It is assumed for the purposes of the development to follow that there are small salt inclusions distributed throughout the matrix. Each salt inclusion is surrounded by a limited number of solvent molecules, and

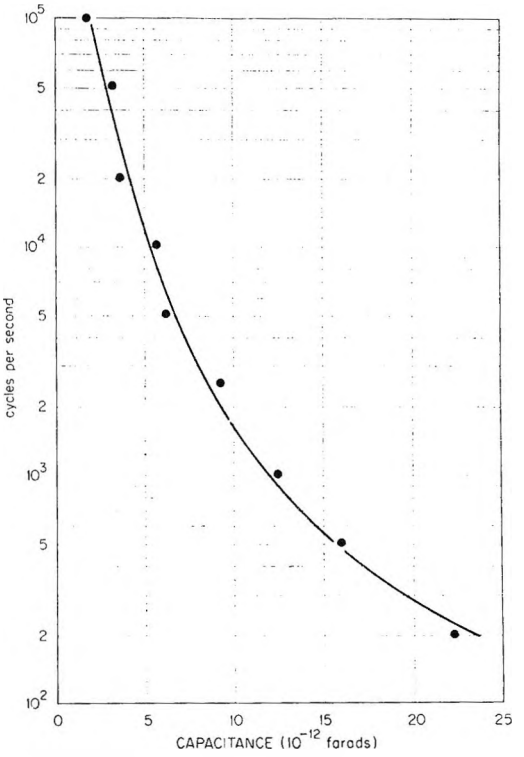

Figure 1. Capacitance *vs.* frequency for an NaCl-filled matrix.

polar solvents appear to give enhanced effects. The polar nature of the solvent molecules tends to keep the solvent molecules at the boundary between the included salt and the matrix. The salt inclusions together with the matrix produce a certain dielectric constant. Thermal motion agitates some of the salt molecules at the boundary between the salt and the solvent. The agitation, solvation, and the difference in the potential between the surfaces will cause a separation of the ions composing the free molecules, and a large dipole is

(2) L. G. Christophorou and R. N. Compton, *Health Physics*, **13**, 1277 (1967).

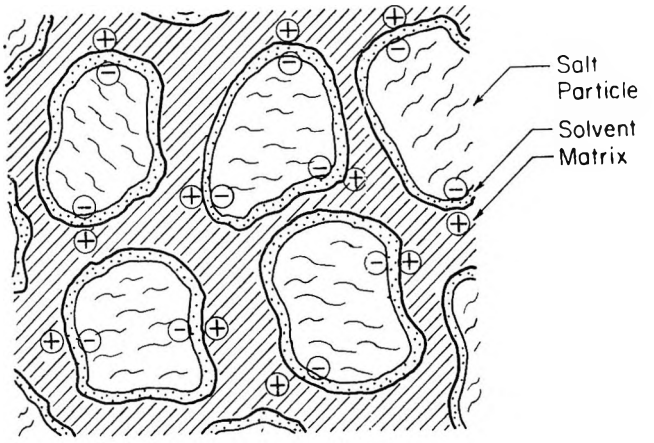

Figure 2. Proposed model of a matrix pore.

formed across the solvent bounding layer. As the temperature is increased, more and more of these dipoles are formed with a resultant increase of the polarizability of the matrix. More and more electric double layers form throughout the matrix. This concept is similar to the double-layer concept at the interface of a liquid and a solid.[3] Here, however, one is dealing with very thin layers of solvent molecules between two bounding surfaces of different materials. Empirically one finds an effectively infinite separation of salt ions, whose number increases exponentially with the reciprocal of the absolute temperature. Figure 1 shows that the large capacitance is essentially a low-frequency phenomenon.

For example, consider one inclusion of salt molecules, shown schematically in Figure 2. The matrix used for most of this work had pores ranging in size from 100 to 1000 Å.[4] Consider a pore 500 Å in diameter with about 1% of the mass water and the other 99% NaCl. NaCl in the cystalline form is approximately twice as dense as water. This would mean the water layer is about 1.7 Å thick, or nearly a monolayer thick. Experimentally, the major capacitance effect disappears or is masked below about 1% moisture content. This perhaps indicates that there has to be approximately a monolayer of solvent present to produce the predominant effect, and this effect disappears at lower temperatures, perhaps because the matrix absorbs or binds the water. The implication is that free solvent is what produces the major effect. With the disappearance of a continuous bounding layer, no more ions are excited across the layer. A residual effect remains which is perhaps partly due to a double layer formed at the interface of the remaining solvent and the matrix.

Empirically it was observed that an effective dielectric constant characteristic of the matrix–salt combination was seen by the dissociating molecules. For the wood matrix this effective dielectric constant was very nearly the macroscopic low-temperature measured value. For ceramic matrices one had to multiply the measured dielectric constant by some factor. For ceramic matrices used, the effective dielectric constant was about one-half that of the macroscopic low-temperature measured value. Hereafter the dielectric constant K will be the relative effective dielectric constant.

In considering the effect of the dielectric constant one can use an analogy to the solid-state hydrogen model. That is, the molecule sees an average dielectric constant of the matrix immediately surrounding it, and the energy levels are reduced[5] by a factor of approximately $1/K^2$.

Now consider the resistivity characteristics. There are several possible mechanisms for the observed changes in resistivity with temperature. The changes can obviously be attributed to the activation of carriers by thermal means. It is noted from the curves in the experimental section that this activation is Boltzmann in nature. In the case being considered, one would first suspect ionic carriers since one is dealing with ionic compounds dispersed in a matrix. If the ions or molecules were tied to specific locations, one might suspect hole or electronic conduction. It is believed that here the ions are tied in the dry limit. The predominant carriers are considered to be electrons or holes as the following arguments indicate.

Types of Carriers

The thermoelectric results mentioned in the experimental section indicate whether positive or negative carriers predominate. If one were to suppose that there were two or three different sources of carriers, then one could assume a relation of the form

$$G = Ae^{-E_1/kT} + Be^{-E_2/kT} + C$$

where G is the conductivity, A, B, C, E_1, and E_2 are constants, k is Boltzmann's constant, and T is the absolute temperature. The C was added in case there was a nontemperature-dependent term. This would result, however, in a curved line on a semilog plot if A and B were comparable in magnitude. The results generally give straight lines over a large range on a semilog plot after a transition point is passed. This indicates that one temperature-dependent mechanism predominates. One can obtain a pronounced increase in the slope by decreasing the solvent content. As the solvent content is decreased, the slope increases to a certain limit. Thereafter the slope does not change, no matter how small the solvent content is made, provided the temperature is not below that required to dissociate the salt in the presence of the solvent. This change in slope represents a transition from ionic to either electronic or hole conduction. Once the transition point is passed, no other transitions are observed even after the sample

(3) D. P. Benton and G. A. H. Elton, *Trans. Faraday Soc.*, **49**, 1225 (1953).

(4) D. H. Everett and F. S. Stone, ref 1, p 367.

(5) A. Many, Y. Goldstein, and N. B. Grover, "Semiconductor Surfaces," North-Holland Publishing Company, Amsterdam, 1965, p 50.

becomes a good insulator. This occurs in the limit of small solvent contents (generally less than 10% of the matrix weight). Both electrons and holes are probably present at any given time, but the mobilities apparently are quite different for the cases to be discussed. This allows one to separate the effects of the electron and hole carriers. It is conceivable that a case might arise where the mobilities were the same and the sample would appear to be intrinsic. In one case (for NaCl) apparently negative carriers predominated at the lower temperatures and at higher temperatures hole conduction appeared. Probably there is some ionic conduction when the matrix is in its driest state, but this contribution is very small and perhaps relatively constant with temperature change. Predominant ionic conduction is also ruled out by the following argument.

If one had ionic conduction, the matrix would become strongly polarized after dc current had flowed for even a short time. This was not observed. In addition, the resistance slopes are too large to assume ionic conduction. Other authors have also proposed electronic and hole carriers for conduction where absorbed molecules are present.[6]

The Basic Equations

Assuming electronic or hole conduction in the dry limit, one would infer that dissociation of the molecule occurs first and then electrons or holes are provided by one of the resulting two ions. This would provide holes from the cation or electrons from the anion. If this were the case, one would conclude that the activation energy is the sum of the dissociation energy and the ionization energy of either electrons or holes. The type of mechanism for the conveyance of electrons or holes after their release is discussed below. For the release of a charge carrier (electron or hole), the following relation was empirically found to hold

$$J = Ce^{-(E_d+I)/K^2kT}$$

where J is the current density, E_d is the ionic dissociation energy, I is the ionization energy, k is Boltzmann's constant, T is the absolute temperature, and C is a constant. In the low solvent case the solvent binding energy and the coulomb energy are neglected.

Conduction here can be explained as a surface mechanism. For example, one can have electron or hole conduction along grain boundaries and damaged surfaces as well as increased conduction at surfaces due to surface states. Several possible surface conduction mechanisms are present here. The mechanisms of surface conduction are discussed by numerous authors, for example Many, *et al.*[7]

Considering that the capacitance varies exponentially with $1/T$, what type of mechanism would provide such a relation? In the case at hand, one is dealing with small pores in a matrix. One would expect a few solvent molecules and a few salt molecules in each pore. Thermal agitation would keep a constant turmoil present in a specific pore. As the temperature is increased, the turbulence would increase until the agitation and polar nature of the solvent molecules dissociates a salt molecule. The solvent molecules tend to shield the resultant ions from one another. Some of the ions may migrate to the pore surface at the interface between water molecules and the matrix. It is probable that the Maxwell–Wagner interfacial mechanism contributes to holding the ions and perhaps other charges apart.[8] The net result is that a dipole is formed in the pore. As the temperature increases, more and more dipoles are produced. This results in an increase of the polarizability with increasing temperature, and thus the dielectric constant increases. One would eventually have a dipole or dipoles in each pore. Finally, one would expect a saturation to occur with all the possible dipoles having been produced. This saturation would result in a ferroelectric behavior.

It was observed in some samples that the dielectric constant apparently rose very rapidly at the highest temperatures. This apparent rapid increase in dielectric constant was probably due chiefly to drying of the sample at the higher temperatures, so that loss of solvent caused some slope change. In addition, the number of ionic or other carriers would increase somewhat at higher temperatures.

From the earlier description of the increase in polarizability, one would expect the polarizability to increase according to a relation of the type

$$P = P_0e^{-(E_d)/K^2kT} + P_1$$

where P is the polarizability, P_0 is a constant, P_1 is the low-temperature polarizability, and K is the low-temperature dielectric constant (measured near liquid nitrogen temperature.) A possible cohesive energy of the salt molecules has been neglected. Although cohesive energy would be expected for a large number of molecules per pore the results did not indicate a need for this. Also it proved unnecessary to add the energy of solvation to E_d for the relatively small amounts of solvent used in these experiments.

At this point consider the application of the above formulas to the two classes of carriers previously discussed. Define EA to be the electron affinity of the atom, molecule, or radical which becomes the anion. For negative carriers (electrons from the anion) the following equations can be written

$$I = RK^2$$

(6) W. T. Eriksen, H. Statz, and G. A. deMars, *J. Appl. Phys.*, **27**, 133 (1957).

(7) A. Many, Y. Goldstein, and N. B. Grover, ref 5, pp 1–496.

(8) K. W. Wagner, *Arch. Electrotech.*, **2**, 371 (1914).

and

$$I - EA = K^2E$$

Eliminating K gives

$$EA = I(1 - E/R)$$

I is the magnitude of the ionization energy of the molecule, atom, or radical which becomes the cation while E and R are the magnitudes of the slopes of the capacitance and resistance *vs.* $1/T$ curves, respectively, multiplied by the Boltzmann constant.

For positive carriers a similar relation can be written

$$2I - EA = RK^2$$

and

$$I - EA = K^2E$$

Elimination of K yields

$$EA = I(2 - R/E)/(1 - R/E)$$

Thus the resulting relations are independent of K. This is important since K often is not directly measurable.

It has been emphasized that the slope of the log capacitance *vs.* the reciprocal of the absolute temperature curve is proportional to the dissociation energy of the molecule. This is true over a certain temperature range. At low temperatures, however, a small residual slope usually appears instead, probably due to solvent attachment to pore boundaries. Also at the higher temperatures, breaks may occur due to impurities in the matrix and salt and perhaps other conduction mechanisms entering the picture. In the NaCl curve in the Results section, the slightly larger slope is probably due to positive carriers. Also, in polyatomic molecules, different bonds will be broken at different locations in the curve with resulting slope changes. One should be able to peel parts of the molecules off one by one and look at successive dissociation energies.

Some problems will doubtless occur in the study of matrix dispersion. There will be more or less interaction of the included molecule with the matrix. An attempt should be made to use a matrix compatible with the molecule to be placed in it. That is, a matrix should be found that does not interact chemically with the molecule. For polyatomic molecules one might have the problem of dissociation in the "wrong" place. The molecule might come apart at an unexpected bond. Thus one might get rather unexpected results. This emphasizes the point that a series of curves under differing conditions (such as different solvent contents and matrices) should be run for each molecule being studied.

Experimental Techniques

For resistance measurements a General Radio 1230A electrometer together with a Simpson multimeter were used. Resistances measured ranged from around 5000 ohms to about 10^{12} ohms, so both of these instruments were necessary. Voltages were measured with the electrometer mentioned above. The voltages measured included thermoelectric voltages. For capacitance measurements, a General Radio 1650A impedance bridge was employed. Most measurements of capacitance were made at 1000 Hz using the oscillator included in the bridge. For the capacitance *vs.* frequency curves an audio oscillator (Hewlett-Packard Model 200CD) was used in conjunction with the bridge.

In measuring resistance using the dc equipment mentioned above, instantaneous measurements were the rule to eliminate any possible polarization and hysteresis effects.

Initially there was some problem with scatter due to lack of intimate contact between the sample and the thermocouple used for temperature measurement. This was corrected by taping the iron–constantan thermocouple directly to the sample. Temperature measurements were made using a Leeds and Northrup 8690 potentiometer. An ice water reference junction was used to help ensure accuracy. The general method of measurement was to heat the sample to the high temperature desired in a styrofoam container. The sample was then allowed to cool rapidly and measurements were taken as the sample cooled. This process was used because the heat-up time was generally quite long, and there was a chance that device characteristics might change with time. The rather rapid cooling virtually eliminated device characteristic changes from solvent loss. Cooling below room temperature was accomplished using Dry Ice and liquid nitrogen.

A glance at the capacitance and resistance curves indicates that scatter was usually very small. Some scatter was apparent in curves where the capacitance being measured was very small. This scatter was chiefly caused by difficulty in reading the scale of the bridge to 0.1 pF. The absolute error in the resistance readings was at most 8% of full scale readings for resistances above 3×10^{10} ohms, and 2% of full scale for lower resistances. Readings were taken as near full scale as possible. Most of the errors are probably caused by scale changes because relative errors are more important than absolute errors in the determination of slopes. There was no scale change in the capacitance readings and thus the slope errors were minimized. Note that the low-temperature capacitance, B, which was usually near 15 pF., was subtracted from each reading. There was an absolute possible error of ± 1 pF indicated for the bridge which was probably the same for the B value and the other readings. This essentially means that the error in capacitance readings is chiefly caused by difficulties in reading the scale.

Thermoelectric measurements were made using the 1230A electrometer. The sample whose thermoelectric power was to be measured was mounted on an aluminum cup by means of conductive silver paint. A thermocouple was mounted on the opposite end, again

by silver paint. The cup was filled with ice and ice water, the temperature of the warm end was read, and the thermoelectric voltage between the cup and one of the leads of the thermocouple was read on the electrometer. The voltages were as high as 100 millivolts for a 20° gradient. No attempt was made to read the thermoelectric voltage in the limit of a very small temperature gradient, which defines the thermoelectric power, since only the sign of the carriers was desired. As a check, the ice water was poured out and hot water poured in to see that the measured thermoelectric voltage changed sign. The whole assembly of the cup and mounting was shielded by grounded metal. Very high input impedances were often used on the electrometer (between 10^{12} ohms and infinity). In measuring the thermoelectric voltage, due to the high impedance of many samples, there was a problem with charges from the atmosphere collecting on the probe and giving erroneous readings. For this reason the results were checked and double checked, and the leads were shorted between readings. A better method needs to be found to check these thermoelectric voltages to eliminate possible ambiguities in some of the measurements. The probe charge buildup was observed both with and without the sample present.

Resistance and capacitance measurements were taken in a small styrofoam container. This type of oven worked very well for the temperature range used. Rapid heat exchange with the surroundings was prevented. A 25-W tungsten lamp was used as a heating element to raise the temperature in the oven. A variac was used to control the rate of heating and cooling.

Samples were prepared as follows. The matrix material was cut to the desired shapes and then boiled in distilled water for removal of volatile substances. Three to eight hours or more was allowed for letting the concentrated salt solution soak into the matrix. The soaking time depended on the thickness of the sample.

The resistors made were generally 1/4 × 1/4 × 1-in. samples. The capacitors used 1 × 1-in. stainless steel or nickel plates with 0.05-in. dielectrics. Fringing effects were neglected. An estimated error of about 10% in capacitance measurements is assumed, caused mainly by lack of flatness of the dielectrics. This would cause an error in the measured dielectric constant, which was avoided by solving the capacitance and resistance curves simultaneously and eliminating the dielectric constant.

Contacts to resistors were made by merely pushing a wire into the matrix. For ceramics, however, pressure contacts were used. It would probably be better to use conducting pastes to make contact to ceramic samples. This would tend to reduce the resistance as well as prevent possible slipping during handling. It was found that nichrome was very stable for most of the constituents used.

The contact problem for devices and parameter determination has not been completely solved. The molecules used tended to react at least slightly with the contacts. There is also the problem of electrolysis at the contacts. It is believed that part of this problem has been solved by using a catalyst at the contacts to cause recombination of the evolved hydrogen and oxygen when alternating current is used. Other contacts might be tried, such as conducting ceramics and organics. With the capacitor, direct metal contact with the dielectric could be prevented by using a very thin layer of another high K dielectric but this would be defeating some of the main purposes of the device. This coating method could be used in the molecular parameter determination process, however.

Various contact methods can be used. One can paint on a colloidal suspension of metal or carbon and let it dry or even bake it on if the solution has not already been put in. Several paints are available on the market for this type of application. The contacts used would be a function of the chemical constituents used. In some cases it may be desirable to use platinum contacts. If the contacts can be pushed in, platinum wire could be used, or if it is desired to paint on the contacts, one could use a platinum colloidal suspension. Pressure contacts might be used for temporary experiments. An easy method of applying soft metals such as gold and aluminum is to rub them into the ceramic. It should be noted for contacts (especially for high work function contacts) some nonohmic effects may come into play. Electrodeless plating of contacts might also be used, especially if the contacts are put on the matrix before the chemical constituents are diffused into the matrix.

The preparation of ceramic samples was similar to that of the yellow pine wood matrices. The porous ceramic was boiled for approximately 12 hr in a concentrated salt solution and then dried to the desired moisture content.

It was found that to obtain a specific moisture content, the easiest way was to dry the samples at about 120° for about 4 hr. This removed the free moisture. Next the samples were allowed to pick up moisture from the atmosphere until the desired concentration was attained. Determination of moisture contents was made with an Ainsworth Type 24N balance. This scale was also used to determine how much salt was in the matrix after drying for about 4 hr at 120°. No attempt was made to drive off all attached moisture. As will be apparent from the results, a fairly wide range of solvent contents was investigated.

Results

The base capacitance or low-temperature capacitance, B, of the sample was obtained near −100°. If any temperature dependence of the capacitance was ob-

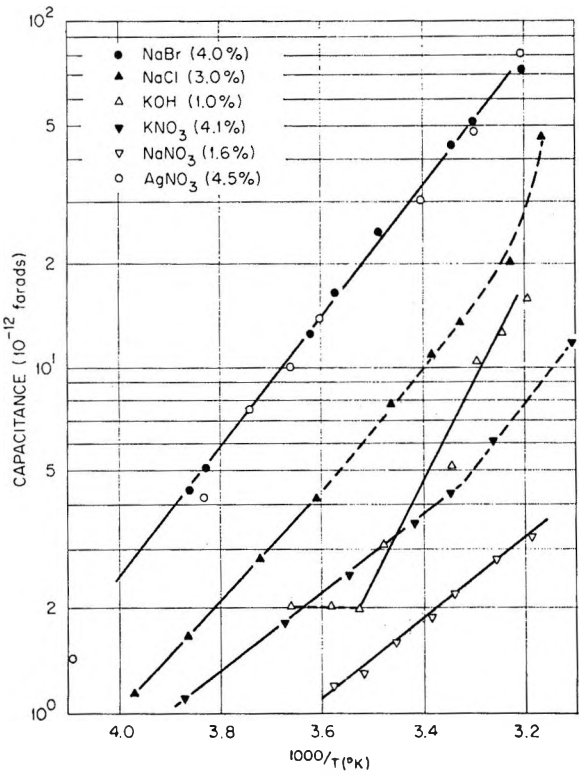

Figure 3. Capacitance *vs.* the reciprccal of the absolute temperature for several different salts included in various matrices.

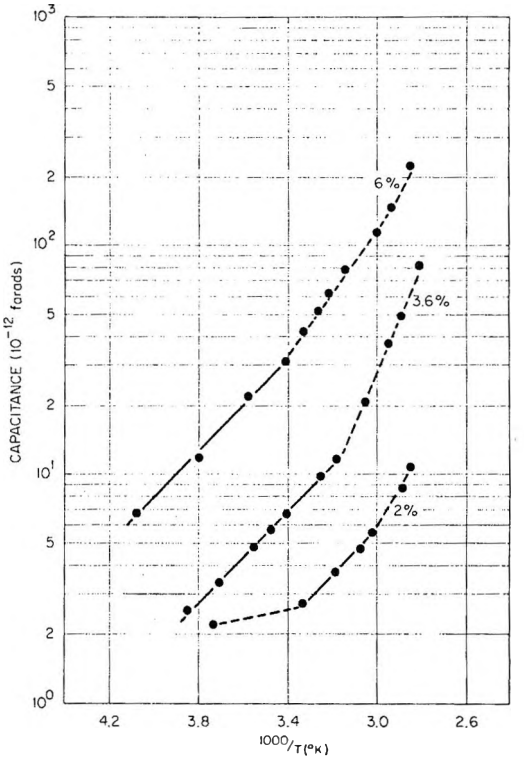

Figure 5. Capacitance *vs.* the reciprocal of the absolute temperature for KCl in a matrix for three different moisture contents.

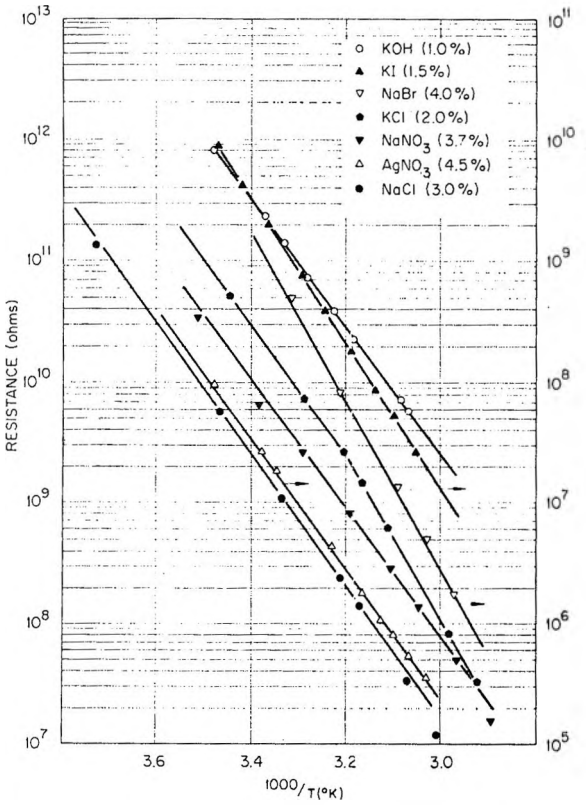

Figure 4. Resistance *vs.* the reciprocal of the absolute temperature for several salts included in various matrices.

served around −100°, the sample's temperature was lowered to liquid nitrogen temperature. In most cases, however, very little change in capacitance was observed for temperature variations below −50°. This of course depended on the amount of water present. Except for a few experiments described later, water was the solvent used to obtain the data reported here. Note that B is subtracted from all other capacitance values before they are plotted.

A KCl sample was tested for changes in capacitance with an applied field of 45 V across the capacitor. No appreciable change was noted, so it was assumed the capacitance was approximately independent of small fields. More tests should be run at higher fields. It may be possible to find cases where a field dependence is present. Weak magnetic fields also produced no observable effects at a fixed temperature.

Some diatomic molecules will be considered first. There are KCl, KI, NaCl, and NaBr. See Figures 3, 4, 5, and 6. Note that the dashed lines represent departures from the constant slope predicted by the theory and are not used in the calculations. The E values were 0.195, 0.286, 0.317, and 0.346 eV, respectively. The R values were 1.35, 1.20, 1.12, and 1.37 eV, respectively. The resultant electron affinities together with the sign of the thermoelectric power are given in Table I. The photodetachment value of the electron affinity of the atom which becomes the anion is listed for comparison. The moisture percentage is listed on each

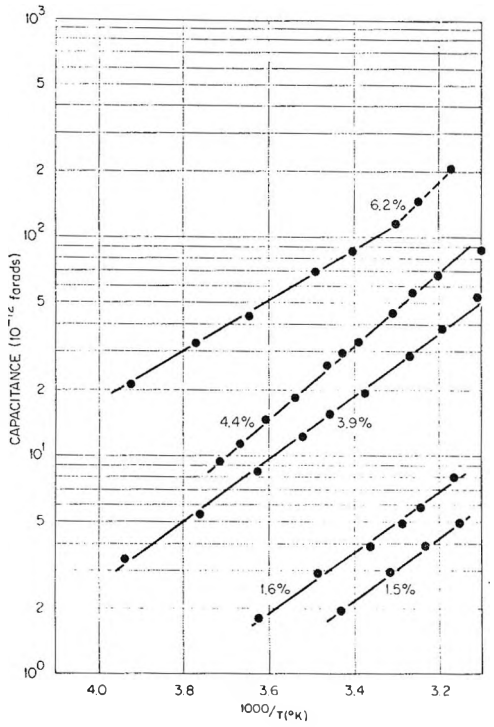

Figure 6. Capacitance *vs.* the reciprocal of the absolute temperature for KI in a matrix for five different moisture contents.

graph. The ionization energies used for K and Na were 4.32 and 5.12 eV, respectively. Note for KCl the resultant dissociation energy is 0.73 eV, giving an effective dielectric constant of 1.87 for the matrix and salt. Note also for KCl that the R used was for the greatest slope of the resistance curve. Two slopes are present because these data were taken in the dry limit. Data indicate that when the capacitance slope disappears, the resistance slope gives the ionization energy of the cation. The R from the lowest slope is 1.15 giving a RK^2 value of 4.30 eV as compared to 4.32 eV for the ionization energy. The ionization energies used in this and the succeeding data were taken from National Bureau of Standards Circular No. 467, Volumes 2 and 3. The work was done by C. E. Moore and published in 1958.

With lower moisture contents there is a higher temperature switch to the residual slope referred to in the theory. As the water content is increased, this occurs at lower and lower temperatures. With higher moisture contents, however, the straight portion of the curve disappears more quickly with increasing temperatures due to changes in moisture content.

Now consider the KOH graphs in Figures 3 and 4. KOH was tried in a wood matrix initially. It destroyed the matrix. A ceramic matrix was tried at about 2% moisture content. Much scatter was present in the capacitance curve with an abrupt drop in the capacitance between 39 and 36°. The data were rerun at 1% moisture content, but scatter was still present.

Table I: Summary of Results[a]

	Electron affinity of radical which becomes anion, eV (experimental)	Electron affinity of radical which becomes anion, eV (photodetachment)	Sign of carriers
KCl	3.59 ± 0.08	3.613 ± 0.003	+
KI	2.98 ± 0.08	3.063 ± 0.003	+
NaBr	3.39 ± 0.08	3.363 ± 0.003	+
NaCl	3.67 ± 0.08	3.613 ± 0.003	−
$AgNO_3$	3.43 ± 0.10	3.88[b]	−
KNO_3	3.43 ± 0.10	3.88[b]	−
$NaNO_3$	3.43 ± 0.10	3.88[b]	−
$CuSO_4$	3.0 ± 0.5[d]	...	−
$FeSO_4$	3.1 ± 0.5[d]	...	−
$MgSO_4$	3.3 ± 0.5[d]	...	−
KNO_2	2.46 ± 0.08	≥3.0[c]	−
KOH	1.9 ± 0.3	1.83 ± 0.005	−

[a] A summary of the most important data from twelve molecules used in this investigation. The photodetachment values are from ref 9 except as specified. [b] This value is a calculated value. See K. B. Yadzimoshii, *Izv. Akad. Nauk SSSR, Ser. Khim. Khim.*, **411**, 453 (1947). [c] L. M. Branscomb, *Phys. Rev.*, **148**, 11 (1966). [d] Values based upon measured relative dielectric constants and the assumption that the carriers were coming from SO_4^{2-}. The value of the electron affinity is for SO_4^- and is probably a lower limit because of the way the dielectric constants were measured.

The data look rather poor, but note that the capacitance is very low and other effects might be present. The scatter is at least partly due to the large pores in the matrix. The electron affinity for OH from these data is 1.9 ± 0.3 eV. This scatter emphasizes the need for more matrix research.

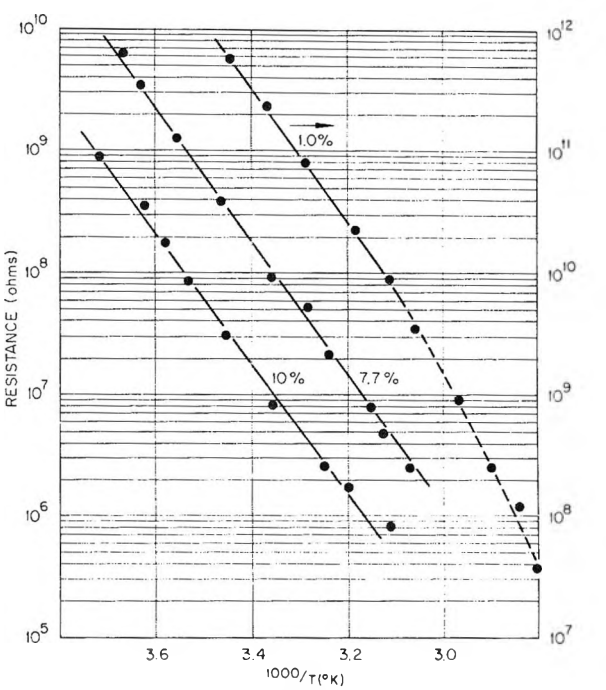

Figure 7. Resistance *vs.* the reciprocal of the absolute temperature for KNO_3 in a matrix for three different moisture contents.

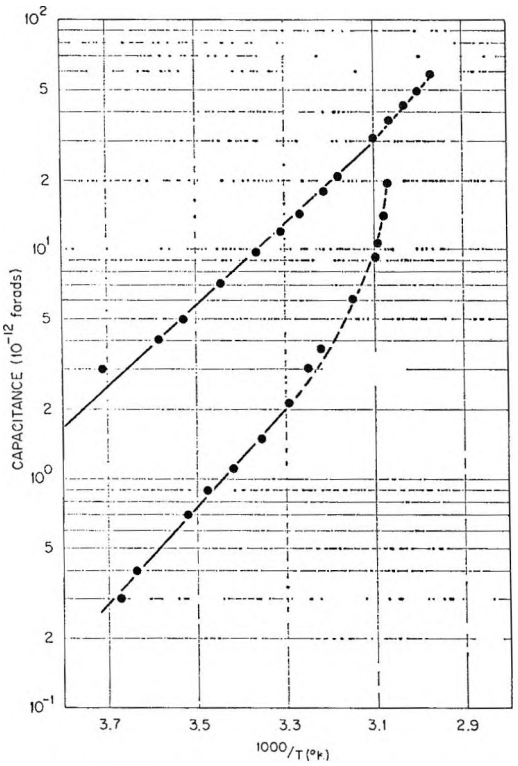

Figure 8. Capacitance *vs.* the reciprocal of the absolute temperature for KNO_2 in two different matrices, Al_2O_3 and wood.

Notice with KI in Figure 6 there was a switch over to greater slope at the 4.4% moisture content. This sudden switching was observed in KI and other molecules. This emphasizes the point that one should use only low solvent contents, and several solvent content curves should be run for each molecule. This switching may have represented some type of resonance at this particular solvent content.

The three nitrate molecules considered were KNO_3, $NaNO_3$, and $AgNO_3$ (see Figures 3, 4, and 7). Negative carriers were indicated for all three molecules. The electron affinities obtained were 3.43 ± 0.08, 3.98 ± 0.08, and 4.64 ± 0.08 eV, respectively. The corresponding E values were 0.226, 0.233, and 0.414 eV and the R values were 1.07, 1.05, and 1.08 eV. These corresponded to dissociation energies of 0.89, 1.14, and 2.90 eV. All of the electron affinities should be the same, but they are not. Some insight into the reason for this can be gained by solving for the effective dielectric constants for each of the matrices. Using $RK^2 = I$, the values obtained (the cations had I values of 4.32, 5.12, and 7.54 eV, respectively) for K are 2.01, 2.21, and 2.64. These values are somewhat higher than the measured values, except for 2.01. The minimum experimental dielectric constant was 1.90 for the KNO_3 matrix. That is, the dielectric constant was greater than or equal to 1.90. This sets a limit on the possible error in the electron affinity. The 2.01 value is very close to the experimental value. For the wood matrix, calculated values are obtained which are near measured values in the diatomic molecules. A plot of the above dielectric constants *vs.* the ionization energies of the cations yields approximately a straight line. The net effect is an apparent reduction of the dissociation energy at large dissociation energies. Apparently what is happening is that the NO_3^- ion splits in some manner to reduce the measured dissociation energy. The effect increases with the increase in the ionization energy of the cation. It is observed that one can approximately correct the dissociation energies by multiplying the ratio of the calculated to the measured dielectric constants by the calculated dissociation energies. For $NaNO_3$, for example, $2.21/1.84 \times 1.14$ equals 1.37. Subtract 1.37 from 5.12 and one obtains 3.75 ± 0.5 eV (after taking into account the possible error) for the electron affinity of NO_3. A similar value is obtained for the $AgNO_3$ molecule. Thus, the value chosen for the electron affinity of NO_3 is 3.43 ± 0.10 eV since the theory fits best for KNO_3. This points out the fact that one needs to analyze a polyatomic molecule from several different approaches. Compare the value obtained for the electron affinity of NO_3 with the calculated value of 3.88 eV. See footnote *b* of Table I.

Now note Figures 8 and 9. As a demonstration that matrices other than wood manifest similar behavior, a fairly coarse Corning fritted glass filter was tried as a matrix, as well as wood, for KNO_2. There tended to be more scatter with the ceramic matrix, but valid data resulted. The electron affinity obtained from the ceramic matrix was 2.6 eV with a water content of about

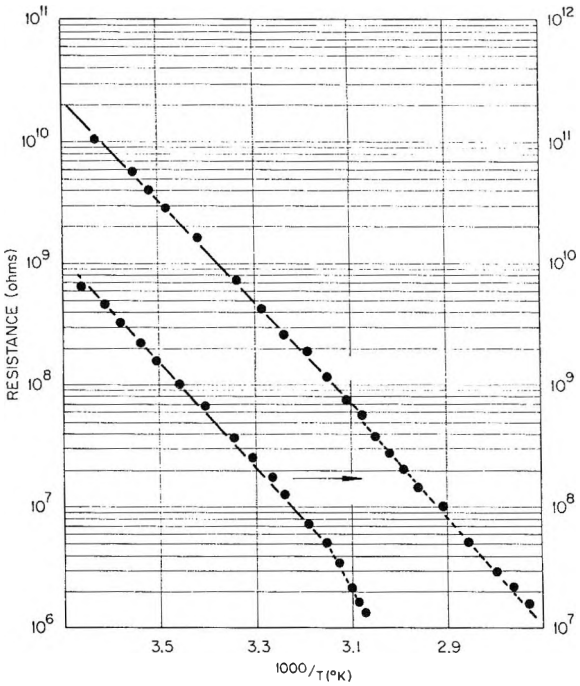

Figure 9. Resistance *vs.* the reciprocal of the absolute temperature for KNO_2 in two different matrices, Al_2O_3 and wood.

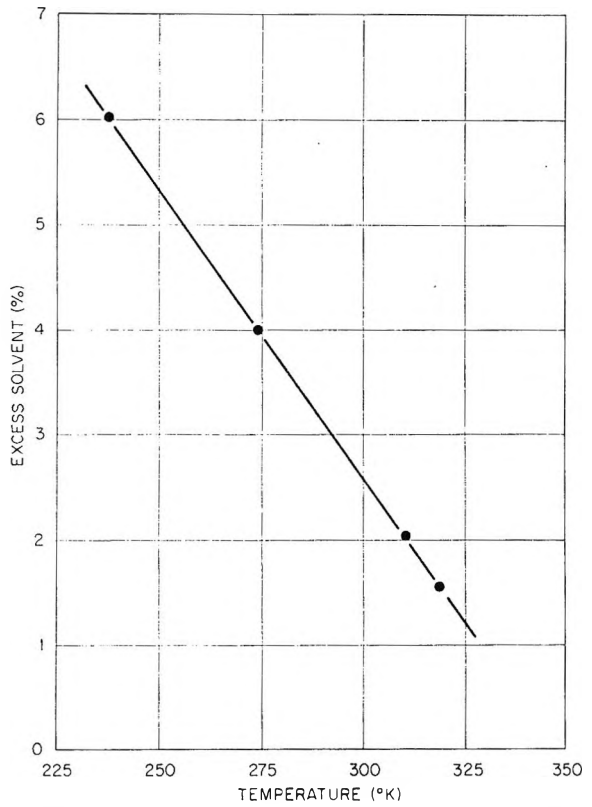

Figure 10. Temperature *vs.* water content for the onset of the residual slope.

1% of the matrix weight (with an E of 0.42 and an R of 1.08). The error in this was at least ±0.1 eV due to the scatter and small capacitances being measured. The wood matrix yielded an electron affinity of 2.46 ± 0.08 eV. One can compare these values with ≥3.0 eV obtained by photodetachment.[9] Obviously, the value for the electron affinity which was measured for NO_2 is rather low. This could be explained by the fact that it is not known what energy state NO_2^- is in when it comes off. It could come off in any one of a number of unknown vibrational energy states. This would reduce the apparent electron affinity.

Another reason for the low value obtained is the possibility that KNO_2 breaks down further than into just K^+ and NO_2^-. Consider the reaction

$$KNO_2 \longrightarrow K^+ + NO_2^- \longrightarrow K^+ + NO + O^-$$

This is, perhaps, indicated by the large capacitance slope and relatively small resistance slope. This points out the fact that the electron affinities obtained by this method should be less than or equal to the actual values.

As a test for other solvents, methanol was tried as the solvent for KNO_2 in a wood matrix. The capacitance effect was present as in the case of a water solvent. The chief difference noted was that the loss factor was less by a factor of about 10 than for the comparable water–salt–matrix system. Solvents such as ethanol, kerosene, and amyl alcohol were also tested with varying results. The smaller polar molecules as solvents seem to provide the largest capacitance effects. Note that for these solvents the salt was put in first with water, the sample was dried, and then the new solvent soaked into the matrix.

For more information on KCl see Figure 10. The solvent content *vs.* the absolute temperature is plotted here for points where the residual slope, previously referred to, set in. Note that for larger water contents the major capacitance effect sets in at lower temperature, or lower energies are required to cause dissociation. It is anticipated that curves of this type will provide knowledge concerning the form of the potential between the atoms or radicals composing a molecule.

Loss factors in capacitance measurements for the molecules studied varied considerably. Since the conductivity increased with temperature, the loss increased somewhat with temperature. Loss factors at room temperature with capacitances approximately $2B$ were typically 0.25. For a room temperature capacitance of $5B$, the dissipation factor was typically 0.40.

Summary

The values for electron affinities obtained for the diatomic molecules used in this investigation were very close to the generally accepted photodetachment values. This method may, thus, provide another tool for obtaining electron affinities and other molecular parameters. The simplicity of the measurements should be emphasized. Merely soaking a solution into a matrix and taking capacitance and resistance measurements is very easily accomplished.

An important result of this research is the possible electronic devices (such as extremely sensitive thermistors and very high dielectric constants and relatively low losses for capacitors). At present the electronic devices are not perfected, but the effects are there. It should be only a matter of time before practical devices can be developed.

Other materials for matrices need thorough testing. For example, the Linde molecular sieves, more ceramics, and other suitable materials can be used for a matrix. In wood there is such a variation in micropore sizes that it is obvious that it would be better to try matrices with uniform pore sizes. Also wood tends to age with the passage of time. The electronic characteristics of the matrix will be quite dependent on the pore size as well as the anisotropy. For example, one might try silica gel with pore sizes of the order of 20 Å.[10]

With ionic compounds there is always the problem of at least some ionic conduction. Prevention of ionic

(9) R. S. Berry and C. W. Reimann, *J. Chem. Phys.*, **38**, 1540 (1963).

(10) D. H. Everett and F. S. Stone, ref 1, p 272.

conduction in capacitors could be accomplished by sealing the ions in the pores as suggested earlier. Ionic conduction devices might be desirable in some cases, especially if alternating current was used and ionic recombination can be accomplished. If the molecular parameters described here are desired, most of these problems are automatically circumvented because currents can be kept low and temporary.

Lattice and hydration energies were early considered. A neglect of these quantities, however, provided (for at least the diatomic molecules considered) electron affinities which were within the experimental error of values found by photodetachment. For this reason it was considered desirable for the present study to neglect the additional quantities. There is probably cancellation of surface, lattice, and hydration energies which permits a neglect of these quantities for a number of molecules. This was considered a major advantage of the experiment. Investigation is continuing with some molecules apparently showing some hydration effects at low solvent contents. When this further study has progressed sufficiently the results will be published. Hydration could help explain the progressive apparent increase in the calculated dielectric constant for the nitrates studied.

It has been reasoned that the released carrier leaves behind a neutral particle and thus I should be reduced by K rather than K^2. In other words

$$J = Ce^{-(E_d+KI)/K^2kT}$$

If one takes into account the experimental results, this equation does not apply. Consider the case where E_d is much smaller than I. This is very often the case. For example, look at the parameters for KCl. For this situation one would need to multiply the experimental obtained resistance slopes by approximately K to fit the new equation. If K were approximately 2 as was found for most cases in this paper, one would need to approximately double the empirical resistance slope values. The value of 2 for K was found both by experimental measurement and by solving the two basic equations. Observe that the total process, dissociation plus ionization, leaves two net charges. K^2 arises, in the hydrogen model, from a reduction in energy caused by a field decrease due to the interposition of a dielectric between two charges.

The Diffusion of Hydrogen in Boron–Palladium Alloys[1a]

by K. D. Allard, Ted B. Flanagan,

Chemistry Department, University of Vermont, Burlington, Vermont

and E. Wicke

Institut für physikalische Chemie Universität Münster, Münster, Germany *(Received June 23, 1969)*

The diffusion of hydrogen in a series of boron–palladium alloys has been investigated using an electrochemical relaxation technique. Results show that the values of the diffusion coefficients determined at $n_H \rightarrow 0$, where n_H = H/Pd, atomic ratio, decline steadily with boron content from that of pure palladium. This behavior is in marked contrast to that of substitutional alloys of palladium. The dependence of the diffusion coefficients upon boron content supports the view that in these alloys boron occupies interstitial sites. A quantitative theory is advanced which satisfactorily explains the results.

Introduction

Before about 1960, data reported for the diffusion of hydrogen in palladium have been very divergent.[1b] Recently, however, data reported from different laboratories have been in excellent agreement. For example, in the low hydrogen content α phase, values selected from five different investigations give an energy of activation within 300 cal/mol of each other, ΔE_a = 5730 ± 150 cal/mol,[2-6] and correspondingly good agreement for the absolute magnitudes of the diffusion constants. This close agreement extends over a very wide temperature range, *i.e.*, from −78 to 379°.[2,6] In

(1) (a) This research was performed at the Institute für physikalische Chemie der Universität Münster, Germany; (b) *e.g.*, R. M. Barrer, "Diffusion in Metals," Cambridge University Press, 1951.

(2) O. M. Katz and E. A. Gulbranson, *Rev. Sci. Instrum.*, **31**, 615 (1960).

(3) J. Simons and T. B. Flanagan, *J. Phys. Chem.*, **69**, 358 (1965).

(4) G. Bohmholdt and E. Wicke, *Z. Phys. Chem.* (Frankfurt am Main), **56**, 133 (1967).

(5) G. Holleck and E. Wicke, *ibid.*, **56**, 155 (1967).

(6) H. Züchner, Diplomarbeit, Münster, Germany (1967).

addition there have been several investigations at a single temperature[7–9] which also agree quite well with those cited above. The experimental techniques employed for these determinations have been quite different, ranging from conventional gas-phase permeation techniques[2] to an electrochemical relaxation method.[5] It is now clear that the major cause of the discrepancies in the past has been that the degree of cleanliness, and catalytic activity of the surface was insufficient for the rapid establishment of the $H_2 \rightleftarrows 2H$ equilibrium at the surface; *i.e.*, the early investigators were not measuring solely bulk diffusion but the slow surface reaction contributed to their measured rates. An exception to these remarks is the research of Jost and Widman.[10] They employed palladized palladium spheres at higher temperatures and obtained diffusion constants comparable to those of the recent studies.

The diffusion system of hydrogen in palladium and its alloys constitutes a most important tool for basic studies of solid-state interstitial diffusion. The hydrogen content can be varied over wide limits in pure palladium and in certain palladium alloys.[11] The electronic and geometric properties of the metal substrate can be altered in a controlled manner by the appropriate choice of substitutional alloy partner. The thermodynamics of absorption are known for palladium–hydrogen and for many alloys of palladium with hydrogen.[11] Experiments utilizing isotopic substitution of deuterium or tritium can be readily carried out. Neutron diffraction and scattering studies have located the positions and measured the vibrational frequencies of the hydrogen atoms in the palladium lattice.[12,13] Finally, of all the possible systems involving interstitial diffusion in metals, the diffusion of hydrogen is probably the most amenable to fundamental interpretation.

A new electrochemical technique for the determination of diffusion coefficients in palladium and its alloys was recently developed by Holleck and Wicke.[5] This relaxation technique consists of potentiostatically charging an electrode to a uniform concentration profile. This uniform profile is then perturbed by the electrolytic addition or subtraction of an increment of hydrogen. During the perturbation a constant flux of hydrogen passes through the surface of the specimen. The relaxation of the nonuniform concentration profile thus established is followed by measurements of the electrode potential of the specimen as a function of the time. (The electrode potential can be related to the concentration at the surface if equilibrium absorption data are available.) For specimens of various geometries the diffusion equation can be solved exactly. Flat plates have been employed here.

The absorption of hydrogen by boron–palladium alloys has been investigated by Sieverts and Brüning[14] and more recently by Burch and Lewis[15] and Husemann.[16] Schaller[17] and Brodowsky have also investigated the absorption of boron itself by palladium. Indirect evidence suggests that boron atoms occupy interstitial sites within the palladium lattice;[14–16] *e.g.*, the lattice expansion which occurs upon boron addition is greater than one would expect on the basis of a substitutional alloy.

Holleck and Wicke[5] and Bohmholdt and Wicke[4] have reported values of the diffusion coefficient of hydrogen in several palladium-rich alloys for both high and low values of n_H where n_H is the atomic hydrogen-to-metal ratio. In the low hydrogen content region, which is the region of interest here, the value of $D_{n_H \to 0}$ (25°) changes upon alloying with substitutional metals from 2.6×10^{-7} cm^2 sec^{-1} (Pd) to 2.3×10^{-7} cm^2 sec^{-1} (10% Ag/Pd), 1.95×10^{-7} cm^2 sec^{-1} (25% Ag/Pd), and 1.95×10^{-7} cm^2 sec^{-1} (5% Sn/Pd). Thus the values of $D_{n_H \to 0}$ do not fall off appreciably from that of pure palladium for additions of substitutional metals up to approximately 25 atomic per cent. This behavior has been supported by additional work in this laboratory using the relaxation method[18] and by Züchner[19] using a breakthrough time technique[7] with membranes. In addition, Küssner[20] and also Makrides and coworkers[21] have reported values of $D_{n_H \to 0}$ of 3×10^{-7} cm^2 sec^{-1} and 3.5×10^{-7} cm^2 sec^{-1} at 25°, respectively, for a 25% silver–palladium alloy.

Since boron is believed to form an interstitial alloy with palladium, in contrast to those systems studied to date, it is of interest to examine the dependence of $D_{n_H \to 0}$ upon the atomic ratio of boron in the alloy.

Experimental Section

The alloys in the form of thin plates containing 0.035, 0.075, 0.135, 0.175 and 0.208 atomic boron-to-palladium ratio, n_B, were prepared by H. Schaller (Institut für physikalische Chemie, Münster). Their

(7) M. Devanathan and Z. Stachurski, *Proc. Roy. Soc.*, **A270**, 90 (1962).

(8) M. von Stackelberg and F. Ludwig, *Z. Naturforsch.*, **19a**, 93 (1964).

(9) D. N. Jewett and A. C. Makrides, *Trans. Faraday Soc.*, **61**, 932 (1965).

(10) W. Jost and A. Widman, *Z Phys. Chem.*, **B29**, 247 (1935).

(11) F. A. Lewis, "The Palladium–Hydrogen System," Academic Press, New York, N. Y., 1967.

(12) J. E. Worsham, M. K. Wilkinson, and C. G. Shull, *J. Phys. Chem. Solids*, **3**, 303 (1957).

(13) J. Bergsma and J. A. Goedkoop, *Physica*, **26**, 744 (1960).

(14) A. Sieverts and K. Brüning, *Z. Phys. Chem.*, **168A**, 411 (1934).

(15) R. Burch and F. A. Lewis, private communication.

(16) H. Husemann, Ph.D. Dissertation, Münster, 1968, and H. Husemann and H. Brodowsky, *Z. Naturforsch.*, **23a**, 1693 (1968).

(17) H. J. Schaller, Diplomarbeit, Münster, 1967.

(18) K. Allard and T. B. Flanagan, to be published.

(19) H. Züchner, Ph.D. Dissertation, Münster, 1969.

(20) A. Küssner, *Z. Phys. Chem.* (Frankfurt am Main), **36**, 383 (1963).

(21) M. Lord, S. Axelrod, K. Brummer, and A. Makrides, *J. Electrochem. Soc.*, **110**, 179 (1963).

preparation and properties are described elsewhere.[17,22] In the alloys employed here as quenched from elevated temperature there was no phase segregation, *i.e.*, the boron was homogeneously distributed within the palladium matrix. The thicknesses of the specimens were from 3.8×10^{-3} ($n_B = 0.175$) to 9.0×10^{-3} cm ($n_B = 0.075$) and the areas were typically 1 cm^2. The thicknesses of the rolled specimens were determined by carefully measuring an edge with a measuring microscope. Ten such measurements were made for each specimen and an average value was employed. The standard deviations were from approximately 8 to 17% of the average value except for the sample with $n_B = 0.208$ which was larger. It is believed that these large deviations are introduced by the cutting process itself and are much greater than any irregularities present in the plates themselves.

The specimens were carefully cleaned and rubbed with fine emery paper prior to their activation by deposition of platinum black on both sides of the plate. It has been shown elsewhere that the diffusion results obtained using this technique for a palladium alloy are identical whether palladium or platinum black is used for the activation.[18] The samples were sealed into tubes with epoxy resin so that only the alloy was exposed to the electrolytic solution. The solution was 1 N H_2SO_4. Measurements were made in a glass reaction vessel which was placed inside a plexiglass container through which water was circulated at the temperature of the run ($\pm 0.2°$).

Experimental details can be seen elsewhere;[5] the only significant modification was that a recorder with a faster response and chart speed was employed (Siemens Kompensograph). Typical currents and times employed for the perturbation were 3×10^{-5} A and 4 sec, respectively. Results were obtained using both anodic and cathodic currents for perturbation. There were no systematic differences in the results obtained with either method. The electrode potential (*vs.* nhe) was approximately 120 mV before a run was commenced. After the perturbation the potential was changed from this value by ± 1 mV.

For the determination of a diffusion coefficient for a given alloy, anodic and cathodic runs were made consecutively until a total of ten runs were completed. Between the runs the specimen returned to a stable electrode potential indicative of a uniform concentration profile. All ten runs were analyzed and averaged for the value of the diffusion coefficient reported, the standard deviation usually amounting to about 11% of the average. The electrode potential employed here, 120 mV *vs.* nhe, corresponds to a small hydrogen content and so the measured value of D should be the limiting, concentration-independent value, $D_{n_H \to 0}$. In the palladium–hydrogen system an electrode potential of 120 mV (30°) corresponds to a hydrogen content of H/Pd (atomic ratio) $\lesssim 0.001$.[23]

Diffusional Relaxation

The diffusion equation can be solved for the perturbation and its subsequent relaxation process. Rather simple approximations for the evaluation of the experimental data can be obtained, as will be shown, if the flux of hydrogen passing into or out of the specimen is constant with time during the course of the perturbation. In order to approximate this condition, the cathodic or anodic currents employed for the perturbation were maintained constant. The flux of hydrogen atoms into or out of the surface may not correspond to the Faradaic current because in the case of a cathodic perturbation some of the discharged hydrogen atoms may recombine at the surface and be evolved into solution as molecular hydrogen, or alternatively in the anodic case additional hydrogen atoms may arrive at the surface from molecules dissolved in the solution.

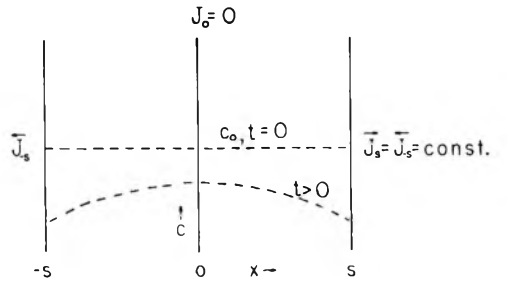

Figure 1. Schematic drawing of concentration profiles before and after application of perturbation.

From the known solubility of hydrogen molecules in the electrolyte at $p_{H_2} \cong 10^{-4}$ atm (the pressure corresponding to 120 mV at 30°) it can be estimated that the magnitude of the contribution of the forward or reverse steps of the reaction $H_{2(solution)} \rightleftarrows 2H$ is negligible compared to the measured flux during typical perturbations, *e.g.*, 3×10^{-5} A for 4 sec. It can be assumed therefore that constant current implies constant flux. This conclusion is supported by the close agreement of the experimental data with the exact solution of the diffusion equation (below). In addition, if the hydrogen flux into the specimen were to vary with time, it would not be expected that its time variation would be identical for the anodic and cathodic perturbations. The close agreement of the results for the two types of perturbation argues that the flux is indeed invariant with time.

For the initial and boundary conditions of $c = c_0$ at $t = 0$ and $(\partial c/\partial x)_0 = 0$ and $(\partial c/\partial x)_{\pm s} = -J_{\pm s}/D$ (Figure 1), Crank[24] gives for the concentration at $t = t_0$

(22) H. Brodowsky and H. Schaller, *Trans. Met. Soc. AIME*, **245**, 1015 (1969).

(23) E. Wicke and G. Nernst, *Ber. Bunsenges. Phys. Chem.*, **68**, 224 (1964).

(24) J. Crank, "Mathematics of Diffusion," Clarendon Press, Oxford, 1956, p 58.

$$f(x) = c_0 + \frac{J_s s}{D}\left\{\frac{Dt_0}{s^2} + \frac{3x^2 - s^2}{6s^2} - \frac{2}{\pi^2}\sum_{m=1}^{\infty}\frac{(-1)^m}{m^2}\exp\left(\frac{-Dm^2n^2t_0}{s^2}\right)\cos\frac{m\pi x}{s}\right\} \quad (1)$$

where s is the half-thickness of the specimen and t_0 is the duration of the perturbation. The subsequent relaxation of the perturbation under the experimental conditions of $(\partial c/\partial x)_{0,\pm s} = 0$ is given as[24]

$$c(x,t) = \frac{1}{s}\int_0^s f(x')dx' + \frac{2}{s}\sum_{n=1}^{\infty}\exp\left(\frac{-D\pi^2n^2t}{s^2}\right)\times \cos\frac{n\pi x}{s}\int_0^s f(x')\cos\frac{n\pi x'}{s}\,dx' \quad (2)$$

where $f(x)$ is given by eq 1 and x' is the variable of integration. At $x = s$ it can be shown that eq 2 reduces to

$$c(x,t) - c(s,\infty) = \frac{2J_s s}{D\pi^2}\sum_{n=1}^{\infty}\frac{1}{n^2}\times \exp(-\alpha t n^2)[1 - \exp(-\alpha t_0 n^2)] \quad (3)$$

where $\alpha = D\pi^2/s^2$. The summation can be replaced by integrals for small values of αt_0 so that eq 3 can be approximated by

$$c(s,t) - c(s,\infty) = \frac{2J_s s}{D\pi^2}\left[\int_1^{\infty}\frac{\exp(-\alpha t n^2)}{n^2}dn + \frac{\exp(-\alpha t)}{2} - \int_1^{\infty}\frac{\exp(-\alpha(t+t_0)n^2)}{n^2}dn - \frac{\exp(-\alpha(t+t_0))}{2}\right] \quad (4)$$

where the $(1/2)\exp(-\alpha t)$ and $(1/2)\exp(-\alpha(t + t_0))$ terms are included to make the integrals better approximations to the summation. If eq 4 is integrated by parts, eq 5 results

$$c(s,t) - c(s,\infty) = \frac{2J_s s}{D\pi^2}\left\{\frac{3}{2}\exp(-\alpha t) - \frac{3}{2}\exp(-\alpha(t+t_0)) - \sqrt{\alpha t\pi}\,erfc\sqrt{\alpha t} + \sqrt{\alpha(t+t_0)\pi}\,erfc\sqrt{\alpha(t+t_0)}\right\} \quad (5)$$

For small values of $\sqrt{\alpha t}$ and $\sqrt{\alpha(t + t_0)}$ eq 5 can be approximated by

$$c(s,t) - c(s,\infty) = \frac{2J_s s}{D\pi^2}\left\{-\frac{\alpha t_0}{2} + \sqrt{\alpha\pi}\,(\sqrt{t+t_0} - \sqrt{t})\right\} \quad (6)$$

Because the data are obtained in regions of hydrogen content where Sieverts' law is valid, $P_{H_2}^{1/2} = \exp(-EF/RT) = K_H n_H$, measured electrode potentials (*vs.* nhe) can be substituted for concentrations at $x = s$. Following this substitution and using $c = n_H/V_{Me}$, where V_{Me} is the molar volume of the hydrogen-containing alloy, and expanding $\exp(E_\infty - E)F/RT$ to the first power (this is a good approximation since experimentally $|E_\infty - E|$ is less than 1 mV) brings eq 6 to the form

$$E(s,\infty) - E(s,t) = \frac{-\alpha t_0}{2K} + \frac{\sqrt{\alpha\pi}}{K}\{\sqrt{t+t_0} - \sqrt{t}\} \quad (7)$$

where

$$K = \frac{\pi^2 D}{2J_s s K_H V_{Me}}\frac{F}{RT}\exp(-E_\infty F/RT)$$

If $E(s,\infty) - E(s,t)$ is plotted against $\sqrt{t+t_0} - \sqrt{t}$, the value of D can be obtained from the slope S, and the intercept I, *i.e.*

$$D = 4I^2s^2/S^2\pi t_0^2 \quad (8)$$

Instead of replacing the summation in eq 3 by integrals it may be computed exactly for selected values of α, t_0, and t. For this purpose an IBM 360 Computer was utilized using values of α from 3×10^{-4} to 10^{-3} in steps of 10^{-4} and from 10^{-3} to 10^{-2} in steps of 10^{-3} and from 10^{-2} to 4×10^{-2} in steps of 10^{-2}. Values of t_0 were from 2 to 15 sec in steps of 1 sec and t in steps of 1 sec to 15 or 100 sec. The summation was carried out until the value of a term in the sum was less than 10^{-5} of the sum up to that term or alternatively when 237 terms were included in the summation. The first criterion was met in most cases before 237 terms were evaluated.

The availability of the nearly exact value for the summation allows the approximate treatment to be evaluated. Table I shows some typical errors introduced by the approximation used in obtaining eq 6. It can be seen from Table I that the approximation is extremely good except when α is large, ≥ 0.1 and t_0 is large.

Table I: Comparison of "Exact" Sum, $\sum_{n=1}^{\infty}\frac{1}{n^2}e^{-\alpha t n^2}(1 - e^{-\alpha t_0 n^2})$, with the Approximation to the Sum, $(-\alpha t_0/2) + \sqrt{\alpha\pi}\{\sqrt{t+t_0} - \sqrt{t}\}$, for Typical Values of α, t_0 and t

α	t_0, sec	t, sec	Exact sum	Approximation (eq 6)
3×10^{-4}	3	4	0.01937	0.01932
1×10^{-3}	3	4	0.03469	0.03462
1×10^{-3}	10	4	0.09262	0.09247
1×10^{-3}	3	14	0.01988	0.01990
1×10^{-2}	3	4	0.09946	0.09915
1×10^{-1}	3	4	0.21194	0.2123
1×10^{-1}	15	14	0.19248	0.228
1×10^{-1}	30	14	0.23524	1.394

For large values of α a more suitable approximation is that previously employed by Holleck and Wicke[5] in which a parabolic initial condition is obtained for the solution of eq 1 when t_0 is large and the terms of the sum may be neglected. When this parabolic distribution is inserted into eq 2 and the summation is limited to the first term, then the following equation results

$$E(s,t) - E(s,\infty) = \text{const} \exp(-D\pi^2 t/s^2) \quad (9)$$

Alternatively, for small times and again under conditions where the parabolic initial distribution holds, t_0 large, the plate can be treated as a semi-infinite medium[25] and the general solution is

$$c(x,t) = \frac{1}{2\sqrt{\pi Dt}} \int_0^\infty \varphi(\xi)\{\exp(-(\xi - x)^2/4Dt) + \exp(-(\xi + x)^2/4Dt)\}\,d\xi \quad (10)$$

This can be evaluated for the initial parabolic distribution, $\varphi(\xi)$, which extends up to a thickness r, $r < s$, *i.e.*

$$\varphi(\xi) = \begin{cases} c_0 - a(r - \xi)^2 & (\xi \leq r) \\ c_0 & (\xi \geq r) \end{cases}$$

It is convenient here to consider the surface to be located at $x = 0$ rather than $x = \pm s$ as in the derivations of eq 9 and 11. If erfcz is approximated by the summation

$$\frac{1}{\sqrt{\pi}} \exp(-z^2)\left[1/z - \frac{1}{2z^3} + \ldots\right]$$

where $z = s^2/4Dt$ and $s^2 \gg 4Dt$, then the following expression results

$$[c(0,\infty) - c(0,t)]/[c(0,\infty) - c(0,0)] = 3Dt/s^2 - 6\sqrt{Dt}/S\sqrt{\pi} + 1 \cong \left[1 - \frac{\sqrt{3Dt}}{s}\right]^2 \quad (11)$$

and

$$\sqrt{E(0,\infty) - E(0,t)} = \sqrt{E(0,\infty) - E(0,0)} - \sqrt{E(0,\infty) - E(0,0)}\,[3Dt/s^2]^{1/2} \quad (12)$$

where measured electrode potentials (*vs.* nhe) have been substituted for concentrations in eq 11 in going to eq 12 using relationships given above. The diffusion coefficient is obtained from the slope of the plot of $\sqrt{E(0,\infty) - E(0,t)}$ *vs.* $t^{1/2}$ and the intercept at $t = 0$.

Results and Discussion

Some typical diffusion runs are shown in Figure 2 (0.175 atomic ratio boron, 30°). A typical analysis of diffusional data *via* eq 7 is shown in Figure 3. The matching of the "exact" summation (eq 3) with the experimental data is shown also in Figure 2 where the value of α and the multiplicative factor before the summation are determined from the slope and intercept of eq 7. It can be seen that the experimental data and the values from the "exact" solution agree reasonably well especially with regard to the shape of the curves. This agreement helps to justify the assumption discussed above that the flux is constant during the perturbation.

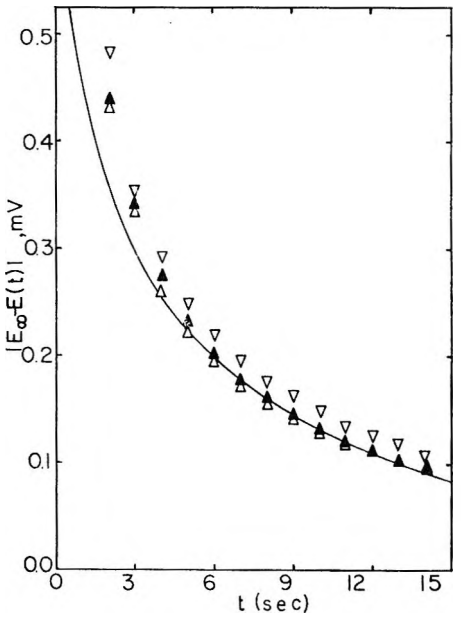

Figure 2. Typical relaxation data obtained for several runs, △, ▲, ▽; n_B = 0.175, 30°. Solid curve calculated from eq 7.

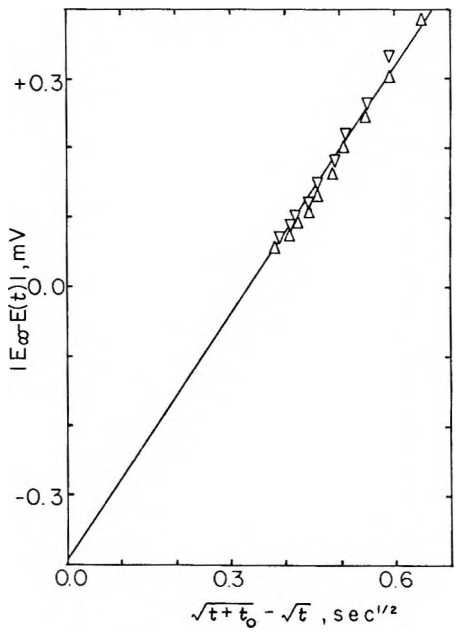

Figure 3. Plots of experimental values of $|E_\infty - E(t)|$ *vs.* $\sqrt{t + t_0} - \sqrt{t}$ at 30° for n_B = 0.175. $E_\infty = E(s,\infty)$ and $E(t) = E(s,t)$.

Figure 4 shows an analysis of data with eq 12 using the 0.035 atomic ratio boron alloy where, among the alloys investigated here, eq 12 should be most ap-

(25) W. Jost, "Diffusion," Academic Press, New York, N. Y., 1960, p 33.

plicable, *i.e.*, $D_{n_H \to 0}$ is large. Each bar represents the spread of values obtained for ten anodic and cathodic runs. The deviation from straight line behavior observed at large times is expected from the assumptions employed in the derivation of eq 12.

Data were obtained for alloys of 0.035, 0.075, 0.137, 0.175, and 0.208 atomic ratio boron using eq 7, 9, and 12. Within experimental error results generally agree except for alloys of $n_B \geq 0.137$ where the more exact analysis is needed (eq 7). The latter analysis gave smaller diffusion coefficients; these coefficients are the more correct for alloys of $n_B \geq 0.137$.

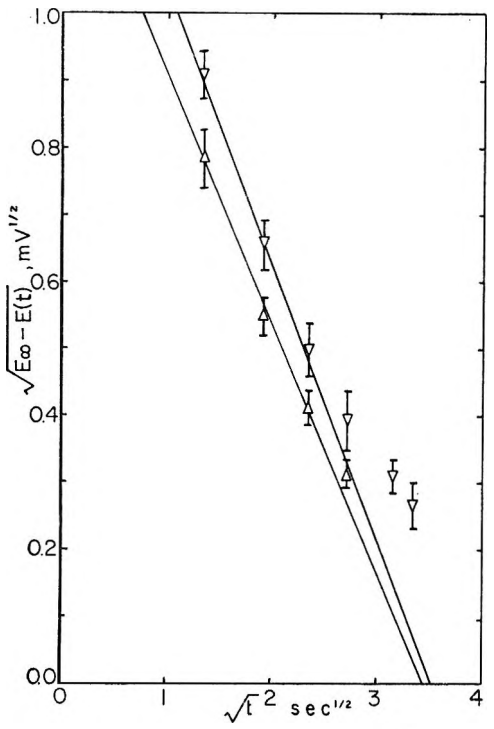

Figure 4. Typical relaxation data plotted as $\sqrt{E_\infty - E(t)}$ *vs.* $\sqrt{t}$; $n_B = 0.035$, 30°. $E_\infty = E(0, \infty)$ and $E(t) = E(0,t)$.

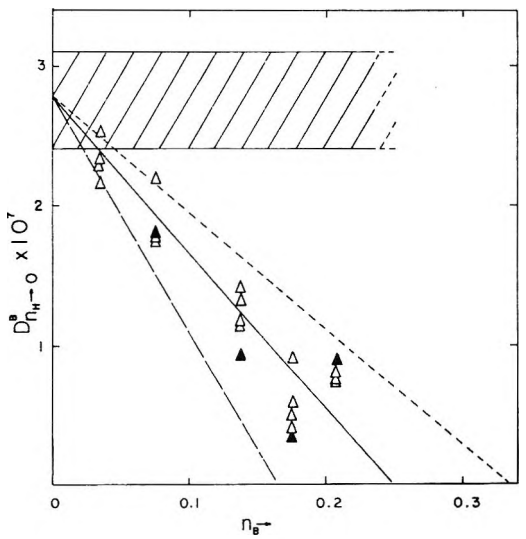

Figure 5. Values of $D^B{}_{nH \to 0}$ *vs.* n_B (30°). ▲, data evaluated using eq 7; △, data evaluated by eq 9 and 12 and averaged. Each point represents the average of 10 runs. Solid line, calcd by eq 13; dashed line calcd by eq 17; broken line calcd by eq 18. The shaded area indicates comparable data as plotted against added metal content for substitutional alloys.[18,19]

Values of the diffusion coefficients are shown in Figure 5 (30°). The behavior of the diffusion coefficients for the boron–palladium alloys is in marked contrast to that of the substitutional alloys which have been investigated to date (Figure 5). This contrast, in itself, strongly supports the view that boron occupies interstitial rather than substitutional positions in the palladium matrix.

Activation energies of 5.8 ± 2.0 kcal/mol and 5.8 ± 0.8 kcal/mol were determined for the diffusion of hydrogen at $n_H \to 0$ for the alloys with $n_B = 0.137$ and 0.175, respectively, from 0 to 71°. These values are essentially unchanged from that of pure palladium.[2-6]

It has been suggested that hydrogen diffuses through pure palladium *via* the tetrahedral holes from one octahedral interstitial site to another;[4] this constitutes the lowest energy pathway. The decline in the values of $D^B{}_{n_H \to 0}$ with boron content—despite the fact that the energy of activation remains unchanged—suggests that the presence of boron blocks possible diffusion paths for the hydrogen. It will be assumed that each isolated boron atom in the alloy matrix completely blocks all eight of its surrounding, neighboring tetrahedral interstitial holes as diffusion pathways for hydrogen atoms. There are $N/4$ unit cells in a specimen containing N palladium atoms and $2N$ tetrahedral holes. The fraction of blocked tetrahedral holes is $4n_B$ so that the diffusion coefficient at $n_H \to 0$ in the first, rough approximation is given by

$$D^B{}_{n_H \to 0} = D^{Pd}{}_{n_H \to 0}[1 - 4n_B] \qquad (13)$$

and

$$dD^B{}_{n_H \to 0}/dn_B = -4D^{Pd}{}_{n_H \to 0}$$

This relationship is shown by the full line in Figure 5; it agrees quite well with the experimental data. By contrast, the assumption that boron blocks all twelve surrounding octahedral sites does not predict a slope in good agreement with the experimental data.

An alternative analysis of the dependence of $D^B{}_{n_H \to 0}$ upon n_B can be made in analogy to Rayleigh's treatment of electrical conductivity of heterogeneous systems.[26,27] If spherical particles of insulating material are uniformly dispersed in a conducting medium such that the total fractional volume occupied by the spherical particles is v and $v \ll 1$ then, following Rayleigh[26]

$$K = K_0 \frac{1 - v}{1 + v/2}$$

(26) Lord Rayleigh, *Phil. Mag.*, **34**, 481 (1892).

(27) G. S. Frey, *Z. Elektrochem.*, **38**, 260 (1932).

where K and K_0 are the conductivities of the heterogeneous system and pure system, respectively. For the problem at hand the conductivities must be replaced by diffusion coefficients

$$D^{B}_{n_H \to 0} = D^{Pd}_{n_H \to 0} \frac{1 - v}{1 + v/2} \quad (14)$$

and more specifically v ($v \ll 1$) is the volume fraction of domains (approximately spherical) in the metallic lattice which are blocked for hydrogen diffusion by the boron atoms. The term $1 - v$ in eq 14 represents the mean fraction of cross-sectional area free for hydrogen diffusion, whereas the term $1 + v/2$ accounts for the lengthening of the diffusional paths since a diffusing particle may bypass a blocked domain *via* a curved path (the labyrinth factor). For $v \ll 1$ eq 14 can be approximated by

$$(D^{B}/D^{Pd})_{n_H \to 0} = 1 - (3/2)v \quad (15)$$

In order to calculate v as a function of the atomic ratio, n_B, the following three assumptions can be made.

(i) Each boron atom in an octahedral hole blocks just this site for hydrogen diffusion. Since the octahedron covers one-sixth of the unit cell volume the following relation results

$$1 - \frac{3}{2}v = 1 - \frac{3}{2}\frac{N_B(a_0^3/6)}{N_{Pd}(a_0^3/4)} = 1 - n_B \quad (16)$$

where a_0 is the unit cell size and N_B and N_{Pd} are the number of boron and palladium atoms, respectively.

(ii) Besides blocking the octahedral site which it occupies, the boron atom blocks the surrounding 8 tetrahedral holes.

$$1 - \frac{3}{2}v = 1 - \frac{3}{2}\frac{N_B(a_0^3/6 + 8a_0^3/24)}{N_{Pd}(a_0^3/4)} = 1 - 3n_B \quad (17)$$

(iii) The boron atom blocks the entire unit cell within which it is situated.

$$1 - \frac{3}{2}v = 1 - \frac{3}{2}\frac{N_B a_0^3}{N_{Pd}(a_0^3/4)} = 1 - 6n_B \quad (18)$$

Assumption (i) leads to results which are quite inconsistent with the data shown in Figure 5 whereas assumptions (ii) and (iii) bracket the data except for the alloy with $n_B = 0.035$, where the experimental scatter exceeds the narrow spread in the predicted values (Figure 5). The simple approximation (eq 13) is included within the slopes predicted by eq 17 and 18. These results indicate that with regard to hydrogen diffusion the boron atom really blocks the 8 tetrahedral holes which surround its own octahedral site.

Equations 15–18 are valid for very small values of v only. When the boron content, n_B, increases in the palladium lattice, the blocked volume fraction, v, increases more slowly than in direct proportion to n_B because of overlapping effects; *i.e.*, boron atoms will occupy adjacent pairs and triples of octahedral holes. This effect tends to bend the straight line shown in Figure 5 as n_B increases. On the other hand, the labyrinth factor decreases more rapidly with increasing v than according to $1/(1 + v/2)$. The addition of these two opposing effects tends to create the linear grouping of the measured points in Figure 5 far beyond the limits of the expected validity of eq 15 through 18.

The obvious success of these simple models supports the view that boron occupies interstitial sites in the palladium lattice and also provides evidence that hydrogen diffusion occurs *via* the tetrahedral holes. The fact that the energy of activation is unchanged from that of pure palladium, in contrast to the behavior of some of the more concentrated substitutional alloys,[4,5] further supports the idea that the hydrogen is blocked completely by the boron; *i.e.*, the hydrogen atoms diffuse through regions of the lattice very much like through pure palladium.

The result that boron is able to block all eight surrounding tetrahedral holes is noteworthy. The hydrogen atom (screened proton) must pass within 1.68 Å of the boron or hydrogen atom when it diffuses through the tetrahedral hole (using the lattice parameter of pure palladium). To a first approximation the presence of hydrogen atoms in the octahedral interstices does not block the passage of other hydrogen atoms.[4] Using standard formulas for shielding[28] of the proton and the +3 boron ion using the density-of-states of pure palladium[29] and a separation of 1.68 Å, the repulsion between the shielded proton or boron ion and the octahedral proton should be negligible. It must be assumed, therefore, that the blocking results instead from the distortion of the tetrahedral holes by the presence of the boron atoms in the interstitial positions. The palladium atoms in the base of the tetrahedron adjacent to the boron interstitial will be distorted more than the apex palladium atom. This distortion seems to raise the activation energy for passage through tetrahedral holes to a value large enough to effectively block diffusion within the temperature range investigated.

It should be mentioned in conclusion that this is one of the first examples of diffusional data yielding structural information. Figure 5 clearly shows a marked contrast in the hydrogen diffusion behavior of the boron–palladium alloys with that of the substitutional alloys and this contrast constitutes rather strong evidence that these boron alloys are not substitutional but interstitial.

(28) J. Ziman, "Principles of the Theory of Solids," Cambridge University Press, 1964.

(29) *E.g.*, F. E. Hoare in "Electronic Structure and Alloy Chemistry of the Transition Elements," P. A. Beck, Ed., John Wiley & Sons, New York, N. Y., 1963.

Acknowledgments. The authors are indebted to Dipl.-Phys. H. J. Schaller (Universität Münster) for the preparation of the alloys and to Dr. E. Weltin (University of Vermont) for his assistance in the computer programming. T. B. F. was supported at the Institut für physikalische Chemie, Münster, as a Fulbright Research Scholar, and acknowledgment is made to the donors of the Petroleum Research Fund, administered by the American Chemical Society, for an International Faculty Award. K. D. A. is indebted to the Deutsche Forschungsgemeinschaft for a fellowship.

Relationships between Divalent Cation Distributions and Residual Water Content in Metal Cation Faujasite-Type Zeolites

by E. Dempsey and D. H. Olson

Mobil Research and Development Corporation, Central Research Division Laboratories, Princeton, New Jersey 08540
(Received June 2, 1969)

Relations between divalent cation site occupancy and residual water content for faujasite-type zeolites are presented. For site I′ and II′ occupancies the relations seem well established. For site I occupancy the relation is weaker and shows exceptions; tentative explanations for these exceptions are given. The relations suggest that for zero water content sites I′ and II′ should be empty.

Several workers have postulated that retained water molecules (or related species) in the sodalite cages of activated faujasite-type zeolites play an important role in determining the cation distribution in the materials.[1-5] Since the catalytic activity of these materials may be a function of both the amount of retained water and the cation distribution, the following relations between these two factors may be of interest. The curves defining the dependences of site I′ and II′ occupancies[6] upon water content seem well-founded and show no exceptions for a range of Si/Al ratios: for site I, the dependence of occupancy upon water content is more tentative. Since natural faujasite crystals fit the same relations as do synthetic X zeolites, we do not distinguish between the two groups of materials other than in their Si/Al ratios.

Recently it was shown theoretically that divalent ions in zeolites having the faujasite structure have a strong electrostatic preference for the site at the center of symmetry in the hexagonal prisms of the structure.[5] However, preliminary X-ray work on specimens vacuum-dehydrated at 400° (see Table I) showed that some of these cations remain in a site adjacent to the electrostatically preferred one (site I′ instead of site I). Confidence in the theoretical predictions led to the proposals that residual water in the zeolites produced the apparently anomalous site occupation and that the size and the nature of the divalent cation should play a role in determining the amount of retained water. Subsequently, X-ray evidence for the presence of this water was in fact found.[7]

In our X-ray investigations, we have observed an apparent near complementarity between the occupancies of sites I and I′ for divalent cation X zeolites. It appears that the occupancies N_I, $N_{I'}$ per unit cell of these sites follow (at least approximately) the rule

$$N_{I'} = 2(16 - N_I) \qquad (1)$$

i.e., whenever a site I is unoccupied, the two adjacent sites I′ are occupied. This is, of course, reasonable on electrostatic and symmetry grounds.

Figure 1 (based upon the data of Table I[8,9]) illustrates the point just made. In the figure the various site

(1) J. V. Smith, J. M. Bennett, and E. Flanigen, *Nature*, **215**, 241 (1967).

(2) T. I. Barry and L. A. Lay, *J. Phys. Chem. Solids*, **29**, 1395 (1968).

(3) J. M. Bennett and J. V. Smith, *Mat. Res. Bull.*, **3**, 865 (1968).

(4) J. M. Bennett, J. V. Smith, and C. L. Angell, *ibid.*, **4**, 77 (1969).

(5) E. Dempsey, *J. Phys. Chem.*, **73**, 3660 (1969).

(6) Sites I lie at centers of hexagonal prisms. Sites II lie on six-ring faces of sodalite units, on the large cavity side. Sites I′ and II′ lie on the other sides of the respective six-rings of the unprimed sites, within the sodalite cages.

(7) D. H. Olson, *J. Phys. Chem.*, **72**, 1400 (1968).

(8) D. H. Olson, unpublished work.

(9) J. V. Smith and J. M. Bennett, *Mat. Res. Bull.*, **3**, 633 (1968).

Table I: Summary of Nonframework Atom Sites

Heat treatment (vacuum)		CaFj,[9] 14 hr, 475°	CaX,[7] 16 hr, 400°	SrX,[7] 16 hr, 400°	SrX(D),[8] 16 hr, 680°[b]	NiFj,[11] 16 hr, 400°
Site occupancy: cations per unit cell	I	14.2 (3)	7.5 (5)	11.2 (3)	6.1 (1)	10.6 (1)
	I′	2.6 (4)	17.3 (6)	7.0 (6)	12.0 (2)	3.2 (3)+ 1.9 (6)[a]
	II′	...	9.0 (10)	4.2 (8)	6.4 (4)	1.9 (6)
	II	11.4 (4)	17.3 (6)	19.5 (6)	20.3 (2)	6.4 (2)
II′ OW–water oxygen/u.c.		...	10.5 (19)	5.4 (15)	7.7 (15)	1.9 (15)

[a] There are two site I′ peaks assigned to nickel ions. The smaller is 2.0 Å from OW scattering matter; for reasons given in the Appendix, only this number is included in Figure 1. [b] The set of points for SrX(D) (SrX vacuum calcined for 16 hr at 680°) represents an attempt to decrease the water content of an SrX sample. Before the sample was sealed off, a trace of water was inadvertently readsorbed. (We also found 23 water molecules per unit cell coordinated to Sr^{2+} ions in site II.)

occupancies for the relevant zeolite are plotted against the site II′ water content (bottom line of Table I) to give a vertical array of points for a given specimen. The crosses in the figure represent the site I′ points derived from relation 1 and the site I occupancies, and we see that, while the relation holds well for the CaX zeolite, it gives only an upper limit for the site I′ occupancies for Ca faujasite and SrX. The Ni faujasite and SrX (D) results do not obey relation 1 (the anomalous points are shown as open circles in Figure 1), so crosses are omitted for these zeolites; further discussion of these results is given below.

For equation 1 to hold rigorously, the crosses in Figure 1 should coincide with the site I′ points. The SrX and Ca faujasite points indicate that about one in sixteen of the hexagonal prisms have neither site I nor site I′ cations associated with them. Figure 1 also shows evidence for a correlation of the cation occupancies of sites I′ and II′ with the amount of water within the sodalite cages; clearly the numbers of cations in the two sites within the sodalite cage are functions of the amounts of water in site II′. (It should be kept in mind that the amount of residual water is a function of the temperature and duration of the heat treatment, *i.e.*, the residual water values shown in Figure 1 may not represent definite hydrates.) This finding is in agreement with the general comments of Barry and Lay.[2] Since the extrapolated lines pass near or through the origin, it is clear that with no residual water there should be no divalent cations in the sodalite cages.

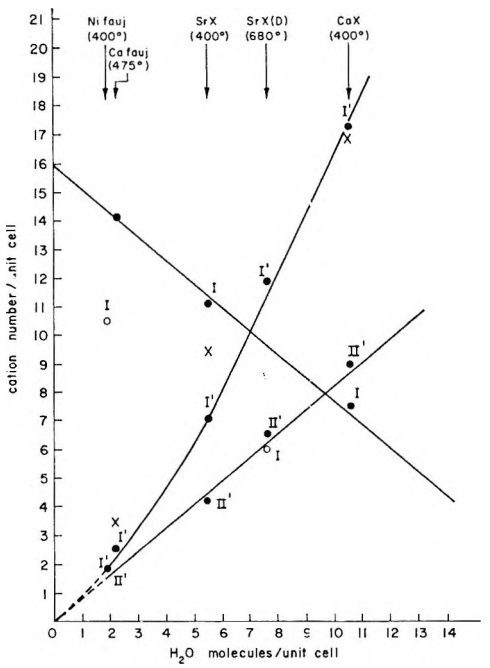

Figure 1. Correlation of cation occupancies of various sites in faujasite-type zeolites with water content in site II′. Points considered to be anomalous are marked as open circles and are discussed in the text. Error limits on the points are given in Table I.

From Figure 1, the site II′ cations bear almost a one-to-one relation to the number of water molecules in the sodalite cage for both X and Y zeolites. For the Ni faujasite, the site I′ occupancy is also almost equal to the water content, but as the number of cations in the structure increases (with decrease in Si/Al ratio, on going to X materials), the site I′ cation/water ratio increases toward 2. Hence, for the zeolites of Figure 1, the total number of cations coordinated to the residual water oxygen varies from two to three. The results also suggest that Y materials may be more readily dehydrated than X materials.

Looked at from a more causal viewpoint, Figure 1 illustrates the suggestion made earlier[5] that, for a given Si/Al ratio, the polarizing power of the cation governs the amount of water retained in the zeolite. For the SrX and the CaX materials, which were given the same calcination treatment, the zeolite containing the smaller cation is less easily dehydrated than is that containing the larger cation. Thus, more calcium ions than strontium ions are retained in sites I′ in association with water molecules. It is also striking that the line joining the site I occupancies for these two zeolites in Figure 1 extrapolates, for zero water content, to a cation number near 16: in other words, for zero water content (and zero site I′ content), site I, in the hexagonal prism,

has close to 100% occupancy; this is another aspect of relation 1. The best straight line through the X zeolite site I points actually passes through 15, whereas we have drawn the best line through these points and the maximum site I occupancy number 16. This we justify on the basis of the significance of the maximum occupancy and the theoretical energy calculations[6] mentioned above. Furthermore, the Ca faujasite results of Smith and Bennett,[9] fitted to the I′ occupancy curve (which is well established by four points), agree best with the line through (0, 16) (see below). Ni faujasite appears not to obey relation 1, although one of the site I′ and the site II′ cation numbers do appear to correlate with the residual water content of the zeolite; the problem (unlike that of the SrX case, where the site I number lies on the site I line) lies with the sites I. A possible explanation is given in the Appendix.

Into Figure 1 we have also incorporated the data of Smith and Bennett[9] for the site I and site I′ occupancies for CaY faujasite calcined to 475°. The points have been placed on the graph at the position of best fit since Smith and Bennett give no water content for their specimen; from the data we would predict that their sample had a residual water content of about 2–3 molecules per unit cell.

The anomalously low site I occupancy for SrX(D) is taken to indicate that some of the hexagonal prisms have been damaged by dehydroxylation, and no longer accept the doubly charged cations, so that the theoretical site I content of ten cations (from Figure 1) is reduced to six. This is consistent with the accepted view[10] that dehydroxylation replaces negatively charged tetrahedral Al sites by positively charged Si and oxygen-defect sites (or at least sites that act as Lewis bases). One would infer from Figure 1 that about 25% of the hexagonal prisms, (10–6)/16, have been affected. The fact that the water content of SrX(D) and the I′ and II′ occupancies fit correctly with the lines of Figure 1 suggests that the sodalite cage–water cation complex follows the same rules whether or not the material is dehydroxylated. It also suggests that cations that in the absence of dehydroxylation would occupy sites I, move into sites II as dehydroxylation proceeds.

Appendix

Since we have included Ni faujasite in Table I and in Figure 1 (for the reason that the site II′ and one of the site I′ occupancies fit our correlation with residual water content), we have the obligation to discuss the apparent anomalies in the Ni faujasite results. Because this discussion, based as it is on a single set of data, involves a higher degree of speculation than the discussion in the text, we have relegated it to an Appendix.

The anomalies in the Ni faujasite results are (1) the site I point for Ni faujasite does not lie on the site I line through the point (0, 16) and (2) there are two site I′

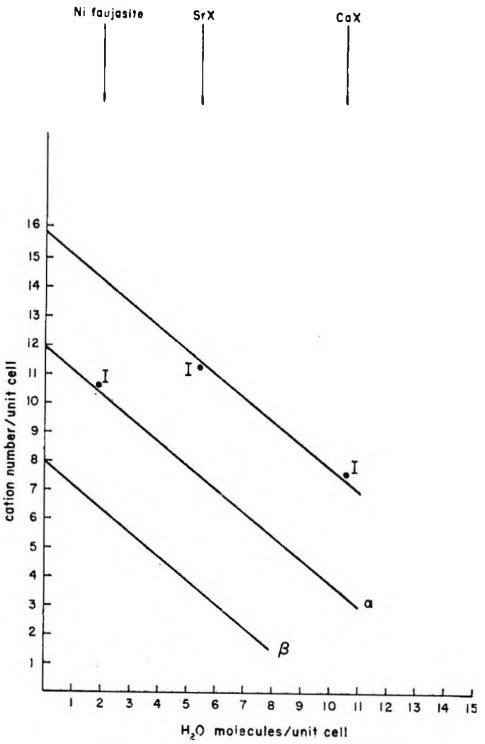

Figure 2. Tentative correlation of the dependence of site I occupancy on water content and charge concentration on hexagonal prisms of the structure. Top line corresponds to a zeolite of Si/Al $\leq$ 2:1; lines α and β correspond to zeolites of Si/Al $\sim$ 2.43:1 and $\sim$ 3:1, respectively.

occupancies (for different site I′ positions), only one of which we have included in Figure 1.

Regarding point 2, it was shown in ref 11 that the ions of the 1.9 occupancy of site I′ lie well away from their nearest hexagonal prism oxygen ions and are coordinated to water oxygens; their coordination to water oxygens justifies their inclusion in Figure 1. The ions of the 3.2 occupancy, on the other hand, are closely coordinated to hexagonal prisms oxygens, and they are not directly coordinated to water oxygens; the latter point justifies their omission from Figure 1. Clearly this is a different site I′ occupancy from that discussed in the text, where site I′ is occupied only because of residual water: Figure 1 and relation 1 imply that removal of this water empties site I′.

The difference between X zeolite and faujasite lies primarily in the Si/Al ratio. Suppose we idealize faujasite to be centrosymmetric and to have the Si/Al ratio 2.43.[12,13] Then each sodalite cage will have seven Al ions, to be distributed over four hexagonal prism faces. This will result in a unit cell in which 12 centro-

(10) J. B. Uytterhoeven, L. G. Christner, and W. K. Hall, *J. Phys. Chem.*, **69**, 2117 (1965).

(11) D. H. Olson, *ibid.*, **72**, 4366 (1968).

(12) E. Dempsey in "Molecular Sieves," Society of Chemical Industry, 1968, p 293.

(13) E. Dempsey, G. H. Kuehl, and D. H. Olson, *J. Phys. Chem.*, **73**, 387 (1969).

symmetric hexagonal prisms will have four Al ions (and a corresponding net negative charge of four) and the remaining four centrosymmetric hexagonal prisms will have only two Al ions (and a net negative charge of 2).[14-16]

Let us say now that relation 1 holds for zeolites all of whose hexagonal prisms carry at least four Al ions. The relation then holds only for materials for which Si/Al $\leq$ 2: *i.e.*, if we generalize relation 1 to

$$N_{I'} = 2(p - N_I) \qquad (2)$$

where p is the number of hexagonal prisms per unit cell carrying at least four Al ions, then only for Si/Al $\leq$ 2 is $p = 16$.

For Si/Al = 2.43:1, $p = 12$. In the case of Ni faujasite, $N_{I'} = 1.9$ and from relation 2 the occupancy of site I should thus be 11. This compares well with the figure 10.6 found experimentally. The line α in Figure 2. passing through (0, 12) should thus give site I occupancies as a function of water content for zeolites having Si/Al = 2.43:1. Similarly, for zeolites of Si/Al = 3:1, the line (β) passing through (0, 8) and parallel to the other two lines should give the site I occupancies.

Hitherto we have neglected the size of the cation under discussion. It seems clear[11] that for a cation to occupy site I, the adjacent six oxygen ions have to fit to the cation. For relatively large cations, the fit may be easy. On the other hand, for small cations, considerable strain energy may have to be put into the zeolite framework to accommodate the ions in site I. This strain energy will operate against any gain in electrostatic energy, and variations in the strain energy with variations in cation size will work against the general validity of relations 1 and 2.

Consider now the four hexagonal prisms of our idealized faujasite that have only two Al ions. We conjecture that the strain energy mentioned above will be large for Ni^{2+}. Taking this in conjunction with the reduced charge on the hexagonal prisms, there will be little driving force for Ni^{2+} ions to enter these hexagonal prisms. (Larger ions like Ca^{2+} may in fact still occupy all sites I—despite a reduced charge on some hexagonal prisms—if little strain energy is involved. This argument is supported by the Ca faujasite data in Figure 1, if our placement of the data is correct.)

Thus we may expect that associated with the four hexagonal prisms carrying only two Al ions there may be Ni^{2+} ions in sites I'. These ions will not have to coordinate to water to retain their positions and, consequently, they will lie closer to the hexagonal prism faces than will those ions that do coordinate to water. Possibly the 3.2 cations occupying the second site I' position for Ni faujasite (see Table I) are ions of this type.

(14) Although this discussion does not include trivalent ions, it is striking that Smith and Bennett, studying La faujasite at room temperature[15] and at 420°,[16] found about 11.8 La ions in sites I; this correlates well with the 12-hexagonal prisms carrying 4 Al ions.

(15) J. M. Bennett and J. V. Smith, *Mat. Res. Bull.*, **4**, 867 (1968).

(16) J. M. Bennett and J. V. Smith, *ibid.*, **4**, 7 (1969).

A Simple Model of Interdiffusion with Precipitation

by F. Helfferich and A. Katchalsky

Shell Development Company, Emeryville, California 94608 and Weizmann Institute of Science, Rehovoth, Israel (*Received June 17, 1969*)

A mathematical treatment of interdiffusion of two substances, A and B, forming a precipitate AB when the solubility product is exceeded, is presented. In contrast to previous work, precipitation is included as a flow in the differential equation rather than being specified as a boundary condition. The calculations are for unidimensional diffusion without convection in a diffusion layer (gel or membrane) between semiinfinite reservoirs, and with the assumption that the precipitate will not impede diffusion.

Introduction

Since Liesegang's discovery[1] in 1896 that interdiffusion of silver nitrate and potassium bichromate in a gelatin gel leads to periodic precipitation, the field of gel precipitation has continued to attract the interest of experimentalists and theoreticians. The classical supersaturation theory of Wilhelm Ostwald[2] and its experimental verification was reviewed by Freundlich[3] and

(1) R. E. Liesegang, *Naturw. Wochenschr.*, **11**, 353 (1896).

(2) W. Ostwald, *Z. Phys. Chem.* (Leipzig), **22**, 289 (1897).

(3) H. Freundlich, "Kapillarchemie," Vol. 2, 4th ed., Akademische Verlagsgesellschaft m.b.H., Leipzig, 1932, p 701.

Van Hook[4] and was more recently put on a quantitative basis by Wagner.[5] During the past two decades, Hirsch-Ayalon[6] studied membranes in which a $BaSO_4$ precipitate was formed by interdiffusion of $Ba(OH)_2$ and H_2SO_4. In 1948, Ouchterlony[7] described an important method for the study of antigen–antibody interaction by following precipitation in agar gels. Subsequently Oudin[8] developed a "single-diffusion" method for antigen–antibody reactions, in which a column of gel loaded with antibody is overlaid with antigen solution. A theoretical analysis of antigen–antibody precipitation by interdiffusion in gels was carried out by Ouchterlony,[9] Preer,[10] and Engelberg,[11] while the theory of single-diffusion precipitation was worked out in an elementary way by Hermans,[12] Becker,[13] and in a more careful and advanced form by Spiers and Augustin.[14] A detailed mathematical treatment of the two-dimensional diffusion in gel systems is found in the papers of Aladjem, *et al.*[15]

It is noteworthy that all previous theories treat the precipitating system by the equations of free diffusion, according to the mathematical methods summarized in the classical monograph of Crank.[16] The precipitation in the critical range of concentrations is introduced as *a boundary condition* and never treated explicitly in the transport equations themselves. Since recent work on nonequilibrium thermodynamics[17] permits the treatment of generalized flows of various kinds and provides a method for the description of their coupling with conventional flows, the flow of precipitation j will be introduced as a new flow. The aim of this paper is to evaluate the precipitation flow explicitly and to specify its coupling with the diffusion flows of the reactants.

System and Premises

For the sake of simplicity, the treatment will be essentially confined to the elementary, ideal case specified below. A few extensions will be examined in the last section.

We consider two nonelectrolytes, A and B, which reversibly form with one another a precipitate AB

$$A + B \rightleftharpoons AB\downarrow \qquad (1)$$

when the solubility product is exceeded. Thus, the concentrations of A and B (assumed to equal the activities) in equilibrium with the precipitate obey the condition

$$C_A C_B = K = \text{constant} \qquad (2)$$

It is assumed that the rate of precipitation is exclusively controlled by the diffusional supply of A and B, *i.e.*, that equilibrium of reaction 1 is attained instantaneously and that there is no supersaturation.

It is also assumed that the precipitate will not impede diffusion, a safe assumption for only the initial phases of precipitation. Eventually, the precipitate will of course clog the diffusion layer, and the theory will then no longer be applicable.

The system under consideration consists of two semiinfinite reservoirs, each containing a solution of one of the reactants, and joined by a permeable plug of length d and uniform cross section (see Figure 1).

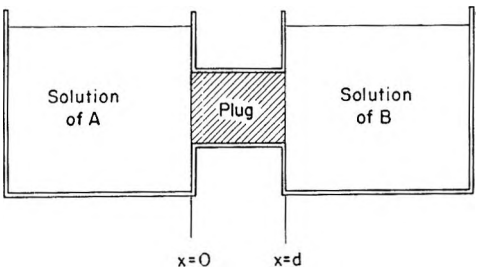

Figure 1. System studied.

The solutions are well mixed so that the concentrations at $x = 0$ and $x = d$ remain constant throughout the process

$$\text{at } x = 0,\ C_A = C_A^\circ \text{ and } C_B = 0 \qquad \text{for } t \geq 0 \qquad (3)$$

$$\text{at } x = d,\ C_A = 0 \text{ and } C_B = C_B^\circ$$

The system is taken to be isothermal; it is assumed that there is no convection, no osmotic or electroosmotic flow, and that the diffusion coefficients are independent of concentration.

Under the specified conditions and assumptions, the system can be expected to attain a steady state. The approach to this state will be discussed later after its concentration profiles and precipitation flow have been calculated.

(4) A. van Hook, in "Colloid Chemistry," Vol. 1, J. Alexander, Ed., Reinhold Publishing Corp., New York, N. Y., 1944, p 513.

(5) C. Wagner, *J. Colloid Sci.*, 5, 85 (1950).

(6) P. Hirsch-Ayalon, *Rec. Trav. Chim.*, **75**, 1065 (1956); *ibid.*, **79**, 382 (1960); *J. Polymer Sci.*, **23**, 697 (1957); see also C. J. Van Oss and Y. S. L. Heck, *Rev. Immunol*, **27**, 27 (1963).

(7) Ö. Ouchterlony, *Arkiv. Kemi Mineral. Geol.*, **26B**, No. 14 (1948).

(8) J. Oudin, *Compt. Rend.*, **222**, 115 (1946).

(9) Ö. Ouchterlony, *Arkiv Kemi*, **1**, 43 (1949).

(10) J. R. Preer, Jr., *J. Immunol.*, **77**, 52 (1956).

(11) J. Engelberg, *ibid.*, **82**, 467 (1959).

(12) J. J. Hermans, *J. Colloid Sci.*, **2**, 387 (1947).

(13) E. L. Becker, J. Munoz, C. Lapresle, and L. Le Beau, *J. Immunol.*, **67**, 501 (1951).

(14) J. A. Spiers and R. Augustin, *Trans. Faraday Soc.*, **54**, 287 (1958).

(15) F. Aladjem, R. W. Jarvis, R. L. Paldino, and J. A. Lackner, *J. Immunol.*, **83**, 221 (1959).

(16) J. Crank, "The Mathematics of Diffusion," The Clarendon Press, Oxford, 1956.

(17) S. R. de Groot, and P. Mazur, "Non-Equilibrium Thermodynamics," Interscience Publ., Inc., New York, N. Y., 1962.

Basic Equations

The equations of continuity of A and B at every point in the plug are

$$\frac{\partial C_A}{\partial t} = -\text{div}\, J_A - j$$

and

$$\frac{\partial C_B}{\partial t} = -\text{div}\, J_B - j$$

where j, a function of x and t, is the local precipitation flow (*i.e.*, number of moles AB per unit volume and per unit time deposited in the plane x at time t).

For the unidimensional case under consideration, div $= \partial/\partial x$, and, if diffusional flows J_A and J_B are governed by concentration-independent diffusion constants D_A and D_B, respectively

$$J_A = -D_A \frac{\partial C_A}{\partial x}$$

and

$$J_B = -D_B \frac{\partial C_B}{\partial x}$$

so that

$$\frac{\partial C_A}{\partial t} = D_A \frac{\partial^2 C_A}{\partial x^2} - j; \quad \frac{\partial C_B}{\partial t} = D_B \frac{\partial^2 C_B}{\partial x^2} - j \qquad (4)$$

The boundary conditions are as stated in eq 3. The following additional restrictions apply. Precipitation does not occur where the concentration product is smaller than the solubility product, so that

$$t \geq 0, \quad 0 \leq x \leq d \quad \begin{cases} C_A C_B < K \quad (j = 0) & (5a) \\ C_A C_B = K \quad (j \geq 0) & (5b) \end{cases}$$

The solubility product imposes the restriction

$$t \geq 0, \quad 0 \leq x \leq d, \quad C_A C_B \leq K \qquad (6)$$

A brief comparison with similar systems involving chemical reactions or adsorption is instructive. In such cases, too, the continuity conditions contain a sink term, but of a different nature. For example, with a first-order reaction of the diffusing species i the continuity condition is

$$\frac{\partial C_i}{\partial t} = D_i \frac{\partial^2 C_i}{\partial x^2} - kC_i$$

where k is a reaction rate constant.[18] The reaction giving rise to the sink term $-kC_i$ takes place wherever $C_i > 0$, the reaction rate depends on the rate constant and the concentration, and no restriction is imposed on the concentration. In our problem, the precipitation reaction takes place only where the concentrations are high enough to meet condition 5b, and the precipitation rate is not limited by a rate constant, with the result that a rigid ceiling is imposed on the concentrations by condition 6.

Qualitative Features

The expected shape of the steady-state concentration profiles of A and B is shown schematically in Figure 2. Within the plug, precipitation cannot occur in the immediate neighborhood of either surface because, here, the concentration of one solute is negligible while that of the other is finite. Precipitation, thus, is restricted to some zone between x' and x'' in the interior of the plug. In the regions outside of the precipitation zone the steady-state profiles must be linear. Within the precipitation zone the profiles must be positively curved, as shown, because for both A and B the flux to a plane from the supply side must exceed the flux away from that plane, as precipitate is deposited in the plane.

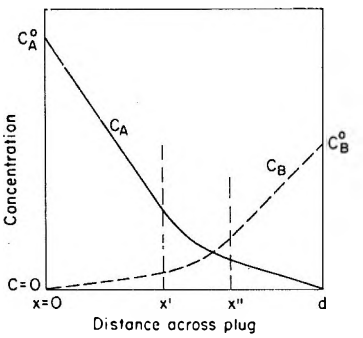

Figure 2. Properties of steady-state concentration profiles (schematic).

Even at the boundaries of the precipitation zone the profiles cannot be discontinuous or have abrupt changes in curvature. A discontinuity in the profile would entail an infinite flux, and an abrupt change in curvature would require an infinite precipitation rate, at the respective location. Neither is compatible with steady-state behavior.

Solution for Steady State

In the steady state

$$\partial C_A/\partial t = 0; \quad \partial C_B/\partial t = 0 \qquad (7)$$

Also, the partial derivatives $\partial/\partial x$ and $\partial^2/\partial x^2$ can be written as total derivatives d/dx and d^2/dx^2, respectively, and j becomes a function of x only.

Subtracting the two eq 4 from one another to eliminate j one obtains with eq 7

$$D_A \frac{d^2 C_A}{dx^2} - D_B \frac{d^2 C_B}{dx^2} = 0 \qquad (8)$$

(18) Reference 16, eq 8.6.

Integrating twice over x one obtains

$$D_A C_A - D_B C_B = ax + b$$

where the constants a and b are determined by the boundary conditions 3. The solution is

$$\alpha C_A - C_B = \alpha C_A^\circ - \frac{x}{d} Q \tag{9}$$

where

$$\alpha \equiv D_A/D_B; \quad Q \equiv \alpha C_A^\circ + C_B^\circ$$

Equation 9 holds over the entire range $0 \leq x \leq d$ since eq 7 is valid whether or not $j = 0$.

Now, we restrict ourselves to the precipitation zone $x' \leq x \leq x''$, the location of whose boundaries will be determined later. Within this zone, condition 5b applies. Thus one can substitute in eq 9 $C_B = K/C_A$ or $C_A = K/C_B$. With these substitutions eq 9 gives the concentration profiles of A and B, respectively, in the precipitation zone ($x' \leq x \leq x''$)

$$C_A(x) = \frac{1}{2\alpha}\left\{\alpha C_A^\circ - \frac{x}{d} Q + \left[\left(\frac{x}{d} Q - \alpha C_A^\circ\right)^2 + 4\alpha K\right]^{1/2}\right\} \tag{10}$$

$$C_B(x) = \frac{1}{2}\left\{\frac{x}{d} Q - \alpha C_A^\circ + \left[\left(\frac{x}{d} Q - \alpha C_A^\circ\right)^2 + 4\alpha K\right]^{1/2}\right\} \tag{11}$$

[only the roots having physical significance are given in eq 10 and 11].

The precipitation flow is calculated as follows. According to eq 4 and 7

$$j = D_B \frac{d^2 C_B}{dx^2} \tag{12}$$

Differentiating eq 11 twice with respect to x and multiplying with D_B one obtains with eq 12

$x' \leq x \leq x''$;

$$j = \frac{2D_A D_B K (D_A C_A^\circ + D_B C_B^\circ)^2}{\left\{\left[\frac{x}{d} D_B C_B^\circ - \left(1 - \frac{x}{d}\right) D_A C_A^\circ\right]^2 + 4 D_A D_B K\right\}^{3/2} d^2} \tag{13}$$

The precipitation flow is finite in the entire range and, as is apparent from the denominator of eq 13, has its maximum where

$$\frac{x}{d} D_B C_B^\circ = \left(1 - \frac{x}{d}\right) D_A C_A^\circ$$

so that

$$\left(\frac{x}{d}\right)_{j_{max}} = \frac{D_A C_A^\circ}{D_A C_A^\circ + D_B C_B^\circ} \tag{14}$$

provided, of course, that this location is in the range of precipitation, between x' and x''.

The simplest way of calculating the boundaries x' and x'' of the precipitation zone is as follows: since j, according to eq 13, is finite throughout, the second derivative d^2C_B/dx^2 must also be finite in view of eq 12. The first derivative dC_B/dx therefore is a continuous function of x, and the profile $C_B(x)$ shows no abrupt change in slope even at the boundaries x' and x''. Thus, the slopes of the profile of B in the regions $0 \leq x \leq x'$ and $x'' \leq x \leq d$ (where the profile is linear) must equal the slopes of the profile at x' and x'', respectively, as given by eq 11 for the zone $x' \leq x \leq x''$. The slopes in the outer regions are

$$0 \leq x \leq x'; \quad \frac{dC_B}{dx} = \frac{C_B(x')}{x'} \text{ and}$$

$$\frac{dC_A}{dx} = \frac{C_A(x') - C_A^\circ}{x'} \tag{15}$$

$$x'' \leq x \leq d; \quad \frac{dC_B}{dx} = \frac{C_B^\circ - C_B(x'')}{d - x''} \text{ and}$$

$$\frac{dC_A}{dx} = -\frac{C_A(x'')}{d - x''} \tag{16}$$

Differentiating eq 11 with respect to x

$$x' \leq x \leq x''; \quad \frac{dC_B}{dx} = \frac{Q}{2d}\left\{1 + \frac{\frac{x}{d} Q - \alpha C_A^\circ}{\left[\left(\frac{x}{d} Q - \alpha C_A^\circ\right)^2 + 4\alpha K\right]^{1/2}}\right\} \tag{17}$$

Setting $x = x'$ in eq 17 equating to eq 15, inserting $C_B(x')$ from eq 11, and solving for x', one obtains

$$x' = \frac{[(D_A C_A^\circ)^2 + 4 D_A D_B K] d}{2 D_A C_A^\circ (D_A C_A^\circ + D_B C_B^\circ)} \tag{18}$$

Setting $x = x''$ in eq 17, equating to eq 16, and solving for x'' one obtains

$$x'' = \frac{[2 D_A C_A^\circ D_B C_B^\circ - 4 D_A D_B K + (D_B C_B^\circ)^2] d}{2 D_B C_B^\circ (D_A C_A^\circ + D_B C_B^\circ)} \tag{19}$$

It is readily verified that eq 18 and 19 meet, as required, the material balance condition

$$\int_{x=x'}^{x=x''} j\,dx = (J_A)_{x=0} - (J_A)_{x=d} + (J_B)_{x=0} - (J_B)_{x=d}$$

By inserting the values of x' and x'' from eq 18 and 19 in eq 10 and 11 we find that the precipitation boundary at the C_A° side corresponds to $C_A(x') = C_A^\circ/2$ and $C_B(x') = 2K/C_A^\circ$ while on the C_B° side $C_A(x'') = 2K/C_A^\circ$ and $C_B(x'') = C_B^\circ/2$.

A necessary condition for precipitation to occur at all is that the precipitation zone exists, *i.e.*, that $x' < x''$.

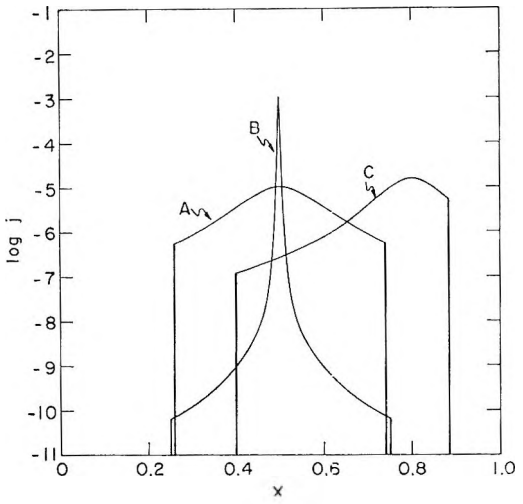

Figure 3. Local precipitation flow j in steady state as a function of x, calculated for the parameter values. (A) $D_AC_A^\circ = 10^{-16}$, $D_BC_B^\circ = 10^{-6}$, $D_AD_BK = 10^{-18}$, $d = 1$; (B) $D_AC_A^\circ = 10^{-6}$, $D_BD_B^\circ = 10^{-6}$, $D_AD_BK = 10^{-16}$, $d = 1$: and (C) $D_AC_A^\circ = 2.10^{-6}$, $D_BC_B^\circ = 0.5 \times 10^{-6}$, $D_AD_BK = 10^{14}$, $d = 1$.

With eq 18 and 19 this condition is seen to be equivalent to

$$C_A^\circ C_B^\circ > 4K \tag{20}$$

Condition 20 is as one should expect. If, and only if, this condition is not met, can one draw linear concentration profiles for both A and B through the entire plug without having the product C_AC_B anywhere exceed the solubility product. [The linear profiles are $C_A(x) = (1 - x/d)C_A^\circ$ and $C_B(x) = (x/d)C_B^\circ$. With these profiles, the product C_AC_B has its maximum at $x = d/2$, *i.e.*, in the center of the plug. At this location, $C_AC_B = C_A^\circ C_B^\circ/4$.]

The following general properties of the system in the steady state can be deduced from the equations. If the boundary concentrations C_A° and C_B° barely exceed the limit set by condition 20, precipitation occurs only in a narrow zone around the center of the plug and is slight. If the boundary concentrations are increased, the precipitation zone widens and precipitation becomes heavier and develops an increasingly sharp maximum at the location given by eq 14. The larger the ratio $D_AC_A^\circ/D_BC_B^\circ$, the more are the precipitation zone and the location of maximum precipitation shifted toward the reservoir containing B. However, the boundaries x' and x'' of the precipitation zone always remain on opposite sides of the center $x = d/2$ of the plug.

Calculated functions $j(x)$ for three different cases are shown in Figure 3.

Attainment of the Steady State

That the steady state is indeed attained if the plug initially contains neither A nor B will now be illustrated with two simple limiting cases.

The initial condition is

$$t = 0; \quad 0 < x < d; \quad C_A = 0; \quad C_B = 0 \tag{21}$$

For both cases we assume equal diffusion coefficients and equal boundary concentrations for A and B

$$D_A + D_B = D; \quad C_A^\circ = C_B^\circ = C^\circ \tag{22}$$

For the boundary concentrations we assume

$$\text{Case 1: } C^{\circ 2} \cong 4K \tag{23}$$

$$\text{Case 2: } C^{\circ 2} \ll K \tag{24}$$

In both cases there will be an initial period of time during which no precipitation occurs at all. For this period, with $j = 0$, the solutions of eq 3 and 4 with the conditions 1, 21, and 22 are well known to be[19]

$$C_A(x, t) = C^\circ\left(1 - \frac{x}{d}\right) - \frac{2C^\circ}{\pi}\sum_{n=1}^{\infty}\left\{\frac{1}{n}\exp\left[-Dt\left(\frac{n\pi}{d}\right)^2\right]\sin\frac{n\pi x}{d}\right\} \tag{25}$$

$$C_B(x, t) = C^\circ\frac{x}{d} - \frac{2C^\circ}{\pi}\sum_{n=1}^{\infty}\left\{\frac{1}{n}\exp\left[-Dt\left(\frac{n\pi}{C}\right)^2\right]\sin\frac{n\pi(d - x)}{d}\right\} \tag{26}$$

One can readily verify that, at the center of the plug,

$$x = \frac{d}{2}; \quad \left[\frac{\partial(C_AC_B)}{\partial x}\right]_t = 0; \quad \left[\frac{\partial^2(C_AC_B)}{\partial x^2}\right]_t < 0$$

Accordingly, at any time t the concentration product C_AC_B has its maximum value at the center of the plug. This is therefore the location where precipitation will first occur.

In Case 1 [condition 23], the time-dependent solutions 25 and 26 hold until the steady state is almost attained. Only when the profiles have become almost linear does precipitation start at the center of the plug. At this stage, the time-dependent solution is almost identical with the steady-state solution, which also gives almost linear profiles and precipitation only in the immediate neighborhood of the center.

In Case 2 (condition 24), the steady-state solution gives a sharp precipitation maximum at the center of the plug. At this location, therefore, the steady-state concentration profiles are strongly curved while being almost linear on either side (see eq 12). The time-dependent solution, on the other hand, shows that precipitation starts at the center at a very early time, t_p, namely, when C_AC_B first attains the solubility product at this location. From then on, C_A and C_B at the center remain unchanged because of the symmetry properties of the system (eq 22) and thus act as a constant internal boundary condition

$$t \geq t_p; \quad x = d/2; \quad C_A = C_B = 2K^{1/2}$$

(19) Reference 16, eq 4.22 with $C_0 = 0$, $C_1 = 0$.

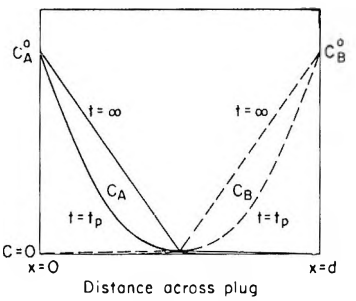

Figure 4. Concentration profiles at beginning precipitation ($t = t_p$) and at steady state ($t = \infty$), for case 2 (conditions 21, 22, and 24).

In layers with constant boundary concentrations on both sides the concentration profiles are known to straighten out completely. They would thus do so in the regions $0 \leq x < d/2$ and $d/2 < x \leq d$ if precipitation would remain restricted to the center alone. The fact that the precipitation zone spreads lets the profiles retain an insignificant residual curvature, but this does not obscure the tendency of the profiles to approach the steady-state shape. Figure 4 illustrates this behavior.

It is interesting that the time required to attain the steady state in case 2 is shorter by about a factor 4 than in the analogous case without precipitation. The time required is proportional to the square of layer thickness,[20] and in case 2 the plug acts essentially as two layers of thickness $d/2$ each, with steady-state conditions being approached simultaneously in both.

With regard to the transient behavior in the general case, it will merely be noted that the location at which precipitation begins is determined only by the ratio D_A/D_B and is independent of the boundary concentrations C_A° and C_B°. For $D_A = D_B$, precipitation begins at the center of the plug, even if $C_A^\circ \neq C_B^\circ$. In this particular case, the precipitation maximum gradually shifts with time from the center to its eventual steady-state location off center, toward the side at which the boundary concentration is lower (*e.g.*, see curve C in Figure 3). Indeed, that the point of beginning precipitation coincides with that of maximum steady-state precipitation, as under the simple condition 22, is the exception rather than the rule.

Extensions

The treatment can be extended to systems with other stoichiometries. For the general case the precipitation reaction can be written as

$$mA + nB \rightleftharpoons A_mB_n\downarrow \qquad (27)$$

If $m = n$, the treatment presented before applies without change, except that care must be taken to define the constant K in accordance with condition 6 rather than identify it with the actual solubility product, which then becomes K^m. If $m \neq n$, the coefficients m and n must appear as factors in the sink terms in eq 4 and as coefficients in conditions 5 and 6. The occurrence of m and n as exponents leads to the need of solving third- or higher-order algebraic equations to calculate the concentration profiles. The resulting equations are rather unwieldy or must be given in implicit form, but no fundamental difficulties are encountered.

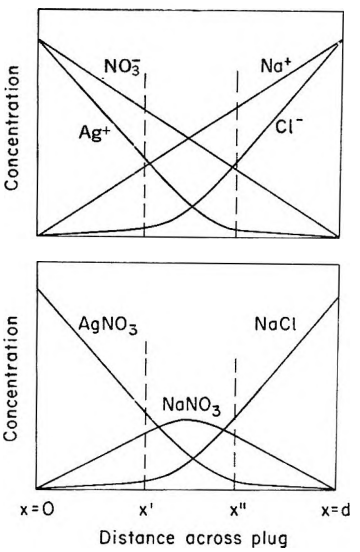

Figure 5. Steady-state concentration profiles for interdiffusion of $AgNO_3$ and NaCl (schematic). The upper diagram shows the profiles of the ions Ag^+, Na^+, NO_3^-, and Cl^-; the lower diagram is an equivalent representation showing the profiles of the salts $AgNO_3$, NaCl, and $NaNO_3$.

Particularly interesting systems are those in which the solutes are electrolytes. Consider, for example, interdiffusion of $AgNO_3$ and NaCl with precipitation of AgCl. Taking Ag^+, NO^-_3, Na^+, and Cl^- as the solutes, one may write for the fluxes and continuity conditions

$$J_i = -D_i\left(\frac{\partial C_i}{\partial x} + z_iC_i\frac{F}{RT}\frac{\partial \varphi}{\partial x}\right) \qquad (28)$$

$$\frac{\partial C_i}{\partial t} = D_i\left(\frac{\partial^2 C_i}{\partial x^2} + z_iC_i\frac{F}{RT}\frac{\partial^2 \varphi}{\partial x^2}\right) - \omega j \qquad (29)$$

(i = Ag^+, NO_3^-, Na^+, or Cl^-; $z_i = +1$ for Ag^+ and Na^+, $z_i = -1$ for NO_3^- and Cl^-; $\omega = 1$ for Ag^+ and Cl^-; $\omega = 0$ for NO_3^- and Na^+; φ = electric potential; F = Faraday constant; R = gas constant; T = absolute temperature). Electroneutrality and absence of electric current impose the restrictions

$$\sum_i z_iC_i = 0; \quad \sum_i z_iJ_i = 0 \qquad (30)$$

Unfortunately, because of the electric-potential terms the differential equations are nonlinear and defy explicit integration. However, an approximation is readily

(20) Reference 16, eq 4.27.

given. If all four diffusion coefficients can be regarded as equal, then no gradient of the electric potential arises. With this simplification, the treatment in the previous sections becomes directly applicable with A = Ag^- and B = Cl^-, and the profiles of the non-reacting ions NO_3^- and Na^+ are linear (see Figure 5). One can easily verify that profiles for Ag^+ and Cl^- as given in eq 10 and 11, respectively, and linear profiles for NO_3^- and Na^+ indeed satisfy eq 28 and 29 without the electric-potential term and also conform to the restrictions 30.

Provided that all diffusion coefficients can be regarded as equal and that the reacting ions have equal valences, the behavior is the same as pointed out above, irrespective of the valences of the nonreacting ions. For example, the treatment can be applied without change to the systems Ag_2SO_4–NaCl, $AgNO_3$–$BaCl_2$, and $BaCl_2$–Na_2SO_4. On the other hand, if the reacting ions have different valences, as in the system $AgNO_3$–Na_2S, the remarks made in connection with eq 27 apply.

It must be stressed, however, that the behavior of electrolyte systems in practice may be more complicated. For example, the studies of $BaSO_4$ precipitation by Hirsch-Ayalon[6] seem to indicate that in this system selective sorption of ions on the precipitate plays an important role. In such cases, the simple treatment outlined here can merely serve to assess which effects will arise from interdiffusion and precipitation alone and which will require other, more complex explanations.

On the Mechanism of Ion Exchange in Crystalline Zirconium Phosphate.

II. Lithium Ion Exchange of α-Zirconium Phosphate[1]

by A. Clearfield and J. Troup

Department of Chemistry, Clippinger Graduate Research Laboratories, Ohio University, Athens, Ohio 45701
(Received July 16, 1969)

The ion-exchange behavior of α-zirconium phosphate crystals titrated with lithium ion and the behavior of the lithium-exchanged crystals back-titrated with HCl have been determined. The titration curves exhibit a hysteresis loop which arises from the presence of different phases during the forward and back titrations. When lithium ion replaces protons, two phases, $Zr(LiPO_4)_{1.33}(HPO_4)\cdot 4H_2O$ and the unexchanged crystals, are present up to 66% of exchange. At higher levels of exchange only the latter phase is present, the excess lithium ion being held in solid solution. However, at about 80% of exchange the fully exchanged phase, $Zr(LiPO_4)_2\cdot 4H_2O$, forms. These two phases persist, in concentrations dependent on the total lithium content of the solid, until 100% replacement of the protons, whereupon only the latter phase is obtained. When HCl is added to $Zr(LiPO_4)_2\cdot 4H_2O$, about 5% of the lithium ions are replaced without phase change. Thereafter, a two-phase region is obtained. The two phases are the slightly protonated fully exchanged phase and $Zr(LiPO_4)_{1.33}(HPO_4)_{0.67}\cdot 4H_2O$. When greater than 33% of the Li^+ has been replaced by protons, gelatinous zirconium phosphate begins to form. At the completion of the titration the solid phase is completely converted into gel. These results are incompatible with the idea proposed earlier that α-zirconium phosphate contains two types of protons of differing acidity.

Introduction

Crystalline zirconium phosphate exists in several polymorphic forms.[2] The most stable form is α-zirconium phosphate (α-ZrP), which is prepared by refluxing zirconium phosphate gels in phosphoric acid.[3] α-ZrP has a layered structure,[4] each layer consisting of zirconium atoms lying very nearly in a plane and bridged by phosphate groups situated above and below the plane. Adjacent layers are arranged in such a way as to create zeolitic cavities with rather restricted entrances into the cavity. In a previous paper of this series, details of the sodium ion exchange with α-ZrP were given.[5] This paper describes the behavior of lithium ion exchange on α-ZrP. Isotherms for the Li^+–

(1) Acknowledgment is made to the donors of the Petroleum Research Fund, administered by the American Chemical Society, for support of this work under Grant No. 1993-A3.

(2) A. Clearfield, R. H. Blessing, and J. A. Stynes, *J. Inorg. Nucl. Chem.*, **30**, 2249 (1968).

(3) A. Clearfield and J. A. Stynes, *ibid.*, **26**, 117 (1964).

(4) A. Clearfield and G. D. Smith, *Inorg. Chem.*, **8**, 431 (1969).

(5) A. Clearfield, W. L. Duax, A. S. Medina, G. D. Smith, and J. R. Thomas, *J. Phys. Chem.*, **73**, 3423 (1969).

Na^+ and Li^+–K^+ systems have been determined by Torracca.[6]

Experimental Section

Crystalline α-ZrP was prepared by refluxing a zirconium phosphate gel in 12 *M* phosphoric acid for 24 hr. Analytical and X-ray data showed that the product was as described earlier.[3,5] Potentiometric titrations were carried out at 25° in a constant-temperature water bath as reported previously.[2] X-Ray diffraction patterns of the solid at different stages of exchange and the dehydration experiments were carried out in the same fashion as for the sodium ion system.[5]

Analytical Data. Analysis of the solid exchangers was carried out by first dissolving a weighed amount (~0.25 g) in a platinum dish containing 13 ml of water and 2 ml of concentrated hydrofluoric acid. The solution was transferred to a 250-ml beaker, the dish being rinsed thoroughly with distilled water. The solution was then diluted to a volume of 50 ml, and 7.5 ml of perchloric acid was added. Zirconium was then precipitated with cupferron and ignited to oxide. The phosphate in the filtrate was determined colorimetrically as the blue phosphomolybdate after destroying the organic matter with perchloric acid. Lithium was determined by atomic absorption analysis (Jarrell-Ash Model 82375C).

Results

Ion-Exchange Studies. The lithium ion titration curve of α-ZrP crystals and the curve of the lithium exchanged crystals back-titrated with acid are shown in Figure 1. As in the case of the sodium ion curves the irreversibility of exchange was found to stem from the presence of different phases during the forward and back titrations.[5] The forward titration curve may be divided into two regions. The first region was found to extend from just beyond zero exchange to 66% lithium ion uptake as indicated by the arrow in Figure 1. X-Ray diffraction patterns revealed the presence of two phases of composition $Zr(LiPO_4)_{1.33}(HPO_4)_{0.67}\cdot 4H_2O$. This latter phase was the only one present at 66% of exchange. At all lower levels of exchange several X-ray reflections of the original α-ZrP crystals were present. The presence of α-ZrP was confirmed by heating the samples to 800°. This converted unexchanged α-ZrP into zirconium pyrophosphate which was easily detected (even in very small quantities) in the X-ray patterns. Analysis of the 66% phase gave 25.3% Zr, 51.5% PO_4, 2.64% Li, 21.2% H_2O (loss on ignition) [Calcd for Zr $(LiPO_4)_{1.33}(HPO_4)_{0.67}\cdot 4H_2O$: 25.3% Zr, 52.2% PO_4, 2.55% Li, 21.4% H_2O]. The 66% exchanged phase will be designated as phase A (1.33 $Li^+\cdot 4H_2O$).[7] Its X-ray pattern is given in Table I.

The second region of the forward titration curve was found to extend from 67 to 100% of exchange. Two phases were also present in this region but not over the entire range of compositions. The two phases are phase A (1.33 $Li\cdot 4H_2O$) and the fully exchanged phase Zr $(LiPO_4)_2\cdot 4H_2O$. Analysis of the latter phase, equilibrated at 60% relative humidity, gave 25.2% Zr, 51.0% PO_4, 3.82% Li, 19.63% H_2O (loss on ignition) [Calcd for Zr $(LiPO_4)_2\cdot 4H_2O$: 25.0% Zr, 51.5% PO_4, 3.77% Li, 19.57% H_2O]. This phase has been designated phase F ($2Li^+\cdot 4H_2O$), and its X-ray pattern is given in ref 6. The similarity of the X-ray patterns of phase A (1.33 $Li^+\cdot 4H_2O$) and phase F ($2Li^+\cdot 4H_2O$) made it difficult to distinguish these two phases. However, phase A appeared to be the only one present up to 80% of exchange. Beyond this point mixtures of phase A and phase F were obtained, and at the final end point of the titration only F remained. This behavior differs from that of sodium ion exchange where two phases were present over the whole range of compositions.

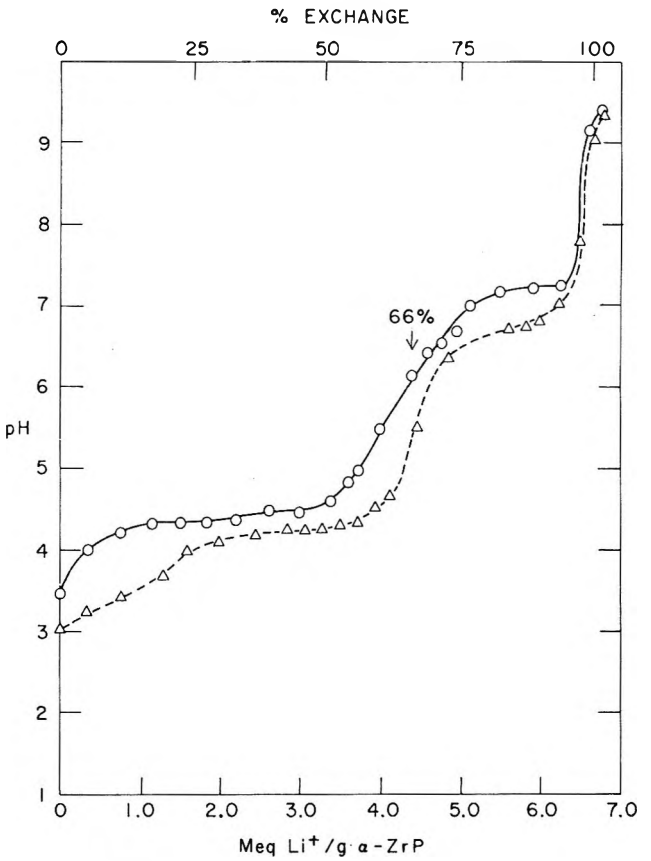

Figure 1. Lithium ion potentiometric titration curve for α-ZrP. Titrant: forward direction, 0.2 *N* LiCl + 0.0916 *N* LiOH, —○—; backward direction, 0.2 *N* LiCl + 0.1021 *N* HCl, - -△- -.

At the completion of the forward titration, the solid sample was not filtered off and reslurried with 0.2 *N* LiCl. Rather it was retitrated as is with 0.1021 *N* hydrochloric acid. Since 82 ml of solution had been added in the forward titration, the ratio of solution to

(6) E. Torracca, *J. Inorg. Nucl. Chem.*, **31**, 1189 (1969).

(7) See ref 5 for an explanation of this nomenclature.

Table I: X-Ray Diffraction Pattern of Phase A ($1.33Li^+ \cdot 4H_2O$)

d, Å	I/I_0
10.0	100
5.05	10
4.56	10
4.35	5
4.21	5
4.11	12
3.89	20
3.66	5
3.59	6
3.55	8
3.41	5
3.30	10
3.23	5
3.10	10
2.99	5
2.83	5
2.71	5

10 additional reflections to 1.94

solid exchanger was greater in the back titration. However, this should not lower the pH appreciably as is in fact observed in Figure 1. This hysteresis is caused by the initial formation of a solid solution of hydrogen ion in phase F rather than the formation of a two-phase system as in the forward titration. The amount of hydrogen ion which can be incorporated into phase F was not determined with accuracy but appears to be small (~5%). Beyond this composition range two phases, A and F, are obtained, but phase F may still retain some of the protons.

As the titration was continued beyond the 33% hydrogen ion addition, gelatinuous zirconium phosphate was found to form instead of α-ZrP crystals. Thus, at the completion of the back titration only gel ZrP remained. This was not due to hydrolysis as the phosphate content of the solutions in equilibrium with the exchanger was found to be less than 1% of the total phosphate in the exchanger.

Dehydration Studies. The dehydration behavior of phase A ($1.33\ Li^+ \cdot 4H_2O$) was found to be extremely complicated. It lost water slowly on standing in air at room temperature and more rapidly in a desiccator over drying agents. At least four phases of varying water content were detected. These phases are listed in Table II and identified by their interlayer separation (the first strong reflection in the X-ray patterns). The water contents of these partially hydrated phases are not known with certainty because of the difficulty of obtaining them free of other phases. However, an extended dehydration study has been undertaken and will be reported upon later. The dehydration behavior of phase A is summarized in the diagram below.

$$\text{phase A} \xrightarrow[\text{or } P_2O_5]{\text{dry in air}} \text{mixture of phases A, B, C, D} \xrightarrow[2\text{ days}]{P_2O_5}$$

$$\text{mixtures of phases B, C, D} \xrightarrow{50\text{–}80^\circ} \text{mixtures of phases C and D} \xrightarrow{110\text{–}130^\circ} \text{phase D} \xrightarrow{185\text{–}400^\circ} \text{phase E} \xrightarrow{450^\circ}$$

$$\text{phase J} \xrightarrow{800^\circ} LiZr_2(PO_4)_3$$

The dehydration of the fully lithium ion exchanged phase F ($2Li^+$) was also found to be complex. The phases are identified in Table III. Phases F, H, and I were reported by Torracca.[6]

Table II: Phases Formed by Dehydrating Phase A ($1.33Li^+ \cdot 4H_2O$)

Phase and probable composition	Interlayer spacing, Å	H_2O/Li
Phase B ($1.33Li^+ \cdot 3.3H_2O$)	8.55	2.5
Phase C ($1.33Li^+ \cdot 1.33\ H_2O$)	7.30	1.0
Phase D ($1.33Li^+ \cdot 0.67H_2O$)	7.84	0.5
Phase E ($1.33Li^+$)	7.00	0

Table III: Phase F and Its Dehydration Products

Phase and probable composition	Interlayer spacing, Å	Temp of formation, °C
Phase F ($2Li^+ \cdot 4H_2O$)	10.1	Room temp
Phase G ($2Li^+ \cdot 2\text{–}3H_2O$)	8.80	Room temp
Phase H ($2Li^+ \cdot H_2O$)	7.87	80–100
Phase I ($2Li^+$)	7.05	185–375
Phase J ($2Li^+$)	6.24	400–805

On standing in air phase F ($2Li^+$) lost water slowly with the formation of phase G. However, this phase transformation occurred rapidly over drying agents. Complete conversion into phase G was observed when 5.25% or 1 mol of water was lost. However, it was also the only phase present up to observed water losses of at least 8.75% or 1.8 mol. Thus, this phase is thought to exist over the range of compositions containing 2–3 mol of water and is represented as phase G ($2Li^+ \cdot 2\text{–}3H_2O$). Further water losses resulted in mixtures of phase G and phase H. This latter phase was obtained in a pure state by heating these mixtures to 138°. The total water loss was 13.62% or 2.78 mol so that phase H is close to a monohydrate. It is represented as phase H ($2Li^+ \cdot H_2O$) in Table III.

Heating phase F ($2Li^+ \cdot 4H_2O$) at 185° converted it into phase I. In 4 hr at 375° the water loss was 19% or very close to 4 mol of water. At 185° about 3 days is required for the complete conversion of phase F ($2Li^+ \cdot 4H_2O$) into phase I ($2Li^+$). Above 375° phase I is converted into another anhydrous phase, phase J ($2Li^+$). Phase J is stable to at least 800°. Conversion into phase J was slow at 400° but rapid at 600°. Phase A when heated above 450° also gave phase J but as a solid

solution containing Li^+ and H^+ since at 800° it was converted into $LiZr_2(PO_4)_3$.

Discussion

The exchange behavior of lithium ion on α-ZrP is unlike the behavior exhibited by sodium ion. With the latter ion the first end point occurs at exactly 50% of exchange.[5] Thus, in the region of 0–50% of exchange two phases, phase A ($Na^+ \cdot 5H_2O$) and α-ZrP, are present. A second two-phase region exists in the range of 50–100% of exchange. The two phases present in the second region are phase A ($Na^+ \cdot 5H_2O$) and phase D ($2Na^+ \cdot 3H_2O$). No solid solutions were observed in this system, and the results were interpreted in terms of the presence of two types of hydrogen ions of differing acidity.[5] The results with the lithium–hydrogen system are incompatible with this idea. Since phase A ($1.33\ Li^+ \cdot 4H_2O$) forms immediately upon addition of lithium hydroxide, some of each type of hydrogen ion must have been displaced. Yet the pH remains constant up to 50% of exchange. Thus, the exchange behavior and pH must depend on the structure of both the newly formed phase as well as the phase undergoing exchange. A more complete understanding of the exchange mechanism would obviously result from a knowledge of the structure of the exchanged phases. Such a study is now underway.

The multitude of phases formed during the dehydration of the lithium exchanged phases must result from the contraction of the α-ZrP layers as water is removed. Thus, in analogy with the sodium ion case,[5] the interlayer distances are taken to be synonymous with the first intense reflection undergoing extensive shifts in the powder patterns. Not all of the resultant phase changes are reversible so that it is possible to alter the nature of the exchanger by partially dehydrating it. This had been demonstrated by Torracca for the lithium exchanged crystals[6] and opens the possibility of producing a host of new exchangers.

An interesting feature of the lithium ion exchange is the formation of gel zirconium phosphate in the back titration. The only detectable phase present before gel formation became extensive was phase A. Thus, the replacement of lithium ion in this phase by protons must involve a difficult structural rearrangement which results in disordering of the crystal lattice.

Capillary Behavior of Viscous Liquids[1]

by Richard L. Kissling and Paul H. Gross

Department of Chemistry, University of the Pacific, Stockton, California 95204 *(Received February 5, 1969)*

A new method is proposed by which flow curves can be determined over wide ranges of shear stress for microquantities of moderately to highly viscous liquids. The method incorporates a modification of the Rabinowitsch derivation for the true rate of shear at a capillary wall. According to the Rabinowitsch expression, the true rate of shear at the capillary wall can be obtained by multiplying the apparent rate of shear at the wall based on the volumetric flow rate by a correction factor, $(3 + b)/4$. The number b is obtained as the slope of a log–log plot of the apparent rate of shear *vs.* the shear stress at the wall. For a liquid undergoing flow due to the action of capillary rise, the log–log plot in the Rabinowitsch development can be simplified to give b as the slope of log dh/dt *vs.* log $(h_\infty - h)/h$, where dh/dt is the velocity of flow at height h, and h_∞ is the final equilibrium weight. The true rate of shear at the capillary wall is then expressed as $[(3 + b)/R](dh/dt)$ and the shear stress at the capillary wall as $^1/_2\rho g R[(h_\infty - h)/h]$. A knowledge of the experimental quantities rate of rise, final equilibrium height, liquid density, and capillary radius enables one to determine the true rate of shear and shear stress relationships and to construct the corresponding flow curve. The log–log treatment of capillary rise rate data indicates that the contact angle constancy and rate of wetting are factors which must be considered in such an experimental technique. Progressively larger deviations from unity and linearity in the slope of the log–log plots are observed as the capillary bore becomes larger and, also, as the shear stress increases. These deviations are attributed to the fact that the rate of wetting under these conditions is slow in comparison to the rate of capillary ascent. Prewetting the capillary wall eliminates these deviations in the log–log plot, and among unwetted capillaries these deviations become less important when very small-bore capillaries are used. If the contact angle is different from zero, but constant over a wide range of shear stress, the log–log plot will be linear with a slope of unity. However, the viscosity calculated from the flow curves under these conditions is higher than that obtained from the smaller bore capillaries. This difference is attributable to capillary bore dimensions and can be used to calculate contact angles under kinetic conditions. The capillary rise method was used to determine the flow curve of a pseudoplastic liquid.

Introduction

The ordinary capillary viscometers (Ostwald, Cannon–Fenske, Ubbelohde, etc.) provide measurements made at the same, or very nearly the same, driving pressure, and are not necessarily applicable for use with non-Newtonian liquids, with which measurements should be made at a number of different driving pressures. Several capillary viscometers have been designed for use with non-Newtonian systems.[2,3] Most of them are not satisfactory for use at low stresses and, hence, cannot provide data for a reliable extrapolation to zero stress. This is a serious inadequacy, since it is generally accepted that in the case of such systems as non-Newtonian polymer solutions, the quantity of greatest interest is the intrinsic viscosity at low shear stress, a quantity that must be determined by extrapolation of data obtained at low shear stresses.

The common phenomenon of capillary rise has been utilized in simple methods for the determination of the viscosities of microquantities of liquids. Flory[4] has used the rising-column method to determine the viscosity of molten linear polyesters; Stow, Horowitz, and Elliott[5] have applied the technique to the high viscosity range; Elliott[6] has designed and constructed a rising-column capillary viscometer for the determination of the viscosities of polymer melts and solutions at low shear rates. Although these methods incorporate external driving pressures, the technique has not been used to determine flow curves.

Many other approaches to the capillary rise phenomenon have dealt in considerable detail with the theoretical aspects of the dynamics associated with capillary rise, but reliable experimental data substantiating the theoretical work have been somewhat limited. The equations for a liquid rising in a capillary column are often so complicated that in order to correlate experimentally determined parameters to the theory, many simplifying assumptions must be made concerning the basic nature of the motion of the liquid in the tube which may or may not exhibit Poiseuille flow.

Washburn,[7] in considering the capillary rise problem, stated that the distance necessary for the establishment

(1) Presented before the Division of Physical Chemistry at the 155th National Meeting of the American Chemical Society, San Francisco, Calif., April 1968; taken in part from the dissertation submitted by R. L. Kissling to the Graduate School of the University of the Pacific in partial fulfillment of the requirements for the Degree of Doctor of Philosophy.

(2) (a) P. J. Flory and T. G Fox, *J. Amer. Chem. Soc.*, **73**, 1904 (1951). (b) S. H. Maron and R. J. Belner, *J. Appl. Phys.*, **26**, 1457 (1955).

(3) A. W. Sisko, *J. Colloid Interfac. Sci.*, **15**, 89 (1960).

(4) P. J. Flory, *J. Amer. Chem. Soc.*, **62**, 1057 (1940).

(5) F. S. Stow, Jr., K. H. Horowitz, and J. H. Elliott, *J. Colloid Sci.*, **4**, 321 (1949).

(6) J. H. Elliott, *Trans. Soc. Rheol.*, **12**, 573 (1968).

(7) E. W. Washburn, *Phys. Rev.*, **17**, 273 (1921).

of Poiseuille flow could be made vanishingly small by choosing a capillary of sufficiently small bore.

Rense[8] has used a stroboscope and motion picture camera to photograph the ascent of water in a capillary tube, and has derived a semiempirical equation for the motion of the liquid in the tube. The derivation of this equation is based on the assumption that the rise of water in a capillary tube is turbulent; *i.e.*, there are frictional-pressure drops which are attributed to variable and incoherent resistive forces accompanying the rapidly changing velocity during ascent.

Pickett[9] disagrees with the conclusion reached by Rense that the rise of water in capillary tubes produces turbulent flow because the Reynolds number for the particular system is far too low for the occurrence of turbulence. He concludes that the rise of water in a capillary tube is in agreement with a theory that takes into account surface tension, viscosity, and density of the fluid and the corresponding capillary, viscous, gravitational, and inertial forces.

Brittin[10] developed a theory for the dynamics of capillary rise by making certain assumptions as to the nature of the motion of the liquid in the tube. The most important assumptions were that the same forces act on the liquid when it is in an accelerated state of motion as when it is in a steady state, that the surface tension is constant, that the angle of contact between the meniscus of the liquid and the tube wall is constant, and that the wetting of the tube is not a rate-determining factor for the motion. This theory leads to a second-order nonlinear differential equation whose solution represents the motion of the liquid in the tube.

The results of a study by Ligenza and Bernstein[11] indicate that the rise of a liquid in a fine vertical capillary may be accurately represented by the solution to a differential equation of motion in which the rate of change of momentum of the contents of the capillary is assumed to be negligible. In addition, the authors contend that the rate of wetting and the rate of assumption of constant (zero) contact angle are apparently sufficiently rapid compared with the rate of ascent that they need not be considered. As a consequence of these simplifications in both the experimental and theoretical treatments of the general problem of liquid rise in fine capillaries, Ligenza and Bernstein present an equation for a rapid and simple method of estimating the viscosity of micro-quantities of liquids, but which does not allow determination of the flow curve, since it is based on Newtonian behavior.

LeGrand and Rense[12] present several of the obvious factors which must be considered in a rigorous treatment of the differential equation of motion for a liquid rising in a capillary column. (a) The rise involves a nonsteady-state condition, and at least in the earlier stages, is impulsive. The fact that a mass of liquid is in motion below as well as above the opening to the capillary must be considered. (b) The vital factor in effecting the rise is surface tension. However, the question of angle of contact is very pertinent. Does this remain constant during the accelerating rise, or does it vary in a predictable, regular way? (c) The possible presence of turbulence over some of the column of liquid cannot be ignored despite low values of Reynolds number. We are here dealing with a nonsteady-state flow and boundary conditions are important. If the meniscus assumes a concave shape, how can the upward speed of flow be greatest at the center without an adjustment at the boundary? Likewise, on entering the tube itself, the liquid must adjust suddenly to new conditions of flow, and turbulence may result. (d) Viscosity contributes in producing frictional force, probably in the same sense as in ordinary streamline flow. Slipping along the walls of the tube should be considered.

Most of the investigators cited above used liquids of low viscosity in their studies, and, as a consequence, a rigorous experimental analysis of the flow curve was not carried out.

In discussing the mechanics of flow in capillaries, the conditions customarily set forth are[13] (1) the flow must be steady; (2) there are no radical and tangential components of the velocity; (3) the axial velocity is a function of the distance from the axis alone; (4) there is no slippage at the wall; (5) the tube is sufficiently long that end effects are negligible; (6) the fluid is incompressible; (7) there are no external forces; (8) isothermal conditions prevail throughout; and (9) viscosity does not change appreciably with the change in pressure along the tube.

From the remarks of LeGrand and Rense which are cited above, it is apparent that certain of these conditions are not fulfilled in the capillary rise process. Compare (1) and L&R (a), (2) and L&R (c), and (4) and L&R (d). A rigorous mathematical treatment of the capillary rise phenomenon is not possible as long as the degree and magnitude of the tangential velocity components are unknown.

It seems, however, that the mentioned inconsistencies would become less important as the capillaries become smaller and the rate of rise becomes slower. By investigation of the rise of highly viscous liquids in small bore capillaries, it might be possible to find the limit beyond which these inconsistencies are no longer important, *i.e.*, for very small capillary diameters the flow curves should become independent of the dimensions of the capillary.

(8) W. A. Rense, *J. Appl. Phys.*, **15**, 436 (1944).

(9) G. Pickett, *ibid.*, **15**, 623 (1944).

(10) W. E. Brittin, *ibid.*, **17**, 37 (1946).

(11) J. R. Ligenza and R. B. Bernstein, *J. Amer. Chem. Soc.*, **73**, 4636 (1951).

(12) E. J. LeGrand and W. A. Rense, *J. Appl. Phys.*, **15**, 456 (1944).

(13) J. R. van Wazer, J. W. Lyons, K. Y. Kim, and R. E. Colwell, "Viscosity and Flow Measurement; A Laboratory Handbook of Rheology," Interscience Publishers, New York, N. Y., 1963, p 189.

This "limiting flow curve" would then represent the true flow curve. The problem was whether such conditions could be realized experimentally.

Mathematical Relationships

During the capillary rise, the liquid is subjected, at least in principle, to the whole range of shear stresses and shear rates, so that the determination of the total flow curve should be possible by following the capillary rise from the start to the equilibrium height. It will be seen that the determination of the flow curve at very high stresses presents technical difficulties (section II).

Since both the shear stress and rate of shear vary with capillary radius, it is essential that the flow curve be constructed by using shear stress and shear rates for the same point in the capillary. The shear stress at the wall of the capillary is

$$s_w = \frac{\gamma}{h}\cos\theta - {}^1/_2\rho g R \tag{1}$$

where γ is the surface tension, R is the radius of the capillary tube, θ is the contact angle of the liquid meniscus with the wall of the capillary tube, g is the gravitational constant, h is the height of the liquid column, and ρ is the density of the liquid. For a liquid which completely wets the wall of the capillary tube, $\cos\theta$ becomes unity and the expression for stress becomes

$$s_w = \frac{\gamma}{h} - {}^1/_2\rho g R \tag{2}$$

Substitution of the equivalent expression for surface tension

$$\gamma = {}^1/_2\rho g R h_\infty \tag{3}$$

(where h_∞ is the final equilibrium height of the liquid column in the capillary) into eq 2 yields the following expression for shear stress at the capillary wall

$$s_w = {}^1/_2\rho g R\left(\frac{h_\infty - h}{h}\right) \tag{4}$$

The rate of shear at the wall is more difficult to determine from experimental data. For its calculation, a correction is applied to the rate of shear which has been calculated from the volumetric flow rate of the fluid.

According to the Rabinowitsch expression[14] the true rate of shear at the capillary wall can be obtained by multiplying the apparent rate of shear at the wall based on the volumetric flow rate, Q, by a correction factor, $(3 + b)/4$. The number b is obtained as the slope of a log–log plot of the apparent rate of shear *vs.* the shear stress at the wall, *i.e.*, $\log(4Q/\pi R^3)$ *vs.* $\log s_w$.

$$\left(\frac{-dv}{dr}\right)_w = \left(\frac{3 + b}{4}\right)\left(\frac{4Q}{\pi R^3}\right) \tag{5}$$

$$b = \frac{d\log(4Q/\pi R^3)}{d\log s_w} \tag{6}$$

Equation 5 is an entirely general expression irrespective of the fluid. If it is found that b is nearly constant over wide ranges of shear stress for non-Newtonian fluids, it is generally sufficient to obtain one average slope and make all corrections by multiplying a constant correction factor. If this is not the case, the slope should be taken at given shear stresses and the correction factors corresponding to the given slopes applied to each apparent rate of shear.

The volume flow rate due to capillary rise in a cylindrical column per unit time is described by

$$Q = \pi R^2\left(\frac{dh}{dt}\right) \tag{7}$$

The Rabinowitsch expression for the true rate of shear at the capillary wall then becomes

$$\left(\frac{-dv}{dr}\right)_w = \left(\frac{3 + b}{R}\right)\left(\frac{dh}{dt}\right) \tag{8}$$

Substitution of eq 4 and 7 into eq 6 for the shear stress and volume flow rate terms, respectively, yields

$$b = \frac{d\log(4/R)(dh/dt)}{d\log {}^1/_2\rho g R(h_\infty - h)/h} \tag{9}$$

and, subsequently

$$b = \frac{d\log(dh/dt)}{d\log(h_\infty - h)/h} \tag{10}$$

The value of b can, therefore, be determined from the slope of a plot of $\log(dh/dt)$ *vs.* $\log(h_\infty - h)/h$. The value of b can then be introduced into eq 8 in order to obtain the true rate of shear at the capillary wall.

A knowledge of the experimental quantities, rate of rise $\Delta h/\Delta t$, final equilibrium height h_∞, liquid density ρ, and capillary radius R enables one to calculate the true rate of shear and shear stress relationships and to construct the corresponding flow curve.

The steps by which flow curves were determined from the capillary rise rate data can be summarized as follows. (a) The capillary rise is followed with a cathetometer, and time increments Δt are recorded for corresponding height increments Δh. The quotients $\Delta h/\Delta t$ are then plotted against the respective mean heights h. (b) From the smooth curve drawn through the $\Delta h/\Delta t$ *vs.* h plot, values of dh/dt are interpolated at selected values of h. Values of the term $(h_\infty - h)/h$ are also computed at these selected h points. (c) A plot of $\log(dh/dt)$ *vs.* $\log(h_\infty - h)/h$ is made. The term b is obtained from the slope. (d) The values of b and dh/dt are introduced into the expression for the true rate of shear, $[(3 + b)/R]\,(dh/dt)$, the value of which is plotted against the shear stress, ${}^1/_2\rho g R(h_\infty - h)/h$, to

(14) B. Rabinowitsch, *Z. Phys. Chem.* (Leipzig), **145A**, 1 (1929).

yield the flow curve over the range of shear stresses and shear rates investigated.

Experimental Procedures

In order to be able to obtain accurate capillary rise rate measurements, a highly viscous liquid, preferably of definite composition, had to be used. Octa-O-methyl sucrose reached its equilibrium height at 40° only after about 24 hr and was readily synthesized from sucrose by a procedure similar to that described by Kuhn and Trischmann.[15]

Octa-O-methyl Sucrose. Sucrose, 8 g (2.3×10^{-2} mol), was dissolved in 200 ml of N,N-dimethylformamide (DMF). An excess of 16 ml of methyl iodide, 80 g of barium oxide, and 4 g of barium hydroxide octahydrate were added to the solution. The mixture was shaken for 4 days and then filtered. The precipitate was washed with 10 ml of DMF, and the combined filtrates were poured into an equal volume of cool, distilled water. The product was extracted with 90 ml of chloroform (3×30 ml). The chloroform layer was washed with water and dried over anhydrous sodium sulfate. The chloroform was then distilled *in vacuo* leaving a pale yellow syrup. This syrupy product was further distilled at 165° (0.075 mm). The product resulting from this last distillation was subjected to further methylation by dissolving it in 150 ml of DMF and shaking with a total of 6 ml methyl iodide, 36 g of BaO, and 1.2 g of $Ba(OH)_2$ which were added in 4 portions at 36-hr intervals. After filtration, it was washed and extracted as before. After the chloroform was distilled *in vacuo*, the syrupy product was distilled under 0.035–0.040 mm. Two constant-boiling fractions were collected at 145 and 160°, respectively. The fraction boiling at 145° was subjected to a second distillation. This operation yielded 3.5 g (33%) of syrup boiling at 145–47° (0.040 mm). $[\alpha]^{25}_D = +70.4°$ ($c = 3.5$, methanol). $n^{22}_D = 1.4566$. Bredereck, *et al.*,[16] report bp = 115° (0.001 mm), $[\alpha]^{20}_D = +70.1°$ (methanol), and $n^{22}_D = 1.4560$ for octa-O-methyl sucrose.

Octa-O-propionyl Sucrose. Octa-O-propionyl sucrose was synthesized according to a method reported by Hurd and Gordon.[17] Sucrose, 20 g (5.8×10^{-2} mol), was dissolved in 145 ml of pyridine. An excess of 75 ml of propionic anhydride was added to the solution. The solution was shaken for 72 hr, poured into cold, dilute hydrochloric acid, and the product was extracted with 500 ml of dichloromethane. The dichloromethane layer was washed with 400 ml of 0.5 *N* hydrochloric acid (4×100 ml), followed by three successive washings with equal volumes of distilled water. The dichloromethane was then washed with 400 ml of 5% potassium bicarbonate (4×100 ml), followed by three more successive washes with distilled water. The dichloromethane layer was dried over magnesium sulfate, stirred, and filtered. The dichloromethane was distilled *in vacuo*. The syrup was further distilled under

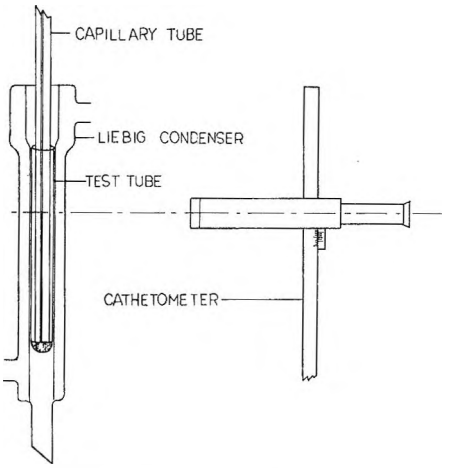

Figure 1. Capillary rise rate apparatus.

0.070 mm with a constant-boiling fraction being collected at 266–274°. A second distillation of the collected product yielded a syrup boiling at 265–267° (0.065 mm). $[\alpha]^{28}_D = +53.4°$ ($c = 4$, chloroform). $n^{21}_D = 1.4668$. After a 10-month period, the syrup crystallized to give a white crystalline material melting at 44.0–45.5°. Hurd and Gordon[17] report the melting point to be 45–46°.

1,1-Di(α-decalyl)-hendecane.[18] The small, carefully synthesized and purified sample of 1,1-di(2-decalyl)-hendecane was obtained from Dr. Joseph Dixon, American Petroleum Institute Project No. 42, Department of Chemistry, The Pennsylvania State University, University Park, Pa. The viscosities and densities of the liquid over a wide range of temperatures and pressures are reported by Lowitz, *et al.*[18]

Polystyrene Solutions. Two polystyrene solutions were chosen to illustrate that the flow curve determination technique would be applicable for non-Newtonian systems. Solutions with equal concentrations of polystyrene in toluene (a "good" solvent) and decalin (a "poor" solvent) were studied and compared.

Polystyrene, possessing a nominal molecular weight of 1.8×10^6 and a M_w/M_n ratio of less than 1.2, was used to prepare the two solutions. The solutions were prepared by adding a weighed quantity of the polystyrene to the particular solvent, and allowing the dissolution of the sample to occur by stirring overnight. The polystyrene was obtained from the Pressure Chemical Company, Pittsburgh, Pa.

Capillary Rise Rate Apparatus. The experimental apparatus used to determine the flow curve from capil-

(15) R. Kuhn and H. Trischmann, *Chem. Ber.*, **94**, 2258 (1961).

(16) H. Bredereck, G. Hagelloch, and E. Hambsch, *ibid.*, **87**, 35 (1954).

(17) C. D. Hurd and K. M. Gordon, *J. Amer. Chem. Soc.*, **63**, 2657 (1941).

(18) The sample designation for 1,1-di(α-decalyl)-hendecane used by the American Petroleum Institute Project No. 42 is P.S.U. 122. D. A. Lowitz, J. W. Spencer, W. Webb, and R. W. Schiessler, *J. Chem. Phys.*, **30**, 73 (1959).

lary rise measurements is illustrated in Figure 1. The Liebig condenser was sealed at the bottom and stoppered at the top. In order that adequate reproducibility be achieved in the rate of rise measurements, it is imperative that the capillary walls be extremely clean and free of absorbed matter. The cleaning procedure adopted was similar to that given by Davis and Rideal.[19]

The capillary is inserted into the apparatus and 30–40 min is allowed for complete temperature equilibrium. The end of the capillary is then touched to the surface of the liquid as one stopwatch is started. The cathetometer is raised a small height increment and as the liquid meniscus passes the horizontal hairline of the cathetometer eyepiece, the stopwatch is stopped and a second watch is simultaneously started. The cathetometer is then raised another increment and the process is repeated. This whole procedure is repeated throughout the desired extent of capillary rise. The time increments, Δt, are recorded for the corresponding height increments, Δh. The quotients, $\Delta h/\Delta t$, are then calculated and plotted against the respective mean heights, h. After the best smoothed curve is drawn through the experimental points, values of the quantity dh/dt are interpolated from the curve at selected values of h. The average deviation of the experimental points, $\Delta h/\Delta t$, from the smoothed curve in the rate of rise curves amounts to about 1–2%.

Capillary Equilibrium Height and Radii. The final height for the larger capillary was determined by first drawing the liquid meniscus by slight suction well above the anticipated equilibrium height and allowing it to descend to its equilibrium position. Light pressure was then applied to force the liquid meniscus slightly below its equilibrium position, allowing it to ascend to its equilibrium position. The final equilibrium height is taken as the average between the descending and ascending equilibrium positions. In most cases the difference between ascending and descending positions was negligible. The equilibrium heights for the capillaries of smaller radius were determined mathematically from the relationship, which is valid for constant temperature, $h_{\infty 2} = h_{\infty 1}R_1/R_2$, where $h_{\infty 1}$ and R_1 are the experimentally determined equilibrium height and radius, respectively, of the larger capillary and $h_{\infty 2}$ and R_2 are the equilibrium height and radius, respectively, of the smaller capillary. The capillary radii were determined by calibration with mercury.

Liquid Density. The density of octa-O-methyl sucrose was determined by a method described by Alber[20] which makes use of a cg specific gravity pipet. The specific gravity pipet used in this work was obtained from the Arthur H. Thomas Company, Philadelphia, Pa.

Results and Discussion

I. Flow Curves from Capillary Rise Rate Measurements. As a representative example, the "rate of rise" curve (Figure 2), the log–log plot (Figure 3), and the flow curves (Figure 4) for octa-O-methyl sucrose at 40° are shown. We have used the method to determine the viscosity–temperature behavior between 5 and 80°. Data, together with densities and surface tensions, are presented in Table I.

Figure 2. In the early portions of the ascent, the velocity is rapid due to the high shears tress (low height, h, values) but continually decelerates as the shear stress becomes less (increased height, h, values).

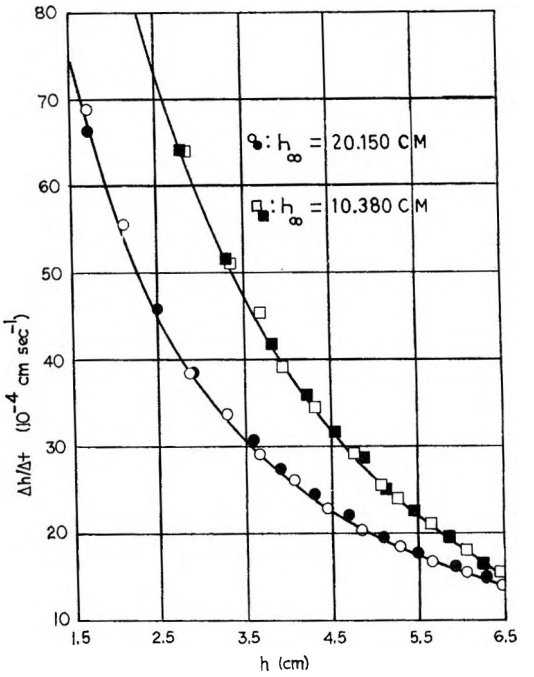

Figure 2. Rate of rise curves of octa-O-methyl sucrose at 40°: O, $R = 2.61 \times 10^{-3}$ cm; □, $R = 5.07 \times 10^{-3}$ cm; darkened symbols represent duplicate determinations.

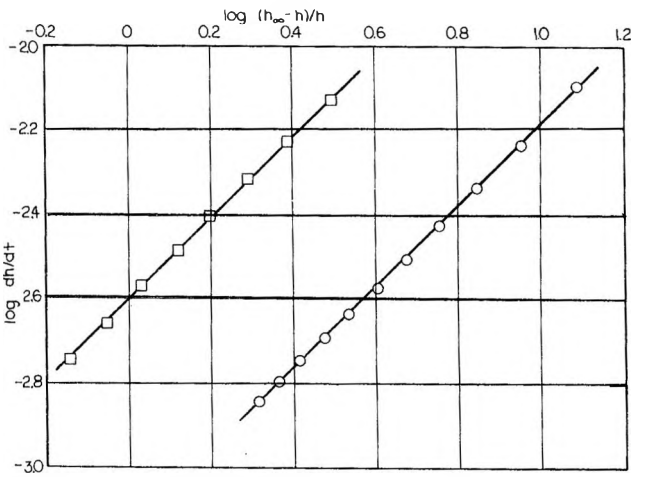

Figure 3. Log–log plots of octa-O-methyl sucrose at 40°: O, $R = 2.61 \times 10^{-3}$ cm; □, $R = 5.07 \times 10^{-3}$ cm.

(19) J. T. Davis and E. K. Rideal, "Interfacial Phenomena," Academic Press, New York, N. Y., 1963.

(20) H. K. Alber, *Ind. Eng. Chem., Anal. Ed.*, 12, 764 (1940).

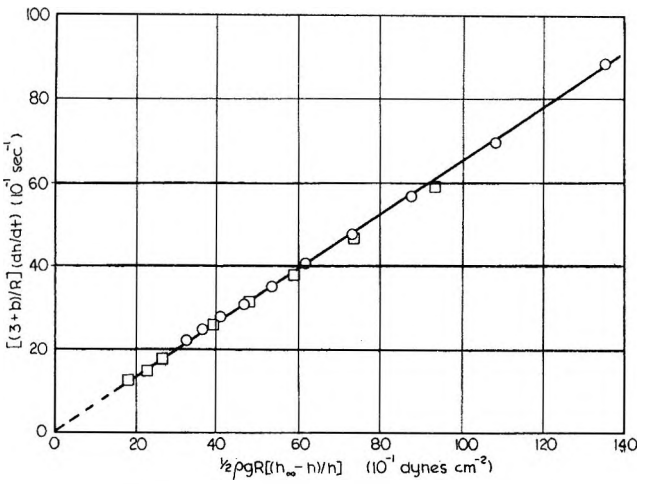

Figure 4. Flow curve of octa-O-methyl sucrose at 40°: O, $R = 2.61 \times 10^{-3}$ cm; □, $R = 5.07 \times 10^{-3}$ cm.

Duplicate experimental data (darkened symbols) are included. From this diagram it can be seen that it is possible to achieve very good reproducibility.

Figure 3. The slope of the log–log plot is seen to be essentially unity for both capillaries over the whole range of stresses and shear rates. This tends to support the validity of the method and shows that octa-O-methyl sucrose has Newtonian flow behavior as is to be expected for a pure liquid. Figure 3 is representative of the log–log plots obtained for other temperatures. The only exception to this was a deviation from the slope of unity in the log–log plot at 5° in the early portion of the capillary rise. We made this anomaly the subject of a more detailed investigation (section II).

Figure 4. Both capillaries used gave the same curves within the experimental accuracy of the method. From the reproducibility of duplicate measurements the accuracy could be estimated.

II. Non-Newtonian Behavior, Contact Angle Variation, and Rate of Wetting during Capillary Rise. For Newtonian liquids undergoing smooth laminar flow, the value of b in eq 8 is unity. The cases in which $b > 1$ represent pseudoplastic flow and the corresponding flow curves bend toward the rate of shear axis. Dilatant flow behavior is generally indicated where $b < 1$, and such flow curves bend toward the stress axis.

Our data for octa-O-methyl sucrose in section I supported the validity of the experimental method since we obtained identical flow curves using capillaries of different bore dimensions. The only anomaly which appeared was a deviation from the slope of unity for the log–log plot at 5° in the early portion of the capillary rise. This anomaly, along with a more detailed investigation into the influence of capillary bore dimensions on capillary rise phenomena, as well as flow curves of non-Newtonian liquids, are the subjects of section II.

The four liquids utilized in this study were octa-O-propionyl sucrose, 1,1-di (α-decalyl)-hendecane, and two polystyrene solutions.

Tables II–IV summarize the densities, surface tensions, and apparent viscosities obtained from the data collected in this investigation. Figures 5–10 illustrate the treatment of the data.

Table I: Density, Surface Tension, and Viscosity of Octa-O-methyl Sucrose

	T, °C				
	5°	20°	40°	60°	80°
ρ, g cm^{-3}	1.248	1.227	1.197	1.168	1.142
γ, dyn cm^{-1}	35.0	32.8	30.8	28.9	26.9
η_A, P	66.7	11.6	1.54	0.456	0.193

Table II: Density, Surface Tension, and Viscosity of Octa-O-propionyl Sucrose

	T, °C			
	20° (supercooled)	55°	70°	85°
ρ, g cm^{-3}	1.236	1.183	1.161	1.136
γ, dyn cm^{-1}	31.5	27.3	25.8	24.6
η_A, cP	4.65–5.20 $\times 10^5$	1.75×10^3	4.11×10^2	1.44×10^2

Table III: Density, Surface Tension, and Viscosity of 1,1-Di(α-Decalyl)-Hendecane

	T, °C		
	5°	10°	60°
ρ, g cm^{-3}	0.9408	0.9376	0.9067
γ, dyn cm^{-1}	32.3	31.6	27.9
η_A, cP	7.73×10^4	3.29×10^4	1.10×10^{2a}

[a] A value of 1.21×10^2 cP was reported by D. A. Lowitz, *et al.*[18] It is noted that the authors standardized their rolling ball viscometer with water, *i.e.*, a liquid of a very much lower viscosity.

Table IV: Density, Surface Tension, and Viscosity of Polystyrene Solutions at 30°

	Solvent	
	Toluene (4 g/100 ml)	Decalin (4 g/100 ml)
ρ, g cm^{-3}	0.848	0.911
γ, dyn cm^{-1}	24.7	29.0
η_A, cP	133–147	209

In the analysis of the capillary rise phenomenon, the significance of the log–log plot takes on a unique character. In several instances the slope of the log–log plot was unity except in the early portions of the capillary rise (high shear stresses) where the slope bent and became less than unity (Figures 5 and 6). This was attributed to a slow rate of wetting. Justification of this

premise is based on the results obtained with octa-O-propionyl sucrose at 20.0°. The capillary rise in the largest available capillary ($R = 10.67 \times 10^{-3}$ cm) was observed for a dry capillary and also in the case where the capillary was prewetted. In the case where there

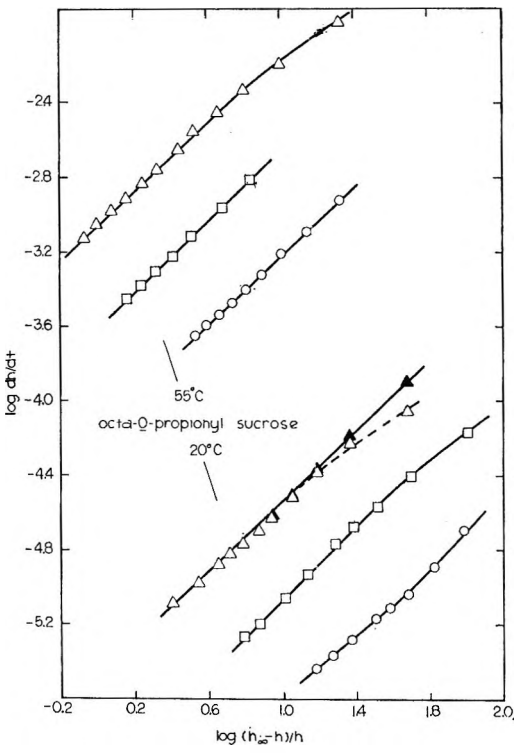

Figure 5. Log–log plots of octa-O-propionyl sucrose: △, $R = 10.67 \times 10^{-3}$ cm (▲, prewetted capillary); □, $R = 5.07 \times 10^{-3}$ cm; ○, $R = 2.61 \times 10^{-3}$ cm.

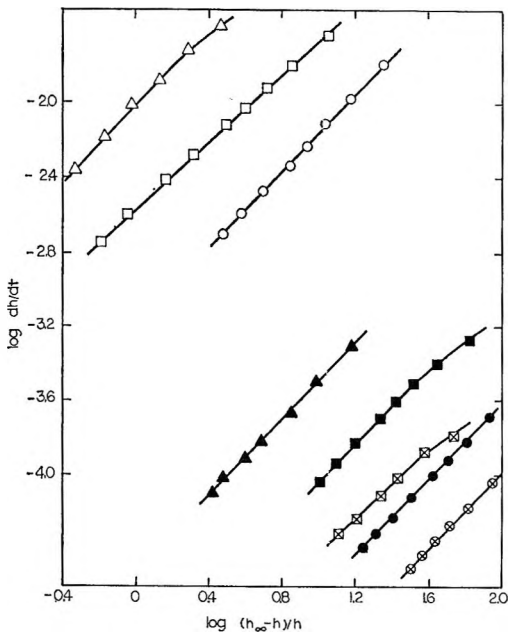

Figure 6. Log–log plots of P.S.U. 122: ▲, △, $R = 10.67 \times 10^{-3}$ cm at 10 and 60°, respectively; ⊠, ■, □, $R = 5.07 \times 10^{-3}$ cm at 5, 10, and 60°, respectively; ⊗, ●, ○, $R = 2.61 \times 10^{-3}$ cm at 5, 10, and 60°, respectively.

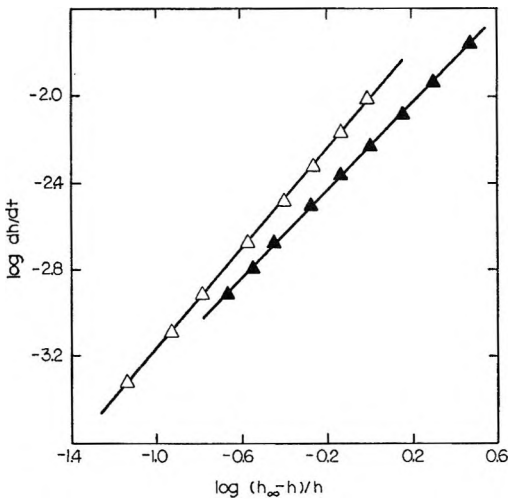

Figure 7. Log–log plots of polystyrene solutions at 30°, 4 g/100 ml: ▲, decalin as solvent; △, toluene as solvent.

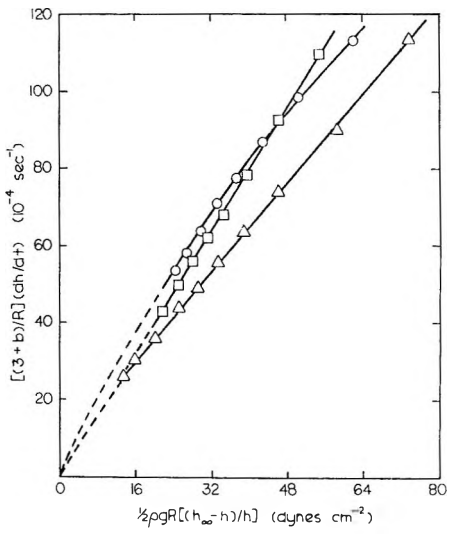

Figure 8. Flow curves of octa-O-propionyl sucrose at 20°: △, $R = 10.67 \times 10^{-3}$ cm; □, $R = 5.07 \times 10^{-3}$ cm; ○, $R = 2.61 \times 10^{-3}$ cm.

was no prewetting there was a definite bending of the slope toward less-than-unity values at the higher stresses in the log–log plots. However, prewetting the capillary eliminated virtually all curvature in the high shear stress portion of the log–log plot. Further substantiation of the slow wetting rate phenomenon was based on the observation that capillaries of smaller radii exhibited decreased departures from linearity in the log–log plots of octa-O-propionyl sucrose at 20 and 55° and of P.S.U. 122 at 5, 10, and 60° (Figures 5 and 6).

The results of this investigation indicate that departures from unity or linearity in the log–log plots for capillary rise flow at low heights, h, are attributable to a time lag in the attainment of a zero-contact angle. In other words, the rate of wetting is slower than the rate of capillary ascent. A flattening of the meniscus would

yield contact angles greater than zero and, hence, it would be necessary to include the cos θ term in eq 4 which would subsequently lead to the following expression for the shear stress at the capillary wall

$$s_W = {}^1/_2\rho g R\left[\frac{h_\infty \cos\theta - h}{h}\right] \qquad (11)$$

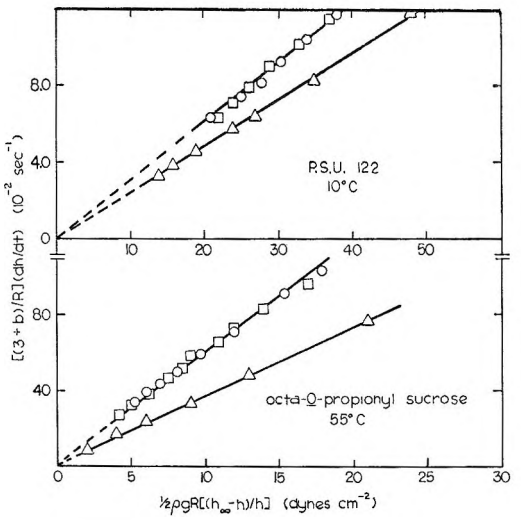

Figure 9. Flow curves of octa-O-propionyl sucrose at 55° (bottom) and P.S.U. 122 at 10° (top): △, $R = 10.67 \times 10^{-3}$ cm; □, $R = 5.07 \times 10^{-3}$ cm; ○, $R = 2.61 \times 10^{-3}$ cm.

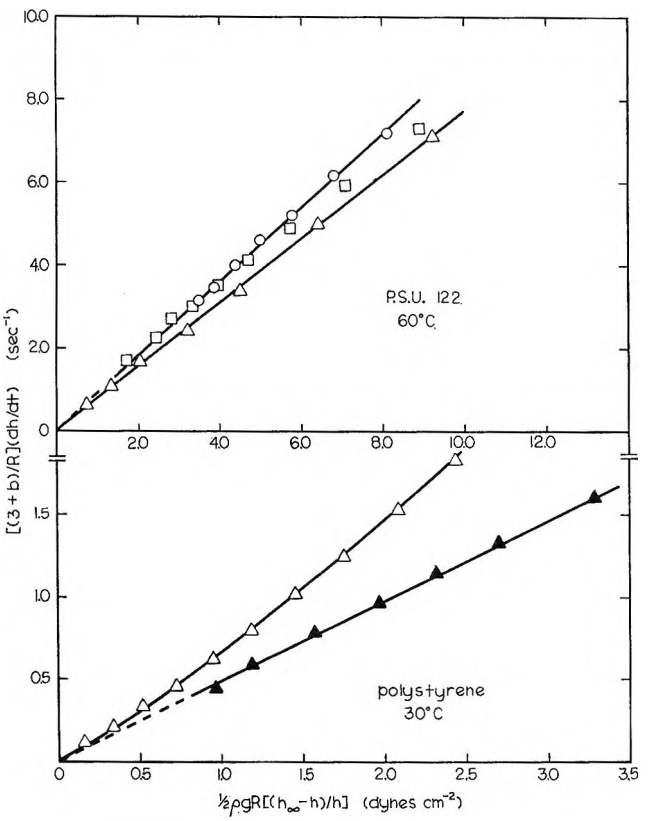

Figure 10. (Bottom) Flow curves of polystyrene solutions at 30°, 4 g/100 ml: ▲, decalin as solvent and △, toluene as solvent. (Top) Flow curves of P.S.U. 122 at 60°: △, $R = 10.67 \times 10^{-3}$ cm; □, $R = 5.07 \times 10^{-3}$ cm; ○, $R = 2.61 \times 10^{-3}$ cm.

Now it can be seen that for cases in which the capillary wall was not completely wetted and the contact angle was greater than zero, cos θ would be less than unity and would yield a stress less than that calculated on the assumption zero contact angle attainment. In other words, for a given rate of shear the "observed" shear stress would appear greater than the true shear stress. As the rise proceeds, the ascent becomes slower and the contact angle decreases. Consequently, as the high shear stresses become smaller, the "observed" shear stress comes closer to the true shear stress.

Even though the log–log plot may be linear with a slope of unity, our data suggest that the contact angle may not be zero. It demonstrates that the contact angle is constant. In several cases the log–log plot involving the largest capillary ($R = 10.67 \times 10^{-3}$ cm) gives a linear slope close to unity, yet the corresponding flow curve yields a viscosity higher than that obtained by the other two capillaries. Figures 8–10 illustrate this observation. In the case of octa-O-propionyl sucrose at 55° this increase in the viscosity amounts to about 60% over that obtained with the other two capillaries. Assuming a zero-contact angle for the capillary rise in the two smaller capillaries, the contact angle in the large capillary can be estimated by equating the complete expression for shear stress (eq 11) to the shear stress of the smaller capillaries at a given rate of shear. When this operation was carried out for the above example, a contact angle of 42–47° was obtained over the stress range of 7–21 dyn cm^{-2}.

For octa-O-propionyl sucrose at 20.0° the viscosity depicted by the flow curve of the larger capillary is about 27% greater than that obtained from the data of the two smaller capillaries, and this amounts to a calculated contact angle of 31–34° over the stress range of 24–58 dyn cm^{-2}.

The same treatment can be applied to P.S.U. 122 at 10.0 and 60.0° (Figures 9 and 10). At 10.0° the deviation in viscosity in the large capillary is 28%, and corresponds to an estimated contact angle of 36–38° over the stress range of 20–40 dynes cm^{-2}. At 60.0° the deviation in viscosity is 18%, whereupon the contact angle is calculated to be 19–23° over the stress range of 3–11 dyn cm^{-2}.

Compared to the stress ranges of often several 100%, these contact angle variations correspond to stress changes of only a few per cent. Thus, it is easy to see that a contact angle, different from zero, can stay constant over an extended range of shear stress. In this connection, Elliot and Riddiford[21] also find advancing contact angles to be independent of velocity at low velocity.

Is the assumption of zero contact angle for the smaller capillaries justified? It should be pointed out that

(21) G. E. P. Elliot and A. C. Riddiford, *J. Colloid Interfac. Sci.*, **23**, 389 (1967).

there are about equal differences between bores of the three capillaries used. Yet, the differences in the flow curves for the two smaller capillaries are well within the experimental error of the measurements. From this it can be safely concluded that a limit is reached here, at which the viscosity and the flow curve determinations become independent of the capillary bore dimensions. Since the rate of rise becomes smaller with smaller bore, there is relatively more time for the wetting process to take place and the contact angle will become smaller and, for very small capillaries, zero. Obviously, this limit was reached for the two smallest capillaries.

Rate of rise measurements were conducted on two polystyrene solutions in order to establish whether the method would be applicable for determining flow curves of non-Newtonian, pseudoplastic materials. Figure 7 depicts the log–log plots for solutions of polystyrene in toluene and of polystyrene in decalin, both at a concentration of 4 g/100 ml. The log–log plot of the toluene solution gives a slope of 1.15 and was, therefore, typically pseudoplastic. Close inspection of the flow curves (Figure 10) reveals that the curve bends toward the rate of shear axis, and the apparent viscosities range from 174 cP at a stress of 0.20 dyn cm^{-2} to 133 cP at 2.40 dyn cm^{-2}. In contrast, the log–log plot and flow curve for polystyrene in decalin is Newtonian and is explainable on the basis that decalin is a poor solvent; the polymer chains do not unravel and interact with each other as they would in the case of a good solvent like toluene.

With solutions like these, as opposed to pure liquids, another difficulty has to be considered. The surface concentration and, hence, the surface tension may change during the capillary rise because of the constant wetting of new capillary wall surfaces. Although we have not done it, this effect could be investigated with the technique of prewetting the capillary as described above.

The "pseudo-dilatant" behavior due to the wetting effect at high shear rates in the early portions of the capillary rise was disclosed as systematic experimental error and is not included in the flow curves. However, most noticeably for octa-O-propionyl sucrose at 20° and with the smallest capillary, the slope of the log–log plot becomes less than unity. This departure from unity at very low shear rates corresponds to true dilatant flow behavior, the effect of which is revealed in the flow curve (Figure 8). Since true dilatant flow behavior is generally associated with dispersed phase systems, it becomes interesting to speculate about its nature in a typically homogeneous, chemically pure material, such as octa-O-propionyl sucrose which is suppercooled at 20°. A recent hypothesis concerning the nature of the liquid state[22,23] allows one to calculate the size of the molecular aggregations. For our higher viscosities, the diameters a of the aggregations are of the order of 10^{-6} cm, at the lower limit of colloidal particle size.

Acknowledgment. R. L. Kissling expresses his gratitude for the financial assistance contributed by the National Science Foundation Graduate Traineeship, Summer 1967.

(22) P. H. Gross, *Rheol. Acta*, **3**, 286 (1964).
(23) P. H. Gross and H. K. Zimmerman, *ibid.*, **3**, 294 (1964).

The Induction Effect in Studies of Solute Diffusion According to the Frit Method

by Michael J. Eitel

Department of Chemistry, Northeastern University, Boston, Massachusetts 02115
(Received May 26, 1969)

In experimental applications of the frit method, polymeric solutes have often exhibited initial diffusion rates that are anomalously rapid. The possibility has been considered that the nonideal induction effect was caused by allowing insufficient time during a diffusion-controlled frit-filling procedure, prior to actual diffusion experiments. If the latter experiments start out with a reasonable diffusion profile as the initial distribution of solute within the frit, then the features of the observed anomalous induction effect are predictable by computation. Controlled experimentation with aqueous solutions of sucrose demonstrated that nonideal induction effects are attainable even with a nearly ideal solute. Experimentally determined diffusion plots for this solute agree well with computed predictions, and the relation is examined between these data and results obtainable for low mobility solutes. Calculations show that the considered type of experimental imperfection does not interfere with the validity of diffusion coefficient determinations by the frit method.

Introduction

A convenient gravimetric means for determining diffusion coefficients of dissolved solutes is afforded by the frit method, in which the rate of change in apparent weight is determined for a solution-filled frit while submerged in a thermostated bath of solvent.[1,2] The method requires that the solution density is a linear function of the solute concentration, and the porous frit must satisfy a number of requirements in order to perform favorably in these experiments; but numerous experimental investigations have demonstrated that the method is suitable for determining diffusion coefficients of both nonpolymeric and polymeric solutes.[3] Using calibration procedures described elsewhere,[2] a meaningful solute diffusion coefficient is determinable from the slope of the straight portion of a semilog plot for the apparent solution weight *vs.* time. At small times, prior to the expiration of an induction period, a curved portion of the diffusion plot is encountered even if the solute behaves ideally. Many nonpolymeric solutes have shown the detailed characteristics of nearly ideal induction effects, but diffusion experiments with high-polymer solutes have often shown an initial change in apparent weight that is anomalously rapid.[3,4]

In the present investigation, a possible cause of this nonideal phenomenon is considered in detail. Reasons are presented below why the effect can be ascribed to an experimental imperfection, although thermodynamic nonideality can also make significant contributions. Finally, a type of imperfection that can account for the observed phenomena is treated mathematically, and the results from controlled experimentation are reported.

Preliminary Considerations

In detailed studies of diffusion phenomena, one must be aware of conditions, which derive from the dependence of diffusion effects on solute activity rather than concentration. The activity effects can be coped with if one postulates that some simple functional relation exists between the diffusion coefficient and the prevailing local solute concentration.[5,6] In particularly interesting cases the thermodynamic nonideality has been found responsible for substantial increases in the diffusion coefficient at increased polymer concentration.[7] Unfortunately, such concentration effects are not detectable in experiments considered here, for computational predictions have shown that observations of diffusion into a solvent bath can provide only indications of the diffusion coefficient at near-infinite dilution.[6,8] If the diffusion coefficient is assumed to increase linearly with concentration, then computed results[8] actually predict induction effects that are similar to the described type. This finding may explain many observed nonideal induction effects, and deviations from ideality should be observable even if frits of various thicknesses are employed in experimentation. But in one polymer–solvent system we have detected such nonideal behavior only in experiments with a thick frit, while nearly ideal behavior prevailed in a thinner frit.[4] It appears that this phenomenon cannot be ascribed solely to thermodynamic nonideality.

As an alternative explanation, it is considered here that the encountered nonideal behavior may be due to an experimental imperfection that is likely to occur

(1) G. Schulze, *Z. Phys. Chem.*, **89**, 168 (1914).

(2) F. T. Wall, P. F. Grieger, and C. W. Childers, *J. Amer. Chem. Soc.*, **74**, 3562 (1952).

(3) F. T. Wall and C. W. Childers, *ibid.*, **75**, 3550 (1953).

(4) H.-W. Ko and M. J. Eitel, *Macromolecules*, **1**, 364 (1968).

(5) J. Crank, "The Mathematics of Diffusion," Oxford University Press, London, 1956.

(6) F. T. Wall and R. C. Wendt, *J. Phys. Chem.*, **62**, 1581 (1958).

(7) A. Haug and G. Meyerhoff, *Makromol. Chem.*, **53**, 91 (1962).

(8) H. K. Frensdorff, *J. Polymer Sci.*, **A2**, 353 (1964).

with polymeric solutes. In conformance with such reasoning, it had been proposed that large induction effects can result if a coating of polymer solution adhered to the frit surface at the instant of immersion into the solvent bath.[3] However, it is difficult to accept that a measurable amount of adhering solute can persist in contact with well agitated solvent during the whole length of the induction period (typically up to 60 min).

In an attempt to explain the observed nonideal behavior, it is considered here that other experimental shortcomings are encountered primarily in working with those solutes which diffuse slowly. In the approach taken here, attention is focused onto the process that introduces solute into the frit, prior to the described diffusion experiments. Ordinarily, the frit-filling procedure relies on diffusion mechanisms in order to bring about a gradual equalization of solute concentrations between a reservoir of solution and a solvent-filled frit. Since the experimental procedure must get by with limited soaking times, some nonuniformity in the concentration profile across the frit must be accepted as an imperfection. At the end of the described procedure, higher local concentrations prevail near the surface of the frit than in its interior, and under a fixed set of conditions, the difference between the considered local concentrations is larger for a solute that diffuses slowly. When subsequent experimentation exposes the frit to pure solvent, then the excess concentration, from the surface regions of the frit, becomes depleted rapidly. For a frit of such a history the rate of solute removal should exceed the rate that is observable if the same amount of solute were distributed uniformly. These arguments enable us to account qualitatively for an accelerated solute removal from the frit.

Mathematical Treatment of the Consecutive Diffusion Processes

In a quantitative treatment of the consecutive filling and depletion steps, the assumption is made that the frit surfaces are maintained at the bath concentration C_0 during the soaking process. Then the concentration profile at the beginning of the depletion process is given as

$$C(x) = C_0 - \frac{4C_0}{\pi} \sum_{n=1}^{\infty} \frac{(-1)^{n-1}}{2n-1} e^{-(2n-1)^2 \alpha D_0 t_0} \times \cos (2n-1)\pi x/L \quad (1)$$

where $\alpha = \pi^2/L^2$, and L is the thickness of the frit; D_0 is the diffusion coefficient at the temperature of the filling step, and t_0 is the time of filling. Using a cosine expansion of unity for the interval $(-L/2 \leq x \leq L/2)$, eq 1 can be cast in the form

$$C(x) = \frac{4C_0}{\pi} \sum_{n=1}^{\infty} \frac{(-1)^{n-1}}{2n-1} [1 - e^{-(2n-1)^2 \alpha D_0 t_0}] \times \cos (2n-1)\pi x/L \quad (2)$$

In order to adapt this result to the interval $0 \leq \chi \leq 1$, one lets $\chi = (x + L/2)/L$, and it follows that

$$C(\chi) = \frac{4C_0}{\pi} \sum_{n=1}^{\infty} \frac{1 - e^{-(2n-1)^2 \alpha D_0 t_0}}{2n-1} \sin (2n-1)\pi\chi \quad (3)$$

This formulation is compatible with a literature result that applies to the continued diffusion from an arbitrary interim profile $g(\xi)$, if like conditions are maintained at the boundaries of the interval. In terms of the dummy variable ξ, the general result[9] can be written

$$C(\chi, t_0 + t) = 2 \sum_{m=1}^{\infty} e^{-m^2 \alpha Dt} \sin m\pi\chi \int_0^1 g(\xi) \sin m\pi\xi d\xi \quad (4)$$

where D and t are the diffusion coefficient and the diffusion time for the depletion experiment. When this equation is applied to the initial concentration profile in eq 3, many integrals make no contribution, since

$$\int_0^1 \sin (2n-1)\pi\xi \sin m\pi\xi d\xi = 0 \qquad (m \neq 2n-1)$$

Nonzero integrals are obtained only when $m = 2n - 1$ and hence a single summation suffices to combine eq 4 and 3. After the indicated integration the result is

$$C(\chi, t_0 + t) = \frac{4C_0}{\pi} \sum_{n=1}^{\infty} \frac{1 - e^{-(2n-1)^2 \alpha D_0 t_0}}{2n-1} e^{-(2n-1)^2 \alpha Dt} \times \sin (2n-1)\pi\chi \quad (5)$$

Further term-by-term integration of this equation over all values of χ is justified, since the summations of eq 5 and 6 converge uniformly for all positive values of t. Finally, the average concentration within the frit is obtained to be

$$\bar{C}(t_0 + t) = \frac{8C_0}{\pi^2} \sum_{n=1}^{\infty} (2n-1)^{-2} \times [1 - e^{-(2n-1)^2 \alpha D_0 t_0}] e^{-(2n-1)^2 \alpha Dt} \quad (6)$$

This result is surprisingly similar to the corresponding relation that applies to experiments, which start with completely filled frits (the only difference being the nonunity contents of the bracket in eq 6). Despite these similarities, detailed numerical calculations are required to demonstrate that amplified induction effects are described by eq 6.

Computed Results

The evaluation of eq 6 was performed conveniently by a FORTRAN computer program using trial values of $\alpha D_0 t_0$ and αDt: a value of 0.1 required about 20

(9) For example, see R. V. Churchill, "Modern Operational Mathematics in Engineering," McGraw-Hill, New York, N. Y., 1944, p 201.

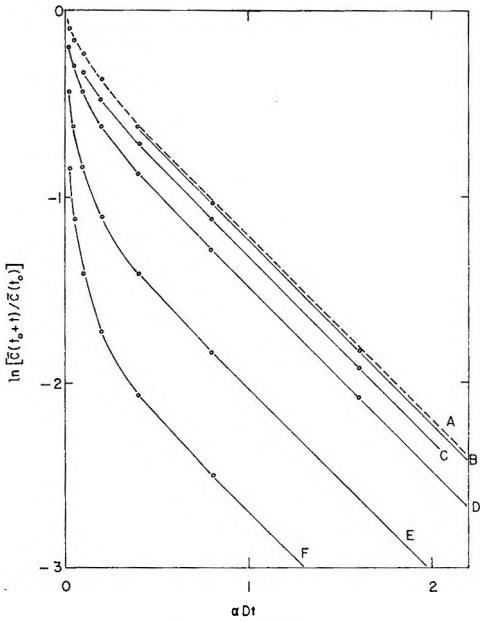

Figure 1. Calculated diffusion plots showing induction effects. Curves A, B, C, D, E, and F, were computed for the values of $\alpha D_0 t_0$: ∞, 1.6, 0.8, 0.4, 0.1, and 0.025, respectively

terms, and twice as many terms were needed at a value of 0.025. In these computations, we insisted that the ratio $(1 - \exp[-(2n - 1)^2 \alpha D_0 t_0])/(2n - 1)^2$ was decreased by two orders of magnitude, before the summation was terminated.

In order to describe the induction effect conveniently, the quantity $\ln[\bar{C}(t_0 + t)/\bar{C}(t_0)]$ was plotted *vs.* αDt, as shown in Figure 1. The induction effect was found to be confined to a time range that is only weakly affected by the filling conditions. After expiration of the induction period, the plots of Figure 1 were found to attain the theoretical slope of unity. This finding shows that undistorted diffusion coefficients are determinable from semilog diffusion plots, after the induction effect has subsided. Therefore, we conclude that an incomplete filling procedure does not subtract from the validity of the diffusion coefficient determinations, but an amplified induction effect can be generated by the considered experimental imperfection.

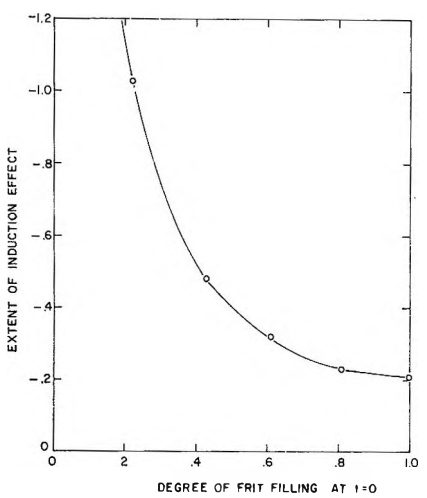

Figure 2. The effect of frit-filling on the magnitude of the induction effect. Abscissa, computed values of $C(t_0)/C_0$; ordinate, intercepts of linear extrapolations of $\ln [\bar{C}(t_0 + t)/\bar{C}(t_0)]$ to $t = 0$ (obtained from Figure 1).

Our computer evaluation of eq 6 permitted the simultaneous determination of the fractional degree of filling at $t = 0$ (given by $\bar{C}(t_0)/\bar{C}_0$), using eq 6. These results enabled us to present an alternate graphical characterization of the induction effect, shown in Figure 2. In this graph, extrapolations (to $t = 0$) for the linear trends of diffusion plots (in Figure 1) were used as a quantitative measure of the induction effect. As discussed elsewhere,[4] the extrapolation value of $\ln (8/\pi^2)$ is indicated in the ideal case, for a completely filled frit at $t = 0$. Figure 2 shows that small deviations from complete filling matter little, but if the average initial concentration within the frit is substantially lower than the saturation value, then greatly amplified induction effects can be obtained.

Experimental Section

The theoretical predictions were followed up by experimentation in which the frit-filling and depletion processes were carried out under controlled conditions. In this work we employed solutions of a nonpolymeric solute whose diffusion characteristics in frit experiments had been found to be virtually ideal.[4] It was the aim of the experimental investigation to demonstrate that even a well-behaved solute can exhibit the features of a nonideal induction effect, if this is warranted by the particular procedure that was employed for pretreatment of the frit.

Apparatus and procedure used here were essentially as described elsewhere.[4] The frit used in this investigation had been designated as Frit II in a prior publication.[4] The frit-filling procedure was carried out to a controlled extent using an agitated bath of aqueous 0.125 *M* sucrose, thermostated at 34°. There is reason to believe that these solutions were quite stable, since spot-checks revealed that the solution remained at a pH of 7.00 ± 0.02. After a predetermined frit-filling time, the frit was transferred quickly to a water bath thermostated at the same temperature, and determinations of submerged frit weight were then carried out as previously described.[3,4]

Results and Discussion

The experimental results are summarized in Figure 3. Data are reported for four diffusion runs with different frit-filling times, as indicated in the caption of Figure 3. The illustration also shows the results of predictive calculations based on eq 6. All data shown can be correlated using a common value of the diffusion parameter $(\pi^2 D/L^2) = 1.6 \times 10^{-4}$ sec^{-1}. The ex-

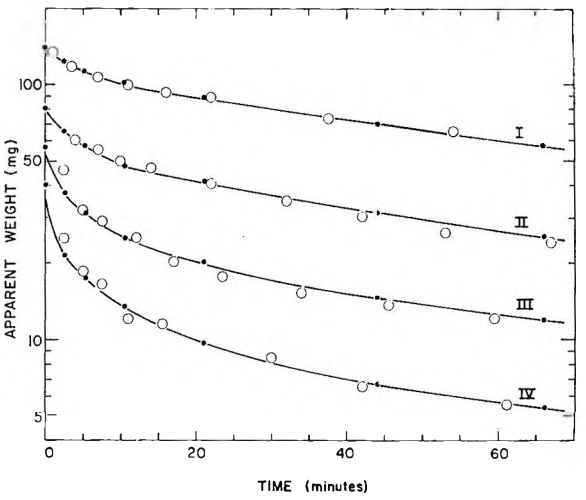

Figure 3. Open circles, diffusion data for "depletion" experiments with sucrose at 34°. Curves I, II, III, and IV were obtained after preconditioning the frit in aqueous 0.125 M sucrose solution for 90, 33, 12, and 5 min, respectively. Solid circles, computed results, based on eq 6. The computations employed a single value of $D\alpha = 1.6 \times 10^{-4}$ sec^{-1} together with values of t_0 and t pertaining to experimentation.

perimental data show no significant deviations from the computed curves.

Compared to some polymeric solutes, which have exhibited nonideal induction effects, sucrose has a diffusion coefficient (6.4×10^{-6} cm^2/sec at 34°) that is about twenty times as large. In view of this rough comparison of the D values for the two types of solutes, it is apparent that the same magnitudes of the product (αDt) are attained if the time of experimentation with the polymer is twenty times as long. The diffusion equations stipulate that the product (αDt) is the variable (see Figure 1) that measures the progress of the diffusion process, such as the duration of the induction effect. In equivalent manner, the quantity ($\alpha D_0 t_0$) describes the extent to which frit-filling was accomplished before the depletion experiments were started. Therefore, we estimate that the frit must be soaked in the described polymer solution about twenty times as long in order to attain the same degree of frit-filling as is attainable with sucrose.

On the basis of this reasoning, one calculates that the frit becomes filled to the same extent upon pretreatment for 90 min with sucrose solution and upon pretreatment with the chosen polymer solution for a duration of 30 hr. The latter condition approximates the experimental procedure followed in reported experiments,[3,4] and the former type of frit history applies to experiments whose results are summarized in the top curve of Figure 3. According to eq 6, one predicts that the depletion experiments should generate data along diffusion plots of identical shape, provided that the time scale is adjusted to correspond to comparable values of (αDt). However, even the top curve of Figure 3 is exhibiting a pronounced nonideal induction effect, as revealed by quantitative considerations described below.

For a frit that is initially filled uniformly with a solute whose diffusion behavior is ideal, the following diffusion equation is valid[4] at all t values that are not very small.

$$\log|w| = -0.4343D\alpha t + \log[(8/\pi^2)|w_0|] \qquad (7)$$

Here w_0 and w are the contributions of the solute to the apparent frit weights at $t = 0$ and at other times t. The equation describes the linear portion of diffusion plots for $\log|w|$ *vs.* t. According to eq 7 the intercept of a graphical extrapolation to zero time is related to $\log|w_0|$. However, the latter quantity can be determined independently of eq 7 from a nonlinear extrapolation of the experimental data, and eq 7 then stipulates that the distance between the two extrapolation values should be given by $\log(8/\pi^2)$. In the top graph of Figure 3 the two extrapolation values are found to be log 104 and log 140, respectively, and their difference is calculated to be 0.133, while the absolute value of $\log(8/\pi^2)$ is 0.0907. The discrepancy between these numbers shows that considerable nonideality prevails in experiments with sucrose at a soaking time of 90 min.

As noted above, the nonideal features of these experimental data should also apply to typical experiments with polymeric solutes. It appears that the considered type of experimental imperfection is likely to be encountered when solutes are investigated, whose rates of diffusion are inherently slow. We conclude that the proposed mechanism provides a plausible explanation for some characteristics of previously reported anomalous induction effects.

Some Considerations of the Electrolyte Used to Maintain Constant Ionic Strength in Studies on Concentration Stability Constants in Aqueous Solutions. Application to the Polarographic Evaluation of Thallium (I) Complexes

by A. M. Bond

Department of Inorganic Chemistry, University of Melbourne, Parkville, Victoria 3052 Australia
(Received May 26, 1969)

In studies of metal ion complexes formed in solution, the magnitudes of equilibrium constants existing between the various species are usually sought. Ideally, these constants are obtained from relationships between activities of each of the species present under equilibrium conditions. Often, however, the activities are unknown and concentrations instead of activities must be used. These latter concentration equilibrium constants, as distinct from activity equilibrium constants, are a function of the ionic strength of the medium and consequently must be evaluated from sets of measurements all made at the same ionic strength. Most studies to date on concentration equilibrium constants, such as stability constants of metal ion complexes in aqueous media, have arbitrarily chosen perchlorate or nitrate media to maintain the ionic strength constant, with the assumption that this added perchlorate or nitrate electrolyte is noncomplexing toward the metal ion being studied. Furthermore, as a consequence of this attitude, little quantitative information on the actual stability of perchlorate or nitrate complexes is available. In this work, consideration is given to errors and effects introduced into results obtained for concentration stability constants in making the assumption that the added electrolyte is noncomplexing with special reference toward the commonly used polarographic method for determining stability constants. Results are then given for stability constants of perchlorate, nitrate, and chloride complexes of thallium(I), obtained by the polarographic method, using fluoride solutions as the noncomplexing medium, to show that perchlorate and nitrate may not always be the best choice as an inert electrolyte and that thought at least should always be given to possible alternatives.

Introduction

In solution studies of complex ion species formed between metal ions and ligands, the magnitudes of all the equilibrium constants existing between the various species in solution are usually sought. The equilibrium constants arise from equilibria involving formation of complexes of the type $ML_n^{(x-ny)+}$ from interaction of metal ion species M^{x+} with ligand L^{y-}.

For simplicity, the equilibria present in solution can be represented by a general equation of the type

$$M^{x+} + nL^{y-} \overset{\beta n}{\rightleftharpoons} ML_n^{(x-ny)+} \qquad (1)$$

In this equation, βn is the equilibrium constant, usually referred to as the "stability constant," and n represents the number of ligands of L^{y-} attached to the central metal ion M^{x+} to give the metal ion complex $ML_n^{(x-ny)+}$.

βn, the stability constant, is mathematically related to the activities of each of the species represented in eq 1 by an expression

$$\beta n = \frac{(\text{activity } ML_n^{(x-ny)+})}{(\text{activity } M^{x+})(\text{activity } L^{y-})^n} \qquad (2)$$

In terms of concentrations of the various species [ ] and activity coefficients γ, this expression in eq 2 becomes

$$\beta n = \frac{(\gamma_{ML_n}{}^{(x-ny)+}\ [ML_n^{(x-ny)+}])}{(\gamma_M{}^{x+}[M^{x+}])(\gamma_L{}^{y-}[L^{y-}])^n} \qquad (3a)$$

or by rearrangement

$$\beta n = \frac{(\gamma_{ML}{}^{(x-ny)+})}{(\gamma_M{}^{x+})(\gamma_L{}^{y-})^n} \frac{[ML_n^{(x-ny)+}]}{[M^{x+}][L^-]^n} \qquad (3b)$$

It can be seen therefore that βn can be measured if either the activities are known or alternatively both activity coefficients and concentrations are known. Many analytical or instrumental techniques used to measure stability constants, however, measure or indicate concentration only. Furthermore, the activity coefficients are generally not known nor can they be calculated easily and reliably except at low ionic strengths, so that in many cases and especially at high ionic strength, the stability constant βn cannot, strictly speaking, be evaluated. However, a related quantity, which may be designated $\beta n'$, can be evaluated using concentrations instead of activities and neglecting activity coefficients. This quantity $\beta n'$ appears frequently in the literature, although it is quite often mistakenly referred to as a βn value.

The relationship between βn and βn′ and the procedure of neglecting activity coefficients and using

concentrations instead of activities can be seen as follows.

Rearrangement of eq 3b leads to

$$\beta n \left\{ \frac{(\gamma^{M^{x+}})(\gamma^{L^{y-}})^n}{(\gamma^{ML_n^{(x-ny)+}})} \right\} = \left\{ \frac{[ML_n^{(x-ny)+}]}{[M^{x+}][L^{y-}]} \right\} = \beta n' \quad (4)$$

Since the activity coefficients are a function of ionic strength I, then it follows that $\beta n'$ is related to βn by a function of ionic strength, $F(I)$, *i.e.*

$$\beta n' = F(I)\beta n \quad (5)$$

Equation 5 implies that $\beta n'$ values should be quoted at the particular ionic strength at which they were measured to be of any thermodynamic significance. In the special case where the ionic strength is low and approaches zero, βn and $\beta n'$ will be equal, as with these conditions activity coefficients approach unity and concentration equals activity. Under other conditions, which are usually the case in practical measurements, βn and $\beta n'$ values are quite different in magnitude, and calculated $\beta n'$ values to be of any significance need to be reported with the ionic strength at which they were measured.

In many of the common techniques for measuring stability constants, for instance electroanalytical methods such as potentiometry and polarography, the ligand concentration L^{y-} is varied over quite a wide concentration range while the analytical metal ion concentration is maintained at a considerably lower value relative to the ligand concentration. Graphical plots, statistical methods or other numerical methods of calculation, of functions of potential, current or some other variable, *vs.* concentration of ligand, allows $\beta n'$ to be evaluated.

The ionic strength for evaluation of $\beta n'$ can be maintained constant for all ligand concentrations by always adding sufficient calculated, additional electrolyte to bring the ionic strength up to a particular value after allowing for contribution by the species M^{x+}, L^{y-}, $ML^{(x-y)+}$ etc., already present in solution. In this manner $\beta n'$ can be calculated at a particular ionic strength I. Obviously the nature and type of electrolyte added to maintain the ionic strength constant will be critical in calculation of $\beta n'$ values and care needs to be made in choosing the particular electrolyte to be used.

For instance, if an equilibrium of the type $M^{x+} + nL^{y-} \rightleftharpoons ML_n^{(x-ny)+}$ is being studied, an important requisite of the added electrolyte AB is that it should be noncomplexing towards M^{x+}.

In most work A is chosen to be Li^+, Na^+, or K^+ and B is either ClO_4^- or NO_3^-, but unfortunately most often without thought as to whether the choice is the best possible. It should always be remembered that it is possible that in some complex ion systems, weaker complexes than perchlorate, and certainly nitrate, can exist. If they do, then more reliable answers can be obtained for $\beta n'$ values as compared with those obtained by using perchlorate or nitrate. Often, of course, these two will be the best available "noncomplexing" media, but at least thought should be given to alternatives. As an example of this, the possibility of using fluoride electrolytes to maintain constant ionic strength in studies on thallium(I) complexes was investigated and results are reported using the polarographic method. Consideration is also given to the effect of the contribution of AB to the value obtained for $\beta n'$ in the polarographic method.

Experimental Section

All chemicals used were of reagent grade purity. All measurements were made at (30 ± 0.1)°. Oxygen-free nitrogen was used to deaerate the solutions. The concentration of thallium(I) used was approximately 2×10^{-4} *M;* the ligand concentrations and concentrations of added fluoride electrolytes added to maintain constant ionic strength are shown in Tables I–V.

All measurements were made on solutions of pH 5.5–6.5. In this pH range it was assumed that both complex formation of fluoride ion by hydrogen ion and thallium(I) by hydroxide ion are negligible.

Polarograms were obtained using the Metrohm Polarecord E.261. Ac polarography was carried out using the Metrohm Ac Modulator E.393 with an ac voltage of 10 mV, rms at 50 cps. To minimize cell impedance, the modulating ac voltage was applied through an auxiliary tungsten electrode. Rapid polarographic techniques and controlled drop times for the dropping mercury electrode (dme) of 0.16 sec were achieved with a Metrohm Polarographie Stand E.354. The dme had a capillary constant $m^{2/3}t^{1/6} = 1.93$ (in distilled water at zero applied potential *vs.* Ag–AgCl electrode) for drop time $t = 4.4$ sec.

Reversibility of the electrode reaction $Tl^+ + e \rightleftharpoons Tl$ (amalgam) was verified for each solution as follows. (i) ac polarograms were completely symmetrical and the ac half band-width was (96 ± 2) mV for all drop times between 0.16 and 4.4 sec. (ii) Plots of E_{de} *vs.* $\log (i)/(id - i)$ were linear with slope (60 ± 1) mV for all drop times between 0.16 and 4.4 sec. (iii) Half-wave potentials ($E_{1/2}$) from ac polarography and summit potentials (E_s) from ac polarography coincided. (iv) $E_{1/2}$ and E_s values were independent of drop time over the range 0.16 to 4.4 sec.

ORION Fluoride Activity Electrode, Model 94-09 was used to measure the concentration or activity of free fluoride ion present in thallium(I) and other solutions.

Results and Discussions

(*a*) *Complexes of Thallium(I).* Examination of tables[1] gives the stability constants (β_1 or β_1' values)

(1) "Stability Constants of Metal-Ion Complexes," Special Publication No. 17, The Chemical Society, London, 1964.

of some typical thallium(I) complexes. It can be seen that in general they are extremely weak as most values lie in the range 1–20. Furthermore, most values have been obtained using perchlorate media to maintain constant ionic strength. However, β_1 for the perchlorate complex of thallium(I) has been measured as 1.0.[2] In addition, in some of the methods of measurement used, the concentration of perchlorate used to maintain the ionic strength constant is considerably greater than the ligand concentration and results obtained by allowing for perchlorate complexing could be quite different from those in which perchlorate complexing is neglected. Obviously the use of nitrate for which $\beta_1 = 2.15$[3] would even be more unsatisfactory than perchlorate for use as a medium to maintain constant ionic strength if effects of nitrate complexing are to be neglected.

Solubility measurements[4] have shown that the fluoride complex of thallium(I), like perchlorate, is also very weak, with a value of $\beta_1 = 1.2$ being obtained. On the other hand, potentiometric studies maintaining an ionic strength of 1.0 with $NaClO_4$[5] indicated no evidence of any fluoride complex formation, and analysis of results suggested in fact that the fluoride complexes may be weaker than the perchlorate complexes. Thus, as the results for β_1 for the fluoride and perchlorate complexes were obtained by different methods and under different conditions, then after taking into account the experimental errors and the evidence from potentiometry, it is quite conceivable that the fluoride complex of thallium(I) is in fact weaker than that of the perchlorate complex.

In view of the uncertainty as to whether the fluoride or perchlorate complex of thallium(I) is weaker, an investigation was therefore carried out to test the relative complexing effects of fluoride and perchlorate toward thallium(I) and to evaluate results for other complexes of thallium(I) when fluoride media are used to maintain constant ionic strength. The technique used for these measurements was that of polarography, since the electrode reaction $Tl + e \rightleftharpoons Tl$ (amalgam) is reversible,[6] and the interpretation of results is relatively simple.

(*b*) *The Polarographic Method for Evaluation of Concentration Stability Constants.* Since the electrode reaction for thallium(I) at the dme was shown to be reversible in this work, the polarographic equation derived by DeFord and Hume[7] can be used to calculate the nature and magnitude of thallium(I) complexes formed in solution. The DeFord–Hume equation can be expressed as

$$F_0(X) = \sum_n \beta n' C_L^n = \text{antilog}\left\{0.434 \frac{nF}{RT} \times [(E_{1/2})_f - (E_{1/2})_c] + \log \frac{(id)_f}{(id)_c}\right\} \quad (6)$$

where the symbol $F_0(X)$ is introduced for convenience to represent the experimentally measurable quantity on the right-hand side of the equation, $\beta n'$ is the concentration stability constant of the nth complex, C_L is the concentration of the complex forming substance and the subscripts f and c refer to the free ion and complexed ion, respectively. Other symbols are those conventionally used in polarography.

The function $F_1(X) = (F_0(X) - \beta_0')/C_L$ is now introduced by DeFord and Hume, where β_0' is the stability constant of the zero complex and is of course, unity. If $F_1(X)$ is plotted against C_L, and is extrapolated to $C_L = 0$, then the value of $F_1(X)$ at the intercept equals β_1'. Likewise, the value β_2' is given by the value $F_2(X)$ at the intercept when the function $F_2(X) = (F_1(X) - \beta_1')/C_L$ is plotted against C_L and is extrapolated to $C_L = 0$. The formation constants of higher complexes (if present) may be determined similarly.

As a consequence of the nature of the $F_n(X)$ functions, a plot of $F_n(X)$ *vs.* C_L for the last complex will be a straight line parallel to the concentration axis, and this allows the determination of the number of complexes.

(*c*) *The Effect of the Noncomplexing Electrolyte on the Polarographic Method for Evaluation of Stability Constants.* Experimentally, the values $(E_{1/2})_f$ and $(id)_f$ are evaluated from the polarogram obtained in the absence of complexing ligand (*i.e.* when the ionic strength is maintained at I solely by added noncomplexing electrolyte). $(E_{1/2})_c$ and $(id)_c$ are evaluated from polarograms obtained when the concentration of ligand is C_L and ionic strength I is maintained by added noncomplexing electrolyte. For instance, if 1:1 electrolytes are used, then concentration of added "noncomplexing" electrolyte will be $(I - C_L)$.

If, however, complexing of the socalled "noncomplexing" electrolyte is considered, then the values $(E_{1/2})_f$ and $(id)_f$ used can be shown to be in error slightly and the true values of these quantities $(E_{1/2})_t$ and $(id)_t$ will be related to the experimentally measured values $(E_{1/2})_f$ and $(id)_f$ by an equation

$$\sum_j \beta j' C_z^j = \text{antilog}\left\{0.434 \frac{nF}{RT} [(E_{1/2})_t - (E_{1/2})_f] + \log \frac{(id)_t}{(id)_f}\right\} \quad (7)$$

where j = jth the complex of noncomplexing ligand,

(2) R. A. Robinson and C. W. Davies, *J. Chem. Soc.*, 574 (1937).

(3) V. S. K. Nair and G. H. Nancollas, *ibid.*, 318 (1957).

(4) R. P. Bell and J. H. B. George, *Trans. Faraday Soc.*, **49**, 619 (1953).

(5) R. O. Nilsson, *Arkiv Kemi*, **10**, 363 (1957).

(6) I. M. Kolthoff and J. J. Lingane, "Polarography," Vol. II, 2nd ed, Interscience, New York, N. Y., 1952, pp 520–521.

(7) D. D. DeFord and D. N. Hume, *J. Amer. Chem. Soc.*, **73**, 5321 (1951).

C_z is the concentration of added "noncomplexing" electrolyte, and $\beta j'$ is the stability complex of the "noncomplexing" ligand. Similarly, when mixtures of complexing ligand and noncomplexing electrolyte are present, measured values of $(E_{1/2})_c$ and $(id)_c$ are slightly in error and values actually being measured will be $(E_{1/2})_{(c1+c2)}$ and $(id)_{(c1+c2)}$, where subscript (c1 + c2) represents a contribution of complexing from ligand L^{y-} at concentration C_L and "noncomplexing electrolyte at concentration C_z.

If the usual case is considered in which the complexing strength of ligand is very much greater than that of the "noncomplexing" electrolyte, then it can be simply shown that calculated values of $F_0(X)$ will essentially be correct as the measured quantity $[(E_{1/2})_f - (E_{1/2})_{(c1+c2)}]$ will be almost the same in magnitude as the correct difference which should be used $[(E_{1/2})_t - (E_{1/2})_c]$ and relative errors will be small. The term log $(id)_f/(id)_c$ is normally very small as $(id)_f$ and $(id)_c$ for a constant concentration of thallium are usually approximately equal and as the term makes little contribution to $F_0(X)$, it is often neglected (*e.g.*, ref 8) so that any effects on this term due to the "noncomplexing" electrolyte need not be considered in consideration on $F_0(X)$ values.

In the case in which the complexing strength of the ligand is not much greater than that of the "noncomplexing" electrolyte, *i.e.*, $(E_{1/2})_f$ and $(E_{1/2})_c$ are similar, then experimentally measured differences between $[(E_{1/2})_f - (E_{1/2})_{(c1+c2)}]$ and the correct value for this term $[(E_{1/2})_t - (E_{1/2})_c]$ will be quite important and large relative errors in calculated values of $F_0(X)$ will be introduced.

If the extreme case is now considered in which the overall stability of the complex whose value is being measured is less than the overall stability of the "non-complexing" electrolyte then the apparent, experimentally measured values of $[(E_{1/2})_f - (E_{1/2})_c]$, could be negative which would give an undefinable value of $F_0(X)$. What needs to be done in this case to calculate a sensible value of $F_0(X)$ is to reverse the definition of the complexing and "noncomplexing" ligand.

For thallium(I) complexes, $\beta n'$ values generally fall in the category of weak to very weak complexes, and even the perchlorate complex is not very much weaker than most other complexes. Many polarographic studies of thallium(I) and other metal–ion complexes have been carried out using sodium or lithium perchlorate as the "noncomplexing" electrolyte to maintain the ionic strength constant; however, consideration to contributions of perchlorate to the $\beta n'$ value obtained, which could be extremely significant have normally been neglected. As the activity coefficients of the perchlorate system are generally unknown,[9] it is difficult to make any quantitative corrections to allow for perchlorate complexing, but alternative media to perchlorate which could be less complexing than perchlorate could be sought.

In the case of thallium(I), as previously mentioned, the nitrate complex is stronger than the perchlorate complex so this rules out the use of nitrate; however, the fluoride complex could well be weaker, so that an improved "noncomplexing medium" to perchlorate in which to evaluate thallium(I) complexes may be fluoride. To test whether in fact fluoride is a weaker complex than perchlorate, $E_{1/2}$ values for the thallium(I) electrode reaction can be measured in various mixtures of perchlorate and fluoride while the ionic strength is maintained at I. Furthermore, $\beta n'$ values for other complexes of thallium(I), such as nitrate and chloride, can be calculated at varying ionic strengths maintained by fluoride. Results from these studies can be compared with those obtained in the literature in which perchlorate has been used to maintain constant ionic strength.

(*d*) *Use of ac and Rapid Polarographic Measurements for Thallium(I) Complexes.* For thallium(I) complexes, which are extremely weak, the shift in half-wave potential $[(E_{1/2})_f - (E_{1/2})_c]$ due to complex formation is extremely small. Hence relative errors in calculating $F_0(X)$ values for weak complexes are very large.[10] Thus, ac polarographic measurements, in which the summit potential (E_s) is used instead of half-wave potential $(E_{1/2})$, and the wave height $(id\sim)$ is used instead of diffusion current (id) were used in place of conventional methods. Results from previous work[10] showed that the reproducibility of the ac method was higher than the dc method, so that more reliable values of $F_0(X)$ and hence $\beta n'$ could be obtained because ac polarographic measurements improve the precision of measurement of shifts in half-wave potential.[10]

Ac measurements have also been used previously in studies of complex ions;[11-15] further advantages of the method over dc measurements are reported in these studies.

The only requisite for use of ac measurements is that the electrode reactions should be reversible. The appearance of an ac wave is not a sufficient criterion for reversibility as was reported quite frequently in the early ac literature, as it has also now been shown to be possible to get ac waves for quasi-

(8) J. Heyrovsky and J. Kuta, "Principles of Polarography," Academic Press, New York, N. Y., 1966, pp 147-154.

(9) J. E. Prue and A. J. Read, *J. Chem. Soc.*, A1812 (1966).

(10) A. M. Bond, *J. Electroanal. Chem.*, **20**, 223 (1969).

(11) S. L. Gupta and M. K. Chatterjee, *J. Electroanal Chem.*, **8**, 245 (1964).

(12) S. L. Gupta, J. N. Jaitly, and R. N. Soni, *J. Indian Chem. Soc.*, **42**, 384 (1965).

(13) S. L. Gupta and M. K. Chatterjee, *Indian J. Chem.*, **4**, 22 (1966).

(14) S. L. Gupta and M. K. Chatterjee, *Rev. Polarog.*, **14**, 198 (1967).

(15) A. M. Bond, *J. Electroanal. Chem.*, **23**, 277 (1969).

reversible[16] and irreversible[17] electrode reactions. The earlier reported advantage made by some workers that it is unnecessary to analyze the ac polarograms for reversibility in studies on complex ions[11] is thus, unfortunately, incorrect, as has been pointed out in a recent review article by Hume.[18] However, for the thallium(I) electrode reaction, ac as well as dc reversibility has been established by several criteria, as mentioned in the experimental section, and ac measurements will be valid.

When ac polarographic measurements are used, eq 6 can be solved as

$$F_0(\mathrm{X}) = \sum_n \beta n' C_L^n = \text{antilog}\left\{0.434\,\frac{nF}{RT}\,[(E_s)_f - (E_s)_c] + \log\frac{(id\sim)_f}{(id\sim)_c}\right\} \quad (8)$$

Experimentally, it has been found that for a constant concentration of thallium(I) $(id\sim)_f$ is approximately equal to $(id\sim)_c$, so that the above expression can be simplified by neglect of the term $\log (id\sim)_f/(id\sim)_c$ to give eq 9, which was used subsequently in some calculations.

$$F_0(\mathrm{X}) = \sum_n \beta n' C_L^n = \text{antilog}\ 0.434\,\frac{nF}{RT}\,[(E_s)_f - (E_s)_c] \quad (9)$$

Rapid polarographpic ac and dc techniques, using short controlled drop times of 0.16 sec and fast scan rates of potential of 0.5 V/min, were also used in this work. This allowed a considerable time saving in recording of polarograms, compared with the conventional polarographic technique using longer drop time and slower scan rates. Furthermore, maxima which were found to be present with conventional dc polarography for the thallium(I) chloride complex system were not observed under conditions of rapid polarography. The uses and advantages of rapid polarographic techniques in studies of complex ions have been investigated recently,[15] and as the thallium(I) electrode reaction was found to be reversible under rapid polarographic conditions, as well as with conventional polarographic conditions, thallium(I) complexes were conveniently and easily evaluated from measurements using the rapid technique.

Table I: Analysis of $F_n(\mathrm{X})$ Functions for Thallium(I)-Perchlorate System. $I = 1.0$, $\beta_1' = 0.32 \pm 0.04$

$[NaClO_4]$	[NaF]	$-E_s$ vs. Ag/AgCl, V	$id\sim$ μA	$F_0(X)$	$F_1(X)$
0.00	1.00	0.4220	0.238	1.00	...
0.20	0.80	0.4239	0.239	1.071	0.36
0.40	0.60	0.4252	0.242	1.112	0.28
0.60	0.40	0.4274	0.246	1.190	0.32
1.00	0.00	0.4298	0.249	1.289	0.29

(*e*) *The Thallium(I)-Fluoride–Perchlorate System.* Table I shows the values of E_s and $id\sim$ obtained for various mixtures of NaF–$NaClO_4$ at an ionic strength of 1.0. These results indicate that the fluoride complex of thallium(I) is in fact weaker than the perchlorate complex (*i.e.*, $\beta n'$ perchlorate < $\beta n'$ fluoride at ionic strength 1.0). However, the shift in E_s in going from an ionic environment of completely fluoride medium to completely prechlorate medium is only 8 mV. This rather small change for a complete change in ionic environment could well be due to factors other than complex formation. For instance, junction potentials and activity coefficients, which are assumed to be constant for all measurements, could alter slightly with change in ionic environment.[9,19] Unfortunately, the limit of solubility of NaF prevents concentrations greater than 1 *M* in sodium fluoride being used to determine if larger shifts in E_s occur at higher fluoride concentrations. Mixtures of KF–$KClO_4$, LiF–$LiClO_4$, and NH_4F–NH_4ClO_4, which could possibly have been used as alternatives to NaF–$NaClO_4$ mixtures to provide higher fluoride concentrations, were not usable because of insolubility of $KClO_4$, LiF, and NH_4ClO_4.

Ideally, to confirm whether the fluoride complex is weaker than the perchlorate complex, it would have been desirable to conduct an experiment in which E_s in say 4 *M* fluoride could have been compared to E_s in 3 *M* fluoride–1 *M* perchlorate, and 2 *M* fluoride–2 *M* perchlorate. In such an experiment, high concentrations of perchlorate could have been added without altering the ionic environment as drastically as in going from 1 *M* fluoride–0 *M* perchlorate to 0 *M* fluoride–1 *M* perchlorate. In view of solubility problems, this was not possible and the best mixture that could be obtained was a comparison of E_s in 4 *M* $NaClO_4$ and E_s in 3 *M* $NaClO_4$–1 *M* NaF. At the ionic strength of 4.0, however, $\beta n'$ values of both species would be so small that changes in E_s due to complex formation would only be expected to be of the order of experimental error of measurement of E_s, so that results are not particularly meaningful. Results of this experiment, which showed a difference in E_s of 3 mV, were, however, at least again consistent with fluoride complexes being weaker than perchlorate at an ionic strength of 4.0.

The polarographic results, therefore, in agreement with the potentiometric results of Nilsson,[5] suggest that fluoride forms less stable complexes than perchlorate at ionic strengths greater than 1, although

(16) D. E. Smith, in "Electroanalytical Chemistry," Vol. I, A. J. Bard, Ed., Marcel Dekker, Inc., 1966, Chapter I.

(17) D. E. Smith and T. G. McCord, *Anal. Chem.*, **40**, 474 (1968).

(18) D. N. Hume, *Anal. Chem.*, **38**, 261R (1966).

(19) R. A. Robinson and R. H. Stokes, "Electrolyte Solutions," 2nd ed, Butterworth and Co., Ltd., London, 1959, Chapter 15.

this point has still to be proved conclusively. The polarographic results, however, do certainly indicate that fluoride formed complexes must be weaker than can be detected polarographically. If any further information on fluoride complexation is to be obtained then a different technique of polarography must be used.

To verify that the fluoride complexing of thallium(I) is extremely small and to assess its order of magnitude a series of experiments were carried out with an ion-selective fluoride electrode.

The potential of an ion-selective fluoride in solution is directly related to the activity of the free uncomplexed fluoride ion present according to an equation

$$E = E_c - \frac{RT}{F} \ln a_{F^-}$$

where E is the electrode potential corresponding to fluoride activity a_{F^-} and E_c is a constant.

Alternatively, the fluoride electrode can be used to measure the concentration of free fluoride ion using an equation of the form

$$E = E_c' - \frac{RT}{F} \ln [F^-]$$

which applies for measurements made at constant ionic strength or at low ionic strengths where activities and concentrations are very nearly equal. In this equation E_c' is a new constant different from, but related to, E_c.

To test for thallium complexing of fluoride, the potential of the fluoride electrode *vs.* sce was measured for each of the solutions: (a) 1 M $NaClO_4$ + 5 × 10^{-5} M NaF; (b) 1 M $NaNO_3$ + 5 × 10^{-5} M NaF; (c) 0.1 M $NaClO_4$ + 5 × 10^{-5} M NaF; (d) 0.1 M $NaNO_3$ + 5 × 10^{-5} M NaF; and (e) distilled water + 5 × 10^{-5} M NaF.

Thallium(I) was then added to solution (a) up to a concentration of 0.1 M keeping the ionic strength constant. With this two thousand-fold excess of thallium(I), no change in potential of the electrode was observed. This means that within the limits of experimental error (±1 mV), no change in the activity or concentration of free fluoride ion has occurred and that no detectable thallium(I) fluoride complex formation exists. In this experiment, as distinct from the polarographic work, the ionic environment remains essentially unaltered for all measurements and the junction potentials and activity coefficients would certainly be expected to be constant.

The above experiment with the fluoride electrode in 1.0 M $NaClO_4$ and 5 × 10^{-5} M NaF was repeated with addition of zinc(II), cadmium(II), magnesium(II), and silver(I) instead of thallium(I). These four metal ions are all known to form weak complexes with fluoride ion[1] and addition of these to the solution altered the potential of the fluoride electrode in a manner consistent with the lowering of free fluoride concentration due to complex formation.

Addition of vast excesses of thallium(I) to solutions (b), (c), (d), and (e) also left unaltered the potential of the fluoride ion electrode and these results prove conclusively that the fluoride complexes of thallium(I), if they exist, must be extremely weak.

It can be shown quite simply that under conditions in which the metal ion concentration is in a vast excess over the concentration of fluoride ion that β_1' is given by an expression

$$\beta_1' = \frac{(C_{TF^-} - C_{F^-})}{(C_{F^-})} \frac{1}{C_{TM}}$$

where C_{TF^-} and C_{TM} are the analytical or total fluoride and metal ion concentrations, respectively, and C_{F^-} is the concentration of free or uncomplexed fluoride ion.

For the fluoride ion electrode, when a change in potential ΔE occurs on addition of a large excess of metal ion to the solution containing fluoride then ΔE is related to β_1' by an expression

$$\beta_1' = \left\{\text{antilog} \frac{\Delta EF}{2.303RT} - 1\right\} \frac{1}{C_{TM}}$$

In this work with thallium(I), C_{TM} was 0.1 M and the smallest ΔE that could have been detected would have been 1 mV so that β_1' must be less than {antilog 0.0167 − 1}10 (*i.e.*, less than about 0.4). Thus it can be concluded that the complex TlF must have a stability constant of a very low value and certainly less than 0.4.

Therefore it has been shown clearly that thallium(I) fluoride complexes if they exist must be extremely weak. Furthermore, potentiometric[5] and polarographic results indicate that at an ionic strength of 1.0, β_1'(fluoride) is probably less than β_1'(perchlorate). Thus fluoride could be better than but certainly should be at least as good as perchlorate in the role of a "noncomplexing" supporting electrolyte in which to study thallium(I) complexes.

Assuming that the fluoride complexing of thallium(I) is in fact less than that of perchlorate, then the thallium(I)–perchlorate complex system can be evaluated polarographically by the DeFord–Hume method.

Table I shows that a value of $\beta_1' = 0.32 \pm 0.04$ for the complex $TlClO_4$ is obtained by analysis of $F_n(X)$ functions, if fluoride complexing is neglected and shifts in E_s are attributed to perchlorate complexing only.

(*f*) *The Thallium(I)–Fluoride–Nitrate System.* Tables II and III show that analysis of $F_n(X)$ functions obtained in KNO_3–KF media give values of $\beta_1' = 0.65 \pm 0.05$ and $\beta_1' = 0.37 \pm 0.04$ for the $TlNO_3$ complex at ionic strengths of 1.0 and 4.0, respectively. These results indicate conclusively that the fluoride

Table II: Analysis of $F_n(X)$ Functions for Thallium(I)–Nitrate System. $I = 1.0$, $\beta_1' = 0.62 \pm 0.05$

[KNO_3]	[KF]	$-E_s$ vs. Ag/AgCl V	id~ μA	$F_0(X)$	$F_1(X)$
0.00	1.00	0.4233	0.234	1.000	...
0.20	0.80	0.4280	0.252	1.112	0.56
0.40	0.60	0.4318	0.258	1.256	0.64
0.60	0.40	0.4348	0.259	1.402	0.67
1.00	0.00	0.4380	0.262	1.565	0.57

Table III: Analysis of $F_n(X)$ Functions for Thallium(I)–Nitrate System. $I = 4.0$, $\beta_1' = 0.37 \pm 0.04$

[KNO_3]	[KF]	$-E_s$ vs. Ag/AgCl, V	id~ μA	$F_0(X)$	$F_1(X)$
0.00	4.00	0.4349	0.212	1.000	...
0.50	3.50	0.4400	0.215	1.199	0.40
1.00	3.00	0.4432	0.219	1.330	0.33
2.00	2.00	0.4504	0.220	1.745	0.37
3.00	1.00	0.4569	0.220	2.239	0.41

Table IV: Analysis of $F_n(X)$ Functions for Thallium(I)–Chloride System. $I = 1.0$, $\beta_1' = 2.1 \pm 0.1$

[KCl]	[KF]	$-E_s$ vs. Ag/AgCl, V	id~ μA	$F_0(X)$	$F_1(X)$
0.00	1.00	0.4233	0.234	1.000	...
0.25	0.75	0.4350	0.242	1.514	2.06
0.50	0.50	0.4433	0.252	1.998	2.00
0.75	0.25	0.4500	0.250	2.603	2.14
1.00	0.00	0.4555	0.250	3.214	2.21

Table V: Analysis of $F_n(X)$ Functions for Thallium(I)–Chloride System. $I = 4.0$, $\beta_1' = 1.00 \pm 0.02$, $\beta_2' = 0.36 \pm 0.05$

[KCl]	[KF]	$-E_s$ vs. Ag/AgCl, V	id~ μA	$F_0(X)$	$F_1(X)$	$F_2(X)$
0.00	4.00	0.4349	0.212	1.000	...	...
0.50	3.50	0.4482	0.222	1.590	1.180	0.36
1.00	3.00	0.4585	0.228	2.291	1.291	0.29
2.00	2.00	0.4772	0.232	4.618	1.809	0.40
3.00	1.00	0.4892	0.234	7.254	2.085	0.36
4.00	0.00	0.5000	0.238	10.76	2.440	0.36

complex of thallium(I) is considerably weaker than the nitrate complex. The literature values of $\beta_1 = 1.8$–2.8[20] are difficult to compare with the β_1' values obtained in this work, as no readily obtainable values of activity coefficients are available to convert β_1' values to β_1. However, the order of magnitude observed in which β_1 ($I = 0$) $> \beta_1'$ ($I = 1.0$) $> \beta_1'$ ($I = 4.0$) is at least the anticipated result.

(g) *The Thallium(I)–Fluoride–Chloride System.* Table IV shows that analysis of $F_n(X)$ functions obtained in KCl–KF media gives a value of $\beta_1' = 2.1 \pm 0.1$ for the complex TlCl at an ionic strength of 1.0. Table V and the graphical method of evaluation of $F_n(X)$, as presented in Figure 1, give values of $\beta_1' = 1.00$ and $\beta_2' = 0.36$ for the complexes TlCl and $TlCl_2^-$, respectively, at an ionic strength of 4.0. The percentage distribution of the various species present in the thallium(I)–chloride complex ion system shown in Figure 2 indicates that very little $TlCl_2^-$ is present at chloride concentrations up to 1 *M*, so that it is not surprising that at an ionic strength of 1.0, in which the maximum ligand chloride ion concentration is 1.0 *M*, no $TlCl_2^-$ is detected. Other studies at an ionic strength of 4.0 maintained by sodium perchlorate or lithium perchlorate,[5,21] have similarly indicated two chloride complexes of thallium(I). However, polarographic studies maintaining the ionic strength at 1.0 and 2.0 with sodium perchlorate,[22,23] reported only TlCl. Consequently, it can be seen that good agreement is obtained for results as to the number of complexes of thallium maintaining ionic strength constant by either perchlorate or fluoride media. Literature values given for $\beta n'$ vary over quite a wide range,[24] so that comparison of results using perchlorate and fluoride as the noncomplexing media is rather difficult. However, results do indicate both fluoride and perchlorate complexes of thallium(I) are

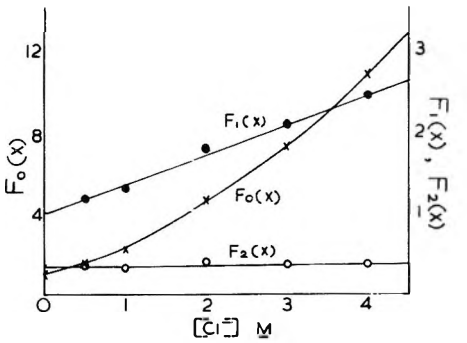

Figure 1. Graphical method of analysis of $F_n(X)$ functions for the thallium(I)–chloride system. $I = 4.0$, $T = 30°$.

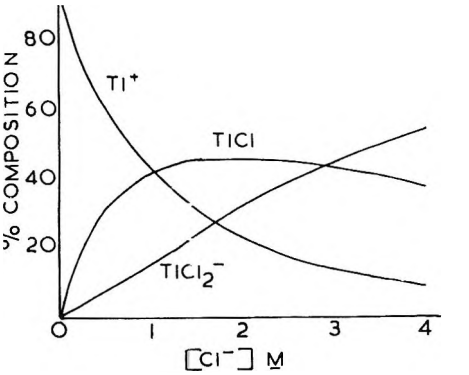

Figure 2. Distribution of the various species present in the thallium(I)–chloride system. $I = 4.0$, $T = 30°$.

(20) Same as ref 1, p 174.

(21) F. Ya. Kul'ba, V. E. Mironov, and V. A. Fedorov, *Zh. Neorg. Khim.*, 6, 1586 (1961).

(22) C. J. Nyman, D. K. Roe, and R. A. Plane, *J. Amer. Chem. Soc.* 83, 323 (1961).

(23) D. Banerjea and I. P. Singh, *J. Indian Chem. Soc.*, 39, 353 (1962).

(24) Same as ref 1, pp 294–296.

extremely weak and that fluoride is most satisfactory as an alternative "noncomplexing" medium to the commonly used perchlorate. β_1 values in the literature vary over the range 3–5,[24] so that it can be seen again that the expected result of $\beta_1(I=0) > \beta_1'(I = 1.0) > \beta_1'(I = 4.0)$ is obtained for chloride complexes of thallium(I).

Summary of Polarographic Results

Polarographic results have indicated that the fluoride complex of thallium(I) could be weaker than the perchlorate complex. Consequently, fluoride electrolytes should be better than or at least as good as perchlorate as a "noncomplexing" electrolyte in studies on concentration stability constants of thallium(I) complexes. The use of fluoride as a noncomplexing" medium to maintain constant ionic strength at 1.0 in polarographic studies has given values of $\beta_1' = 0.32$, 0.65, and 2.1 for the complexes $TlClO_4$, $TlNO_3$, and TlCl, respectively. At an ionic strength of 4.0, values of $\beta_1' = 0.37$ and 1.00 and $\beta_2' = 0.36$ for the complexes $TlNO_3$, TlCl and $TlCl_2^-$, respectively, were obtained.

Basicity Constants of Cyclopolymethylenetetrazoles in Formic Acid Solutions

by Ronald H. Erlich and Alexander I. Popov

Department of Chemistry, Michigan State University, East Lansing, Michigan 48823 *(Received July 31, 1969)*

Electrical conductance measurements have been carried out on six cyclopolymethylenetetrazoles varying from trimethylenetetrazole to undecamethylenetetrazole as well as on 6,6′-dichloro- and 6,6′-dibromopentamethylenetetrazoles in formic acid solutions at 25°. Basicity constants defined by the reaction $Tz + HCOOH \rightleftarrows TzH^+ + HCOO^-$ as well as limiting equivalent conductances have been calculated by the Fuoss–Shedlovsky method from the conductance data. It is shown that while the above tetrazoles do not have any detectable proton affinity in aqueous solutions the unsubstituted cyclopolymethylenetetrazoles act as fairly strong monoprotic bases in formic acid solutions. The length of the hydrocarbon chain does not influence the basic strength of the tetrazole ring, but the inductive effect of the halogens essentially divests the ring of its proton affinity.

Previous studies on cyclopolymethylenetetrazoles have shown that these compounds can form fairly stable

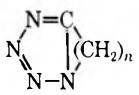

complexes with transition metal ions[1-3] and with halogens.[4] The compounds act as unidentate ligands. It is interesting to note, however, that qualitative studies in aqueous solutions indicate essentially complete absence of proton affinity[1-5] although a claim has been made[5] for the preparation of a solid complex $PMT \cdot H_2SO_4$ (PMT = pentamethylenetetrazole). It has also been shown that the tetrazole ring can be protonated in a strongly protogenic solvent such as formic acid and the pK_b value for PMT has been determined in this solvent both by potentiometric[6] and by conductometric measurements.[7] It should be noted that for the study of very weak bases formic acid is a much better solvent than acetic acid since not only does the former have a greater acidic strength, but also, owing to its high dielectric constant of 56.1, the formation of ion pairs is minimized.

Recently a number of new polymethylenetetrazoles have been synthesized[8] with n varying from 3 to 11, as well as two halogenated derivatives of PMT, namely, 6,6′dichloro- and 6,6′-dibromopentamethylenetetrazoles.[9] It was of interest to us to see if the variation in the length of the hydrocarbon chain or the halogen substitution had any influence on the proton affinity of the tetrazoles.

(1) A. I. Popov and R. D. Holm, *J. Amer. Chem. Soc.*, **81**, 3250 (1959).

(2) F. M. D'Itri and A. I. Popov, *Inorg. Chem.*, **5**, 1670 (1966); **6**, 597, 1591 (1967).

(3) D. M. Bowers and A. I. Popov, *ibid.*, **7**, 1594 (1968).

(4) A. I. Popov, C. C. Bisi, and M. Craft, *J. Amer. Chem. Soc.*, **80**, 6513 (1958).

(5) A. Dister, *J. Pharm. Belg.*, **3**, 190 (1948).

(6) A. I. Popov and J. C. Marshall, *J. Inorg. Nucl. Chem.*, **19**, 340 (1961).

(7) T. C. Wehman and A. I. Popov, *J. Phys. Chem.*, **72**, 4031 (1968).

(8) F. M. D'Itri and A. I. Popov, *J. Amer. Chem. Soc.*, **90**, 6476 (1968).

(9) F. M. D'Itri, Ph.D. Thesis, Michigan State University, 1968.

Table I: Conductances of Some Cyclopolymethylenetetrazoles in Formic Acid at 25°

C_3MT		C_4MT		C_5MT	
10^3C	Λ	10^3C	Λ	10^3C	Λ
4.852	31.57[a]	6.825	42.32[a]	3.628	39.19[a]
10.26	28.29	10.59	39.94	8.398	36.91
16.91	25.09	12.34	38.86	14.05	33.39
22.40	23.15	18.34	35.76	18.98	31.00
26.91	21.89	21.39	34.40	23.08	29.37
31.58	20.78	25.19	32.96	27.44	27.91
6.26	30.72[b]	29.56	31.50	31.14	26.84
10.63	28.25	33.69	30.34	33.86	26.16
15.95	25.41	39.75	28.84	38.01	25.21
21.43	23.36	47.97	27.16	43.23	24.15
25.28	22.22	6.209	42.55[b]	48.12	23.27
30.12	20.99	10.18	40.04	4.235	37.83[b]
		14.46	37.49	8.295	35.48
		20.00	34.78	11.45	33.54
		23.71	33.24	15.73	31.32
		26.58	32.23	20.50	29.24
		31.04	30.81	23.24	28.23
		42.62	27.91	27.53	26.87
		51.09	26.27	30.32	26.10
				33.50	25.27
				36.50	24.58
				41.64	23.53

C_6MT		C_7MT		$C_{11}MT$	
10^3C	Λ	10^3C	Λ	10^3C	Λ
2.790	34.06[a]	2.732	32.58[a]	5.233	29.71[a]
5.299	33.98	6.064	32.92	7.794	28.21
8.532	31.92	9.457	30.54	11.35	26.13
12.37	29.58	12.77	28.72	13.82	24.88
15.07	28.18	18.37	26.27	16.54	23.70
17.13	27.26	22.23	24.88	20.26	22.34
19.65	26.21	26.04	23.70	22.00	21.77
21.56	25.50	31.57	22.32	24.48	21.04
24.11	24.66	35.02	21.58	27.02	20.36
26.33	23.99	46.15	19.62	29.82	19.69
29.84	23.03	2.790	34.59[b]	36.42	18.34
3.3019	34.65[b]	6.274	33.92	2.896	29.80[b]
7.165	32.89	9.737	31.62	4.875	29.69
10.78	30.53	13.62	29.35	6.872	28.56
14.30	28.57	16.94	27.73	9.043	27.30
18.16	26.79	22.29	25.64	11.88	25.72
21.08	25.67	25.11	24.69	14.07	24.65
24.32	24.56	29.32	23.49	15.67	23.96
27.12	23.76	33.44	22.46	17.77	23.11
31.03	22.70	43.55	20.47	19.96	22.33
33.25	22.17			21.42	21.84
38.87	20.99			28.17	19.97

6,6′-Dichloro-C_5MT		6,6′-Dibromo-C_5MT	
10^3C	Λ	10^3C	Λ
2.776	0.05446	2.657	0.09847
7.888	0.05144	5.308	0.1254
13.18	0.05418	8.573	0.1330
18.07	0.06252	11.65	0.1359
24.08	0.06774	14.34	0.1438
32.00	0.07507	17.83	0.1477
38.47	0.08066	20.03	0.1488
47.14	0.08378		

[a] First run. [b] Second run.

Experimental Section

The solvent (B & A 98–100% formic acid) was allowed to stand 48 hr over anhydrous copper sulfate. It was then slowly vacuum distilled through a 1-m Vigreux column at about 20 mm pressure. The retained middle fraction was placed in a 6-l. separatory funnel under nitrogen atmosphere and subjected to at least four fractional freezings. The pure formic acid obtained in this manner had a freezing point of about 8.5°. It was stored frozen until ready for use. The specific conductance of this product was 1×10^{-5} ohm^{-1} cm^{-1}, slightly better than the best literature value.[7]

The cyclopolymethylenetetrazoles were all prepared by the methods of D'Itri.[8,9] To remove any possible conducting impurities such as the azide ion, etc., the tetrazoles were dissolved in a minimum amount of 50:50 water–ethanol solution to which was then added 5 ml of concentrated sulfuric acid and enough 0.3 *M* $KMnO_4$ to completely oxidize the azide as evidenced by the permanent purple color of the excess permanganate. The tetrazoles were extracted into chloroform, evaporated to dryness, and recrystallized several times from the recommended solvent mixtures.[9] Since tri- and tetramethylenetetrazole have reasonably high vapor pressure, they were further purified by sublimation under vacuum. Although pentamethylenetetrazole will sublime, it yielded a gray product indicating that some decomposition had taken place; therefore, only recrystallization from ether was used to purify the latter. The remainder of the cyclopolymethylenetetrazoles do not have sufficiently high vapor pressure to allow vacuum sublimation even at temperatures near their melting points.

An attempt was also made to measure the basicity constants for 6,6′-dichloro- and 6,6′-dibromopentamethylenetetrazole. These tetrazoles were obtained from Dr. D'Itri of this laboratory and used without further purification.

The apparatus and procedures used in this investigation have been described previously.[7]

In general, the upper limit of concentration was determined by the Fuoss equation, $C_{max} = 3.2 \times 10^{-7}D^3$, where D is the dielectric constant of the solvent, since at high concentrations, the laws of dilute solutions may no longer apply.[10] Even for most dilute solutions the specific conductance of the solvent was less than 5% of the specific conductance of the solutions.

Results and Discussion

Proton affinity of PMT in aqueous solutions was tested by the following two methods. Distilled water was purged with purified nitrogen until the pH of the solution was 7.00. Enough solid PMT was added to make the solution 0.1 *M* in this solute. No change in

(10) R. M. Fuoss, *J. Amer. Chem. Soc.*, 57, 2604 (1935).

Table II: Basicity Constants and Limiting Equivalent Conductances at 25°

Tetrazole	Run 1		Run 2	
	pK_b	Λ_0	pK_b	Λ_0
C_3MT	1.79 ± 0.03[a]	41.70 ± 1.17[a]	1.86 ± 0.03	43.32 ± 1.23
C_4MT	1.74 ± 0.03	57.33 ± 1.10	1.76 ± 0.03	57.58 ± 1.53
C_5MT	1.88 ± 0.01	55.05 ± 1.06	1.84 ± 0.01	51.87 ± 0.92
C_6MT	1.82 ± 0.02	45.91 ± 0.98	1.94 ± 0.03	48.96 ± 1.03
C_7MT	1.87 ± 0.02	46.23 ± 0.98	1.76 ± 0.05	44.52 ± 1.96
$C_{11}MT$	1.91 ± 0.03	41.86 ± 1.04	1.83 ± 0.03	40.07 ± 0.93

[a] Standard deviations.

pH was observed. Likewise PMT was added to a dilute solution of acetic acid at pH of 5.00, and again there was no change in the acidity of the solution.

Conductance data were obtained for eight cyclopolymethylenetetrazoles in anhydrous formic acid. These data were analyzed by the methods of Fuoss and Shedlovsky[11] using a FORTRAN program run on a CDC 3600 computer. The values of equivalent conductance *vs.* concentration are shown in Table I while the values of pK_b where K_b is the equilibrium constant for the reaction

$$Tz + HCOOH \rightleftarrows TzH^+ + HCOO^-;$$

$$K_b = \frac{(TzH^+)(HCOO^-)}{(Tz)}$$

and the values of the equivalent conductance at infinite dilution are shown in Table II along with the standard deviations for these data. It should be noted that the tetrazoles act as monoprotic bases.

The unsubstituted cyclopolymethylenetetrazoles in formic acid solutions behaved as fairly strong electrolytes. The basicity constants shown in Table II do not vary appreciably with length of the hydrocarbon chain. On the other hand, halogen substitution drastically decreases the basic strength of the cyclopolymethylenetetrazoles to such extent that it becomes impossible to measure their basicity constant even in formic acid solutions. In fact, it is seen from Table I that at a given concentration the molar conductance of the dihalo derivatives is nearly three orders of magnitude lower than the conductance of the unsubstituted cyclopolymethylenetetrazoles. Comparison of the conductances of the chloro and the bromo derivatives also indicates the greater electron-withdrawing effect of the former halogens.

Acknowledgment. This work was supported by Research Grant MH-07825 from the Institute of Mental Health. R. H. E. gratefully acknowledges a predoctoral fellowship from the U. S. Public Health Service.

(11) R. M. Fuoss and T. Shedlovsky, *J. Amer. Chem. Soc.*, **71**, 1496 (1949).

Osmotic Coefficients of Aqueous Sodium Chloride Solutions from 125 to 130°[1a]

by Chia-tsun Liu and W. T. Lindsay, Jr.[1b]

Westinghouse Research Laboratories, Pittsburgh, Pennsylvania 15235 *(Received June 30, 1969)*

Osmotic coefficients have been determined by vapor pressure lowering measurements on aqueous sodium chloride solutions of 0.1, 0.25, 0.5, and 1.0 *m* concentrations at 25° intervals from 125 to 300°. Apparatus and methods are described. The results of this work extend high-temperature osmotic coefficient data to concentrations on the dilute side of the osmotic coefficient minimum. They are consistent with limiting slopes and with concentration and temperature trends established by other data at higher concentrations and/or lower temperatures. High-temperature osmotic coefficient data now seem adequate for calculation of excess thermodynamic quantities for both water and salt up to 300°.

Introduction

There have been very few investigations of aqueous electrolyte solutions at high temperatures that have yielded results of good precision. Accurate and precise data are needed to determine how structural and other temperature-sensitive changes in water affect solution properties. Sodium chloride solutions have perhaps been studied more extensively than any other system at temperatures over 100°, yet little useful thermodynamic information even on sodium chloride was available until Gardner, Jones, and de Nordwall[2] recently completed a study of osmotic coefficients for the 1–3 *m* concentration range. We report here the results of osmotic coefficient determinations by vapor pressure-lowering measurements in the concentration range of 0.1–1 *m*. The data now seem adequate for calculation of activity coefficients and excess thermodynamic quantities, for salt as well as water, with reasonable assurance up to 300°. It is expected that data extending over such a wide temperature range will provide a new dimension for test and evaluations of the several competing theories for chemical potentials of strong electrolytes in aqueous solutions of moderate concentration. If this expectation is realized, these results may help shed light on the nature of electrolyte solutions at ordinary temperatures in addition to providing useful information about high-temperature solutions.

Experimental Section

The experimental method consisted of measurement of the difference in gas pressures required to balance the vapor pressures of solution and pure water in two separate pressure cells held at identical temperatures in an oil bath. Although simple in principle, the method is complicated at high temperatures by the high vapor pressures and the aggressive attack of water and solutions on materials. The unique features of apparatus and techniques that were developed for this work are described briefly in the following parts of this section. More detail is given elsewhere.[3]

Vapor Pressure Cells. As shown in Figure 1, the vapor pressure cells consist of two main parts: a lower body, made of Inconel Alloy 600 and fitted with a platinum cup to contain the solution, and a pressure-sensing head made of AISI Type 304 stainless steel, containing a stainless steel bellows isolating water vapor in the cell. The construction is such that it is impossible for leaking gaskets to allow intermixing of water vapor and pressurizing gas. Bellows position is sensed by a linear variable differential transformer (LVDT) located above the oil bath, with the LVDT magnetic core attached to the top of the bellows by a connecting rod within a pressurized tube. The LVDT coil windings sense movement of the magnetic core and bellows inside the pressure system. The coil windings are supported by an outer, unpressurized tube to avoid pressure effects in position sensing. A hydrogen diffuser is provided to remove gas generated by corrosion reactions between steam and the cell materials.

Temperature Control. A "double thermostating" system was adopted for this work. Two identical cells were installed in a symmetrical manner in a massive aluminum block, as shown in cross-sectional view in Figure 2. This entire assembly was immersed in a vigorously stirred oil bath regulated to ±0.001°.

(1) (a) Presented in part at the 151st National Meeting of the American Chemical Society, Pittsburgh, Pa., March 1966, and at the 153rd National Meeting, Miami Beach, Fla., April 1967; (b) to whom correspondence should be addressed.

(2) E. R. Gardner, P. J. Jones, and H. J. de Nordwall, *Trans. Faraday Soc.*, 59, 1994 (1963).

(3) A detailed description of all features of the apparatus and procedures is given by W. T. Lindsay, Jr., and Chia-tsun Liu in "Vapor Pressure Lowering of Aqueous Solutions at Elevated Temperatures," OSW Research and Development Progress Report No. 347. Available from Superintendent of Documents, U. S. Government Printing Office, Washington, D. C. 20402.

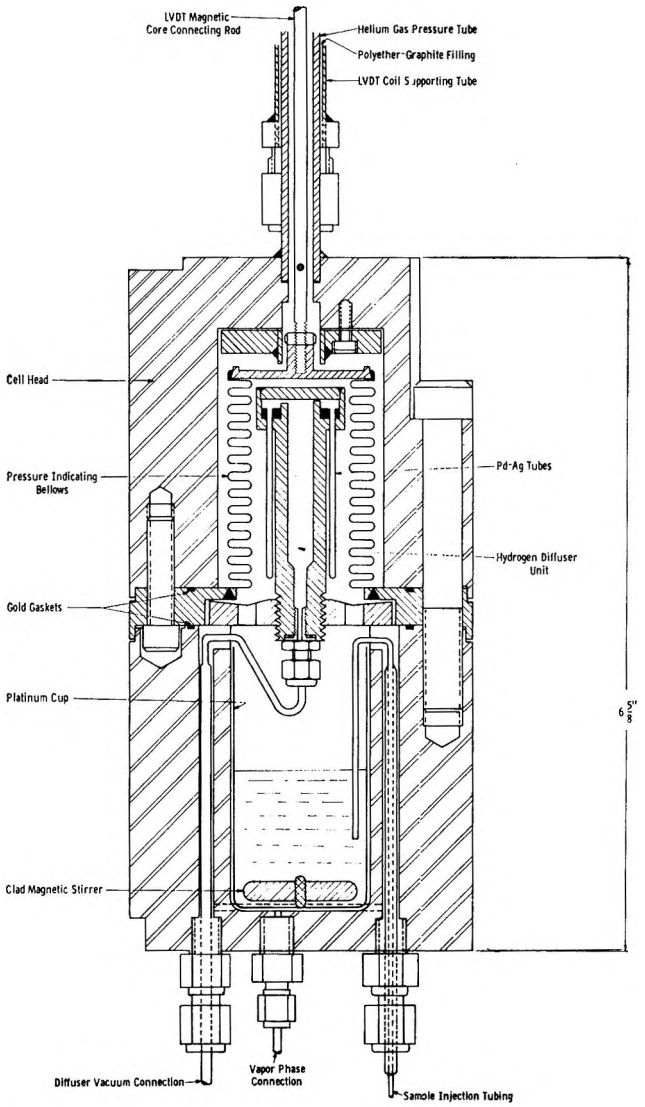

Figure 1. Cross sectional view of vapor pressure cell.

Preliminary experiments with resistance thermometers installed in dummy cells indicated a maximum difference of 0.0004° to be expected between the temperatures of the two cells. Temperatures during the vapor pressure measurements were determined with a Leeds and Northrup Model No. 8163 platinum resistance thermometer calibrated against the laboratory standard thermometer throughout the temperature range of the measurements. It was used with a Leeds and Northrup Model 8067, Type G-2 Mueller bridge, whose calibration was checked against NBS-certified standard resistors. The thermometer was located in a well extending into the bath fluid. Although the measured temperature is of the bath fluid rather than the interior of the cells, the difference between these temperatures cannot be very large after equilibration. Differences between the measured temperature and the actual cell temperatures have a second-order effect on the results if the two cells are at the same temperature.

Differential Pressure Measurement. Vapor pressures were balanced by helium gas pressure applied to the bellows in the two cells. The pressurization system was adapted for automatic control during extended equilibration periods. Fine adjustment of pressure was accomplished manually when measurements were being taken. The bellows–LVDT sensing systems for vapor pressure balance were calibrated for effects of temperature and pressure on shift of null position. The total shift on change of conditions from vacuum at 25° to 1250 psi

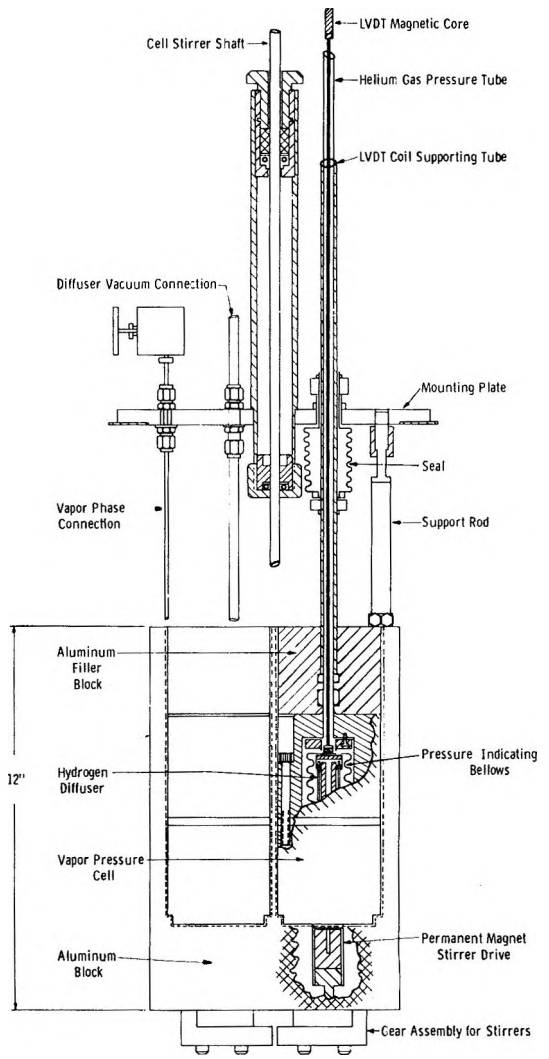

Figure 2. Assembly of vapor pressure cells in aluminum thermostat block.

at 300° was equivalent to about 2 mm pressure difference, which was compensated mechanically by adjustment of the sensing coil position for each temperature of measurement. The precision of pressure balancing was better than ±0.1 mm. Differences in balancing gas pressures were determined for most of the runs by a high-pressure, mercury filled differential manometer, described elsewhere.[4] The manometer has

(4) W. T. Lindsay, Jr., and T. S. Bulischeck, accepted for publication in *Rev. Sci. Instrum.*

a differential pressure measurement capacity up to 2500 mm at total pressures to 3000 psi, with a differential pressure measurement reproducibility of about ±0.1 mm. Differential pressures exceeding the capacity of the manometer were determined by a calibrated Texas Instruments quartz-spiral Bourdon gauge in a pressure capsule.

Preparation of Cells. Experience showed that extreme care was necessary in cleaning the cells to prevent accumulation of noncondensable gases during the measurements. The gases, primarily CH_4 and CO_2, are apparently generated by contact of nonvolatile organic compounds with water and steam and are not eliminated by a simple evaculation and baking of the cells before use. Successful cleaning of the cells was accomplished by the following combination of procedures: (1) initial rinsing and ultrasonic cleaning of all parts with reagent grade acetone and trichloroethylene, followed by steam cleaning at atmospheric pressure for several hours; (2) exposure of the interior of the assembled and sealed cells to steam at 700 to 800 psi and 300° for 2 full days followed by removal of steam and evacuation at this temperature; and (3) a final overnight baking at 150° under vacuum.

Preparation of Solutions. Solutions were prepared immediately before use from dried reagent grade sodium chloride and triply distilled water. Degassed water was withdrawn by syringe from the bottom of a boiling vessel and injected into an evacuated bottle containing a known weight of the salt. Additional degassing was caused to occur by boiling of the contents of the bottle with continued evacuation, followed by mixing and weighing of the remaining contents of the sealed bottle. Thirty-five milliliters of solution was withdrawn from this bottle by syringe and injected into the cooled evacuated solution cell through platinum–iridium alloy capillary tubing. An equal volume of degassed pure water was injected into the evacuated reference cell.

Conduct of Runs. The capillary tubes used for sample injection were crimped off and sealed by gold brazing the ends. The entire assembly as shown in Figure 2 was then placed in the bath and heated first to 125.00°, where the absolute pressures in each cell could be checked by the manometer. When all indications were favorable and conditions were stable, the differential vapor pressure was determined by repeated measurements over a several-hour period. Measurements were made successively at 25° intervals from 125.00 to 300.00° and then again at 125.00° to determine any effects of the operational period at higher temperatures. Equilibration periods before measurements were 16 to 48 hr at the lower temperatures, while 6 to 10 hr was sufficient at the higher temperatures. Figure 3 illustrates the precision of the measurements obtained in a typical run. Mass spectrometric analyses were used to determine the quantity and composition of any noncondensable gases present after the final measurements on each solution. After opening of the cells, the solution and water remaining were checked for changes in volume and such properties as pH, electrical conductivity, and total dissolved solids.

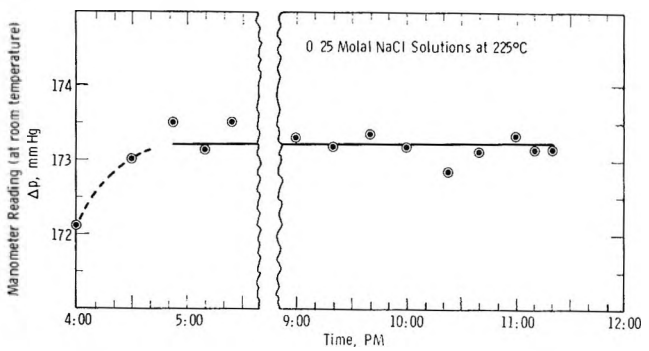

Figure 3. Typical experimental plot of pressure difference measurements illustrating constancy of measurements.

Results

Measurements were made on solutions nominally 0.1, 0.25, 0.5, and 1.0 *m*. The results of runs not showing acceptable constancy or reproducibility of differential pressure measurements or otherwise not meeting acceptance criteria were discarded, and the runs were repeated. Duplicate sets of measurements were obtained at nominally 0.1 *m* and 1.0 *m* to establish reproducibility and to obtain firmer results. The considerable number of differential pressure measurements obtained after equilibration at each temperature (Figure 3 is typical) were averaged, the manometer null difference correction was applied, and the differential pressures were corrected to the density of mercury at 0°. The final corrected difference Δp is the difference between the vapor pressure of pure water p_0 and the vapor pressure of the solution p at the same temperature. Concentrations of solutions at each temperature were calculated from the initial concentration (as determined from the preparation on a weight basis) by using the known volume of the cell, the initial volume of liquid, and the density of steam. Expansion of the liquid solution was approximated by the expansion of pure liquid water.

Table I contains the experimental results. The poorest reproducibility was obtained at the temperatures and concentrations giving the smallest vapor pressure lowering. Consequently, the results at 125° for 0.1 *m* have been discarded, and the values in the table for 0.1 *m* solutions at 150, 175, and 200° are averages of two or three duplicate runs of somewhat poorer reproducibility than the others. These averages should be given a weight equal to the other individual results.

The osmotic coefficients reported in Table I are all applicable to the solution when under a total pressure

Table I: Experimental Results of Vapor Pressure Lowering Measurements for Sodium Chloride Solutions

T, °C	Molality	$\Delta p = p_0 - p$, mm	Osmotic coefficient ϕ at $p = p_0$
125.00	0.2458	14.47	0.9153
	0.5309	30.17	0.8881
	1.0039	58.31	0.9155
150.00	0.1013	12.02	0.8820[a]
	0.2463	29.99	0.9060
	0.5328	62.44	0.8770
	0.9967	118.46	0.8970
	1.0061	118.91	0.8921
175.00	0.1021	23.78	0.8995[b]
	0.2472	56.78	0.8891
	0.5360	117.76	0.8549
	0.9590	211.37	0.8643
	1.0045	221.49	0.8653
200.00	0.1025	42.67	0.8880[a]
	0.2486	100.62	0.8683
	0.5409	213.01	0.8497
	0.9641	377.97	0.8527
	1.0149	399.11	0.8563
	1.0170	397.20	0.8504
225.00	0.1064	72.64	0.8502
	0.2507	172.44	0.8588
	0.5484	353.60	0.8098
	0.9718	636.55	0.8301
	1.0228	672.28	0.8339
	1.0365	679.92	0.8313
250.00	0.1077	120.62	0.8400
	0.2536	277.34	0.8227
	0.5596	587.83	0.7957
	0.9829	1028.65	0.8006
	1.0342	1076.47	0.7971
275.00	0.1095	197.24	0.8298
	0.2580	442.58	0.7947
	0.9988	1615.32	0.7633
	1.0506	1675.18	0.7534
300.00	0.1124	320.52	0.8102
	0.2644	691.95	0.7474
	1.0220	2487.53	0.7128
	1.0743	2568.79	0.7010

[a] Average value of three experimental results. [b] Average value of two experimental results.

equal to the vapor pressure of pure water at each temperature. They were calculated by the expression

$$\phi = \frac{1000}{\nu m M_1 RT}\left[RT \ln \frac{p_0}{p} - \int_p^{p_0} \xi dP - V_1^{\circ}(l)\Delta p\right] \quad (1)$$

In this expression, ϕ is the osmotic coefficient, ν is 2, m is molality, M_1 is the molecular weight of water, R is the gas constant, T is absolute temperature, and p is the vapor pressure of the solution as determined by $p_0 - \Delta p$. The first term in the brackets gives the familiar form of the expression applicable at low vapor pressures, the second term gives the correction for deviation of the vapor from the perfect gas law, and the third term is an adequate approximate correction for isothermal compression of the solution from its own vapor pressure to the vapor pressure of pure water. The analytical

Table II: Contribution of Terms to Calculation of Osmotic Coefficients[a]

	0.25 m NaCl solution			
T, °C	ϕ	= T_1	+ T_2	+ T_3
125	0.91525	0.94187	−0.02536	−0.00126
150	0.90595	0.94944	−0.04097	−0.00252
175	0.88907	0.95597	−0.06229	−0.00460
200	0.86827	0.96694	−0.09074	−0.00793
225	0.85879	1.00237	−0.13030	−0.01328
250	0.82269	1.02209	−0.17843	−0.02097
275	0.79473	1.07339	−0.24561	−0.03304
300	0.74743	1.13339	−0.33459	−0.05137

[a] Headings T_1, T_2, T_3 refer in sequence to the three terms of eq 1. Significant figures are those carried in calculations and do not indicate experimental precision.

expressions given by Smith, Keyes, and Gerry[5] were used for the integrand ξ of the second term in the brackets, for $V_1^0(l)$, the molar volume of pure water at its saturation pressure (an approximation for the partial molar volume of water in the solution), and for calculation of p_0. When each of the terms in the brackets of eq. 1 is multiplied by the common factor, we have the osmotic coefficient as the sum of three terms. Table II shows the relative magnitudes of the three contributing terms for the typical case of 0.25 m solutions. Note that term T_2, the effect of gas imperfection for the vapor, is not negligible at any of the temperatures and becomes very large at 300°. We believe, however, that the properties of pure water vapor are sufficiently well known that uncertainties in the constants used for this correction have a negligible effect on the osmotic coefficients. Note also that the third term T_3, correcting the pressure to p_0, is not insignificant at the higher temperatures. We estimate that the maximum error in osmotic coefficient introduced by use of the molal volume of pure water in this term, rather than the partial molar volume of water in solution, is 0.0002, occurring at 1 m and 300°.

Discussion

The duplicate runs for approximately 1.0 m solutions at temperatures 150, 175, 250, 275, and 300°, and the triplicate runs for this concentration at 200 and 225°, give one measure of the reproducibility of the determinations. Neglecting the effects of the small concentration differences among these solutions of nominally 1.0 m, the average deviations of the osmotic coefficients in Table I range from around ±0.002 at the lower temperatures up to ±0.005 at 275° and ±0.006 at 300°. This degree of reproducibility is consistent with the sources of random error in the measurements

(5) L. B. Smith, F. G. Keyes, and H. T. Gerry, *Proc. Am. Acad. Arts Sci.*, **69**, 137 (1934). See also J. H. Keenan and F. G. Keyes, "Thermodynamic Properties of Steam," John Wiley & Sons, Inc., New York, N. Y., 1936.

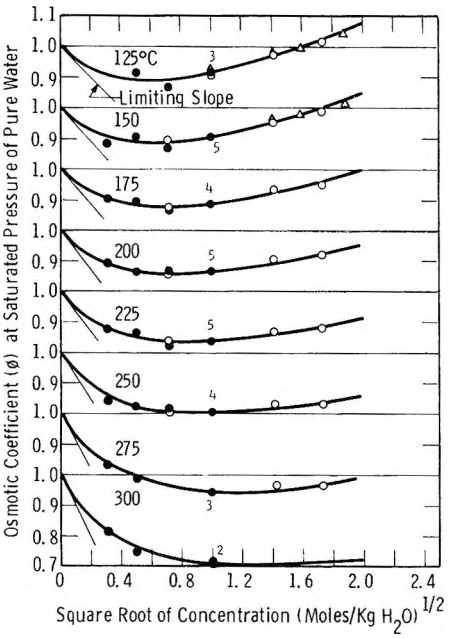

Figure 4. Concentration dependence of high-temperature osmotic coefficients for sodium chloride solutions. Filled circles, this work; open circles, Gardner, *et al.*,[2,6] triangles, Fabuss and Korosi.[7] Numbers indicate multiple points.

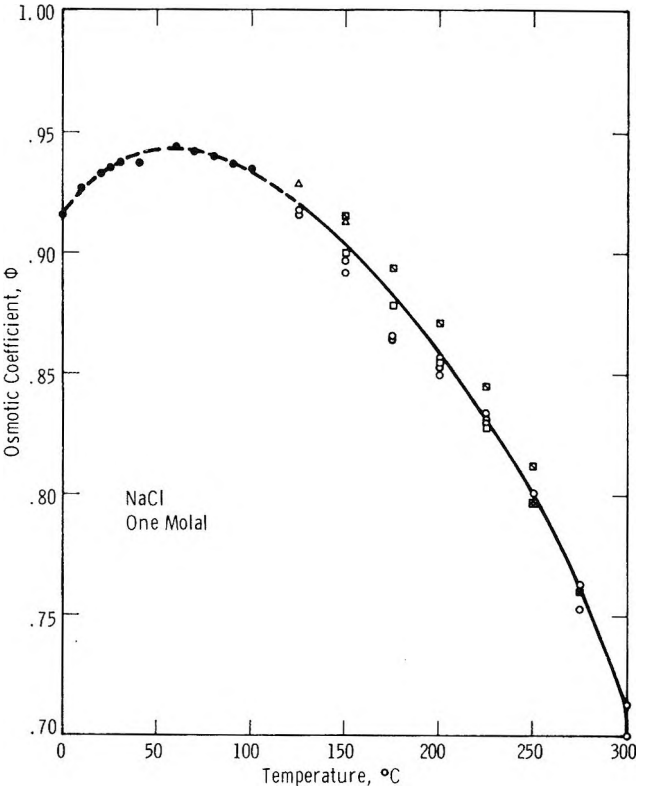

Figure 5. Temperature dependence of osmotic coefficients for 1 *m* sodium chloride. Open circles, this work; open squares, Gardner, *et al.*[2] filled square, Gardner, *et al.*[2], extrapolated to 275°; squares with diagonal, Gardner[6]; triangles, Fabuss and Korosi[7]; filled circles, low-temperature data tabulated in standard texts.[8]

and is perhaps as good as can be expected, considering the experimental difficulties.

Figure 4 shows the results of Table I compared with all other known osmotic coefficient data at high temperatures on plots of osmotic coefficient *vs.* square root of concentration. The data for the Harwell group shown on this plot include both the first published report[2] and more recent results.[6] We have extended extrapolation of the Harwell data to 275° for more direct comparison with our results at that temperature. The osmotic coefficients attributed to Fabuss and Korosi[7] were calculated by us from their reported p/p_0 data. Examination of Figure 4 shows that the osmotic coefficient data from the several sources correlate reasonably well with concentration and with the indicated Debye–Hückel limiting slopes at each temperature. At 1 *m* there is a multiplicity of data which cannot be shown as separate points on a plot of this scale.

The concentration dependence below 1 *m* is now fairly well established for sodium chloride solutions at high temperatures, since our results extend to solutions on the dilute side of the osmotic coefficient minimum. Correlation of the data by relations reducing to the Debye–Hückel limiting slope at high dilution should therefore be sufficiently accurate to allow calculation of activity coefficients and excess thermodynamic quantities for the salt by integration of the Gibbs–Duhem equation.

Figure 4 shows that the principal effect of increasing temperature is a progressive decline in osmotic coefficients for moderately concentrated solutions and a decreasing importance of concentration-dependent effects tending to raise the osmotic coefficients at higher concentrations. Figure 5 shows the temperature dependence for osmotic coefficients at 1 *m* on a larger scale plot. Here it is seen that the high-temperature data are in good accordance with the temperature-dependent trend established by earlier measurements[8] at lower temperatures. Comparison may also be made on a plot of this scale among the high-temperature results from the various investigating groups. The solid line on Figure 5 and the solid lines on Figure 4 represent a correlation equation of the extended Debye–Hückel type with temperature-dependent parameters determined by fitting the high-temperature data from 125 to 300° at all concentrations.

Although the effect of temperature on osmotic coefficients above 100° is superficially in accord with a decreasing extent of hydration and/or an increasing degree of association of the salt ions, we believe these

(6) E. R. Gardner, *Trans. Faraday Soc.*, **65**, 91 (1969). We are grateful to Dr. Gardner for making some of his results available to us before publication.

(7) B. M. Fabuss and A. Korosi, *Desalination*, **1**, 139 (1966).

(8) H. S. Harned and B. B. Owen, "The Physical Chemistry of Electrolytic Solutions," 3rd ed, Reinhold Publishing Company, Inc., New York, N. Y., 1958. R. A. Robinson and R. H. Stokes, "Electrolyte Solutions," 2nd ed, Academic Press, Inc., New York, N. Y., 1959.

possibilities must be examined carefully and compared with other factors that may have an influence on thermodynamic properties, particularly the effects of water structure breakdown, for a proper evaluation of the significance of the data. Such an evaluation is assisted by inspection of the temperature and concentration dependence of excess free energies, enthalpies, and entropies for both water and salt. A succeeding paper will deal with correlation of all available high-temperature osmotic coefficient data, calculation of activity coefficients and excess functions for salt as well as water, and some interpretations of the significance these have for aqueous solutions at both high and low temperatures.

Acknowledgments. This work was performed under contract from the Office of Saline Water. We are indebted also to Mr. T. S. Bulischeck for assistance in construction of apparatus and conducting the experiments, and to many others at Westinghouse Research Laboratories who contributed to various phases of the work. We also wish to acknowledge useful and informative discussions with Professors R. M. Fuoss and H. S. Frank.

Complete Equilibrium Constants, Electrolyte Equilibria, and Reaction Rates[1]

by William L. Marshall

Reactor Chemistry Division, Oak Ridge National Laboratory, Oak Ridge, Tennessee 37830
(Received May 15, 1969)

Application of the complete equilibrium constant ($K°$), which includes solvent as a reactant, has revealed recently several additional correlations of aqueous electrolyte behavior. Of particular importance, the conventionally derived standard state change in molar volumes (ΔV) between products and reactants (excluding solvent) is shown experimentally to be proportional merely to the compressibility of the solvent; the significance of this relationship is discussed. All other conventional thermodynamic properties can be calculated as a function of both pressure and temperature from the variation of $K°$ and k (the assumed net change in waters of solvation) with temperature (only) and from the known pressure–volume–temperature behavior of the solvent. Analogous behavior for rate constants is considered, with the product being the activated complex. There appears to be no significant effect of viscosity on the complete constants within the precision of measurements. Several comparisons of the description of ionization behavior by means of $K°$, fugacity, and activity coefficients are presented. From these comparisons over wide ranges of pressure, temperature, and dioxane–water mixed solvent compositions, the overall utility of fugacity, with its defined relationship to chemical potential, is questioned in that the use of $K°$ simplifies the description of electrolyte–solvent equilibria. A knowledge of fugacities (and/or activity coefficients) is unnecessary, and therefore the complete constant would appear to have much potential usefulness.

Complete Ionization Constants

Isothermal ionization equilibria in aqueous fluids can be described by complete ionization constants ($K°$)

$$K° = \frac{[M(H_2O)^{+}_{m}][A(H_2O)^{-}_{n}]}{[MA(H_2O)_j][H_2O]^k} = K/[H_2O]^k \quad (1)$$

where $K°$ and k (the assumed average net change in waters of solvation upon dissociation of solvated ion-pair species $MA(H_2O)_j$) are found to vary only with temperature, K is a conventional constant (or quotient) that varies both with temperature and pressure, j, m, and n represent average waters of solvation, and all concentrations are expressed in moles per liter at a total pressure P.[2-4]

The conventional constant does not distinguish between contact ion pairs, ion pairs containing a discrete

(1) Research sponsored by the U. S. Atomic Energy Commission under contract with the Union Carbide Corp. Presented before the Division of Physical Chemistry at the 158th National Meeting of the American Chemical Society, New York, N. Y., Sept 7–12, 1969.

(2) E. U. Franck, *Z. Phys. Chem.* (Frankfurt am Main), **8**, 107, 192 (1956).

(3) W. L. Marshall and A. S. Quist, *Proc. Natl. Acad. Sci. U. S.*, **58**, 901 (1967).

(4) A. S. Quist and W. L. Marshall, *J. Phys. Chem.*, **72**, 1536 (1968).

number of water molecules between ions,[5-7] and those of any other degree of solvation. The parameter k, therefore, appears to be a statistical term representing the net change in solvation number, on ionization, from the average extent of solvation of the various ion pairs to a corresponding average for the ions. Calculated thermodynamic functions, like those ordinarily obtained from conventional constants, must be considered on this basis.

The conventional constant is obtained for the solute species in reference states at infinite dilution at the particular pressure on the system, and for H_2O in a reference state of pure solvent at the same pressure. Under these conditions, the activity coefficients are always defined to be unity. Ordinarily at low temperature and atmospheric pressure, and at infinite dilution of electrolyte, the activity of water is taken also as unity (a constant) and is deleted from the equilibrium expression. In the present approach, the activity of water is defined to be equivalent to its analytical molarity (C_{H_2O}). The standard states are therefore hypothetical 1 M solutions for all reacting species (eq 1). With the above definitions, the standard states are functions both of temperature and pressure. We have found that virtually all ionization behavior in aqueous media adheres to this relationship not only at 25–800° at pressures to 4000 bars but also in dioxane–water solutions at 25–100° where dioxane is considered to be an inert diluent and where C_{H_2O} is simply the analytical molarity of water in the mixed solvent[4] (however, see Appendix). Although the standard free energies of reactants and products will indeed change with pressure, with the model (eq 1) and definitions used it would appear that the complete differences in these standard free energies ($\Delta G°$) are invariant with pressure.

By substituting $55.51d$ for $[H_2O]$ in eq 1, where d is the density of water, taking the logarithm of the resulting equation, and differentiating with respect to pressure (P) at constant temperature (T), the following expressions are obtained

$$\ln K = \ln K° + k \ln C_{H_2O} \quad (2)$$

$$= \ln K° + k \ln 55.51 + k \ln d \quad (3)$$

$$\left(\frac{\partial \ln K}{\partial P}\right)_T = k\left(\frac{\partial \ln d}{\partial P}\right)_T \quad (4)$$

$$= k\beta \quad (5)$$

where β is the compressibility of water. Thus, it is experimentally found that the isothermal change in the logarithm of a conventional ionization constant with pressure is merely proportional to the compressibility of the solvent, relating to the specific electrolyte equilibrium by the constant k. A stringent test of this relationship is shown in the lower section of Figure 1 where log K (molar ionization) for sodium iodide in an aqueous supercritical fluid is plotted against log C_{H_2O} at

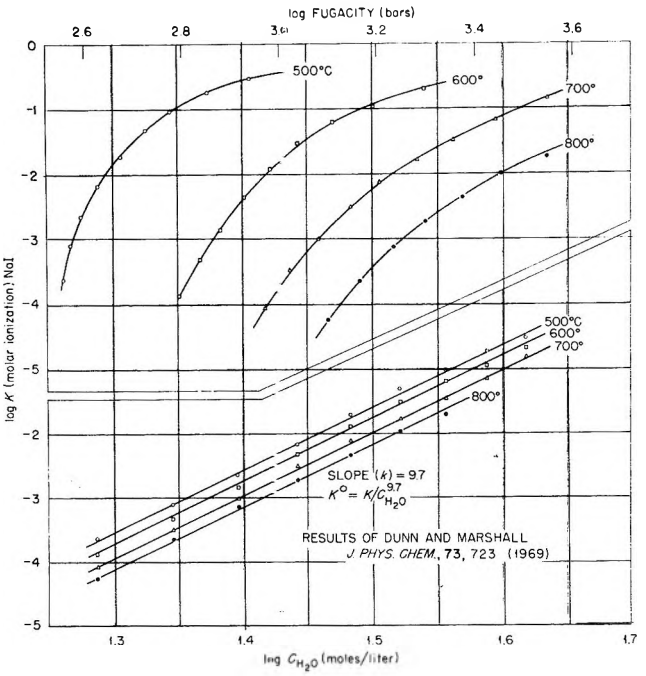

Figure 1. Contrast in the dependence of K(molar ionization) for NaI on the fugacity and the molar concentration of water, 500–800°.

several temperatures from 500 to 800° and at pressures from 1000 to 4000 bars.[8] The linear relationships verify the adherence to eq 2–5 and reflect the dependence of the conventional constant K on the change in concentration of the substance water to maintain a truly constant $K°$. Figure 1 shows also that the slope k at high temperature becomes independent both of temperature and pressure for these particular 1–1 salt equilibria.[2-4,8]

Fugacity and Concentration

Comparative plots in the upper section of Figure 1 of the logarithm of the fugacity of water *vs.* the same values of log K(NaI) as in the lower section provide no linearity. With the use of fugacity, however, the standard state of water is taken to be invariant with pressure, and consequently pressure activity coefficients for solute species should be introduced to maintain pressure-independent standard states also for these species. These activity coefficients could be calculated in a manner to account for the nonlinearity in the plots of Figure 1, as discussed in the next section. By the definition of fugacity, its defined[9] relationship to chemical potential,[10] and the defined direct proportionality of

(5) M. Eigen and K. Tamm, *Z. Elektrochem.*, **66**, 93, 107 (1962).

(6) G. Atkinson and S. Petrucci, *J. Phys. Chem.*, **70**, 3122 (1966).

(7) G. Atkinson and S. K. Kor, *ibid.*, **71**, 673 (1967).

(8) L. A. Dunn and W. L. Marshall, *ibid.*, **73**, 723 (1969).

(9) G. N. Lewis, *Proc. Am. Acad.*, **36**, 145 (1900); **37**, 49 (1901); **43**, 259 (1907); *Z. Phys. Chem.* (Leipzig), **38**, 205 (1901); **61**, 129 (1907).

(10) J. W. Gibbs, *Trans. Conn. Acad. Sci. U. S.*, **3**, 108, 343 (1875–1878).

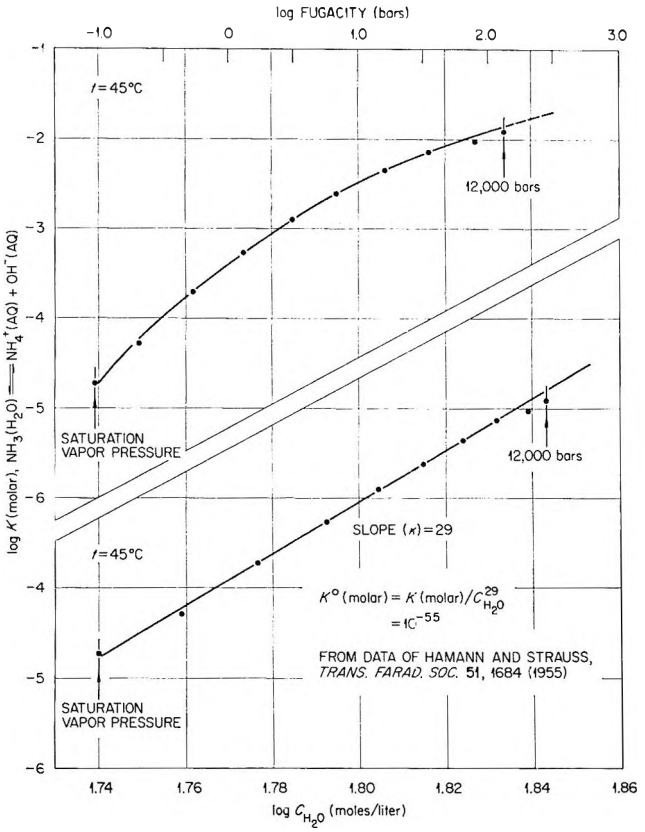

Figure 2. Contrast in the dependence of K(molar ionization) for ammonia on fugacity and on the molar concentration of water, 45° and 1–12,000 bars.

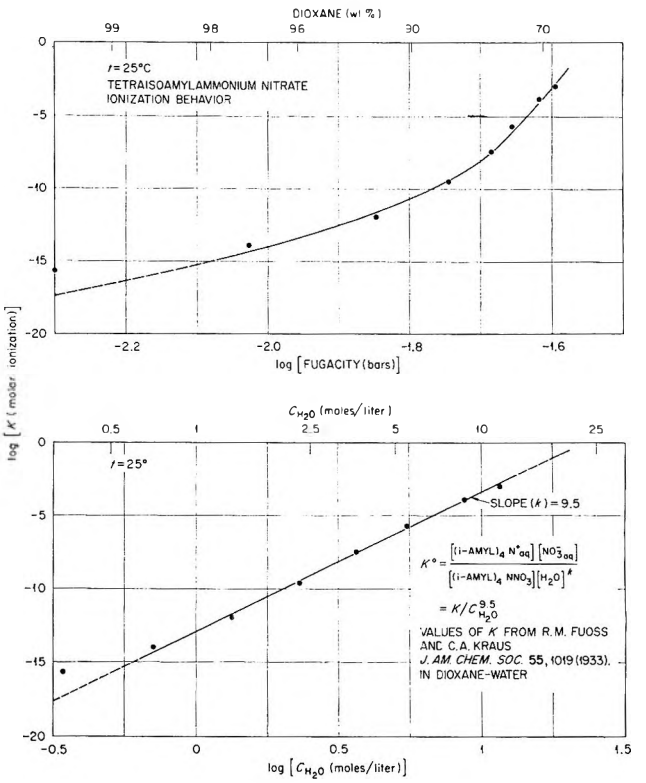

Figure 3. Contrast in the dependence of K (molar ionization) for tetraisoamylammonium nitrate on the fugacity and molar concentration of water; dioxane–water solvent mixtures at 25°, saturation vapor pressure.

activity to fugacity,[9] this interpretation is proper but appears to provide no simple relationship. All fugacities were determined from the thermodynamic tables of Pistorius and Sharp[11] and the recent data of Maier and Franck;[12] these values compared reasonably well with those of Anderson.[13]

Aside from the monotonic curvatures of log K *vs.* log f_{H_2O} shown in Figure 1, there would appear to be an additional complication in the use of fugacity at lower pressures. As the supercritical fluid approaches ideality at very low pressures, both $(\partial \log f_{H_2O}/\partial \log C_{H_2O})_T$ and $(\partial \log f_{H_2O}/\partial \log P_{H_2O})_T$ approach unity. Under these conditions, and with the assumption that the log K − log C_{H_2O} plots continue to remain linear, all plots of log K(NaI) *vs.* log f_{H_2O} would approach a slope of 9.7 for the examples shown (Figure 1). Isothermal plots of log f_{H_2O} *vs.* log C_{H_2O} or *vs.* log P_{H_2O} over the entire range of pressure from 1 to 4000 bars, and at 500–800°, produce S-shaped curves, with the greatest expected deviation occurring at the lower temperatures. Accordingly, a plot of log K *vs.* log f_{H_2O} (with the restriction of an assumed linearity of log K *vs.* log C_{H_2O} to the lowest pressures) would also produce an S-shaped curve, suggesting an additional complexity in the description of log K by means of fugacity in the region of supercritical fluid.

A good example of adherence at low temperature of values of K to eq 2–5, and to an extremely high pressure, is shown in the lower half of Figure 2 where the excellent molal ionization constants for ammonia in aqueous solution at 45° and from 1 to 12,000 bars of pressure obtained by Hamann and Strauss[14] were converted into molar units and plotted as log K(molar) *vs.* log C_{H_2O}. (The use of log K(molal) produces mathematically a slope of $(k - 1)$ rather than k, but only concentration units can be used in defining $K°$ since the *molality* of water is independent of pressure.) A comparative plot of log K(molar) *vs.* log f_{H_2O} in the upper half of Figure 2 does not show linearity. Fugacities were calculated from the tables of Pistorius–Sharp and of Sharp.[11]

An example[15] of linear behavior of log K *vs.* log C_{H_2O} in dioxane–water solutions at saturation vapor pressure at 25° to an extremely low water concentration is shown in the lower half of Figure 3. (Many other examples of linearity at higher values of C_{H_2O} in this

(11) C. W. F. T. Pistorius and W. E. Sharp, *Amer. J. Sci.*, **258**, 757 (1960); W. E. Sharp, University of California Report No. UCRL-7118 (1962).

(12) S. Maier and E. U. Franck, *Ber. Bunsenges. Phys. Chem.*, **70**, 639 (1966).

(13) G. M. Anderson, *Geochim. Cosmochim. Acta*, **28**, 713 (1964).

(14) S. D. Hamann and W. Strauss, *Trans. Faraday Soc.*, **51**, 1684 (1955).

(15) R. M. Fuoss and C. A. Kraus, *J. Amer. Chem. Soc.*, **55**, 1019 (1933).

mixed solvent system, where dioxane acts chiefly as a diluent, are cited and plotted elsewhere.[3,4,16,17] Although dioxane is not expected or found to be completely inert to water,[18] or to electrolytes, the considerably greater preferential solvation (by water) appears not to allow any deviation from linearity in the log K *vs.* log C_{H_2O} plots until extremely low concentrations of water ($< 0.5\ M$) are reached (Figure 3). Comparative plots in Figure 3 of the same values of log K *vs.* log f_{H_2O} do not provide linearity. The fugacities were evaluated from the data at 25° of Hovorka, Schaefer, and Dreisbach[19] for the saturation vapor pressure of water over dioxane–water solvent mixtures.

Activity Coefficients, Fugacity, and Complete Constants

To provide an unambiguous description of a complete ionization constant with the definition of pressure-independent standard states, and according to convention, a new constant ($K^{\circ\prime}$) can be written

$$K^{\circ\prime} = \frac{C_{M+}C_{A-}\gamma_{M+}\gamma_{A-}}{C_{MA}\gamma_{MA}b_{H_2O}{}^{s}f_{H_2O}{}^{s}} \tag{6}$$

where γ_i is a pressure activity coefficient of species i, b is a proportionality constant for converting fugacity (f) of water into activity in molar units, s is a parameter implied to have the same physical meaning as k in eq 5, and the quotient ($C_{M+}\ C_{A-}/C_{MA-}$) corresponds to K. Taking logarithms of eq 6, replacing ($\gamma_{M+}\gamma_{A-}/\gamma_{MA}$) by Γ_p, and differentiating with respect to pressure at constant temperature

$$\left(\frac{\partial \ln K^{\circ\prime}}{\partial P}\right)_T = \left(\frac{\partial \ln K}{\partial P}\right)_T + \left(\frac{\partial \ln \Gamma_p}{\partial P}\right)_T - s\left(\frac{\partial \ln f_{H_2O}}{\partial P}\right)_T = 0 \tag{7}$$

With the use of the experimental relationship of eq 2–5 and with the assumption that $s = k$

$$\left(\frac{\partial \ln \Gamma_p}{\partial P}\right)_T = k\left[\left(\frac{\partial \ln f_{H_2O}}{\partial P}\right)_T - \beta\right] \tag{8}$$

If s is not equal to k, or varies with pressure, then eq 8 becomes more complicated by the addition of the terms s and $(\partial s/\partial P)_T$, which are not easily evaluated. The right-hand side of eq 8 can be calculated from the PVT properties of the solvent and a plot of log K *vs.* log C_{H_2O}, but a moderately large number of parameters are needed for a mathematical description in terms of a single variable such as pressure. In the limit of ideal gas behavior where $P \rightarrow 0$, $(\partial \ln f_{H_2O}/\partial P)_T \rightarrow \beta$ and therefore $(\partial \ln \Gamma_p/\partial P)_T \rightarrow 0$.

In an alternate approach where fugacity is not introduced but concentration units are retained, pressure activity coefficients are still included to maintain standard states independent of pressure, and C_{M+}, C_{A-}, and C_{MA} still approach zero, we can write

$$K^{\circ\prime\prime} = \frac{C_{M+}C_{A-}\Gamma_p}{C_{MA}C_{H_2O}{}^{k}\gamma_{H_2O}{}^{k}} = \frac{K\Gamma_p}{C_{H_2O}{}^{k}\gamma_{H_2O}{}^{k}} \tag{9}$$

Taking the logarithms of eq 9, differentiating with respect to pressure, and again using the observed relationship of eq 2–5 yields the unique relationship

$$\left(\frac{\partial \ln \Gamma_p}{\partial P}\right)_T = k\left(\frac{\partial \ln \gamma_{H_2O}}{\partial P}\right)_T \tag{10}$$

Or, if all activity coefficient terms are combined

$$\left(\frac{\partial \ln (\Gamma_p/\gamma_{H_2O}{}^{k})}{\partial P}\right)_T = 0 \tag{11}$$

and there is no distinction between the use of pressure-independent or pressure-dependent standard states. The introduction of fugacities and/or activity coefficients appears therefore to be unnecessary for describing these equilibria, and the equilibrium behavior of water ($C_{\text{electrolyte}} \rightarrow 0$) is described only by its analytical concentration. These observations would suggest that concentration ultimately might provide a better basis for a relationship to a chemical potential than pressure.

The Volume Change (ΔV)

The isothermal changes in conventional constants (molar or molal units) with pressure are conventionally related to a change (ΔV) in partial molar volumes between products and reactants in their standard states where the standard states are allowed to vary with the pressure on the system.[20] This derivation arises from the use of the Gibbs potential and the defined relationship between chemical potential and fugacity. Thus

$$\left(\frac{\partial \ln K}{\partial P}\right)_T = \frac{-\Delta V}{RT} \tag{12}$$

Equating eq 5 and 12 yields

$$\Delta V = -kRT\beta \tag{13}$$

The term ΔV can therefore be calculated from the compressibility of the solvent, with knowledge of the stoichiometry of the complete equilibrium. Conversely,

(16) W. L. Marshall, *Rev. Pure Appl. Chem.*, **18**, 167 (1968); *Rec. Chem. Progr.*, **30**, 61 (1969).

(17) L. A. Dunn and W. L. Marshall, *J. Phys. Chem.*, **73**, 2619 (1969).

(18) S. K. Garg and C. P. Smyth, *J. Chem. Phys.*, **43**, 2959 (1965).

(19) F. Hovorka, R. A. Schaefer, and D. A. Dreisbach, *J. Amer. Chem. Soc.*, **59**, 2753 (1937).

(20) (a) B. B. Owen and S. R. Brinkley, *Chem. Rev.*, **29**, 461 (1941); (b) H. S. Harned and B. B. Owen, "The Physical Chemistry of Electrolytic Solutions," Reinhold Publishing Corp., New York, N. Y., 1958, pp 14, 15.

k can be calculated from an accurate knowledge of ΔV at one pressure and the compressibility of the solvent at the same pressure. The quantity ΔV thus represents the difference in standard state partial molar volumes between solute products and reactants under the conditions of the standard state reaction and is essentially equal to zero (expressed as $\Delta V°$) when the complete equilibrium is considered.

Hamann and Lim earlier found a linear relationship of partial molar volumes ($\bar{V}$) of strong electrolytes with the compressibility at 1 atm of several solvents.[21] The present approach to ΔV is certainly consistent with their earlier, unique observation on the behavior of $\bar{V}$.

The above relationship (eq 13) can be correlated directly with a usual concept of the partial molar volume ($\bar{V}_i$) of a species i

$$\bar{V}_i = V_I - V_{E_i} \tag{14}$$

where $\bar{V}_I$ is the intrinsic volume of the species and V_{E_i} is the volume of electrostriction of the solvent due to interaction with species i. There are numerous papers in the literature relating to this and similar approaches. References to most of these papers are included in an extensive review article by Conway[22] and in a recent paper by Panckhurst.[23] Very recently, King has presented volume changes for the ionization of several acids where he expands the basic eq 14 to include volume terms relating to void spaces and specific hydrogen bonding.[24] Of particular mention are relatively recent theoretical and experimental studies of Ellis,[25] Hills,[26] Yeager, *et al.*,[27] Conway, Verrall, and Desnoyers,[28] Hepler,[29] Glueckauf,[30] Benson and Copeland,[31] Padova,[32] Hamann,[33] and Distèche and Distèche.[34] These various investigators have observed and discussed unique relationships of partial molar volumes, in many cases under wide conditions of temperature[25,26,33] and pressure.[25,26,33,34] The recent papers of Dunn and of Millero and Drost-Hansen on molar volumes of electrolytes should also be mentioned.[35]

In this present paper, we can correlate ΔV (eq 12 and 13) with a physical model in the following manner. For a conventional ionization equilibrium

$$MA(\text{solvated}) \rightleftharpoons M^+(\text{solvated}) + A^-(\text{solvated}) \tag{15}$$

let

$$\Delta V = (V'_{M^+(I)} + V''_{H_2O(S)} - V'''_{H_2O(C)}) + (V'_{A^-(I)} + V''_{H_2O(S)} - V''_{H_2O(C)}) - (V'_{MA(I)} + V'''_{H_2O(S)} - V'''_{H_2O(C)}) \tag{16}$$

where (I), (S), and (C) refer to the intrinsic volume (I) of the species, *i.e.*, the unsolvated ionic or molecular volume, the volume of the solvation shell (S), and the initial free volume of solvent (C) *consumed* to form the solvation shell. The terms, V'_{H_2O}, V''_{H_2O}, and V'''_{H_2O} refer to volumes of solvent interacting with species M^+, A^-, and MA, respectively. With this description, each of the several combined terms ($V_{H_2O(S)} - V_{H_2O(C)}$) corresponds to the term $-V_{E_i}$ of eq 14. The common terms in eq 16 can be combined to yield

$$\Delta V = \Sigma V_{(I)} + \Sigma V_{H_2O(S)} - \Sigma V_{H_2O(C)} \tag{17}$$

where the three terms on the right-hand side are the respective differences in the common values between product and reactants, with each species in its respective standard state. We now can assume that over a wide range of pressure the difference in the intrinsic volumes ($\Sigma V_{(I)}$) will be (essentially) zero, and therefore by combining eq 13 and 17

$$\Delta V = \Sigma V_{H_2O(S)} - \Sigma V_{H_2O(C)} = -kRT\beta \tag{18}$$

In addition, it appears reasonable to conclude that

$$\left(\frac{\partial \Sigma V_{H_2O(S)}}{\partial P}\right)_T \ll \left(\frac{\partial \Sigma V_{H_2O(C)}}{\partial P}\right)_T \tag{19}$$

With this latter assumption, eq 18 can be differentiated with respect to pressure at constant temperature to yield

$$\left(\frac{\partial \Delta V}{\partial P}\right)_T = -kRT\left(\frac{\partial \beta}{\partial P}\right)_T \cong -\left(\frac{\partial \Sigma V_{H_2O(C)}}{\partial P}\right)_T \tag{20}$$

From eq 20, it would appear again that ΔV is essentially a function of the PVT properties of the solvent. Further correlations of volume changes are to appear in a subsequent paper.[36]

(21) S. D. Hamann and S. C. Lim, *Aust. J. Chem.*, **7**, 329 (1954).

(22) B. E. Conway, *Ann. Rev. Phys. Chem.*, **17**, 481 (1966).

(23) M. H. Panckhurst, *Rev. Pure Appl. Chem.*, **19**, 45 (1969).

(24) E. J. King, *J. Phys. Chem.*, **73**, 1220 (1969).

(25) A. J. Ellis, *J. Chem. Soc., A*, 1138 (1968); 660 (1967); 1579 (1966); A. J. Ellis and I. M. McFadden, *Chem. Commun.*, 516 (1968).

(26) G. J. Hills, *Rev. Pure Appl. Chem.*, **18**, 153 (1968).

(27) R. Zana and E. Yeager, *J. Phys. Chem.*, **71**, 521 (1967); L. Goldfarb and E. Yeager, Ultrasonics Research Laboratory, Western Reserve University, Technical Report No. 32, Jan 1968.

(28) B. E. Conway, R. E. Verrall, and J. E. Desnoyers, *Z. Phys. Chem.* (Leipzig), **230**, 157 (1965); *Trans. Faraday Soc.*, **62**, 2738 (1966); J. E. Desnoyers, R. E. Verrall, and B. E. Conway, *J. Chem. Phys.*, **43**, 243 (1965).

(29) L. G. Hepler, *J. Phys. Chem.*, **69**, 965 (1965).

(30) E. Glueckauf, *Trans. Faraday Soc.*, **61**, 914 (1965).

(31) S. W. Benson and C. S. Copeland, *J. Phys. Chem.*, **67**, 1194 (1963).

(32) J. Padova, *J. Chem. Phys.*, **39**, 1552 (1963).

(33) (a) S. D. Hamann, "Physico-Chemical Effects of Pressure," Butterworth and Co. Ltd., London, 1957; (b) S. D. Hamann *Ann. Rev. Phys. Chem.*, **15**, 349 (1964).

(34) A. Distèche and S. Distèche, *J. Electrochem. Soc.*, **112**, 350 (1965); A. Distèche, *ibid.*, **109**, 1084 (1962); A. Distèche, *Rev. Sci. Instr.*, **30**, 474 (1959).

(35) L. A. Dunn, *Trans. Faraday Soc.*, **64**, 1898, 2951 (1968); **62**, 2348 (1966); F. J. Millero, *J. Phys. Chem.*, **72**, 4589 (1868); *Limnol. Oceanogr.*, **14**, 376 (1969); F. J. Millero and W. Drost-Hansen, *J. Phys. Chem.*, **72**, 1758 (1968); *J. Chem. Eng. Data*, **13**, 330 (1968).

(36) W. L. Marshall, in preparation.

Conventional Thermodynamic Functions from Complete Constants

All conventional thermodynamic properties as a function of both pressure and temperature can be calculated from a knowledge of K° and k varying with temperature (only), and with the known PVT properties of the solvent. Rearranging eq 2 and differentiating with respect to $1/T(^\circ\mathrm{K})$ at constant pressure, where K° and k are functions only of temperature, yields

$$\frac{\mathrm{d} \ln K^\circ}{\mathrm{d}(1/T)} = \left(\frac{\partial \ln K}{\partial(1/T)}\right)_P - k\left(\frac{\partial \ln C_{H_2O}}{\partial(1/T)}\right)_P - \ln C_{H_2O}\left(\frac{\mathrm{d}k}{\mathrm{d}(1/T)}\right) \quad (21)$$

From the van't Hoff isochore,[20b] $(\partial \ln K/\partial(1/T))_P = -\Delta H/R$, where ΔH is the conventionally defined change in enthalpy (excluding solvent) between products and reactants in their standard states at pressure P. By substituting $55.51d$ for C_{H_2O} in eq 21 the second term on the right-hand side can be shown to equal $k\alpha T^2$ where α is the coefficient of thermal expansion of the solvent. By making these two substitutions into eq 21 and rearranging, the following expression for ΔH is obtained

$$\Delta H = -R\left[\frac{\mathrm{d} \ln K^\circ}{\mathrm{d}(1/T)} + \ln C_{H_2O}\left(\frac{\mathrm{d}k}{\mathrm{d}(1/T)}\right) + k\alpha T^2\right] \quad (22)$$

With values of ΔV and ΔH from eq 13 and 22

$$\Delta E = \Delta H - P\Delta V \quad (23)$$

and from eq 2, with a value of ΔH (eq 22)

$$\Delta G = \Delta G^\circ - kRT \ln C_{H_2O} \quad (24)$$

$$\Delta S = (\Delta H - \Delta G)/T \quad (25)$$

where ΔE and ΔS are the conventional changes in internal energy and entropy, respectively, and ΔG and ΔG° are the conventional and complete changes in Gibbs free energy which are equal to $-RT \ln K$ and $-RT \ln K^\circ$, respectively. Again, all functions refer to changes in the standard states. When k is invariant with temperature, *i.e.*, for 1–1 electrolyte salts at 400–800°,[4,8,37] the term $\ln C_{H_2O}(\mathrm{d}k/\mathrm{d}(1/T))$ in eq 21 and 22 is zero, and in addition a ΔH° for the complete reaction can be evaluated with the van't Hoff isochore directly from $(\mathrm{d} \ln K^\circ/\mathrm{d}(1/T))$.[8] However, where k changes with temperature, ΔH° cannot be calculated by this method since K° as a function of temperature must refer to the same stoichiometry for the complete equilibrium in order to apply the van't Hoff isochore. The conventional thermodynamic functions, like ΔV, would appear not to represent complete changes in standard-state properties since one of the reactants, the solvent, is omitted from the description of the equilibrium.

Ionization Behavior in Dioxane–Water and Water at High Pressures

From the few studies of ionization equilibria at 25° of a salt ($MgSO_4$ or $MnSO_4$) both in dioxane–water mixtures[38] at saturation pressure and in (pure) water at high pressures,[39] the value of k was found to be essentially the same in either solvent system.[4] In contrast, a plot of $\ln f_{H_2O}$ *vs.* $\ln K$ for these two salts shows a sharp break in the curve at the common boundary of the two solvent systems where the two slopes are

$$\left(\frac{\partial \ln f_{H_2O}}{\partial \ln K}\right)_T = 6.7 \text{ (from fugacities over dioxane–water mixtures)} \quad (26)$$

$$= 0.036 \text{ (from (pure) water at high pressures)}$$

For both systems $M_{H_2O} \rightarrow 55.34$, saturation vapor pressure (25°). This behavior may not be unexpected, but it does stress the observation of greater complexity in the use of fugacity to describe these particular equilibria as contrasted to the use of the complete constant. The values of fugacity (for H_2O) over dioxane–water mixtures were evaluated from the data cited previously[19] and those at high pressure from the tables of Pistorius and Sharp.[21]

Dielectric Constant and Complete Constant

The use of the complete constant can replace theories invoking the macroscopic dielectric constant of the solvent[3,4] and terms that are functions of the nearest approach of ions in correlating the behavior of $(\partial \ln K/\partial P)_T$. Where, for example, this latter interpretation was used, agreement of the calculated K (ionization) for lanthanum ferricyanide at 2000 bars with the experimental value[40] diverged approximately −6 to +12% depending on the theory used. The present interpretation, of considerably less complexity, allows agreement throughout by ±1%, or within the experimental scatter of the reported K's.[40]

In a very recent paper on a solvolysis reaction, Fagley and Oglukian have found no (theoretical) correlation of the rate constant in dioxane–water solvent mixtures with a change in macroscopic dielectric constant.[41] Their overall interpretation of reaction rates, analogous to the concept of a complete constant, is discussed in the next section.

(37) (a) A. S. Quist and W. L. Marshall, *J. Phys. Chem.*, **72**, 684 (1968); (b) *ibid.*, **72**, 2100 (1968).

(38) H. S. Dunsmore and J. C. James, *J. Chem. Soc.*, 2925 (1951); G. Atkinson and C. J. Hallada, *J. Amer. Chem. Soc.*, **84**, 721 (1962).

(39) F. H. Fisher, *J. Phys. Chem.*, **66**, 1607 (1962); F. H. Fisher and D. F. Davis, *ibid.*, **69**, 2595 (1965).

(40) S. D. Hamann, P. J. Pearce, and W. Strauss, *ibid.*, **68**, 375 (1964).

(41) T. F. Fagley and R. L. Oglukian, *ibid.*, **73**, 1438 (1969).

Complete Rate Constants and Functions of Activation

Complete Rate Constants in Dioxane–Water Solvents. While reaction kinetics involving the solvent comprises a large field of study, particularly in organic chemistry,[42] relatively few investigations have been made in dioxane–water solvents. Most recently, however, Fagley and Oglukian have found approximate linearity in a plot of log r (a specific reaction rate constant—the symbol k is used by them) *vs.* log C_{H_2O} to low concentrations of water in dioxane–water mixtures.[41] They also show that the logarithm of a conventional quotient representing a steady-state equilibrium is proportional to log C_{H_2O} to extremely low concentrations of water, allowing deduction of the primary solvolysis of phthalic anhydride. A particular slow rate process is the subsequent, additional solvolysis. In their paper, they make an analogous interpretation to that of the complete equilibrium constant and discuss a pure (or complete) rate constant unperturbed by solvent composition, but with a particular complication.[43] In this approach, as they and others have reasoned,[44] the number of waters of solvation in the activated complex is obtained. With rate constant measurements at other temperatures, complete (or pure) thermodynamic functions for activation processes accordingly can be obtained.

Complete Rate Constants at High Pressures. A similar approach can be applied to the change in conventional specific rate constants (r) with pressure in a pure solvent, where log r is plotted against log C_{H_2O} to obtain a complete rate constant (r°) that is independent of pressure. For these processes at high pressures a conventional volume change of activation ($\Delta V^\pm$) is expressed by

$$\Delta V^\pm = -k^\pm RT\beta \qquad (27)$$

where $k^\pm$ is the assumed net change in bound solvent molecules between the activated complex and the reactants. All other conventional and complete thermodynamic functions of activation can be calculated accordingly by equations directly analogous to eq 21–25, where symbols for the conventional and complete functions of activation are substituted for those corresponding to equilibrium processes.

A good example of the logarithmic proportionality of a rate constant to the molar concentration of the solvent is observed from the very recent, highly accurate results of Baliga and Whalley for the hydrolysis of methyl and isopropyl bromide to pressures of 3000 bars at temperatures from 40 to 80°.[45] When their isothermal values of r (the symbol k is used by them) are converted into log r and are plotted against log C_{H_2O}, the average random deviation from a linear relationship is less than $\pm 0.5\%$, except under particular, high-pressure conditions (methyl bromide at 60 and 70°; isopropyl bromide at 50°) where they state that a second mechanism of hydrolysis occurs, and except for two data points at 50 and 100 bars (isopropyl bromide, 40°) that deviate sharply by -2.5%. The random deviation of less than 0.5% can be compared with a maximum deviation from linearity of about 7 and 10% for the same values of log r plotted against pressure, the examples being for isopropyl bromide at 50 and 40°, respectively.[46] Of course, linearity is *not* to be expected for these latter plots, but the contrasting observation stresses the significance of the simple correlation with solvent *concentration* and the active participation of solvent in the reaction. The slope, $(\partial \log r/\partial \log C_{H_2O})_T$, is 9.40 for the hydrolysis of isopropyl bromide at all three temperatures (40, 50, and 60°) and 10.13 for the corresponding hydrolysis (the mechanism at low pressure) of methyl bromide at 60, 70, and 80°. This slope is the value of $k^\pm$ in eq 27, from which $\Delta V^\pm$ and, subsequently, the other thermodynamic functions of the activation process can be calculated.

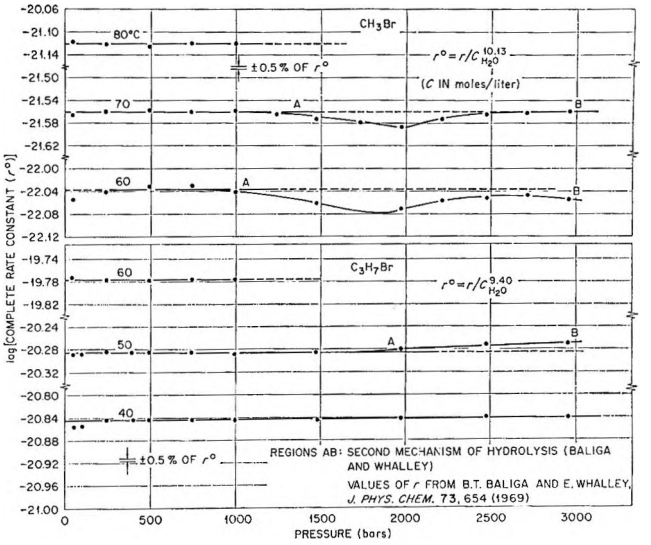

Figure 4. Isothermal invariance of the complete rate constant (r°) for the hydrolysis of methyl bromide and isopropyl bromide calculated from conventional rate constants (r) of Baliga and Whalley.[45]

The isothermal constancy with pressure of the complete rate constant (r°)

$$r^\circ = r/C^{k^\pm}{}_{H_2O} \qquad (28)$$

is shown in Figure 4. The separate values of r° were calculated from the separate experimental values of r of Baliga and Whalley,[45] from a value of $k^\pm$ that is constant both with pressure and temperature, and with the use of PVT data for water.[11] The divergences

(42) For a relatively recent summary, with many references, see E. R. Thornton, "Solvolysis Mechanisms," Ronald Press Co., New York, N. Y., 1964.

(43) See ref 41, eq 3c *et seq.*

(44) R. P. Bell, J. P. Millington, and J. M. Pink, *Proc. Roy. Soc.*, **A303**, 1 (1968).

(45) B. T. Baliga and E. Whalley, *J. Phys. Chem.*, **73**, 654 (1969).

(46) See ref 45, Figure 2.

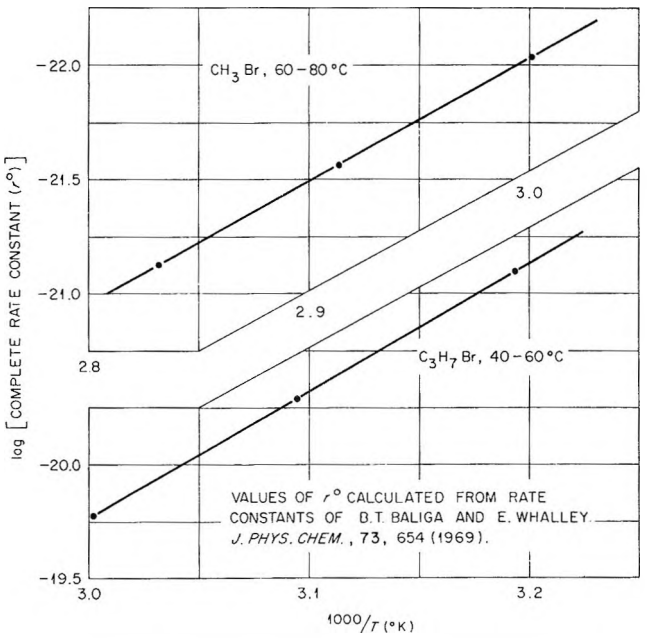

Figure 5. Logarithm of the complete rate constant (r°) *vs.* T^{-1}(°K) for the hydrolysis (first mechanism) of isopropyl bromide and methyl bromide; these constants are dependent only on temperature.

(regions AB) at high pressures for methyl bromide at 60 and 70° and for isopropyl bromide at 50° correspond to the proposed second mechanism of hydrolysis,[45] and therefore the constancy of r° and of $k^\pm$ (eq 28) would not be expected to apply under these conditions. Deviations in the two calculated values of r° for isopropyl bromide at 50 and 100 bars and 40° also stand out sharply.

The logarithms (base 10) of the averaged values for the complete rate constants (r°), dependent only on temperature, are −20.844, −20.285, and −19.776 for the hydrolysis of isopropyl bromide at 40, 50, and 60°, and −22.038, −21.559, and −21.121 for methyl bromide at 60, 70, and 80°, respectively. These values for the first (low pressure) mechanism defined by Baliga and Whalley are plotted against $1/T(°K)$ to yield the two linear relationships shown in Figure 5. Since $k^\pm$ is constant with temperature (and pressure), each slope of Figure 5 yields the complete enthalpy of activation ($\Delta H^{\pm\circ}$) by the equation

$$\frac{d \ln r^\circ}{d(1/T(°K))} = -\frac{\Delta H^{\pm\circ}}{R} \quad (29)$$

It is seen from Figure 5 that the values of $\Delta H^{\pm\circ}$, in addition to being independent of pressure, are independent also of temperature within the precision of the measurements. From values of the complete Gibbs enthalpy of activation ($\Delta G^{\pm\circ}$) calculated from the equation

$$\Delta G^{\pm\circ} = -RT \ln r^\circ \quad (30)$$

Table I: Thermodynamic Values ($\Delta H^{\pm\circ}$, $\Delta S^{\pm\circ}$) of Activation and $k^\pm$ for the Hydrolysis (First Mechamism) of Isopropyl Bromide (40–60°) and Methyl Bromide (60–80°) at 1–3000 Bars[a]

Compound	$k^\pm$	$\Delta H^{\pm\circ}$, kcal mol^{-1}	$\Delta S^{\pm\circ}$, kcal mol^{-1} deg^{-1}
Isopropyl bromide	9.40	+25.4 ± 0.2	−14.06 ± 0.02
Methyl bromide	10.13	+24.6 ± 0.3	−26.81 ± 0.02

[a] Caclulated from the rate constants of Baliga and Whalley.[45]

and values of $\Delta H^{\pm\circ}$, corresponding values of the complete entropy of activation ($\Delta S^{\pm\circ}$) are obtained; these values, like $\Delta H^{\pm\circ}$, are found also to be independent of temperature (and pressure).

Table I lists the values of $k^\pm$, $\Delta H^{\pm\circ}$, and $\Delta S^{\pm\circ}$, together with their estimated uncertainties, for the hydrolysis of isopropyl bromide and methyl bromide evaluated from the excellent data of Baliga and Whalley.[45] It is interesting to note that $\Delta H^{\pm\circ}$ has nearly the same value for the two compounds, yet $\Delta S^{\pm\circ}$ for methyl bromide is almost double the corresponding value for isopropyl bromide.

From the three values for one compound (Table I) and the PVT properties of the solvent water, all conventional and complete functions for the first mechanism rate process can be calculated and might be predicted outside of the range of experimental study. This simplicity of description is analogous to that exhibited by complete ionization equilibria of alkali halides at 400–800° where k, ΔH°, and ΔS° are independent of both temperature and pressure.[8] Since the complete volume change ($\Delta V^{\pm\circ}$) is equal to zero

$$\Delta A^{\pm\circ} = \Delta G^{\pm\circ} \quad (31)$$

$$\Delta E^{\pm\circ} = \Delta H^{\pm\circ} \quad (32)$$

where $\Delta A^{\pm\circ}$ and $\Delta E^{\pm\circ}$ are the complete Helmholtz free energy of activation and the complete internal energy of activation, respectively.

Similar Approaches. The role of the solvent in systems under varying high pressure in the formation of the activated complex has not been neglected by other investigators.[26,47,48] In most interpretations, values of $\Delta V^\pm$ are related partially to electrostriction of the solvent in the formation of the activated complex. This approach is similar to the usual interpretation of ΔV for equilibrium processes[22-33] as discussed in a previous section. Changes in degree of solvation between the complex and reactants also have been considered in relationship to pressure and dielectric constant.[47,48] The apparent number of moles of solvent electrostricted in the activation process has been con-

(47) See ref 33a, pp 137–196; ref 33b.

(48) K. E. Weale, "Chemical Reactions at High Pressures," E. and F. N. Spon, Ltd., London, 1967.

sidered and discussed by Hills.[26] The present concept of a complete rate constant independent of pressure (although the effect of viscosity should be considered; see next section) would appear to provide considerable predictability of r and the functions of activation with a lesser number of parameters than otherwise required.

Viscosity, Reaction Rates, and Equilibria

For reactions, the variation in the viscosity (η) of the solvent with pressure or with composition of mixed solvent might be expected to have a proportionate influence on rate constants (r) and should be considered. At one time, changes in rate constants with pressure were proposed to be related completely to an effect of viscosity,[49] but the inconsistency of this hypothesis was mentioned later.[50] Some nonlinearity in the plot of log r *vs.* log C_{H_2O} might be expected if the effect of viscosity is significant *unless* log C_{H_2O} *vs.* log η_{H_2O} also provides a linear relationship or unless the change in viscosity with pressure is very small compared to the change in the rate constant. A plot of log r from the data of Baliga and Whalley[45] for the hydrolysis of isopropyl bromide at 40° and to 3000 bars *vs.* log η yields a nonlinear relationship, and therefore any simple effect of viscosity does not appear to be masked in the linear log r–log C_{H_2O} plots. Similarly for equilibrium processes, plots of log K (molar ionization) at high pressures *vs.* log η yield nonlinear relationships both at low and at supercritical temperatures. The aqueous ionization constants of Hamann and Strauss[14] for ammonia at 45° and to 12,000 bars (see Figure 2) and the ionization constants of NaCl[37a] and NaI[8] (see Figure 1) at 500° and to 4000 bars were the examples of constants defining equilibrium behavior under extreme conditions that were plotted. The viscosities used were those of Bett and Cappi at low temperature[51a] and of Dudziak and Franck at supercritical temperatures.[51b]

By the above criterion, it appears that viscosity does not have any significant effect either on rate constants or on equilibrium constants, at least under conditions where the viscosity of the solvent is not excessively high. At very high viscosities, any effect probably would be observed first in the behavior of rate constants rather than equilibrium constants. At equilibrium, some cancellation of the effect of viscosity might be expected in the ratio of forward and reverse rate constants that defines K.

Application to Environmental Sciences

Practical application of the complete equilibrium constant can provide greater ease in the interpretation of electrolyte equilibria. In geochemistry or oceanography, the stoichiometric constant k for a particular salt might be determined in dioxane–water solutions at saturation vapor pressure and then used in calculating the ionization equilibrium in water at high pressures. It would appear that this approach could be used at any temperature where the value of k is known. In general, at 25° k for 1–1 salts is approximately 6.5 and for 2–2 salts is approximately 10.[4] At higher temperatures, the value of k for NaCl increases from 6.4 (in dioxane–water) at 25°[3,4] to 7.8 (in dioxane–water) at 100°[17] and to a constant 10.2 (in water) at 400–800°.[37a] These observations appear further to commonly relate ionization behavior in the two solvent media.[17] Acids and bases, however, give different values of k in dioxane–water solutions than in water at high pressures, possibly reflecting acid–base interaction with dioxane.[4] By knowing the value of k, it should be possible to obtain the ionization behavior of a particular salt well outside the experimental range of pressure, for example, in the supercritical fluid region of water at very low or high pressures.

The value of k at temperatures from 400 to 800° for several 1–1 salts in water solution is independent of temperature and pressure.[2–4,8,17] In addition, the standard enthalpy $\Delta H°$ and standard entropy $\Delta S°$ for the complete equilibrium are found also to be essentially independent of T and P.[8] Since $\Delta G° = (\Delta H° - T\Delta S°) = -RT \ln K°$, the complete thermodynamic description of a particular salt in this supercritical region is given essentially by three single numbers, k, $\Delta H°$, and $\Delta S°$.[8] This apparent simplicity allows considerable economy in describing ionization equilibria at these high temperatures.

Conclusion

The observations presented here and elsewhere[3,4,8] question the overall utility of fugacity, from which activity is defined, in that a simpler approach can be taken that reduces considerably the number of parameters necessary for description of equilibria. In a dense fluid such as liquid water, where solvent and solute species are in intimate contact, a "true" solvation number must more or less be arbitrarily defined. While the parameter k may not represent a "true" net change in solvation number by other definitions, it appears to be definable in this manner for the model of a complete equilibrium. The large values of k for the ionization behavior of acids and bases and for certain acidic and basic salts may reflect the ionization behavior of the solvent water, where the particular k is a combined value of k's from two or more competitive equilibria.

The use of the complete constants, where electrostatic interactions of solute species have been eliminated by extrapolation to infinite dilution, appears to eliminate the necessity for pressure activity coefficients over

(49) E. A. Moelwyn-Hughes, "Kinetics of Reactions in Solution," Oxford University Press, Oxford, 1947, p 346.

(50) See ref 33a, p 161.

(51) (a) K. E. Bett, and J. B. Cappi, *Nature*, **207**, 620 (1965); (b) K. H. Dudziak and E. U. Franck, *Ber. Bunsenges. Phys. Chem.*, **70**, 1120 (1966).

wide ranges of pressure at both low and high temperatures and even the need for standard states at a specified single pressure. It is the belief, therefore, that fugacity with its defined relationship to chemical potential (μ), $\mu = \mu^\circ + RT \ln f$, where μ° is the chemical potential in a standard state, might ultimately be replaced by another approach that describes equilibria with greater simplicity.

Appendix

Association Constants from Conductance Measurements. Recently, Fuoss, *et al.*, have included the $C^{3/2}$ terms in the earlier conductance equation[52] to calculate electrolyte association constants (K_A, where $1/K_A = K$-(molar ionization)) from conductance measurements of solutions to 0.1 M.[53] For the new values of K_A for particular electrolytes (NaCl, KCl, CsI) in dioxane–water mixed solvents, the relation between log K_A and log C_{H_2O} is not as linear as that for the previously published values for these same electrolytes derived from conductance measurements at concentrations only to 0.01 M.[54] The earlier values of K_A[54] obtained in dioxane–water solvent mixtures containing high concentrations of water show a large degree of uncertainty, but for most of these values the midpoints of their uncertainty limits[55] still fit reasonably well to linear log K_A–log C_{H_2O} plots.

When K_A is calculated from a set of conductance measurements obtained at successively higher concentrations, it would appear that increasing reliance on particular terms in the theoretical equation is necessary to believe completely in the physical significance of the calculated K_A. For example, additional species may appear at higher concentrations, necessitating modified terms. Conversely, a calculation of K_A from conductances of a set of solutions at very low concentrations requires less dependence on theory and more reliance on the high accuracy of the measurements. In the most recent treatments,[53] the sharp minimum in values of the standard deviation of fit when plotted against arbitrarily varied values of the parameter K_A certainly restricts the value of K_A necessary to fit the equivalent conductances to 0.1 M. However, the earlier values[54] calculated from conductances to 0.01 M without using the $C^{3/2}$ terms may have greater physical significance, although possessing greater uncertainty especially in dioxane–water compositions of high concentrations of water. (At these high water concentrations, an assumed value of the ion size was used in the calculations.[54]) This author is inclined to prefer the earlier values of K_A of Fuoss, *et al.*, in dioxane–water solvent mixtures of low water concentrations and to apply the complete equilibrium constant derived therefrom to obtain values of K_A (or K, molar ionization) at high concentrations of water and in pure water as solvent.

(52) (a) R. M. Fuoss and L. Onsager, *J. Phys. Chem.*, **61**, 668 (1957); (b) R. M. Fuoss, *J. Amer. Chem. Soc.*, **81**, 2659 (1959).

(53) (a) R. M. Fuoss and K.-L. Hsia, *Proc. Nat. Acad. Sci. U. S.*, **57**, 1550 (1967); (b) K.-L. Hsia and R. M. Fuoss, *J. Amer. Chem. Soc.*, **90**, 3055 (1968); (c) Y.-C. Chiu and R. M. Fuoss, *J. Phys. Chem.*, **72**, 4123 (1968); (d) I. D. McKenzie and R. M. Fuoss, *ibid.*, **73**, 1501 (1969).

(54) (a) R. W. Kunze and R. M. Fuoss, *ibid.*, **67**, 911 (1963); (b) J. E. Lind and R. M. Fuoss, *ibid.*, **65**, 999 (1961); (c) J. E. Lind and R. M. Fuoss, *ibid.*, **65**, 1414 (1961).

(55) See ref 54, values obtained from the figures.

The Apparent and Partial Molal Volume of Aqueous Sodium Chloride Solutions at Various Temperatures

by Frank J. Millero

Contribution No. 1134 from the Institute of Marine Sciences, University of Miami, Miami, Florida 33149
(Received June 6, 1969)

The apparent, ϕ_V, and partial, $\bar{V}_2$, molal volumes of dilute (0.01 to 1.0 *m*) aqueous NaCl solutions have been determined as a function of temperature (0 to 55°) from precision density measurements. The Debye–Hückel theoretical limiting slope for the ϕ_V and $\bar{V}_2$ as a function of the square root of molar concentration is approached at all temperatures studied. The deviations of ϕ_V and $\bar{V}_2$ are strongly dependent on temperature. These results indicate that ion–ion interactions are strongly related to the effect of temperature on the structure of the hydrated ions or the structure of water between the interacting ions. Ion pairing (cation–anion) is examined as a possible cause for the observed deviations and a general method of calculating association constants from $\bar{V}_2$ data is presented. Stoichiometric association constants, $K_A^* = 0.35$, 0.18 and 0.11, respectively, at 0, 25, and 55°, were found to represent the $\bar{V}_2$ data over the concentration range from 0.25 to 1.0*c*.

Introduction

The concentration dependence of the apparent and partial molal volume can be a very useful tool in elucidating ion–ion interactions. Earlier workers[1-4] found that the apparent molal volumes of electrolytes vary with the square root of the molar concentration (over a wide concentration range) by the linear equation

$$\phi_V = \phi_V^\circ + S_V^*\sqrt{c} \qquad (1)$$

where the experimental slope, S_V^*, varied with electrolyte type and charge. Redlich and Rosenfeld,[5] however, predicted that a constant limiting slope should be obtained for a given electrolyte charge type (at constant temperature and pressure). Redlich and Meyer[6] have calculated the theoretical limiting law slope, S_V, and recommend that ϕ_V be extrapolated using eq 2, where b_V is an arbitrary constant. Results

$$\phi_V = \phi_V^\circ + S_V\sqrt{c} + b_V c \qquad (2)$$

of a number of recent studies[7-16] at 25° have confirmed the limiting slope for a number of 1–1, 2–1, 2–2, 3–1, and 4–1 electrolytes. Dunn[17] and Franks and Smith[13] have also shown that the limiting law slope is approached for some 1–1, 2–1, and 2–2 electrolytes from 0 to 65°. Their results show that S_V increases in a regular manner with increasing temperature as predicted,[6] although S_V^* decreases with increasing temperature between 0 to ~40°[2,3] and increases with increasing temperature above 50°.[18-20] Thus, at low temperatures the deviations from the limiting law are positive (b_V is positive) and at high temperatures the deviations are negative (b_V is negative).

At present no one has offered an explanation for the cause of the change in sign of b_V as a function of temperature. This study was made to provide ϕ_V data that could be used to examine the types of ion–ion interactions responsible for the observed temperature dependence of b_V. Our results represent an independent study that confirms the predictions of Redlich and coworkers[5,6] and offers a possible explanation for the cause of the deviation of ϕ_V and $\bar{V}_2$ from the limiting law as a function of temperature.

(1) D. O. Masson, *Phil. Mag.* (7), **8**, 218 (1929).

(2) A. F. Scott, *J. Phys. Chem.*, **35**, 2315 (1931).

(3) W. Geffcken, *Z. Phys. Chem.*, **A155**, 1 (1931).

(4) H. S. Harned and B. B. Owen, "The Physical Chemistry of Electrolytic Solutions," ACS Monograph No. 137, Reinhold Publishing Corp., New York, N. Y., 3rd ed, 1958.

(5) O. Redlich and P. Rosenfeld, *Z. Electrochem.*, **37**, 705 (1931); *Z. Phys. Chem.*, **A155**, 65 (1931).

(6) O. Redlich and D. Meyer, *Chem. Rev.*, **64**, 221 (1964).

(7) L. G. Hepler, M. M. Stokes, and R. H. Stokes, *Trans. Faraday Soc.*, **61**, 20 (1965).

(8) F. Vaslow, *J. Phys. Chem.*, **70**, 2286 (1966); **73**, 3745 (1969).

(9) B. E. Conway, R. E. Verrall, and J. E. Desnoyers, *Trans. Faraday Soc.*, **62**, 2738 (1966).

(10) R. E. Verrall and B. E. Conway, *J. Phys. Chem.*, **70**, 3961 (1966).

(11) F. H. Spedding, M. J. Pikal, and B. O. Ayers, *ibid.*, **70**, 2440 (1966).

(12) J. E. Desnoyers and M. Arel, *Can. J. Chem.*, **45**, 359 (1967).

(13) F. Franks and H. T. Smith, *Trans. Faraday Soc.*, **63**, 2586 (1967).

(14) H. E. Wirth, *J. Phys. Chem.*, **71**, 2922 (1967).

(15) F. J. Millero, *ibid.*, **71**, 4567 (1967).

(16) L. A. Dunn, *Trans. Faraday Soc.*, **62**, 2348 (1966); **64**, 1898 (1968).

(17) L. A. Dunn, *ibid.*, **64**, 2951 (1968).

(18) B. M. Fabuss, A. Korosi, and A. K. M. Shamsul Huq., *J. Chem. Eng. Data*, **11**, 325 (1966).

(19) I. M. Rodnyanskii, V. I. Korobkov, and I. S. Galinker, *Zh. Fiz. Khim.*, **36**, 2216 (1962).

(20) A. J. Ellis, *J. Chem. Soc., A*, 1579 (1966); 660 (1967); 1138 (1968).

Experimental Section

The NaCl used in this study was reagent grade Baker Analyzed. The salt was recrystallized from doubly distilled water, dried at 200°, and stored in a desiccator. All the solutions were made by weight with doubly distilled water, degassed to prevent the formation of bubbles on the magnetic float during a run. Aliquot amounts of solution were analyzed by heating to dryness before and after an experimental run to determine the concentration of the solution. This was necessitated by the fact that at higher temperatures evaporation occurred.

The magnetic float used to make the density measurements has been described in detail elsewhere.[15,21] The density measurements were made by the weight dilution technique[15] and on single stock solutions.[21] Both methods agreed within the experimental error of the apparatus (~1 ppm).

The temperature of the bath was set to ±0.02° with Brooklyn thermometers and regulated to better than ±0.001° with a Hallikainen thermoregulator. During an experiment the temperature was monitored with a Hewlett-Packard quartz crystal thermometer and recorder.

Table I: The Density of Aqueous Sodium Chloride Solutions

0°	
Molality	$-1000(d^\circ - d)$
0.010197	0.4626
0.010202	0.4658
0.020642	0.9404
0.027023	1.2304
0.039766	1.8039
0.064991	2.9370
0.101802	4.5734
0.121250	5.4364
0.138813	6.2204
0.154619	6.9174
0.168565	7.5324
0.181614	8.1064
0.201120	8.9584
0.204419	9.0874
0.214681	9.5354
0.224209	9.9534
0.344756	15.1684
0.505906	22.0264
0.684443	40.8267

5°	
Molality	$-1000(d^\circ - d)$
0.010202	0.4505
0.010333	0.4561
0.039987	1.7535
0.161465	7.0100
0.356409	15.2847
0.475759	20.2607
0.684443	28.8041
0.963232	39.9755

15°	
Molality	$-1000(d^\circ - d)$
0.010202	0.4346
0.014082	0.6014
0.028880	1.2284
0.064991	2.7497
0.102122	4.3094
0.121337	5.1074
0.153610	6.4524
0.202320	8.4714
0.351101	14.5824
0.505906	20.8554
0.683549	27.8257
0.963647	38.6596

25°	
Molality	$-1000(d^\circ - d)$
0.010021	0.4167
0.039766	1.6417
0.052243	2.1589
0.103490	4.2519
0.120759	4.9440
0.162253	6.6329
0.201720	8.2289
0.212622	8.6609
0.280763	11.3876
0.309342	12.5349
0.347819	14.0509
0.506771	20.3229
0.683549	27.1339
0.963647	37.7490

35°	
Molality	$-1000(d^\circ - d)$
0.010021	0.4078
0.010197	0.4169
0.039766	1.6189
0.064769	2.6210
0.094630	3.8135
0.201720	8.0575
0.280763	11.1735
0.341607	13.5375
0.506771	19.8925
0.682655	26.6407
0.963647	37.0685

45°	
Molality	$-1000(d^\circ - d)$
0.009845	0.3991
0.071519	2.8615
0.160602	6.3763
0.248683	9.7996
0.356468	13.9788
0.382848	14.9407
0.524054	20.3310
0.689310	26.5351
0.963647	36.6100
0.965352	36.7507

55°	
Molality	$-1000(d^\circ - d)$
0.010111	0.4024
0.040458	1.6029
0.065311	2.5872
0.120759	4.7557
0.162253	6.3734
0.249190	9.7273
0.356911	13.8484
0.474686	18.2944
0.682655	26.0961
0.963232	36.3404

Results

The density of dilute aqueous solutions (0.01 to 1.0 m) of NaCl have been determined at 0, 5, 15, 25, 35, 45, and 55° using a magnetic float densitometer. The results of the difference between the density of water[22] and the density of the solutions, $d^\circ - d$, at various molal concentrations are given in Table I. The apparent molal volumes, ϕ_V's, of these solutions were calculated from the equation[4]

$$\phi_V = \frac{1000\,(d^\circ - d)}{dd^\circ m} + \frac{M}{d} \tag{3}$$

The ϕ_V's as a function of molar concentration, $c = md^\circ 1000/(1000 + \phi_V md^\circ)$, at each temperature were fit to the Redlich and Meyer equation (eq 2)[6] by a least-square best fit method. The Debye–Hückel limiting slope, S_V, is approached at all temperatures. Table II lists the apparent molal volume at infinite dilution, $\phi_V^\circ = \bar{V}_2^\circ$, and the deviation constant, b_V, at various temperatures and the results obtained by other workers.[2,3,8,13,17,20,21,23-29] The results agree very well with the recent work of Dunn[17] over this same temperature range.

The partial molal volumes, $\bar{V}_2$ for the NaCl solutions were calculated from the ϕ_V's and its concentration dependence using the equation[4]

$$\bar{V}_2 = \phi_V + \left[\frac{1000 - c\phi_V}{2000 + c^{3/2}(\partial\phi_V/\partial\sqrt{c})}\right]\sqrt{c}\,(\partial\phi_V/\partial\sqrt{c}) \tag{4}$$

(21) F. J. Millero, *Rev. Sci. Instrum.*, **38**, 1441 (1967).
(22) G. S. Kell, *J. Chem. Eng. Data*, **12**, 66 (1967).
(23) I. W. Duedall and P. K. Weyl, *Rev. Sci. Instrum.*, **38**, 528 (1965).
(24) E.-an. Zen, *Geochim. Cosmoch. Acta.*, **12**, 103 (1957).
(25) A. Kruis, *Z. Phys. Chem.*, **B34**, 1 (1936).
(26) H. E. Wirth, *J. Amer. Chem. Soc.*, **62**, 1128 (1940).
(27) G. Jones and S. M. Christian, *ibid.*, **59**, 484 (1937).
(28) K. Fajans and O. Johnson, *ibid.*, **64**, 668 (1942).
(29) A. F. Scott and R. W. Wilson, *J. Phys. Chem.*, **38**, 951 (1934).

Table II: The Partial Molal Volume of NaCl in Water at Infinite Dilution and the Deviation Constants from the Limiting Law (eq 2 and 5) at Various Temperatures

T, °C	$\phi V^\circ = V_2^\circ$, ml mol^{-1}	b_V, ml l. mol^{-1}	b_V', ml l. mol^{-1}	Rms, ml mol^{-1}
0.0	12.855, 12.94[a] 12.58,[b] 13.1[c] 12.36,[d] 12.4[e]	1.348, 1.20[a]	2.662, 2.37[a]	±0.06
5.0	14.175, 14.02[a] 14.15,[f] 14.03[g]	0.682, 0.85[a]	1.341, 1.68[a]	±0.03
15.0	15.577, 15.62[a]	0.369, 0.30[a]	0.717, 0.58[a]	±0.05
25.0	16.624, 16.61[a,h] 16.65,[f] 16.64[g,i] 16.67,[j] 16.62[k]	0.048, 0.018[a]	0.079	±0.04
35.0	17.280, 17.16[a] 17.3,[l] 17.25[m]	−0.127, −0.095[a]	−0.271, −0.21[a]	±0.05
45.0	17.592, 17.65[a]	−0.250, −0.41[a]	−0.519, −0.85[a]	±0.04
55.0	17.913, 17.76[a] 18.2,[n] 17.96[o]	−0.628, −0.43[a]	−1.267, −0.85[a]	±0.04

[a] Reference 17; the results at 0° have been estimated from the results at 0.05° using $\bar{E}_2^\circ = 0.25$ ml/mol deg. [b] Reference 23, estimated from results at 0.8° using $\bar{E}_2^\circ = 0.25$ ml/mol deg. [c] Reference 24. [d] Reference 2. [e] Reference 3. [f] Reference 13. [g] Reference 8. [h] Reference 25. [i] Reference 21. [j] Reference 26. [k] Reference 27. [l] Reference 28. [m] Reference 29. [n] Reference 20 at 50°. [o] Reference 2 at 50°.

The resulting partial molal volumes have been fit to the equation

$$\bar{V}_2 = \bar{V}_2^\circ + 1.5S_V\sqrt{c} + b_V'c \qquad (5)$$

The b_V' constants are given in Table II along with the results calculated from Dunn's data.[17] Figures 1, 2, and 3 show a plot of the relative partial molal volume, $\bar{V}_2 - \bar{V}_2^\circ$, *vs.* $\sqrt{c}$ at 0, 25, and 55°.

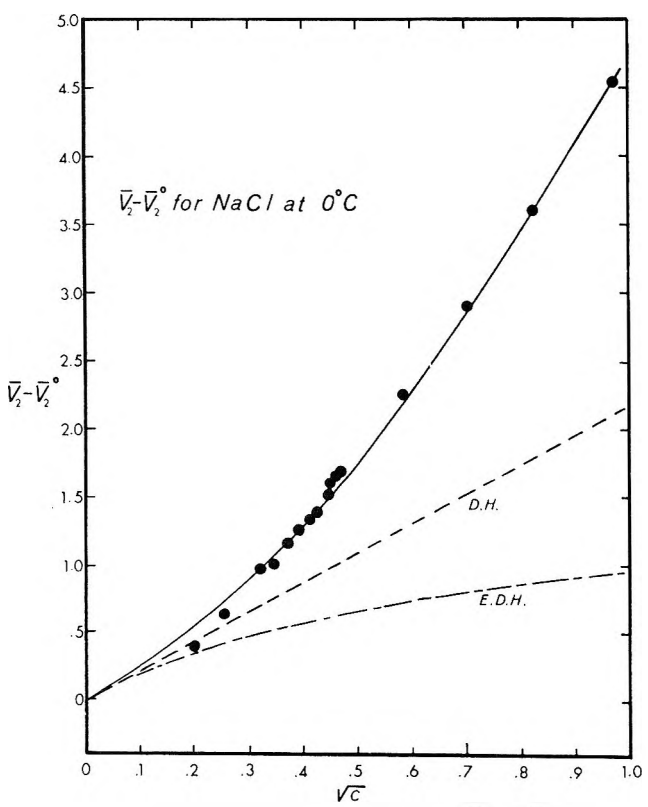

Figure 1. The relative partial molal volume, $\bar{V}_2 - \bar{V}_2$, of NaCl in water at 0° plotted *vs.* $\sqrt{c}$. D. H. is the Debye–Hückel limiting slope and E. D. H. is the extended Debye–Hückel limiting slope including the ion-size parameter.

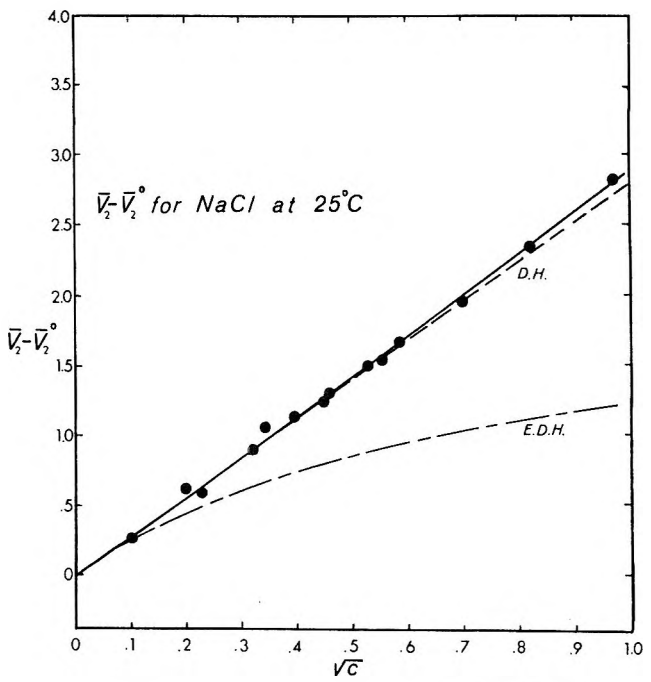

Figure 2. The relative partial molal volume, $\bar{V}_2 - \bar{V}_2$, of NaCl in water at 25° plotted *vs.* $\sqrt{c}$. (D. H. and E. D. H. have the same meaning as in Figure 1).

A more complete equation for the relative partial molal volume as a function of concentration taking into consideration the ion-size parameter, $\dot{a}$, (in angstrom units) is given as[4,30]

(30) B. B. Owen and S. R. Brinkley, Jr., *Ann. N. Y. Acad. Sci.*, **51**, 753 (1949).

$$\bar{V}_2 - \bar{V}_2^\circ = \frac{1.5S_V\sqrt{c}}{1 + A\mathring{a}\sqrt{c}} + \frac{W_V c}{(1 + A\mathring{a}\sqrt{c})^2} + K_V c \quad (6)$$

where $A = 0.3286$ at 25° for a 1–1 electrolyte, $W_V/\mathring{a}$ = constant ($\partial \ln D/\partial P - \beta - 2\partial \ln \mathring{a}/\partial P$), and K_V is an empirical constant that must be evaluated from the data.[4,30] If we assume that the $\mathring{a}$ parameter is independent of pressure,[4,11,31] the W_V term is very small and can be neglected in dilute solutions, and the extended limiting law for the relative partial molal volume becomes

$$\bar{V}_2 - \bar{V}_2^\circ = \frac{1.5S_V\sqrt{c}}{1 + A\mathring{a}\sqrt{c}} \quad (7)$$

Using an ion-size parameter of 4.0 Å for NaCl,[4] we have calculated the extended limiting law at 0, 25, and 55°. The results are shown in Figures 1, 2, and 3. As found for the rare earth salt solutions,[11] the inclusion of the ion size predicts negative deviations from the limiting law. The experimental $\bar{V}_2 - \bar{V}_2^\circ$ results are greater than the results calculated from the extended limiting law at all temperatures (*i.e.*, positive deviations occur), unlike the results using only the limiting slope. By adjusting the ion-size parameter it is possible to represent the experimental results within experimental error. We obtain $\mathring{a} = -2.16$, 0.15 and 1.64 Å, respectively, at 0, 25, and 55°. Since negative values or values less than the crystal radius (2.76 Å) for the ion-size parameter are meaningless, the extended limiting law is unable to account for the observed changes in $\bar{V}_2 - \bar{V}_2^\circ$ as a function of concentration and temperature.

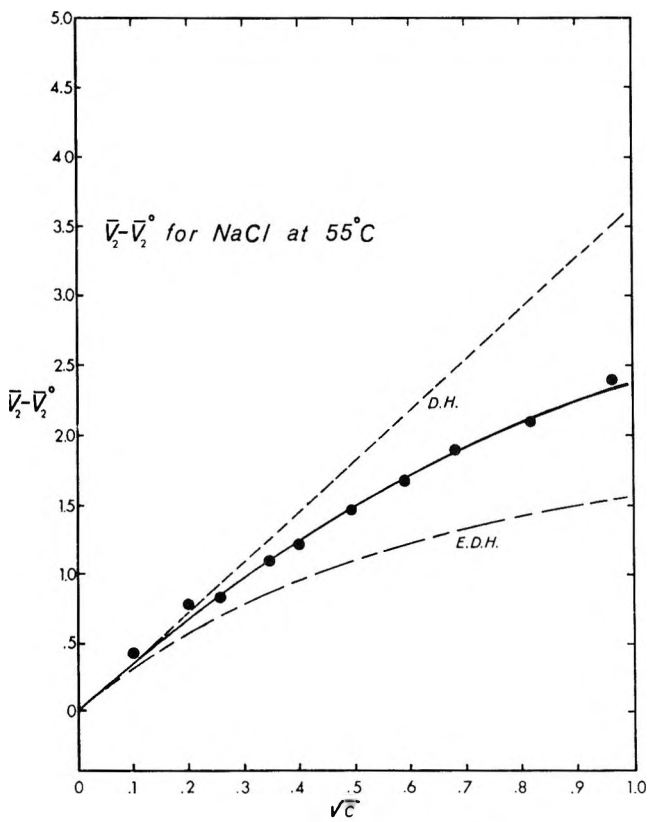

Figure 3. The relative partial molal volume, $\bar{V}_2 - \bar{V}_2^\circ$, of NaCl in water at 55° plotted *vs.* $\sqrt{c}$. (D. H. and E. D. H. have the same meaning as in Figure 1).

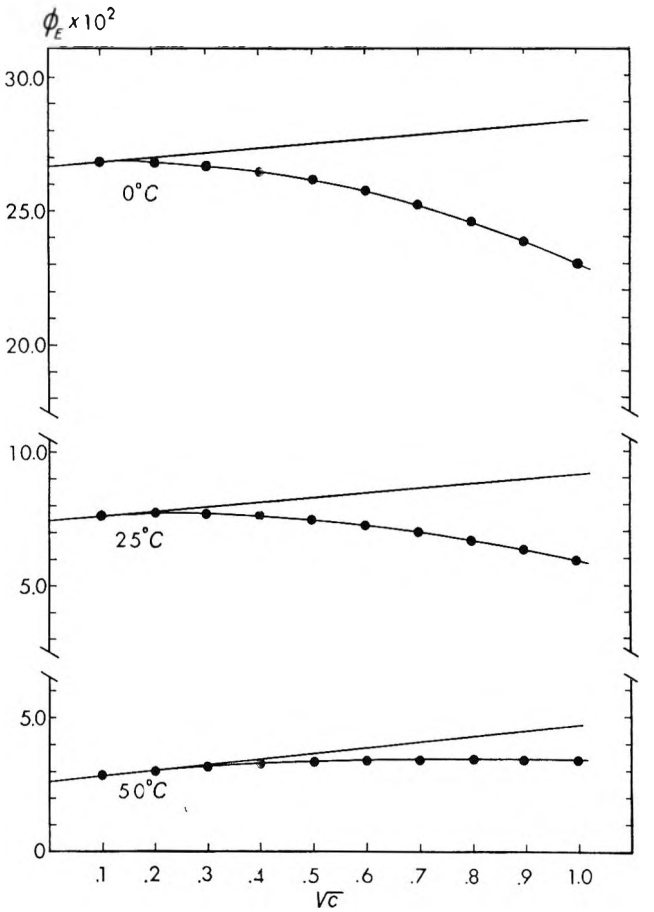

Figure 4. The apparent molal expansibility, ϕ_E, of NaCl in water plotted *vs.* $\sqrt{c}$ at 0, 25 and 55°. The straight line is the limiting slope, S_E.

The apparent molal expansibility, $\phi_E = \partial\phi_V/\partial T$, can be calculated from eq 2 by differentiating with respect to temperature

$$\phi_E = \phi_E^\circ + (\partial S_V/\partial T - \alpha S_V/2)\sqrt{c} + (\partial b_V/\partial T - b_V\alpha)c \quad (8)$$

where $\phi_E^\circ = \bar{E}_2^\circ$, the partial molal expansibility at infinite dilution and $\alpha = -(1/c)(\partial c/\partial T)$ is the expansibility of the solution. Gucker[32] has shown that α can be replaced by α°, the expansibility of pure water, to concentrations of several molar without serious error. Over the temperature range of 0 to 65° the α° of water[22] varies from -68 to 544×10^{-6} deg^{-1}; thus, in dilute solutions eq 8 reduces simply to

$$\phi_E = \phi_E^\circ + S_E\sqrt{c} + b_E c \quad (9)$$

(31) J. Poirer, *J. Chem. Phys.*, 21, 965 (1953).

(32) F. T. Gucker, Jr., *J. Amer. Chem. Soc.*, 56, 1017 (1934).

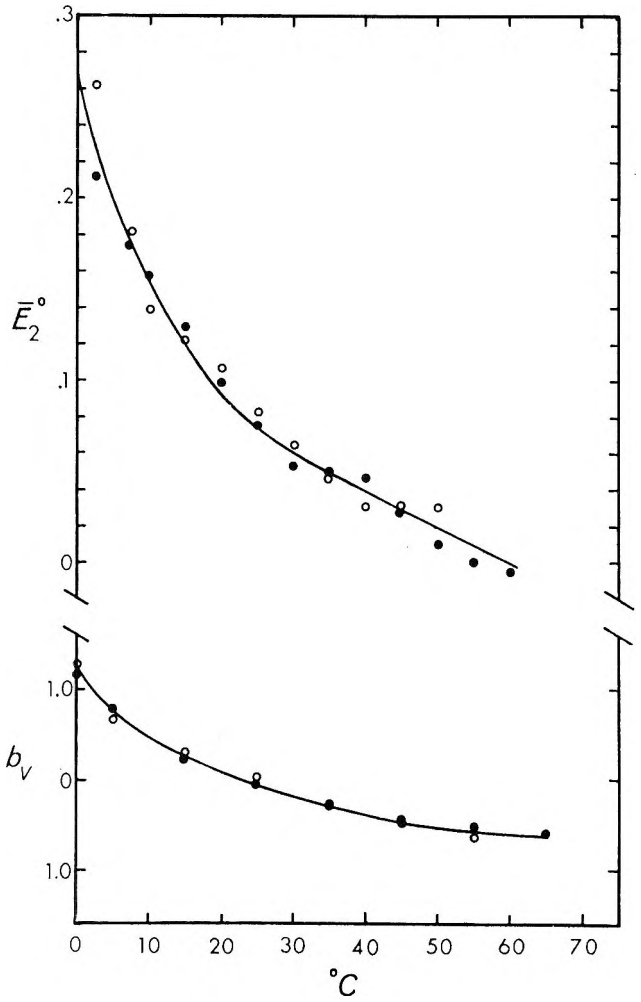

Figure 5. The partial molal expansibility, $E_2°$, of NaCl at infinite dilution and the deviation constant, b_V, plotted *vs.* temperature. (The open circles were calculated from our work and the closed circles were calculated from Dunn's work, Table II, and the curves were calculated by differentiating eq 10 and 12).

where $S_E = \partial S_V/\partial T$ and $b_E = \partial b_V/\partial T$. To aid in the calculation of ϕ_E from this equation, we have fit $\phi_V°$, S_V, and b_V to the equations

$$\bar{V}_2° = A + Bt + Ct^2 + Dt^3 + Et^4 \quad (10)$$

$$S_V = A' + B't + C't^2 + D't^3 \quad (11)$$

$$b_V = A'' + B''t + C''t^2 \quad (12)$$

where $A = 12.901$, $B = 2.6597 \times 10^{-1}$, $C = -6.7854 \times 10^{-3}$, $D = 9.8371 \times 10^{-5}$, $E = -5.9778 \times 10^{-7}$ (with an rms of 0.05 ml/mol); $A' = 1.4447$, $B' = 1.6799 \times 10^{-2}$, $C' = -8.4055 \times 10^{-5}$,[6] $D' = 5.5153 \times 10^{-7}$ (with an rms of 0.0005 ml mol$^{-3/2}$ l.); and $A'' = 1.144$, $B'' = -5.300 \times 10^{-2}$, $C'' = 4.163 \times 10^{-4}$ (with an rms of 0.1 ml mol^{-2} l.). By differentiating these equations with respect to temperature combined with eq 9, we have calculated ϕ_E as a function of $\sqrt{c}$. The results are shown in Figure 4. At low temperatures ϕ_E shows large negative deviations from the limiting law; however, at high temperatures the deviations are small. Figure 5 shows a plot of $\bar{E}_2°$ and b_V as a function of temperature calculated by differentiating eq 10 with respect to temperature and from eq 12, as well as the results obtained directly from Table II. Our results for $\bar{E}_2°$ and b_V agree very well with the recent work of Dunn[17] over the entire temperature range.

An examination of $\bar{E}_2°$ and b_V of NaCl solutions as a function of temperature (Figure 5) indicates that both ion–water and ion–ion interactions are strongly dependent upon temperature. The positive values of $\bar{E}_2°$ and b_V at low temperatures appear to be a unique feature of aqueous solutions. At high temperatures both $\bar{E}_2°$ and b_V are negative as one might expect. ($\bar{E}_2°$ is negative in most other solvents[33,34] and $\bar{E}_2°$ should be negative according to the simple Born model for ion–solvent interactions[35] and b_V should be negative according to the extended Debye–Hückel limiting law). There appears to be a similarity in the effect of temperature on ion–ion and ion–water interactions.

Discussion of Results

The deviation of ϕ_V and $\bar{V}_2$ from the limiting law as a function of temperature cannot be explained by a simple extension of the Debye–Hückel interionic attraction theory (*i.e.*, including the ion-size parameter). The positive deviations from 0 to ~30° are, in fact, the opposite of what is predicted by the extended theory. If we assume that the extended limiting law (with a reasonable value for the ion-size parameter) can be used to describe the ideal concentration dependence of $\bar{V}_2$ in dilute solutions, we obtain positive deviations over the entire temperature range. We will now briefly examine the possible cause of this positive deviation.

At infinite dilution the Na^+ and Cl^- ions are far from each other, each interacting with the surrounding water molecules in its own unique way. The $\bar{V}°$ of Na^+ and Cl^- ions can be represented by three major components.[34-37]

$$\bar{V}°(\text{ion}) = \bar{V}°(\text{cryst}) + \bar{V}°(\text{elect}) + \bar{V}°(\text{disord}) \quad (13)$$

The effect of temperature on the $\bar{V}°$ of the Na^+ and Cl^- ions can be represented by two major components[35,36]

$$\bar{E}°(\text{ion}) = \bar{E}°(\text{elect}) + \bar{E}°(\text{disord}) \quad (14)$$

where (cryst) is the crystal partial molal component, (elect) is the electrostriction partial molal component and (disord) is the disordered or void space partial molal component. At low temperatures the disordered

(33) R. W. Gurney, "Ionic Processes in Solutions," McGraw-Hill Book Co., Inc., New York, N. Y., 1953.

(34) F. J. Millero, *J. Phys. Chem.*, **72**, 3209 (1968).

(35) F. J. Millero, *ibid.*, **72**, 4589 (1968).

(36) F. A. Millero in "A Treatise on Skin," Vol. I, R. H. Elden, Ed., Interscience Publishers, New York, N. Y., 1970, Chapter 11.

(37) F. J. Millero, *J. Phys. Chem.*, **73**, 2417 (1969).

partial molal component is the predominant factor and at high temperatures the electrostriction partial molal component is the predominant factor. The large temperature dependence of $\bar{E}^\circ$(ions) has been attributed to the effect of temperature on the outer hydrated water molecules, $\bar{E}^\circ$(disord).[35,36] Since $\bar{E}^\circ$(disord) appears to be related to the structure of the solvent,[35,36] it is not possible to state with certainty that the changes in $\bar{E}^\circ$(ion) are due to changes in ion–water or water–water interactions.

With an initial increase in salt concentration the interactions between the ions can be adequately represented by the Debye–Hückel interionic attraction theory. That is, the volume of the system will increase with increasing concentration as predicted by the limiting law. When the ions come close together, the hydrated water molecules begin to interact and deviations from the limiting law occur. Since the interactions between the hydrated ions are related to the magnitude of the ion–water interactions, the large temperature dependence of the deviations can be interpreted as being due to changes in the structure of the bulk water between the interacting ions or the structure of the hydrated interacting ions. For example, the large positive deviations at low temperatures can be attributed to the structure of water between the interacting ions being able to transmit the interactions, or the deviations can be attributed to interactions of the hydrated water molecules surrounding the interacting ions. These two effects are indistinguishable and both effects appear to be related to the structure of water.

There are three types of interactions to consider that can possibly cause the deviation from the limiting law; cation–cation, Na^+–Na^+, anion–anion, Cl^-–Cl^-, and cation–anion, Na^+–Cl^-. From the volume of mixing data of simple salt solutions[36,38-42] with a common cation and common anion at constant ionic strength, cation–cation and anion–anion interactions appear to be very small in dilute solutions. The volumes of mixing the simple salts HCl–NaCl, LiCl–NaCl, KCl–NaCl, and $NaClO_4$–NaCl[36,38-42] are all small and negative; thus, one might predict that the volume change due to cation–cation (Na^+–Na^+) and anion–anion (Cl^-–Cl^-) interactions would be negative and small in dilute NaCl solutions. By using the general rule describing structural hydration interactions, recently developed by Desnoyers, *et al.*,[43] we arrive at a similar conclusion. For the ions Na^+ and Cl^-, the incompatibility of the cospheres of Na^+–Na^+ and Cl^-–Cl^- ions results in a repulsion causing a decrease in volume and the compatibility of the co-spheres of Na^+–Cl^- ions results in an attraction causing an increase in volume.

Therefore, the positive deviations from the extended limiting law in the NaCl system appear to be due to cation–anion (Na^+–Cl^-) interactions. We can thus examine the positive deviations of the $\bar{V}_2$ from the extended limiting law by using Bjerrum's model for the formation of ion pairs.[44] The basic assumption of this approach is that the ion–ion interactions responsible for the deviations can be represented by the formation of cation–anion ion pairs. When the ion pair is formed, electrostricted water molecules would be released, thus causing the positive deviations from the extended limiting law.

Although some workers[4,45] have interpreted the activity and conductance data of NaCl solutions without considering ion pairing, the recent conductance work of Chiu and Fuoss[46] and the activity coefficient calculations of Eigen and Wicke[47] does indicate that ion pairing may be important. Thus, we will examine the $\bar{V}_2$ of NaCl solutions by assuming that the observed deviations are due to ion pairing.

The formation of the ion pair, $NaCl^\circ$, can be represented by the equation

$$Na^+ + Cl^- = NaCl^\circ \qquad (15)$$

The volume change for the formation of the ion pair, $\Delta\bar{V}$(ion pair), is given by

$$\Delta\bar{V}(\text{ion pair}) = \bar{V}(NaCl^\circ) - \bar{V}(Na^+) - \bar{V}(Cl^-) \qquad (16)$$

where ($\bar{V}NaCl^\circ$) is the partial molal volume of the ion pair and $\bar{V}(Na^+)$ and $\bar{V}(Cl^-)$ are the partial molal volumes of the free ions. The volume change for the formation of the ion-pair would be expected to be positive due to the individual ions releasing some or all of their electrostricted water when the ion pair is formed. By examining the positive deviations from the extended limiting law, it is possible to calculate the degree of association or the fraction of ions that are complexed, α, by the following techniques.

If we apply the additivity principle (Young's rule)[48] to the components of the salt mixture (Na^+, Cl^- and $NaCl^\circ$), we obtain

$$\bar{V}(\text{obsd}) = (1 - \alpha)\bar{V}(Na^+) + (1 - \alpha)\bar{V}(Cl^-) + \alpha\bar{V}(NaCl^\circ) \qquad (17)$$

(38) H. E. Wirth, *J. Amer. Chem. Soc.*, **59**, 2549 (1939); *J. Phys. Chem.*, **67**, 2339 (1963).

(39) H. E. Wirth and F. N. Collier, *J. Amer. Chem. Soc.*, **72**, 5292 (1950).

(40) H. E. Wirth, R. E. Lindstrom, and R. E. Johnson, *J. Phys. Chem.*, **67**, 2239 (1963).

(41) H. E. Wirth and W. L. Mills, *J. Chem. Eng. Data*, **13**, 102 (1968).

(42) H. E. Wirth and A. LoSurdo, *ibid.*, **13**, 226 (1968).

(43) J. E. Desnoyers, M. Arel, G. Perron, and C. Jolicoeur, *J. Phys. Chem.*, **73**, 3346 (1969).

(44) N. Bjerrum, *Kgl. Danske Videnskab. Selskab. Mat. Fys. Medd.*, (9), **7**, 1 (1929).

(45) C. W. Davies, "Ion Association," Butterworth and Co. Inc., Washington, D. C., 1962.

(46) Y. -Chech Chiu and R. M. Fuoss, *J. Phys. Chem.*, **72**, 4123 (1968).

(47) M. Eigen and E. Wicke, *ibid.*, **58**, 702 (1954).

(48) T. F. Young and M. B. Smith, *ibid.*, **58**, 716 (1954).

where α is the fraction of ions complexed, $(1 - \alpha)$ is the fraction of free ions, and $\bar{V}$(obsd) is the observed partial molal volume at total concentration c_T. If we solve for the fraction of complexed ions, α, we obtain

$$\alpha = \frac{\bar{V}(\text{obsd}) - \bar{V}(Na^+) - \bar{V}(Cl^-)}{\bar{V}(NaCl^\circ) - \bar{V}(Na^+) - \bar{V}(Cl^-)} \quad (18)$$

where $\bar{V}(Na^+) + \bar{V}(Cl^-)$ is the partial molal volume of the free ions. The numerator of this equation will be designated as $\Delta\bar{V}$(excess) to denote that it represents the change in volume over and above the extended Debye–Hückel limiting law (eq 5 minus eq 7). The denominator to this equation is equal to $\Delta\bar{V}$(ion pair) given by eq 16($\bar{V}$(ion pair) minus eq 7). Thus, we have

$$\alpha = \Delta\bar{V}(\text{excess})/\Delta\bar{V}(\text{ion-pair}) \quad (19)$$

Recently, various other workers[49-52] have used a similar equation to examine ion-pairing effects in aqueous solutions and earlier workers[4] have used these techniques in reverse to calculate the apparent molal volume of weak acids. The problem of using this equation to calculate the fraction of ions that are paired is associated with the lack of knowledge of $\bar{V}(NaCl^\circ)$ or $\Delta\bar{V}$(ion pair). If a contact ion pair is formed, one would expect $\bar{V}(NaCl^\circ)$ to be equal to the sum of the crystal volume including void space effects (*i.e.*, $\bar{V}$(cryst) + V(disord)); however, if a solvent-separated or outer sphere ion pair is formed, $\bar{V}(NaCl^\circ)$ will also have some electrostriction contributions and will be difficult to estimate.

By using the simple model for the components of $\bar{V}^\circ$(ions) at infinite dilution (eq 13), we can estimate $\bar{V}(NaCl^\circ)$ for the contact ion pair from the sums of $\bar{V}^\circ$(cryst) + $\bar{V}^\circ$(disord) for the Na^+ and Cl^- ions. Using the semiempirical equations[53,54]

$$\bar{V}^\circ(\text{int}) + \bar{V}^\circ(\text{disord}) = 4.48r^3 \quad (20)$$

$$\bar{V}^\circ(\text{int}) + \bar{V}^\circ(\text{disord}) = 2.52r^3 + 3.14r^2 \quad (21)$$

for the ions (where r is the crystal radius), we obtain, respectively, $\bar{V}^\circ(NaCl^\circ)$ = 30.4 and 30.2 ml/mol at 25°.

Using $\bar{V}(NaCl^\circ)$ = 30.3 ml/mol and assuming that it is independent of concentration and temperature, we have estimated $\Delta\bar{V}$(ion pair) from 0.25 to 1.0c at 0, 25, and 55°. Combining these values with $\Delta\bar{V}$(excess) taken from Figures 1, 2, and 3, we have calculated the fraction of ions complexed, α, using eq 18 (by an iterative method). The resulting α's are given in Table III at various temperatures and concentrations. The stoichiometric association constants, K_A^*, given by the equation

$$K_A^* = (NaCl^\circ)/(Na^+)(Cl^-) = \alpha/(1 - \alpha)^2 c_T \quad (22)$$

were also calculated and the results are given in Table III. Since the stoichiometric constants do not vary strongly with concentration or ionic strength, the average K_A^* can be equated with the thermodynamic association constant, K_A (*i.e.*, within experimental error). We obtain $K_A^* = K_A = 0.35 \pm 0.03$, 0.18 ± 0.01, and 0.11 ± 0.01 l/mol, respectively, at 0, 25, and 55°. These results can be compared to $K_A = 0.92$ at 25° obtained by Chiu and Fuoss (using $\hat{a} = 6.11$ Å), $K_A = 0.16$ at 20° obtained by Eigen and Wicke[47] (using $\hat{a} = 5.0$ Å) and $K_A = -0.26$ at 100° obtained by Dunn and Marshall.[55] From the best straight line through $\log K_A^*$ *vs.* $1/T$, we obtain the heat of association of the ion pair, $\Delta H_A = -0.8 \pm 0.3$ kcal/mol. Due to the large number of assumptions made in these calculations, the results should be considered with some reservations.[56] The calculations do show that ion pairing can be used to explain the positive deviations from the extended limiting law within experimental error.

Table III: Calculations of the Stoichiometric Association Constant For NaCl Solutions at Various Temperatures

c_T	$\alpha \times 100$ 0°	25°	55°	K_A^* 0°	25°	55°
0.25	6.8	4.4	3.6	0.31	0.19	0.15
0.36	9.4	6.0	4.5	0.32	0.19	0.14
0.49	12.4	7.0	5.4	0.33	0.19	0.12
0.64	15.8	9.5	6.2	0.35	0.18	0.11
0.81	19.6	11.4	6.9	0.37	0.18	0.10
1.00	23.8	13.3	7.4	0.41	0.17	0.09
			Av	0.35 ± 0.03	0.18 ± 0.01	0.11 ± 0.01

In future work, we plan to use the general techniques described in this paper to examine ion-pair formation in salt systems where this type of ion–ion interaction is the dominant effect as adjudged from other physical measurements.

Acknowledgment. The author wishes to thank Col. Jonathan Knox for making the density measurements, Dr. F. Vaslow, Dr. J. E. Desnoyers, and coworkers for making their manuscript available prior to publication, and Dr. Lawrence Dunn and Dr. W. L. Marshall for their comments. The author wishes to acknowledge the support of the Office of Naval Research (Contract NONR 4008(02)) and the National Science Foundation (GA-17386) for this study.

(49) T. G. Spiro, A. Revesz and J. Lee, *J. Amer. Chem. Soc.*, **90**, 4000 (1968).

(50) H. E. Wirth, *J. Phys. Chem.*, **71**, 1922 (1967).

(51) R. E. Lindstrom and H. E. Wirth, *ibid.*, **73**, 218 (1969).

(52) F. J. Millero, *Limnol. Oceanogr.*, **14**, 376 (1969).

(53) P. Murkerjee, *J. Phys. Chem.*, **65**, 744 (1961).

(54) B. E. Conway, R. E. Verrall, and J. E. Desnoyers, *Z. Phys. Chem.*, **230**, 157 (1965).

(55) L. A. Dunn and W. L. Marshall, *J. Phys. Chem.*, **73**, 2619 (1969). It should be noted that a plot of our K_A^* values and the value at 100° from this study is a linear function of temperature (within experimental error).

(56) Since the numerical value for K_A depends upon the ion-size parameter used, the K_A results obtained by various experimental techniques may vary significantly. Thus, the agreement of our K_A values with those obtained by other workers is as well as can be expected. Personal communication, R. M. Fuoss, 1969.

Apparent Molar Volumes and Temperatures of Maximum Density of Dilute Aqueous Sucrose Solutions

by John E. Garrod and Thelma M. Herrington

Department of Chemistry, The University, Reading, Berkshire, England *(Received June 9, 1969)*

Apparent molar volumes for solutions of sucrose and water are determined over a large range of concentration using both pycnometric and dilatometric techniques. The temperatures of maximum density of dilute sucrose solutions are found. For the interaction between sucrose and water, a rigid particle model combined with an attractive square-well potential is assumed. On this model the attraction between sucrose and water increases with temperature. It is also shown that a solution of sucrose and water cannot be considered to be "semiideal dilute" since a necessary criterion between the activity coefficients is not satisfied.

There has been considerable interest recently[1] in the effect of hydrogen-bonding solutes on the temperature of maximum density of water. Whether a solute raises or lowers the temperature of maximum density depends on the rate of change of the solute–solvent intermolecular forces with temperature. The partial molar volume of the solute at infinite dilution is a measure of these intermolecular forces. Sucrose was chosen as its behavior should be typical of a solute which hydrogen bonds with water. The apparent molar volumes of dilute sucrose solutions were determined so that accurate extrapolation to infinite dilution could be made. Previous density measurements[2] on sucrose solutions were carried out on solutions too concentrated to allow an accurate extrapolation. The dependence of the lowering of the temperature of maximum density of water on the molality of the solute is directly related to the rate of change with temperature of the partial molar volume of the solute. Our results were compared with previous measurements of the temperature of maximum density of sucrose solutions;[3] good agreement was obtained between our own measurements of the temperature of maximum density of dilute sucrose solutions and the temperature dependence of the partial molar volume of sucrose.

Theory

The apparent molar volume, ${}^{\phi}V$, is defined by

$$ {}^{\phi}V = (V - n_1\bar{V}_1^{\circ})/n_2 \qquad (T \text{ constant}) \qquad (1) $$

where V is the total volume of the solution, $\bar{V}_1^{\circ}$, is the molar volume of pure solvent and n_1 and n_2 are the number of moles of solvent and solute respectively. In principle, ${}^{\phi}V$ can be determined from density measurements; the appropriate equation is

$$ {}^{\phi}V = \left\{\frac{1000 + mM_2}{\rho} - \frac{1000}{\rho_1^{\circ}}\right\} \Big/ m \qquad (2) $$

where m is the molality of the solution, M_2 is the molar mass of solute, ρ_1° is the density of pure solvent, and ρ is that of the solution. For a 1 m solution, the error in molality, δm, must be $\sim 10^{-4}$ mol kg^{-1} and $\delta(\rho_1^{\circ} - \rho)$, $\sim 10^{-5}$ g cm^{-3} to give an accuracy of 0.01 cm^3 in ${}^{\phi}V$, whereas, for a 0.1 m solution, δm must be $\sim 10^{-5}$ mol kg^{-1} and $\delta(\rho_1^{\circ} - \rho)$, $\sim 10^{-6}$ g cm^{-3} for the same accuracy in ${}^{\phi}V$. Thus, at concentrations greater than 0.5 m, density determinations with an Ostwald pycnometer give ${}^{\phi}V$ with sufficient accuracy, but at lower concentrations another method must be used.

Consider mixing a small volume of a concentrated solution containing n_2 moles of solute and of apparent molar volume ${}^{\phi}V_{\text{Init.}}$ with a much larger volume of pure solvent; then the apparent molar volume of the resulting solution is given by

$$ {}^{\phi}V_{\text{Final}} = {}^{\phi}V_{\text{Init.}} + \Delta V/n_2 \qquad (3) $$

where ΔV is the volume change on mixing. Thus, if ${}^{\phi}V_{\text{Init.}}$ is known with an accuracy of 0.01 cm^3 mol^{-1} from pycnometer densities, and $\Delta V/n_2$ can be determined with a similar accuracy, ${}^{\phi}V_{\text{Final}}$ is known to ± 0.02 cm^3 mol^{-1} in the final dilute solution.

Experimental Section

Materials. The sucrose was supplied by the research department of Tate and Lyle, Ltd. It was dried in a vacuum oven at 60° before use. The conductivity water used for preparing the solutions was made by passing distilled water through a cation–anion exchange resin: the specific conductance was 5×10^{-8} ohm^{-1} cm^{-1}. As a further check on any impurities, a large sample (approximately 1000 g) was evaporated slowly to dryness; it was found that any nonionic impurities present were less than one part in 10^6.

(1) F. Franks and H. T. Smith, *Trans. Faraday Soc.*, **64**, 2962 (1968); F. Franks and B. Watson, *ibid.*, **63**, 329 (1967).

(2) I. F. Schneider, D. Schliepake, and A. Klimmek, *Zucker*, **16**, 17 (1963).

(3) G. Wada and S. Umeda, *Bull. Chem. Soc. Jap.*, **35**, 646 (1962).

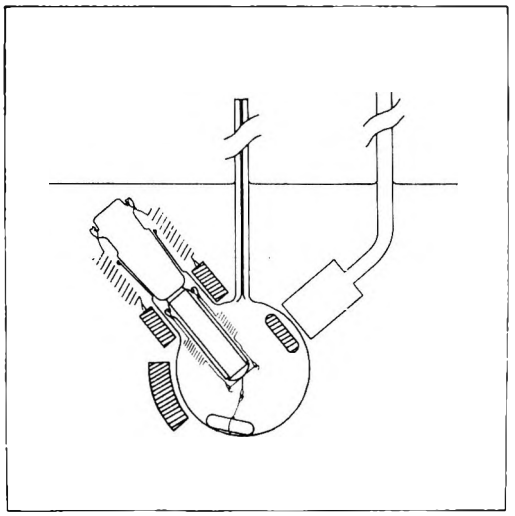

Figure 1. The dilatometer (not to scale).

The conductivity water was outgassed on a water pump and then further degassed by keeping at 10° above thermostat temperature for several hours for the measurements at 25°.

Apparatus. The thermostat used was an insulated copper tank containing 220 l. of demineralized water; a plate glass window was mounted in one side of the tank so that manipulation of the contents of the dilatometer could be readily observed. The tank was thoroughly stirred and its temperature controlled by a mercury–decane regulator. For measurements below room temperature, chilled water was passed through a coil immersed in the tank. The temperature of the tank was determined with an N.P.L. certified platinum resistance thermometer and a transformer ratio bridge to ±0.001°.

Ostwald–Sprengel type pycnometers made of Pyrex glass, of volume 25 cm³ and with 0.1-cm diameter capillary tubing were used to determine the densities of the concentrated sucrose solutions. Duplicate density determinations agreed to $\pm 1 \times 10^{-5}$ g cm^{-3}.

The dilatometer illustrated in Figure 1 is similar in construction to that described by Hepler, Stokes, and Stokes.[4] It is essentially a large flask of known volume with a precision bore capillary tube attached which can be mounted vertically in the thermostat. Changes in volume of the contents of the dilatometer are observed by measuring the height of liquid in the capillary tube with a cathetometer. A glass tube joined to the stopper of the flask forms part of a capsule to hold the concentrated solution. The glass lid of the capsule, shaped like a plano-convex lens, is a ground fit; it is lightly greased with stopcock grease, or pure petroleum jelly for the lowest temperatures, and held in place with light springs. The same capsule of volume 11 cm³ was used throughout but two sizes of flask were used; flask A was of volume 1100 cm³ with a 0.075-cm diameter capillary and flask B was 250 cm³ with a 0.15-cm capillary. Flask A was used for a final concentration of less than 2×10^{-2} *m* and flask B from 2×10^{-2} to 1×10^{-1} *m*.

To determine $\Delta V/n_2$ to 0.01 cm³ mol^{-1}, δn_2 must be $\sim 10^{-5}$ mol and $\delta \Delta V$ known to one part in 10^7 for an initial 1 *m* solution and a change in meniscus height of 10 cm. To have an error in δn_2 of $\pm 10^{-5}$ mol, the number of moles in one cubic centimeter of the initial solution must be known to $\pm 10^{-6}$ and the capsule volume to ±0.01 cm³. The total volume of the flask is only required to calculate the final molality of the dilute solution; it was in fact determined to ±0.1 cm³.

Technique

All solutions were used within 3 days of making up, as it was found that in certain samples biological action could be observed within 2 weeks (see also Robinson and Stokes[5]). The capsule of the dilatometer was filled with a concentrated solution of known density at thermostat temperature and inserted into the flask filled with degassed conductivity water also at thermostat temperature (for water, $(\partial p/\partial T)_V \simeq 4$ atm °K^{-1}). The dilatometer was then carefully checked for entrapped air bubbles and left to equilibrate in the thermostat; a magnetic stirrer was used to speed up the attainment of equilibrium. After about 30 min, the level of the meniscus was observed every 5 min until it was constant to ±0.001 cm for two consecutive readings. This took about 1 or 2 hr, depending on the temperature. The capsule lid was then slid off by pulling on the attached Teflon encased magnet with a powerful permanent magnet adjacent to the outside of the flask. The solution was stirred to mix thoroughly. Observations of the meniscus height were taken as before until two consecutive readings agreed to ±0.001 cm; this was achieved within about 1 hr of mixing. Lines etched on the capillary tube were used to check that no movement of the dilatometer assembly occurred.

A volume change of one part in 10^8 was detectable with the large dilatometer, and one part in 10^7 with the small dilatometer. However, a volume change of one part in 10^7 is equivalent to a change in the average temperature of the thermostat of 5×10^{-4}°, a change in room temperature of 10°(0.5°) or a change in atmospheric pressure of 133 N m^{-2}. Except on days of very rapidly changing barometric pressure, these conditions were easily satisfied for the time of 1 hr taken in complete mixing.

The principal sources of error were (a) the change in pressure due to changes in the hydrostatic head of

(4) L. G. Hepler, J. M. Stokes, and R. H. Stokes, *Trans. Faraday Soc.*, 61, 20 (1965).

(5) R. A. Robinson and R. H. Stokes, *J. Phys. Chem.*, 65, 1954 (1961).

liquid in the capillary and (b) the change in temperature of the liquid displaced from the flask into the capillary. In (a) a change in height of 1 cm of liquid in the capillary is theoretically equivalent to a volume change of 1 part in 10^7. The maximum change in height observed was 10 cm. The effect of pressure on the meniscus height was determined experimentally and was in fact found to be about 3 parts in 10^8 for a 1 cm change in meniscus height. Calibration curves were plotted for both flasks and appropriate corrections applied. For (b) a difference between room temperature and thermostat temperature of 15° corresponds to a volume change of 5 parts in 10^8 for a change in meniscus height of 10 cm (0.5 cm); a correction was applied.

Temperature of Maximum Density. The temperature of maximum density of each dilute sucrose solution left in the dilatometer after mixing at 5° was found by measuring the change in meniscus height with temperature. The temperature of the thermostat was regulated to within ±0.001°; temperature differences were determined to ±0.01° using a 6° Beckmann thermometer calibrated at 5°C against the N.P.L. certified platinum resistance thermometer. Measurements of meniscus height were made with a cathetometer to ±0.001 cm at 0.2° intervals with ±1.5° of the temperature corresponding to the minimum in meniscus height, θ_m(observed). The dilatometer attained thermal equilibrium with the thermostat within 0.5 hr of a temperature change; readings of meniscus height were taken every few minutes until two consecutive readings agreed to ±0.001 cm. The plot of meniscus height *vs.* temperature was approximately symmetrical (parabolic) about θ_m(observed) for each solution.

The temperature, θ_m(observed), corresponding to the minimum in meniscus height is not the true temperature of maximum density of that solution because of the thermal expansion of the dilatometer itself. Each dilatometer was calibrated by doing a run using pure water ($\theta_m = 3.98°$) and the true temperature of maximum density of each solution determined as explained below. The values of θ_m are estimated to be accurate to ±0.04°. The fact that the emergent stem of the dilatometer was at room temperature was calculated to affect θ_m by less than 0.001°(0.02°).

Now the measured volume change is equal to the expansion of the liquid of volume V less the expansion of the Pyrex glass dilatometer, so that

$$A\,dh \simeq dV - dV_g \qquad (4)$$

where A is the cross-sectional area of the capillary, V_g is the volume of the vessel, and V is the volume of solution. If we write

$$V_g = V_g^\circ[1 + \alpha_g\theta] \qquad (5)$$

and

$$V = V^*[1 + \alpha(\theta - \theta_m)^2] \qquad (6)$$

where θ is the temperature, θ_m is the true temperature of maximum density of the solution, V^* is the volume of solution at θ_m, α_g is the coefficient of expansion of the glass vessel, and α the coefficient of expansion of the solution, then

$$dh/d\theta = K + 2V^*\alpha(\theta - \theta_m)/A \qquad (7)$$

where $K = -V_g^\circ\alpha_g/A$ and is a constant for the particular vessel.

Accordingly, if $\Delta h/\Delta\theta$ is plotted against θ for pure water then K is equal to the value of $\Delta h/\Delta\theta$ at $\theta = 3.98°$. For each solution $\Delta h/\Delta\theta$ is then plotted against θ and when $\Delta h/\Delta\theta$ is equal to K then $\theta = \theta_m$ for that solution.

The temperature of maximum density could have been obtained by plotting h against θ and then correcting θ_m(observed) by the difference [θ_m(observed) − θ_m] of pure water for that dilatometer; however, this assumes that the coefficient of expansion of the solution is equal to that of water.

Results

Determinations of the densities of the concentrated solutions were made at 5, 15, and 25°. The pycnometers were calibrated with conductance water immediately after a density measurement; buoyancy corrections were applied to the masses. Densities for the concentrated solutions are given in Table I. Values for the density of water were taken from the compilation of Tilton and Taylor.[6] Values for the apparent molar volumes were calculated at these molalities; these values were plotted together with values at other molalities calculated from data in the literature and the results smoothed graphically to give the apparent molar volumes recorded in Table I as $^\phi V_{\text{initial smoothed}}$. Values for the apparent molar volume were calculated at 25° and 15° from the density data of Schneider,[2] at 25° from the data of Mantovani and Indelli,[7] and at 5° from extrapolation of Plato's data.[8] The values of the apparent molar volume and molality obtained on diluting the concentrated solution in the dilatometer are recorded in Table I as $^\phi V_{\text{Final}}$ and final molality. The smoothed values of the initial apparent molar volumes were used in calculating the apparent molar volumes of the dilute solutions.

The apparent molar volumes at each temperature

(6) L. W. Tilton and J. K. Taylor, *J. Res. Nat. Bur. Stand.* **18**, 205 (1937).

(7) G. Mantovani and A. Indelli, *International Sugar Journal*, **68**, 104 (1966).

(8) F. Plato, *Kaiserlichen-Normal-Eichungs Kommision, Wiss. Abh.* 2, 153 (1900). F. T. Bates, "Polarimetry and Saccharimetry of the sugars," National Bureau of Standards Circular 440, U. S. Government Printing Office, Washington, D. C.

Table I: Densities and Apparent Molar Volumes of Sucrose Solutions

$10^2 \times$ mass fraction of sucrose	Density/ g cm^{-3}	Initial molality/ mol kg^{-1}	$^{\phi}V_{\text{Initial smoothed}}$/ cm^3 mol^{-1}	$10^2 \times$ Final molality/ mol kg^{-1}	V_{Final}/ cm^3 mol^{-1}
		5.00°			
Water	0.999964				
24.836	1.10693	0.9653	209.16	0.759	207.60
39.748	1.18078	1.9272	210.52	1.296	207.64
48.117	1.22555	2.7093	211.41	6.465	207.72
52.683	1.25100	3.2527	211.93	1.820	207.68
54.623	1.26231	3.5166	212.18	7.558	207.80
		15.00°			
Water	0.999101				
24.536	1.10310	0.9498	211.19	0.747	209.96
27.074	1.11484	1.0846	211.36	3.306	210.04
36.437	1.16019	1.6747	212.02	1.167	209.98
37.412	1.16513	1.7462	212.10	4.775	210.05
48.091	1.22141	2.7065	213.01	6.433	210.03
48.265	1.22263	2.7254	213.02	1.628	209.97
54.900	1.25968	3.5563	213.69	7.572	210.10
		25.00°			
Water	0.997047				
13.082	1.04961	0.4397	212.04	0.379	211.43
15.670	1.10606	0.5428	212.16	0.458	211.50
16.913	1.06589	0.5947	212.23	0.497	211.48
24.713	1.10047	0.9589	212.66	0.750	211.49
28.404	1.11757	1.1590	212.89	0.875	211.52
51.433	1.23516	3.0938	214.60	6.955	211.61
55.372	1.25726	3.6247	214.97	1.920	211.54

Table II: Sucrose: Coefficients of the Polynomial

$$^{\phi}V = V_2^{\ominus} + RT\left\{\frac{1}{2}A'm + \frac{1}{3}B\dagger' m^2 + \frac{1}{4}C\dagger' m^3 + \frac{1}{5}D\dagger' m^4\right\}$$

T/°C	$\bar{V}_2^{\ominus}$ cm^3 mol^{-1}	$A' \times 10^4$/ kg mol^{-1} atm^{-1}	$B\dagger' \times 10^6$/ kg^2 mol^{-2} atm^{-1}	$C\dagger' \times 10^6$/ kg^3 mol^{-3} atm^{-1}	$D\dagger' \times 10^8$/ kg^4 mol^{-4} atm^{-1}
5.00	207.62	1.752	−5.61	20.18	−3.16
15.00	209.97	1.166	−1.13	−0.20	
25.00	211.49	1.107	−1.64	1.15	

were fitted by least squares to a polynomial in the molality. The best fitting polynomial was found using the null hypothesis, *i.e.*, the polynomial is assumed to be the best fit which gives the minimum value of $\delta_p^2/(n-p-1)$, where δ_p^2 is the sum of the squares of the deviations, n the number of points, and p the degree of the polynomial. If we write (see later)

$$^{\phi}V = \bar{V}_2^{\ominus} + RT\left\{\frac{1}{2}A'm + \frac{1}{3}B\dagger' m^2 + \frac{1}{4}C\dagger' m^3 + \frac{1}{5}D\dagger' m^4 + \ldots\right\} \quad (8)$$

where $\bar{V}_2^{\ominus}$ is the partial molar volume of sucrose at infinite dilution, T the absolute temperature, and m the molality, then the coefficients of the best fitting polynomial are given in Table II. The pycnometric data were given twice the weighing of the dilatometric data. (The results were compared with calculations giving the data equal weighting: the value of $\bar{V}_2^{\ominus}$ was not affected; A' was altered by 2% and the higher coefficients by rather more). The degree of the polynomial did not affect $\bar{V}_2^{\ominus}$, but A' was affected by 5%.

Table III: Temperature of Maximum Density of Sucrose Solutions

$10^2 \times$ Molality/ mol kg^{-1}	θ_m/ °C	$\Delta\theta_m$/ °K
Water	(3.98)	
0.759	3.84	−0.14
1.296	3.70	−0.28
3.464	3.46	−0.52
4.965	3.16	−0.82
6.465	2.92	−1.06
7.558	2.68	−1.30

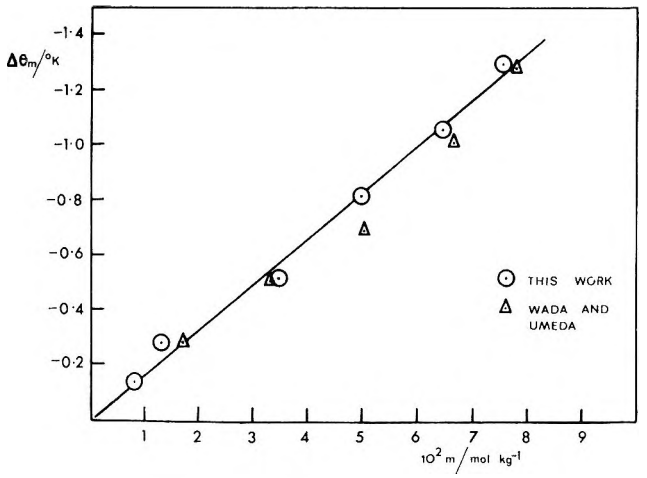

Figure 2. Lowering of the temperature of maximum density of water by sucrose at low values of the molality.

The change in the temperature of maximum density of water produced by a solute is defined by

$$\Delta\theta_m/°C = \theta_m/°C - 3.98 \quad (9)$$

The observed values of θ_m and $\Delta\theta_m$ for dilute sucrose solutions are given in Table III. The data are plotted in Figure 2 together with data obtained by Wada and Umeda.[3]

Discussion

(*i*) *Partial Molar Volumes.* Let us write for the Gibbs energy of a solution of mole ratio $\bar{m}$[9,10]

$$G/N_1kT = \mu_1°/kT + \bar{m}\mu_2^{\ominus}/kT - \bar{m} + \ln \bar{m} + \frac{1}{2}A_{22}\bar{m}^2 + \frac{1}{3}B_{222}\bar{m}^3 + \frac{1}{4}C_{2222}\bar{m}^4 + \frac{1}{5}D_{22222}\bar{m}^5 + \ldots \quad (10)$$

where $\bar{m} = N_2/N_1$ (N_1 and N_2 are the number of molecules of solvent and solute, respectively) and the coefficients A_{22} etc. are functions of temperature and pressure only. Then for the partial molecular volume of the solvent

$$\bar{v}_1 = \bar{v}_1° - kT\left\{\frac{1}{2}\left(\frac{\partial A_{22}}{\partial p}\right)_T\bar{m}^2 + \frac{2}{3}\left(\frac{\partial B_{222}}{\partial p}\right)_T\bar{m}^3 + \frac{3}{4}\left(\frac{\partial C_{2222}}{\partial p}\right)_T\bar{m}^4 + \frac{4}{5}\left(\frac{\partial D_{22222}}{\partial p}\right)_T\bar{m}^5 + \ldots\right\} \quad (11)$$

where $\bar{v}_1°$ is the molecular volume of pure solvent, and for the solute

$$\bar{v}_2 = \bar{v}_2^{\ominus} + kT\left\{\left(\frac{\partial A_{22}}{\partial p}\right)_T\bar{m} + \left(\frac{\partial B_{222}}{\partial p}\right)_T\bar{m}^2 + \left(\frac{\partial C_{2222}}{\partial p}\right)_T\bar{m}^3 + \left(\frac{\partial D_{22222}}{\partial p}\right)_T\bar{m}^4 \ldots\right\} \quad (12)$$

where $\bar{v}_2^{\ominus}$ is the partial molecular volume of the solute at infinite dilution. Thus the total volume, V, of the solution is given by

$$V/N_1 = \bar{v}_1° + m\bar{v}_2^{\ominus} + kT\left\{\frac{1}{2}A_{22}'m^2 + \frac{1}{3}B'_{222}m^3 + \frac{1}{4}C_{2222}'m^4 + \frac{1}{5}D'_{22222}m^5 + \ldots\right\} \quad (13)$$

where the dash represents differentiation with respect to pressure, and the apparent molar volume is given by

$${}^{\phi}V = \bar{V}_2^{\ominus} + RT\left\{\frac{1}{2}A'm + \frac{1}{3}B'm^2 + \frac{1}{4}C'm^3 + \frac{1}{5}D'm^4 + \ldots\right\} \quad (14)$$

where m is now the molality, $\bar{V}_2^{\ominus}$ the partial molar volume of the solute at infinite dilution, and $A' = (1000/M_1)^2A_{22}'$, $B' = (1000/M_1)^3B_{222}'$ etc. (M_1 is the molar mass of solvent.)

According to the theory of McMillan and Mayer,[11] for a solution of a solute in a solvent the osmotic pressure, Π, is given by

$$\Pi/kT = \rho + B_{22}{}^*\rho^2 + B_{222}{}^*\rho^3 + \ldots \quad (15)$$

where ρ is the number density of the solute. Hill[12] has shown that the coefficients A_{22} etc., may be related to the coefficients $B_{22}{}^*$ etc. For example

$$A_{22}\bar{v}_1° = 2B_{22}{}^{*\circ} - \bar{v}_2^{\ominus} + b_{11}° \quad (16)$$

where $B_{22}{}^{*\circ} = b_{02}°$; $b_{02}°$ is the cluster integral for two molecules of solute in pure solvent and $b_{11}°$ is the cluster integral for one molecule of solute and one of solvent in pure solvent. In relating coefficients higher than A_{22} (*i.e.*, B_{222} etc.) to the coefficients $B^{*\circ}$, it must be remembered that these equations are only applicable in dilute solutions when $\gamma - 1 \simeq \ln\gamma$; in more concentrated solutions

$$\ln\gamma = A_{22}m + B\dagger m^2 + \ldots \quad (17)$$

$$B\dagger = B_{222} - \tfrac{1}{2}A_{22}{}^2 \text{ etc.} \quad (18)$$

Thus, instead of eq 14 in general we write

$${}^{\phi}V = \bar{V}_2^{\ominus} + RT\left\{\frac{1}{2}A'm + \frac{1}{3}B\dagger'm^2 + \frac{1}{4}C\dagger'm^3 + \frac{1}{5}D\dagger'm^4 + \ldots\right\} \quad (8)$$

It is preferable to determine the coefficients A' etc., from the functional dependence of the apparent molar

(9) T. L. Hill, *J. Amer. Chem. Soc.*, 79, 4885 (1957).

(10) J. E. Garrod and T. M. Herrington, *J. Phys. Chem.*, 73, 1877 (1969).

(11) W. G. McMillan and J E. Mayer, *J. Chem. Phys.*, 13, 276 (1945).

(12) T. L. Hill, *J. Chem. Phys.*, 30, 93 (1959).

volume on the molality rather than that of the molar volume as it can be seen from eq 8 and 13 that the polynomial is of lower degree.

Stigter[13] has used eq 16 together with activity coefficient[14] and osmotic pressure[15] data on sucrose solutions to evaluate b_{11}°. He finds $N_0 b_{11}^\circ = -257$ cm^3 mol^{-1}. Now, according to Garrod and Herrington[10] eq 69

$$b_{11}^\circ = -\bar{v}_2^\infty + kT\kappa \tag{19}$$

where κ is the isothermal compressibility of the solvent. Values for $N_A B_{11}^{*\circ}$ for sucrose and water calculated from our values for $\bar{v}_2^\infty$ are given in Table IV. Compressibility data for water were taken from Peña and McGlashan.[16] The magnitude of $N_0 B_{11}^{*\circ}$ increases slightly with temperature.

We can consider $B_{11}^{*\circ}$ as being composed of an attractive and a repulsive contribution from the intermolecular forces. Now

$$B_{11}^{*\circ} = 4\pi \int_0^\infty (1 - e^{-\omega^{11}/kT}) r^2 \, dr \tag{20}$$

where ω^{11} is the potential of average force between one molecule of solute and one of solvent in the pure solvent, including averaging of the force over all rotational coordinates. Let R_{12} be the distance of closest approach between the centers of two molecules; then

$$B_{11}^{*\circ} = 4\pi \int_0^{R_{12}} (1 - e^{-\omega^{11}/kT}) r^2 dr + 4\pi \int_{R_{12}}^\infty (1 - e^{-\omega^{11}/kT}) r^2 dr = S + \phi \tag{21}$$

where S is the repulsive and ϕ the attractive contribution. The signs of the integrals can be obtained from considerations of the magnitude of ω^{11}. In the region $0 < r < R_{12}$, ω^{11} is mostly positive and very much greater than kT, so that S is positive. For $R_{12} < r < \infty$, ω^{11} is negative and comparable with kT so that ϕ is negative. Thus the sign and magnitude of $B_{11}^{*\circ}$ depend on the relative magnitudes of S and ϕ.

For two hard spheres $B_{11}^{*\circ}$ is given [17] by

$$B_{11}^{*\circ} = \frac{\pi}{6} (R_1 + R_2)^3 \tag{22}$$

where R_1 and R_2 are the diameters of the spheres. Isihara[18] has evaluated $B_{22}^{*\circ}$ for noninteracting rigid ellipsoids; he finds that

$$B_{22}^{*\circ} = f(4v_2) \tag{23}$$

where v_2 denotes the particle volume and f is equal to unity for a sphere but increases when the particles become more asymmetrical. If we take formulas 2, 4, and 21 from his paper and remember that $B_{11}^{*\circ}$ must reduce to the case of two hard spheres when the eccentricity, $\epsilon = 0$, then for a hard sphere of radius a_1 and a hard prolate ellipsoid with long axis $2b_2$ and short axis $2a_2$

$$B_{11}^{*\circ} = \frac{4}{3}\pi a_1^3 + \frac{4}{3}\pi a_2^2 b_2 + 2\pi a_1 b_2 \left[a_2 \left\{ (1 - \epsilon^2)^{1/2} + \frac{\sin^{-1}\epsilon}{\epsilon} \right\} + a_1 \left(1 + \frac{1 - \epsilon^2}{2\epsilon} \ln \frac{1 + \epsilon}{1 - \epsilon} \right) \right] \tag{24}$$

where $\epsilon^2 = (b_2^2 - a_2^2)/b_2^2$.

A model of sucrose was constructed using Corey–Pauling models and taking into account crystallographic data[19] which showed that there are two H bond linkages between the pyranose and furanose rings. The molecule may be approximated by a prolate ellipsoid with semiaxes 5.9 Å and 3.5 Å. The water molecule was assumed to be a sphere of radius 1.52 Å. It was found that for a rigid sucrose and water molecule

$$S = 588 \pm 5 \text{ cm}^3 \text{ mol}^{-1}$$

This may be compared with Stigter's[12] values of 655 cm^3 mol^{-1}; he used values of $\bar{v}_2^\infty$ for sucrose to calculate values of a_2 and b_2. Thus at 25°, the attractive contribution to $B_{11}^{*\circ}$ is given by

$$N_A \phi = N_A B_{11}^{*\circ} - N_A S = -378 \text{ cm}^3 \text{ mol}^{-1}$$

A very approximate estimate of the effect of hydrogen bonding on the attractive part of $B_{11}^{*\circ}$ may be made by considering the sucrose molecule to be a right angled parallelepiped surrounded by a square-well potential. Then

$$\phi = 2 \int_{a_2}^{D + a_2} \int_{a_2}^{D + a_2} \int_{b_2}^{D + b_2} (1 - e^{-\omega^{11}/kT}) dx dy dz \tag{25}$$

where D is the width of the well. ω^{11} is taken *arbitrarily* to be -4.0 kcal mol^{-1} at 25°; this is the mean of the values given for the enthalpy of formation of the H bond in methanol and in water by Pimentel and McClellan.[20] D is found to be 0.72 Å, which is a reasonable figure for atomic vibrations in the O–H ··· O bond. The absolute magnitude of ϕ decreases slightly with increasing temperature (Table IVA), assuming that the rigid particle contribution to $B_{11}^{*\circ}$ is unchanged. If we assume that D is constant then ω^{11} decreases with decreasing temperature,

(13) D. Stigter, *J. Phys. Chem.*, **64**, 118 (1960).

(14) G. Scatchard, W. J. Hamer, and S. E. Wood, *J. Amer. Chem. Soc.*, **60**, 3061 (1938); R. A. Robinson and D. A. Sinclair, *ibid.*, **56**, 1830 (1934).

(15) H. N. Morse, *Publ. Carnegie Inst. Wash.*, 198 (1914).

(16) M. Diaz Peña and M. L. McGlashan, *Trans. Faraday Soc.*, **55**, 2018 (1959).

(17) B. H. Zimm, *J. Chem. Phys.*, **14**, 164 (1946).

(18) A. Isihara, *ibid.*, **18**, 1446 (1950).

(19) G. A. Jeffrey and R. D. Rosenstein, *Advan. Carbohyd. Chem.*, **19**, 11 (1964).

(20) G. C. Pimentel and A. L. McClellan, "The Hydrogen Bond," W. H. Freeman and Co., New York, 1960.

Table IV

A. Sucrose. Attractive Contribution to the Solute–Solvent Interaction Coefficient

T/C°	$RT\varkappa$/ cm³ mol⁻¹	$N_A B_1{}^{*\circ}$/ cm³ mol⁻¹	$N_A\phi$/ cm³ mol⁻¹	ω^{11}/ kcal mol⁻¹
5.0	1.14	206.48	−382	−3.74
15.0	1.13	208.84	−379	−3.87
25.0	1.13	210.36	−378	(−4.00)

B. Tertiary butanol: Attractive Contribution to the Solute–Solvent Interaction Coefficient

T/C°	$\bar{V}_2{}^{\phi}$/ cm³ mol⁻¹	$RT\varkappa$/ cm³ mol⁻¹	$N_A B_{11}{}^{*\circ}$/ cm³mol⁻¹	$N_A\phi$/ cm³ mol⁻¹	ω^{11}/ kcal mol⁻¹
0.5	88.0[a]	1.6[b]	86.4	−146.6	−3.67
5.0	87.9	1.7	86.2	−146.8	−3.73
25.0	87.8	2.3	85.5	−147.5	(−4.00)

[a] Reference 21. [b] $\varkappa$ calculated from a value at 20° using the same temperature coefficient as for 1-propanol. Int. Crit. Tables, Vol. III (1928); W. Brzostowski and T. M. Hardman, Bulletin de l'Academie Polonaise des Sciences, Vol XI, 447 (1963).

as shown in Table IVa. On the other hand, if we assume that ω^{11} is independent of temperature, then D increases with temperature (Table VI).

(*ii*) *The Temperature of Maximum Density.* Let us rewrite eq 13 in the form

$$V = 55.51\,\bar{V}_1{}^{\circ} + m\bar{V}_2{}^{\phi} + RT\left\{\frac{1}{2}A'm^2 + \frac{1}{3}B\dagger' m^3 \ldots\right\} \quad (26)$$

and for the temperature dependence of the molar volume of water in the neighborhood of its temperature of maximum density θ_m

$$\bar{V}_1{}^{\circ} = \bar{V}_1{}^{\circ *}\,[1 + \alpha_1(\theta - \theta_m)^2] \quad (27)$$

Then, substituting (27) into (26) and differentiating with respect to temperature gives for the solution at its temperature of maximum density, θ_m

$$\Delta\theta_m = -\frac{1}{2}\frac{[\partial\bar{V}_2{}^{\phi}/\partial T]_{\theta_m}}{55.51\,\alpha_1\bar{V}_1{}^{*\circ}}m - \frac{1}{4}R\frac{[\partial(TA')/\partial T]_{\theta_m}}{55.51\,\alpha_1\bar{V}_1{}^{*\circ}}m^2 + \ldots \quad (28)$$

The first term on the right-hand side of eq 28 is the "ideal dilute" contribution to $\Delta\theta_m$, $\Delta\theta_m$(ideal dilute), and the second term is the nonideal dilute contribution, $\Delta\theta_m$(nonideal dilute). Note that the first term is linear in the molality whereas the second term is a function of the square of the molality.

Now from (16) and (19)

$$A_{22}\bar{v}_1{}^{\circ} = -2b_{02}{}^{\circ} + 2b_{11}{}^{\circ} - kT\varkappa \quad (29)$$

Thus, $\Delta\theta$(nonideal dilute) is a measure of solute–solute and solute–solvent interaction, but from (19), $\Delta\theta$(ideal dilute) is a measure of solute–solvent interaction alone.

Table V: Analysis of the Effect of the Solute–Solvent Interaction on the Temperature of Maximum Density

	ζ/°K· mol⁻¹ kg	ξ/°K· mol⁻² kg²	χ/°K· mol⁻³ kg³
t-Butyl alcohol[a]	4.2	−10.3	3.8
Ethanol[a]	1.5	−2.0	0.3
Ethylene glycol[a]	−3.2	−0.4	
Glycerol[a]	−4.1	−1.5	
Sucrose[b] (experimental)	−18.3	2×10^1	
Sucrose[b] (calculated)	−18	6	
Sucrose[a]	−16	2	

[a] Wada and Umeda, ref 3. [b] Our data.

If we assume that $[\partial\bar{V}_2{}^{\phi}/\partial T]_{\theta_m}$ and $[\partial(TA')\partial T]_{\theta_m}$ are constant for small values of $\Delta\theta$, then we can rewrite eq 28 as

$$\Delta\theta_m = \zeta m + \xi m^2 + \chi m^3 + \ldots \quad (30)$$

so that if $\Delta\theta_m/m$ is plotted against m, the intercept will be ζ and the coefficient of m, ξ.

In Table V our values of ζ and ξ, obtained by a least-squares fit for sucrose are compared with those of Wada and Umeda.[7] Also given in the table are values for tertiary butanol, ethanol, ethylene glycol, and glycerol obtained by appropriate least-squares fits to their data. Also given in Table V are values of ζ and ξ for sucrose calculated using our experimental data for $\bar{V}_2{}^{\phi}$ and A' as functions of temperature; least-squares fits for these latter two quantities as functions of temperature gave

$$\bar{V}_2{}^{\phi}/\text{cm}^3\,\text{mol}^{-1} = 206.13 + 3.18\,10^{-1}\,(t/°\text{C}) - 4.15\,10^{-3}\,(t/°\text{C})^2 \quad (31)$$

$$A'/\text{kg mol}^{-1}\,\text{atm}^{-1} = 2.244\,10^{-4} - 1.11\,10^{-5}\,(t/°\text{C}) - 2.6\,10^{-7}\,(t/°\text{C})^2 \quad (32)$$

The values used for α_1 and $\bar{V}_1{}^{*\circ}$ were $8.0\,10^{-6}°\text{K}^{-2}$ and 18.02 cm³ mol⁻¹, respectively. The agreement obtained for ζ is good; the poor agreement for ξ is probably due to the rapid variation of A' with temperature in the neighborhood of 5°. It can be seen from the variation of the sign and magnitude of $B\dagger'$, $C\dagger'$, and $D\dagger'$ with temperature that a quantative analysis is not justified.

The sign and magnitude of ζ which gives the "ideal dilute" or "solute–solvent" contribution to $\Delta\theta_m$ is determined by $[\partial\bar{V}_2{}^{\phi}/\partial T]_{\theta_m}$. ζ varies from small and positive for tertiary butanol to large and negative for sucrose. For sucrose $[\partial\bar{V}_2{}^{\phi}/\partial T]_{\theta_m}$ is positive so that $\partial\phi/\partial T$ is positive and $-\partial\omega^{11}/\partial T$ is positive as shown in Table IVA; for tertiary butanol on the other hand $[\partial\bar{V}_2{}^{\phi}/\partial T]_{\theta_m}$ is negative[21]: if we assume

(21) F. Franks and H. T. Smith, *Trans. Faraday. Soc.*, **64**, 2962 (1968).

Table VI: Variation of D with Temperature, ($\omega^{11} = -4.0$ kcal mol^{-1})

	D/Å	
T/°C	Sucrose	t-Butyl alcohol
0.5		0.43
5.0	0.61	0.45
15.0	0.66	
25.0	0.72	0.52

the tertiary butanol molecule to be a sphere of radius 3.0 Å, then the rigid particle contribution to $B_{11}{}^{*\circ}$ is 233 cm^3 mol^{-1}. Thus for tertiary butanol $\partial\phi/\partial T$ is negative but, as shown in Table IVB, $-\partial\omega^{11}/\partial T$ is positive and almost identical with that for sucrose. On the other hand, if we consider ω^{11} to be independent of temperature then the width D of the attractive square-well potential for tertiary butanol increases with temperature in a very similar manner to that for sucrose (Table VI).

The sign and magnitude of ζ determines the sign of $\Delta\theta_m$ in dilute solutions and, on our model, although $\Delta\theta_m$ is different in both sign and magnitude for tertiary butanol and sucrose, the temperature dependence of the depth or width of the attractive square well potential is almost the same in each case.

"Semiideal" Solutions. We investigated the application of the concept of a "semiideal dilute" solution in the analysis of our results. The concept of a "semiideal" solution was first introduced by Scatchard[22] and refined by Robinson and Stokes.[23] A "semiideal" solution is defined as one in which all the departures from ideal behavior are attributed to chemical reactions, and the activity of each actual species in the solution is equal to its actual mole fraction when the chemical reactions have reached equilibrium. We *define* a "semiideal dilute" solution as one in which the activity of the solvent on the Raoult's law scale is equal to its actual mole fraction and the activity of each solute species on the Henry's law scale is equal to its actual mole fraction when the chemical reactions have reached equilibrium.

However, using our concept of a "semiideal dilute" solution, a certain inequality (eq 40) must be satisfied by the activity coefficients of solute and solvent and we found that this criterion was not obeyed for solutions of sucrose and water.

Let us assume that in a solution of sucrose and water, we have the species S, SW, SW_2 etc. in equilibrium. Then

$$\lambda_{SW} = \lambda_S\lambda_W \qquad \lambda_{SW_2} = \lambda_S\lambda_W{}^2, \text{ etc.} \tag{33}$$

where λ is the absolute activity. Equilibrium constants are then given by

$$K_1 = a_{SW}/a_S a_W,\ K_2 = a_{SW_2}/a_S a_W{}^2 \text{ etc.}, \tag{34}$$

where a_W is the Raoult's law activity of the water and a_S, a_{SW} etc. are the Henry's law activities of the solute species on the mole fraction scale.

Let η_S, η_W etc. represent the *actual* mole fractions of each species present at equilibrium, then

$$\eta_S + \eta_W + \eta_{SW} + \eta_{SW_2} + \ldots = 1 \tag{35}$$

from the definition of mole fraction. Then, substituting (34) into (35)

$$1 - \eta_S - \eta_W = \eta_{SW} + \eta_{SW_2} + \ldots = K_1 a_S a_W + K_2 a_S a_W{}^2 + \ldots \tag{36}$$

Thus $1 - \eta_S - \eta_W$ must be positive, *i.e.*

$$\eta_S + \eta_W < 1 \tag{37}$$

Now if the actual solvent present is ideal on the Raoult's law scale, and the actual solute present is ideal on the Henry's law mole fraction scale, the inequality (37) becomes

$$a_W + \gamma_{x,s}x_S < 1 \tag{38}$$

where $\gamma_{x,s}$ is the activity coefficient of the solute on the Henry's law mole fraction scale. Now

$$\gamma_{x,s} = \gamma_{m,s}[1 + mM_1/1000] \tag{39}$$

where $\gamma_{m,s}$ is the activity coefficient of the solute on the Henry's law molality scale, and M_1 is the molar mass of solvent. Then, from (38) and (39)

$$a_W + \gamma_{m,s}\, mM_1/1000 < 1 \tag{40}$$

Equation 40 was tested using the experimental data of Robinson and Stokes.[5] The results are recorded in Table VII. It can be seen from the table

Table VII: Sucrose: Test of "Semiideal Dilute" Behavior

Molality	$a_W + \gamma_{m,s}mM_1/1000$
0.01	1.00000
0.1	1.00002
0.4	1.0003
1.0	1.002
6.0	1.157

that the inequality is not obeyed even for 0.01 m solutions, so that a solution of sucrose and water cannot be considered to be "semiideal dilute."

Acknowledgment. We wish to thank Professor R. A. Robinson for helpful advice and the the S.R.C. for a research studentship to J. E. G.

(22) G. Scatchard, *J. Amer. Chem. Soc.*, **43**, 2387 (1921).

(23) R. H. Stokes and R. A. Robinson, *J. Phys. Chem.*, **70**, 2126 (1966).

The Thermodynamic Properties of Liquids, Including Solutions. I. Intermolecular Energies in Monotonic Liquids and Their Mixtures[1]

by Maurice L. Huggins

Arcadia Institute for Scientific Research, 135 Northridge Lane, Woodside, California 94062 *(Received July 7, 1969)*

The intermolecular interaction energies in liquids, including solutions, can be related to the intermolecularly contacting surface areas of the segments of which the molecules are composed, to the contact energies per unit contact area (for each type of contact), and to an equilibrium constant, relating the contact areas of the different types to their contact energies. Equations based on these ideas can be used to deduce the magnitudes of the parameters involved from heat of vaporization and heat of mixing data. These parameters can then be used for other systems containing the same types of segments, to predict heats of vaporization, heat of mixing curves, and derived quantities. As simple examples, CCl_4, $SiCl_4$, $SnCl_4$, $TiCl_4$, C_6H_6, c-C_6H_{12}, and their mixtures are considered. Each of these substances is treated as monotonic: containing only one type of intermolecularly contacting group. Heat of mixing curves for pairs of these compounds conform quantitatively to the theoretical equations.

Introduction

This series of papers is a result of an attempt to apply certain ideas, first developed for polymer solutions,[2-5] to solutions in general. One aim is to deduce the parameters needed to relate the thermodynamic properties of polymer solutions to their composition from experimental data on liquids, including solutions, of low molecular weight. In the process of developing and testing the theory, it soon became evident that it yields results for the low-molecular-weight systems that are of considerable interest and use in themselves, without regard to their possible application to systems containing high-molecular-weight components.

This theory can be considered an extension and refinement of the theories of Hildebrand[6,7] and Scatchard.[8] It also embodies some concepts related to those in the "quasi-chemical" treatment of Guggenheim,[9] further developed by Prigogine.[10] It differs from these other treatments, however, in several important respects. These differences are responsible for the more quantitative agreement with experiment now obtained. Moreover, the new theory is much more readily applicable to systems containing molecules that contain segments that are chemically different.

This first paper in the series deals with fundamental ideas and equations concerned with the cohesive energies in liquids and with the application of these ideas and equations to a few simple liquids and their mixtures.

Fundamental Ideas

Interaction energies between pairs of atoms fall off quite rapidly, in general, as the interatomic distance increases. By far the largest part of the intermolecular energy in a liquid comes from the interactions between pairs of atoms in adjacent molecules that are closest together. Moreover, in comparing different liquids of similar type or solutions of different concentrations, the sum of the intermolecular energies that are not due to close atom pair interactions changes but little. There is thus ample justification for concentrating attention on the close neighbor interactions, as the writer has done in other applications of the "structon" theory.[11-14]

The structure of any liquid, except perhaps one containing only monatomic molecules, is too complex and too little known to permit the calculation of the total intermolecular energy by direct summation of the atom-to-atom interaction energies. Also, pres-

(1) Preliminary reports of the theory outlined in this paper have been presented at the 155th and 157th National Meetings of the American Chemical Society, San Francisco, Calif., April 1968, and Minneapolis, Minn., April 1969 [see *Polymer Preprints*, **9**, 558 (1968) and **10**, 334 (1969)] and in a lecture at Kent State University [*J. Paint Technol.*, **41**, 509 (1969)].

(2) M. L. Huggins, *Ann. N. Y. Acad. Sci.*, **43**, 1 (1942).

(3) M. L. Huggins, *J. Polym. Sci.*, **16**, 209 (1955).

(4) M. L. Huggins, "Physical Chemistry of High Polymers," John Wiley & Sons, Inc., New York, N. Y., 1958, Chapter 6.

(5) M. L. Huggins, *J. Amer. Chem. Soc.*, **86**, 3535 (1964).

(6) J. H. Hildebrand and R. L. Scott, "Solubility of Nonelectrolytes," 3rd ed, Reinhold Publishing Corp., New York, N. Y., 1950.

(7) J. H. Hildebrand and R. L. Scott, "Regular Solutions," Prentice-Hall, Inc., Edgewood Cliffs, N. J., 1962.

(8) G. Scatchard, *Chem. Rev.*, **3**, 321 (1931).

(9) E. A. Guggenheim, "Mixtures," Clarendon Press, Oxford, 1952.

(10) I. Prigogine, "The Molecular Theory of Solutions," North-Holland Publishing Co., Amsterdam, 1957.

(11) M. L. Huggins, *J. Phys. Chem.*, **58**, 1141 (1954).

(12) M. L. Huggins, *Bull. Chem. Soc. Jap.*, **28**, 606 (1955).

(13) M. L. Huggins, *Macromolecules*, **1**, 184 (1968).

(14) M. L. Huggins, *Inorg. Chem.*, **7**, 2108 (1968).

ent knowledge of the dependence of these interaction energies on interatomic distances is, except for the interactions between simple ions,[15,16] insufficient. Even in the very important case of H···H interactions, this is unfortunately true.[17,18]

For these reasons it is necessary to use a model, hoping that it will approximate sufficiently well the actual liquid and yet be simple enough to yield relationships that can be applied to experimental measurements on actual solutions. The model to be described appears to meet these requirements.

Each molecule is considered to have a molecular surface, with the surfaces of neighboring molecules in mutual contact. If the molecules contain segments that are chemically different, such that different types of segments would be expected to interact differently with segments of other molecules, the molecular surface is considered to be composed of the segment surfaces of the component segments. For example, a normal alkane molecule is treated as consisting of two methyl segments and $n - 2$ methylene segments.

Some of the molecular surfaces and segment surfaces do not contact other surfaces, but it seems reasonable to assume (except for molecules making *intra*molecular contacts, such as those composed of long flexible chains) that *for each segment type the average intermolecularly contacting segment surface area is constant at a given temperature, regardless of variations in the types and numbers of other segments.*

In general, a segment surface can make contact with surfaces of segments of the same kind or of other kinds. It is assumed that *for each kind of segment–segment contact, the average contact energy per unit area of contact is constant at a given temperature, regardless of variations in the types and areas of other contacts.*

The relative contact areas of the different types should be such as to minimize the free energy. It is assumed, therefore, that *the relative contact areas are governed by one or more equilibrium constants, these constants being related in an appropriate way to the interaction energies per unit contact area.*

With the foregoing assumptions one can derive equations relating the cohesive energy in a given system to the numbers of segments of the different types, the average intermolecularly contacting surface area for each type of segment–segment contact, and one or more equilibrium constants (if there are two or more kinds of segments). These equations can be tested against experiment. The parameters, once determined, should be applicable to many systems containing the same segments or segment–segment contacts. The experimentally determined dependence of the parameters on temperature and pressure should be useful in extending our knowledge of atomic and molecular interactions. Observed departures from the theoretical relationships deduced from the model will require theoretical or experimental explanation.

Equations

Let types of segments be designated by subscripts α, β, etc., and types of segment–segment contact by subscripts $\alpha\alpha$, $\alpha\beta$, $\beta\beta$, etc. Let the intermolecularly contacting surface areas in 1 mol of substance or mixture be designated by σ_α, σ_β, etc. Let the average intermolecularly contacting surface area per mole (Avogadro's number) of single segments of the α (or β, etc.) type be designated by σ_α° (or σ_β°, etc.). Let the average areas of intermolecular contact per mole for the different types of contact be designated by $\sigma_{\alpha\alpha}$, $\sigma_{\alpha\beta}$, $\sigma_{\beta\beta}$, etc. Let the average energies per unit contact area for the different types of intermolecular contact be designated by $\epsilon_{\alpha\alpha}$, $\epsilon_{\alpha\beta}$, $\epsilon_{\beta\beta}$, etc. In general these energies are attraction energies, hence negative, in accordance with convention. (The unit area need not be specified, since the quantities obtained are either products of the form $\sigma\epsilon$ or ratios, such as $\sigma_\beta/\sigma_\alpha$.)

If, in a given system, there is but one type of segment, hence only one type of contact, the total intermolecular energy (the negative of the cohesive energy) per mole is obviously

$$E = \sigma_{\alpha\alpha}\epsilon_{\alpha\alpha} = n_\alpha\sigma_\alpha^\circ\epsilon_{\alpha\alpha}/2 \tag{1}$$

where n_α is the number of α-type segments per molecule.

If there are two types of segment, hence three types of contact

$$E = \sigma_{\alpha\alpha}\epsilon_{\alpha\alpha} + \sigma_{\beta\beta}\epsilon_{\beta\beta} + \sigma_{\alpha\beta}\epsilon_{\alpha\beta} \tag{2}$$

$$\sigma_\alpha = 2\sigma_{\alpha\alpha} + \sigma_{\alpha\beta} \tag{3}$$

$$\sigma_\beta = 2\sigma_{\beta\beta} + \sigma_{\alpha\beta} \tag{4}$$

The equilibrium constant, relating the contact areas of the three types, I define by the equation

$$K = \frac{\sigma_{\alpha\beta}^2}{4\sigma_{\alpha\alpha}\sigma_{\beta\beta}} \tag{5}$$

The 4 in the denominator is included to make K equal to 1 for perfect randomness of contact formation, with no preference for either of the two possible contact types as an α (or β) segment is added, hypothetically, to an equimolal mixture.

The equilibrium constant can reasonably be related to the contact energies by an equation of the form

$$K = A\exp(-\Delta\epsilon/kT) \tag{6}$$

where

$$\Delta\epsilon = 2\epsilon_{\alpha\beta} - \epsilon_{\alpha\alpha} - \epsilon_{\beta\beta} \tag{7}$$

(15) M. L. Huggins, *J. Chem. Phys.*, 5, 143 (1937).

(16) M. L. Huggins and Y. Sakamoto, *J. Phys. Soc. Jap.* 12, 241 (1957).

(17) M. L. Huggins, *Makromol. Chem.*, 92, 260 (1966).

(18) M. L. Huggins in "Structural Chemistry and Molecular Biology," A. Rich and N. Davidson, Ed., W. H. Freeman and Co., San Francisco, Calif., 1968, p 761.

If there are more than two segment types, more than one K is required. The K, A, k, and $\Delta\epsilon$ constants in eq 5, 6, and 7 should then be given subscripts $K_{\alpha\beta}$, etc.

The k in eq 6 is not the Boltzmann constant, since its magnitude must depend on the choice of the unit of area and since the unit contact areas are not independent entities like gas molecules. The coefficient A is related to steric and other factors, in addition to $\Delta\epsilon$, affecting the relative amounts of the different types of contact. For present purposes no use need be made of eq 6; neither A nor k needs to be evaluated. The significance of A will, nevertheless, be briefly discussed at the end of the next section. Further discussion can well be postponed until after sufficient values of the temperature dependence of the solution parameters have been accumulated.

From eq 3, 4, and 5 one can readily deduce

$$\sigma_{\alpha\beta} = \frac{-2(\sigma_\alpha + \sigma_\beta)[1 - (1 + y)^{1/2}]}{K'} \quad (8)$$

$$\sigma_{\alpha\alpha} = \frac{\sigma_\alpha}{2} + \frac{(\sigma_\alpha + \sigma_\beta)[1 - (1 + y)^{1/2}]}{K'} \quad (9)$$

and

$$\sigma_{\beta\beta} = \frac{\sigma_\beta}{2} + \frac{(\sigma_\alpha + \sigma_\beta)[1 - (1 + y)^{1/2}]}{K'} \quad (10)$$

where

$$K' = 4\left(\frac{1}{K} - 1\right) \quad (11)$$

and

$$y = \frac{K'\sigma_\alpha\sigma_\beta}{(\sigma_\alpha + \sigma_\beta)^2} \quad (12)$$

Substitution of these equations into eq 2 yields, for the molal interaction energy

$$E = \frac{\sigma_\alpha\epsilon_{\alpha\alpha}}{2} + \frac{\sigma_\beta\epsilon_{\beta\beta}}{2} - \frac{(\sigma_\alpha + \sigma_\beta)\Delta\epsilon}{K'} \times [1 - (1 + y)^{1/2}] \quad (13)$$

CCl_4, $SiCl_4$, $SnCl_4$, $TiCl_4$ and Their Mixtures

As first examples the tetrachlorides of C, Si, Sn, and Ti will be considered. Each will be treated as a "monotonic" substance, containing only one kind of atom or group, with regard to intermolecular interactions. For our purpose, that group ("segment," in the preceding theoretical development) might either be considered as a chlorine atom attached to an atom of C, Si, Sn, or Ti, or as the whole molecule. These two alternatives are equivalent, except that the σ_{MCl_4} obtained by the latter procedure will be four times the $\sigma_{Cl(M)}$ obtained by the former procedure. For simplicity, the latter procedure will be used here. Equation 1 then applies, with $n_\alpha = 1$.

The propriety of treating these substances as monotonic might be questioned, especially in the cases of $SnCl_4$ and $TiCl_4$, since these compounds can add chloride ions and some organic chlorides to form complexes in which the coordination number of the metal ion is 6. Perhaps, in a mixture with CCl_4 for instance, Sn (or Ti) atoms "make contact" with some of the Cl (C) atoms. If so, the molecules can still be treated as monotonic, but the magnitudes of the $\sigma^\circ_{MCl_4}$ and $\epsilon_{\alpha\beta}$ constants will be different from what they would be without the M···Cl contacts.

The magnitude of the molal intermolecular energy, hence also that of the product $\sigma_\alpha\epsilon_{\alpha\alpha}$, can be estimated from the standard heat of vaporization, ΔH_v°, with the aid of the following equations

$$\Delta H_v^\circ = \Delta E_v^\circ + P\Delta V^\circ \quad (14)$$

$$\Delta E_v^\circ = -E_{\text{mol interactions}} + \Delta E_{\text{internal}} + \Delta E_{\text{external}} \quad (15)$$

ΔV° is the molal volume of the ideal gas minus that of the liquid. $E_{\text{mol interactions}}$ is the intermolecular energy in the liquid (the negative of the cohesive energy), designated in eq 1 merely as E. $\Delta E_{\text{internal}}$, the difference between the energies of vibration and rotation of the atoms and groups within the molecules in the gaseous and liquid states, is probably close to zero. $\Delta E_{\text{external}}$ is the difference between the energies of translation and rotation of the whole molecules in the gaseous state and the energies of vibration, torsion, and (in some cases) rotation of the whole molecules in the liquid state. These external energies in the liquid are difficult to estimate accurately. For the present I shall follow Bagley and coworkers[19] in putting

$$\Delta E_{\text{external}} = -3RT/2 \quad (16)$$

for molecular liquids of the sort dealt with here. This may well be inaccurate and have to be modified later, especially when dealing with more polar compounds. Fortunately, inaccuracies in the E values do not affect the accuracy of the treatment of heats of mixing, to be dealt with presently, or other solution properties.

From the foregoing relationships, assumptions, and approximations

$$E = -\Delta H_v^\circ + P\Delta V^\circ - 3RT/2 \quad (17)$$

Values of E, calculated by this equation for the liquids considered here, are listed in Table I. They may be in error by 1 kcal or more, but the differences between the values for different compounds are probably correct to within 0.1 or 0.2 kcal.

Mixtures of pairs of these compounds can be treated, for present purposes, as ditonic systems, containing

(19) E. B. Bagley, T. P. Nelson, J. W. Barlow, and S-A. Chen, submitted for publication.

Table I: Intermolecular Energies in the Pure Liquids

Compound	Temp, °C	$\Delta H_v°$, kcal/mol	$P\Delta V°$,[e] kcal/mol	E, kcal/mol
CCl_4	20	7.83[a,b]	0.58	−8.12
$SiCl_4$	20	7.24[a,b]	0.58	−7.53
$SnCl_4$	20	9.77[a,c]	0.58	−10.08
$TiCl_4$	20	8.80[a,c]	0.58	−9.11
CCl_4	25	7.77[a,b]	0.59	−8.07
C_6H_6	25	8.102[d]	0.590	−8.40
c-C_6H_{12}	25	7.908[d]	0.590	−8.21

[a] F. D. Rossini, D. D. Wagman, W. H. Evans, S. Levine, and I. Jaffe, "Selected Values of Chemical Thermodynamic Properties," National Bureau of Standards, Circular 500, U. S. Government Printing Office, Washington, D. C., 1952. [b] D. D. Wagman, W. H. Evans, V. B. Parker, I. Halow, S. M. Bailey, and R. H. Schumm, "Selected Values of Chemical Thermodynamic Properties," National Bureau of Standards, Technical Note 270-3, U. S. Government Printing Office, Washington, D. C., 1968. [c] C. E. Wicks, "Thermodynamic Properties of 65 Elements—Their Oxides, Halides, Carbides and Nitrides," Bureau of Mines Bulletin 605, U. S. Government Printing Office, Washington, D. C., 1963. [d] "Selected Values of Physical and Thermodynamic Properties of Hydrocarbons and Related Compounds," American Petroleum Institute Research Project 44, Tables 5p (1945) and 7p (1948). [e] Calculated from the densities of the liquid and the ideal gas at 1 atm pressure.

just two types of "segments." As with the pure compounds, it is convenient to take the segments as the same as the molecules, although one might validly take them as quarter molecules: a chlorine atom attached to a specified central atom. It would not be justified, however, to assume that a chlorine atom attached to one type of central atom (*e.g.*, C) has the same intermolecularly contacting surface area and the same contact energies as a chlorine atom attached to another type of central atom (*e.g.*, Si).

The excess enthalpy per mole or molar heat of mixing, essentially equal to the molar energy change on mixing, is the difference between the actual enthalpy (or energy) of 1 mol of solution and the sum of the molar enthalpies (or energies) of the components, each multiplied by its mole fraction in the solution

$$\tilde{H}^E = H - x_1H_1 - x_2H_2 = E - x_1E_1 - x_2E_2 \quad (18$$

From eq 1, with $n_\alpha = 1$ for the pure compounds and eq 13, with σ_α and σ_β equal to $x_1\sigma_\alpha°$ and $x_2\sigma_\beta°$ respectively

$$\tilde{H}^E = \frac{-(x_1\sigma_\alpha° + x_2\sigma_\beta°)\Delta\epsilon}{K'}\left[1 - \left(1 + \frac{K'x_1\sigma_\alpha°x_2\sigma_\beta°}{(x_1\sigma_\alpha° + x_2\sigma_\beta°)^2}\right)^{1/2}\right] \quad (19$$

or

$$\tilde{H}^E = \frac{-\sigma_\alpha°\Delta\epsilon}{K'}[1 + x_2(r-1)]\left\{1 - \left[1 + \frac{K'r(x_2 - x_2^2)}{[1 + x^2(r-1)]^2}\right]^{1/2}\right\} \quad (20)$$

where

$$r = \sigma_\beta°/\sigma_\alpha° \quad (21)$$

If K is exactly 1, K' is zero and eq 20 reduces to

$$\tilde{H}^E = \frac{\sigma_\alpha°\Delta\epsilon}{2}\left[\frac{r(x_2 - x_2^2)}{1 + x_2(r-1)}\right] \quad (22)$$

The heat of mixing thus depends on the concentration (x_2) and on three parameters: K (or K'), r, and the product $\sigma_\alpha°\Delta\epsilon$. From sufficiently accurate measurements of $\tilde{H}^E$ as a function of the composition of the solution, these three parameters can be determined.

The accuracy of determination of the parameters can be increased if, as in the present instance, data are available (for a single temperature) for more pairwise mixtures than the number of segment types. Use can then be made of the additional requirement that the r values must be mutually consistent. Also, if data for a single mixture are available at a series of temperatures, it can reasonably be required that

Table II: Parameters for Mixtures[a]

Components α	Components β	Temp, °C	K	$\sigma_\beta°/\sigma_\alpha°$	$\sigma_\alpha°\Delta\epsilon$	$\sigma_\beta°\Delta\epsilon$	$-\sigma_\alpha°\epsilon_{\alpha\alpha}$	$-\sigma_\beta\epsilon_{\beta\beta}$	$-\sigma_\alpha°\epsilon_{\alpha\beta}$	$-\sigma_\beta°\epsilon_{\alpha\beta}$	$\sigma_\alpha°(\epsilon_{\alpha\beta} - \epsilon_{\alpha\alpha})$	$\sigma_\beta°(\epsilon_{\alpha\beta} - \epsilon_{\beta\beta})$
CCl_4	$SiCl_4$	20.2	1.00	1.230	0.306	0.376	16.24	15.06	14.09	17.33	2.15	−2.27
CCl_4	$SnCl_4$	20.2	1.00	1.290	0.490	0.632	16.24	20.16	15.69	20.23	0.55	−0.07
CCl_4	$TiCl_4$	20.2	7.0	1.70	0.193	0.328	16.24	18.22	13.38	22.75	2.86	−4.53
$SiCl_4$	$SnCl_4$	20.2	1.00	1.05	0.506	0.531	15.06	20.16	16.89	17.71	−1.83	2.45
$SiCl_4$	$TiCl_4$	20.2	1.0	1.38	0.277	0.383	15.06	18.22	13.96	19.33	1.10	−1.11
$SnCl_4$	$TiCl_4$	20.2	1.0	1.32	0.32	0.425	20.16	18.22	16.83	22.19	3.33	−3.97
C_6H_6	CCl_4	25	1.00	1.080	0.214	0.232	16.80	16.14	15.76	17.02	1.04	−0.88
C_6H_6	C_6H_{12}	25	1.00	1.112	1.411	1.569	16.80	16.42	15.07	16.77	1.73	−0.35
CCl_4	C_6H_{12}	25	1.00	1.030	0.278	0.286	16.14	16.42	15.90	16.38	0.24	0.04

[a] Units for the quantities in the last eight columns are kilocalories per mole.

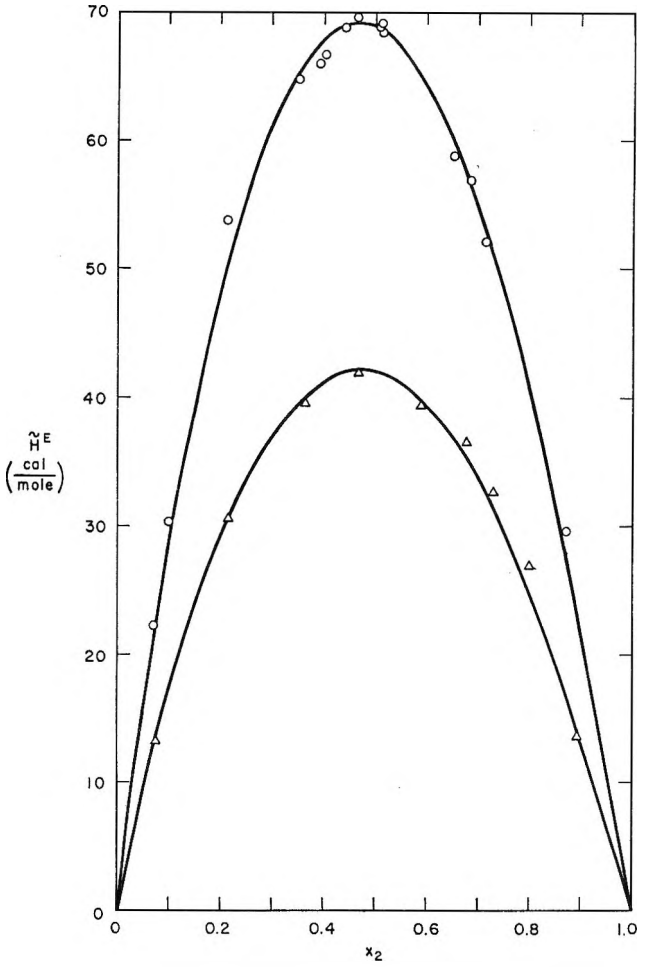

Figure 1. Heats of mixing for CCl_4 + $SnCl_4$ (○) and CCl_4 + $SiCl_4$ (△) at 20.2°; data from ref 20. The curves represent eq 22 with the parameters of Table II, columns 5 and 6.

the values for each parameter lie on a smooth curve when plotted against the temperature.

The parameter determinations are readily made with an electronic computer or a computing desk calculator such as the Hewlett-Packard 9100A.

Kolbe and Sackmann[20] have published heat of mixing data at 20.2° for the six pairwise mixtures obtainable from the chlorides of C, Si, Sn, and Ti. The parameters given in Table II, columns 4–6, give good agreement with their data, apparently within the probable limits of experimental error, judged from the scatter of the data points about smooth curves (see Figures 1–4). The agreement is poorest for the $SiCl_4$ + $TiCl_4$ solutions, for which the experimental results seem to be relatively inaccurate.

Neglecting possible systematic errors in the experimental results and assuming the other parameters to be exactly correct, the probable error in each of the values in columns 4–6 is estimated to be a few units in the last decimal place shown, except for the solutions containing $TiCl_4$ as a component. For these the probable error might be a few units in the next to the last decimal place. If the other parameters

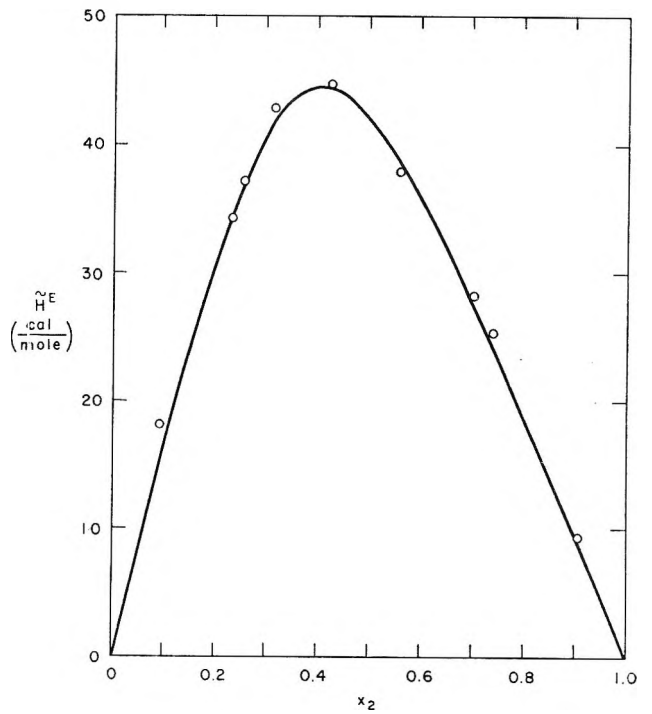

Figure 2. Heats of mixing for CCl_4 + $TiCl_4$ at 20.2°; data from ref 20. The curve represents eq 22 with the parameters of Table II, columns 4, 5, and 6.

are allowed to vary also, any one parameter value might be varied by perhaps ten times this "probable error," without spoiling the agreement unreasonably. With the additional requirement that the r values be consistent, the permissible variation is between these two extremes. The precision of the parameter determinations will, of course, increase as more and better data on these systems and on other systems containing one or more of the same components become available.

The figures in columns 7 to 13 of Table II were calculated from those in columns 5 and 6 and the E values in Table I by means of eq 1, 7, and 21. Because of the uncertainties in the E values, already discussed, the individual values in columns 8 to 11 may well be in error by 1 kcal or more. For comparing relative values, however, and for use in predicting $\sigma^\circ\Delta\epsilon$ values for other systems containing one of the same components, the values in these columns are given to the second decimal place, *i.e.*, to 10 cal. It is to be expected that revisions of these figures will have to be made, as better experimental data are obtained and as more systems are treated.

The data require that the equilibrium constant K be close to unity, even though $\sigma_\alpha^\circ\Delta\epsilon$ and $\sigma_\beta^\circ\Delta\epsilon$ are not zero, except for the solutions of $TiCl_4$ with CCl_4 and perhaps for those of $TiCl_4$ with $SiCl_4$ and $SnCl_4$. (The $SiCl_4$ + $TiCl_4$ data are such as to make a reliable

(20) A. Kolbe and H. Sackmann, *Z. Phys. Chem.* (Frankfurt am Main), 31, 281 (1962).

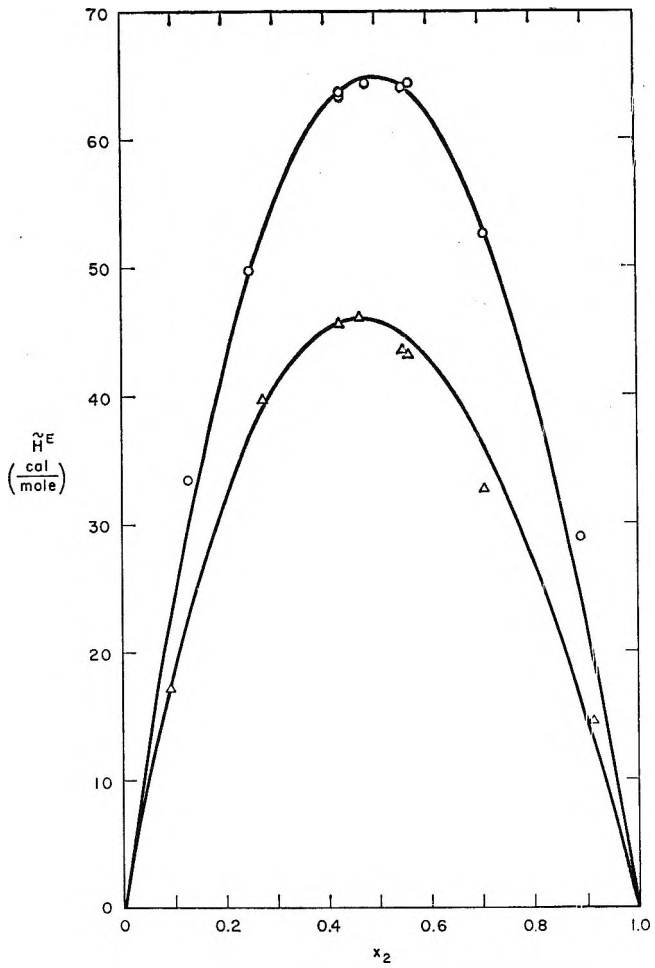

Figure 3. Heats of mixing for $SiCl_4$ + $SnCl_4$ (○) and $SnCl_4$ + $TiCl_4$ (△) at 20.2°; data from ref 20. The curves represent eq 22 with the parameters of Table II, columns 5 and 6.

determination of K impossible. The $SnCl_4$ + $TlCl_4$ data are satisfied as well by K and r parameters of 2.0 and 1.34, respectively, as by the 1.0 and 1.32 in the table. Increasing the r value would necessitate some adjustment of parameters for some of the other solutions.) This may at first seem surprising. Formally, it may be interpreted as indicating a value of the factor A, in eq 6, different from unity. This factor must allow for the fact that the unit areas of segment surface do not behave independently with regard to making contacts with other segment surfaces, since all the unit areas of each segment surface are connected together. The shapes of the segment surfaces must also be involved, as well as other factors.

Perhaps more important is the fact that the difference between the interaction energies of a given segment type for contacts with like and unlike segments is, in the examples being considered, of the order of magnitude of the gas constant times the absolute temperature, roughly 0.6 kcal/mol. Illustrating this, columns 12 and 13 of Table II show the differences between the average intermolecular energy for a mole

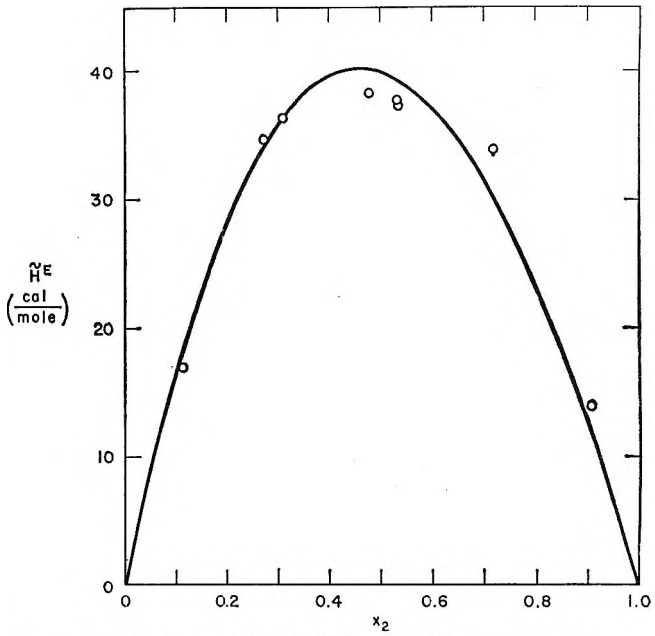

Figure 4. Heats of mixing for $SiCl_4$ + $TiCl_4$ at 20.2°; data from ref 20. The curve represents eq 22 with the parameters of Table II, columns 5 and 6.

of molecules in contact only with molecules of the same type and for a mole of molecules in contact only with molecules of the other type. For most

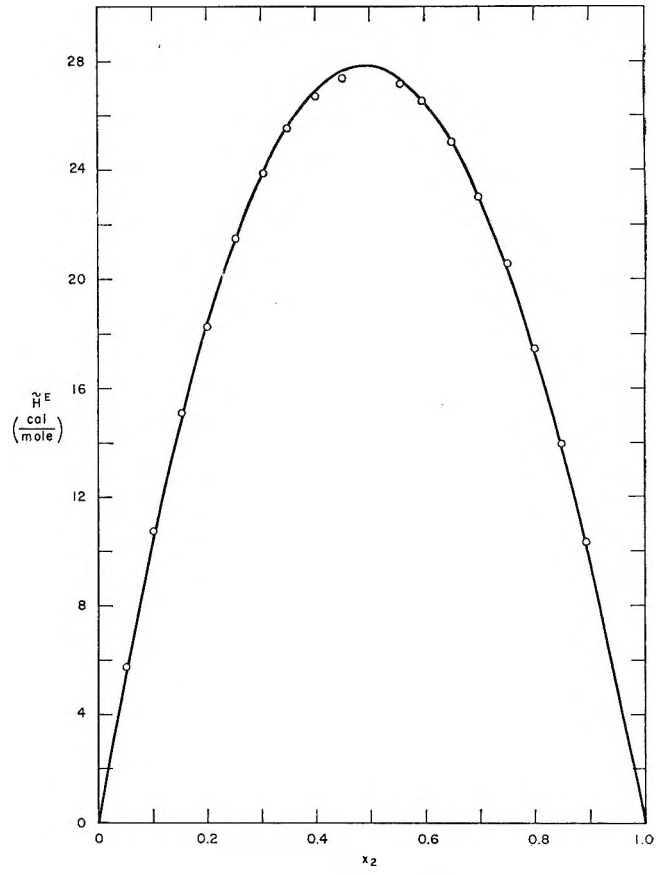

Figure 5. Heats of mixing for C_6H_6 + CCl_4 at 25°; data from ref 21. The curve represents eq 22 with the parameters of Table II, columns 5 and 6.

of the solutions the values in these columns are not more than a few times RT, indicating that changes in intermolecular contacts take place quite readily, hence frequently. However, column 13 shows relatively large negative values for the solutions of $TiCl_4$ with CCl_4 and $SnCl_4$. This means that $TiCl_4$ molecules attract CCl_4 and $SnCl_4$ molecules considerably more strongly than they attract other $TiCl_4$ molecules. It will be interesting to see if accurate data for the $SiCl_4$ + $TiCl_4$ system will lead to a similar result.

It thus seems likely that, except for the solutions of $TiCl_4$ with CCl_4 (and possibly those of $TiCl_4$ with $SiCl_4$ and $SnCl_4$), the magnitudes of the differences in contact energies for the different types are insufficient to prevent practically perfect random mixing of the molecules. This does not, of course, lead to athermal mixing. These solutions appear to be "regular" solutions, in the Hildebrand sense.[6,7]

Benzene, Cyclohexane, and Their Mixtures with Each Other and with Carbon Tetrachloride

As further examples, C_6H_6, c-C_6H_{12}, and their solutions with each other and with CCl_4 will be considered.

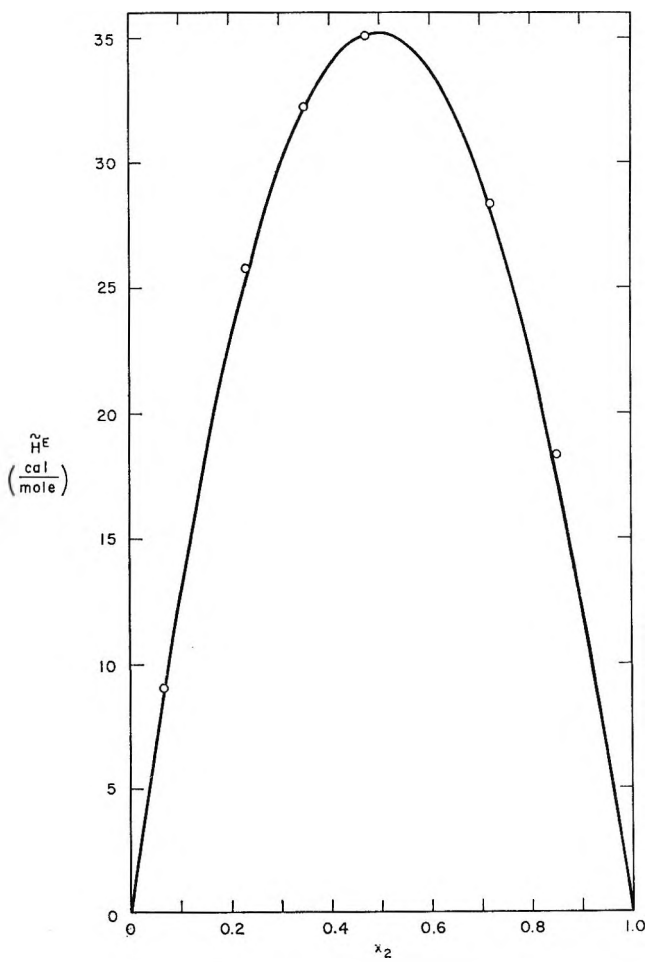

Figure 6. Heats of mixing for CCl_4 + c-C_6H_{12} at 25°; data from ref 23. The curve represents eq 22 with the parameters of Table II, columns 5 and 6.

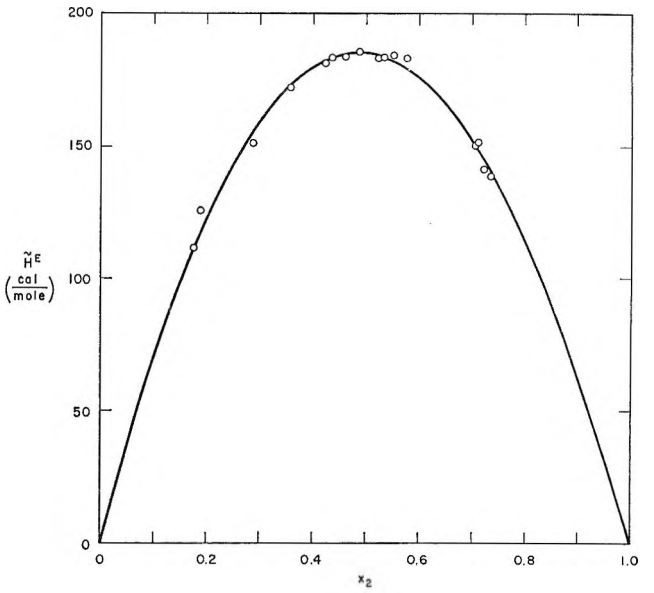

Figure 7. Heats of mixing for C_6H_6 + c-C_6H_{12} at 25°; data from ref 24. The curve represents eq 22 with the parameters of Table II, columns 5 and 6.

Again, each of these will be treated as monotonic. One might, alternatively, treat benzene and cyclohexane molecules each as ditonic, their central cores making contact directly with hydrogen or chlorine atoms of other molecules, but for our present purpose this is not necessary. Each molecule as a whole can be considered as a single "segment."

For pure benzene and pure cyclohexane the magnitudes of the intermolecular energy, per mole, and so of the $\sigma_\alpha\epsilon_{\alpha\alpha}$ products can be estimated as was done for the tetrachlorides. Making the same assumptions and approximations, the E values listed in Table I are obtained.

Heats of mixing of solutions of benzene and carbon tetrachloride at 25° have been reported by a number of groups of researchers. The older data have been carefully reviewed and compared with their own new data by Larkin and McGlashan.[21] Their data appear to be the most accurate that cover a wide range of composition. They will be used here. It should be noted, however, that the true values are probably a little higher (about 0.2 cal/mol for an equimolar mixture), as noted by Larkin, Fenby, Gilman, and Scott[22] and at the conclusion of the Larkin–McGlashan paper. One suspects that the data used here for the C_6H_6 + C_6H_{12} and CCl_4 + C_6H_{12} solutions are also slightly in error, perhaps by a similar amount. For all three mixtures the data are here used as published, with the realization that the magnitudes of the parameters, especially the $\sigma_\alpha{}^\circ\Delta\epsilon$ parameters, and other quantities

(21) J. A. Larkin and M. L. McGlashan, *J. Chem. Soc.*, 3425 (1961).

(22) J. A. Larkin, D. V. Fenby, T. S. Gilman, and R. L. Scott, *J. Phys. Chem.*, **70**, 1959 (1966).

derived from them may have to be modified slightly later.

For the $CCl_4 + C_6H_{12}$ system heats of mixing reported by Adcock and McGlashan[23] and for the $C_6H_6 + C_6H_{12}$ system those published by Peña and Martín[24] are used. It may be noted that Peña is a former collaborator of McGlashan.

The parameters obtained for the three systems, by equations and procedures like those used for the mixtures of tetrachlorides, are included in Table II. The close agreement with the individual data points is shown in Figures 5–7.

For each of these three systems, as with most of the tetrachloride mixtures, a value of K equal to unity, corresponding to a regular solution, is found to yield satisfactory agreement. Mutually consistent values of r are obtained. As shown in columns 12 and 13, the energy differences for different types of close neighbors are quite small.

Summary and Conclusion

A new theory for the molecular interaction energies in pure liquids and liquid solutions has been described. Equations have been presented for liquids containing only one or two chemically different types of molecules or segments. Some of the parameters can be determined, roughly, from heats of vaporization; others, more accurately, from heats of mixing. According to the theory, the parameters should be transferable from one system to others (at the same temperature) containing the same segments or combinations of segments. This has been tested with regard to mixtures of two monotonic substances at different concentrations and with regard to the relative contacting surface areas of different segment types. Quantitative agreement with accurate heat-of-mixing data has been obtained.

Extensions and further applications of the theory will be presented in future papers.

Acknowledgment. In the development of this theory I have had discussions with many other scientists. For their comments and suggestions I am very grateful. I also want to acknowledge my great indebtedness to the experimenters who have provided, in the scientific literature, the excellent data that I have used, and am using, to test my theory and various tentative hypotheses.

(23) D. S. Adcock and M. L. McGlashan, *Proc. Roy. Soc., Ser. A*, **226**, 266 (1954).

(24) M. D. Peña and F. F. Martín, *An. Real Soc. Espan. Fis. Quim., Ser. B*, **59**, 323 (1963).

Derivation of a Surface Tension Equation for Mixed Organic Liquids from a Binary Surface Tension Equation

by H. S. Chang

Soo Doo Women's Teachers College, Ha Wang Siq Ri, Seoul, Korea *(Received May 28, 1969)*

There is as yet no method of calculation of surface tension for three or more component organic solutions. In this paper the author attempts to derive surface tension equations from a binary system. The two mathematical procedures used for calculating the surface tensions of liquids are (i) a step by step method using a binary surface tension equation and (ii) using ratio differences of physical properties of only the first and last liquids and the mean of different coefficient values of the mixtures.

$$\sigma = \sigma_1 - \frac{RT}{\Sigma} \ln (X_1 + X_2 C)$$

$$\sigma = \sigma_1 - \left(\frac{\bar{\sigma}_{x \cdot y}}{\bar{\sigma}_x \cdot \bar{\sigma}_y}\right)\left(\frac{RT}{\Sigma}\right) \ln(X_1 + X_2 C)$$

When the values from the two equations are compared with experimental data, the value calculated by the mean difference coefficient method is nearer the experimental value. The comparison of calculated and experimental values shows that surface tensions of more-than-three-component organic liquid mixtures are around 24.77–25 dyn/cm.

Introduction

Expressions of surface tension for binary liquid mixtures have been derived with three different physical parameters, such as activity, distribution, and absorption constants. These expressions have basically the same form, the only difference between them being the values of the physical properties of liquids that were used in the equation.

For the surface tension of a binary system this is given as $\sigma = \sigma_1 - RT/\Sigma \ln (X_1 + X_2 C)$[1]; $C = \exp \cdot (\sigma_1 - \sigma_2/RT)\Sigma$, σ = surface tension for the mixture, σ_1 = surface tension for liquid 1, σ_2 = surface tension for liquid 2, R = gas constant, T = temperature, Σ = area, X_1 = mole per cent for liquid 1, X_2 = mole per cent for liquid 2, C = parameter (value given later).

Not only the surface tension for binary liquids, but also that for a multicomponent system can be calculated by this equation. (A multicomponent system may contain organic and inorganic liquids. In this paper, only organic liquids are discussed.)

Experimental Section

Measurements of surface tension were made with a Du Nöey tensiometer. In this experiment, a thermos flask was used to regulate the temperature during the measurement. The temperature of the flask was constant to $\pm 1°$.

Discussion

To express surface free energy, one must consider all the factors affecting it. Surface free energy is the summation of intermolecular energy, bulk phases, surface energy differences, and energy values from attraction in the lattice.

The expression for binary surface free energy is given by[1]

$$\frac{\partial \Delta F}{\partial n_{1s}} = \Delta F_1^0 + KT \ln \frac{X_{1s}}{X_1}$$

$$\frac{\partial \Delta F}{\partial n_{2s}} = \Delta F_2^0 + KT \ln \frac{X_{2s}}{X_2}$$

If one considers the other factors, where $A = 1$, $B = 2$

$$\frac{\Delta F}{A} = \frac{\Delta F_1^0}{A_{1s}} + \frac{KT}{A_{1s}} \ln \frac{X_{1s}}{X_1} + (X_1 \Delta F_1^0 + X_2 \Delta F_2^0) \times$$

$$\frac{(N_1 + N_2)A_1}{N_{1s}A_{1s} + N_{2s}A_2} = \sigma_1^0 + \frac{KT}{A_{1s}} \ln \frac{X_{1s}}{X_1} +$$

$$\frac{A_1 - A_{1s}}{A_{1s}}\left(\sigma_1^0 + \frac{KT}{A_1} \ln \frac{X_{1s}}{X_1}\right) + (X_1 \sigma_1^0 + X_2 \sigma_2^0) \times$$

$$\left(\frac{N_1 + N_2}{N_1 A_1 + N_2 A_2} - 1\right)\frac{A_1}{A_{1s}} = \sigma_1^0 + \frac{KT}{A_{1s}} \ln \frac{X_{1s}}{X_1} + p \ldots$$

(1) J. W. Belton and M. G. Evans, *Trans. Faraday Soc.*, **41**, 1. (1945).

then

$$\sigma = \sigma_1 + \frac{KT}{A}\log\left(\frac{X_{1s}}{X_1}\right) = \sigma_2 + \frac{KT}{A}\log\left(\frac{X_{1s}}{X_1}\right)$$

$$\sigma = \sigma_A + \frac{KT}{A}\log\left(\frac{X_{As}}{X_A}\right) - \left(\sigma_B + \frac{KT}{A}\right)\log\left(\frac{X_{Bs}}{X_B}\right)$$

$$= \sigma_A + \frac{KT}{A}\log\left(\frac{X_{As}}{X_A}\cdot\frac{X_B}{X_{Bs}}\right) = \sigma_B + \frac{KT}{A}\log 1$$

$$= \sigma_A + \frac{KT}{A}\log\left(\frac{X_{As}}{X_A}\cdot\frac{X_B}{X_{Bs}}\right) = \sigma_B + \ldots$$

$$\therefore \sigma = \sigma_A - \sigma_B + \frac{KT}{A}\log\left(\frac{X_{As}}{X_A}\cdot\frac{X_B}{X_{Bs}}\right)$$

Introducing here a parameter C which has the value

$$C = \left(\frac{X_{1s}}{X_1}\right)^{a_2}\left(\frac{X_2}{X_{2s}}\right)^{a_1} \times \exp\frac{X_1a_1(\Delta F_2^0 - \Delta F_1^0) + X_2a_2(\Delta F_2^0 - \Delta F_1^0)}{KT}$$

$$\log C = a_1\log\left(\frac{X_{1s}}{X_1}\right) + a_2\log\left(\frac{X_2}{X_{2s}}\right) \times \left\{\frac{X_1a_1 + X_2a_2}{KT} \times (\Delta F_2^0 - \Delta F_1^0)\right\}$$

Then

$$\sigma = \sigma_A - \sigma_B + \frac{KT}{A}\log\left(\frac{X_{As}}{X_A}\cdot\frac{X_B}{X_{Bs}}\right) = \frac{KT}{A}\log C$$

Calculating and introducing from the above equations[2]

$$X_1a_1\Delta F_2^0 - X_1a_1\Delta F_1^0 + X_2a_2\Delta F_2^0 - X_2a_2\Delta F_1^0 =$$

$$X_1a_1(\Delta F_2^0 - \Delta F_1^0) + (\Delta F_2^0 - \Delta F_1^0)X_2a_2 =$$

$$\Delta F_2^0(X_1a_1 + X_2a_2) - \Delta F_1^0(X_1a_1 + X_2a_2)$$

$$\sigma = \sigma_A^0X_1 + \sigma_B^0X_2$$

$$\sigma = \sigma_A^0 + \sigma_B^0\frac{X_2}{X_1} = \sigma_A^0 + \left(\frac{KT}{A}\log C\right)\frac{X_2}{X_1}$$

$$= \sigma_A^0 + \left(\frac{KT}{A}\log\frac{CX_2}{X_1}\right) \quad X_1 = X_2$$

$$\sigma = \sigma_A^0 - \frac{KT}{A}\log(X_1 + X_2C)$$

The above equation expresses the surface tension of a binary liquid. From this equation, three-component surface tension values can be calculated. Schmidt extended this method of ratio differences for binary mixtures to the surface tension of multicomponent mixtures $n = 1, 2, 3, 4 \ldots$ In the first method, the surface tension for any two liquids is calculated from the two-liquid surface tension equation and from this the other liquid values are calculated, again using the two-liquid surface tension equation. This method of calculating surface tensions of mixtures may be called the step-by-step method.

Table I: Binary Liquid Surface Tensions at 20°, 1 Atm

Mixture	Method I: Surface tensions	Method I: Av dev	Method II: Surface tension	Method II: Av dev	Exptl Data
Acetone–benzene	27.19	−1.29	...	...	28.48
Carbon tetrachloride–benzene	27.18	−1.36	...	...	28.54
Carbon tetrachloride–ethyl ether	22.42	46.05	...	...	22.37
Chloroform–ethyl ether	23.46	0.24	...	...	23.70
Chloroform–ethyl alcohol	24.60	0.51	...	...	25.11
Acetone–ethyl alcohol	23.86	0.31	...	...	23.55

The second method of calculating surface tensions of multicomponent liquid systems uses ratios of activity coefficients or ratios of any physical properties, that is

$$\left(\frac{X_{1s}}{X_1}\right)\left(\frac{X_{2s}}{X_2}\right); \text{ or } \left(\frac{X_{2s}}{X_2}\right)\left(\frac{X_{3s}}{X_3}\right)$$

In the binary surface tension equation this mole per cent part becomes

$$\left(\frac{X_{1s}}{X_1}\right)^{a_1}\left(\frac{X_2}{X_{2s}}\right)^{a_2}$$

and

$$\left(\frac{X_{2s}}{X_2}\right)^{a_2}\left(\frac{X_3}{X_{3s}}\right)^{a_3}$$

where a_1 = area for liquid 1, a_2 = area for liquid 2, a_3 = area for liquid 3, and $a_1 = a_2 = a_3$. For the three-component system the coefficients in the equation will be[2]

$$\left(\frac{X_{1s}}{X_1}\right)^{a_1}\left(\frac{X_2}{X_{2s}}\right)^{a_2}; \left(\frac{X_{2s}}{X_2}\right)^{a_2}\left(\frac{X_3}{X_{3s}}\right)^{a_2}$$

giving simply

$$\left(\frac{X_2}{X_{2s}}\right)^{a_2}\left(\frac{X_{2s}}{X_2}\right)^{a_3} \quad a_2 = a_3$$

Similary for the parameter c, only the ratios in physical properties of the first and the last liquids appear

$$\left(\frac{X_{1s}}{X_1}\right)^{a_1}\left(\frac{X_{3s}}{X_3}\right)^{a_3}$$

(2) R. L. Schmidt, *J. Phys. Chem.*, **71**, 1152 (1967).

This shows that for a three or more component system, surface tensions may be calculated from physical properties of the first and the last components.

Surface tension calculated with this method will look as though it was for only the first and the last components with the inclusion of a mean difference coefficient. Mean difference coefficients are used to take average values of physical properties.

The mean difference coefficient is given by $\bar{\sigma}_{x \cdot y}/\bar{\sigma}_x \cdot \bar{\sigma}_y$ where $\bar{\sigma}_{x \cdot y}$ is the mean value of the first liquid X

Table II: Three-Liquid Surface Tensions at 20°, 1 Atm

Mixtures	Method I		Method II		Exptl data
	Surface tension	Av dev	Surface tension	Av dev	
Acetone–benzene–carbon tetrachloride	26.67	0.04	26.69	0.07	26.63
Benzene–carbon tetrachloride–ethyl ether	24.97	0.23	24.79	0.05	24.74
Carbon tetrachloride–ethyl ether–chloroform	23.88	0.12	23.83	0.07	23.76
Ethyl ether–chloroform–ethyl alcohol	23.38	0.06	23.37	0.05	23.32
Chloroform–ethyl alcohol–acetone	25.07	0.33	24.79	0.05	24.74
Ethyl alcohol–acetone–benzene	23.75	0.60	23.30	0.15	23.15

Table III: Four-Liquid Surface Tensions at 20°, 1 Atm

Mixtures	Method I		Method II		Exptl data
	Surface tension	Av dev	Surface tension	Av dev	
Acetone–carbon tetrachloride–benzene–ethyl ether	23.97	0.57	24.60	0.06	24.54
Benzene–carbon tetrachloride–ethyl alcohol–acetone	24.77	0.38	24.45	0.06	24.39
Chloroform–acetone–benzene–carbon tetrachloride	23.85	0.54	24.47	0.08	24.39
Carbon tetrachloride–ethyl ether–chloroform–ethyl alcohol	22.39	0.02	23.37	1.00	22.37
Ethyl alcohol–benzene–acetone–carbon tetrachloride	27.64	0.39	27.31	0.06	27.25
Ethyl ether–chloroform–ethyl alcohol–acetone	25.98	0.02	25.86	0.06	25.80

Table IV: Five-Liquid Surface Tensions at 20°, 1 Atm

Mixtures	Method I		Method II		Exptl data
	Surface tension	Av dev	Surface tension	Av dev	
Acetone–benzene–carbon tetrachloride–ethyl ether–chloroform	25.44	0.47	25.02	0.05	24.97
Benzene–carbon tetrachloride–ethyl ether–chloroform–ethyl alcohol	24.28	0.27	25.09	0.07	25.03
Carbon tetrachloride–ethyl ether–acetone–chloroform–benzene	23.79	0.34	24.37	0.06	24.31
Acetone–ethyl ether–benzene–carbon tetrachloride–chloroform	24.13	0.27	23.45	−0.94	24.39
Acetone–chloroform–benzene–ethyl ether–carbon tetrachloride	25.74	0.55	25.25	0.06	25.11
Acetone–benzene–carbon tetrachloride–ethyl ether–chloroform	23.51	0.50	24.06	0.05	24.01

times the mean value of the last liquid Y, and $\bar{\sigma}_x$ and $\bar{\sigma}_y$ the mean values for all the single liquids X and for all are single liquids Y, respectively.

X and Y are any components in the mixture where Y is not the same as X; multicomponent systems are divided for calculation is into X, Y binary systems.

$$\sigma = \sigma_1 - \left(\frac{\bar{\sigma}_{x \cdot y}}{\bar{\sigma}_x \cdot \bar{\sigma}_y}\right)\frac{RT}{\Sigma} \ln (X_1 + X_2 C)$$

is the surface tension value for the mixture. The data in the second column of Tables I–IV were calculated from the above equation. This equation gives better agreement with the experimental value than values obtained from the step-by-step equation.

From the five different surface tension values, it can be seen that the surface tension of more-than-three component mixtures of hydrocarbons is about 25 dyn/cm.

Study of Protonic Transfers in the Ammonia–Silica Gel System by Infrared and Pulsed Proton Magnetic Resonance Spectroscopy and by Conductivity Measurements

by J. J. Fripiat,[1] C. Van der Meersche,[2] R. Touillaux,[1] and A. Jelli[2]

Laboratoire de Physico-Chimie Minérale, Institut des Sciences de la Terre, Heverlee, Belgium *(Received December 27, 1968)*

As shown by infrared spectroscopy, ammonia adsorbed by the hydroxylated surface of Aerogel is partially converted into ammonium, the ratio of the NH_4^+/NH_3 surface concentrations being approximately 0.3 at the monolayer coverage and at 20°. Ammonium is strongly hydrogen bonded to ammonia, suggesting a possible proton transfer along the N–N axis. Dielectric measurements reinforce this hypothesis since, at the frequency of 1592 cps, the conductivity seems mainly due to the proton exchange process, the "gross" diffusion coefficient being 0.5×10^{-11} cm^2 sec^{-1}. The "gross" diffusion coefficient involves proton tunneling along the N···N axis and reorientation of orbitals, the rate limiting process being probably the rotational motion. From this model and pulsed nuclear magnetic resonance experiments, the proton spin–lattice relaxation rate (T_1^{-1}) in adsorbed ammonia is probably mostly contributed by the proton transfer in the $NH_4^+ + NH_3$ exchange process while the proton spin–spin relaxation rate (T_2^{-1}) is mainly due to rotational motions of the adsorbed species. The jump frequency along the N···N axis is approximately 0.5×10^9 sec^{-1} at the monolayer coverage and at 25°, in good agreement with the jump frequency in the liquid ammonia–ammonium system. The activation energy of the proton transfer is of the order of 5 kcal mol^{-1} and the activation energy of the molecular rotational motion is approximately 3 kcal mol^{-1}. The sum of these activation energies is close to the activation energy obtained for the "gross" diffusion coefficient.

Introduction

The surface of amorphous silica is partially covered by silanol groups and, depending on the partial pressure of water vapor, by one or several layers of water molecules. These molecules are hydrogen bonded to each other and to the silanol groups.

Both the silanol groups and the water molecules in contact with the surface have acid properties[2] and, therefore, their protons must have an appreciable mobility. This contribution aims to define the mobile character of the surface protons of an Aerogel by following their reaction with ammonia by various techniques. Because of the complexity of the system, it appears highly desirable to obtain a first approximate model for the adsorbed phase from infrared spectroscopy and dielectric measurements and then, in light of this information, to compare the expected nuclear magnetic relaxation times of the hydrogen nuclei contained in the adsorbed species to those obtained experimentally. In agreement with this program, Packer[3] concluded a review paper on the nuclear relaxation studies of adsorbed molecules by saying that

(1) (a) The University of Louvain and M.R.A.C. (Tervuren). (b) Research Associates at Glaverbel.

(2) J. J. Fripiat, A. N. Jelli, G. Poncelet, and J. V. André, *J. Phys. Chem.*, 69, 2185 (1965).

(3) K. J. Packer, "Progress in NMR Spectroscopy," Vol. 3, J. M. Emsley, J. Feeney, and L. H. Sutcliffe, Ed., Pergamon Press, Ltd., London, 1968, p 81.

"the investigation of high surface area adsorbents solely by nuclear spin relaxation is unlikely to yield unambiguous informations but in conjunction with other methods, it can give detailed informations about adsorbate–adsorbent interactions."

The infrared study has been limited to the bending vibrations region. In spite of numerous studies[4-8] that have been carried out on the spectroscopic characteristics of NH_3 adsorbed on silica gels and porous glass, no extensive data exist on the 6–7-μ region where the deformation bands (ν_4) of NH_3 and NH_4^+ clearly appear. Peri[4] has been able to identify the $-NH_2$ species in the region of the stretching bands in Aerogel outgassed at 800°. Low, *et al.*,[5,8] come to a similar conclusion for Vycor glass and, moreover, they have shown the existence of the B:NH_3 interaction. Chapman and Hair,[6a] Felden,[6b] and Boyle, *et al.*,[7] consider that a band appearing at 3450 cm^{-1} is caused by the formation of NH_4^+ but Low, *et al.*,[5] point out that this band may be misinterpreted because of the proximity of the stretching band of $-NH_2$. The symmetric deformation mode of NH_3 appears at 950 cm^{-1} (938–962 cm^{-1}) in the gaseous state and at 1050 cm^{-1} for NH_3 adsorbed on silica gel. This frequency shift is interpreted by Cant and Little[9] as due to the formation of a hydrogen bond with the surface silanols. From this review, the presence of NH_4^+ on silica surfaces appears at the least as uncertain: the overlapping of the OH, NH, and $^+$NH stretching modes precludes any clear conclusion.

The dielectric properties of ammonia adsorbed on silica have been studied by Waldman,[10,11] who has observed a strong dielectric absorption for the NH_3–silica gel system between 10^2 and 10^6 cps in the temperature range of -175 to 20°. The intensity of the absorption peaks varies with frequency and temperature, which suggests a contribution of the Maxwell–Wagner effects. A clear discontinuity in the increase in intensity of the absorption peaks is observed at the completion of the first layer.

Folman, *et al.*,[12,13] have studied the dielectric absorption of NH_3 adsorbed on porous Vycor glass pretreated above 450°. For an adsorbent having a moderate concentration of OH groups, two bands are found in the temperature range 250–350°K at the frequency of 23.6 Mc/sec, the potential barriers corresponding to the orientation of NH_3 on these two sites being 1.98 and 2.56 kcal mol^{-1}. The latter is assigned to NH_3 possibly adsorbed on boron while the former is probably due to NH_3 hydrogen bonded to surface hydroxyls.

Fiat, *et al.*,[14,15] have measured the proton longitudinal (T_1) and transversal (T_2) relaxation times in ammonia adsorbed on a Vycor porous glass. The main results may be summarized as follows. T_1 and T_2 depend greatly on the degree of coverage (θ) because of a broad distribution of the correlation times assigned to two kinds of motions: (1) Diffusion of adsorbed NH_3 also influences the interactions between NH_3 and the surface silanol groups. Assuming that the NH_3 adsorption energy is approximately equal to the activation energy of the diffusion process, the correlation time for this process ranges from 3×10^{-9} to 4×10^{-7} sec at 20°. (2) The correlation time obtained from dielectric measurements for the rotation of NH_3 on its adsorption site does not correlate with that deduced from nmr.

Fiat, *et al.*, did not consider the possible influence of a proton transfer from NH_4^+ to NH_3 nor the diffusion or rotation of NH_4^+, probably because of the high temperature pretreatment applied to the porous glass. Under the milder outgassing conditions adopted here, an appreciable fraction of adsorbed NH_3 might be converted into NH_4^+.

The multiphase behavior observed by Zimmerman, *et al.*,[16-18] and by Woessner[19-21] for the H_2O–silica gel system has not been observed. Indeed, it has never been possible to find any evidence of the existence of multiple relaxation times. This could be due to the large pores (average radius 400 Å) characterizing the Aerogel sample, in agreement with Winkler's[22] conclusions that multiple relaxation times are observed for water adsorbed by microporous silica gel only. It must also be pointed out that with the instrument used in this work, the signal due to the relaxation of surface hydroxyl groups or of NH_3 at low degree of coverage ($\theta < 0.3$) is not measurable. The pulse nuclear magnetic resonance technique (pnmr) is less sensitive than the usual nmr spectroscopy. However, it offers the advantage of getting rid of the lack of homogeneity of the magnetic field.

(4) J. Peri, *J. Phys. Chem.*, **70**, 2937 (1966).

(5) M. J. D. Low, N. Ramasubramanian, and V. V. Subba Rao, **71**, *ibid.*, 1726 (1967).

(6) (a) I. D. Chapman and M. L. Hair, *J. Catal.*, **2**, 145 (1963); (b) M. Felden, *Compt. Rend.*, **249**, 682 (1959).

(7) T. W. Boyle, W. J. Gaw, and R. A. Ross, *J. Chem. Soc.*, 240 (1965).

(8) M. J. D. Low and N. Ramasubramanian, *J. Phys. Chem.*, **70**, 2740 (1966).

(9) N. W. Cant and L. M. Little, *Can. J. Chem.*, **45**, 3055 (1967).

(10) M. H. Waldman, *Cahiers Phys.*, **60**, 9 (1955).

(11) M. H. Waldman, *J. Phys. Radium*, **17**, 426 (1956).

(12) U. Feldman and M. Folman, *Trans. Faraday Soc.*, **60**, 440 (1964).

(13) I. Lubezky, U. Feldman, and M. Folman, *ibid.*, **61**, 2 (1965).

(14) D. Fiat and J. Reuben, Proceedings of the XIVth Colloque Ampère, Ljubljana, 1966, p 1143.

(15) J. Reuben, D. Fiat, and N. Folman, *J. Phys.*, **45**, 311 (1966).

(16) J. R. Zimmerman, B. G. Holmes, and J. A. Lasater, *J. Phys. Chem.*, **60**, 1157 (1956).

(17) J. R. Zimmerman and W. E. Brittin, *ibid.*, **61**, 1325 (1957).

(18) J. R. Zimmerman and J. A. Lasater, *ibid.*, **62**, 1157 (1958).

(19) D. E. Woessner, *J. Chem. Phys.*, **37**, 647 (1962).

(20) D. E. Woessner, *ibid.*, **39**, 2783 (1963).

(21) D. E. Woessner and J. R. Zimmerman, *J. Phys. Chem.*, **67**, 1590 (1963).

(22) H. Winkler, *Wiss. Z. Karl-Max-Univ. Leipzig, Math. Naturwiss. Reihe*, **4**, 913 (1965).

Surface Properties of Aerogel and NH_3 Adsorption Isotherms

The "Aerogel" used for this study was prepared as described by Imelik and Carteret,[23] by precipitating a concentrated solution of sodium silicate by formic acid. The specific surface area was 135 m^2/g and the average pore radius was about 400 Å. The Na and Fe contents were both of the order of 6×10^{-6} g-atom/g of SiO_2. The surface hydroxyl content determined by a procedure described by Fripiat and Uytterhoeven[24] was about 0.8×10^{-3} silanol group/g of SiO_2. In the films that were used for infrared spectroscopic studies and that were obtained by pressing the powder at approximately 300 kg/cm^2, 10^{-3} mol of H_2O/g remained after outgassing at 100°. At about 250° and under a better vacuum ($\sim 10^{-5}$ mm), the water was almost completely removed.

It is probable that outgassing the powdered sample *in vacuo* removes the hydration water at a lower temperature. After pretreatment at 130° under vacuum, Van Tongelen, Uytterhoeven, and Fripiat[25] measured a hydroxyl content (H_2O and silanol) of 2.5×10^{-3} OH/g of SiO_2 by the diborane technique.

The ammonia adsorption isotherms are shown in Figure 1. The data obtained after outgassing under vacuum at 120 and 200° agree fairly well whereas the isotherm measured for the sample outgassed at 20° shows a weaker adsorption.

If a cross section area of 13 $Å^2$ is assigned to an adsorbed ammonia molecule, the monolayer coverage is achieved for 1.8×10^{-3} mol of NH_3 adsorbed per gram, under an ammonia equilibrium pressure of about 1 mm. The isotherm is thus rather steep at low pressure, suggesting an appreciable contribution of a chemisorption process.

Determination of the Nature of the Adsorbed Species by Infrared Spectroscopy

The most interesting spectral region for the identification of the adsorbed species ranges between 6 and 7.5 μ. It covers the bending band of water and the asymmetric deformation bands of ammonia and NH_4^+. Unfortunately, a Si–O harmonic or combination band also appears approximately at 6 μ and interferes with the bending band of water and the asymmetric deformation band of ammonia.[26] Figures 2A and 2B summarize the results obtained in absorbance, for a film outgassed at 120°, or in transmission, for a film outgassed at 200°.

Three bands at 1450, 1500, and 1600 cm^{-1}, respectively, can be assigned to the adsorbed species. The Si–O vibration band, the H_2O bending band, and the gaseous NH_3 deformation band (that can be present in the cell) contribute to the ir beam absorption in the 1640-cm^{-1} region.

Regardless of the outgassing temperature, the bands due to the adsorbed species are modified in a similar way according to the surface coverage. At low degree of

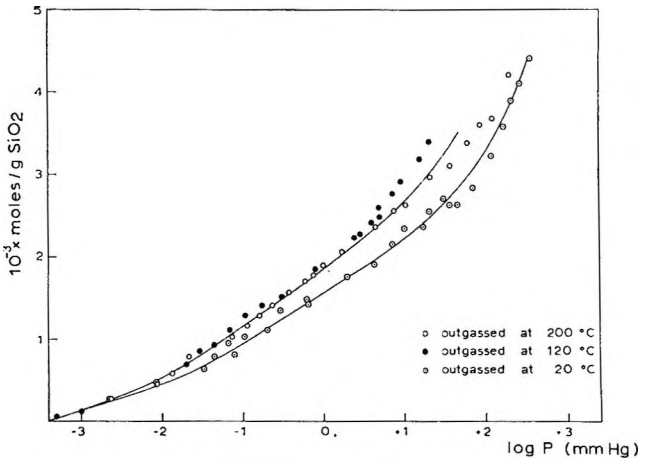

Figure 1. Adsorption isotherms of ammonia on Aerogel at 20° after outgassing at 20, 120, and 200°.

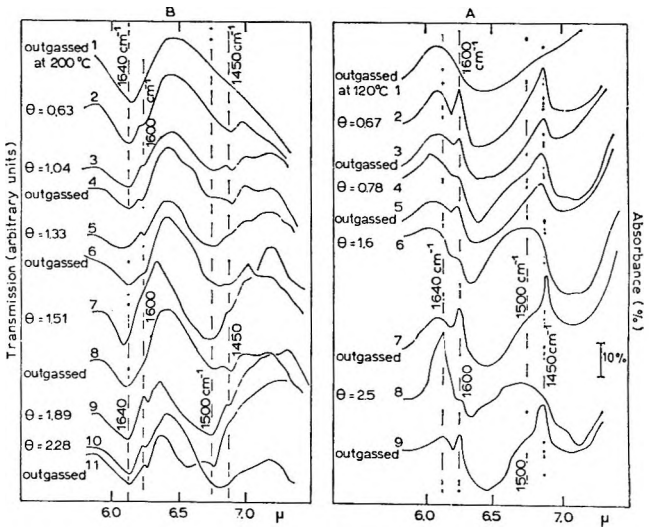

Figure 2. Infrared spectra of adsorbed species at increasing coverage degree (θ). A, Gel initially outgassed at 120° and B, initially outgassed at 200° under a residual pressure of 10^{-6} mm. Outgassing between the adsorption steps is carried out for a few minutes at a pressure of about 10^{-3} mm at 20°.

surface coverage ($\theta < 1$), the most intense bands are observed at 1450 and at 1600 cm^{-1} (*cf.* curve 2, Figure 2A and curves 2 and 3, Figure 2B).

The decrease in intensity of the band at 1600 cm^{-1} when the pressure is quickly reduced to 10^{-3} mm at room temperature is more pronounced than that of the band at 1450 cm^{-1}. For $\theta \simeq 1$, the band at 1500 cm^{-1} increases (*cf.* curves 2 and 3, Figure 2A and curve 4, Figure 2B). At this stage, reducing the pressure to 10^{-3} mm at room temperature weakens the intensity

(23) B. Imelik and Y. Carteret, *Bull. Soc. Chim. France*, 864 (1951).

(24) J. J. Fripiat and J. B. Uytterhoeven, *J. Phys. Chem.*, 66, 800 (1962).

(25) M. Van Tongelen, J. B. Uytterhoeven, and J. J. Fripiat, *Bull. Soc. Chim. France*, 2318 (1965).

(26) L. H. Little and M. V. Mathieu, *Actes Intern. Congr. Catalyse, 2e Paris*, 1, 771 (1961).

of the band at 1500 cm^{-1} relative to that at 1600 cm^{-1} (*cf.* curves 3 and 4, Figure 2A and curves 4 and 5, Figure 2B).

When $\theta > 1$, the 1500-cm^{-1} band grows more intense than that at 1450 cm^{-1}, whereas the band at 1600 cm^{-1} gets weaker (*cf.* curves 6 and 8, Figure 2B and curves 5, 7, and 9 Figure 2A). Outgassing the sample at this point reinforces the band at 1600 cm^{-1} and weakens the band at 1500 cm^{-1} (*cf.* curves 5 and 6, 7 and 8 of Figure 2A; 6 and 7, 8 and 9 of Figure 2B).

These observations can be interpreted assigning (1) the band at 1600 cm^{-1} to the asymmetric deformation of NH_3 molecules isolated on the surface; (2) the band at 1450 cm^{-1} to the asymmetric deformation of NH_4^+ formed by the transfer of a proton belonging either to a silanol group or to a water molecule, and (3) the band at 1500 cm^{-1} to the asymmetric deformation of NH_4^+ hydrogen bonded to NH_3.

For $\theta < 1$, the NH_3 and NH_4 species are isolated from each other: the most noticeable bands are observed at 1600 cm^{-1} and at 1450 cm^{-1}. Evacuation of gaseous NH_3 in equilibrium with the adsorbed phase influences more NH_3 than NH_4^+, which suggests, as it can be expected, that the latter is more strongly adsorbed than the former. At higher surface coverage ($\theta \simeq 1$), the adsorbed species come closer to each other and NH_4^+–NH_3 "units" are formed giving rise to the band at 1500 cm^{-1} whereas the band at 1600 cm^{-1} is weakened. For $\theta > 1$, the concentration in hydrogen-bonded ammonium increases furthermore and the band at 1500 cm^{-1} becomes the most intense. The weakening of the 1600-cm^{-1} band for $\theta > 1$ could be interpreted by a decrease of the charge of the transition moment caused by the polarity of the ^+N–H·N bond.

In summary, the infrared spectroscopy provides two types of information on the nature of the adsorbed species.

Firstly, it shows the simultaneous presence of NH_3 and NH_4^+ from the very beginning of the adsorption process. The integrated intensity of the NH_4^+ band is apparently larger than that of the band at 1600 cm^{-1} but the absorption coefficient of the ammonium asymmetric deformation band is approximately seven times larger than the absorption coefficient of the ammonia asymmetric deformation band (Fripiat, *et al.*[27]). When $\theta \simeq 1$, a rough estimate leads to a NH_4^+/NH_3 ratio of about 30%.

Secondly, infrared spectroscopy shows the formation of $^+NH\cdots N$ hydrogen bonds and thus it suggests indirectly a possible proton transfer along the ^+N–N axis.

Conductivity and Dielectric Constant Measurements

At room temperature, as shown further, the only phenomenon that can be measured, at frequencies lower than 20×10^3 cps, consists of an ionic conductivity process. To induce Debye's dipolar absorption in this frequency range, it is necessary to slow down the molecular movements by lowering the temperature.

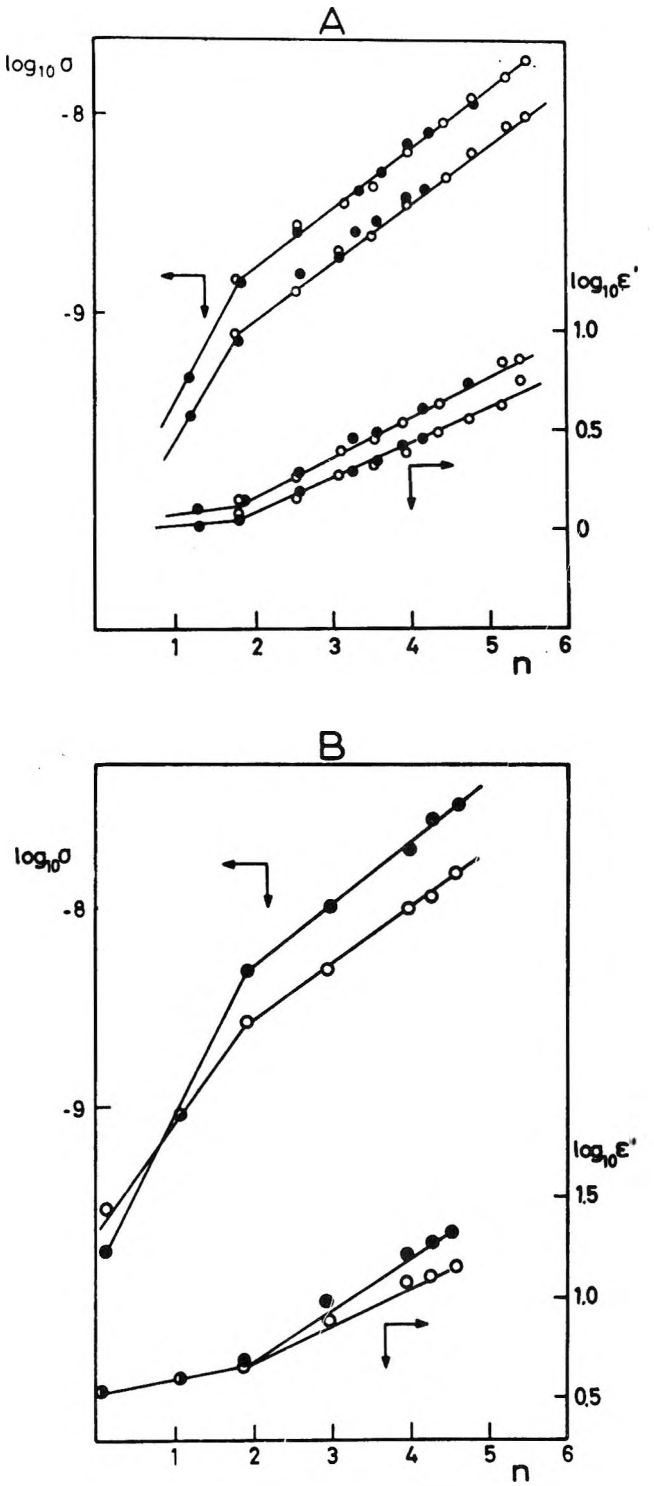

Figure 3. Variation of log σ and log ϵ' as function of the number (n) of NH_3 molecules removed from the gas phase. Aerogel pretreated at 120°, residual pressure 10^{-6} mm. A, measurements at 20°; ○, adsorption; ●, desorption. The two sets of results correspond to two different pellets. B, measurements at 40° (○ and ● different pellets). Frequency, 1592 cps.

(27) J. J. Fripiat, A. Léonard, and J. B. Uytterhoeven, *J. Phys. Chem.*, 69, 3274 (1965).

Dielectric measurements have thus been performed down to −190°.

A Wayne–Kerr ac bridge operated at frequencies from 2×10^2 to 2×10^4 cps allows one to measure simultaneously the parallel conductance and capacitance of the pellets.

The study of the dispersion of the real (ϵ') and imaginary (ϵ'') terms of the complex dielectric constant with respect to the frequency demonstrates that, at room temperature, the main phenomenon is the absorption of the electrical energy by free charge carriers: ϵ'', as well as ϵ', decrease steadily at increasing frequency at any specified degree of coverage. Therefore, under these conditions, the model suggested earlier[2] may be adopted: charge carriers (e) have to jump over the potential barrier U in order to move from one equilibrium position to the next. The specific conductivity σ is then given by

$$\sigma = n_p \nu \frac{e^2(2l)^2\rho}{kT} \exp\left(+\frac{4\pi(e)^2 h n_p}{kTA}\right) \quad (1)$$

where n_p is the number of charge carriers per unit weight; ρ, the density of the sample; ν, the number of "jumping attempts" per second; and $2l$, the distance between two equilibrium positions. A is the surface area and h the distance between the surface and the conduction level. As shown in Figure 3, for sections of the adsorption isotherms

$$\sigma = \sigma_0 e^{m\theta} \quad (2)$$

and

$$\epsilon' = \epsilon_0' e^{p\theta} \quad (3)$$

where m and p are temperature-independent constants and θ, the degree of surface coverage. From relationships 2 and 3, it follows that the tangent of the loss angle is an exponential function of θ

$$\tan \delta = \frac{4\pi\sigma_0}{\omega\epsilon_0'} \exp(m - p)\theta \quad (4)$$

It does not depend on the surface coverage for $m \rightarrow p$. A clear discontinuity can be observed in Figure 3 for $n \simeq 1.8$; *i.e.*, for $\theta = 1$. When $\theta < 1$, the conductivity increases steeply whereas the dielectric constant varies but slightly. When $\theta > 1$, the dielectric constant and the conductivity increase in an almost parallel way but the conductivity increases less quickly than when $\theta < 1$.

By assuming the protons to be the main charge carriers, the interpretation of these observations seems rather obvious. The steep increase of σ for $\theta < 1$ would reflect the increasing concentration in NH_4^+ and the multiplication of the relays for protonic transfer ($NH_4^+ \rightarrow NH_3$). The loss factor would grow exponentially with θ. As soon as the ammonia molecules acting as relays for the protonic transfers are in sufficient number, the loss factor would become almost independent of θ. Indeed, for $\theta > 1$, $m \rightarrow p$ and thus, according to eq 4, the loss factor does not vary furthermore with the surface coverage.

In order to account for the slope of log σ against n in Figure 3, it is easily demonstrated that n_p/n should be approximately 10^{-2} for $\theta \simeq 1$ assuming that h is approximately equal to 1 Å.

Should the charge carriers be the ammonium cations, n_p would be of the order of $0.3n$ for $\theta \simeq 1$, since from the intensity of the NH_4^+ and NH_3 deformation bands, this concentration seems a reasonable estimation. Accordingly m should be 30 times higher than the experimental value.

In the range of kilometric electromagnetic waves, Debye dipolar absorption phenomena caused by the rotation of adsorbed molecules or by surface defects are expected to show up at low temperature. Effectively, two main domains of absorption have been observed. The first is well defined and appears between −120 and −60°. The second one is observed between −180 and −130° and is broader and less intense (ϵ'' max <10).

In the first domain, the temperature at which the maxima of the absorption bands can be observed does not shift in terms of frequency, but the band intensity increases considerably as the frequency decreases. It is therefore probable that these bands have to be assigned to a Maxwell–Wagner effect of dielectric heterogeneity, according to Freymann and Soutif.[28]

In the second domain (−180 to −130°) the absorption bands are broader and weaker. Their intensities do not vary in a considerable way with the frequency. Because of the impossibility to compute the activation energy in this temperature range, it seems very hazardous to assign them to any defined process. Assuming that they correspond to the rotation of NH_3, a band should appear at −170° at a frequency of 5×10^3 cps if the rotation period were $\tau_r = 2 \times 10^{-10} e^{3000/RT}$ sec. Such a period is of the order of magnitude of those found by Folman,[12] *et al.*

Proton Magnetic Relaxation Times Measurements

A 2-g sample of Aerogel contained in a Pyrex (15-mm id) tube is outgassed either at 20 or 200° until a pressure lower than 10^{-6} mm is reached. The sample is then equilibrated at the desired pressure of gaseous ammonia at room temperature until constant pressure and the tube is then sealed. The number of NH_3 molecules removed from the gas phase is obtained from the adsorption isotherms in Figure 1.

The BKR 302 pulse spectrograph, made by Brücker, coupled with a 14-kG Varian magnet, allows one to measure T_2 according to the spin-echo technique if T_2 is larger than 10^{-3} sec. Below 10^{-3} sec, T_2 is obtained from the decay curve of the first pulse. The error provoked by the magnetic field inhomogeneity does not affect markedly the T_2 measurement for such short

(28) A. Freymann and M. Soutif, "La Spectroscopie Hertzienne Appliquée à la Chimie," Dunod, Paris, 1960.

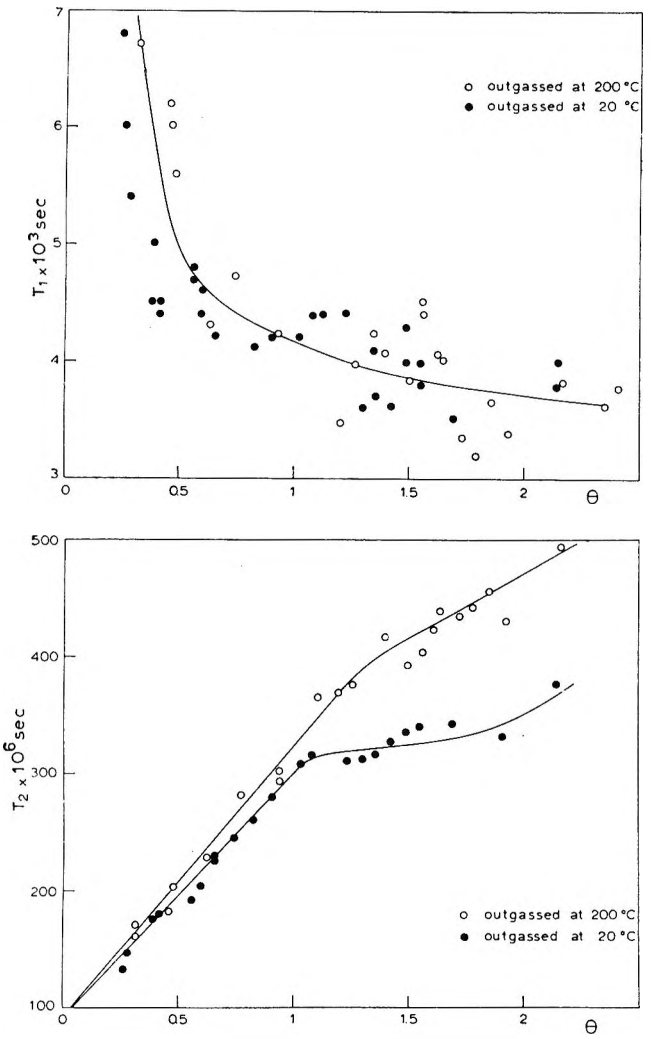

Figure 4. Top, variation of T_1 as function of θ at 20°; bottom, variation of T_2 as function of θ at 20°.

transversal relaxation times. T_1 is computed from the ratio of the signal amplitudes of two $\pi/2$, $\pi/2$ consecutive pulses in function of the time interval between them. The repetition time of the pulse sequence was 40×10^{-3} sec at a temperature close to the room temperature. It was increased up to 200×10^{-3} sec at $-100°$.

The temperature of the (sample + probe) system can be lowered and controlled from 20 to $-100°$ by blowing cold, dry air. Several experiments were performed in order to make sure that no appreciable NH_3 desorption occurs in the course of the sample cooling process. Measurements above 30° are unfortunately not possible because of NH_3 desorbing from the gel.

The error on T_2 is of the order of $\pm 10 \times 10^{-6}$ sec while T_1 is only reproducible within $\pm 250 \times 10^{-6}$ sec.

The instrument response is checked periodically using Fe^{3+} aqueous solutions in the concentration range of 10^{18} to 10^{21} ions per cm^3 and by comparing the $T_1 \simeq T_2$ results with those obtained by Bloembergen, Purcell, and Pound[29] and Gabillard.[30] The relaxation times obtained from experiments performed on separate NH_3–Aerogel systems prepared within a year are in very good agreement. Also, T_2 obtained by pnmr compares within $\pm 5\%$ with T_2 derived from the width of the nmr absorption band measured with the Varian DP60 spectrometer.

The variations of T_1 and T_2, either at increasing degree of coverage at constant temperature (20°) or at decreasing temperature and at a specified degree of coverage, are shown in Figures 4, 5, and 6 for the gels outgassed either at 20 or at 200°. For the measurements performed at 20°, T_2 increases linearly with θ in the range $0.3 < \theta < 1.0$, whereas T_1 decreases rapidly within the same limits. At higher degrees of coverage, T_1 scatters along a slightly decreasing function while T_2 increases but more slowly. In this range, a clear distinction is observed between the two pretreatment temperatures whereas at lower degrees of coverage the results do not differ appreciably. As shown in Figure 7, the main variation of T_1/T_2 occurs within the monolayer range.

For the measurements performed at decreasing temperature on samples maintained at specified degrees of coverage (Figures 5 and 6), only the results obtained for samples outgassed at 200° are shown. In the range $0.3 < \theta < 1.0$, they do not differ significantly from those obtained after outgassing at 20°. In all cases T_1 increases and T_2 decreases when the temperature is lowered: below $-80°$ the relaxation signal disappears. In all cases, T_1 levels in the temperature range from 5 to $-25°$. A leveling of T_2 occurs simultaneously but it is more apparent at low than at high degree of coverage. As measurements at temperatures higher than 30° cannot be performed without causing an appreciable NH_3 desorption, it is impossible to claim that a minimum value of T_1 is actually reached at approximately 25°. In spite of any clearer experimental evidence, this basic assumption will be maintained at all degrees of coverage. The reason for this will become clearer further but it must already be realized that this is the weakest point of this experimental section.

Provisional Model

The protonic transfers involved in the ammonia–silica gel surface interactions may be summarized as

$$\left.\begin{aligned} AH + NH_3 &\rightleftarrows A^- + NH_4^+ \\ NH_4^+ + NH_3 &\longrightarrow NH_3 + NH_4^+ \end{aligned}\right\} \quad (5)$$

where AH represents an acidic surface site. This could be either a silanol group or a residual water molecule. The protonation process represented by eq 5 may be divided into two steps as shown in eq 6

(29) N. Bloembergen, E. Purcell, and R. Pound, *Phys. Rev.*, **73**, 679 (1948).

(30) R. Gabillard, *Rev Sci.*, **90**, 307 (1952).

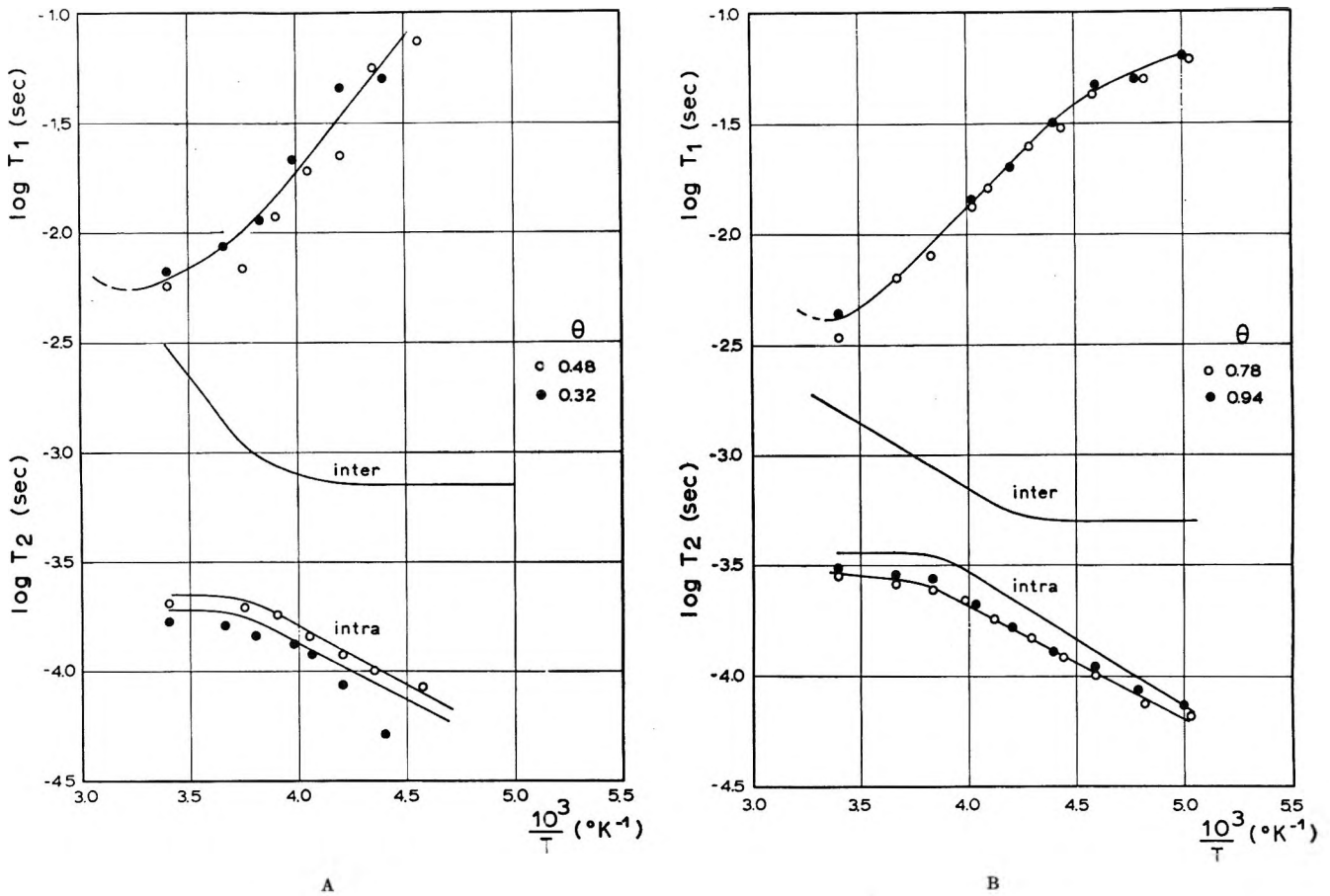

Figure 5. Variation of log T_1 and log T_2 as function of $1/T$ (°K). The upper curve is obtained assuming that the diffusional motion only contributes to T_1^{-1}, according to eq 13. Lower curve, best fitting curve of the experimental results obtained for T_2.

$$\left.\begin{aligned} AH &\rightleftharpoons A^- + H^+ \quad (K_1) \\ NH_3 + H^+ &\rightleftharpoons NH_4^+ \quad (K_2) \end{aligned}\right\} \tag{6}$$

leading to an equilibrium between the NH_4^+ and NH_3 species

$$K = K_1K_2 \tag{7}$$

where

$$K_2 = \frac{nx}{n(1-x)[H^+]} \tag{8}$$

x represents the ratio $[NH_4^+]/[NH_3]$ and n the number of NH_3 molecules removed from the gas phase. At 20°, x is of the order of magnitude of 0.3 for $\theta \simeq 1$, according to the corrected intensities ratio of the NH_4^+/NH_3 asymmetric deformations, and $[H^+]/n \simeq 10^{-2}$, according to the slope (m) of the empirical relationship (2). The monolayer coverage being achieved for $n \simeq 1.8 \times 10^{-3}$ mol, it follows that $K_2 \simeq 0.29 \times 10^5$ mol^{-1}. This corresponds to a pK_a of 4.46 in reasonable agreement with the usual value of 4.75 assigned to NH_4^+ at 25°.

From these data and from the infrared spectroscopy results, the following conclusions appear to be acceptable: (1) upon adsorption, NH_3 is partially transformed into NH_4^+ by a proton transfer from a surface silanol group or from a strongly acidic residual water molecule;[2] (2) the main contribution to the electrical conductivity is due to free protons coming from the dissociation of NH_4^+, since the $[H^+]/n$ ratio deduced from conductivity measurements leads to a reasonable evaluation of K_2; and (3) the conduction relays are probably the NH_3 molecules, the strong $^+NH\cdots N$ hydrogen bond, at the origin of the band at 1500 cm^{-1}, favoring the proton translation along the $N\cdots N$ axis.

The calculation of the proton diffusion coefficient from conductivity measurements (D_0) may then be attempted using the preexponential factor in eq 1 and taking into account that $n_p/n = 10^{-2}$ for $\theta \simeq 1$ and that $\rho = 2$. At the monolayer coverage, it is found that $D_0 = 0.5 \times 10^{-11}$ cm^2 sec^{-1}. From the data in Figure 3, the activation energy amounts to approximately 8 kcal.

In order to displace a proton from one point on the surface to another, a NH_4^+ cation has to direct one among its protons toward the free orbital of a NH_3 molecule and after the proton capture by the latter, the same reorientation process involving an other NH_3 molecule must occur. In the system H_3O^+–H_2O,

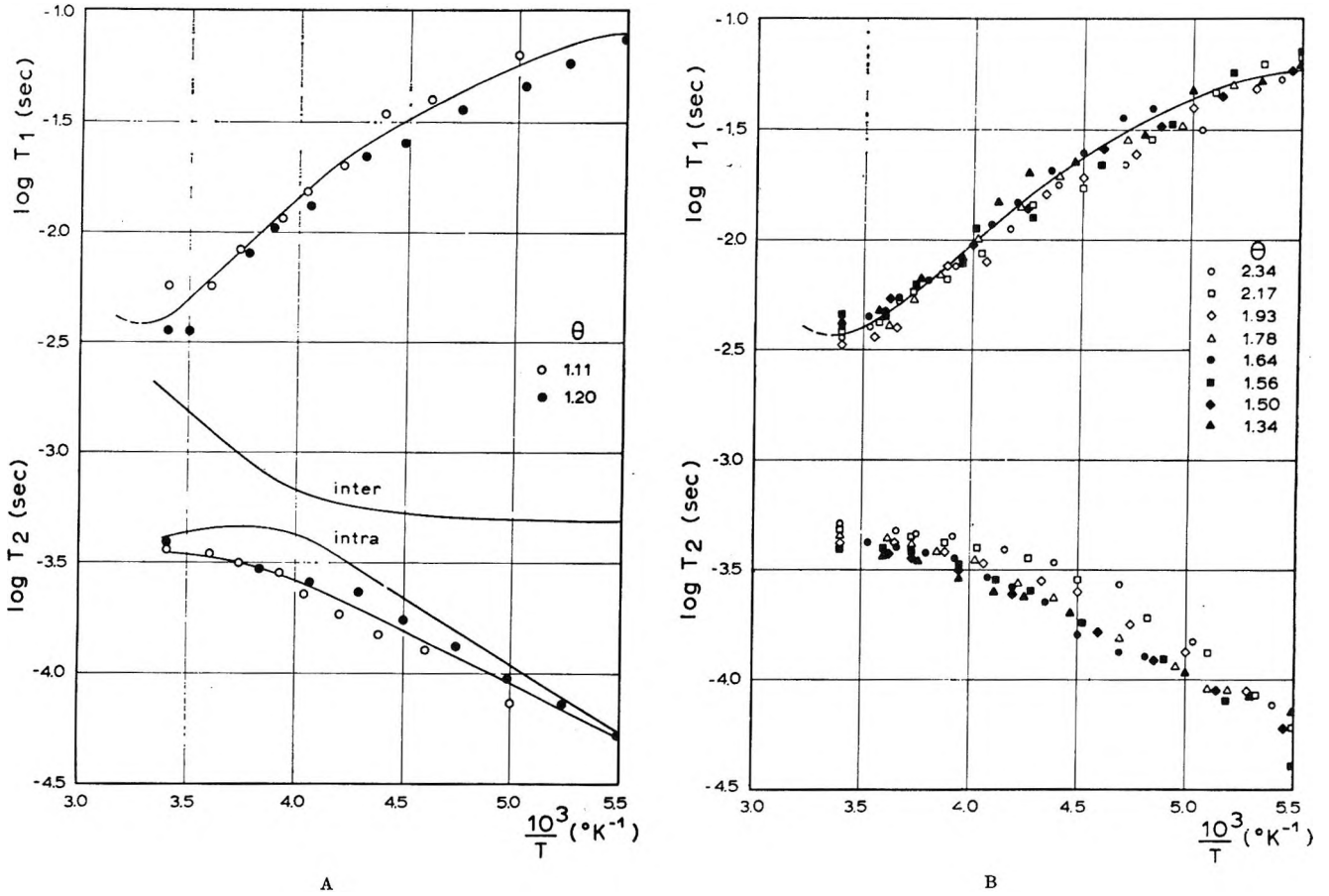

Figure 6. Same legend as in Figure 5.

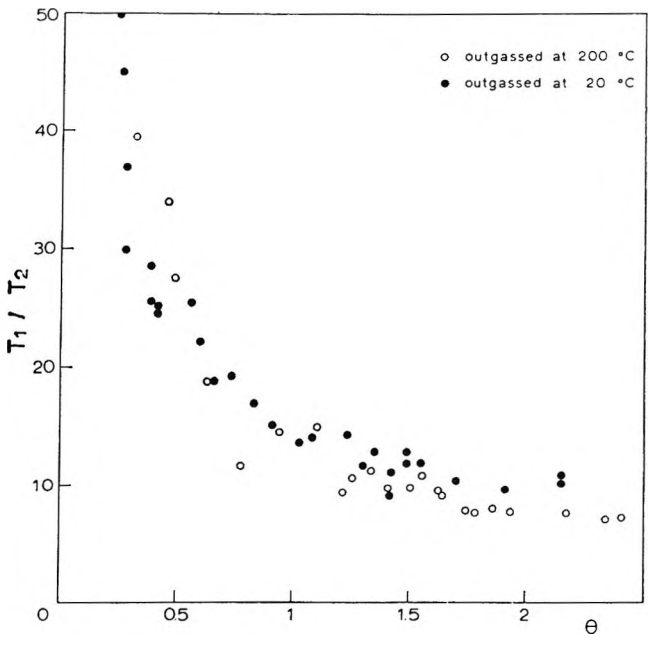

Figure 7. Variation of T_1/T_2 as function of θ at 20°.

Conway, *et al.*,[31] have shown that the limiting rate process for the proton diffusion is the orientation motion and not the tunneling rate along the O···O axis. At 25°, the probability of a such a suitable orientation diminishes by a factor of 0.25×10^{-3} the theoretical mobility computed from the tunneling rate. It seems appropriate to assume that a similar situation exists in the NH_4^+–NH_3 system. Let ν be the jump frequency deduced from the diffusion coefficient, $D_c = \nu(2l)^2$, accounting for the tunneling–reorientation processes and let ν_j be the jump frequency of the proton motion along the N–N axis in a $^+NH_4$–NH_3 pair, involving the tunneling only. D_c may be considered as a "gross" diffusion coefficient while $\nu_j(2l^*)^2$ represents the diffusion coefficient at the microscopic scale across the potential barrier along the $^+NH\cdots N$ hydrogen bond (barrier width = $2l^*$). According to the findings of Conway, *et al.*, ν/ν_j is of the order of 10^{-3} and thus ν_j should be about 10^8 for $2l^*$ approximately equal to 1 Å.

In contrast with the conductivity measurements, the proton magnetic relaxation mechanism experiences in the first place protonic motions occurring in the neighborhood of a proton taken as reference and, to a much lesser extent, the proton translation on relatively long distances. It may thus be expected that the proton jump along the N···N axis as well as the rotation of the adsorbed species has to be taken into consideration in

(31) B. E. Conway, J. O. M. Bockris, and H. J. Linton, *J. Chem. Phys.*, 24, 832 (1956).

the model proposed to account for the proton relaxation mechanisms, observed by the pnmr technique.

Theoretical Models Proposed for the Proton Magnetic Relaxation Mechanisms

According to Bloembergen, Purcell, and Pound,[29] an isotropic motion characterized by a single correlation time gives rise to a relaxation mechanism whose longitudinal and transversal relaxation rates are ruled by the so-called spectral intensity functions $J(\nu)$. The molecules are considered as vehicles bearing the magnetic nuclei from point to point and each magnetic moment takes part in the random translational or rotational motion of the molecules. The local magnetic field generated by the magnetic moments at any point is thus a fluctuating function of the time. The Fourier spectral components at the frequency ν of this function are the J functions. Assuming simultaneous isotropic (tridimensional) rotational and translational (bidimensional) motions on a surface, O'Reilly and Poole[32] have adapted the BPP relationships as follows

$$\left.\begin{aligned}\frac{1}{T_{1\,\mathrm{intra}}} &= \frac{3}{10}\frac{j\gamma^3\hbar^2}{r^6}\times\left[\frac{\tau_r}{1+\omega_0^2\tau_r^2}+\frac{4\tau_r}{1+4\omega_0^2\tau_r^2}\right]\\ \frac{1}{T_{2\,\mathrm{intra}}} &= \frac{3}{10}\frac{j\gamma^4\hbar^2}{r^6}\times\left[\frac{3}{2}\tau_r+\frac{5}{2}\frac{\tau_r}{1+\omega_0^2\tau_r^2}+\frac{\tau_r}{1+4\omega_0^2\tau_r^2}\right]\end{aligned}\right\} \quad (9)$$

$$\left.\begin{aligned}\frac{1}{T_{1\,\mathrm{inter}}} &= \frac{3j\gamma^4\hbar^2N\pi}{80Da^2}\times\left[5-\frac{\omega_0a^2}{4D}\left(\frac{1}{2}\cot^{-1}\frac{\omega_0a^2}{8D}+4\cot^{-1}\frac{\omega_0a^2}{4D}\right)\right]\\ \frac{1}{T_{2\,\mathrm{inter}}} &= \frac{3j\gamma^4\hbar^2N\pi}{80Da^2}\times\left[5-\frac{\omega_0a^2}{4D}\left(\frac{5}{4}\cot^{-1}\frac{\omega_0a^2}{8D}+\cot^{-1}\frac{\omega_0a^2}{4D}\right)\right]\end{aligned}\right\} \quad (10)$$

the intramolecular and intermolecular contributions arising from the rotational and translational motions, respectively. D is the diffusion coefficient, N the number of protons per unit surface area, γ the proton gyromagnetic ratio, and ω_0 the radiofrequency field pulsation; j is the number of magnetic interactions undergone by one specified proton within the molecule ($j = 3$ for NH_4^+, $j = 2$ for NH_3, and $j = 1$ for H_2O). This factor has been introduced by Hubbard[33] by considering, as a first approximation, that the relaxation rate is the sum of the relaxation rates of each protonic pair. The r value in eq 9 is the H–H distance, *i.e.*, 1.63 Å in NH_3 or 1.68 Å in NH_4^+. At increasing surface concentrations, however, it is necessary to consider, in the rotational contribution, the interactions with protons belonging to other molecules orbiting near the one taken as reference.

This may be obtained by replacing the proportionality factor in relationship 9, $T_{2\,\mathrm{intra}}^{-1}$ by $C' = {}^3/_{10}\cdot\gamma^4\hbar^2j(1/r^6 + \pi N/2b^4)$, where b is the smallest interprotonic distance between two adsorbed species. Actually $N\pi/2b^4$ is a small fraction of r^{-6}.

In eq 10, a is the smallest distance between diffusing species, either two "vehicles" bearing the magnetic moments or two diffusing protons in the case of a proton exchange process. In the first case a should be of the order of the molecular diameter while in the second case it might be smaller.

Qualitatively similar descriptions of the variations of T_1 or T_2 with respect to the temperature are derived from eq 9 and 10. $T_{1\,\mathrm{intra}}$ should pass through a minimum at a temperature where $\omega_0\tau_r = 0.6154$ while $T_{1\,\mathrm{inter}}$ should reach this minimum at a temperature where $\omega_0a^2/4D = 0.8$. Accordingly, T_2 should decrease exponentially with temperature and at $T_{1\,\mathrm{min}}$ the ratio T_1/T_2 should be close to 1.6 or to 1.87 for the intramolecular or for the intermolecular contribution, respectively. These variations are easily understood by considering the temperature dependence either of the correlation time, $\tau_r = \tau_{r0}e^{+E_{\mathrm{rot}}/RT}$, or of the diffusion coefficient, $D = D_0e^{-E_D/RT}$.

As outlined in the experimental section, if we assume that the minimum of the longitudinal relaxation rate is obtained approximately at 25° regardless of the degree of coverage, then the experimental results of eq 9 and 10 would represent the increasing wing of function T_1 and the decrease of T_2 when the temperature is progressively lowered. However, as shown in Figure 7, the T_1/T_2 ratio at $T_{1\,\mathrm{minimum}}$ is far above the theoretical value obtained from eq 9 or 10. Moreover the leveling of T_2 on the high temperature side is in contradiction with the theoretical relationship. Such a situation has been observed in various systems, for instance by Resing, *et al.*,[34] for water adsorbed on charcoal, by Krüger and Helcke[35] for water in protein, or by Touillaux, *et al.*,[36] for water adsorbed by montmorillonite.

In the two former examples, in order to account for the discrepancy between the observed and theoretical T_1/T_2 ratio at $T_{1\,\mathrm{minimum}}$, a log normal distribution of the rotational correlation times was assumed

(32) D. E. O'Reilly and C. P. Poole, *J Phys. Chem.*, **67**, 1762 (1963).

(33) P. S. Hubbard, *Phys. Rev.*, **108**, 1153 (1958); *ibid.*, **111**, 1746 (1958).

(34) H. A. Resing, J. K. Thompson, and J. J. Kreb, *J. Phys. Chem.*, **68**, 1621 (1964).

(35) G. J. Krüger and G. A. Helcke, Proceedings of the XIVth Colloque Ampere, Ljubljana, 1966, p 1136.

(36) R. Touillaux, P. Salvador, C. Van der Meersche, and J. J. Fripiat, *Israel J. Chem.*, **6**, 337 (1968).

$$k(\tau_r)\, d \ln (\tau_r/\tau^*) = \frac{B}{\sqrt{\pi}} \exp(-B^2Z^2)\, dZ \quad (11)$$

where $Z = \ln (\tau_r/\tau_r^*)$ and where B is proportional to the width of the distribution function; $\tau^* = \exp(\overline{\ln \tau_r})$ where $\overline{\ln \tau_r}$ is the average value of $\ln \tau_r$.

In the present NH_3–Aerogel system, this hypothesis fails to reconcile the experimental and theoretical data. Another possibility has been invoked by Woessner,[21] who has shown, on a theoretical basis, that an anisotropic rotational motion is characterized by a $(T_1/T_2)_{min}$ ratio larger than that obtained at $T_{1\ minimum}$ from eq 9. Unfortunately, this theory was not applicable as such to the present situation.

For water adsorbed on montmorillonite, where a similar situation was met, Touillaux, *et al.*,[36] have observed that the experimental data could be adequately explained by assuming that the translational motion rules the spin–lattice relaxation rate T_1^{-1}, while the spin–spin relaxation rate, T_2^{-1}, is contributed by both the rotational and translational motions. This model will be considered again and refined but it must be emphasized that it cannot be checked directly. It is only possible to obtain indirect evidences about its validity by comparing the conclusions issuing from its application to the present situation with those deduced earlier from infrared spectroscopy and dielectric measurements.

Suggested Model. Assuming a distribution of the diffusion coefficients appears, at first sight, as a preliminary requirement in order to account for the fluctuation of the diffusion rate experienced by nuclei moving, within a time of the order of T_2, on sites characterized by different adsorption energies. Since the diffusion coefficient (D) is proportional to the translational speed, it seems logical to assume a Maxwellian distribution of D such as

$$K(D) = \frac{4}{\alpha^3\sqrt{\pi}} D^2 e^{-D^2/\alpha^2} \quad (12)$$

where $\langle D \rangle = 2\alpha/\sqrt{\pi}$. From eq 3 it follows

$$T_{1\,\mathrm{inter}}^{-1} = \frac{C}{a^2\alpha^3}\left[5\int_0^\infty De^{-D^2/\alpha^2}\, dD - \frac{\omega_0 a^2}{4}\left(\frac{1}{2}F_1 + 4F_2\right)\right] \quad (13)$$

$$T_{2\,\mathrm{inter}}^{-1} = C\left[\frac{5}{2\alpha a^2} - \frac{\omega_0}{4\alpha^3}\left(\frac{5}{4}F_1 + F_2\right)\right] \quad (14)$$

where

$$F_1 = \int_0^\infty \left(\cot^{-1}\frac{\omega_0 a^2}{8D}\right) e^{-D^2/\alpha^2}\, dD$$

$$F_2 = \int_0^\infty \left(\cot^{-1}\frac{\omega_0 a^2}{4D}\right) e^{-D^2/\alpha^2}\, dD$$

and

$$C = \frac{12j}{80}\gamma^4\hbar^2 N\sqrt{\pi}$$

F_1 and F_2 have been tabulated for $10^{-4} < \alpha < 10^{-11}$ cm^2 sec^{-1} and for $0.5 < a < 2.5$ Å. For a specified degree of coverage, the shortest distance between two diffusing species, *i.e.*, a, may be considered as constant since the nuclei surface density is constant. Therefore $(\delta T_{\mathrm{inter}}^{-1}/\delta\alpha)_a$ must be zero when the minimum value of T_1 is obtained at constant degree of coverage. This condition is fulfilled for

$$A = \frac{3B}{\alpha} + \frac{C_1}{C_2}a^{-2}\alpha \quad (15)$$

where

$$B = \left(\frac{1}{2}F_1 + 4F_2\right) \text{ and } A = \left(\frac{\delta B}{\delta\alpha}\right)_a$$

The calculation procedure is then performed as follows for $\theta < 1$. From the numerical tables, the pairs of (α,a) variables that correspond to any specified T_1C are obtained. $T_{1\ \mathrm{inter}}$ is known experimentally since it is assumed that the translational motion contributes mostly to the T_1^{-1} relaxation rate.

For $T_{1\ \mathrm{minimum}}$, α is plotted against a and the pair of (α,a) values that fulfill eq 15 is then determined. At constant α, a is kept constant regardless of the temperature and then, from the tables and measured T_1, α is obtained at various temperatures, assuming

$$\alpha = \alpha_0 e^{-E_{\mathrm{dif}}/RT}$$

The same procedure is repeated for each degree of coverage. The numerical results at 25° are shown in Table I and in Figure 8.

Table I: α, a, and D Parameters of the Translational Motion at 25° Assuming a Maxwellian Distribution of the Diffusion Coefficients or Neglecting this Distribution

		Maxwellian distribution		No distribution	
		α, cm^2 sec^{-1} × 10^8	$\langle D \rangle$, cm^2 sec^{-1} × 10^8		D, cm^2 sec^{-1} × 10^8
θ	a, Å			a, Å	
0.4	1.15	(2.2)[a]		1.2	1.7
0.85	1.305	2.2	2.50	1.33	2.1
1	1.35	2.2		1.37	2.2

[a] Uncertain.

If the Maxwellian distribution is neglected, D and a may be obtained using more simply $T_{1\ \mathrm{inter}}^{-1}$, eq 10, and the minimum condition for T_1, *i.e.*, $\omega_0 a^2/4D = 0.8$. As shown in Table I, in the range of the minimum value of T_1, the average diffusion coefficient $\langle D \rangle$ and the diffusion coefficient D as well as the a parameters are close to each other.

It is important to point out that a does not vary

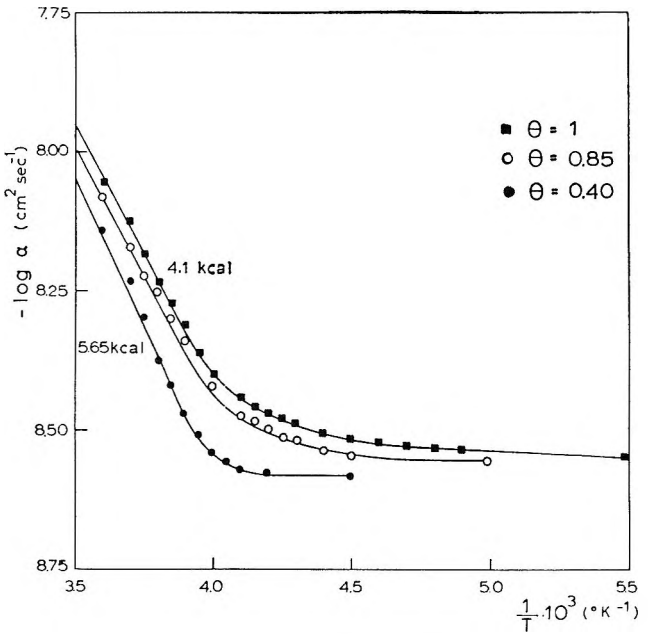

Figure 8. Activation energy of the proton diffusion process.

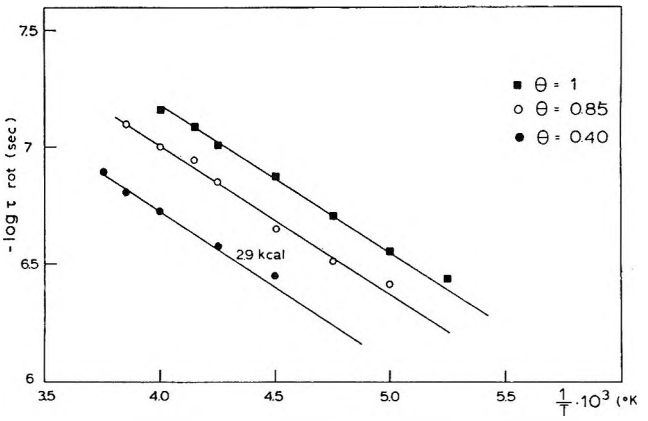

Figure 9. Activation energy obtained for the rotational correlation time, computed from eq 9, $T_{2\ \mathrm{intra}}^{-1}$.

noticeably with θ, and that it represents only 60% of the NH_3 or NH_4^+ diameter. The same remark still holds assuming j to be 2 instead of 3.

The contribution of the translational motion to the spin–spin relaxation rate, obtained by introducing into eq 14 the α and a parameters, is represented by the solid lines, entitled "inter" in Figures 5 and 6.

The intramolecular contribution obtained from $T_{2\ \mathrm{intra}}^{-1} = T_{2\ \mathrm{experim}}^{-1} - T_{2\ \mathrm{inter}}^{-1}$ is also shown in Figures 5 and 6.

The activation energy of the rotational correlation time (Figure 9) amounts to 2.9 kcal mol^{-1} for $0.4 < \theta < 1$ below $-10°$. The leveling of $T_{2\ \mathrm{intra}}$ at higher temperature might indicate that another relaxation mechanism is operating. The leveling of $T_{2\ \mathrm{inter}}$ at low temperature will be discussed later.

Discussion

The arbitrary character of the model suggested for the nuclear relaxation mechanisms originates essentially from the assumption that the main contribution to the spin–lattice relaxation rate is assigned to a diffusional motion. It must thus be checked with respect to the provisional model obtained for the proton transfer and, in particular, the significance of the short a distance and the meaning of diffusion activation energies (Figure 8) vanishing at low temperature are to be examined critically.

Since T_1 is a quadratic function of a and that a is 60% smaller than the molecular diameter, it might be accepted that the diffusion species is neither NH_4^+ nor NH_3, the error on T_1 being certainly much lower than three times its value. If the proton diffuses from one molecular species to another, according to the $NH_4^+ + NH_3$ exchange process, the a parameter would be smaller than the H–H distance in NH_3 or NH_4^+. Consider for instance the situation wherein NH_4^- approaches NH_3; the shape of the potential function across the N–N axis shows, near NH_3, a second well whose minimum is of course higher in the energy scale than the bottom of the first well, containing the NH_4^+ proton to be exchanged. Let us imagine that another NH_4^+ cation approaches the

$$\mathrm{H—N^+—H \cdots N—H}$$

association. The electrostatic repulsion will lift up the first well, favoring the proton transfer into the second well, an orbital of the first nitrogen atom being now available, after reorientation, for further hydrogen bonding with the closest NH_4^+ neighbor. During the proton jump, the a parameter is probably shorter than the H–H distance in NH_4^+ or NH_3, *i.e.*, $a < 1.6$ Å.

In agreement with this proposal, it is significant to point out that the decrease of the activation energy with decreasing temperature appears to be a common feature of proton exchange reactions, as shown by Bell.[37]

This is a consequence of the correction introduced in order to account for the tunnel effect. The observed activation energy E^* is always lower than the real value E.

At high temperature, $(E^* - E)$ becomes very small. Assuming, for instance, a barrier width of 1 Å and E = 6.2 kcal, the theory proposed by Bell predicts that E^* = 5.2 kcal at 270°K and $E^* \simeq 0$ at 195°K. For E = 4.1 kcal, one finds E^* = 3.8 kcal at 280°K and $E^* \simeq 0$ at 160°K. The width of 1 Å, used in these computations, was obtained by subtracting from the ^+N–H··N bond length (2.98 Å, according to Pauling[38]) the N–H bond length ($\simeq$1 Å).

Actually, as shown in Figure 8, the activation energy tends to vanish at 240°K for θ = 0.4 and at 200°K for

(37) R. P. Bell, "The Proton in Chemistry," Cornell University Press, Ithaca, N. Y., 1959.

(38) L. Pauling, "The Nature of the Chemical Bond," Cornell Univsrsity Press, Ithaca, N. Y., 1965.

$\theta = 1$, the observed values being 5.6 kcal mol^{-1} and 4.1 kcal for $\theta \simeq 0.4$ and $\theta \simeq 1$, respectively.

Therefore both the short a parameter and the decrease of the activation energy at low temperature are in general agreement with the features expected for a proton transfer reaction between adsorbed NH_4^+ and NH_3. Another indirect argument in favor of the suggested model is obtained by considering the jump frequency (ν_j) between two adjacent positions. The diffusion coefficient on a surface is related to ν_j and to the distance ($2l^*$) between two sites as follows

$$\nu_j = 4D(2l^*)^2 \tag{16}$$

From Table I, it follows that $\nu_j = 0.55 \times 10^9$ sec^{-1} for $\theta \simeq 1$ at 25° and $a \simeq 2l^*$. This figure compares well with that deduced from the unimolecular rate constant k_1 determined by Clutter and Swift[39] by high resolution nmr spectroscopy for the $NH_4^+ + NH_3$ proton transfer in liquid ammonia at the same temperature

$$k_1 = \nu_j \frac{[NH_3]}{[NH_4^+]} = 6.9 \times 10^9 \text{ sec}^{-1}$$

From the ir results, $[NH_4^+]/[NH_3]$ was estimated to be approximately 0.3 for $\theta \simeq 1$ and thus, for this concentration, $\nu_j = 2.1 \times 10^9$ sec^{-1}.

Therefore the proton jump frequency obtained from T_1 assuming that a protonic translational motion contributed mostly to the spin–lattice relation time is in good agreement with that obtained in the homogeneous NH_4^+–NH_3 system. Some additional observations in favor of this conclusion are listed below.

(a). The rotational motion, which represents the main contribution to T_2^{-1}, is characterized by a correlation time

$$\tau_r = 2 \times 10^{-10} e^{2900/RT} \text{ sec} \tag{17}$$

This might correspond to the diffuse dielectric absorption bands observed between −140 and −180°, assuming a broad distribution of the correlation time.

(b). The sum of the activation energies of both the rotation of the adsorbed species and the proton exchange process approximates 8 kcal. This result agrees well with the activation energy obtained for the protonic conductivity. As emphasized previously, this may be expected since the conduction process requires a succession of protonic tunneling and molecular reorientation processes.

In summary, in the NH_3–Aerogel system a fast proton transfer reaction seems to determine the spin–lattice relaxation rate, while the spin–spin relaxation rate appears as being mainly influenced by a rotational motion. The D and τ_r parameters of these motions are probably characterized by distribution functions reflecting the surface heterogeneity.

(39) D. R. Clutter and T. J. Swift, *J. Amer. Chem. Soc.*, 90, 601 (1968).

The Neptunium(VII)–(VI) Couple in Sodium Hydroxide Solutions[1]

by A. J. Zielen and D. Cohen

Chemistry Division, Argonne National Laboratory, Argonne, Illinois 60439 *(Received July 21, 1969)*

Controlled potential coulometry and conventional potentiometry established the existence of a reversible neptunium(VII)–(VI) couple in sodium hydroxide solutions. A study of the hydroxide ion dependence indicated the half-reaction to be $e^- + NpO_5^{3-} + H_2O = NpO_4^{2-} + 2OH^-$. The formal potential of the couple in 1 *M* sodium hydroxide at 25° *vs.* the normal hydrogen electrode was determined to be 582.1 ± 0.45 mV. Electrolysis was found to be an excellent preparative method for both Np(VII) and Np(VI) in alkaline solution, and controlled potential coulometry can be directly applied as a quantitative analytical method for the Np(VII) content. Infrared absorption spectra of Np(VII) and Np(VI) in 1 *M* NaOH were determined; a single band at about 1100 cm^{-1} was found for both species.

Introduction

The preparation of heptavalent neptunium has been one of the most interesting recent discoveries in actinide chemistry. Krot and Gel'man[2] found that ozone will readily oxidize neptunium (and plutonium) in alkaline hydroxide solution to a higher valence. The dark green neptunium solution was shown to be in the Np(VII) oxidation state by a hydrogen peroxide titration, and the new state was readily interpreted as the loss of neptunium's last 5f electron. A more detailed report of the initial discovery has since appeared and also a summary of other methods, including electrolysis, for preparing Np(VII).[2b,c] A convenient review (in English) covering this work is given by Spitsyn.[3]

We repeated and confirmed the ozone oxidation of neptunium in basic solution and then tried oxidation by electrolysis. The electrolytic oxidation and reduction worked so well, an investigation of the electrochemistry of Np(VII) was initiated. This study had three main parts. First, controlled potential coulometry established the existence of a reversible couple with a 1-equiv change in oxidation state: Np(VII) + e^- $\rightleftharpoons$ Np(VI). Second, the formal potential of the couple in 1 *M* sodium hydroxide was determined and adherence to the Nernst equation was checked over a wide range of neptunium concentration ratios. Third, the hydroxide ion dependence of the couple was studied to help establish the nature of the oxidation–reduction reaction and the structure of the ions.

Experimental Section

Reagents. Initially pure neptunium(VI) in 1 *M* perchloric acid served as the starting point in the preparation of all solutions. The use of Np(VI) stock solutions has the advantage that the radiolysis products (mainly hydrogen peroxide) from the α decay of ^{237}Np are not allowed to accumulate; the only effect is the reduction of Np(VI) to Np(V) at about 0.80% per month.[4] Pure Np(V) solutions in 1 *M* perchloric acid were prepared by reduction of Np(VI–V) mixtures with solid sodium nitrite, precipitation with sodium hydroxide, and solution of the washed neptunium(V) hydroxide in perchloric acid. The initially pure Np(VI) stocks were prepared from pure Np(V) solutions in 1 *M* perchloric acid by electrolysis at 1.38 V with a potentiostat. (All voltages listed, unless otherwise noted, are with respect to the normal hydrogen electrode or nhe.)

Ozone was obtained as a 1–2% solution in oxygen by a conventional ozonator discharge apparatus. Tank ozone, dissolved in chlorotrifluoromethane ("Freon 13") and supplied by the Matheson Co., was also used and found very convenient. With a fresh tank, the ozone concentration is about 15 mol %, and this greatly shortens reaction times.

A carbonate-free, 5 *M* solution of sodium hydroxide was prepared by diluting a 50% solution of reagent NaOH. The stock solution was stored in a polyethylene bottle with an Ascarite–CO_2 adsorption tube inlet, and samples were removed by siphon action. Standardization was by potentiometric, weight buret titration against NBS potassium acid phthalate. A recheck standardization 5 months after preparation showed a titer increase of only 0.02%. The sodium hydroxide stock served as a secondary standard in titrating perchloric acid solutions.

The water used for all solutions was of conductivity grade. It was prepared by redistilling distilled water under oxygen pressure successively through cupric oxide at 800° and manganese dioxide at 250°.[5] All other materials were reagent grade, commercial preparations.

(1) Based on work performed under the auspices of the U. S. Atomic Energy Commission.

(2) (a) N. N. Krot and A. D. Gel'man, *Dokl. Akad. Nauk SSSR*, **177**, 124 (1967); (b) N. N. Krot, M. P. Mefod'eva, T. V. Smirnova, and I. A. D. Gel'man, *Radiokhimiya*, **10**, 412 (1968); (c) V. I. Spitsyn, N. N. Krot, M. P. Mefod'eva, and A. D. Gel'man, *Dokl. Akad. Nauk SSSR*, **181**, 128 (1968).

(3) V. I. Spitsyn, *Rec. Chem. Progr.*, **29**, 243 (1968).

(4) A. J. Zielen, J. C. Sullivan, and D. Cohen, *J. Inorg. Nucl. Chem.*, **7**, 378 (1958).

(5) Unpublished still design by E. H. Appelman of this Laboratory.

Preparation of Basic Np(VII) and Np(VI) Solutions. All Np(VII) stock solutions were 1 *M* in NaOH with neptunium ranging from 0.001–0.01 *M*. Initially, oxidation by ozone or electrolysis was carried out on a suspension of pure nepunium(VI) hydroxide in sodium hydroxide solution. This followed the recommendation of Krot, *et al.*[2b] (who warn that the presence of Np(V) greatly reduces the yield of soluble neptunium). This was later found to be very poor advice, and a suspension of neptunium(V) hydroxide proved, in fact, to be the best starting material.

When Np(VI) served as the starting material, the dark brown hydroxide suspension thoroughly obscured the solution and the course of the reaction. Of more importance, it was virtually impossible, even with overnight oxidation times, to prepare a "clean" Np(VII) solution that did not contain unreacted solid Np(VI). On the other hand, neptunium(V) hydroxide is almost colorless, and it is oxidized directly to a pink Np(VI) solution without any trace of the bothersome neptunium(VI) hydroxide precipitate. This heterogeneous reaction is somewhat slow, perhaps lasting 30–60 min, but its end is easily noted since no appreciable amount of Np(VII) can be formed until all the Np(V) has been consumed. At this point, the intense green Np(VII) color starts to develop and the oxidation from Np(VI) to Np(VII) is smooth and rapid.

For the ozonization preparations, appropriate amounts of neptunium and sodium hydroxide were placed in 50- or 100-ml volumetric flasks, O_3 was bubbled through the solution for 2–4 hr, excess O_3 was swept out by O_2 bubbling, and the solution was diluted to the mark. If necessary, solid Np(VI) was then removed by centrifuging. The free hydroxide ion concentration of the solution was calculated from the amount of base added and the following ozonization reaction, which anticipates NpO_5^{3-} as the Np(VII) species

$$3OH^- + NpO_2 \cdot OH + O_3 = NpO_5^{3-} + O_2 + 2H_2O \quad (1)$$

The electrolysis preparations were carried out in 100-ml weighing bottle cells at a cylindrical platinum gauze electrode with a calculated (individual wire) surface area of 85 cm². The combined guard tube-counter electrode (Figure 2) and potentiostat will be discussed later. Electrolysis conditions are not critical. Generally a constant current of 100 mA was passed until vigorous oxygen evolution was observed from the dark green, almost black, Np(VII) solution; this invariably required less than 1 hr to prepare, say, 100 ml of 0.01 *M* Np(VII). Neptunium(VI) stocks could then be conveniently prepared by electrolytic reduction of Np(VII), again at a constant current of 100 mA, until vigorous hydrogen evolution occurred from the bright pink Np(VI) solution.

The electrolysis preparation of Np(VII) proved to be much faster and simpler than the ozonization method. The one disadvantage was that it was necessary to determine the hydroxide ion concentration of the electrolysis stocks by titration. This was done by adding a small excess of standard perchloric acid, which converts Np(VII) into Np(VI), followed by backtitration with standard 0.1 *M* NaOH. When neptunium(VI) hydroxide started to precipitate from the still slightly acid solution, a two- to threefold excess of sodium nitrite solution was added, immediately reducing all the neptunium to the soluble Np(V) state. Titration was continued to a pH 7 end point using a calibrated pH meter and glass electrode. Neptunium(V) hydroxide does not precipitate until the pH exceeds 8. The following reactions summarize the titration procedure, and again we anticipate the Np(VII) and basic Np(VI) species

$$4NpO_5^{3-} + 20H^+ = 4NpO_2^{2+} + O_2 + 10H_2O \quad (2)$$

$$NpO_4^{2-} + 4H^+ = NpO_2^{2+} + 2H_2O \quad (3)$$

$$H_2O + 2NpO_2^{2+} + NO_2^- = 2NpO_2^+ + NO_3^- + 2H^+ \quad (4)$$

Thus the net corrections applied were four and three excess hydrogen ions consumed, respectively, for Np(VII) and Np(VI). However, there is some uncertainty as to whether nitrogen dioxide or nitrate ion should be the major product of reaction 4. Under the conditions used in this work, the maximum error possible in the calculated hydroxide ion concentration would have been 0.7%, which corresponds to 0.36 mV in the formal potential determination.

Neptunium(VII) solutions decompose because of slow water oxidation. Stability data on five solutions in 1 *M* NaOH at 25° and usually covering only the first 6–8 hr after preparation gave decomposition rates ranging from 1 to 5% per day. Catalysis by trace impurities was probably an important factor. The best stability results were obtained by electrolysis preparation coupled with storage in the dark. The useful life of a Np(VII) stock generally ended with the appearance of a brown Np(VI) precipitate. This varied from a few days to 2 weeks both because of the range of Np(VII) decomposition rates and because metastable, supersaturated Np(VI) solutions are readily obtained. The latter effect was very marked in the Np(VI) stocks prepared by electrolysis, which were 20-fold more concentrated than the direct solution of neptunium(VI) hydroxide in base. Two such electrolysis Np(VI) stocks were prepared, each about 0.007 *M* in 1 *M* NaOH. Precipitation eventually occurred from both solutions; however, one lasted only 24 hr and the other for 7 days with no obvious reason for the difference.

The absorption spectrum of Np(VII) was checked against the reported results[2,3] using a Cary Model 14

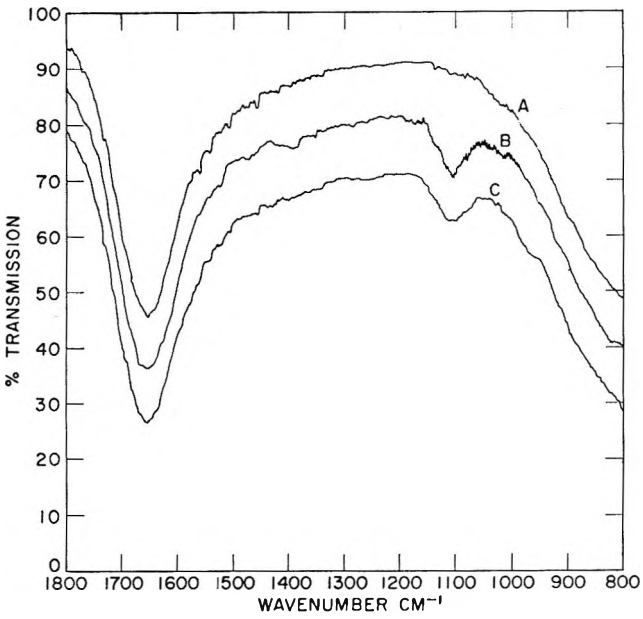

Figure 1. Infrared absorption spectra of A, 1 *M* NaOH solvent; B, 6.1 × 10^{-3} *M* Np(VII); C, 6.5 × 10^{-3} *M* Np(VI). Path length was 0.025 mm.

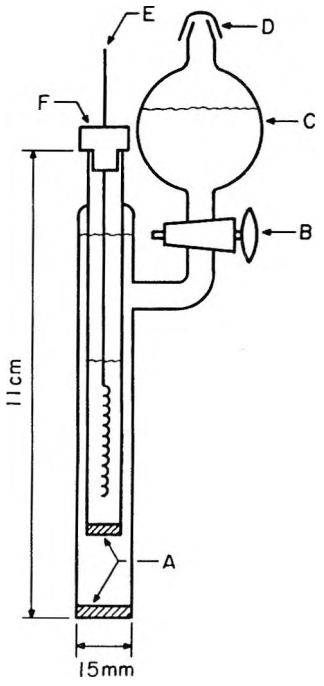

Figure 2. Combined counter flow shield tube and counter electrode compartment used for controlled potential coulometry. A, fine frits; B, Teflon stopcock; C, ~50-ml reservoir bulb; D, standard taper cap with 1-mm diameter air vent drilled in side (not shown); E, platinum spiral counter electrode; F, loose fitting Teflon cap with air vent (not shown).

recording spectrophotometer. The agreement was good. Our best values locate the two main absorption peaks at 411 and 616 mμ with respective 25° molar absorptivities of 1397 and 395. Krot, *et al.*,[2b] give mean 1 *M* NaOH values of 1403 and 387 at 410 and 625 mμ. However, the Russian work does not mention the most significant feature of the spectrum, namely the existence of regularly spaced fine structure bands superimposed on the main peaks. We observed seven such bands in the region 393–520 mμ with an average separation and standard deviation of 1034 ± 132 cm^{-1}; and in the region 590–775 mμ, five bands separated by 1036 ± 368 cm^{-1} were noted. Similar fine structure has been interpreted as symmetrical vibrations in metal–oxygen bonds and helped to establish the -yl ions, MO_2^+ and MO_2^{2+}, for uranium, neptunium, and plutonium.[6-8]

The infrared absorption spectra of 1 *M* NaOH solutions of Np(VI) and Np(VII) were also determined. The only area of interest in the region 400–4000 cm^{-1} is shown in Figure 1. A single band was found for both neptunium species, a fairly sharp peak for Np(VII) at 1105 cm^{-1} and a broader band for Np(VI) between 1070 and 1130 cm^{-1}. The spectra were obtained with a Beckman Infrared-12 instrument by use of a Wilks Scientific Corp. "mini-cell" (0.025-mm path length) with AgCl windows. Similar results were also obtained with a Beckman Infrared-10. However, it should be emphasized that the neptunium solutions used were very dilute (~6 m*M*) compared to the short path length, and weaker infrared bands may have remained undetected or obscured by the solvent.

Electrolysis Equipment. The controlled potential coulometer used for all coulograms and electrolysis analyses is an operational amplifier-type instrument very similar to the design of Stephens and Harrar.[9] A Non-Linear Systems, Inc., Model V35B digital voltmeter with five-figure readout (±0.01%) is applied to the full output of a Philbrick Model UPA-2 integrator amplifier. The integrator input circuit was designed to give an approximate output of 1 V/C with a total capacity of 100 C. Electrical calibration of the integrator as described by Kelley, *et al.*,[10] routinely gave values reproducible to 0.01%. Analytical work was customarily done on Np(VII) and Np(VI) samples of 10–20 μequiv with an anticipated accuracy of 0.1%.

The cells used were 1-oz weighing bottles with Teflon caps machined to fit the standard taper. The working electrode was a 45-mesh gauze platinum cylinder, 1 × 0.75 in. in diameter and height, spot-welded to a 50-mil platinum wire. The calculated (individual wire) electrode area was 54 cm^2. The combined shield tube and counter electrode compartment is illustrated in Figure 2. This simple device, a

(6) R. Sjoblom and J. C. Hindman, *J. Amer. Chem. Soc.*, **73**, 1744 (1951).

(7) M. Kasha, *J. Chem. Phys.*, **17**, 349 (1949).

(8) R. H. Betts and B. G. Harvey, *ibid.*, **16**, 1089 (1948).

(9) F. B. Stephens and J. E. Harrar, U. S. Atomic Energy Commission Report UCRL-7165 (1963).

(10) M. T. Kelley, H. C. Jones, and D. J. Fisher, *Anal. Chem.*, **31**, 488 (1959).

compact version of the counter flow shield tube suggested by Eckfeldt and Shaffer,[11] completely eliminates the need for silica gel or agar plugs. The hydrostatic head in the reservoir bulb gives a reverse flow through each frit that prevents mixing of the anode and cathode compartments. Knoeck and Diehl[12] have recently demonstrated that the counter flow shield tube can be used in coulometric work of the highest precision (0.001%).

The shield tube assembly was centrally mounted in the electrolysis cell by means of the Teflon cap and inserted inside the platinum gauze cylinder. Holes in the cap also provided support for an inert gas inlet (N_2 or Ar), the reference electrode, and an entry port for the samples. Rapid mixing was achieved by use of a 0.875 × 0.25 in. magnetic stirring bar run at the highest possible speed. Before each run the platinum gauze electrode was cleaned by heating in a gas flame.

Two different coulometric analyses were used: Np(VI) to Np(V) in 1 *M* perchloric acid at 0.89 V and Np(VII) to Np(VI) in 1 *M* sodium hydroxide at 0.34 V, both potentials *vs.* nhe. In either case, 10–12 ml of supporting electrolyte was prereduced at the control potential; cell currents fell to a background level of less than 10 μA usually in about 5 min. At this point, without interruption of the electrolysis or change in the control potential, the neptunium sample was added from a plastic 1-oz weight buret used as previously described.[13] Reduction of the neptunium was rapid with a half-time of 30–40 sec; the cell current returned to the background level in 8–10 min. Generally a second and third sample were added in sequence to the same cell, all without interruption of the electrolysis. Corrections for faradaic background were applied,[14] but blank corrections were not needed, probably because the continuous electrolysis procedure eliminates the charging current that occurs if the potentiostat is turned off and on.

Coulograms were obtained as a variation of controlled potential coulometry. To maintain the initial (calculated) hydroxide ion concentration, the counter flow shield tube was replaced with a conventional guard tube with a fine frit and a plug of 5% agar in 0.5 *M* sodium perchlorate; generally, there was no preelectrolysis of the supporting electrolyte. As soon as the potentiostat was turned on, the control potential was adjusted to zero cell current (taken as ±10 μA), and the integrator was then engaged. This was the initial reading. Additional points were obtained by allowing the passage of a suitable coulomb increment and then adjusting the applied potential to zero current. Relative formal potentials were obtained by using Yan's[15] method to calculate the inflection point of the sigmoid coulogram curves. Usually the inflection point could be obtained within an accuracy of 1–3 mV, but difficulty was sometimes encountered if the coulomb increments were too small. As a standard procedure, two independent Yan calculations using every other point were made for each coulogram, and the mean of the two results was taken as the final value.

Potentiometric Measurements. Potential measurements were made on cells of the type

$$\mathrm{Pt,Hg,HgO|1}\ M\ \mathrm{NaOH}\|(A - B - pC - qD)\ M\ \mathrm{NaOH},\ B\ M\ \mathrm{NaClO_4},\ C\ M\ \mathrm{Na}_p\mathrm{Np(VI)},\ D\ M\ \mathrm{Na}_q\mathrm{Np(VII)|Pt} \quad \text{(I)}$$

Cell I can be broken down into the half-reactions or couples

$$2e^- + HgO + H_2O = Hg + 2OH^- \quad (5)$$

$$e^- + 0.5mH_2O + Np(VII)^{p-} = Np(VI)^{q-} + mOH^- \quad (6)$$

$$E_5 = E_5^\circ - 0.5k \log \left(\frac{y_{OH^-}^2}{a_w}\right)_{1,0} \quad (5a)$$

$$E_6 = E_6^\circ - k \log \frac{[Np(VI)][OH^-]^m}{[Np(VII)]a_w^{0.5m}} \left(\frac{y_{VI}y_{OH^-}^m}{y_{VII}}\right)_{A,\beta} \quad (6a)$$

$$E_I = E_6 - E_5 + E_j + E_j'' \quad (7)$$

In the above and subsequent equations, brackets indicate concentrations on the moles per liter scale, the y's are the respective molar activity coefficients, a_w is the water activity, E_j and E_j'' are liquid-junction potentials that will be discussed shortly, and the other symbols are self-evident or have their customary meaning. The subscript system applied to the activity coefficient and water activity terms indicates the total sodium ion and the equivalent perchlorate ion concentrations. The latter quantity was defined as $\beta = B + pC + qD$; with both C and D relatively small ($\leq 7 \times 10^{-3}$ *M*), it was assumed a solution of $(A - \beta)$ *M* NaOH + β *M* $NaClO_4$ would be equivalent to the actual neptunium solution of cell I as the medium factor for both activity coefficient and liquid-junction potential behavior. Thus the subscript 1,0 indicates a pure 1 *M* NaOH solution.

The nominal value $A = 1$ was not always achieved in the solution make-up for the cell I experiments. To bring this into account, the liquid-junction potential of cell I was broken into the junctions E_j and E_j''; the latter quantity tends to zero as A approaches 1

$$1\ M\ \mathrm{NaOH}\overset{E_j}{\|}(1-\beta)\ M\ \mathrm{NaOH},\ \beta\ M\ \mathrm{NaClO_4}\overset{E_j''}{\|}(A-\beta)\ M\ \mathrm{NaOH},\ \beta\ M\ \mathrm{NaClO_4}$$

To evaluate E_j and to express the formal potential of

(11) E. L. Eckfeldt and E. W. Shaffer, Jr., *Anal. Chem.*, **37**, 1534 (1965).
(12) J. Knoeck and H. Diehl, *Talanta*, **16**, 181 (1969).
(13) A. J. Zielen, *Anal. Chem.*, **40**, 139 (1968).
(14) L. Meites and S. A. Moros, *ibid.*, **31**, 23 (1958).
(15) J. F. Yan, *ibid.*, **37**, 1588 (1965).

couple 6 with respect to the normal hydrogen electrode, measurements were also made on cells of the type

$$\mathrm{Pt,H_2}|(1-\beta)\ M\ \mathrm{NaOH},\ \beta\ M\ \mathrm{NaClO_4}||\ 1\ M\ \mathrm{NaOH}|\mathrm{HgO,Hg,Pt} \quad \text{(II)}$$

In basic solution, the nhe has the form

$$e^- + H_2O = 0.5H_2 + OH^- \quad (8)$$

$$E_8 = E_8^\circ - k\log[\mathrm{OH}]\left(\frac{y_{\mathrm{OH}}}{a_w}\right)_{1,\beta} \quad (8a)$$

The potential of cell II can then be written as

$$E_{II} = E_5 - E_8 - E_j \quad (9)$$

This procedure for determining liquid-junction potentials is adapted from the method of Biedermann and Sillén.[16]

The vessels for cells I and II consisted of stubby test tubes, 28 × 90 mm, which fitted snugly into a cup-shaped glass jacket through which water thermostated at 25.00 ± 0.01° was pumped. Holes in a Teflon cap provided entry and support for the electrodes and gas bubbler tubes. Magnetic stirring was employed. Lightly platinized platinum hydrogen electrodes were prepared and used as previously described.[17] Two different types of shiny platinum electrodes were used in the cell I measurements for the Np(VII)–Np(VI) couple: a length of 50-mil wire dipping into the solution and a 5 × 10 mm rectangle of 5-mil foil sealed on the end of a soft glass tube. Invariably the two platinum electrodes agreed within a few hundredths of a millivolt. A few attempts were also made using gold wire as the cell I inert electrode. The unsatisfactory results were drifting potentials about 8–10 mV lower than the platinum values; however, the drift was always toward the platinum potentials.

The Hg–HgO reference electrode used in cells I and II and for all controlled potential coulometry in sodium hydroxide solutions was a completely independent unit with a self-contained 1 *M* NaOH salt bridge. It was constructed of quartz because of the alkali medium and followed the calomel electrode design of Lingane[18] except that the J-form exit was replaced with a straight tip with capillary bore. No special precautions were taken in preparing the electrode other than refluxing the red HgO with boiling water for 5 days.[19] The Hg–HgO electrode assembly was not thermostated other than by use in a 25 ± 1° room. Fortunately the temperature coefficient of the cell (*vs.* nhe) is only −0.2878 mV/deg at 25°.[19] In 5 months of use as a working reference electrode, there was no evidence that the potential varied by more than the temperature uncertainty factor. An entirely similar reference electrode assembly with the $Hg–Hg_2^{2+}$ couple in 1 *M* $HClO_4$ was used for controlled potential coulometry in perchloric acid solutions.

Cell potentials were measured to 0.01 mV with a Leeds & Northrup K-3 potentiometer standardized by two saturated Weston cells calibrated by laboratory standards recently certified by the U. S. National Bureau of Standards. The signs of cells and relative electrode potentials conform to the Stockholm Convention.[20] The molar or moles per liter of solution concentration scale, designated by *M* or [ ], was used throughout.

Results and Discussion

Controlled Potential Coulometry. Coulograms provide a rapid method of obtaining approximate formal potentials and the number of equivalents involved in a reversible couple. However, since background corrections cannot be applied, it is necessary for the current efficiency of the reaction to be near 100%. This condition was easily met for the reduction of Np(VII) to Np(VI), but the reverse process presented experimental problems because the oxidation of water becomes appreciable at potentials necessary to generate high Np(VII)/Np(VI) ratios.

Typical coulograms observed for Np(VII) in 1 *M* NaOH are presented in Figure 3 and show the sigmoid curve expected for a reversible couple. Run A was obtained using a saturated calomel (sce) as the reference electrode. The starting point was a Np(VII) sample that contained an appreciable (~5%) amount of Np(VI). Reduction proceeded smoothly at potentials reasonably near the equilibrium values until the plateau region or end of the Np(VII) to Np(VI) reaction was reached. Further reduction then became very difficult. The current generated for the last reduction point in run A was less than 100 μA even though the applied potential was the maximum −1-V setting of the potentiostat. [To avoid misunderstanding, we repeat that the points in Figure 3 represent equilibrium or zero current potentials and should not be confused with the potentials applied to generate the data points. The generating potentials were always more cathodic or anodic—respectively, for reduction or oxidation coulograms—than the equilibrium potentials.] Oxidation readily occurred upon applying potentials more positive than the plateau region. However, to obtain a coulogram that retraced the reduction cycle as closely as run A, it was necessary to keep the applied oxidation potentials as low as possible concordant with a reasonable flow of current. The highest potential used in run A was 0.45 V until the last three points where 0.55 V was used (all potentials *vs.* sce), and the extra current

(16) G. Biedermann and L. G. Sillén, *Ark. Kemi*, **5**, 425 (1953).

(17) A. J. Zielen, *J. Phys. Chem.*, **67**, 1474 (1963).

(18) J. J. Lingane, 'Electroanalytical Chemistry," 2nd ed, Interscience Publishers, Inc., New York, N. Y., 1958, p 362.

(19) D. J. G. Ives and G. J. Janz, "Reference Electrodes," Academic Press, New York, N. Y., 1961, p 336.

(20) J. A. Christiansen, *J. Amer. Chem. Soc.*, **82**, 5517 (1960).

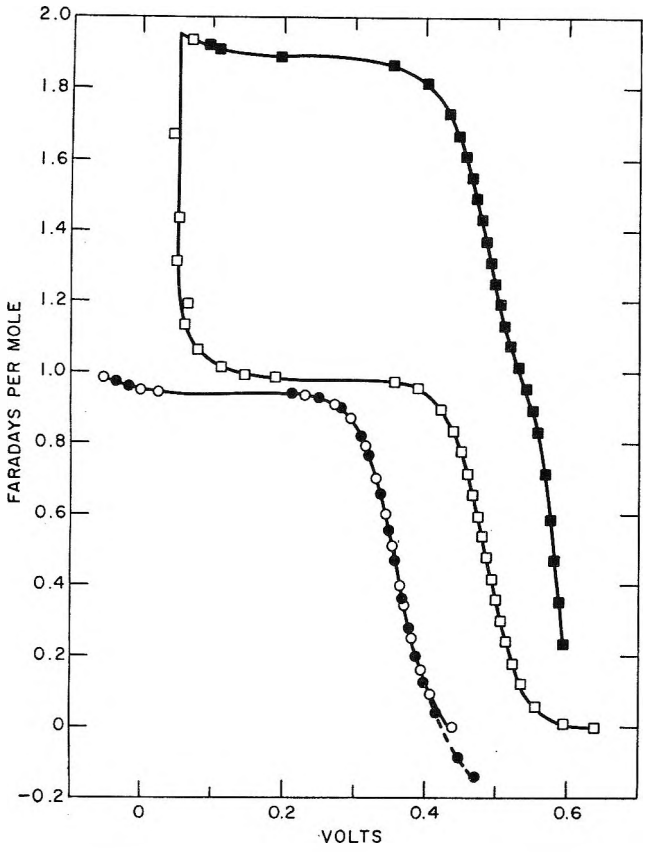

Figure 3. Typical 25° coulograms in 1 *M* NaOH indicating the reversibility and 1-equiv change of the Np(VII)–Np(VI) couple. Open points are reduction and closed points are oxidation; ○, run A *vs.* saturated calomel reference, ΣNp = 7.02×10^{-3} *M* in 0.983 *M* NaOH; □, run B *vs.* Hg–HgO (1 *M* NaOH) reference, ΣNp = 6.42×10^{-3} *M* in 0.984 *M* NaOH.

consumed by water oxidation is clearly visible in the dashed extension.

Curve B illustrates data obtained with the Hg–HgO reference electrode (MMO), which is approximately 0.13 V more negative than the sce. Here, in an effort to start with a pure oxidation state, the Np(VII) sample was preoxidized at 0.8 V (*vs.* MMO) for 1 hr. The reduction coulogram was started *in situ* by lowering the applied potential to the point of zero current. The separation of the initial emf and the observed reduction inflection point was 153 mV, which corresponds to only 0.26% Np(VI) at the starting point. However, the observed faraday per mole plateau value (Table I) was lower than this value by 1.6%. The difference may be within experimental error, or it is possible that relatively pure Np(VII) cannot exist in 1 *M* NaOH for an appreciable time. Any such chemical reduction process would, of course, appear as a loss in the faradays consumed.

The highest reduction potential applied in run B was again the −1-V maximum obtainable from the potentiostat. However, the added range of 0.13 V available with the MMO reference was sufficient to

Table I: Neptunium(VII) Coulograms at 25° in 1 *M* NaOH[a]

Run	Plateau, faradays/mol	Relative formal potential,[b] mV	Equiv in half-reaction
A reduction	0.941	358	0.98
A oxidation	0.951	359[c]	1.02
B reduction	0.981	485	1.00
B oxidation	1.878	488[d]	1.11

[a] See Figure 3 caption for concentration details. [b] Actual observed value *vs.* stated reference. [c] Saturated calomel reference electrode. [d] Hg–HgO reference in 1 *M* NaOH.

reach the stage of hydrogen evolution, which produced the sharp upward turn in the reduction coulogram. The fact that this occurred at an equilibrium potential of 0.05, or 0.15 V on the nhe scale, may be related to the 0.15-V potential for the Pt–$Pt(OH)_2$ couple in 1 *M* hydroxide.[21] There was no evidence of reduction of neptunium below the Np(VI) state.

Upon changing to oxidation potentials, the B coulogram immediately reverted to the plateau and curve of the Np(VII–VI) couple. The highest oxidation potential used was 0.6 V (*vs.* MMO) until the point at 528-mV equilibrium potential was reached. Gradually higher potentials were then applied up to a maximum of 0.9 V, which was used for the last three points. This was done for a better demonstration of the extra coulombs consumed in water oxidation at high potentials.

It should be emphasized that the difference in the A and B coulograms was primarily due to the limited potentiostat range of ±1 V *vs.* the reference electrode used. An anodic downturn similar to B did occur in A (not shown) when more positive potentials were applied, and a cathodic upturn would have occurred in A if an additional ~0.1 V more negative potential had been available.

A summary of quantitative calculations with the coulogram data is presented in Table I. The results clearly indicate a reversible, one electron oxidation–reduction couple. The equivalents in the half-reaction were calculated by doubling the separation, as faradays per mole of neptunium, of the plateau and the inflection point. This procedure is independent of the oxidation state purity of the starting sample, but because of the steep slope, the equivalents evaluation is more sensitive to an inflection point error than the formal potential determination. Distortion of the curve by water oxidation could give high values for both the formal potentials and the number of equivalents. However, the exceptionally high number of equivalents found in the B oxidation cycle probably indicates the occurrence

(21) W. M. Latimer, "The Oxidation States of the Elements and their Potentials in Aqueous Solutions," 2nd ed, Prentice-Hall, Englewood Cliffs, N. J., 1952, p 205.

of another reaction. Reduction of generated Np(VII) by hydrogen remaining after the proceeding severe cathodic electrolysis would be one possibility. Another could be the formation of a $Pt(OH)_2$ film on the freshly reduced platinum electrode.

Controlled potential coulometry was also used in conventional fashion to analyze the Np(VII) concentrations of 1 *M* NaOH solutions. The results were compared with the total neptunium content obtained coulometrically by converting all neptunium into the Np(VI) state with excess perchloric acid[2] followed by controlled potential reduction to Np(V).[22] These experiments were superior to the coulograms in that proper background current corrections could be applied.[14] Ozonization was used with the hope that oxidation to the Np(VII) state would be quantitative. so, this would immediately confirm controlled potential coulometry as an analytical method for Np(VII), and it would also provide a stoichiometry check of the electrolysis reactions and the assumed conversion of Np(VII) to Np(VI) in acid. The autoreduction of Np(VII) by water oxidation was a complication that was countered by correcting the Np(VII) assays to zero time (end of ozonization) by linear extrapolation of the concentration changes observed over a 6–8-hr interval. The corrections to zero time concentrations were relatively small, ranging from 0.10 to 0.25%.

An independent spectrophotometric assay of the total neptunium was obtained by using the Np(V) 980-mμ absorption peak in 1 *M* $HClO_4$ (molar absorptivity = 403). The Np(V) solutions were prepared by acidifying Np(VII) and adding excess sodium nitrite. The spectrophotometric assays were probably accurate to 1–2% as compared to 0.1% or better expected for the coulometric results.[22]

A summary of results obtained with two ozonization experiments is given in Table II. (The individual coulometric analyses are given to indicate the precision attained.) In both cases, 1–2% electrical discharge ozone was used. In run C a large quantity of brown precipitate, presumably a neptunium(VI) hydroxide or neptunate, was removed by centrifuging before proceeding with the analyses. Since the solution would be expected to be saturated with soluble Np(VI), a modified procedure was tried. For run D a smaller amount of neptunium and a much longer ozonization time was combined with a second ozonization for 30 min on the clear supernatant obtained after removal of the brown precipitate. The result was an improved but still disappointing value of 1.6% Np(VI), extrapolated to zero time, in the final solution. The run D result is very close to the plateau value observed in reduction coulogram B. Both experiments demonstrate that either high-purity Np(VII) cannot be prepared (in 1 *M* NaOH) or there is a rapid reduction to a 1–2% Np(VI) mixture—possibly an impurity catalyzed solvent reaction—as soon as the preparative oxidation process is ended.

Table II: Controlled Potential Coulometric Analyses of Np(VII) in 1 *M* NaOH and ΣNp in 1 *M* $HClO_4$[a]

	Run C	Run D
Ozonization time, hr	4.5	15
Yield soluble Np, %	51	90
Np(VII) × 10^3	4.891	4.043
	4.892	4.046
	4.890	4.048
	4.888	
ΣNp × 10^3	5.048	4.109
	5.080	4.116
		4.111
Check ΣNp × 10^3	5.05[b]	4.13[b]
Np(VII)/ΣNp	0.966	0.984

[a] All results as milliequivalents per gram of solution and corrected to zero time. [b] Mean of two spectrophotometric assays.

Another possibility is that the coulometric analysis of Np(VII) gives low results. This cannot be completely discounted; but if true, the error is very subtle since the Np(VII) reduction at a controlled potential is the best behaved and most reproducible coulometric procedure ever observed in this laboratory. The excellent electrolysis performance probably occurs because, under the conditions used, the platinum electrode must be completely coated with an oxide or hydroxide layer; and at 0.15 V, the Pt–$Pt(OH)_2$ couple is far enough removed from the applied potential of 0.34 V to cause no interference. A low coulometric result could occur if some of the Np(VII) were lost by further (chemical) oxidation of the platinum surface; however, this can be ruled out because successive samples were added to the same cell without any observed trend in the results. For the present work the coulometric analysis of Np(VII) was assumed correct, but final confirmation will require a conventional oxidation–reduction titration with a standard reducing agent.

Potentiometric Measurements. Adherence to the Nernst equation over a wide concentration range is the customary practical criterion of reversibility. This test was applied to the Np(VII)–Np(VI) couple by means of the cell I measurements. Independent stock solutions of Np(VII) and Np(VI) and 1 *M* NaOH were prepared and mixed in varying proportions. Basically the experiments were of the titration type where the initial point was a measured volume of one stock, say Np(VI), and subsequent points were obtained by adding measured volumes of the Np(VII) stock. A second series would then be run in reverse order with the Np(VII) stock serving as the starting point. Additive volumes were assumed, and all concentrations were calculated on the basis of make-up from the neptunium stocks.

(22) R. W. Stromatt, *Anal. Chem.*, 32, 134 (1960); U. S. Atomic Energy Commission Report HW-59447 (1959).

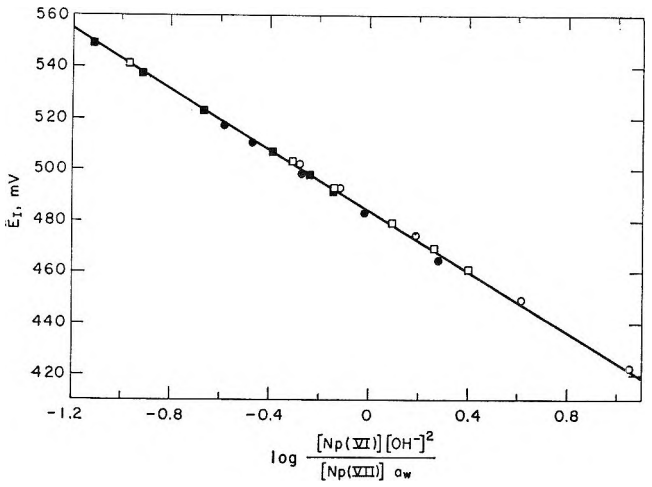

Figure 4. Potentiometric check of Nernst equation behavior for the couple $e^- + H_2O + Np(VII) = Np(VI) + 2OH^-$. The straight line has the theoretical Nerst slope of −59.16 mV; □, Np(VII) stock diluted by successive additions of Np(VI) stock; ○, Np(VI) stock diluted by successive additions of Np(VII) stock; closed points (run E), 0.333×10^{-3} *M* Np(VI) in 1.006 *M* NaOH + 0.0155 *M* $NaClO_4$, 1.462×10^{-3} *M* Np(VII) + 0.069×10^{-3} *M* Np(VI) in 1.153 *M* NaOH + 0.0178 *M* $NaClO_4$; open points (run F), 7.18×10^{-3} *M* Np(VI) in 0.966 *M* NaOH, 6.51×10^{-3} *M* Np(VII) + 0.73×10^{-3} *M* Np(VI) in 0.953 *M* NaOH. All data at 25° *vs.* Hg–HgO (1 *M* NaOH) reference.

Two independent titrations were carried out. In both cases the stocks were standardized by controlled potential coulometry (*cf.* Table II): the Np(VII) by direct analysis plus a ΣNp to give Np(VI) by difference; the Np(VI) stock from a ΣNp acid standardization. Appropriate small adjustments of the Np(VII) stock with time were made by linear interpolation of analyses made at the start and end of the emf measurements. In run E, the Np(VI) was obtained by an overnight equilibration of neptunium(VI) hydroxide with 1 *M* NaOH; the Np(VII) was freshly prepared using tank ozone. For run F, both neptunium solutions were prepared by electrolysis and allowed to stand overnight before use. Solids were removed from the stocks immediately prior to the start of each run by centrifuging, and all standardizations and potential measurements were completed within a single day.

There was some difficulty with upward drifting potentials for the starting point in each series. In the worst case, the drift was almost 2 mV and required about 40 min to establish a potential stable to a few hundredths of a mV over a 10-min period. This was taken as the emf of the initial solution. For all subsequent additions, equilibrium potentials were apparently established within the time of mixing, and the additional data points were taken at about 10-min intervals. In this time interval, there would generally be a downward potential drift of 0.05–0.1 mV, which correlates fairly well with the rates observed for the water reduction of Np(VII). The cell potential for each point was taken as the extrapolated emf value at the time of mixing, and small corrections on the basis of the observed potential drift were then applied to the metal ion ratio in calculating concentrations for the next point.

The E_I cell potential data of runs E and F are summarized in Figure 4. The straight line was drawn with the theoretical 25° Nernst slope of −59.16 mV. The metal ion ratio was the only important variable in the Figure 4 experiments; however, the complete Nernst form was used as the abscissa to include the relatively minor hydroxide ion and water activity corrections. Water activities were calculated from osmotic coefficient data[23] using pure sodium hydroxide solutions of the same sodium ion concentration as the cell solutions. The data of Harned and Hecker[24] supplied the necessary molal–molar conversions.

Liquid-Junction Potentials. Errors produced by liquid-junction potentials were not of great importance in the Figure 4 presentation of the cell I data; however, this was not the case with the experiments to determine the hydroxide ion dependence of the Np(VII)–Np(VI) couple. For this purpose, the cell II measurements were carried out on a series of NaOH–$NaClO_4$ solutions of ionic strength $\mu = 1.000$. The equilibrium hydroxide ion concentrations were determined directly by titration of cell solution samples at the end of the emf runs.

Designating the 1 *M* NaOH value of E_{II} by E_{II}' and combining eq 5a, 8a, and 9

$$E_{II}' = E_5^\circ - E_8^\circ - 0.5k \log(a_w)_{1,0} \qquad (10)$$

and

$$E_{II} - k \log[OH^-] = E_{II}' - E_j' \qquad (11)$$

where

$$E_j' = E_j + k \log\left(\frac{y_{OH}}{a_w}\right)_{1,0}\left(\frac{a_w}{y_{OH}}\right)_{1,\beta} \qquad (12)$$

Thus, E_j', the apparent liquid-junction potential, can be identified with the true junction potential only if the hydroxide ion activity coefficient remains constant. But of course this is the customary assumption with a constant ionic strength medium. The water activity coefficient ratio in eq 12 can be ignored since the same value of $a_w = 0.9660$ was found for both 1 *M* NaOH and $NaClO_4$.[23]

Figure 5 summarizes the cell II data. The smooth curves are the calculated least-squares fit with the Henderson liquid-junction equation assumed as the functional form for E_j[25]

$$E_j = k \log\{1 + [ClO_4^-]f(U)/\mu\} \qquad (13)$$

(23) R. A. Robinson and R. H. Stokes, "Electrolyte Solutions," Academic Press, Inc., New York, N. Y., 1955, p 468.

(24) H. S. Harned and J. C. Hecker, *J. Amer. Chem. Soc.*, **55**, 4838 (1933).

(25) A very lucid discussion is given by D. A. MacInnes, "The Principles of Electrochemistry," Reinhold Publishing Corp., New York, N. Y., 1939, Chapter 13.

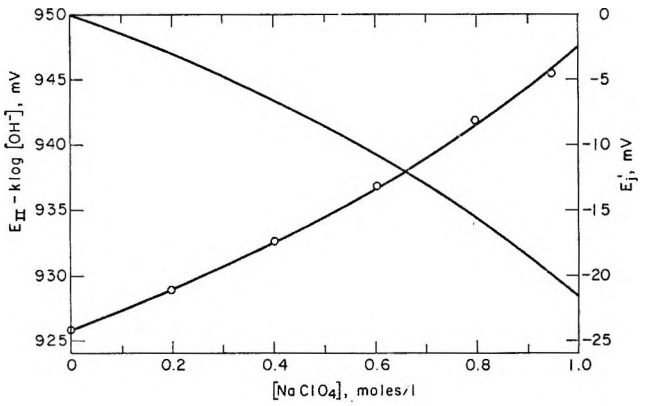

Figure 5. Calibration at 25° of the Hg–HgO (1 *M* NaOH) reference *vs.* the normal hydrogen electrode and determination of the liquid-junction potential 1 *M* NaOH || (1 − β) *M* NaOH + β *M* $NaClO_4$. Data points are $E_{II}' - E_j'$ and refer to left-hand ordinate; curve without points refers to right-hand ordinate scale and is E_j alone. Smooth curves are least-squares calculated values using the functional form of the Henderson liquid-junction equation (see text).

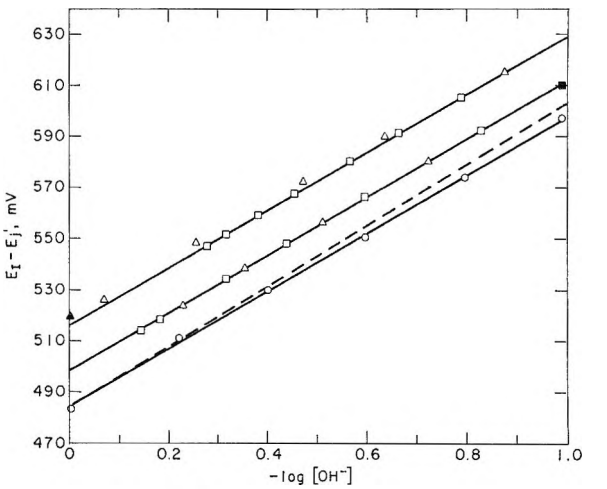

Figure 6. Determination of the hydroxide ion dependence of the Np(VII)–Np(VI) couple. Solid straight lines are the calculated least-squares values, and dashed line illustrates the theoretical Nernst slope for the second-power dependence. Run G (○), inflection points of reduction coulograms, all with ΣNp = 1.9×10^{-3} *M* and μ = 1.005 ± 0.005 (NaOH + $NaClO_4$); run H (■), starting point in potentiometric titration of ~1:1 Np(VII)–Np(VI) mixture in 0.103 *M* NaOH + 0.900 *M* $NaClO_4$; □, titration with 1.000 *M* NaOH; △, titration with 1.000 *M* $HClO_4$ + 1.000 *M* $NaClO_4$; run I, same as run *H* except ▲ indicates starting point with ~96% Np(VII) + 4% Np(VI) in 0.991 *M* NaOH. All data *vs.* Hg–HgO (1 *M* NaOH) reference with junction potential corrections applied. For graphical convenience, all run H ordinates were increased by 10 mV and run I ordinates were decreased by 50 mV.

where $f(U)$ is the mobility of perchlorate ion minus that of hydroxide divided by the sum of the sodium and hydroxide ion mobilities. With $f(U)$ assumed constant and $E_j = E_j'$, the least-squares value and standard deviation of $f(U)$ was −0.570 ± 0.0062, which checks reasonably well with the value −0.528 calculated with limiting equivalent conductances. Our extrapolated value of −21.7 mV for the 1 *M* NaOH||1 *M* $NaClO_4$ liquid-junction potential can be compared to values of −23.4 and −24 mV calculated from the Swedish school studies.[26] The agreement could only be approximate since the latter values were determined in the opposite sense of the present work, namely with a $NaClO_4$ salt bridge and cell solutions with a low NaOH concentration. Thus a long extrapolation was required plus correction[16] from an ionic strength of 3.

The least-squares value and standard deviation of E_{II}' found in Figure 5 was 925.92 ± 0.18 mV. This is in satisfactory agreement with the value 926.25 ± 0.36 mV calculated from eq 10 using the best literature value of 925.81 mV for the cell II standard potential.[19] The observed least-squares value of E_{II}' will be used to convert the observed neptunium formal potentials of cell I into the nhe scale.

Hydroxide Ion Dependence of the Np(VII)–Np(VI) Couple. Two different types of measurements were made to determine the *m* value of eq 6. The first (run G) was a series of reduction coulograms at varying hydroxide ion concentration and μ = 1.005 ± 0.005. Otherwise the coulograms, all *vs.* the MMO reference, were entirely similar to the Figure 3 experiments.

The second series of measurements was potentiometric, using cell I with hydroxide ion concentration as the variable. Again the experiments were of the titration type wherein a Np(VII)–Np(VI) sample, say initially in 0.1 *M* NaOH + 0.9 *M* $NaClO_4$, was first diluted with known volumes of 1 *M* NaOH and then the process was reversed by adding 1 *M* $HClO_4$ + 1 *M* $NaClO_4$. Two independent titrations were made, each with an ionic strength range of 1.011 to 1.003. The first (run H) started with an approximate 1:1 Np(VII)–Np(VI) mixture in dilute base as above, and the second (run I) was carried out in reverse order by starting with a 96% Np(VII) stock in 1 *M* NaOH.

Precise values of the neptunium concentrations were not needed, but the titration experiments did depend on the Np(VII)/Np(VI) ratio remaining constant. This was not the case. Invariably the cell potentials drifted downward, which again was presumed to indicate a slow reduction of Np(VII). The greatest difficulty was encountered in run I where the high Np(VII)/Np(VI) ratio magnified the effect of small changes in the Np(VII) content. To correct all results to the same neptunium ion ratio, the change in emf at the moment of addition of acid or base was obtained by graphical extrapolation of a recorder tracing of the cell potentials. A normalized set of E_I data as function of hydroxide ion concentration was then constructed by adding the Δemf values to the last, and only truly observed, E_I reading. The total corrections by this procedure

(26) (a) B. Carell and A. Olin, *Acta Chem. Scand.*, **14**, 1999 (1960); (b) N. Ingri, G. Lagerström, M. Frydman, and L. G. Sillén, *ibid.*, **11**, 1034 (1957).

amounted respectively to 2.8 and 6.4 mV for runs H and I out of a total potential change of about 80 mV for each run.

The normalized hydroxide dependence data, with the liquid-junction potential corrections of Figure 5 applied, are summarized in Figure 6. In each case the solid line is the least-squares fit, and the one dashed line was drawn to illustrate the theoretical 118.31-mV slope required for an m value of 2. All three runs gave almost identical least-squares slopes. The corresponding m values with the statistical 95% confidence levels were 1.911 ± 0.080 (run G), 1.919 ± 0.019 (run H), and 1.921 ± 0.027 (run I, base added data only).

The acid titration data of run I were not used in the least-squares calculation since they gave a slope significantly lower than any of the other runs. The rejected points, most of which required large drift corrections of about 1 mV, were the most uncertain of all the data. Furthermore, there was the possibility, magnified by the high Np(VII)/Np(VI) ratio, that local excesses during the addition of acid may have destroyed some of the Np(VII). This would lower the observed slope. A similar though very slight trend to lower slope was noted in the acid added data of run H, but there the effect would be minimized by the Np(VII)/Np(VI) ratio of 1.

The NpO_5^{3-} and NpO_4^{2-} Species. At face value the Figure 6 results indicate a nonintegral hydroxide dependence and hence a mixture of Np(VII) and/or Np(VI) species. However, it is simpler and certainly no less reasonable to attribute the observed discrepancy of 4.9 out of 118.3 mV to changing activity coefficients. Effects of the same magnitude have been observed for the Np(VI)–Np(V) couple in acid solutions,[27] and numerous studies of mixed electrolytes at constant ionic strength have demonstrated similar behavior.[28] Therefore, accepting an integral m value, eq 6 can be written as

$$e^- + H_2O + NpO_5^{3-} = NpO_4^{2-} + 2OH^- \quad (14)$$

Of course the Np(VII) and Np(VI) species in eq 14 are not unambiguously established merely by determination of the hydroxide dependence. The assignment is based on three extra considerations. First, in electromigration experiments using a three-compartment electrolysis cell with all the neptunium initially in the center compartment, both Np(VI) and Np(VII) in alkaline solution migrated into the anode compartment. A test run with NpO_2^{2+} in acid solution gave migration into the cathode cell. Thus eq 14 is the simplest selection of anion species with a second-power hydroxide dependence.

The second argument is by analogy with uranium chemistry. The hydrolysis and polymerization of U(VI) is a complicated problem still subject to debate.[29] However, a simplification occurs at pH >12 where the normal uranate UO_4^{2-} becomes the predominant species in solution. The behavior of Np(VI) would be expected to be similar. It should also be noted that if neptunates less hydrolyzed than NpO_4^{2-} are of importance, the hydroxide dependence of eq 6 would tend to be greater than two. Furthermore, the Figure 4 data, which covered a fairly wide range of neptunium concentrations, gave no evidence of polynuclear species.

The third and most direct argument is that a solid Np(VII) compound has been prepared and identified. Krot, *et al.*,[2b] isolated a black crystalline precipitate resulting from the reaction of $Co(NH_3)_6Cl_3$ and Np(VII). The air-dried solid was analyzed as $Co(NH_3)_6NpO_5 \cdot 3H_2O$, and the characteristic Np(VII) absorption spectrum was obtained upon redissolving the solid in alkali.[30]

It might be contended that the reversibility of the Np(VII)–Np(VI) couple precludes the species assigned because of the apparent need to make and break metal–oxygen bonds. This can be easily answered in terms of coordination theory with the NpO_2 unit preserved as the central entity. The Np(VI) and Np(VII) species could then be written as $[NpO_2(OH)_4(H_2O)_2]^{2-}$ and $[NpO_2(OH)_6]^{3-}$, and the couple is readily reversible because of the ease of OH^- and H_2O exchange or replacement. A similar and very attractive hypothesis has been made to rationalize the "uranates" as a systematic group of complex aquohydroxy compounds of uranyl ion.[31] The remarkable similarity of the infrared spectra (Figure 1) also supports the coordination theory structure. On this basis the single band at ~1100 cm^{-1} could be attributed to the asymmetric O–Np–O stretching frequency.[32]

The Formal Potential of the Np(VII)–Np(VI) Couple. The potential of the Np(VII)–Np(VI) couple *vs.* nhe refers to the reaction

$$0.5H_2 + NpO_5^{3-} = NpO_4^{2-} + OH^- \quad (15)$$

and the formal potential of the neptunium couple *vs.* nhe, E_6', is defined by

(27) A. J. Zielen and J. C. Sullivan, *J. Phys. Chem.*, **66**, 1065 (1962).

(28) For example, see H. S. Harned and B. B. Owen, "The Physical Chemistry of Electrolytic Solutions," 3rd ed, Reinhold Publishing Corp., New York, N. Y., 1958, Chapter 14.

(29) A convenient summary is presented by E. A. Ippolitova and N. I. Pechurova in "Investigations in the Field of Uranium Chemistry" (English translation of "Issledovaniya v oblasti khimii urana," V. I. Spitsyn, Ed., Moscow University Publishing House, Moscow, 1961), U. S. Atomic Energy Commission Report ANL-Trans-33, 1964, p 89.

(30) Since preparation of this paper, additional Np(VII) compounds have been reported: $Ba_3(NpO_5)_2 \cdot nH_2O$, $Sr_3(NpO_5)_2 \cdot nH_2O$, and $[Pt(NH_3)_5Cl]NpO_5 \cdot nH_2O$ with $n \sim 1$ for the last compound: N. N. Krot, M. P. Mefod'eva, F. A. Zakharova, T. V. Smirnova, and A. D. Gel'man, *Radiokhimiya*, **10**, 630 (1968).

(31) G. V. Ellert in "Complex Compounds of Uranium" (English translation of "Kompleksnye Soedineniya Urana," I. I. Chernyaev, Ed., Izdatel'stvo "Nauka," Moscow, 1964), Israel Program for Scientific Translations, Jerusalem, 1966, Chapter 4.

(32) L. H. Jones and R. A. Penneman, *J. Chem. Phys.*, **21**, 542 (1953).

$$E_6' = E_{15} + k \log \frac{[\mathrm{Np(VI)}][\mathrm{OH^-}]}{[\mathrm{Np(VII)}]} + E_8^\circ \quad (16)$$

In 1 M sodium ion, the formal potential can also be written as

$$E_6' = E_6^\circ - k \log \left(\frac{y_{\mathrm{VI}} y_{\mathrm{OH}}}{y_{\mathrm{VII}}} \right)_{1,\beta} \quad (17)$$

(It should be noted that y_{OH} appears only to the first power in eq 17 as compared to the half-reaction form given by eq 6a.) To obtain E_6', we define E_{I}' and E_{II}'' as

$$E_{\mathrm{I}}' = E_{\mathrm{I}} + k \log \frac{[\mathrm{Np(VI)}][\mathrm{OH^-}]^2}{[\mathrm{Np(VII)}]a_w} - E_j' \quad (18)$$

$$E_{\mathrm{II}}'' = E_{\mathrm{II}}' + E_8^\circ + k \log(a_w)_{1,0} = 96.96 \text{ mV} \quad (19)$$

The evaluations $E_{\mathrm{II}}' = 925.92$ mV and $(a_w)_{1,0} = 0.9660$ have been given earlier. The quantity E_8°, the standard potential of the hydrogen electrode in base or the hydroxyl electrode, was computed to be 828.07 mV.[33] This is the molar scale value obtained by taking 1.008×10^{-14} for the 25° disassociation constant (molal scale) of water.

Substituting eq 5a, 6a, 7, 10, and 12 into eq 18 and 19

$$E_{\mathrm{I}}' + E_{\mathrm{II}}'' = E_6^\circ - k \log \left(\frac{y_{\mathrm{VI}} y_{\mathrm{CH}}^2}{y_{\mathrm{VII}}} \right)_{A,\beta} + k \log(y_{\mathrm{OH}})_{1,\beta} + E_j'' \quad (20)$$

Equations 20 and 17 become identical at $A = 1$, and if activity coefficients are independent of β in our assumed equivalent media of $(1 - \beta)$ M NaOH + β M $NaClO_4$, or at least as the limiting case of indefinitely dilute neptunium in 1 M NaOH, the final expression for the formal potential is

$$\lim_{A \to 1,\ \beta \to 0} (E_{\mathrm{I}}' + E_{\mathrm{II}}'') = E_6^\circ - k \log \left(\frac{y_{\mathrm{VI}} y_{\mathrm{OH}}}{y_{\mathrm{VII}}} \right)_{1,0} \quad (21)$$

The evaluation of the Np(VII)–Np(VI) couple formal potential *vs.* nhe is given in Figure 7. The presentation is a severe test of the data (the ordinate scale is a 25-fold enlargement over that of Figures 4 and 6) that is intended to summarize the results of this research and to indicate the correction or interpolation needed to obtain the 1 M NaOH formal potential defined by eq 21. All the emf data of this work are included except run B, where the extensive preelectrolysis made the calculated sodium and hydroxide concentrations unreliable, and runs H and I, where accurate values of the Np(VII)/Np(VI) ratio were not determined. The run G point and range represents the least-squares 1 M hydroxide intercept and standard deviation obtained from Figure 6. Even though questionable corrections were required, the run A reduction coulogram *vs.* sce was included because it remains as our only value with a different reference electrode. For run A only, a quantity corresponding to E_{II}' was computed as 241.2 − 8.6 − 10.0 = 222.6 mV. The numbers, in order, represent the 25° potential of the sce;[34] the calculated liquid-junction potential between saturated (~4.2 M) KCl and 1 M NaOH as obtained with the Henderson equation using limiting conductances; and k log $(y_{\mathrm{OH}})_{1,0}$, which was estimated by using $y_{\pm}$ for 1 M NaOH.

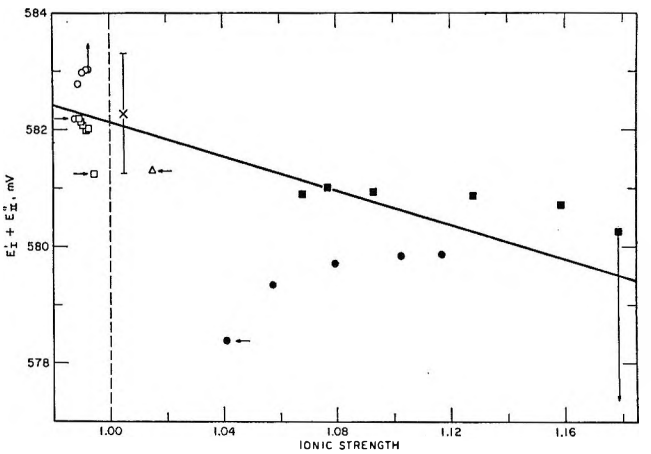

Figure 7. Summary and final evaluation of the Np(VII)–Np(VI) formal potential at 25° *vs.* the normal hydrogen electrode in 1 M NaOH: ○ and □, potentiometric runs E and F, same key as Figure 4, vertical arrows indicate movement of points if E_j'' corrections had been applied (see text); coulometric run A (*vs.* sce), △; coulometric run G, × plotted point and range is the least-squares intercept and standard deviation from Figure 6. Straight line is the calculated least-squares result used for interpolation to $\mu = 1$ value of the formal potential. Points marked with horizontal arrows were rejected in the least-squares calculations (see text).

The fact that the Figure 7 results do not cluster around a single smooth curve indicates hidden bias in each series, probably in the calculated Np(VII)/Np(VI) ratios. The most accurate data set undoubtedly was potentiometric run F, which checked very well with coulometric run G. And, considering the rather dubious calculations needed, the agreement with sce run A was also satisfactory. Potentiometric run E was the poorest data set for two reasons. First, the Np(VI) stock was too dilute to obtain a reliable coulometric standardization, and second, a make-up error in the sodium hydroxide concentration of the Np(VII) stock produced the large variation in ionic strength displayed in Figure 7.

More properly, at least according to eq 17–21, the Figure 7 abscissa should have been sodium ion concentration instead of ionic strength, but the change would have been trivial (range of ΣNp = 0.48 to 7.2×10^{-3} M and β range = 0.005 to 0.022 M). Ionic strength was selected purely for convenience since it slightly spreads out points that otherwise would have been virtually superimposed. The trend with ionic strength—or

(33) Compare ref 21, pp 3, 31, 32; ref 25, pp 252, 253.

(34) Reference 19, p 160.

$[Na^+]$—appears to be slight, but this is a cancellation artifice of the activity coefficient terms and E_j'' of eq 20. Estimated values of E_j'' were calculated with the appropriate form of the Henderson liquid-junction equation; extreme cases are shown as vertical arrows in Figure 7; *i.e.*, the arrows indicate where the points would move if E_j'' estimates had been included in E_I'. Clearly, there would have been no advantage in attempting the E_j'' correction.

Fortunately the correction required from optimum run F to the eq 21 conditions was small and would depend very little on the methods used. The procedure selected was the $\mu = 1$ value of the least-squares straight line through the Figure 7 data. The four points marked with horizontal arrows were not included in the calculation. The sce value was rejected because of the dubious corrections applied. The other three were each initial (upward drifting) points of a titration series, and apparently they had not reached equilibrium since all were significantly lower than the subsequent points of the same set.

The final value and 95% statistical confidence limits of the 25° Np(VII)–Np(VI) formal potential *vs.* nhe in 1 *M* NaOH was found to be 582.1 ± 0.45 mV. An approximate value of 0.61 V in 1 *M* KOH at 25° is given by Spitsyn.[2c,3] The redox potential indicates Np(VII) to be a good oxidizing agent of about the same strength as the alkaline permanganate–manganese dioxide couple, listed as 588 mV by Latimer.[35]

The orginal data of this research are available as a microfilm supplement.[36,37]

Acknowledgment. We acknowledge with pleasure the assistance of Dr. Anne T. Sherren of North Central College, who carried out the infrared measurements and prepared the fine structure assignment in the Np(VII) absorption spectrum.

(35) Reference 21, p 238.

(36) Material supplementary to this article has been deposited as document NAPS-00626 with the ASIS National Auxiliary Publications Service, % CCM information Corp., 909 3rd Ave., New York, N. Y. 10022; remit $1.00 for microfiche or $3.00 for photocopies. Advance payment is required. Make check payable to: ASIS-NAPS.

(37) NOTE ADDED IN PROOF. The most comprehensive English review to date of the Russian work on Np(VII) and Pu(VII) has recently appeared: V. I. Spitsyn, A. D. Gelman, N. N. Krot, M. P. Mefodiyeva, F. A. Zakharova, Yu. A. Komkov, V. P. Shilov, and I. V. Smirnova, *J. Inorg. Nucl. Chem.*, 31, 2733 (1969).

Comments on the Partition Function for Potential Energy

by D. R. Cruise

Propulsion Development Department, Naval Weapons Center, China Lake, California 93555 *(Received January 29, 1969)*

A derivation of the pressure ensemble reported by Jaynes in 1957 is pursued. This theory leads to a partition function for potential energy. When certain approximations for molecular interactions are introduced to this function, a qualitative prediction of critical point phenomena results.

Introduction

The frequency at which a molecule is found in a given total energy state is usually formulated in terms of a partition function[1,2]

$$Q = \sum_{i=1}^{\infty} e^{-\beta\epsilon_i} \tag{1}$$

where

$$\beta = 1/kT \tag{2}$$

k is the Boltzmann constant, and ϵ_i is the energy of the ith state. Further derivations lead to a pressure relation

$$P = RT\left(\frac{\partial \ln Q}{\partial V}\right)_T \tag{3}$$

where R is the universal gas constant. When intermolecular forces are explicitly introduced, eq 3 can be expanded to obtain the virial equation of state

$$\frac{PV}{RT} = 1 + \frac{B(T)}{V} + \frac{C(T)}{V^2} + \cdots \tag{4}$$

The virial expansion has a great theoretical justification and is very accurate in certain regions, but it has two weaknesses. It is difficult in practice to evaluate the high-order coefficients, and the series does not

(1) E. Schrödinger, "Statistical Thermodynamics," Cambridge University Press, Cambridge, 1948.

(2) J. Hirschfelder, C. Curtiss, and R. Bird, "Molecular Theory of Gases and Liquids," John Wiley & Sons, Inc., New York, N. Y., 1964, p 137.

converge in regions approaching the density of the liquid.[3]

In the theory that follows, a complete departure is made from the virial equation of state. This is based on a statistical mechanical derivation made by Jaynes[4] employing an information theory approach. This derivation begins with constraints on energy and volume and proceeds to what is called the pressure ensemble. It thus has an immediate accord with the Duhem theorem, which states that the equilibrium state of a closed system is completely determined by two state variables.[5]

Theory

Let the volume, v, of a molecule be defined as that space within the walls of the container that is closer to the specified molecule than to any other molecule. Such a space would contain regions both inside and outside the molecule. For the first part of the theory, let it be assumed that the potential energy of a molecule depends only on the size of this volume and not on its shape. Further, let it be assumed that molecular volume is a measure upon which the potential energy of the molecule depends

$$\phi = \phi(v) \tag{5}$$

It would appear that molecular interactions cannot be treated when potential energy is defined in this manner because molecular volume is identified only with a particular molecule. This is not the case, however, because molecular volume is implicitly determined by the positions of neighboring molecules. It will later be shown that eq 5 can be modified to treat molecular interactions more explicitly.

If v has a uniform measure,[6] the information theory entropy for an N molecule system is expressed

$$S = -Nk\int \mathrm{f}(v) \ln \mathrm{f}(v)\mathrm{d}v \tag{6}$$

where N may take any value, but in this work is taken as Avogadro's number, and where $\mathrm{f}(v)$ is the frequency of v, which is normalized so

$$\int \mathrm{f}(v)\mathrm{d}v = 1 \tag{7}$$

The potential energy of the system is

$$E = N\int \phi(v)\mathrm{f}(v)\mathrm{d}v \tag{8}$$

and the system volume is

$$V = N\int v\mathrm{f}(v)\mathrm{d}v \tag{9}$$

Using a formalism which minimizes the bias of an observer, Jaynes[4] solves eq 6 subject to the constraints of eq 7, 8, and 9 such that entropy is a maximum. The direct result is

$$\mathrm{f}(v) = \exp(-\alpha - \beta\phi(v) - \gamma v) \tag{10}$$

where α, β, and γ are Lagrange multipliers. The first is obtained directly from eq 7

$$\alpha = \ln \int \exp(-\beta\phi(v) - \gamma v)\mathrm{d}v \tag{11}$$

The others are identified by Jaynes as follows

$$\beta = N/RT \tag{12}$$

and

$$\gamma = NP/RT \tag{13}$$

A partition function may be defined as follows

$$Q \equiv e^{\alpha} = \int \exp(-\beta\phi(v) - \gamma v)\mathrm{d}v \tag{14}$$

This can be called the partition function for potential energy because kinetic energy is not included in eq 8.

Although the above approach is completely heuristic, the pressure ensemble obtained has the same distribution as that derived by Lewis and Siegert.[7] The approach may easily be extended to obtain the following relations.

Potential energy

$$EQ = -N\frac{\partial}{\partial\beta}Q \tag{15}$$

Volume

$$VQ = -N\frac{\partial}{\partial\gamma}Q \tag{16}$$

Heat capacity for potential energy (c_v)

$$(c_v + E^2/RT^2)Q = N^2/RT^2\left(\frac{\partial}{\partial\beta}\right)^2 Q \tag{17}$$

Thermal expansion coefficient (α)

$$(\alpha + VE/RT^2)Q = N^2/RT^2\,\frac{\partial}{\partial\beta}\frac{\partial}{\partial\gamma}Q \tag{18}$$

Isothermal compressibility (χ)

$$(\chi + V/RT)Q = N^2/VRT\left(\frac{\partial}{\partial\gamma}\right)^2 Q \tag{19}$$

Gibbs free energy for potential energy

$$G = -RT \ln Q \tag{20}$$

To use these relations, a potential function must be assumed. The simplest case is to consider the molecules to be point masses with no potential energy at any volume

$$\phi(v) = 0 \quad 0 \leq v \leq \infty \tag{21}$$

(3) J. Hirschfelder, C. Curtiss, and R. Bird, ref 2, p 132.

(4) E. T. Jaynes, *Phys. Rev.*, **106**, 620 (1957) (see also p 269).

(5) I. Prigogine and R. Defay, "Chemical Thermodynamics," translated by D. H. Everett, Longmans, Green and Co., New York, N. Y., 1952, p 188.

(6) E. T. Jaynes, "Information Theory and Statistical Mechanics," Brandeis University Summer Institute Lectures in Theoretical Physics. In Statistical Physics," K. W. Ford, Ed., W. A. Benjamin Inc., New York, N. Y., 1963, p 201.

(7) M. B. Lewis and A. J. F. Siegert, *Phys. Rev.*, **101**, 1227 (1956).

(8) J. Hirschfelder, *et al.*, ref 2, p 30.

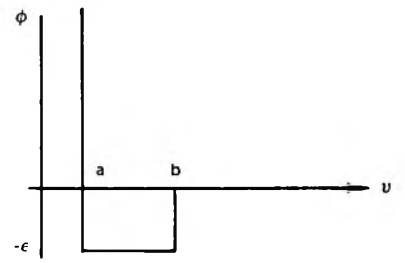

Figure 1. Square well potential.

In this case, the partition function becomes

$$Q = \int_0^\infty e^{-\gamma v} dv = -\frac{1}{\gamma}\left[e^{-\gamma v}\right]_0^\infty = \frac{1}{\gamma} \quad (22)$$

Volume may be obtained from eq 16

$$V = -N\frac{\partial}{\partial \gamma} \ln Q = -N\left(\frac{-1}{\gamma^2}\right)\gamma = \frac{N}{\gamma} = \frac{RT}{P} \quad (23)$$

This is the perfect gas relation.

A hard sphere model without potential is also easy to evaluate

$$\phi(v) = \infty \quad 0 \leq v < b \quad (24)$$

$$\phi(v) = 0 \quad b \leq v \leq \infty \quad (25)$$

Here b is the minimum volume allowed to the molecule

$$Q = \int_b^\infty e^{-\gamma v} dv = \frac{-1}{\gamma}\left[e^{-\gamma v}\right]_b^\infty = \frac{1}{\gamma} e^{-\gamma b} \quad (26)$$

$$V = -N\left(\frac{-1}{\gamma^2} - \frac{b}{\gamma}\right)e^{-\gamma b} \Big/ \left(\frac{1}{\gamma} e^{-\gamma b}\right) = N\left(\frac{1}{\gamma} + b\right) = \frac{RT}{P} + Nb \quad (27)$$

Thus, this assumption leads to the Abel equation of state.

The partition function for a square well potential (Figure 1) has an analytic solution.

$$\phi(v) = \infty \quad 0 \leq v < a \quad (28)$$

$$\phi(v) = -\epsilon \quad a \leq v < b \quad (29)$$

$$\phi(v) = 0 \quad b \leq v \leq \infty \quad (30)$$

The partition function is

$$Q = \int_a^b \exp(\beta\epsilon - \gamma v) dv + \int_b^\infty \exp(-\gamma v) dv \quad (31)$$

which upon integrating becomes

$$Q = \frac{-1}{\gamma} \exp(\beta\epsilon)[\exp(-\gamma b) - \exp(-\gamma a)] + \frac{1}{\gamma} \exp(-\gamma b) \quad (32)$$

From this expression V may be determined

$$V = N\left\{\frac{1}{\gamma} + \frac{\exp(\beta\epsilon)[b \exp(-\gamma b) - a \exp(-\gamma a)] - b \exp(-\gamma b)}{\exp(\beta\epsilon)[\exp(-\gamma b) - \exp(-\gamma a)] - \exp(-\gamma b)}\right\} \quad (33)$$

and with eq 15, the system potential energy may also be determined

$$E = -N\epsilon \frac{\exp(\beta\epsilon)[\exp(-\gamma b) - \exp(-\gamma a)]}{\exp(\beta\epsilon)[\exp(-\gamma b) - \exp(-\gamma a)] - \exp(-\gamma b)} \quad (34)$$

The use of other potential functions, such as the Lennard-Jones[7] function, is numerically possible. Molecular volume, v, may be made proportional to the cube of the intermolecular distance in these functions.

It can be noted that the partition function, eq 14, is a Laplace transform[9]

$$\int_0^\infty e^{-\beta\phi(v)} e^{-\gamma v} dv = L(e^{-\beta\phi(v)}) = Q(\gamma) \quad (35)$$

The inverse transform

$$e^{-\beta\phi(v)} = L^{-1}(Q(\gamma)) \quad (36)$$

with eq 16 allows one to express the potential in terms of system volume

$$\phi(v) = \frac{-1}{\beta} \ln\left\{L^{-1}\left[\exp\left(\frac{-1}{N}\int V(\gamma) d\gamma\right)\right]\right\} \quad (37)$$

Critical Behavior

The theory of the partition function for potential energy may be extended by making more elaborate assumptions about $\phi(v)$. It is unrealistic to assign the same potential energy to a molecule of a given volume regardless of the geometric shape of that space; probably, it is most unrealistic to do this in the vicinity of the critical point. In any case, the theory as developed thus far does not predict critical phenomena.

The task of expressing the potential energy of a molecule as a function of the shape as well as the size of the space it occupies can be simplified by a certain heuristic approximation. Just as the volume occupied by a molecule depends on the position of its neighbors, so also must the shape of that space depend on the volume occupied by its neighbors. This is the basis for the following relation

$$\phi(v) = \int_0^\infty \psi(u,v) f(u) du \quad (38)$$

where $\psi(u,v)$ is the potential of a molecule of size v,

(9) R. V. Churchill, "Operational Mathematics," McGraw-Hill Book Co., Inc., New York, N. Y., 1958.

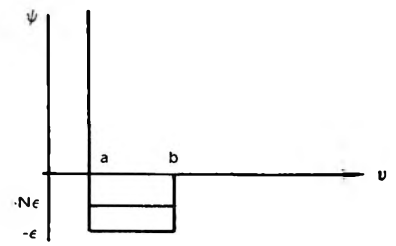

Figure 2. Modified square well potential.

given that its nearest neighbor has size u. This can be extended to two neighbors as follows

$$\phi(v) = \int_0^\infty \int_0^\infty \psi(w,u,v)\mathrm{f}(w)\mathrm{d}w\mathrm{f}(u)\mathrm{d}u \qquad (39)$$

and so on for as many neighbors as one wishes to consider.

As a specific but simple example, consider the following modified square well potential function shown in Figure 2

$$\psi(u,v) = 0 \qquad b < v \leq \infty \qquad (40)$$

$$\psi(u,v) = -\epsilon \qquad a \leq u \leq b \quad a \leq v \leq b \qquad (41)$$

$$\psi(u,v) = -x\epsilon \qquad b < u \leq \infty \quad a \leq v \leq b \qquad (42)$$

Equation 40 states that the potential of a molecule not in the well is zero regardless of the volume of its nearest neighbor; eq 41 states that the potential of a molecule which falls in the well is $-\epsilon$ when its nearest neighbor also falls in the well; but eq 42 states that the potential of a molecule which falls in the well is $-x\epsilon$ when its nearest neighbor does not fall in the well.

The new partition function is obtained by substituting eq 38 into eq 14

$$Q = \int_0^\infty \exp\left[-\beta \int_0^\infty \psi(u,v)\mathrm{f}(u)\mathrm{d}u - \gamma v\right]\mathrm{d}v \qquad (43)$$

This substitution again assumes that volume has a uniform measure in the sense reported by Jaynes.[6]

Q may be broken into two parts

$$Q = Q_1 + Q_2 \qquad (44)$$

where

$$Q_1 = \int_a^b \exp\left[-\beta \int_0^\infty \psi(u,v)\mathrm{f}(u)\mathrm{d}u - \gamma v\right]\mathrm{d}v \qquad (45)$$

and

$$Q_2 = \int_b^\infty e^{-\gamma v}\mathrm{d}v = \frac{1}{\gamma} e^{-\gamma b} \qquad (46)$$

Equations 41 and 42 may then be substituted into eq 45 to obtain

$$Q_1 = \int_a^b \exp\left\{\beta\left[\epsilon \int_a^b \mathrm{f}(u)\mathrm{d}u + x\epsilon \int_b^\infty \mathrm{f}(u)\mathrm{d}u\right] - \gamma v\right\}\mathrm{d}v \qquad (47)$$

Let the following definitions be made

$$\beta^* = \beta\epsilon \qquad (48)$$

$$F_1 = \int_a^b \mathrm{f}(u)\mathrm{d}u \qquad (49)$$

$$F_2 = \int_b^\infty \mathrm{f}(u)\mathrm{d}u \qquad (50)$$

where physically F_1 may be interpreted as the mole fraction of molecules which fall in the well and F_2 that which does not fall in the well. These may be substituted into eq 47, and upon integrating

$$Q_1 = \frac{-1}{\gamma}(e^{-\gamma b} - e^{-\gamma a})e^{\beta^*(F_1 + xF_2)} \qquad (51)$$

Since u can just as well be v in eq 49 and 50, the following are obtained

$$F_1 = Q_1/Q \qquad (52)$$

$$F_2 = Q_2/Q \qquad (53)$$

If one guesses values of F_1 and F_2, they may be substituted into eq 46 and 51 to obtain estimates of Q_1 and Q_2. Then one may employ eq 52 and 53 to obtain new guesses for F_1 and F_2. This procedure may be repeated until convergence is obtained.

It was found that if initial guesses of $F_1 = 1$ and $F_2 = 0$ were used, the final solution was not always the same as when initial guesses of $F_1 = 0$ and $F_2 = 1$ were used. In the case of multiple solutions, one chooses the solution with the largest value of Q because this minimizes Gibbs free energy (see eq 20), which is the thermodynamic potential for a constant β, γ (temperature, pressure) system.[10]

Such a procedure was used to estimate the isotherms of nitrogen (Figure 3). Note that there is a transition region (below the dotted line) where the free energy criterion requires a switch from one solution to another. Above the 126.1°K line only one solution is ever obtained. At the point C′ (which will now be freely called the predicted critical point) a transition occurs between multiple and single solutions.

The problem of determining values of a, b, ϵ, and x for a material such as nitrogen will now be approached. Let r be the ratio of F_1 to F_2

$$r = \frac{F_1}{F_2} = \frac{Q_1}{Q_2} \qquad (54)$$

Equations 46 and 51 may be substituted into eq 54 to obtain

$$r = -[1 - \exp(-\gamma a + \gamma b)]\exp\left[\beta^*\left(\frac{r + x}{r + 1}\right)\right] \qquad (55)$$

Let the following dimensionless quantities be defined

(10) I. Prigogine and R. Defay, ref 5, pp 36, 66–68.

$$\gamma^* = \gamma b \tag{56}$$

$$y = \frac{b - a}{b} \tag{57}$$

Then eq 55 becomes, on rearrangement

$$e^{\gamma^* y} = 1 + r \exp\left[-\beta^*\left(\frac{r + x}{r + 1}\right)\right] \tag{58}$$

In order that there be more than one solution of r (given γ^*, β^*, x, and y), the right-hand member of eq 58 must have maximums and minimums. These may be found by differentiating

$$ye^{\gamma^* y}\frac{d\gamma^*}{dr} = \left[1 - r\beta^*\frac{(r + 1) - (r + x)}{(r + 1)^2}\right] \exp\left[-\beta^*\left(\frac{r + x}{r + 1}\right)\right] \tag{59}$$

By equating $d\gamma^*/dr$ to zero, one obtains the conditions for a maximum or a minimum

$$0 = 1 - r\beta^*\frac{1 - x}{(r + 1)^2} \tag{60}$$

this equation may be solved for r

$$r = \{-2 + \beta^*(1 - x) \pm \sqrt{[2 - \beta^*(1 - x)^2] - 4}\}/2 \tag{61}$$

In order that a maximum or minimum occur for real values of r, the expression under the radical must be positive. If it is negative, there can be only one real root value for r in eq 58. The transition between single and multiple root regions occur when the discriminant is zero

$$[2 - \beta^*(1 - x)^2] - 4 = 0 \tag{62}$$

Solving this equation, one finds the critical value of β^*

$$\beta_c^* = \frac{4}{1 - x} \tag{63}$$

Substituting the result into eq 61, one finds the critical value of r

$$r_c = \left[-2 + \frac{4}{1 - x}(1 - x)\right] = 1 \tag{64}$$

Finally after substitution of eq 63 and 64 into eq 58, one obtains

$$\gamma_c^* = \frac{1}{y}\ln\left[1 + \exp\left(-2\frac{1 + x}{1 - x}\right)\right] \tag{65}$$

The parameters may be fit to a specific material as follows

$$\gamma_c = NP_c/RT_c \tag{66}$$

$$\beta_c = N/RT_c \tag{67}$$

$$\epsilon \cong \frac{1}{N}\Delta E_v = \frac{1}{N}(\Delta H_v - RT) \tag{68}$$

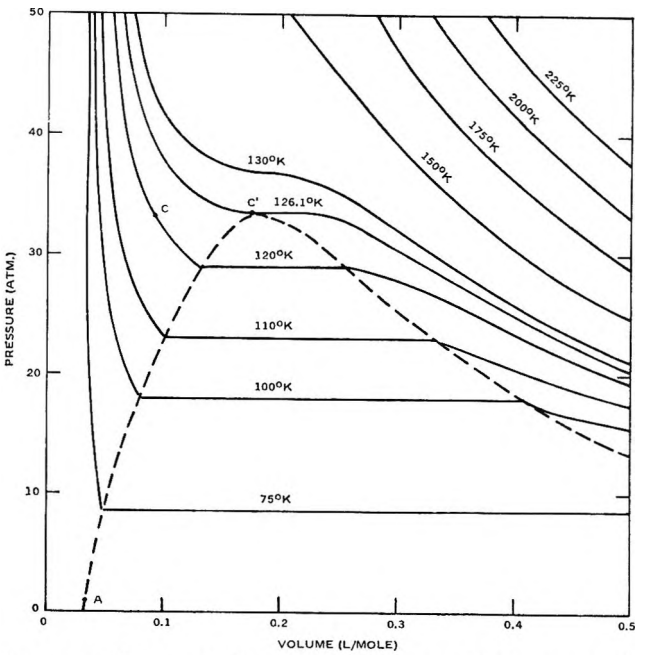

Figure 3. Nitrogen isotherms predicted by modified square well potential showing the qualitative prediction of the critical point C′, but poor quantitative agreement with the true critical point C.

where ΔH_v is the heat of vaporization well below the critical temperature. The latter equation makes the crude assumption that the kinetic energy of molecules does not change due to evaporation. The procedure may be continued as follows

$$\beta_c^* = \beta_c\epsilon \tag{69}$$

$$x = 1 - 4/\beta_c^* \tag{70}$$

The parameters a and b may be estimated by solving the two simultaneous equations

$$(b + a)/2 = \frac{1}{N}V_l \tag{71}$$

$$b - a = \frac{1}{\gamma_c}\ln\left[1 + \exp\left(-2\frac{1 + x}{1 - x}\right)\right] \tag{72}$$

where V_l is the liquid volume at low temperatures and eq 72 is derived from eq 65. The following

$$\beta^* = N\epsilon/RT \tag{73}$$

$$\gamma^* = NbP/RT \tag{74}$$

are then computed for any pressure and temperature.

The expression for volume which yielded the isotherms in Figure 3 is found by the usual operation on the partition function

$$VQ = -N\frac{\partial}{\partial\gamma}Q = -N\left\{\left[\frac{-1}{\gamma} - \frac{b\exp(-\gamma b) - a\exp(-\gamma a)}{\exp(-\gamma b) - \exp(-\gamma a)}\right]Q_1 + \left[\frac{-1}{\gamma} - b\right]Q_2\right\} \tag{75}$$

Since this equals $V(Q_1 + Q_2)$

$$V = -N\left\{F_1\left[\frac{-1}{\gamma} - \frac{b\exp(-\gamma b) - a\exp(-\gamma a)}{\exp(-\gamma b) - \exp(-\gamma a)}\right] + F_2\left[\frac{-1}{\gamma} - b\right]\right\} \quad (76)$$

or

$$V = +Nb\left\{\frac{+1}{\gamma^*} + F_1\left[\frac{1 - (1 - y)\exp(\gamma^* y)}{1 - \exp(\gamma^* y)}\right] + F_2\right\} \quad (77)$$

The parametric values used for nitrogen in Figure 3 are

$$P_c = 33.5 \text{ atm}^{11}$$

$$T_c = 126.1°\text{K}^{11}$$

$V_1 = 0.3465$ l./mol at 77.34°K and 1 atm[11]

$N\epsilon = 1082$ cal/mol at 77.34°K and 1 atm[12]

Discussion

The theory presented gives a respectable qualitative prediction of the critical phenomenon even with a crude square well potential. There is even some quantitative agreement as one proceeds to the right in Figure 3. However, the critical volume predicted (C′) is displaced considerably from the true value (C). The critical pressure and temperature achieved in Figure 3 are, of course, exactly correct because they were used to estimate two of the parameters of the square well model. The point marked (A) is also correct because of the arbitrary way the liquid volume at 1 atm was related to $(a + b)/2$ in eq 71.

The lack of quantitative agreement in the upper left portion of the figure can possibly be attributed to the abnormally high compressibilities predicted by the square well potential. The results obtained encourage further study in (1) the use of more realistic potential functions; (2) the consideration of interactions with more than one neighbor; and (3) the justification of a uniform measure on v space, or the derivation of the true measure.

(11) "Handbook of Chemistry and Physics," Chemical Rubber Publishing Co., Cleveland, Ohio, 1960.

(12) "Selected Values of Chemical Thermodynamic Properties," National Bureau of Standards, Circular 500, U. S. Government Printing Office, Washington, D. C., 1952.

Electron Distribution of Electron-Bombarded Alkylamines and Its Correlation with the Probability of Bond Scission in Their Mass Spectra[1]

by Kozo Hirota, Iwao Fujita, Masao Yamamoto, and Yoshio Niwa

Department of Chemistry, Faculty of Science, Osaka University, Toyonaka, Osaka, Japan
(Received May 29, 1969)

Electron distribution of *n*-propylamine and ethylamine is calculated by means of the CNDO method to study the probability of bond scission in their mass spectra. Electron density of the highest occupied orbital in the skeletal bonds of both amines is found to be the largest on the α-CC bond adjacent to the CN bond. This is in sharp contrast to the equivalent orbital calculation, in which electron density is the largest on the CN bond. The order of scission probability of each bond determined from the mass spectra of propylamine (α-CC bond > CN bond > β-CC bond) can be explained by the MO theory, based on the above electron density. Under the assumption that there exist fast and slow processes in fragmentation of alkylamines, change of scission probability at low energy of the bombarding electron can be explained also. Reliability of the calculated values can be supported by the agreement of the calculated dipole moment with the observed.

Introduction

As far as the mass spectra of the aliphatic and cyclic alkanes are concerned, the correlation[2] that the scission probability of their skeletal bonds is proportional to the positive charge distribution of the highest occupied (HO) orbital at the corresponding bond of the molecular ions seems now to be accepted generally.[3]

However, the use of this correlation to predict the mass spectra of other compounds is not regarded credit-

(1) Report XX on molecular orbital theory for mass spectra.

(2) (a) K. Fueki and K. Hirota, *Nippon Kagaku Zasshi*, **81**, 212 (1960); (b) K. Hirota and Y. Niwa, *J. Phys. Chem.*, **72**, 5 (1968).

(3) J. C. Lorquet, *ibid.*, **73**, 463 (1969); K. Hirota, Y. Niwa, and M. Yamamoto, *ibid.*, **73**, 464 (1969).

able yet. For instance, Lorquet, *et al.*,[4] heavily criticized our attempt to extend this line of research over normal alkylamines.[5] Their criticism against our attempt is due to the calculated result of alkylamines based on the LCBO approximation; *i.e.*, though the charge densities at the CN bond and lone pair are 16 and 71% of the total charge, respectively, we took only the charge distribution of the CC bonds into account in discussing relative scission probability. The above criticism was already expected by us when the research was started. However, because of the following reason, we dared to adopt the above assumption. In our LCBO calculation, charge distribution of the lone pair is included implicitly in that of the CN bond, and the net charge distribution at the CN bond might occupy only a small fraction of the total and even be smaller than that at the α-CC bond adjacent to it. Nevertheless, such a presumption seems not to have been justified by Lorquet's simple calculation, even though details are not shown by them. Final decision of the applicability of the correlation, therefore, has to be postponed until the charge distribution is calculated by a more elaborate MO method than they used.

This is the reason why we began to investigate the problem by adopting the complete neglect of differential overlap (CNDO) method proposed by Pople, *et al.*[6] As the compounds to be studied, ethylamine and *n*-propylamine are adopted in the calculation, and the correlation of the charge density of the HO orbital at each bond with its scission probability is compared with the experiment which is carried out on *n*-propylamine under such a condition as to satisfy the purpose of theoretical discussion.

The result obtained is found favorable for our standpoint; *i.e.*, the experimental scission probabilities of the CN bond and β-CC bond as well as of the α-CC bond can be predicted by our calculation. Besides, if the MO theory is extended more generally than the original theory,[2a] effect of ionizing voltage on the mass spectra can be explained.

Method of Calculation

As is well known, the CNDO method is a semiempirical SCF method of calculating molecular orbitals and is known to be able with success to treat π electrons and lone-pair electrons as well as σ electrons. Therefore, this method is much more elaborate than the LCBO method, which was adopted by Hirota and Itoh.[5] Before entering into the details of calculation, it has to be pointed out that the electron distribution of neutral amines is calculated, but the charge distribution of the corresponding ions is not calculated as Lorquet, *et al.*,[4] did, owing to the reason that both absolute values would be practically the same as already discussed.[2b]

In the calculation, two stable conformations (*i.e.*, *trans* and *gauche* form with respect to the CC bond and lone pair along the CN bond) are adopted as the representative ones of all the possible conformations. They are explained by Figure 1, taking *n*-propylamine as an example. Since the 1s electrons of carbon and nitrogen atoms are amalgamated to the cores, only the orbitals in problem for each amine are numbered in Figure 1, where the lone-pair orbital is numbered to be the first in both forms.

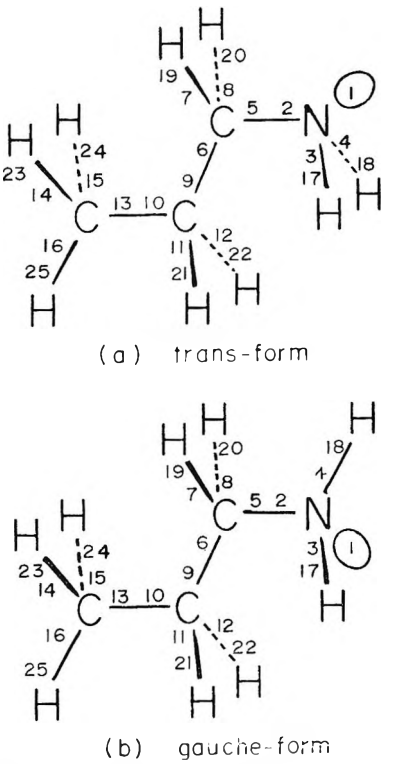

Figure 1. Numbering of atomic orbitals of *n*-propylamine used in the calculation.

Atomic distances of both amines are adopted as follows: C–C, 1.540 Å; C–N, 1.474 Å; C–H, 1.085 Å; N–H, 1.012 Å. All the bond angles are taken to be 109° 28′.

Atomic integrals necessary in the calculation were the same as in the papers of Pople and Segal.[6c] For instance, see Table I where the matrix elements $U_{\mu\mu}$ concerning the μth orbital are assumed to be equal to $-1/2$ (ionization potential + electron affinity). ($U_{\mu\mu}$

Table I: Matrix Elements $U_{\mu\mu}$ (in electron volts)

	H	C	N
s orbital	−7.176	−14.051	−19.316
p orbital	...	−5.572	−7.275

(4) J. C. Lorquet, A. J. Lorquet, and J. C. Leclerc, *Advan. Mass Spectrom.*, **4**, 569 (1968).

(5) K. Hirota and M. Itoh, *Bull Chem. Soc. Jap.*, **39**, 1406 (1966).

(6) (a) J. A. Pople, D. P. Santry, and G. A. Segal, *J. Chem. Phys.*, **43**, S129 (1965); (b) J. A. Pople and G. A. Segal, *ibid.*, **43**, S136 (1965); (c) J. A. Pople and G. A. Segal, *ibid.*, **44**, 3289 (1966).

$= (\mu| - {}^1/_2\nabla^2 - Z_A/r_{1A}|\mu)$, where μ denotes an atomic orbital on atom A, r_{1A} is the distance between the electron and nucleus A, and Z_A is the core charge.) In actual calculation of electron densities, 2s, $2p_x$, $2p_y$, $2p_z$ orbitals of nitrogen and carbon atoms are adopted as the basis set of orbitals, and they are transformed into sp^3-hybrid orbitals after the calculation. Then, their values are summed up in both atoms forming the bond, for the convenience of predicting the scission probability of the bond by use of the values.

The calculation has been carried out on the NEAC-2200 Model 500 computer at the Computer Center of Osaka University.

Experimental Section

Even though mass spectra of *n*-propylamine measured at various ionizing voltages V_i were reported in our previous paper,[7] they are measured again at the repeller voltage V_r of 3 or 0 V, to investigate its effect, because V_r was 10 V in the previous paper. The same spectrometer of high-resolution type is used, which is installed in our department (Hitachi RMU-7HR). Several mass patterns are shown in Table II, where unpublished spectra measured at V_r = 10 V are included.

Table II: Pattern Coefficients of Mass Spectra of *n*-Propylamine

	Effect of ionizing voltage (V_r = 10 V)					
m/e	80 V[a]	50 V	30 V	20 V[a]	15 V	10 V
15	1.2	1.1	0.5			
18[b]	2.1	1.9	2.0	1.6	1.1	
26	1.9	1.5				
27[c]	5.3	5.1	3.0	0.8		
28[c]	9.6	10.0	6.3	1.8		
29[c]	2.6	2.6	2.5	0.9		
30	100.0	100.0	100.0	100.0	100.0	100.0
31	1.8	1.7	1.9	1.5	1.5	
38	0.5	0.3				
39	2.4	2.7	1.7			
40[c]	0.9	0.8				
41[c]	6.0	6.4	5.5	3.9	2.5	
42[c]	3.4	3.8	3.9	1.7	1.0	
43	2.6	2.7	2.6	1.4	0.6	
44	1.2	1.3	1.2	1.2	1.0	
52	0.4	0.3				
54	0.4	0.5				
56	1.1	1.4	1.6	0.7		
58	2.2	2.6	3.0	2.7	3.1	1.5
59p	11.1	13.4	14.0	16.0	23.1	26.3
60	0.4	0.3	0.3	0.6	1.0	

[a] Published data (ref 7). [b] Contribution of H_2O^+ is omitted. [c] Doublet.

There was no intense metastable peak worthy to be mentioned. The metastable peaks are not shown at all in Table II. This neglect is due to our view of the role of metastable peaks in the fragmentation scheme of the mass spectra, because the metastable peaks correspond only to a part of the fragmentation successively produced.

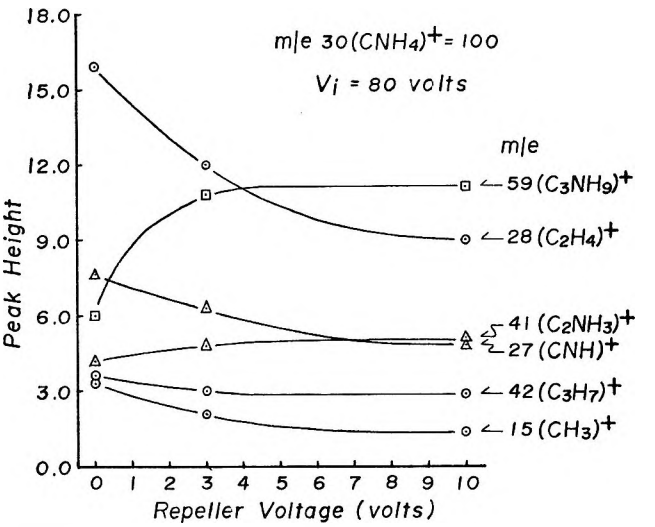

Figure 2. Dependence of main peaks on repeller voltage.

It is expected that if V_r is too low, the ion initially produced should again decompose in the ion source. To investigate this possibility, dependence of main peaks on V_r is shown in Figure 2. From the shape of the curve of the parent ion (*m/e* 59), successive fragmentation would not occur in the ion source if V_r lies between 3 and 10 V at V_i = 80 V.

Results

In calculation, the SCF procedure is repeated until self-consistence is achieved on all coefficients with a tolerance of 0.0001. The results thus obtained are shown in Table III (ethylamine) and Table IV (*n*-propylamine), where the electron densities in each atomic orbital at the HO level are tabulated as are the total densities at each orbital for the reference.

Thereby, the relation between atomic orbitals and relating bond as indicated by Figure 1 is also listed for the next use; also it has to be noted that the same orbital number is given to lone pair in both *trans* and *gauche* forms.

Tables III and IV indicate that about half of the electron density localizes at lone-pair orbitals, irrespective of *trans* and *gauche* forms. This tendency may be generally true in higher alkylamines.

Now from the tables, the electron densities of the HO orbital at the skeletal bonds are calculated from those of the atomic orbitals by the procedure already described. Their normalized values of both amines are shown at the corresponding bonds in Figure 3.

Figure 3 indicates that if the lone pair is put aside from consideration, electron density at the α-CC bond is larger than that at the CN bond. The conclusion

(7) M. Itoh, M. Yamamoto, and K. Hirota, *Nippon Kagaku Zasshi*, 89, 443 (1968).

Table III: Electron Density of the Higher Occupied Orbitals (HO) and the Total Electron Density of Ethylamine[a]

Atomic orbitals			*trans* form		*gauche* form	
Numbering		Relating bond	HO, %	Total	HO, %	Total
N	1	Lone pair	59.1	1.979	52.7	1.973
	2	CN	1.3	1.080	0.5	1.083
	3	NH	1.1	1.077	1.0	1.078
	4	NH	1.1	1.077	1.1	1.075
C-1	5	CN	1.6	0.923	0.9	0.920
	6	CC	8.3	0.992	7.7	0.995
	7	CH	0.8	0.993	1.2	0.988
	8	CH	0.8	0.993	1.3	0.992
C-2	9	CC	13.4	1.017	2.3	1.008
	10	CH	1.4	1.003	0.0	1.003
	11	CH	0.0	1.005	0.2	1.006
	12	CH	0.0	1.005	1.5	1.008
H	13	NH	2.6	0.923	2.6	0.922
	14	NH	2.6	0.923	2.6	0.929
	15	CH	1.7	1.012	17.3	1.028
	16	CH	1.7	1.012	3.3	1.012
	17	CH	0.0	0.994	0.6	0.993
	18	CH	0.0	0.994	3.1	0.991
	19	CH	2.4	0.999	0.1	0.997

[a] All the orbitals of Table III and IV are regarded to be sp^3 hybrid ones for N and C atoms, and their numbering is illustrated in Figure 1.

Table IV: Electron Density of the Highest Occupied Orbitals (HO) and the Total Electron Density of *n*-Propylamine

Atomic orbitals			*trans* form		*gauche* form	
Numbering		Relating bond	HO, %	Total	HO, %	Total
N	1	Lone pair	48.9	1.979	49.2	1.973
	2	CN	1.9	1.084	0.2	1.088
	3	NH	0.8	1.076	0.8	1.077
	4	NH	0.8	1.076	1.6	1.074
C-1	5	CN	1.8	0.922	0.6	0.920
	6	α-CC	10.9	0.993	7.0	0.995
	7	CH	0.6	0.994	0.8	0.990
	8	CH	0.6	0.994	3.0	0.994
C-2	9	α-CC	14.7	1.011	4.1	1.001
	10	β-CC	1.9	0.996	0.0	0.997
	11	CH	0.1	0.996	0.1	0.996
	12	CH	0.1	0.996	1.9	0.999
C-3	13	β-CC	2.7	1.003	0.0	1.001
	14	CH	0.1	1.003	0.2	1.004
	15	CH	0.1	1.003	0.0	1.004
	16	CH	2.1	1.001	0.4	1.002
H	17	NH	2.0	0.924	3.5	0.923
	18	NH	2.0	0.924	2.0	0.930
	19	CH	1.2	1.011	16.1	1.027
	20	CH	1.2	1.011	2.5	1.012
	21	CH	0.2	1.002	0.3	1.001
	22	CH	0.2	1.002	4.1	0.999
	23	CH	0.3	0.998	0.6	0.997
	24	CH	0.3	0.998	0.0	0.997
	25	CH	4.4	1.003	0.9	1.002

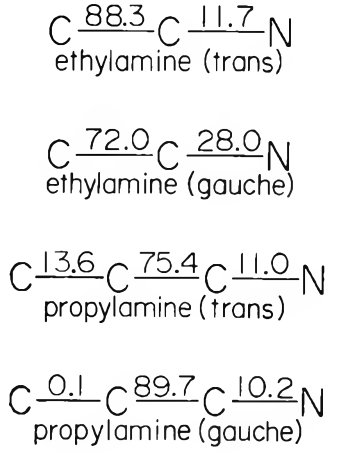

Figure 3. Electron distribution in the highest occupied orbital on skeletal bonds excluding the lone pair.

Table V: Scission Probability of the Skeletal Bonds C^3–C^2–C^1–N

		Bond no.			Reference
		1 (CN)	2 (α-CC)	3 (β-CC)	
Theoretical values					
Present	*trans* form	11.0	75.4	13.6	
	gauche form	10.2	89.7	0.1	
	mean value	10.6	82.6	6.8	
LCBO (old method)		(0.0)	86.5	13.5	5
LCBO (new method)		8.0	80.8	11.2	7
Observed values					
Ionizing voltage[c]	80	8.4[a]	86.9	4.7	
		8.3	86.0	5.7	
		7.2[b]	85.8	7.0	
	50	8.4[a]	85.7	5.9	
	30	7.2[a]	86.8	6.0	
		6.4	89.3	4.3	
	20	4.4[a]	91.8	3.8	
		3.9	94.0	2.1	
		3.2[b]	95.1	1.7	
	15	2.9[a]	94.2	2.9	
		1.8	96.9	1.3	
		0.0[b]	100.0	0.0	
	10	10.0[a]	100.0	0.0	
		0.0	100.0	0.0	

[a] Measured at V_r = 10 V. [b] Measured at 0 V. [c] All new data measured at V_r = 3 V.

is applicable to both *trans* and *gauche* form of *n*-propylamine. This is in sharp contrast to the Lorquet's result based on the LCBO approximation.[4] The above electron distribution, however, is favorable for the MO theory because this CNDO method can predict the scission probability of the CN bond also so that the range of its applicability can be extended more than the case when the simple LCBO approximation was adopted.

Now, experimental scission probabilities of the skeletal bonds of *n*-propylamine are evaluated from the spectra shown in Table II. They are summarized in the lower part of Table V. In the upper part of the table, theoretical scission probabilities are described for comparison with the observed. The calculated scission probabilities obtained by two kinds of the LCBO methods are also compared in Table V. The parameters used in the new LCBO calculation are the empirical ones which give plausible results for several monoamines and diamines.[7,8] Even though two *gauche* forms are possible to *n*-propylamine, simple mean values of both forms are shown in the table, considering the situation that both conformations are not reported to be stable at room temperature.

Discussion

Generally speaking, mean theoretical values agree qualitatively well with the observed above $V_i = 30$ V, irrespective of V_r. It is noteworthy that the agreement is even better than that of the new LCBO method, because the order of bond scission, bond 2 > bond 1 > bond 3, can be given by the present method.

The above satisfactory result gives us an answer to the criticism against our attempt to apply the MO theory to the prediction of the skeletal bond scission of alkylamines. However, explanation of the reason why the scission of bond 2 is larger than the theoretical values at very low V_i would be very desirable, to estimate the range of applicability of the MO theory.

This apparent discrepancy can be explained by the possibility that the electron energy at low V_i is too small to elevate the bombarded molecule to the highly excited (or superexcited) state,[2b] so that it does not have sufficient energy to rupture a bond instantly. Besides, even if the highly excited species would be produced, the most abundant ion in the initial fragmentation process would produce the parent ion CH_3CH_2-$CH_2NH_2^+$, because the electron at the HO orbital exists at the lone pair with the probability of about 50%. In either case, the parent ion includes some excess energy, so that slow fragmentation of the initial ions can occur successively, according to the scheme of the statistical theory. Considering the shape of the potential energy hypersurface of molecular ethylamine ion,[9] fragment ions may be produced overwhelmingly by scission of bond 2. Therefore, because of superposition of this slow fragmentation process on the fast one, the discrepancy between theory and experiment at low V_i can be explained; *i.e.*, scission probability of bond 2 becomes larger as V_i is lowered.

Of course, the above successive fragmentation may occur at high V_i, but it does not proceed actually, judging from the analysis of ions in mass spectra. Only the initial fragmentation seems to occur even at high V_i. This possibility is reasonable also from the fact that sufficient energy is given to the bombarded molecule so as to reach very highly excited state, and most of the fragmentations proceed very fast *via* such species.

By introducing the slow process which occurs more easily as V_i is lowered, existence of the correlation between charge and fragmentation in the fast process may be very plausible as far as *n*-propylamine is concerned. On the other hand, the agreement was also satisfactory when the new LCBO method was adopted in the mass spectra of *n*-butyl-, *n*-pentyl-, *n*-hexyl-, and *n*-heptylamine[7] and several diamines.[8] Considering the situation, the MO theory may be applicable more generally to the alkylamines, at least as a useful tool in the study of mass spectra.

Finally, it has to be mentioned why the theoretical value agrees well with the calculated irrespective of V_r above $V_i = 30$ V. This can be explained by the possibility that V_r plays a role of V_i, especially when V_i is low; *i.e.*, such a role becomes negligibly small at high V_i in comparison to V_r.

Physical Picture of the MO Theory. The above successful results favor the MO theory, but the fundamental assumption on the correlation of charge distribution with the scission probability and the approximation adopted in the actual calculation are not given any firm physical picture. This point cannot reduce the plausibility of the theory, considering that the present knowledge of the electronic state of the molecules at the moment of electron bombardment is still limited.

It has to be mentioned here on the approximation that the positive charge distribution of the molecular ion can be substituted for the electron distribution at the HO orbital of the stable neutral molecule. This approximation may not be a pure assumption, because it may have some connection to the nature of highly excited species, which can be regarded as a positive ion loosely coupled with an electron. Since such species can decompose spontaneously through a kind of autoinizing process, its life is very short. Then, an alternative attempt to calculate the electron density of the ionized molecule instead of the neutral molecule is not necessarily required, though such a proposition can be suggested.

In short, the physical picture of the present theory explained above is not a final model but is a preliminary one. Nevertheless, the approximation to calculate the electron distribution of the neutral molecule instead of its ion may be allowed under the fundamental assumption.

Evaluation of Dipole Moment. To estimate the reliability of the present calculation, the dipole moment of ethylamine is evaluated by use of the total electron density shown in Table III.

The calculated results are 1.77 and 1.67 D for *trans*

(8) M. Yamamoto, M. Itoh, I. Fujita, and K. Hirota, *Nippon Kagaku Zasshi.*, 89, 752(1968).

(9) J. C. Leclerc and J. C. Lorquet, *J. Phys. Chem.*, 71, 787 (1967).

and *gauche* forms, respectively. Their mean value, 1.72 D, agrees fairly well with the observed 1.39 D in benzene solution.[10] Therefore, the electron density calculated by the CNDO method may be reliable and can be used as the basis of our research. This conclusion, in turn, suggests the possibility of applying the LCBO–MO theory as a semiempirical one to the compounds other than alkanes.

Acknowledgment. The authors express their sincere thanks to Dr. Keiji Kuwata for his discussions.

(10) P. Trunel, *Compt. Rend.*, **203**, 563 (1936).

Ground- and Excited-State Geometries of Benzophenone

by Roald Hoffmann and Jerrald R. Swenson

Department of Chemistry, Cornell University, Ithaca, New York 14850 *(Received August 6, 1969)*

The equilibrium geometries of benzophenone and benzaldehyde in ground and (n,π^*) excited states are calculated using the extended Hückel and CNDO/2 methods. The ground state of benzophenone has both phenyl rings twisted out of plane to a C_2 geometry by 38°. The excited state has a considerably steeper potential well for a similar geometry in which the angles of twist are 32°. It appears that the carbonyl group remains locally planar in the excited state. Potential surfaces for the interconversion of enantiomeric minima are reported.

Introduction

Among photochemists benzophenone (**1**) is a most popular molecule. Careful and elegant studies have clarified the mechanism of the classic photochemical reduction of benzophenone to benzpinacol in the presence of hydrogen donors.[1] Benzophenone participates in a

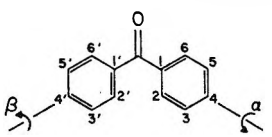

1

number of photochemical 2 + 2 cycloadditions yielding oxetanes,[2] but perhaps the greatest utility of benzophenone is found in its application as an agent for efficient triplet state energy transfer.[3] Equilibrium geometry changes in the excited states of molecules play a most significant role in determining their photochemical behavior. In this contribution we examine possible geometry changes in the (n,π^*) excited state of benzophenone.

The ground-state equilibrium geometry of benzophenone is determined by a balance of steric and conjugative effects. Conjugation of the carbonyl group with the phenyl rings would favor a planar conformation. Steric repulsion between the H_2 and H_2' hydrogen atoms prevents the attainment of coplanarity. Each of the phenyl rings must then be rotated by some angle, α and β (see structure **1**), out of the plane formed by the carbonyl group and the adjacent phenyl carbon atoms. The mode of rotation which most efficiently relieves the steric problems of the planar geometry is a conrotatory one, *i.e.*, α and β as defined in structure **1** both positive and probably of similar magnitude. This was clearly pointed out by Adams,[4] Rodebush,[5] and Jones[6] though the steric prohibition to coplanarity was no doubt apparent to many researchers as soon as the structure of optically active biphenyls was clarified.[7]

(1) G. Ciamician and P. Silber, *Ber.*, **33**, 2911 (1900); **34**, 1530 (1901); C. Weizmann, E. Bergmann, and Y. Hirschberg, *J. Amer. Chem. Soc.*, **60**, 1530 (1938); H. L. J. Bäckström, *Z. Phys. Chem.*, **B25**, 99 (1934); H. L. J. Bäckström and K. Sandros, *Acta Chim. Scand.*, **14**, 48 (1960); A. Schönberg and A. Mustafa, *Chem. Rev.*, **40**, 181 (1947); G. Porter and F. Wilkinson, *Trans. Faraday Soc.*, **57**, 1686 (1961); A. Beckett and G. Porter, *ibid.*, **59**, 2039, 2051 (1963); W. M. Moore, G. S. Hammond, and R. P. Foss, *J. Amer. Chem. Soc.*, **83**, 2789 (1961); G. S. Hammond, W. P. Baker, and W. M. Moore, *ibid.*, **83**, 2795 (1961); J. N. Pitts, Jr., H. W. Johnson, and T. Kuwana, *J. Phys. Chem.*, **66**, 2471 (1962); J. A. Bell and H. A. Linschitz, *J. Amer. Chem. Soc.*, **85**, 528 (1963).

(2) E. Paterno and G. Chieffi, *Gazz. Chim. Ital.*, **39**, 341 (1909); D. Scharf and F. Korte, *Tetrahedron Lett.*, 821 (1963); G. O. Schenck, W. Hartmann, and R. Steinmetz, *Ber.*, **96**, 498 (1963); R. Steinmetz, W. Hartmann, and G. O. Schenck, *ibid.*, **98**, 3854 (1965); J. S. Bradshaw, *J. Org. Chem.*, **31**, 237 (1966); J. W. Hanifin and E. Cohen, *Tetrahedron Lett.*, 1419 (1966); D. R. Arnold, R. L. Hinman, and A. H. Glick, *ibid.*, 1425 (1964); N. C. Yang, *Pure Appl. Chem.*, **9**, 591 (1965); D. R. Arnold, *Advan. Photochem.*, **6**, 301 (1968), and references therein.

(3) Reviewed by A. Terenin in "Recent Progress in Photobiology," E. J. Bowen, Ed., Blackwells, London, 1965, p 3; V. L. Ermolaev, *Usp. Fiz. Nauk*, **80**, 3 (1963).

(4) J. F. Hyde and R. Adams, *J. Amer. Chem. Soc.*, **50**, 2499 (1928); M. E. Maclean and R. Adams, *ibid.*, **55**, 4683 (1933).

(5) M. T. O'Shaughnessy and W. H. Rodebush, *ibid.*, **62**, 2906 (1940).

(6) R. N. Jones, *ibid.*, **67**, 2127 (1945).

Intensity effects on the electronic spectrum of benzophenone were cleverly utilized as a means of obtaining an estimate of the angle of twist of the phenyl groups.[8,9]

Crystal structures of substituted benzophenones[10-13] exhibited approximately equal angles of twist of each ring in the range of 20–35°. The most precise of these[11b] has slightly differing angles: $\alpha \simeq 25°, \beta \simeq 35°$. Recently crystal structures of benzophenone itself have become available.[14,15] A dihedral angle of 56° between the two phenyl rings is reported.[15] Assuming C_2 molecular symmetry, this corresponds to $\alpha = \beta = 33°$.

Discussion

We have carried out approximate molecular orbital calculations of two types—CNDO/2[16] and extended Hückel[17] (EH)—on benzophenone.[18] The first degree of freedom we studied was the conrotatory (C_2 molecular symmetry, $\alpha = \beta$) twisting of the phenyl rings away from the molecular plane. Figure 1 shows the calculated EH results for the ground state and the excited configuration resulting from (n,π^*) excitation. The ground state has a shallow minimum at $\alpha = \beta = 38°$; the excited configuration has a much deeper minimum at a significantly smaller angle of twist, $\alpha = \beta = 32°$. The agreement with the ground-state crystallographic[15] value of $\alpha = \beta = 33°$ is good, and the calculations thus produce the balance of steric and conjugative effects which produces the equilibrium geometry.[19] The CNDO/2 method gave an energy minimum at $\alpha = \beta = 90°$. Similar results were obtained for benzaldehyde. Since the discrepancy with experiment is sizable, we did not pursue calculations with this method any further.

Since unsymmetrical geometries ($\alpha \neq \beta$) have been suggested at various times,[20] we thought it important to allow the molecule the freedom of varying α and β independently. Figure 2 illustrates our calculated potential energy surface for the ground state. The figure shows the range $-90° < \alpha < +90°$, $0° < \beta < 180°$. Other conformations are identical by symmetry with those shown in Figure 2; in fact the only symmetry nonequivalent regions or generators of the figure are two tri-

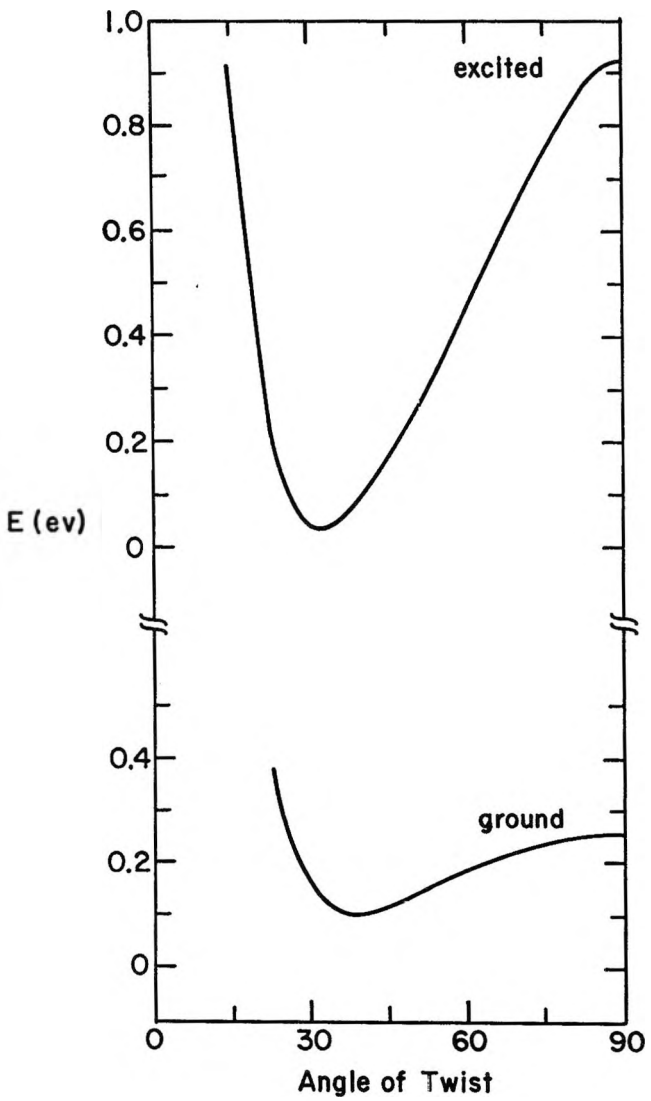

Figure 1. Extended Hückel potential energy curves for the conrotatory twisting of phenyl rings in ground and excited configurations of benzophenone. The energy scale is relative to an arbitrary energy zero, and one different for ground and excited configurations. (Note broken energy scale.)

(7) A fascinating contemporary discussion of this important chapter in the development of modern structural ideas may be found in E. E. Turner and R. J. W. Le Fèvre, *Chem. Ind.* (London), **45**, 831, 883 (1926); F. Bell and J. Kenyon, *ibid.*, **45**, 864 (1926); W. H. Mills, *ibid.*, **45**, 884 (1926); J. Kenner, *ibid.*, **46**, 218 (1927); see also R. Adams and H. C. Yuan, *Chem. Rev.*, **12**, 260 (1933).

(8) E. A. Braude, E. R. H. Jones, H. P. Koch, R. W. Richardson, F. Sondheimer, and J. B. Toogood, *J. Chem. Soc.*, 1890 (1949); E. A. Braude and F. Sondheimer, *ibid.*, 3754 (1954).

(9) R. F. Rekker and W. Th. Nauta, *Rec. Trav. Chim.*, **73**, 969 (1954); **80**, 764 (1961); *Spectrochim. Acta*, **8**, 348 (1957).

(10) 4,4′-Dichlorobenzophenone: J. Toussaint, *Proc. Soc. Roy. Sci. Liege*, **17**, 10 (1948).

(11) 4,4′-Dimethoxybenzophenone: (a) I. L. Karle, H. Hauptman, J. Karle, and A. B. Wing, *Acta Cryst.*, **10**, 481 (1957); (b) H. G. Norment and I. L. Karle, *ibid.*, **15**, 873 (1962).

(12) 3,3′-Dibromobenzophenone: S. Ramaseshan and K. Venkatesan, *Experientia*, **14**, 237 (1958).

(13) 2,2′-Dibromo-4,4′,5,5′-tetramethoxybenzophenone: A. Olivi and A. Ripamonti, *Ric. Sci.*, **28**, 2102 (1958).

(14) E. B. Vul and G. M. Lobanova, *Kristallografiya*, **12**, 411 (1967); *Soviet Phys.-Cryst.* (English Transl.), **12**, 355 (1967).

(15) E. B. Fleischer, N. Sung, and S. Hawkinson, *J. Phys. Chem.*, **72**, 4311 (1968).

(16) J. A. Pople, D. P. Santry, and G. A. Segal, *J. Chem. Phys.*, **43**, S129 (1965); J. A. Pople and G. A. Segal, *ibid.*, **44**, 3289 (1966).

(17) R. Hoffmann, *ibid.*, **39**, 1397 (1963); **40**, 2474, 2480, 2745 (1964); *Tetrahedron*, **22**, 521, 539 (1966), and subsequent papers. In our present calculations we use a hydrogen 1s exponent of 1.3.

(18) We assumed an idealized benzophenone geometry in all our calculations: C=O, 1.25 Å; C(carbonyl)–C(phenyl), 1.50 Å; hexagonal benzene rings with C–C, 1.40 Å; C–H, 1.10 Å; angle C_1CC_1' 120°.

(19) Faithful modeling of the very similar balance in phenyl carbonium ions has also been obtained: R. Hoffmann, R. Bissell, and D. G. Farnum, *J. Phys. Chem.*, **73**, 1789 (1969).

(20) *E.g.*, W. D. Chandler and L. Goodman, *J. Chem. Phys.*, **45**, 4088 (1966); for a review of these suggestions see J. Barassin, G. Queguiner, and H. Lumbroso, *Bull. Soc. Chim. Fr.*, 4707 (1967).

angles: a conrotatory region, $0° < \alpha < 90°$, $0° < \beta < \alpha$ and a disrotatory region $-90° < \alpha < 0°$, $0° < \beta < |\alpha|$. The only minima in this surface are the previously located conrotatory one at $\alpha = \beta = 38°$, and its mirror image, at $\alpha = -38°$, $\beta = 142°$. There are no minima in the disrotatory regions, and geometries such as those with $\alpha = 0°$, $\beta = 90°$ or $\alpha = \beta = 90°$ are saddle points.

The stable conformation of benzophenone is chiral. There arises immediately the problem of mechanisms for the conversion of one enantiomer into the other and the activation energies for such processes. As in the analogous diphenyl methyl system,[19] we consider three possible geared motions for the conversion of one enantiomer into the other. These are shown schematically below. In mechanism 2 the transition state is planar

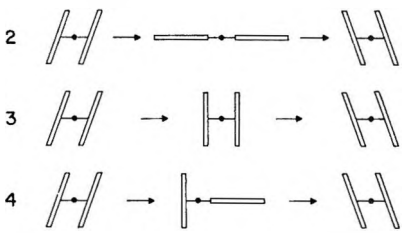

($\alpha = \beta = 0°$); in 3 both phenyl rings are perpendicular to the plane of the carbonyl carbon atom ($\alpha = 90°$, $\beta = 90°$); in 4 one phenyl ring is coplanar and the other is perpendicular ($\alpha = 0°$, $\beta = 90°$). Figure 2, previously presented, contains the requisite information to compare the three reaction paths. Mechanism 2, involving the sterically hindered planar intermediate, has an extremely high activation energy of 3.682 eV. Mechanism 4 is slightly favored over mechanism 3; the calculated activation energy is 0.146 eV for 3 and 0.051 eV for 4. The calculated activation energy for 4 is very small, and the conversion from one enantiomeric form of benzophenone into the other should proceed most easily.

The experimental information available to date on benzophenone clearly demands a small barrier. It is clear that bulky substituents on the benzene rings will increase the barriers to interconversion.[21]

We now turn to a discussion of the excited state. Figure 3 illustrates the extended Hückel surface for the (n,π^*) excited configuration of benzophenone. The angles are defined analogously to Figure 2, but the energy contours are spaced at greater energy intervals. The only minima in this surface are once again the conrotatory ones for $\alpha = \beta = 32°$ and $\alpha = -32°$, $\beta = 148°$. Loci such as $\alpha = 0°$, $\beta = 90°$ remain saddle points. New saddle points occur in the disrotatory regions, *e.g.*, at $\alpha = -57°$, $\beta = 57°$ and $\alpha = 57°$, $\beta = 123°$.

The preference of the excited (n, π^*) configuration for a more nearly planar geometry is significant. The results were anticipated from the examination of the interaction diagram in Figure 4. On the left side of the

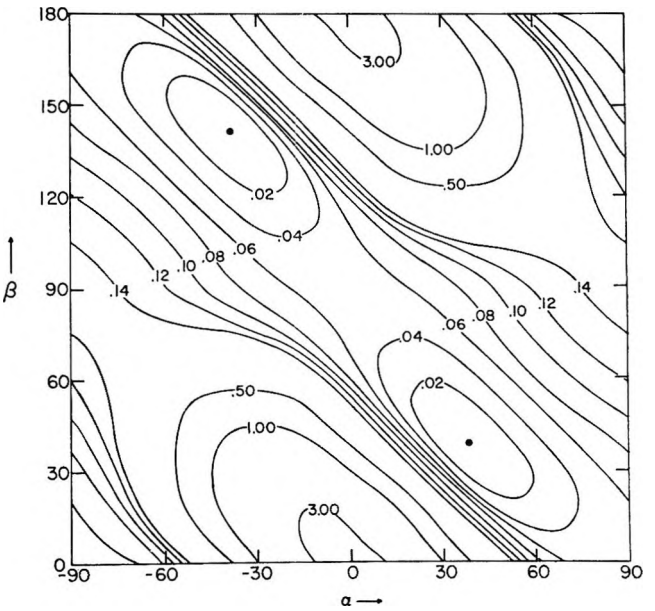

Figure 2. Contour diagram of the extended Hückel potential energy surface for the ground state of benzophenone. The signs of α and β are defined relative to the sense of rotation shown in structure 1. α and β are equal to zero for the planar conformation. The energy contours are in electron volts relative to the marked minima.

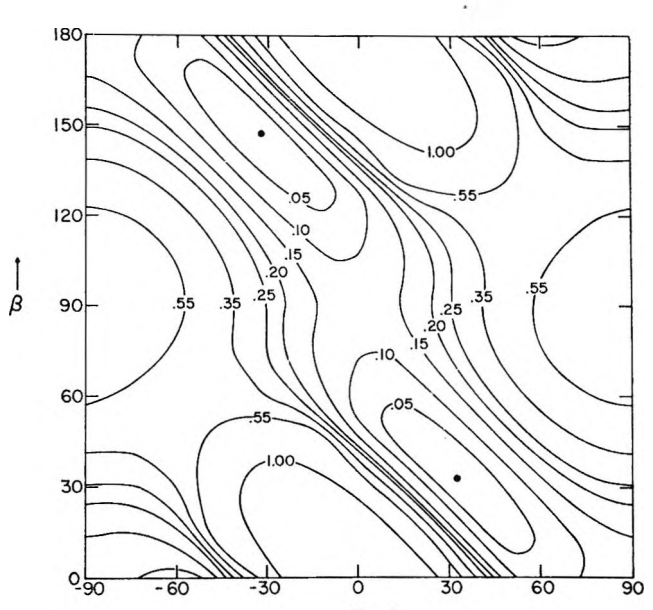

Figure 3. Contour diagram of the extended Hückel potential energy surface for the (n,π^*) excited configuration of benzophenone. See caption to Figure 2 for definition of angles. (Note that the contours in Figure 3 are at greater energy intervals than in Figure 2.)

(21) D. Lauer and H. A. Staab, *Ber.*, 102, 1631 (1969); *Tetrahedron Lett.*, 177 (1968), report some careful studies of such highly hindered benzophenones. Adams (ref 4) attempted to resolve some less hindered derivatives without success. The resolution of a substituted benzophenone has recently been reported: K. V. Narayanan, R. Selvarajan, and S. Swaminathan, *J. Chem. Soc., C*, 540 (1968). This result has been questioned by Lauer and Staab (ref 21).

diagram are the benzene π orbitals, taken twice. On the right side are carbonyl π and π^* orbitals. As a consequence of the greater electronegativity of the oxygen atom the center of energy of the carbonyl orbitals is lower than that of the benzene orbitals. The molecular orbitals may be classified as symmetric, S, or antisymmetric, A, with respect to the molecular C_2 axis. The molecular orbitals are then allowed to interact; minimum interaction would correspond to $\alpha = \beta = 90°$, maximum π-electron interaction would occur at $\alpha = \beta = 0°$. The principal interaction is that of the carbonyl π^* with an unoccupied benzene orbital of the same symmetry. In the resulting stabilized MO, which is principally carbonyl π^*, the benzene π^* MO is mixed in a bonding way. Population of this MO in the (n,π^*) excited state results in both an increase in C–C_1 and C–C_1' bond order and a greater tendency to planarity. The relative depths of ground- and excited-state minima are explained in the same manner. The interaction of benzene and carbonyl orbitals has been previously analyzed with the aid of an interaction diagram.[22,23]

The preceding argument may also be used to account for the stabilization of the disrotatory region as manifested by the removal of the ground-state saddle point at $\alpha = -90°, \beta = 90°$ to $\alpha = -57°, \beta = 57°$. However, in the excited state, the disrotatory region may benefit from another electronic interaction, arising from the proximity of the two benzene rings. The polar valence bond structures **5** and **6** no doubt contribute to the best description of benzophenone. Pentadienyl cations, such as may be seen in part of structure **6**, are expected theoretically[24] and known experimentally[25] to undergo electrocyclic ring closure to cyclopentenyl cations in a conrotatory manner in the ground state and in a disrotatory manner in the excited state. The stabilizing interaction here is from the overlap of the C_2 and C_2' 2p orbitals.

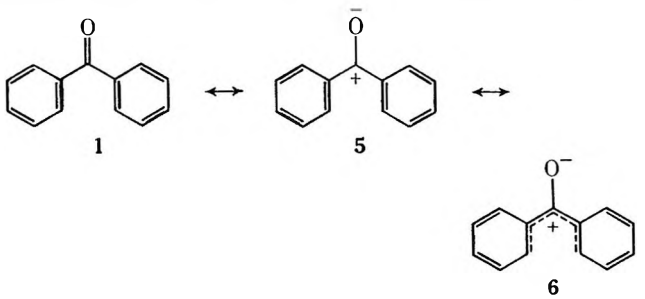

1 **5** **6**

The singlet and triplet (n,π^*) states of formaldehyde[26] are pyramidal. We therefore studied the feasibility of the similar distortion in benzophenone excited states. CNDO/2 results for the formaldehyde excited-state geometry have been presented by Kroto and Santry.[27] The calculated barrier to inversion is small. EH calculations predict an out-of-plane angle of 20° and an inversion barrier of 0.0034 eV. The singlet state has in fact been analyzed to have the oxygen out of the plane of the remaining atoms by 20° and to possess an inversion barrier of ~650 cm^{-1} or 0.080 eV.[26b] Thus both computational methods give much too small inversion barriers, though they confirm nonplanarity.

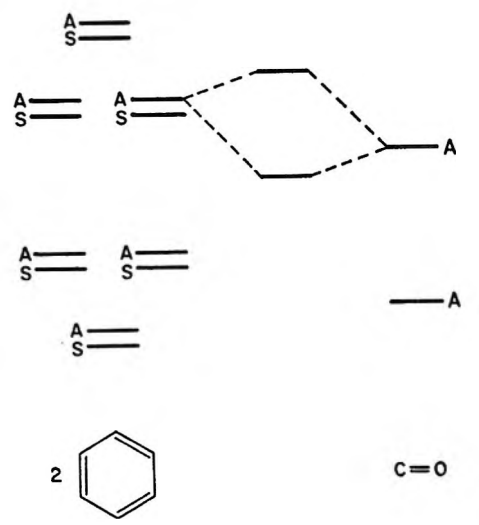

Figure 4. The interaction of the π levels of two phenyl groups with a carbonyl group, as in benzophenone. The levels are classified according to their behavior under C_2. Only the most significant interaction is shown.

For the equilibrium conformation of the excited configuration of benzophenone ($\alpha = \beta = 32°$) we studied a motion of the carbonyl oxygen out of its local molecular plane. The resulting potential energy curve (EH) is compared with that of formaldehyde in Figure 5. The planar conformation remains stable. However, in view of the fact that the EH method severely underestimates the barrier to inversion in formaldehyde, the only reliable conclusion that may be drawn is that the out-of-plane angle in benzophenone (if nonzero at all) is less than it is in formaldehyde.

We also studied an out-of-plane motion of the oxygen at the disrotatory saddle point at $\alpha = -57°, \beta = 57°$. It was found that in the excited state the carbonyl oxygen definitely preferred to move out-of-plane, coming to an equilibrium position bent by 25° down,

(22) S. Nagakura and J. Tanaka, *J. Chem. Phys.*, **22**, 236 (1954); S. Nagakura, *ibid.*, **23**, 1441 (1955); J. Tanaka, S. Nagakura, and M. Kobayashi, *ibid.*, **24**, 311 (1956).

(23) H. Suzuki, "Electronic Absorption Spectra and Geometries of Organic Molecules," Academic Press, New York, N. Y., 1967, p 440; H. Suzuki, *Bull. Chem. Soc. Jap.*, **35**, 1853 (1962); **33**, 613 (1960).

(24) R. B. Woodward and R. Hoffmann, *J. Amer. Chem. Soc.*, **87**, 395 (1965); *Angew. Chem.*, in press; R. Hoffmann and R. B. Woodward *Accounts. Chem. Res.*, **1**, 17 (1968).

(25) R. B. Woodward, "Aromaticity," Special Publication No. 21, The Chemical Society, London, 1967, p 217. D. Kurland, Dissertation, Harvard, 1967; R. Lehr, Dissertation, Harvard, 1968.

(26) (a) G. W. Robinson and V. E. DiGiorgio, *Can. J. Chem.*, **36**, 31 (1958); *J. Chem. Phys.*, **31**, 1678 (1959); (b) J. C. D. Brand, *J. Chem. Soc.*, 858 (1956); (c) V. A. Job, V. Sethuraman, and K. K. Innes, *J. Mol. Spectrosc.*, **30**, 365 (1969).

(27) H. W. Kroto and D. P. Santry, *J. Chem. Phys.*, **47**, 792, 2736 (1967).

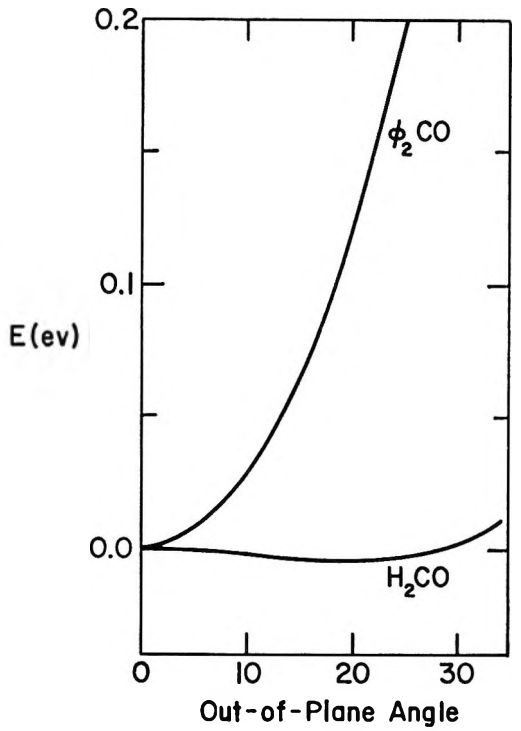

Figure 5. Comparison of calculated out-of-plane bending energy curves of formaldehyde and benzophenone. Both molecules are referred to the same energy zero for a planar geometry. The bending angle is defined in the plane perpendicular to the XCX plane and containing the bisector the XCX of angle. The bending angle is then the angle in the above defined plane by which the oxygen is out of planarity.

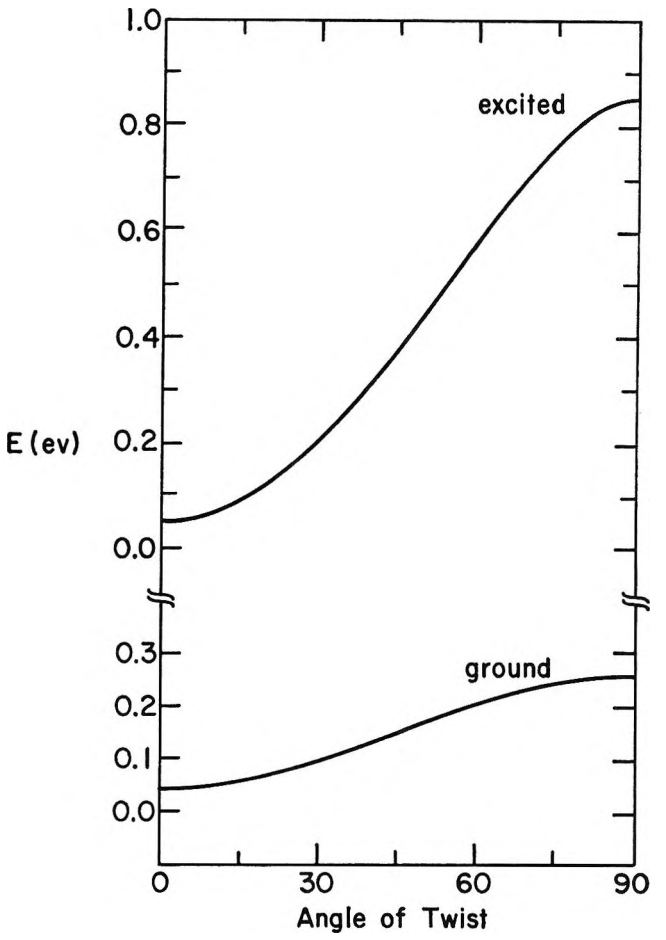

Figure 7. Energy as a function of angle of twist for ground and excited configuration of benzaldehyde. The energy scale is relative to an arbitrary energy zero, different for the two configurations. (Note broken energy scale.)

i.e., below the original plane defined by structure **1**. This placed the oxygen closest to the 6 and 6′ positions. The favored geometry was 0.25 eV below the "planar" excited-state conformation. This is still 0.22 eV above the conrotatory excited-state minima at $\alpha = \beta = 32°$. Readjustment of α and β in the "nonplanar" disrotatory conformation gain only approximately 0.01 eV, so that we remain confident that the only true minima in the excited state are the "planar" conrotatory ones.

The preferred direction of out-of-plane bending at the disrotatory saddle point is nevertheless interesting. One possible explanation of the observed trend may be obtained from examining Figure 6. This shows a projection of C_1, and the carbonyl group on the plane perpendicular to C_1–C_4, for the "planar" disrotatory saddle point, and the two possible motions of an oxygen 25° out of plane. It is clear that better conjugation or overlap of the carbonyl carbon orbital (presumably a hybrid with increasing s character) and the phenyl orbitals is achieved upon oxygen bending in the manner indicated at left.

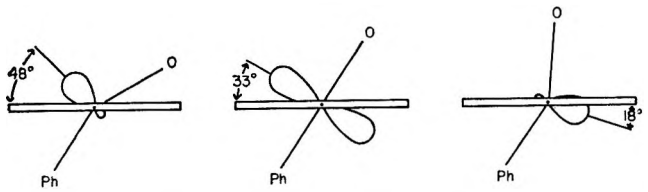

Figure 6. Projection of the left-hand phenyl ring and carbonyl oxygen on the plane perpendicular to the C_1–C_4 axis. The view is from C_4 toward C_1. The front bar is the projection of the right-hand phenyl ring. Three oxygen positions are shown. In the middle we have the disrotatory saddle point geometry, $\alpha = -57°$, $\beta = 57°$, oxygen "planar." At the left the oxygen has been moved "down" 25° (see text and caption to Figure 5), at right "up" 25°.

Our calculations also yielded the ground and excited configuration charge distributions for benzophenone. We consider the CNDO charge distributions more reliable and show below the carbon and oxygen charges computed by this method for a conrotatory geometry with $\alpha = \beta = 35°$

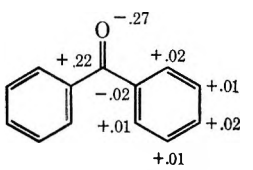

ground-state charge distribution

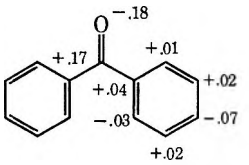

excited-state charge distribution

The charge redistribution in the excited state is not very great. This is the consequence of an "n" orbital which is not localized at oxygen, but significantly delocalized thoughout the molecule. The absence of charge redistribution of a magnitude consistent with the classical picture of a fully localized oxygen lone pair is supported by recent measurements of the dipole moments of benzophenone excited states.[28]

Benzaldehyde has been assumed to have a planar conformation since there is no steric interaction preventing such a conformation. Extended Hückel calculations confirm this assumption. The potential energy curves for the rotation of the aldehyde group away from the plane of the phenyl ring for the ground state and the excited state of benzaldehyde arising from the carbonyl (n,π^*) transition are shown in Figure 7. The calculated barrier to rotation is 0.22 eV for the ground state and 0.79 eV for the excited state. The theoretical analysis is just like that presented for benzophenone, with a predicted higher barrier to internal rotation in the (n,π^*) excited state compared to the ground state.

Acknowledgment. This work was supported by the Petroleum Research Fund of the American Chemical Society and the Public Health Service (GM 13468).

(28) R. M. Hochstrasser and T. S. Lin, *J. Chem. Phys.*, **49**, 4929 (1968).

Energy Parameters in Polypeptides. II. Semiempirical Molecular Orbital Calculations for Model Peptides[1,2]

by J. F. Yan, F. A. Momany,[3] R. Hoffmann, and H. A. Scheraga[4]

Department of Chemistry, Cornell University, Ithaca, New York 14850 *(Received June 30, 1969)*

The EHT and CNDO/2 methods have been used to compute charge distributions, dipole moments, energies for internal rotation, electronic orbital configurations, and electronic spectra of formamide, N-methylformamide, N,N-dimethylformamide, acetamide, N-methylacetamide, N,N-dimethylacetamide, and acetyl-L-proline amide. The CNDO/2 method gives more reliable charge distributions and dipole moments than the EHT procedure. However, the EHT procedure is better for treating internal rotation and provides a physical picture for the preference of the *trans* form of the amide group in peptides. Calculations are also carried out for the changes in the charge distributions, dipole moments, energies for internal rotation, electronic orbital configurations, and electronic spectra of these model compounds as the amide group departs from planarity. Some of the data for acetyl-L-prolineamide are represented in the form of a ψ–ω energy contour diagram.

Introduction

At the present time, conformational energy calculations are being carried out for polypeptides, using *empirical* methods.[5] In conjunction with these studies, an examination is being conducted[6,7] of the underlying theoretical basis of the empirical approaches.

In the first paper[8] of this series (designated here as paper I), a semiempirical method was employed to obtain some of the parameters required for the conformational energy calculations. The method of Del Re[9–11] was used to obtain the σ charges, and dipole moment data (as well as computed values of Pullman and Pullman[12]) were used to obtain the π charges. The resulting total charges on all the atoms of the amino acid residues which commonly occur in proteins were then obtained. A similar calculation of the

(1) This work was supported by research grants from the National Science Foundation (GB-7571X, GB-7160, and GP-8013), from the National Institute of General Medical Sciences of the National Institutes of Health, U. S. Public Health Service (GM-14312 and GM-13468), and from the Eli Lilly, Hofmann-LaRoche, and Smith Kline and French Grants Committees.

(2) Presented before the Division of Biological Chemistry at the 158th National Meeting of the American Chemical Society, New York, N. Y., Sept 1969.

(3) Special Fellow of the National Institute of General Medical Sciences, National Institutes of Health, 1968–1969.

(4) To whom requests for reprints should be addressed.

(5) See, *e.g.*, H. A. Scheraga, *Advan. Phys. Org. Chem.*, **6**, 103 (1968).

(6) K. D. Gibson and H. A. Scheraga, *Physiol. Chem. Phys.*, **1**, 109 (1969).

partial charges in amino acids had been carried out earlier by Del Re, *et al.*,[13] who computed only the σ charges.[14] In the present paper, we apply more rigorous LCAO–MO methods to various model peptide molecules and compute the charge distributions and resulting dipole moments, the energies for rotation about bonds (including the peptide bond, thereby obtaining the energy barrier and the energy difference between the *cis* and *trans* forms[15]), the electronic orbital configuration, and the electronic spectra of these simple amides.

The extended Hückel theory (EHT) of Hoffmann[16] and the approximate SCF–MO theory (CNDO/2) of Pople and Segal[17] are both used in the computations. These methods, which are reasonably good approximations to exact quantum mechanical calculations, can be applied to molecules of the kind considered here. A comparison of the calculated properties obtained with the EHT and CNDO/2 methods provides a narrow bracketing range of the results one might hope to obtain from exact quantum mechanical calculations. They also provide the physical insight required to establish the validity of *empirical*[18,19] conformational energy calculations for polypeptides, the latter molecules being too large for application of even the approximate EHT and CNDO/2 methods.

The molecules treated in this paper are formamide, N-methylformamide, N,N-dimethylformamide, acetamide, N-methylacetamide, N,N-dimethylacetamide, and acetyl-L-prolineamide. Their structural formulas and the nomenclature conventions[15] are illustrated in Figures 1–3.

Method

The EHT and CNDO/2 methods, both of which attempt to approximate a Hartree–Fock solution of the many-electron problem, are described in detail in the original publications.[16,17] These two approximations differ considerably and thus give rise in some cases to differences in physical properties which, however, constitute a narrow range, as indicated above. The EHT theory treats all valence electrons and includes overlap integrals, but neglects all electron repulsion integrals. The CNDO/2 theory is an SCF method which also treats all valence electrons, employs zero differential overlap, but includes electron interactions explicitly.

The input data for the computer programs[20,21] are given in Table I (atomic coordinates, expressed in terms of bond lengths and bond angles given in Table I) and Table II [(1) Slater orbital exponents, (2) values of s and p Coulomb integrals, and (3) bonding parameters, β]. The molecular geometry of the first six molecules was taken from a compilation of peptide structural data in the literature.[5] The experimental values for formamide[22–24] show the largest deviation from the data in ref 5; however, we have used the data of ref 5 for consistency with all the other molecules. For acetyl-L-

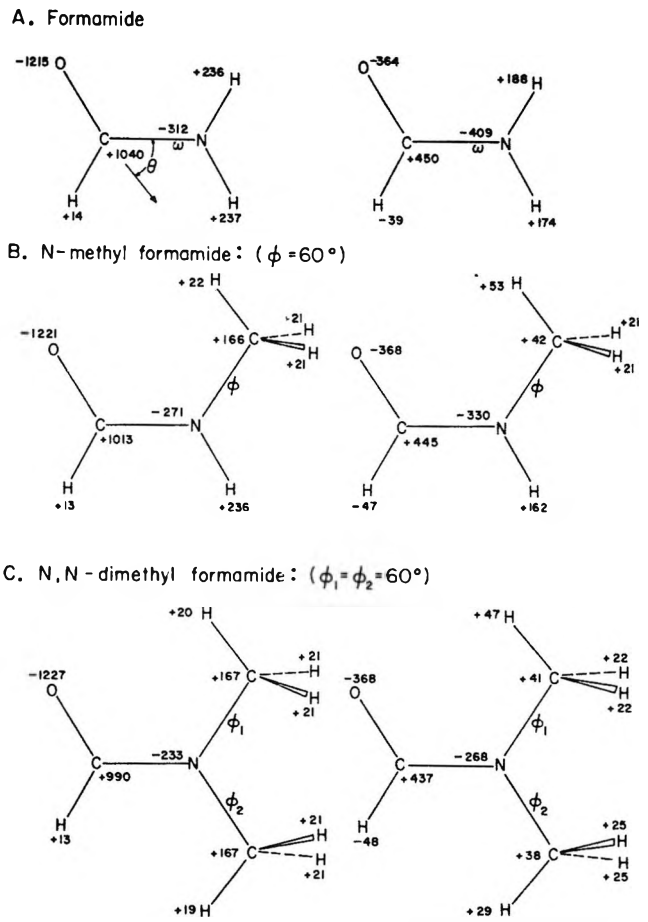

Figure 1. Computed partial charges ($\sigma + \pi$) for the molecules and conformations shown; where not designated explicitly, the conformation is planar; left, EHT (ON); right, CNDO/2 (ON). The values shown should be divided by 100 to obtain electronic charge units. The *trans* conformation (*i.e.*, ω = 0°) is shown in B. The direction of the dipole moment (θ) with respect to the C–N bond is indicated in A; this definition of θ is used for all the molecules considered here.

(7) N. Gō and H. A. Scheraga, *J. Chem. Phys.*, in press.

(8) D. Poland and H. A. Scheraga, *Biochemistry*, **6**, 3791 (1967).

(9) G. Del Re, *J. Chem. Soc.*, 4031 (1958).

(10) G. Del Re, *Theoret. Chim. Acta*, **1**, 188 (1963).

(11) G. Del Re, "Electronic Aspects of Biochemistry," Academic Press, Inc., New York, N. Y., 1963, p 221.

(12) B. Pullman and A. Pullman, "Quantum Biochemistry," Interscience, New York, N. Y., 1963, pp 321 and 661.

(13) G. Del Re, B. Pullman, and T. Yonezawa, *Biochim. Biophys. Acta*, **75**, 153 (1963).

(14) See ref 5, footnote 1, p 133, for further discussion of the differences between the methods of Del Re, *et al.*,[13] and Poland and Scheraga.[8]

(15) J. T. Edsall, P. J. Flory, J. C. Kendrew, A. M. Liquori, G. Nemethy, G. N. Ramachandran, and H. A. Scheraga, *J. Mol. Biol.*, **15**, 399 (1966).

(16) R. Hoffmann, *J. Chem. Phys.*, **39**, 1397 (1963); **40**, 2474, 2480, 2745 (1964).

(17) J. A. Pople and G. A. Segal, *ibid.*, **44**, 3289 (1966).

(18) Further refinement of the computed parameters is being carried out by empirical calculations of crystal structures.[19]

(19) F. A. Momany, G. Vanderkooi, and H. A. Scheraga, *Proc. Natl. Acad. Sci. U. S.*, **61**, 429 (1968).

(20) The version used is substantially that of R. Hoffmann, "EXTHUC—Extended Hückel Theory Calculations," No. 30, QCPE, Indiana University.

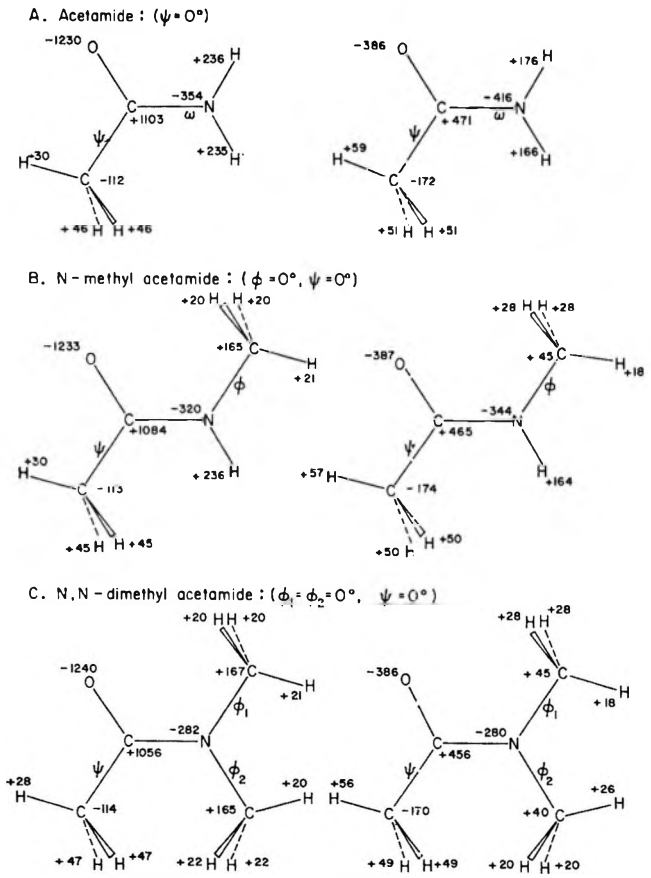

Figure 2. Computed partial charges ($\sigma + \pi$) for the molecules and conformations shown; where not designated explicity, the conformation is planar; left, EHT (ON); right, CNDO/2 (ON). The values shown should be divided by 1000 to obtain electronic charge units. The *trans* conformation (*i.e.*, $\omega = 0°$) is shown in B.

Table I: Molecular Geometry[a,b] of Acetyl-L-prolineamide

Bond distances		Bond angles	
Bond	Bond length, Å	Bond angle	Value, deg
C^{α}_{acetyl}–H	1.09	$\tau[C'C^{\alpha}H]_{acetyl}$	109.5
C^{α}_{acetyl}–C'_{acetyl}	1.53	$\tau[C^{\alpha}C'O]_{acetyl}$	121.0
C'_{acetyl}–O_{acetyl}	1.24	$\tau[C^{\alpha}C'N]_{acetyl}$	118.0
C'_{acetyl}–N	1.34	$\tau[C'NC^{\alpha}]$	121.0
N–C^{α}	1.45	$\tau[NC^{\alpha}C^{\beta}]$	105.0
C^{α}–H	1.00	$\tau[C^{\alpha}C^{\beta}C^{\gamma}]$	106.6
C^{α}–C^{β}	1.50	$\tau[C^{\beta}C^{\gamma}C^{\delta}]$	111.3
C^{β}–C^{γ}	1.47	$\tau[C^{\gamma}C^{\delta}N]$	104.1
C^{γ}–C^{δ}	1.45	$\tau[C^{\delta}NC']$	126.0
C^{δ}–N	1.46	$\tau[NC^{\alpha}C']$	111.0
$C^{\beta,\gamma,\delta}$–H	1.09	$\tau[HC^{\alpha}C^{\beta}]$	112.0
C^{α}–C'_{amide}	1.53	$\tau[HC^{\alpha}C']$	104.0
C'_{amide}–O_{amide}	1.24	$\tau[C^{\alpha}C'O]_{amide}$	120.0
C'_{amide}–N_{amide}	1.32	$\tau[C^{\alpha}C'N]_{amide}$	115.0
N_{amide}–H	1.00	$\tau[C'NH]_{amide}$	123.0

[a] The geometry in this table was maintained fixed for all values of the dihedral angles of internal rotation. The proline ring is planar. [b] The data for all compounds except acetyl-L-prolineamide were taken from Tables 5 and 6 of ref 5, except that the aliphatic C–H bond length was taken as 1.09 Å.

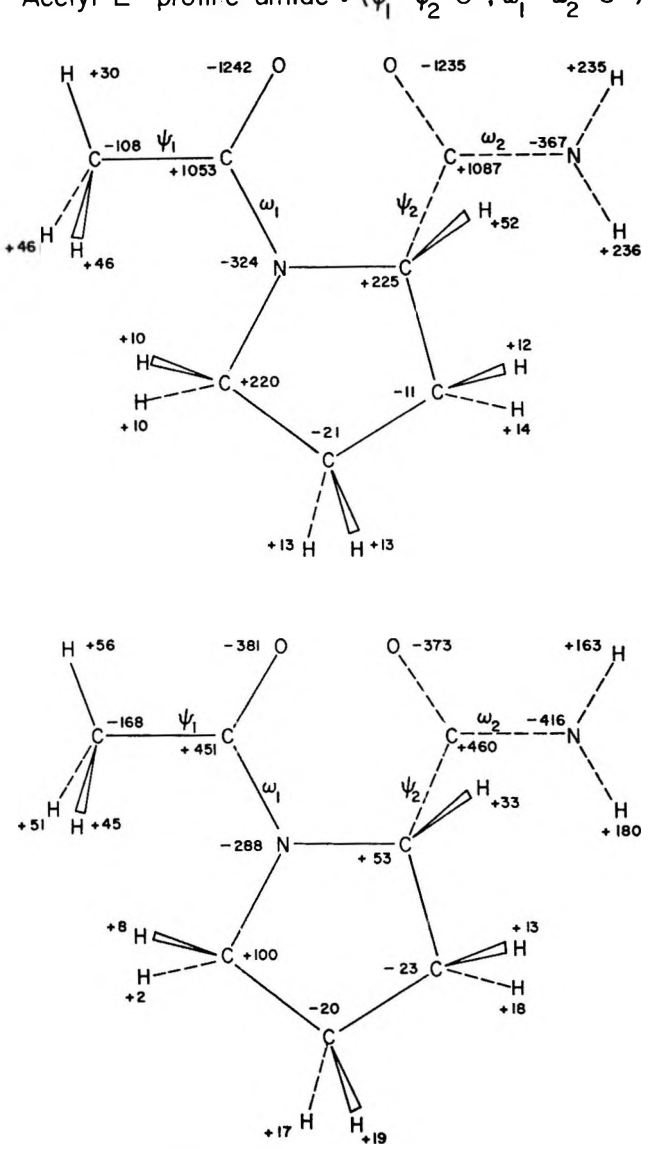

Figure 3. Computed partial charges ($\sigma + \pi$) for the molecules and conformations shown. The portion indicated by the solid lines is planar; top, EHT (ON); bottom, CNDO/2 (ON). The values shown should be divided by 1000 to obtain electronic charge units. The conformation about ω_1 is the *trans* one.

prolineamide, the parameters were selected from a composite of available X-ray data.[25-29] All bond angles

(21) Our version of the CNDO/2 method was written by P. Clark and J. Swenson. A similar program is available; see G. A. Segal, "CNDO/2—Molecular Calculations with Complete Neglect of Differential Overlap," No. 91 QCPE, Indiana University.

(22) C. C. Costain and J. M. Dowling, *J. Chem. Phys.*, **32**, 158 (1960).

(23) R. J. Kurland and E. B. Wilson, *ibid.*, **27**, 585 (1957).

(24) J. Ladell and B. Post, *Acta Cryst.*, **7**, 559 (1954).

(25) Y. C. Leung and R. E. Marsh, *ibid.*, **11**, 17 (1958).

(26) J. Fridrichsons and A. McL. Mathieson, *ibid.*, **15**, 569 (1962).

(27) J. Zussman, *ibid.*, **4**, 493 (1951).

(28) J. Donohue and K. N. Trueblood, *ibid.*, **5**, 419 (1952).

(29) S. Arnott and S. D. Dover, *ibid.*, **B24**, 599 (1968).

Table II: Parameters for EHT and CNDO/2 Methods[a]

Atom	Slater orbital exponent	α(2s)	α(2p)	α(1s)	β
			EHT[b]		
C and C′	1.625	−21.400	−11.400		
O	2.275	−32.300	−14.800		
N	1.950	−26.000	−13.400		
H	1.300			−13.600	
			(CNDO/2)[c]		
C and C′	1.625	−14.051	−5.572		−21.00
O	2.275	−25.390	−9.111		−31.00
N	1.950	−19.316	−7.275		−25.00
H	1.300			−7.176	−9.00

[a] The α's are the usual valence state ionization potentials in the EHT method and are the averages of the ionization potentials and electron affinities in the CNDO/2 method. The α's and β are expressed in electron volts. β is an estimate of the resonance integral. [b] Reference 16. [c] Reference 17.

and bond lengths were maintained constant (rigid geometry) in the calculations reported here, to avoid increase in computational time, even though it is recognized (and confirmed from some preliminary calculations with flexible geometry) that the results will be somewhat altered by this restriction. All other input data are given in the original papers.[16,17]

The output from the programs includes (1) the calculated energy levels and total energy of the molecule; (2) the wave functions; (3) the partial charges localized on each atom;[30,31] and (4) the bond order or overlap population. Since these results are obtained for each set of values of the dihedral angles of rotation, it is possible to study the variation of the energy, partial charges, dipole moments, and electronic orbital distributions, with changes in the dihedral angles.

The computational times on an IBM 360/65 computer ranged from 5–20 sec for a single EHT calculation to several minutes for a CNDO/2 calculation. The longer times and cost made it necessary to limit the number of conformations studied by the CNDO/2 method; however, a sufficient number of calculations were performed to map out all the necessary conformational information and to make critical comparisons of the results.

Results and Discussion

The results of the calculations are presented and discussed in five sections: (1) charges, (2) dipole moments, (3) energies for internal rotation, and (4) electronic spectra. All of the molecules, except acetyl-L-prolineamide, are considered together as a group so that differences between these similar molecules may be compared easily; acetyl-L-prolineamide will be treated in section 5.

1. Charges. The computed total charges ($\sigma + \pi$) for the seven molecules considered here, in given conformations, are shown in Figures 1–3. Two features are of interest. First, the charges computed by the two methods differ, in some cases even as far as the sign is concerned; in all cases, the EHT method gives very high charge separation for the carbonyl groups, while the CNDO/2 method gives values for the charges on this group in reasonable agreement with our earlier[8] theoretical studies. Both methods give nearly equivalent charge distributions on the methyl groups and around the nitrogen atom. Second, as found in paper I,[8] the hydrogen atoms of the methyl groups have significant charges.

Since formamide has been examined quite extensively by a number of theoretical approaches, we consider the charge distribution for this molecule in some detail and compare it with that obtained by other methods (see Table III). It can be seen that the CNDO/2 calculations are sensitive to variations in geometry and in the Slater orbital exponent of the hydrogen atom. Differences also arise from the use of the overlap-normalized (ON) Mulliken population analysis as compared to the CNDO/2 population analysis. For example, in the calculations of Pullman and Berthod,[32] the observed differences are due only to experimental differences in geometry from microwave[22] and crystal structure[24] studies. Similarly, in the "*ab initio*" calculations of Basch, *et al.*,[33] differences in charges arose because of

(30) There are two distinct ways in which charges may be assigned to atoms, depending on whether or not the overlap is included in the normalization of the molecular orbitals. The primary output of a CNDO/2 calculation is an electron density derived with the assumption of neglect of overlap. To compare such charges to the Mulliken gross atomic populations,[31] which are computed by the EHT program, it is possible to transform the CNDO/2 electron densities to an overlap-normalized basis (which will be designated as ON throughout this paper). We will have occasion to refer to both types of CNDO/2 population analysis in the course of our discussion.

(31) R. Mulliken, *J. Chem. Phys.*, **23**, 1833, 1841, 2338, 2343 (1955).

(32) A. Pullman and H. Berthod, *Theoret. Chim. Acta*, **10**, 461 (1968).

Table III: Various Charge Distributions for Formamide,[a] in Electronic Units

Atom	EHT[b-d]	(CNDO/2)[b-d]	(CNDO/2)[b,e-g]	(CNDO/2)[e-h]	(CNDO/2)[g-e]
O	−1.215	−0.365	−0.338	−0.336	−0.373
C′	1.040	0.450	0.358	0.356	0.441
N	−0.312	−0.409	−0.236	−0.237	−0.424
H(C′)	0.014	−0.039	−0.046	−0.046	−0.027
H_1	0.236	0.188	0.142	0.120[i]	0.204
H_2	0.237	0.174	0.120	0.142[i]	0.178
	(CNDO/2)[f,g,j,k]	(CNDO/2)[f,g,k,l]	(*ab initio*)[j,m]	(*ab initio*)[j,n]	(*ab initio*)[n,c]
O	−0.354	−0.306	−0.41	−0.377	−0.429
C′	0.348	0.367	0.36	0.258	0.295
N	−0.223	−0.262	−0.86	−0.758	−0.745
H(C′)	−0.044	−0.055	0.17	0.152	0.134
H_1	0.146	0.132	0.37	0.368	0.383
H_2	0.127	0.123	0.37	0.357	0.362

[a] H_1 and H_2 refer to the hydrogen atoms which are *cis* and *trans*, respectively, to the oxygen atom. [b] This work. [c] Exponent for Slater orbital of hydrogen atom = 1.3. [d] Mulliken population analysis (ON) (ref 31). [e] Pople–Gordon geometry (ref 34). [f] Exponent for Slater orbital of hydrogen atom = 1.2 (chosen for comparison with Pople and Gordon data[h]). [g] CNDO/2 population analysis. [h] Calculation by Pople and Gordon (ref 34). [i] We believe that these were interchanged in the Pople–Gordon paper (ref 34). [j] Geometry from microwave data (ref 22). [k] Calculation by Pullman and Berthod (ref 32). [l] Geometry from X-ray data (ref 24). [m] Calculated using a Gaussian orbital basis set (ref 56). [n] Calculated using a Gaussian orbital basis set (ref 33). [o] Geometry from microwave data (ref 23).

Table IV: Charge Distribution around Peptide Bond, in Units of Electronic Charge

Atom	EHT[a,b]	(CNDO/2)[a,c]	(CNDO/2)[a,b]	Ooi, *et al.*[d]	Poland–Scheraga[e]	Brant, *et al.*[f]	Schellman and Oriel[g]
C′	+1.08	+0.36	+0.47	+0.45	+0.32	+0.39	+0.43
O	−1.23	−0.36	−0.39	−0.42	−0.42	−0.39	−0.39
N	−0.32	−0.18	−0.34	−0.30	−0.20	−0.28	−0.30
H(N)	+0.24	+0.10	+0.16	+0.27	+0.20	+0.28	+0.26

[a] For N-methylacetamide in the *trans* form; all other data also pertain to the *trans* conformation. [b] Mulliken population analysis (ON).[30,31] [c] CNDO/2 population analysis. [d] Reference 35. [e] Reference 8. [f] Reference 36. [g] Reference 37.

differences in two reported sets of microwave geometries.[22,23] Likewise, in the calculations reported here and in those of Pople and Gordon,[34] there is an influence of geometry on the resulting charges. However, the results of all the CNDO/2 calculations are in reasonable agreement with each other, while the "*ab initio*" and EHT charges differ from those obtained by the CNDO/2 method. It is clear from previous experience with the EHT method that it tends to exaggerate charge separation in polar molecules. It should also be noted that the size of the basis set and the degree of approach to Hartree–Fock accuracy significantly influence the charge distribution obtained by "*ab initio*" methods. The CNDO/2 results, though sensitive to the parameters and geometry used, appear to provide the most reasonable estimate of the charge distribution in formamide as well as in the other molecules considered here.

Using N-methylacetamide as a model for the polypeptide chain, we obtain the data of Table IV for the charge distribution around the peptide bond. For comparison, the results of other workers are also included in Table IV. The CNDO/2 results are in general agreement with data from the literature,[8,35-37] whereas the EHT data differ considerably. In all the results obtained here, the sum of the peptide group charges is negative, in agreement with the results of paper I.[8] Again, it seems valid to conclude that the charges obtained by the CNDO/2 method are reasonable ones and may be used in conformational energy calculations[5] in which Coulomb's law is applied to point-charge distributions. The most serious omission in the calculation of electrostatic energies in earlier calculations[5] would seem to be the assignment of zero charge to carbon atoms and to the hydrogen atoms

(33) H. Basch, M. B. Robin, and N. A. Kuebler, *J. Chem. Phys.*, **47**, 1201 (1967).

(34) J. A. Pople and M. Gordon, *J. Amer. Chem. Soc.*, **89**, 4253 (1967).

(35) T. Ooi, R. A. Scott, G. Vanderkooi, and H. A. Scheraga, *J. Chem. Phys.*, **46**, 4410 (1967).

(36) D. A. Brant, W. G. Miller, and P. J. Flory, *J. Mol. Biol.*, **23**, 47 (1967).

(37) J. A. Schellman and P. Oriel, *J. Chem. Phys.*, **37**, 2114 (1962).

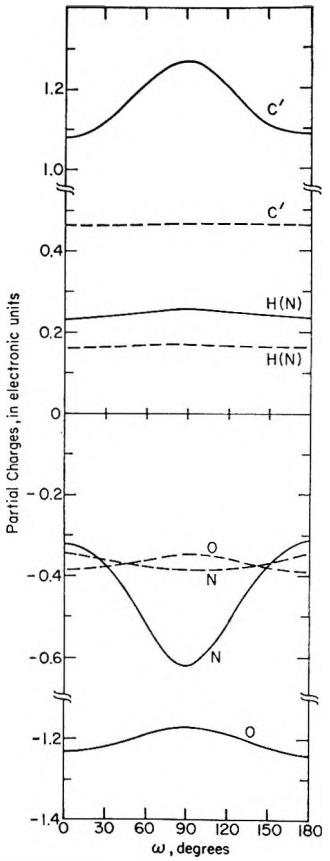

Figure 4. Variation of partial charges on the atoms of the amide group [C′, O, H, H(N)] with ω, for N-methylacetamide. The solid and dashed lines are EHT and CNDO/2 results, respectively.

attached to them; this point will be considered in a later paper of this series.

If ω, the dihedral angle for rotation around the peptide bond, is allowed to vary and the calculations repeated for specific values of ω, we obtain the variations of charge with ω shown in Figure 4. The variations of charge with ω are greater in the EHT than in the CNDO/2 results. The charges on the C′ and N atoms vary most upon rotation about the peptide bond; thus, assuming that the two theoretical methods show the extremes of variation of the partial charges, it appears that a study of the C^{13} chemical shift of the carbonyl carbon may provide information about the electronic distribution as a function of ω. Using our computed bond orders for N-methylacetamide and Pople's theory of carbon chemical shifts,[38] we predict a maximum nmr shift (EHT) of 30 ppm (from $\omega = 0°$ to $\omega = 90°$) and a minimum shift (CNDO/2) of 0.3 ppm. We would expect the true value to lie somewhere between these limits, and that such nmr studies would detect changes in ω by approximately 15° or more. Another conclusion from the data of Figure 4 is that the partial charges are nearly identical at $\omega = 0°$ (*trans*) and $\omega = 180°$ (*cis*) for both methods. This result confirms the use of equivalent charge distributions for conformational calculations for both *cis* and *trans* forms.

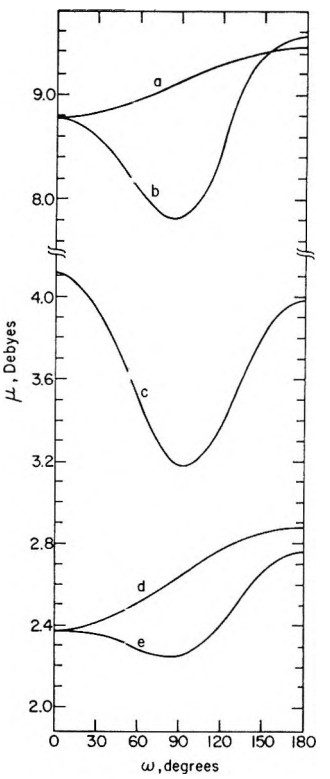

Figure 5. Variation in the dipole moment of N-methylacetamide with ω. Curve a, monopole calculation with EHT charges taken as constant and equal to those of the conformation $\phi = 60°$, $\psi = 0°$, $\omega = 0°$; curve b, monopole calculation with EHT charges as obtained for the conformation of lowest energy for each value of ω; curve c, monopole calculation with CNDO/2 charges and Pople–Segal correction[39] as obtained for the conformation of lowest energy for each value of ω; curve d, monopole calculation with CNDO/2 (ON) charges taken as constant and equal to those of the conformation $\phi = 60°$, $\psi = 0°$, $\omega = 0°$; curve e, monopole calculation with CNDO/2 (ON) charges as obtained for the conformation of lowest energy for each value of ω.

It is of interest to note that the charge on the carbonyl oxygen atom decreases as ω departs from 0 and 180°. Assuming that a hydrogen bond contains an electrostatic contribution, one might expect a departure of ω from 0 and 180° to lead to a reduced strength of a hydrogen bond involving this oxygen atom. An opposite, although weaker effect appears at the amide hydrogen atom, whose charge increases slightly; this might enhance the strength of a hydrogen bond involving this hydrogen atom. These points will be considered in detail in later papers of this series, where their possible effects on helix formation as well as their influence on solvent interactions will be discussed.

The geometrically nonequivalent hydrogens of the methyl groups carry slightly different charges, which *change* by about 0.01 electron upon rotation of the methyl group. These *changes* may most probably be ignored in conformational energy calculations;[5] however,

(38) J. A. Pople, *Mol. Phys.*, 7, 301 (1964).

Table V: Dipole Moments in Debye Units[a,b]

Molecule	EHT (ON)	CNDO/2	CNDO/2 (corrected)[c]	θ,[d] deg	μ, (exptl)[e]	θ (exptl), deg
Formamide	8.75 (T)	2.46 (T)	4.00 (T)	−37.7	3.71[f]	−39.6[f]
N-Methyl-formamide	8.85 (T)	2.40 (T)	3.97 (T)	−38.8	3.82[g]	
N,N-Dimethyl-formamide	9.59 (T)	2.52 (T)	3.83 (T)	−37.8	3.80[g]	
Acetamide	8.78 (T)	2.53 (T)	4.15 (T)	−44.3	3.75,[g] 3.72[h]	
N-Methyl-acetamide	8.80 (T)	2.40 (T)	4.12 (T)	−44.3	3.71 (T),[g] 4.39 (T)[i]	
	9.50 (C)	2.61 (C)	3.98 (C)	−42.5	3.40 (C)[i]	
N,N-Dimethyl-acetamide	9.60 (T)	2.51 (T)	3.97 (T)	−44.3	3.80[g,h]	

[a] Dipole moments were calculated classically, using the charges of the minimum-energy conformation. [b] T and C refer to *trans* and *cis* conformations, respectively. [c] Contribution to the dipole moment due to the displacement of atomic electron charges away from the center of the atom (see ref 34 and 39). [d] See Figure 1 for direction of dipole moment. This column was computed from the CNDO/2 (corrected) results. [e] The value of μ in ref 23 was obtained from microwave data. The values of μ given in footnote *h* of this table may be considered as experimental values since they were calculated from dielectric constants of solutions; the values from footnote *i* of this table and ref 40 are estimates from bond moments. [f] Reference 22. [g] Reference 39. [h] R. M. Meigham and R. H. Cole, *J. Phys. Chem.*, **68**, 503 (1964). [i] W. D. Kumler and C. W. Porter, *J. Amer. Chem. Soc.*, **56**, 2549 (1934).

the significance of the *magnitudes* of these proton charges for conformational energy calculations and for other physical properties, such as proton nmr spectroscopy and ORD, may have to be taken into account.

2. *Dipole Moments.* As a general check on the validity of the computed charges, we may use them to compute dipole moments, μ, which may be compared with experimental values. Dipole moments, computed from the calculated charges, are listed in Table V, together with experimental values. The dipole moments were calculated classically from the EHT and CNDO/2 charges of the minimum energy conformation, taking into account the charges on all of the atoms. Those calculated using the CNDO/2 basis were corrected by adding a term primarily due to the lone-pair electrons, using equations of Pople and Segal.[39] The dipole moments computed with this correction then seem to show the best agreement with experimental results, as was demonstrated earlier[34] for a large number of other molecules, providing additional confidence in the charges computed by the CNDO/2 method.

Figure 5 shows the variation of μ with ω for N-methylacetamide. Different results are obtained depending on whether the charges on each atom are kept constant (at the values for the *trans* form) or are allowed to vary as ω varies. Since we expect the charges to vary with ω (see Figure 4), the usual procedure of ignoring the variation of charge with ω in empirical conformational energy calculations[5] (*i.e.*, the use of curves a or d) is clearly erroneous. However, as already pointed out, the charges are similar at $\omega = 0$ and 180° (although the values of μ differ because of the different geometry); thus, the *same* charges can be used in a comparison of *cis* and *trans* forms in empirical calculations,[5] *provided* ω *does not depart from these values.* Since curve c gives the closest agreement with the *limited* experimental data, we again conclude that the CNDO/2 method provides the best estimate of the charge distribution.

3. *Energies for Internal Rotation.* The effect of steric interactions and conjugation on barriers to rotation has been well documented,[16,41] and the vast amount of literature in this field will not be reviewed here. However, it is necessary to consider the approximations which have been made in treating rotation potentials and nonbonded interactions to use them in conformational analyses of polypeptides and proteins. Hopefully, use of the theoretical methods applied in this paper will shed some light on this very difficult problem. One should expect that most features usually associated with steric interactions will manifest themselves in the computed rotational barriers since interactions among *all* the atoms of the molecule are included in both the EHT and CNDO/2 calculations; however, in the procedures used here, it is not possible to separate out those energies associated with any given type of interaction. Also, while the approximate molecular orbital methods used here do not appear to include the attractive portion of the van der Waals interactions between nonbonded atoms, nevertheless it will be shown that

(39) J. A. Pople and G. A. Segal, *J. Chem. Phys.*, **43**, S136 (1965).

(40) S. Mizushima, T. Simanouti, S. Nagakura, K. Kuratani, M. Tsuboi, H. Baba, and O. Fujioka, *J. Amer. Chem. Soc.*, **72**, 3490 (1950).

(41) For recent work, see: L. C. Allen, *Chem. Phys. Lett.*, **2**, 597 (1968); W. H. Fink and L. C. Allen, *J. Chem. Phys.*, **46**, 2261, 2267 (1967); J. P. Lowe and G. Parr, *ibid.*, **44**, 3001 (1966); for earlier work, see R. M. Pitzer and W. N. Lipscomb, *ibid.*, **39**, 1995 (1963), and references cited therein.

they do give the essential features of the rotational energy functions.

For the purpose of considering the rotational energies, we provide in Table VI a listing of the total energies computed for several conformations. For each molecule, the conformation of lowest energy has been assigned the energy zero.

The energies for rotation about the peptide bond in N-methylacetamide, acetamide, and N-methylformamide, respectively, are shown in Figure 6. The

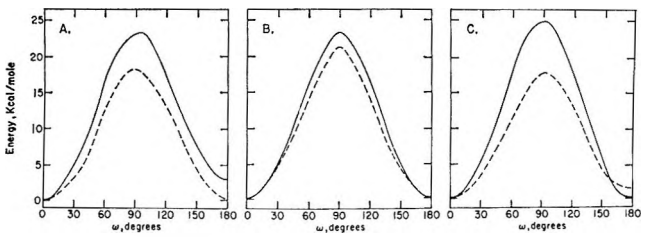

Figure 6. Energy for rotation about the peptide bond in (A) N-methylacetamide, (B) acetamide, and (C) N-methylformamide. The solid and dashed lines are EHT and CNDO/2 results, respectively.

EHT and CNDO/2 methods both give similar shapes and magnitudes for the rotational energy. The energy scales have been normalized to agree at $\omega = 0°$ (the *trans* conformation); hence, the difference in energy between the *cis* and *trans* conformations appears at $\omega = 180°$ (the *cis* conformation). The calculated results are in reasonable agreement with the experimental values shown in Table VII. Unfortunately, there is so much deviation in the experimental results for a given molecule that it is impossible to make any but a qualitative comparison.

In addition to the well-known preference of synthetic and natural polypeptides for the *trans* conformation around the peptide bond, there exists some fragmentary evidence for a *trans* preference in the model compounds N-methylformamide[42] and N-methyl acetamide.[43,44] Neither EHT nor CNDO/2 methods reproduce the somewhat uncertain experimental quantities, but the trend predicted from the EHT calculations, namely a small *trans* preference in N-methylformamide and a greater differential in N-methylacetamide, appears most consistent.

The preference for the *trans* conformation of N-methylformamide may actually be due to consequent proximity of the methyl substituent and the carbonyl oxygen. In the *trans* conformation, the methyl group is *cis* to the carbonyl group. The peptide unit, as a four π-electron system, is isoelectronic with the allyl anion. There exists experimental evidence for the greater stability of a *cis*-methyl allyl anion.[45] Other examples of the stabilization of alkyl substituents *cis* to a four π-electron system are cited by Owen.[46] A theoretical rationalization of the preference for *cis*-methyl groups has been presented.[47] On this basis, we would expect the methyl group to be *cis* to the oxygen in the N-methylformamide (*trans* conformation of the peptide).

In analyzing the still greater preference of N-methylacetamide for a *trans* conformation, one is inclined to attribute a significant role to a destabilization of the *cis* conformation as a consequence of the steric repulsion of the *cis*-methyl groups. The simple steric argument gains support from the following set of numerical observations (Table VI).

1. The barriers to internal rotation of the single methyl groups in N-methylformamide and in acetamide remain small (less than 1 kcal/mol) regardless of the rotation of the amide group out of planarity (see Figure 7).

2. The barriers to internal rotation of the two methyl groups of N-methylacetamide remain small and comparable to the corresponding barriers in N-methylformamide and in acetamide *only* when the angle of twist of the amide, ω, is less than 120°. At greater angles of twist, as the *cis* conformation of N-methylacetamide is approached, the methyl group barriers rise sharply. This magnification of methyl group barriers, obtained by both EHT and CNDO/2 methods, is highly indicative of a sharpening of the potential walls due to steric repulsions.

The steric effect appears to dictate a peculiar geared motion which couples methyl group internal rotations to amide twisting in N-methylacetamide. The data in Table VI yield the following itinerary of optimum ϕ and ψ for a given range of ω.

ω	ϕ	ψ
0,30,60	60	0
90	0	0
120	60	0
150,180	0	0

Figure 7 shows the computed ω dependence of the methyl group rotations in N-methylformamide and in acetamide. The preferred conformations are illustrated in Figures 1B and 2A, respectively. The trends exhibited in Figure 7 result from both calculations, and so it becomes important to present an interpretation.

Both barriers are relatively small at $\omega = 0°$. The

(42) R. M. Badger and H. Rubalcava, *Proc. Nat. Acad. Sci. U. S.* **40**, 12 (1954).

(43) I. Suzuki, *Bull. Chem. Soc. Jap.*, **35**, 540 (1962).

(44) T. Miyazawa, *J. Mol. Spectrosc.*, **4**, 155 (1960).

(45) S. Bank, A. Schriesheim, and C. A. Rowe, Jr., *J. Amer. Chem. Soc.*, **87**, 3244 (1965), and references therein.

(46) N. L. Owen, *Proc. Chem. Soc.*, 264 (1963).

(47) R. Hoffmann and R. A. Olofson, *J. Amer. Chem. Soc.*, **88**, 943 (1966).

Table VI: Total Energies for Various Conformations of Several Molecules[a,b]

	Dihedral angle, deg				Energy, kcal/mol	
	ϕ_1	ϕ_2	ψ_1	ω	EHT	CNDO/2
Formamide				0	0.00	0.00
				30	5.35	
				60	17.79	
				90	25.26	20.29
N-Methylformamide	0			0	0.33	0.25
	60			0	0.00	0.00
	0			30	5.78	
	60			30	5.33	
	0			60	18.26	
	60			60	18.00	
	0			90	25.60	18.22
	60			90	25.62	18.05
	0			120	18.05	
	60			120	17.86	
	0			150	5.87	
	60			150	5.36	
	0			180	0.71	1.41
	60			180	0.09	1.18
N,N-Dimethylformamide	0	0		0	3.47	
	60	0		0	1.40	
	60	60		0	0.00	0.00
	0	0		90	28.42	
	60	0		90	26.77	
	60	60		90	25.81	15.03
Acetamide			0	0	0.00	0.00
			60	0	0.21	0.25
			0	30	5.14	
			60	30	5.41	
			0	60	16.98	
			60	60	17.51	
			0	90	24.01	21.72
			60	90	24.80	22.41
N-Methylacetamide	0		0	0	0.30	0.24
	0		60	0	0.48	0.54
	60		0	0	0.00	0.00
	60		60	0	0.18	0.30
	0		0	30	5.47	
	0		60	30	5.72	
	60		0	30	5.08	
	60		60	30	5.32	
	0		0	60	17.18	
	0		60	60	17.73	
	60		0	60	17.00	
	60		60	60	17.54	
	0		0	90	24.16	18.91
	0		60	90	24.84	19.47
	60		0	90	24.17	18.80
	60		60	90	24.90	19.39
	0		0	120	18.42	
	0		60	120	18.78	
	60		0	120	18.09	
	60		60	120	18.12	
	0		0	150	7.76	
	0		60	150	11.22	
	60		0	150	10.11	
	60		60	150	12.42	
	0		0	180	2.92	−0.09
	0		60	180	7.64	1.19
	60		0	180	6.70	0.75
	60		60	180	18.03	9.01

Table VI (*Continued*)

	Dihedral angle, deg				Energy, kcal/mol	
	ϕ_1	ϕ_2	ψ_1	ω	EHT	CNDO/2
N,N-Dimethylacetamide	0	0	0	0	2.03	
	0	0	60	0	6.76	
	0	60	0	0	0.00	0.00
	0	60	60	0	4.69	
	60	0	0	0	4.08	
	60	0	60	0	15.39	
	60	60	0	0	2.99	
	60	60	60	0	14.26	
	0	0	0	30	6.91	
	0	0	0	60	17.45	
	0	0	0	90	23.14	
	0	0	60	90	23.74	
	0	60	0	90	21.48	
	0	60	60	90	22.12	
	60	0	0	90	21.48	
	60	0	60	90	22.12	
	60	60	0	90	20.52	16.04
	60	60	60	90	21.20	

[a] The dihedral angles are those shown in Figures 1 and 2. [b] For each molecule, the zero value corresponds to the conformation of lowest energy.

Table VII: Barriers to Rotation about the Peptide Bond, and *cis–trans* Energy Difference, in Kilocalories per Mole, for Minimum-Energy Values of ϕ and ψ

Molecule	Barrier (EHT)	Barrier (CNDO/2)	$\Delta E_{cis-trans}$ (EHT)	$\Delta E_{cis-trans}$ (CNDO/2)	Barrier (exptl)	$\Delta E_{cis-trans}$ (other estimates)
Formamide	25.26	20.29			18 ± 3[a]	
					16.8–21.3[b]	
N-Methyl-formamide	25.60 (0–90°)	18.05 (0–90°)			28.0–28.5[d]	
			0.09	1.18, 1.25[c]		>2.0[e]
	25.51 (90–180°)	16.87 (90–180°)			14.0[f]	
N,N-Dimethyl-formamide	25.81	15.03			6.5 ± 0.3[g]	
					22.0 ± 3[h]	
					9.6 ± 1.5[i]	
					21.0[j]	
					21.0[k]	
					20.6[l]	
Acetamide	24.01	21.72				
N-Methyl-acetamide	24.16 (0–90°)	18.80 (0–90°)				
			2.92	−0.09		3.0[d], 1.6[m]
	21.24 (90–180°)	18.89 (90–180°)			14.0[f]	
N,N-Dimethyl-acetamide	20.52	16.04			17.4[j]	
					18.2 ± 3[n]	
					19.0[h]	
					17.5[o]	

[a] B. Sunners, L. H. Piette, and W. G. Schneider, *Can. J. Chem.*, **38**, 681 (1960). [b] H. Kamei, *Bull. Chem. Soc. Jap.*, **41**, 2269 (1968). Values listed are E_a^{rot}. [c] Reference 32. Theoretical value by CNDO/2 method. [d] Reference 43. Estimated from spectroscopic force constants. [e] Reference 42. Estimated from infrared spectroscopic data. [f] T. Miyazawa, *J. Chem. Phys.*, **34**, 691 (1961). Estimated from spectroscopic force constants. [g] E. S. Gore, D. J. Blears, and S. S. Danyluk, *Can. J. Chem.*, **43**, 2135 (1965). Value listed is ΔH^*. [h] H. S. Gutowsky and C. H. Holm *J. Chem. Phys.*, **25**, 1228 (1956). Value listed is ΔF^*. [i] G. Fraenkel and C. Franconi, *J. Amer. Chem. Soc.*, **82**, 4478 (1960). Value listed is E_a^{rot}. [j] M. T. Rogers and J. C. Woodbrey, *J. Phys. Chem.*, **66**, 540 (1962). Value listed is ΔF^*. [k] M. Rabinovitz and A. Pines, *J. Amer. Chem. Soc.*, **91**, 1585 (1969). Value listed is ΔF^*. [l] A. Mannschreck, A. Mattheus, and G. Rissmann, *J. Mol. Spectrosc.*, **23**, 15 (1967). Value listed is ΔF^*. [m] Reference 44. Estimated from infrared spectroscopic data. [n] R. C. Neuman, Jr., and V. Jonas, *J. Amer. Chem. Soc.*, **90**, 1970 (1968). Value listed is ΔF^*. [o] G. N. Ramachandran and V. Sasisekharan, *Advan. Protein Chem.*, **23**, 365 (1968).

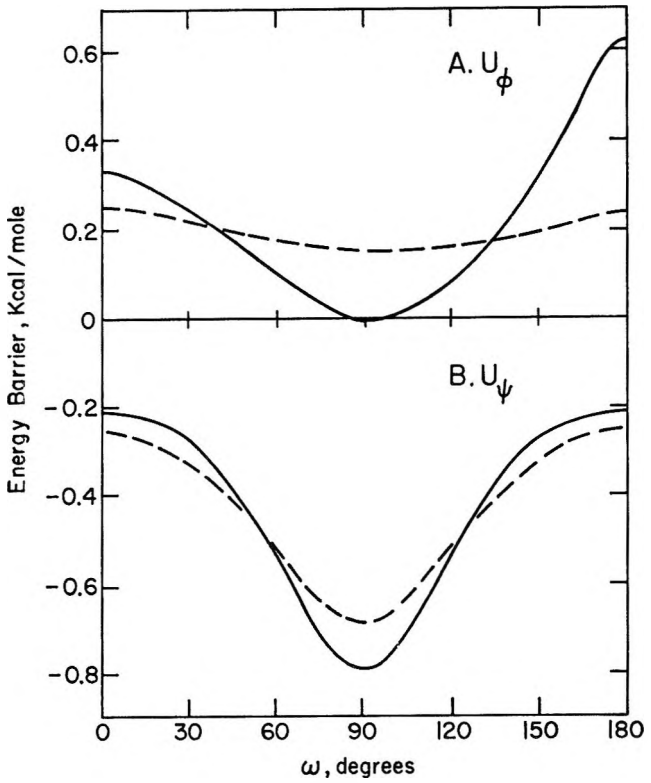

Figure 7. Barriers to rotation of methyl groups as functions of ω for (A) N-methylformamide and (B) acetamide. The solid and dashed lines are EHT and CNDO/2 results, respectively. The values of U_ϕ and U_ψ are the differences in energy $E_{0°} - E_{60°}$ for ϕ and ψ, respectively.

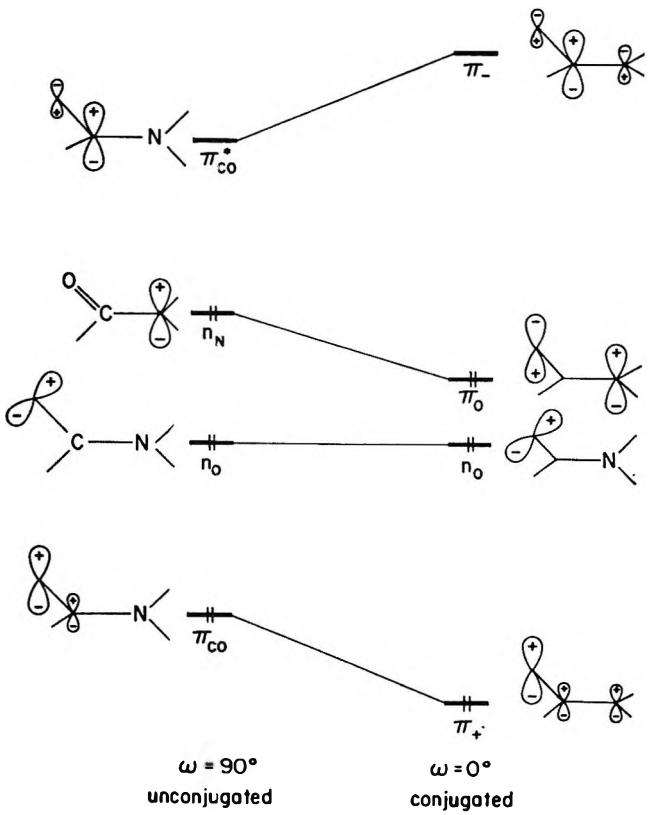

Figure 8. Qualitative description of energy position and composition of molecular orbitals of a typical peptide unit at ω = 90 and 0°. See text for derivation.

rotors are of the form CH_3–XAB with X trigonal. Were A and B equivalent, the barrier would be sixfold, and such barriers are known to be small.[48-51] When A and B are nonequivalent, a threefold component is introduced. This dominates the general barrier shape, but the barrier height generally remains small as long as the trigonal configuration at X is maintained.

The preferred conformations at ω = 0° are easily understood if one recalls that, in propylene[52,53] and acetaldehyde,[54] the conformations in which a hydrogen eclipses the C=C or C=O double bond are favored by 1.98 and 1.16 kcal/mol, respectively. The acetamide case is then entirely analogous to the model compound acetaldehyde. The rise in this barrier as ω approaches 90° may be explained as follows. Whereas the NH_2 and CO groups are conjugated at ω = 0°, the peptide delocalization is broken at ω = 90°, and the carbonyl group is unconjugated. At ω = 0° the peptide delocalization weakens the C=O bond and strengthens the C–N bond, thus making the A,B groups in the CH_3–CAB rotor (A = O, B = NH_2) more equivalent. In the N-methylformamide case at ω = 0 or 180°, the methyl hydrogens prefer to eclipse N–COH, which has partial double bond character, in analogy with propylene and acetaldehyde. As ω is changed to 90°, this double bond character is lost; thus, the NAB rotor has an A (nonconjugated COH) more like a B (H on N) than in the ω = 0° geometry, and the barrier decreases accordingly.

It is appropriate at this point to show that the information we have obtained so far concerning charges and barriers is consistent with a simple molecular orbital description of the peptide bond. The description derived below has some further important consequences for the spectral characteristics of nonplanar peptide units (considered in section 4).

Consider a carbonyl π system interacting with a lone pair on an adjacent amine group. In the absence of interaction or equivalently when the amine group is twisted 90° out of the plane of the carbonyl, the orbitals of the noninteracting systems are as shown at the left of Figure 8. In order of increasing energy these are: a π_{CO} orbital of the carbonyl group which, as a consequence of the greater electronegativity of oxygen, possesses a larger contribution of the oxygen 2p orbital; a lone pair of the carbonyl oxygen, n_O; a lone pair,

(48) E. Tannenbaum, R. J. Myers, and W. D. Gwinn, *J. Chem. Phys.*, 25, 42 (1956).

(49) W. M. Tolles, E. T. Handelman, and W. D. Gwinn, *ibid.*, 43, 3019 (1965).

(50) R. E. Naylor and E. B. Wilson, *ibid.*, 26, 1057 (1957).

(51) H. D. Rudolph and M. Seiler, *Z. Naturforsch.*, 20, 1682 (1965).

(52) E. Hirota, *J. Chem. Phys.*, 45, 1984 (1966).

(53) D. R. Lide and D. E. Mann, *ibid.*, 27, 868 (1957).

(54) R. W. Kilb, C. C. Lin, and E. B. Wilson, *ibid.*, 26, 1695 (1957).

assumed to be pure 2p, of nitrogen, n_N; a low-lying π^*_{CO} orbital of the carbonyl group which, in contrast to the π_{CO} level, is heavy at the carbon atom.

We then "turn on" the interaction between the carbonyl group and the amine or equivalently rotate the amine group into conjugation from its original perpendicular orientation. Perturbation theory is a powerful guide to the interaction of orbitals. As a result of interaction, the orbital energies and wave functions are modified as follows[55]

$$E_i = E_{i0} + \sum_{j \neq i} \frac{|H'_{ij}|^2}{E_{i0} - E_{j0}}$$

$$\psi_i = \psi_{i0} + \sum_{j \neq i} \frac{H_{ij}'\psi_j}{E_{i0} - E_{j0}}$$

The following set of qualitative rules emerges. (1) Orbital interactions are pairwise additive. (2) Energy levels "repel" each other. (3) The extent of interaction between two levels is approximately proportional to some function of their overlap and inversely proportional to their separation in energy. (4) The consequence of the interaction of two orbitals is a mixing of their wave functions in the following manner. The lower energy orbital mixes into itself the upper one in a bonding way, whereas the upper one mixes into itself the lower one in an antibonding manner. The extent of interaction is governed by the same factors as in (3) above.

Applying these guide lines to the case at hand, we obtain the energy shifts and delocalized wave functions shown at the right-hand side of Figure 8. These are justified in the following way. (1) π_{CO} is stabilized by interaction with n_N and mixes into itself the latter orbital in a bonding way. It becomes π_+, the lowest energy allylic orbital. (2) π^*_{CO} is destabilized by interaction with n_N and mixes into itself n_N in an antibonding way. It emerges as π_-. (3) n_O, lying in the nodal plane of the π orbitals, is (to first order) unaffected by the interaction. (4) n_N interacts with both π_{CO} and π^*_{CO}. It is difficult to weigh qualitatively the strength of the two interactions. After interaction n_N takes on the form

$$n'_N = \pi_0 = n_N + c_1\pi^*_{CO} - c_2\pi_{CO}$$

where c_1 and c_2 are the mixing coefficients. The computational methods which we have used disagree on the relative sizes of c_1 and c_2. The EHT calculations place the node in π_0 between C and O, implying $c_1 > c_2$; the CNDO/2 calculations (as well as the "*ab initio*" Gaussian computations[56]) put the node between C and N, implying $c_2 > c_1$. Both procedures agree in that n_N is stabilized as a consequence of interaction.

These qualitative arguments are confirmed in detail by examination of the calculated molecular orbitals, and the important consequences of the interaction are as follows. (1) There exists a sizable barrier to rotation of the amine group out of conjugation. This follows from the increase in energy of π_+ and π_0 as they become π_{CO} and n_N. (2) As the amine group rotates out of planarity there should be some electron transfer from the carbonyl group to the amine nitrogen. Thus, as the rotation occurs, C and O should become more positive and N more negative. This is a consequence of the strong interaction of n_N (donor) with π^*_{CO} (acceptor). On the rotated, unconjugated side, the two electrons in the n_N orbital are all on N while, in the planar, conjugated system, the two electrons in π_0 are mostly on N, but with a significant fraction in the carbonyl group.

(3) As the amine group rotates out of planarity, there should occur a significant red shift and intensity diminution of the $\pi_0 \rightarrow \pi_-$ electronic transition, the first intense band of a peptide group (1700–1950 Å). The energy shift follows from the motion of levels shown in Figure 8. The hypochromic effect follows from the transformation of a $\pi \rightarrow \pi^*$ transition in the planar form to essentially an intramolecular charge-transfer transition, $n_N \rightarrow \pi^*_{CO}$, in the rotated form. The weaker peptide transition, $n_0 \rightarrow \pi_-$, ~2200 Å, should also be shifted to lower energy on twisting, but less than the $\pi_0 \rightarrow \pi_-$ transition.

4. *Electronic Spectra.* Amides are characterized by two primary electronic transitions in the ultraviolet region. A weak transition, occurring at approximately 2200 Å, has been assigned to an $n \rightarrow \pi^*$ excitation, more specifically to $n_0 \rightarrow \pi_-$.[57,53] The intense vacuum ultraviolet transition of peptides is located in the region 1700–1950 Å, and has been assigned to the $\pi_0 \rightarrow \pi_-$ excitation.[57–59] More recently a new band has been observed between the two above-mentioned transitions and has been tentatively assigned to a $n \rightarrow \sigma^*$ excitation.[33]

In the previous section we have outlined the qualitative spectral changes we would expect in a twisted ($\omega \neq 0$ or 180°) peptide chromophore. The calculations confirm our qualitative conclusions. Figure 9 illustrates the one-electron energy gap for $n_0 \rightarrow \pi_-$ and $\pi_0 \rightarrow \pi_-$ excitations as a function of ω, as obtained from EHT calculations. Since these calculations do not include electron interaction explicitly they cannot provide accurate singlet and triplet state energies. The one-electron gap is at best considered as a configuration energy, the average of singlet and triplet states. This is the reason for the "incorrect" ordering of the $n_0 \rightarrow$

(55) J. N. Murrell, "The Theory of the Electronic Spectra of Organic Molecules," John Wiley & Sons, Inc., New York, N. Y., 1963.

(56) M. A. Robb and I. G. Csizmadia, *Theoret. Chim. Acta*, **10**, 269 (1968).

(57) H. D. Hunt and W. T. Simpson, *J. Amer. Chem. Soc.*, **75**, 4540 (1953).

(58) E. E. Barnes and W. T. Simpson, *J. Chem. Phys.*, **39**, 670 (1963).

(59) D. L. Peterson and W. T. Simpson, *J. Amer. Chem. Soc.*, **77**, 3929 (1955); **79**, 2375 (1957).

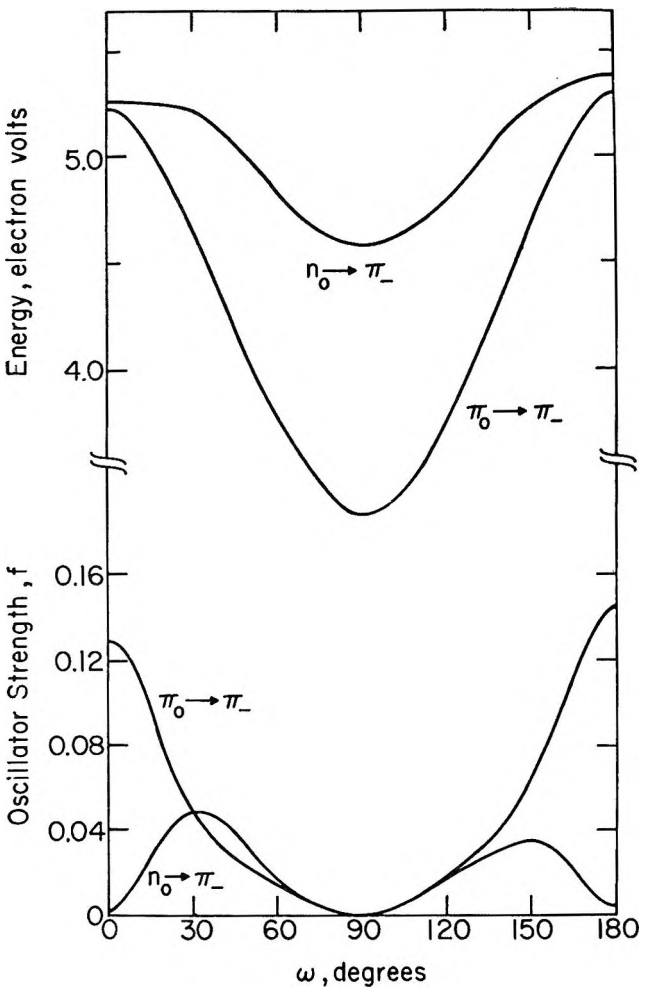

Figure 9. Computed dependence on ω of energies and oscillator strengths for $n_0 \rightarrow \pi_-$ and $\pi_0 \rightarrow \pi_-$ transitions in N-methylacetamide.

π_- and $\pi_0 \rightarrow \pi_-$ transition in Figures 8 and 9. However, *trends* in this configuration energy are, from our experience, reliable indicators of spectral shifts. Figure 9 also shows for the two transitions the calculated oscillator strengths,[60] which are proportional to the intensities of the electronic transition.

The important conclusions are as follows. Both (n,π^*) and (π,π^*) peptide transitions should be red shifted on twisting out of planarity. The effect should be more extreme for the (π,π^*) transition, and so it is likely that, at a certain angle of twist, the two bands might cross. The intensity of the (π,π^*) band should diminish sharply with twisting. The computed intensity of the (n,π^*) band has maxima around $\omega = 30$ and 150°. The latter behavior was not anticipated by our simple argument and remains to be tested experimentally.

There appear to be no proper model compounds, *i.e.*, peptides with ω deviating significantly from 0 or 180°, to test these predictions. One can devise sterically hindered molecules for this purpose, *e.g.*, derivatives of N,N-dimethylacetamide in which all three

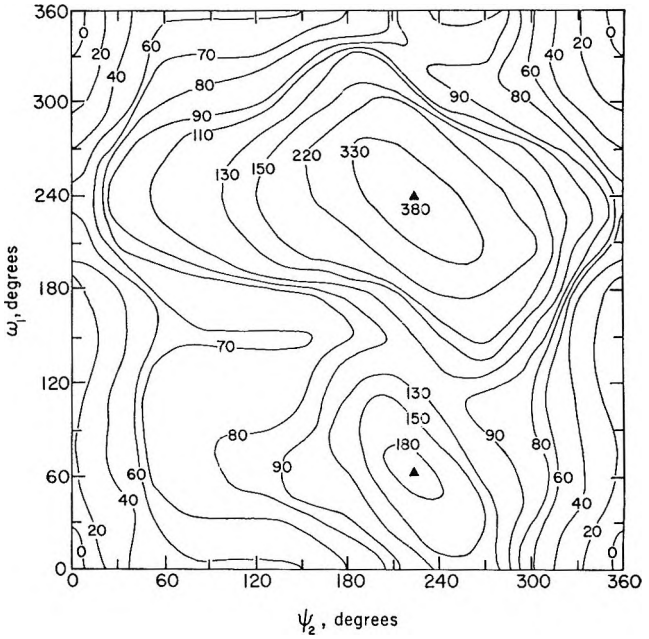

Figure 10. Conformational energy contour diagram (EHT) of acetyl-L-prolineamide for $\psi_1 = \omega_2 = 0°$ at all values of ψ_2 and ω_1. The energies are in units of kilocalories per mole relative to zero around $\psi_2 = \omega_1 = 0°$. The solid triangles refer to maxima in the energy surface.

methyl groups have bulky groups attached to them. The synthesis of some appropriate derivatives is planned in this laboratory.

5. *Acetyl-L-prolineamide.* Since poly-L-proline undergoes a *cis–trans* interconversion,[61] whereas polyamino acids having amide groups with an unsubstituted NH do not, it was of interest to see if the peptide bond in a model proline compound, acetyl-L-prolineamide, differed from that in, say, N-methylacetamide.

The charges of acetyl-L-prolineamide are shown in Figure 3. As in the case of the other N-methyl compounds of Figures 1 and 2, the charges on carbons attached to the proline nitrogen are positive. The other two carbons in the proline ring are slightly negative, as was observed in previous calculations[16] on hydrocarbons.

An energy contour map of ω_1 *vs.* ψ_2, computed at 30° intervals in both angles, using the EHT method, is shown in Figure 10. The large steric hindrances in this molecule lead to very high energies in most of the ψ–ω map. Also, in contrast to the other molecules considered here, the energy function for rotation about the peptide bond is very asymmetric, as illustrated in Figure 11.

From Figure 10, it can be seen, first of all, that, at

(60) These are computed correctly, *i.e.*, with all two-center terms included. We would like to thank J. Howell for making his transition moment program available to us. In Figure 9, the oscillator strength,[55] *f*, has been computed using the calculated transition energies.

(61) I. Z. Steinberg, W. F. Harrington, A. Berger, M. Sela, and E. Katchalski, *J. Amer. Chem. Soc.*, 82, 5263 (1960).

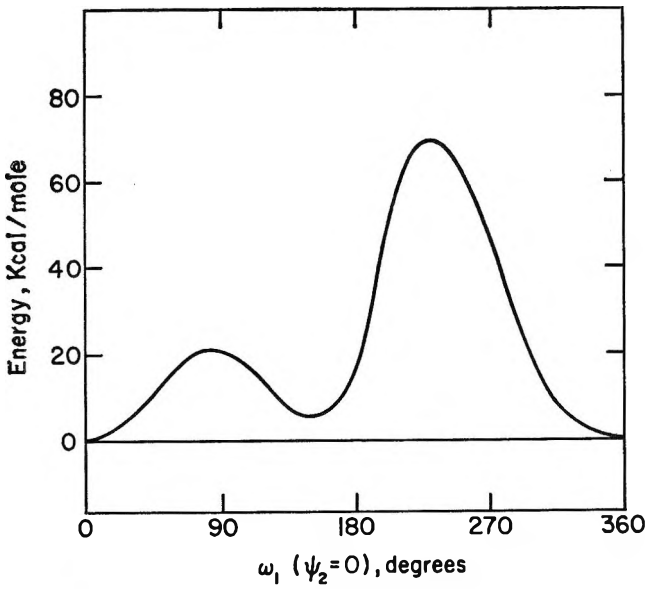

Figure 11. Variation of energy of acetyl-L-prolineamide with ω_1 at $\psi_2 = 0°$ (taken from the data of Figure 10).

$\omega_1 = 0°$ (*trans*), the energy rises rapidly as ψ_2 increases from 0 to 60° and then levels off between $\psi_2 = 60$ and 150°; these high energies are probably the result of interactions between the amine hydrogens and the C^β hydrogens. The very high energy between $\psi_2 = 240$ and 270° (at $\omega_1 = 0°$) arises primarily from interactions between the amine hydrogens and the acetyl oxygen; this bad contact can be relieved somewhat by varying ω from 0 to *ca.* −30°. Thus, for $\omega = 0°$, the range of low-energy values of ψ_2 is very small. A second point of interest in Figure 10 is that the low-energy *cis* conformation (at $\psi_2 = 0°$) lies near $\omega_1 = 150°$ rather than at $\omega_1 = 180°$ (see also Figure 11); *i.e.*, the stable *cis* conformation should be nonplanar. Planarity could be achieved (*i.e.*, the minimum-energy *cis* conformation could be brought to 180°) by changing some bond angles. Available experimental evidence[62,63] indicates that both conditions exist, *i.e.*, some variation in bond angles from "normal" values and also some departure from planarity of the amide group. As in the case of the *trans* conformation, the low-energy path for variation of ψ_2, for the *cis*-amide (*i.e.*, starting from $\omega_1 = 150°$), would involve some variation in ω_1, *viz.*, from $\omega_1 = 150$ to 120° as ψ_2 increases beyond $\sim 210°$.

The activation energy for the *cis–trans* interconversion in poly-L-proline has been found[61,64] to be 20–23 kcal/mol. While the detailed mechanism for this interconversion is not known, it is of interest to consider the activation energy for the reversible thermal *cis–trans* interconversion. Our calculations serve as a model for the latter process. Figure 11 shows the computed energy profile as ω_1 is varied at $\psi_2 = 0°$. The numerical value of the barrier between $\psi_2 = 0$ and 150° is 22.4 kcal/mol which is similar to those of amides with unsubstituted NH groups. Even though the values of $\Delta E_{cis-trans}$ (5.3 and 1.2 kcal/mol by the EHT and CNDO/2 procedures, respectively) are somewhat greater than for N-methylacetamide, poly-L-proline undergoes the *cis–trans* interconversion whereas polyamino acids with unsubstituted NH groups do not. Until we know the mechanism of the *cis–trans* interconversion, and whether stable conformations exist for *cis*-peptides, we cannot account for the difference in behavior between proline and other peptides. Calculations on prolylproline and other dipeptides in the *cis* and *trans* forms, as well as the influence of nonplanarity of the proline ring, are in progress.

Another important feature of Figure 11 is that the barriers between the *trans* (0°) and *cis* (150°) forms differ according to the path; *i.e.*, at $\psi_2 = 0°$, the *cis–trans* conversion would appear to follow a path $\omega_1 = 150°_{min} \rightarrow 90°_{max} \rightarrow 0°_{min}$ rather than the path $\omega_1 = 150°_{min} \rightarrow 240°_{max} \rightarrow 360°_{min}$. According to Figure 10, ψ_2 would probably remain at 0° as ω_1 varies, for the *fixed geometry* used in the calculation of Figures 10 and 11.

A few points on the ψ–ω energy contour diagram of acetyl-L-prolineamide were computed by the CNDO/2 method. The *cis* conformation occurs at 180° and, in general, the barriers due to nonbonded interactions (steric effects) are lower than those found by the EHT procedure.

The availability of these results for acetyl-L-prolineamide, *i.e.*, the accessibility of conformations with nonplanar amide groups, may help rationalize theoretical and experimental results on the optical rotatory properties[65] of this molecule.

Acknowledgments. We wish to thank Mrs. K. Kashuba and Mrs. S. Rosen for invaluable help with the computer programs, and the Cornell Office of Computer Services for use of their facilities.

(62) G. N. Ramachandran and C. M. Venkatachalam, *Biopolymers*, **6**, 1255 (1968).

(63) G. N. Ramachandran, *ibid.*, **6**, 1494 (1968).

(64) A. R. Downie and A. A. Randall, *Trans. Faraday Soc.*, **55**, 2132 (1959).

(65) J. A. Schellman and E. B. Nielsen, "Conformations of Biopolymers," G. N. Ramachandran, Ed., Vol. 1, Academic Press, London, 1967, p 109.

The Stereochemistry of Energetic Chlorine Atom Exchange in Alkyl Halides[1]

by Chien M. Wai and F. S. Rowland

Department of Chemistry, University of California, Irvine, California 92664 *(Received May 9, 1969)*

Energetic chlorine atoms produced in nuclear recoil substitute for Cl atoms in either *meso*- or *dl*-2,3-dichlorobutane with almost complete ($\geq 93\%$) retention of configuration at the asymmetric centers in the gas phase. The same result is obtained for hot chlorine atoms from the nuclear reactions $^{37}Cl(n,\gamma)^{38}Cl$ and $^{40}Ar(\gamma,p)^{39}Cl$.

Introduction

Energetic chlorine atoms are able to replace Cl atoms in alkyl chlorides, both in the gaseous and condensed phases.[2-11] In the present experiments, we have focused our attention on the stereochemistry of the substitution process at an asymmetric carbon atom in an effort toward better understanding of the mechanism of the energetic substitution process. The major experimental difficulty involved in stereochemical experiments with molecules possessing only one asymmetric center is the problem of complete resolution of a racemic mixture into its pure *d*- and *l*- forms. In our case, an additional restriction arises from the relatively short half-lives (<1 hr) of the radioactive chlorine atoms used in these experiments, and eliminates the possibility of complicated multistep chemical processes for the resolution of optical isomers. Our experiments have, therefore, utilized molecules containing two asymmetric centers, the *dl* and *meso* forms of 2,3-dichlorobutane (DCB). These two molecules, differing appreciably in both boiling point and dipole moment, can be readily separated by gas chromatography.[3,5]

The chlorine atoms in our experiments have attained their excess energy through recoil accompanying their formation in the nuclear reactions $^{37}Cl(n,\gamma)^{38}Cl$ or $^{40}Ar(\gamma,p)^{39}Cl$. All of the experimental evidence to date concerning the reactions of these energetic species with alkyl halides is consistent with their interpretation as chemical reactions initiated by neutral chlorine atoms in the electronic ground state, but possessing excess kinetic energy.[4-11] The chemical reactions under study are therefore the isotopic exchange reactions summarized in eq 1 for ^{38}Cl, and the equivalent reactions for ^{39}Cl.

$$^{38}Cl^* + \textit{meso}\text{- or } \textit{dl}\text{-}CH_3CHClCHClCH_3 \longrightarrow \textit{meso}\text{- or } \textit{dl}\text{-}CH_3CH^{38}ClCHClCH_3 + Cl \quad (1)$$

Experimental Section

Chemicals. The *dl* and *meso* forms of 2,3-DCB were prepared in >95% purity by low-temperature stereospecific addition of Cl_2 to *trans*- and *cis*-2-butene, respectively,[12] and then purified by gas chromatography. The actual limitation on purity is set, not by the initial impurity level after preparative gas chromatography, but by the radiation chemical formation of the "opposite" stereoisomer from all radiation (neutron, gamma, etc.) present during the thermal neutron irradiation of the samples. The measured macroscopic fraction of the "opposite" isomer was always less than the fraction of chlorine radioactivity found in that isomeric form, indicating that the radioactivity observed in the form of the inversion product could *not* arise solely from radiation chemical damage to the radioactive, stereochemically pure parent isomer. However, thermal reaction mechanisms of thermalized radiochlorine atoms—such as the reaction suppressed by 1,3-butadiene, as discussed below—could account for all or part of the higher specific activities found for the inversion products.

Experimental Techniques. The details of sample preparation, irradiation, and radio gas chromatographic analysis are adequately described elsewhere, and are essentially unchanged from these previous descriptions.[6,10,13] A typical radio gas chromatogram, taken on a 15-ft tritolylphosphate column with ^{39}Cl radioactivity, is shown in Figure 1. The recorded activities are then corrected for the decay of the particular

(1) This research was supported by AEC Contract No. AT-(11-1)-34, Agreement No. 126, and constituted part of the thesis submitted by C. M. Wai in partial fulfillment of the requirements for the Ph.D. degree at the University of California, Irvine.

(2) J. E. Willard, "Chemical Effects of Nuclear Transformations," Vol. 2, International Atomic Energy Agency, Vienna, 1965, p 221.

(3) F. S. Rowland, C. M. Wai, C. T. Ting, and G. Miller, "Chemical Effects of Nuclear Transformations," Vol. 2, International Atomic Energy Agency, Vienna, 1965, p 333.

(4) R. Wolfgang, *Progr. Reaction Kinetics*, **3**, 97 (1965).

(5) C. M. Wai and F. S. Rowland, *J. Phys. Chem.*, **71**, 2752 (1967).

(6) C. M. Wai and F. S. Rowland, *J. Amer. Chem. Soc.*, **90**, 3638 (1968).

(7) C. M. Wai and F. S. Rowland, *J. Phys. Chem.*, **72**, 3049 (1968).

(8) L. Spicer and R. Wolfgang, *J. Amer. Chem. Soc.*, **90**, 2426 (1968).

(9) C. M. Wai and F. S. Rowland, *ibid.*, **91**, 1053 (1969).

(10) C. M. Wai, Ph.D. Thesis, University of California, Irvine, 1967.

(11) L. Spicer, Ph.D. Thesis, Yale University, 1968.

(12) H. J. Lucas and C. W. Gould, Jr., *J. Amer. Chem. Soc.*, **63**, 2541 (1941).

(13) J. K. Lee, E. K. C. Lee, B. Musgrave, Y.-N. Tang, J. W. Root, and F. S. Rowland, *Anal. Chem.*, **34**, 741 (1962).

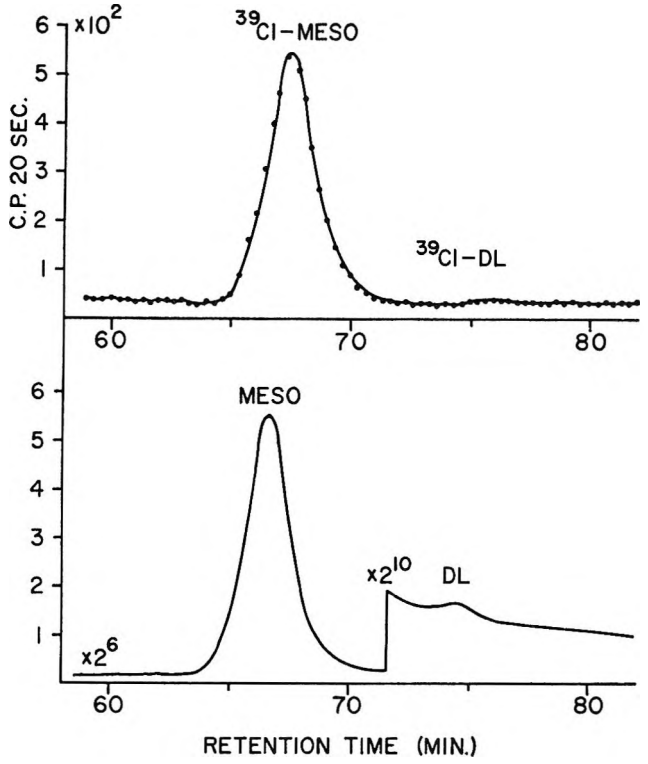

Figure 1. Gas chromatographic records of *meso*- and *dl*-2,3-dichlorobutane peaks from the reactions of energetic ^{39}Cl with *meso*-2,3-dichlorobutane in the gas phase. Upper trace, ^{39}Cl radioactivity; lower trace, thermal conductivity.

isotope during the time between chromatographic peaks.[14]

The chief experimental problem is the low total radioactivity of labeled 2,3-DCB in gas-phase experiments with the pure molecules. This difficulty arises from two factors—the low vapor pressure of the target molecule (about 1.8 cm in room temperature irradiations) and the low absolute percentage yield (<1%) of the isotopically labeled 2,3-DCB as a product of energetic Cl atom reactions. Accurate measurements therefore require high specific radioactivities. For experiments involving the $(n,\gamma)^{38}Cl$ process, the gas samples were irradiated in the core of a nuclear reactor at a neutron flux of 8×10^{12} n/cm² sec. At high total neutron dosages, the amounts of radiation damage are correspondingly higher than in other ^{38}Cl experiments, and macroscopic amounts of radiation products were observed, roughly totalling 5–10% of the original parent material. Under such conditions, radical reactions become a serious side effect, with possibilities for perturbation of the primary hot atom yields. Several radical scavengers were used in these experiments, including Cl_2, NO, O_2, ethylene, isobutene, 1,3-butadiene, and some combinations of these. Butadiene was the most effective scavenger for this system, and prevented the formation (perhaps by diversion into higher molecular weight products) of most of the low molecular weight radiation damage products.

Experiments involving ^{39}Cl were not so limited in the number of target atoms (Ar) as for ^{38}Cl, for which the target atoms were Cl atoms in the parent compound, but of course involve the formation and study of the reactions of ^{39}Cl in the presence of large excesses of argon, a good moderator for the kinetic energy of the chlorine atom. Radiation damage was much less (<1%) than in the ^{38}Cl experiments; the close agreement between the results obtained with both isotopes suggests that subsequent radiation chemical effects in the ^{38}Cl experiments did not seriously perturb the original distribution from hot reactions.

The absolute yields of ^{38}Cl-labeled products were evaluated in comparison to an internal monitor, the nuclear reaction $^{40}Ar(n,\gamma)^{41}Ar$. The sum of all observed volatile radioactive products in the butadiene-scavenged system accounted for approximately 3 ± 1% of the total ^{38}Cl formed, with the observations usually being stopped soon after the emergence of the *dl*-DCB peak. The *meso* and *dl* forms of the target molecule contained about one-tenth of the observed radioactive products, or about 0.3 ± 0.1% of the total ^{38}Cl formed in the system. No measurements of absolute yield were performed with ^{39}Cl experiments, but the absolute yields of ^{38}Cl and ^{39}Cl species in reactions with CH_3Cl have been shown to be the same within the accuracy of the measurements.[6,8,10,11]

Upper Limits for the Failure of Bond Rupture During the $^{37}Cl(n,\gamma)^{38}Cl$ Process. The occurrence of multiple emission of γ radiation with a fortuitous near-cancellation of the momentum vectors is a possible minor process for (n,γ) reactions, and could result in such low recoil energy for the ^{38}Cl atom that it failed to break its original C–^{37}Cl bond. Such processes are not of great concern in the current experiments, since essentially identical results were obtained for ^{39}Cl atoms, whose chemical form prior to the nuclear event was that of monatomic ^{40}Ar. However, limits on possible failure to bond rupture are of interest for ^{38}Cl reactions in general. Gordus and Hsiung have experimentally measured limits in the range 0.1–1.0% for the (n,γ) reaction in various bromides and iodides,[15] but no experiments with ^{38}Cl have been reported. The results from such experiments with *meso*-2,3-DCB are shown in Table I. The yield of labeled 2,3-DCB decreased by a factor of 10–15 in the presence of 76 cm scavenger relative to the yield with 1 cm of scavenger, although failure of rupture of the original bond would be unaffected by the amount of scavenger present. If the residual activity observed in the presence of one atmosphere pressure of scavenger is assumed to be the result of failure to bond rupture in the original process, then the upper limit for the process is about 0.02 ± 0.01%. This is probably an overestimate, since there is no

(14) Half-lives: ^{38}Cl, $t_{1/2}$ = 37.3 min; ^{39}Cl, $t_{1/2}$ = 56 min.

(15) A. A. Gordus and C. Hsiung, *J. Chem. Phys.*, 36, 954 (1962).

Table I: Absolute Yield of *meso*-$CH_3CH^{38}ClCHClCH_3$ from Reactions of Energetic ^{38}Cl with *meso*-2,3-Dichlorobutane As a Function of Scavenger Pressure

	Sample pressure (cm)		
meso-2,3-DCB	1.5	1.5	1.5
1,3-Butadiene	1.0	76	...
Ethylene	...	...	70
	Specific activity[a]		
^{38}Cl-*meso*-2,3-DCB	900 ± 50	65 ± 10	85 ± 10
^{38}Cl-*dl*/^{38}Cl-*meso*	~0.03	...	...
Approximate absolute yield, DCB	0.3%	0.02%	0.03%

[a] Expressed in counts/arbitrary mass unit; all samples were irradiated at 8×10^{12}/n/cm²/sec for 3 min.

experimental reason to believe that further increases in scavenger would not be accompanied by still further reductions in the yield of the labeled parent molecule.

Results and Discussion

Choice of Free Radical Scavenger. When either *meso*- or *dl*-2,3-DCB is neutron irradiated with no other additives present, ^{38}Cl is found in both diastereomers. The radioactivity ratios are not the same from the two parent molecules with each showing a preference for the formation of the labeled parent molecule: the ratio of *meso*-2,3-^{38}Cl,Cl-DCB/*dl*-2,3-^{38}Cl,Cl-DCB from the *dl* target was about 0.30, while the *dl*/*meso* radioactivity ratio from the *meso* target was about 0.18. These observations in unscavenged vapor samples suggested that radical reactions might possibly be involved in the formation of both diastereomers, with some preference for the formation of the more stable *meso* form. Various scavengers were tried, as shown in Tables II and III, in an effort to suppress radical reactions leading to the formation of the labeled 2,3-dichlorobutane molecules. The most successful scavenger in these systems was 1,3-butadiene.

Table II: Relative Yield of *meso*- and *dl*-$CH_3CH^{38}ClCHClCH_3$ from Energetic ^{38}Cl Reactions with Gaseous 2,3-Dichlorobutane in 1,3-Butadiene Scavenged Systems

Target molecule: *dl*-2,3-dichlorobutane

Sample pressure, cm				Product ratio
dl-2,3-DCB	1,3-Butadiene	Ar	Xe	^{38}Cl-*meso*/^{38}Cl-*dl*
1.4	...	...	...	0.35 ± 0.03
1.4	1.0	...	...	0.06 ± 0.02
1.4	1.0	30	...	0.07 ± 0.02
1.4	1.0	...	28	0.06 ± 0.02

Target molecule: *meso*-2,3-dichlorobutane

Sample pressure, cm				Product ratio
meso-2,3-DCB	1,3-Butadiene	Ar	Xe	^{38}Cl-*dl*/^{38}Cl-*meso*
1.5	...	...	...	0.18 ± 0.02
1.5	1.0	...	...	0.05 ± 0.02
1.5	1.0	30	...	0.03 ± 0.01
1.5	1.0	...	31	0.03 ± 0.01

Table III: Effects of Additives on the Relative Yields of *meso*- and *dl*-$CH_3CH^{38}ClCHClCH_3$ from Gas-Phase Reactions of Energetic ^{38}Cl with 2,3-Dichlorobutane

Target molecule: *dl*-2,3-DCB (1.4 cm pressure)

Sample pressures of additives, cm				
O_2	C_2H_4	Ar	Xe	^{38}Cl-*meso*/^{38}Cl-*dl*
2	0	0	0	0.55 ± 0.10
2	0.5	0	0	0.60 ± 0.05
2	0.5	*cis*-CHCl=CHCl		0.56 ± 0.05
2	0	19	0	2.5 ± 0.2
2.2	0	0	17	2.1 ± 0.1
2.0	0.5	17	0	1.44 ± 0.10
2.0	0.5	0	7	0.99 ± 0.05
2.2	0.5	0	17	1.37 ± 0.10
2.0	0.5	0	27	1.45 ± 0.05
2.0	0.5	0	55	1.82 ± 0.15
2.2	1.0	0	17	1.15 ± 0.10
2.2	2.2	0	14	0.87 ± 0.10
2.4	2.1	14	0	0.91 ± 0.09

Target molecule: *meso*-2,3-DCB (1.5 cm pressure)

Sample pressure of additives, cm				
O_2	C_2H_4	Ar	Xe	^{38}Cl-*dl*/^{38}Cl-*meso*
2.0	0	0	0	0.10 ± 0.03
2.0	0.5	0	0	0.13 ± 0.03
2.0	0.5	0	16	0.21 ± 0.05
2.0	0.5	0	55	0.32 ± 0.05
2.0	0.5	16	0	0.24 ± 0.05
2.0	1.0	0	16	0.23 ± 0.05
2.0	2.1	0	14	0.24 ± 0.05

In the presence of O_2 as a scavenger, relatively more ^{38}Cl-*meso* compound was formed than with the pure molecules, while the further addition of ethylene (or dichloroethylene) had little effect on the ratio of labeled diastereomers. The addition of either argon or xenon progressively changes the ratios toward an equilibrium value of 2.5–3.0 for *meso*/*dl* favoring the stabler *meso* by an amount reasonable for room temperature equilibrium between the two diastereomers.[16] The inclusion of ethylene in argon- or xenon-moderated samples altered the *meso*/*dl* ratio from that observed in its absence, but still indicated substantial quantities of both labeled stereoisomers as present.

All of these results shown in Table III are consistent with the presence in the system of two mechanisms of formation for ^{38}Cl-labeled dichlorobutanes—a direct mechanism favoring the formation of the parent compound, and a second mechanism tending to form the two isomers in a near-equilibrium ratio. This second mechanism is most probably a free radical combination mechanism that is not sensitive to suppression by O_2 and/or C_2H_4. We have not attempted further studies

(16) A *meso*/*dl* ratio of 2.5 is obtained in photochlorination experiments involving radical chains. P. S. Fredrick and J. M. Tedder, *J. Chem. Soc.*, 3520 (1961).

of this second mechanism, but speculate that it involves the reactions of thermal ^{38}Cl atoms with radicals. The reaction of Cl atoms with ethylene and chloroethylenes has been shown to be reversible on a rapid time scale,[17,18] while the formation and decomposition of ClO_2 may also be sufficiently fast that thermal Cl atoms are not rapidly removed by reaction with O_2. One would expect rapid reaction of alkyl or chloroalkyl radicals with O_2, but such oxygenated radicals may yet be able to react with thermalized Cl atoms.

The introduction of 1,3-butadiene effects a very marked change in the diastereomeric distribution of ^{38}Cl, as indicated in Table II, almost eliminating the formation of the radioactive nonparent isomer. The success of 1,3-butadiene in eliminating the second, free radical mechanism for the formation of the labeled diastereomers is of course of uncertain origin, since that mechanism itself is unknown, but very probably the low activation energy for radical addition to 1,3-butadiene is the critical factor.[19] In any event, the substitution of ^{38}Cl for Cl in 2,3-DCB proceeds almost entirely with retention of configuration in the presence of 1,3-butadiene.

Experiments with ^{39}Cl. Gas-phase experiments were also carried out using energetic chlorine atoms formed by the $^{40}Ar(\gamma,p)^{39}Cl$ reaction, giving the results summarized in Table IV. The ratios of diastereomeric products in the argon-moderated experiments of Tables II and IV are essentially the same for both ^{38}Cl and ^{39}Cl for samples of equivalent composition.

Table IV: Relative Yield of *meso*- and *dl*-$CH_3CH^{39}ClCHClCH_3$ from Reactions of Energetic ^{39}Cl with Gaseous 2,3-Dichlorobutane

Target molecule: *dl*-2,3-dichlorobutane

Sample pressure, cm			Product ratio
dl-2,3-DCB	1,3-butadiene	Ar	^{39}Cl-*meso*/^{39}Cl-*dl*
1.5	none	30	0.50 ± 0.05
1.5	1.0	30	0.03 ± 0.01

Target molecule: *meso*-2,3-dichlorobutane

Sample pressure, cm			Product ratio
meso-2,3-DCB	1,3-butadiene	Ar	^{39}Cl-*dl*/^{39}Cl-*meso*
1.5	none	30	0.30 ± 0.05
1.5	1.0	30	0.02 ± 0.01

Nature of the Reacting Chlorine Species. Energetic chlorine atoms could be created by nuclear reactions in ionic or excited neutral states, and can readily be transformed into either form as well during subsequent collisions. The great similarity in chemical reaction patterns despite the great differences in the nuclear reactions involved in the formation of ^{38}Cl and ^{39}Cl supports the contention that the reacting chlorine atoms have equilibrated with their surroundings, and are in the same chemical form. The reactive behavior in the presence of xenon and argon is consistent with the moderation of excess kinetic energy of the hot chlorine atoms, as previously shown for the hot isotopic exchange of ^{38}Cl and ^{39}Cl into CH_3Cl.[6]

A possible source of labeled chlorine species in low yield might be the reactions of positively charged ions. Since the ionization potential of Cl (13.01 eV) lies between those of Ar (15.76 eV) and Xe (12.13 eV), samples moderated in these two gases would be expected to exhibit different yield patterns for ionic Cl species, either quantitatively or qualitatively. Since no significant difference was observed between Ar and Xe moderated samples, we conclude that charged Cl species are not appreciably involved in the formation of the substitution products under study.

Observations of the Labeled Inversion Product. Both Tables II and IV indicate that retention of configuration during substitution of energetic Cl-for-Cl is the predominant ($\geq 93\%$) mode of reaction. Nevertheless, a small yield is always found of the radioactive inversion product, in amounts larger than can be accounted for simply through radiation chemical alteration of the parent molecule. These may be genuine yields from an energetic substitution-with-inversion process. However, since they represent approximately 0.01% (.05 × 0.3% absolute yield) of the total ^{38}Cl or ^{39}Cl formed in these systems, no definite conclusions concerning the mechanism for its formation can be reached without extensive further study of radiation damage effects, the free radical mechanism for formation of DCB, etc.

Mechanism for Retention of Configuration. The observation of particular labeled products in gas-phase experiments signifies both that a mechanism for the formation of the particular product exists, and also that this mechanism leaves the product molecule with an excitation energy insufficiently large for secondary reactions to occur under the conditions of the experiment. Studies of the substitution of ^{18}F-for-F[20] and of ^{38}Cl-for-Cl[21] in other molecules have both shown very high levels of excitation in the product molecules, sufficient to cause extensive decomposition with some halomethane molecules. The low vapor pressure of the 2,3-dichlorobutane molecules makes similar studies very difficult, and therefore no information is available concerning the excitation left in the Cl-labeled diastereomers. The mechanism of substitution under discussion is thus the substitution of Cl-for-Cl with

(17) D. C. Tardy and B. S. Rabinovitch, *Trans. Faraday Soc.*, **64**, 1844 (1968).

(18) J. Franklin, P. Goldfinger, and G. Huybrechts, *Ber. Bunsenges.*, **72**, 173 (1968).

(19) $E_{act} \sim 2.5$ kcal/mol. E. W. R. Steacie, "Atomic and Free Radical Reactions," Reinhold Publishing Company, New York, N. Y., 1954.

(20) Y.-N. Tang, T. Smail, and F. S. Rowland, *J. Amer. Chem. Soc.*, in press.

(21) Unpublished experiments by Y.-N. Tang and F. S. Rowland, and by Y.-N. Tang and colleagues.

retention of configuration, *and* with product excitation less than about 4 or 5 eV. The experiments do not furnish any information about the possible existence of gas-phase primary retention *or inversion* reactions which are accompanied by product excitation energies in the >6 eV range.

Energetic substitution with retention of configuration need not be accompanied by extensive motion or adjustment among the other substituent groups, and presumably proceeds by a direct replacement process on a time scale comparable to molecular transit times for energetic chlorine atoms, estimated to be about 10^{-13} to 10^{-14} sec.[22] Analogous observations of retention of configuration during T-for-H substitution have been reported for several experiments with energetic tritium atoms from nuclear recoil.[23-26] The almost complete absence of the inversion product in gas-phase experiments with energetic chlorine atoms implies either that the motions of the substituent groups required for the inversion process take too much time for completion while the hot Cl atom is available for bonding, or else these rapid motions involve so much vibrational excitation energy that the molecules thus formed undergo secondary decomposition within 10^{-10} sec, and hence are not experimentally observed in the gas phase. In effect, the present experiments suggest that the minimum excitation energy for substitution-with-retention is lower than that for substitution-with-inversion; the latter process may well not exist in the gas phase.

Comparison with Liquid Phase Results. We have earlier reported the results of similar experiments involving neutron irradiation of both *meso-* and *dl*-DCB in the liquid phase at room temperature and lower, and in the solid phase.[3] There are two chief differences between the gaseous and condensed phase results: (a) the absolute yield of ^{38}Cl-DCB is roughly a factor of 10 higher in the condensed phases than in the gas phase and (b) appreciable amounts of both diastereomers (28–50% inversion product) were observed from both parent molecules under all experimental conditions. Three factors which can readily enhance the condensed phase ^{38}Cl yields are (1) enhanced collision frequency in the liquid phase, thereby stabilizing excited molecules which decompose under gas-phase conditions; (2) relaxation in the presence of near-neighbor molecules of the energy and momentum requirements of the gas-phase reactions, thus permitting higher direct substitution yields in the condensed phases, and (3) the existence of a cage effect[27,2-4] which may hold reaction partners in close proximity within a solvent cage, *e.g.*, a hot ^{38}Cl atom in the immediate vicinity of a chloro-*sec*-butyl radical produced by the collision of the energetic chlorine atom with a DCB molecule. The ^{38}Cl atom can then become thermalized by further collisions with the solvent molecules (the "cage wall") and finally recombine with the radical still held in the cage. Such a process involves only the few molecules in the immediate solvent layer and will not be affected by normal concentrations of scavenger molecules.

The relative yields of the inversion and retention forms of ^{38}Cl-DCB is about 3:7 for both parent molecules in the liquid phase at 20°,[3] a ratio not affected by the addition of scavengers such as diphenylpicrylhydrazyl or molecular iodine. These results suggest that an additional atom–radical reaction is taking place in the liquid phase responsible for the formation of the opposite diastereomer, with a yield sufficiently large that the direct substitution process is no longer the major source of ^{37}Cl-labeled DCB. Szwarc has estimated the time scale for the cage recombination of acetate radical in isooctane at 65° to be 10^{-7} to 10^{-10} sec,[28] and such a time estimate should be crudely applicable for the combination of ^{38}Cl atoms with chloro-*sec*-butyl radicals. The observation of appreciable inversion product in amounts varying with the temperature of the liquid suggests that the atom–radical combination time is comparable to the time for racemization of the original stereospecificity of chloro-*sec*-butyl radicals. The increasing yield of the inversion product at lower temperatures is consistent with a slightly higher activation energy for the combination process than for the racemization process. An activation energy for racemization of the iodo-*sec*-butyl radical has been calculated as 3.5 kcal/mol[29] while that for thermal diffusion in CCl_4 has been measured as 3.3 kcal/mol.[30] While it is certainly not clear that bulk diffusion measurements should be directly applicable to cage processes, it is plausible that both the combination and racemization processes in our system have activation energies in the 2–4 kcal/mol range, with a slightly higher value for the former. Additional experimentation will be required to subject such a hypothesis to a more quantitative test.

Possible contributions from the other two postulated phase effects—increased stabilization and altered physical restrictions—cannot be confirmed or eliminated in the presence of the dominant mechanism of atom–radical combination.

Acknowledgment. The 2,3-dichlorobutane molecules were prepared by Mr. C. T. Ting.

(22) The velocity of a 5-eV chlorine atom is 5×10^{13} Å/sec.

(23) F. S. Rowland, C. N. Turton, and R. Wolfgang, *J. Amer. Chem. Soc.*, **78**, 2354 (1956).

(24) H. Keller and F. S. Rowland, *J. Phys. Chem.*, **62**, 1373 (1958).

(25) J. G. Kay, R. P. Malsan, and F. S. Rowland, *J. Amer. Chem. Soc.*, **81**, 5050 (1959).

(26) M. Henchman and R. Wolfgang, *ibid.*, **83**, 2991 (1961).

(27) J. Franck and E. Rabinowitch, *Trans. Faraday Soc.*, **30**, 120 (1934).

(28) L. Herk, M. Feld, and M. Szwarc, *J. Amer. Chem. Soc.*, **83**, 2998 (1961).

(29) S. W. Benson, K. W. Egger, and D. M. Golden, *ibid.*, **87**, 468 (1965).

(30) H. Watts, B. J. Alder, and J. H. Hildebrand, *J. Chem. Phys.*, **23**, 659 (1955).

Recoil Tritium Reactions with 1-Butene and 1-Butene-1,1-d_2 in the Gas Phase[1]

by Edward K. C. Lee and F. S. Rowland

Department of Chemistry, University of California, Irvine, California 92664 *(Received May 5, 1969)*

Energetic tritium atoms have been treated with 1-butene and 1-butene-1,1-d_2 over a range of pressures, and in competition with *n*-butane. The primary mechanisms of formation of ethylene and propylene from 1-butene are demonstrated by isotopic labeling to be, as expected, the decomposition of excited *n*-butyl and *sec*-butyl radicals formed in the addition of tritium to the olefinic positions. In each case, a lesser mechanistic route also exists to the formation of the smaller olefins. The decomposition of both excited butyl radicals is pressure dependent, with a larger effect for *sec*-butyl radical indicative of its formation by lower energy tritium atoms. An isotope effect in the yield of propylene from *sec*-butyl-*t** is found, favoring lesser decomposition of the radical formed by terminal addition to $=CD_2$ than to $=CH_2$. The formation of $CH_2{=}CHT$ from $T^* + CH_3CH_2CH{=}CD_2$ is attributed to high excitation energy decomposition of 1-butene-*t*. The tritium-labeled parent molecules formed by substitution of T-for-H show pressure-dependent yields for both butenes and for *n*-butane-*t*. The yield of T-for-CH_3 per position is probably higher for CH_3 in 1-butene than CH_3 in *n*-butane. Detailed comparison of product yields in mixtures with those from single-component systems indicates competition between abstraction and addition in the 1–3 eV range.

Introduction

Earlier studies of the reactions of recoil tritium atoms with the isomeric butene hydrocarbons have shown that the chief reactions occurring in these systems are those given in (1) to (4), as written for 1-butene.[2-8]

$$T^* + CH_3CH_2CH{=}CH_2 \longrightarrow \text{1-butene-}t + H \quad (1)$$

$$\longrightarrow \text{propylene-}t + CH_3 \quad (2)$$

$$\longrightarrow \text{ethylene-}t + C_2H_5 \quad (3)$$

$$\longrightarrow HT + \text{butenyl} \quad (4)$$

Small yields are also observed for the direct T-for-R substitution products, CH_3T and C_2H_5T, in direct analogy with results obtained with saturated hydrocarbons.[7,8] The most important source of propylene-*t* in the 1-butene system is undoubtedly addition to the double bond, forming an excited *sec*-butyl radical, as shown in (5), followed by its subsequent decomposition to the products shown in (2).[2,3] Similarly, the most important source of ethylene-*t* is through the formation of an excited *n*-butyl radical in the primary addition process, as shown in (6), followed by its decomposition to the products of (3). In order simultaneously to study these reactions more thoroughly and to examine

$$T^* + CH_3CH_2CH{=}CH_2 \longrightarrow CH_3CH_2\dot{C}HCH_2T^* \quad (5)$$

$$T^* + CH_3CH_2CH{=}CH_2 \longrightarrow CH_3CH_2CHT\dot{C}H_2^* \quad (6)$$

other mechanistic sources of the same products in lesser yield, we have carried out a comparative study of the reactions of recoil tritium atoms with 1-butene and with 1-butene-1,1-d_2. With $CH_3CH_2CH{=}CD_2$, addition reaction to form the *sec*-butyl-d_2* radical leads to the formation of $CD_2TCH{=}CH_2$, while the isotopic counterpart of (6) will result in the formation of $CHT{=}CD_2$. Lower yield reactions which can then be isotopically distinguished are the direct substitution of T-for-CH_3 as in (7), and substantial disruption of the 1-butene molecule as in (8). Intermolecular comparisons have also been carried out through investigations of competitive systems involving *n*-butane and the two 1-butene molecules.

$$T^* + CH_3CH_2CH{=}CD_2 \longrightarrow CH_2TCH{=}CD_2 + CH_3\cdot \quad (7)$$

$$T^* + CH_3CH_2CH{=}CD_2 \longrightarrow CH_2TCH_2CH{=}CD_2^* + H \quad (8)$$

$$T^* + CH_3CH_2CH{=}CD_2 \longrightarrow CH_3CHTCH{=}CD_2^* + H \quad (8)$$

$$T^* + CH_3CH_2CH{=}CD_2 \longrightarrow CH_2{=}CHT + \dot{C}H{=}CD_2 + H \quad (8)$$

(1) This research has been supported by Atomic Energy Commission Contract No. AT-(11-1)-407 and AT-(11-1)-34, Agreement No. 126.

(2) D. Urch and R. Wolfgang, *J. Amer. Chem. Soc.*, **83**, 2982 (1961).

(3) D. Urch and R. Wolfgang, "Chemical Effects of Nuclear Transformations," Vol. II, International Atomic Energy Agency, Vienna, 1961, p 99.

(4) A. H. Rosenberg and R. Wolfgang, *J. Chem. Phys.*, **41**, 2159 (1964).

(5) J. K. Lee, B. Musgrave, and F. S. Rowland, *J. Amer. Chem. Soc.*, **82**, 3545 (1960).

(6) F. S. Rowland, J. K. Lee, B. Musgrave, and R. M. White, "Chemical Effects of Nuclear Transformations," Vol. II, International Atomic Energy Agency, Vienna, 1961, p 67.

(7) R. Wolfgang, *Progr. Reaction Kinetics*, **3**, 97 (1965).

(8) F. Schmidt-Bleek and F. S. Rowland, *Angew. Chem. (Int. Ed.)*, **3**, 769 (1964).

Table I: Distributions of Tritium-Labeled Products from the Reactions of Recoil Tritium Atoms with 1-Butene, 1-Butene-1,1-d_2, and *n*-Butane

	Target Molecule (RH)											
	1-Butene				1-Butene-1,1-d_2				*n*-Butane			
	Pressures, cm											
RH	68.5	68.5	23.5	6.8	73.1	68.9	19.2	7.0	70.9	19.4	7.9	
O_2	2.1	2.1	2.1	1.8	2.0	2.1	1.5	2.0	1.6	1.6	1.2	
^3He	1.5	1.5	1.5	1.5	1.3	1.3	1.3	1.3	1.3	1.3	1.3	
Products												
HT + DT	113 ± 2	112 ± 2	(112)	(112)	113 ± 2	111 ± 2	(112)	(112)	197 ± 2	(197)	(197)	
Methane-t	4.8 ± 0.2	4.8 ± 0.2	4.5 ± 0.2	4.8 ± 0.4	5.0 ± 0.2	5.2 ± 0.3	5.1 ± 0.5	5.3 ± 0.5	7.5 ± 0.2	7.8 ± 0.3	7.9 ± 0.3	
Ethane-t	1.8 ± 0.2	1.7 ± 0.2	1.6 ± 0.2	1.5 ± 0.3	1.7 ± 0.2	1.8 ± 0.2	1.5 ± 0.3	1.9 ± 0.5	3.9 ± 0.2	3.9 ± 0.2	4.0 ± 0.2	
$CHT{=}CH_2$	33.7 ± 0.4	34.4 ± 0.4	36.9 ± 0.4	38.7 ± 0.7	2.6 ± 0.3	2.4 ± 0.3	2.7 ± 0.3	2.7 ± 0.3	5.9 ± 0.2	8.2 ± 0.2	9.2 ± 0.3	
$CHT{=}CD_2$					32.0 ± 0.4	32.1 ± 0.4	35.0 ± 0.5	36.6 ± 0.6				
Propane-t									3.1 ± 0.2	3.3 ± 0.2	3.4 ± 0.3	
Acetylene-t	1.2 ± 0.1	1.0 ± 0.1	1.1 ± 0.1	1.1 ± 0.3	0.8 ± 0.1	1.0 ± 0.1	1.1 ± 0.1	0.9 ± 0.2				
$CD_2TCH{=}CH_2$					31.4 ± 0.3	31.1 ± 0.3	39.2 ± 0.4	44.9 ± 0.6				
$CH_2TCH{=}CD_2$					2.4 ± 0.5	2.0 ± 0.5	2.1 ± 0.5	2.4 ± 0.5				
Propylene-t	38.8 ± 0.4	39.2 ± 0.4	45.8 ± 0.5	53.7 ± 0.8					1.8 ± 0.2	1.9 ± 0.2	2.1 ± 0.2	
Allene-t	1.0 ± 0.1	1.2 ± 0.1	1.2 ± 0.1	1.6 ± 0.3	0.9 ± 0.1	1.0 ± 0.1	1.3 ± 0.2	1.4 ± 0.3				
n-Butane-t									(100)	98 ± 2	95 ± 2	
1-Butene-t	(83)	(83)	77 ± 2	73 ± 2	(81)	(81)	75 ± 2	73 ± 2	0.5 ± 0.2	0.7 ± 0.2	0.5 ± 0.2	
trans-2-Butene-t	3.4 ± 0.1	3.8 ± 0.1	3.7 ± 0.1	4.5 ± 0.3	3.3 ± 0.1	3.2 ± 0.1	3.1 ± 0.3	3.7 ± 0.3				
cis-2-Butene-t	2.6 ± 0.1	2.7 ± 0.1	2.5 ± 0.1	3.1 ± 0.3	2.3 ± 0.1	2.4 ± 0.1	2.5 ± 0.2	2.3 ± 0.3				

Experimental Section

n-Butane (Phillips Research Grade, 99.98 %), 1-butene (Matheson, CP Grade, 99.0 % minimum), and 1-butene-1,1-d_2 (Merck Sharp and Dohme of Canada) were used after purification in a vacuum line employing freeze–pump–thaw cycles to remove air. The quoted isotopic purity of 1-butene-1,1-d_2 was 95.8 %-d_2, 1.8%-d_1 and 2.4 %-d_0. Oxygen (Linde Co.) was used without purification. ^3He (Mound Laboratory) was used as the source of tritium under neutron irradiation.

The samples were sealed into ampoules made from 1720 Pyrex tubing using conventional vacuum line techniques,[2-8] and irradiated in a nominal neutron flux of 1×10^{11} n/cm^2 sec at 20°.

The analysis of gaseous tritium labeled products was made with a conventional radio gas chromatography setup,[9] with analysis of aliquots on the following three columns:[9-11] (A) 80-ft acetonylacetone column at 0° for C_3–C_4 hydrocarbon analysis, (B) 50-ft propylene carbonate on alumina column at 0° for HT, CH_3T, C_2H_3T, and C_2H_5T analysis and (C) 250-ft (or 150-ft) silver nitrate–ethylene glycol column at 0° for the analysis of isotopic position isomers of tritium and deuterium-labeled olefins. This separation of isotopic isomers is illustrated in Figure 1.

Results

Standard for Comparison of Samples. The distribution of radioactive products from the reactions of recoil tritium atoms with 1-butene, 1-butene-1,1-d_2, and *n*-butane under closely comparable conditions of irradiation and analysis is shown in Table I. In each case, samples were run over about a tenfold range of pressures. In order to facilitate intercomparison of samples, the yields have been normalized to 100 for the yield of *n*-C_4H_9T from *n*-C_4H_{10} at 70.9 cm pressure in the following way. (a) The yields of all products from the 70.9 cm pressure sample of *n*-C_4H_{10} have been expressed relative to *n*-C_4H_{10} as 100; on this basis the yield of HT is 197 from this sample. (b) Assuming that the yield of HT is pressure independent, the *n*-C_4H_{10} samples at other pressures have been expressed relative to a secondary standard that HT = 197. (c) The yields for 1-butene and 1-butene-1,1-d_2 have been normalized to that of *n*-C_4H_9T from *n*-C_4H_{10} through the intermolecular competition experiments of Table II, in which the 70-cm yields of the tritiated parent molecules are found to be 83 and 81, respectively, on the basis of *n*-C_4H_9T = 100; the HT yield from 1-butene is then measured to be 112, while the (HT + DT) yield from 1-butene-1,1-d_2 is also 112. (d) The HT yield from 1-butene and the

(9) J. K. Lee, E. K. C. Lee, B. Musgrave, Y.-N. Tang, J. W. Root, and F. S. Rowland, *Anal. Chem.*, **34**, 741 (1962).

(10) E. K. C. Lee and F. S. Rowland, *ibid.*, **36**, 2181 (1964).

(11) E. K. C. Lee and F. S. Rowland, *J. Amer. Chem. Soc.*, **85**, 897 (1963).

Table II: Distribution of Tritium-Labeled Products from The Reactions of Recoil Tritium Atoms in 1-Butene/*n*-Butane Mixtures

	Pressure, cm					
n-C_4H_{10}	22.6	6.1	2.4	20.4	6.2	3
$CH_3CH_2CH{=}CH_2$	47.8	17.6	8.0	...	...	...
$CH_3CH_2CH{=}CD_2$	...	...	...	49.2	15.9	9
O_2	2.1	1.5	1.5	2.1	1.8	1.3
^3He	1.5	1.5	1.5	1.5	1.5	1.3
Mass peak areas						
n-Butane(A)	4475	1395	545	4,500	1428	482
1-Butene(B)	9080	3718	1776	10,160	3525	2070
Mole ratio = 1.04(B/A)	2.11 ± 0 06	2.78 ± 0.06	3.39 ± 0.08	2.35 ± 0.05	2.57 ± 0.05	4.47 ± 0.10
Products (observed counts of radioactivity)[a]						
HT (+ DT)	56,650	47,760	37,400	59,570	54,380	27,180
CH_3T	2,460	2,110	1,580	2,740	2,480	1,150
C_2H_5T	1,010	510	600	1,020	940	390
Ethylene-*t*	11,090	11,330	9,770	12,250	13,230	7,510
Acetylene-*t*	270	310	170	270	320	130
Propane-*t*	600	520	370	600	550	190
Propylene-*t*	12,130	13,430	12,570	11,480	13,430	8,680
Allene-*t*	320	340	290	310	350	190
n-Butane-*t*(A′)	13,600	9,290	6,370	13,790	11,510	3,800
1-Butene-*t*(B′)	23,920	21,470	17,210	26,120	23,500	13,510
t-2-Butene	1,100	1,080	970	1,070	1,150	610
c-2-Butene	770	750	640	770	770	470
Activity ratio, (B′/A′)	1.75 ± 0.03	2.30 ± 0.04	2.69 ± 0.06	1.90 ± 0.03	2.04 ± 0.03	3.56 ± 0.06
Specific activity ratio (B′/A′)/(B/A)	0.830 ± 0.02	0.828 ± 0.02	0.794 ± 0.02	0.808 ± 0.02	0.794 ± 0.02	0.796 ± 0.02

[a] Intersample comparisons of observed number of counts are not significant since ^3He concentration was not closely monitored.

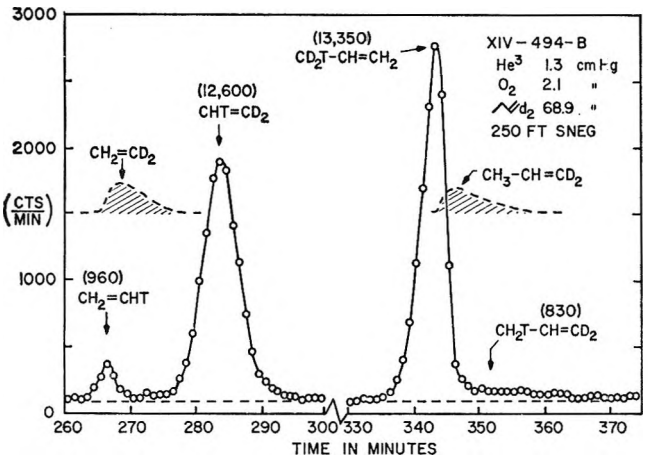

Figure 1. Radio gas chromatographic separation of the isotopic isomers of ethylene and propylene. The shaded peaks are macroscopic mass trace recorded by thermistor detector. The peaks with open circles are tritium radioactivity trace, and the numbers in parenthesis are the observed activity counts for the corresponding peaks.

(HT + DT) yield from 1-butene-1,1-d_2 have both been used as secondary standards, each (fortuitously) equal to 112, for the expression of the relative yields of all products in irradiations not carried out at about 70 cm pressure.

The yields have been so expressed in order to equate as nearly as possible all of the yields of Table I to conditions of equal tritium flux, using the assumption, established in a number of other experiments,[11-13] that the abstraction reactions are essentially pressure independent, while the yields of the hydrocarbon products frequently vary with pressure because of secondary decomposition or isomerization. The accuracy of this assumption in the present system is probably better than ±5%, so that variations of product yield with pressure exceeding such a limitation can definitely be assigned to mechanisms involving secondary reactions either in their formation or removal.

Pressure dependent yields are observed for *n*-C_4H_9T and $CH_2{=}CHT$ from *n*-C_4H_{10} and for 1-butene-*t*, propylene-*t*, ethylene-*t*, allene-*t*, *trans*-2-butene-*t*, and *cis*-2-butene-*t* from reactions with 1-butene. Separation of the isotopic components of propylene-*t* and ethylene-*t* from 1-butene-1,1-d_2 demonstrates clearly that the pressure dependence occurs for the much more abundant product, in each case the labeled olefinic molecule corresponding to decomposition of the excited radical formed by hot T* addition to the double bond.

Competition Experiments. The results from competitive experiments between *n*-C_4H_{10} and each of the

(12) Y.-N. Tang, E. K. C. Lee, and F. S. Rowland, *J. Amer. Chem. Soc.*, **86**, 1280 (1964).

(13) Y.-N. Tang and F. S. Rowland, *ibid.*, **87**, 3304 (1965).

1-butene parent molecules are given in Table II. The data given are the actual number of counts observed in each product, together with the macroscopic composition of the mixtures. The data on the specific activity ratios have been calculated using the measured gas chromatographic peak areas, as corrected for the difference in thermal response constants for the two parent molecules (a factor of 1.04). Within the limits of error on these measurements, the specific activity ratio of 1-butene-*t* *vs.* n-C_4H_9T is 0.82 ± 0.02 at all pressures; the corresponding figure for 1-butene-1, 1-d_2 *vs.* n-C_4H_9T is 0.80 ± 0.02. Comparison of Tables I and II indicates that the approximate constancy of these ratios with pressure changes is the consequence of a simultaneous decrease in the yields of *all* parent molecules at lower pressures because of secondary decomposition processes.

If the distribution of radioactivity among the various products were completely independent of the composition of the mixture, and merely a function of binary collisions between T + parent molecule (and assuming that the moderator characteristics of the components were the same), then the product distribution from binary mixtures should just be a sum of the expected products from the two parent molecules taken separately, with proper normalization for their mole fraction in the mixture. Such a comparison, shown in Table III, indicates that the mixture data of Table II actually

Table III: Additivity of n-Butane–1-Butene Mixtures

	From Table I			From Table II
	n-C_4H_{10}[a]	1-C_4H_8[b]	Total	Total[c]
HT	26,800	32,600	59,400	56,650
CH_3T	1,020	1,380	2,500	2,460
C_2H_5T	530	500	1,030	1,010
C_2H_3T	800	9,800	10,600	11,090
C_2HT	low	320	320	270
C_3H_7T	420	0	420	600
C_3H_5T	240	11,200	11,440	12,130
CH_2=C=CHT	low	290	290	320
n-C_4H_9T	13,600	0	13,600	(13,600)
1-C_4H_7T	70	23,850	23,920	(23,920)
t-2-C_4H_7T	low	1,030	1,030	1,100
c-2-C_4H_7T	low	760	760	770

[a] Sample with 70.9 cm n-C_4H_{10}. [b] Samples with 68.5 cm 1-C_4H_8. [c] Sample with 22.6 cm n-C_4H_{10} and 47.8 cm 1-C_4H_8, normalized to parent molecule yields.

come rather close to being a linear sum of the data for n-C_4H_{10} and 1-butene from Table I. Since we have performed the weighting on a normalized radioactivity basis and not on an absolute yield basis, the mixture data are sensitive to changes in the tritium atom spectra, in the relative distribution of collisions with energy but not to changes in the absolute number of collisions. The near-summation implies that most of the reactions occur with the same relative frequency in n-C_4H_{10} and in 1-butene.

The significant deviations from additivity are the lower total HT yield and the higher yields of C_2H_3T and propylene-*t* in the mixtures, each variation amounting to about 5% of the expected sum from the separate components. Possible deviations from additivity among the products with minor yields are not important for the understanding of the major mechanisms of reaction.

Discussion

Pressure-Dependent Reactions of n-Butane. The small, but measurable, decrease in n-C_4H_9T yield with pressure has been noted earlier,[14] and indicates greater secondary decomposition of excited molecules at the lower pressure. The probable decomposition mechanism is the split into two ethyl radicals, as shown in (9); if these ethyl radicals are still excited, then further decomposition by loss of an H atom, as in (10), can account for the increase in yield of CH_2=CHT at lower pressures. The increase in ethylene-*t* yield does not correspond completely to the decrease in yield of

$$n\text{-}C_4H_9T^* \longrightarrow C_2H_4T + C_2H_5 \qquad (9)$$

$$C_2H_4T^* \longrightarrow C_2H_3T + H \qquad (10)$$

n-C_4H_9T, even after correction for isotopic loss of T in (10), probably indicating that some $C_2H_4T^*$ radicals are stabilized prior to (10), and do not appear among the measured products. However, the differences in yields with pressure are near the margin of accuracy, making precise discussion of the other possible mechanisms of decomposition of n-$C_4H_9T^*$ not very profitable.

No pressure dependence was observed in Table I for the decomposition of CH_3T, C_2H_5T or C_3H_7T from T* + n-C_4H_{10}; however, the accuracy of comparison is very low and a pressure dependence of the magnitude of that found for n-C_4H_9T would *not* be observed. Consequently, we draw no conclusions from these experiments about the magnitude of secondary decomposition for these T-for-alkyl substitution products.[15]

Pressure-Dependent Reactions of 1-Butene and 1-Butene-1,1-d_2. The data for product yields *vs.* pressure for the 1-butene parent molecules demonstrate that the yield of propylene-*t* is more than 40% larger at the lower pressures than at the higher, while that of ethylene-*t* increases by about 15% over the same pressure range. Yield differences in the pressure range 0.1–1.0 atmosphere imply rate constants for the decomposition of the excited radicals of the order of $10^9 \sim 10^{10}$ sec^{-1}, competitive with the rate of collisional deactivation.[16,17]

(14) E. K. C. Lee, Ph.D. Thesis, University of Kansas, 1963.

(15) Unpublished experiments by G. Palino, B. Arezzo, and F. S. Rowland have shown almost complete product decomposition following T-for-alkyl reactions with n-propyl alcohol in the gas phase. See also C. T. Ting and F. S. Rowland, *J. Phys. Chem.*, 74, 445 (1970).

The relatively small change in yield for ethylene-*t* suggests that only a small fraction of *n*-$C_4H_8T^*$ radicals possess rate constants in this range. This finding is consistent with the observation that thermal hydrogen atoms add very preferentially to the terminal position of the double bond, with the formation of *sec*-butyl radicals. Since the formation of *n*-$C_4H_8T^*$ radicals has a higher threshold energy for H(or T) atom addition, this additional energy is added to the internal energy of the excited radical, and leads to decomposition rate constants in excess of 10^{10} sec^{-1}, and therefore to nearly complete decomposition even at one atmosphere total pressure. On the other hand, the addition of H(or T) to the terminal position can occur with thermal hydrogen atoms, and the *sec*-$C_4H_8T^*$ radicals can be formed with energies as low as the exothermicity of the addition reaction itself. *sec*-$C_4H_8T^*$ radicals formed by the addition of tritium atoms of less than 0.4 eV kinetic energy have rate constants for decomposition of 10^7 sec^{-1} or less, and would not decompose in this system, reacting instead as stabilized *sec*-butyl radicals. The yields of ethylene-*t* and propylene-*t* are approximately equal in the 70 cm pressure experiments, indicating that about equal amounts of the two butyl radicals are formed by the initial reactions of *energetic* tritium atoms, as postulated by Urch and Wolfgang.[2,3] The increasing predominance of propylene-*t* at lower pressures reflects the continued formation by lower energy tritium atoms of *sec*-$C_4H_8T^*$ radicals below the threshold for the *n*-$C_4H_8T^*$ addition process.

Isotope Effects. Isotopic differences in the yields of recoil tritium reactions have been established for the processes of substitution, abstraction, and moderation.[7,8,18,19] While several isotopic differences are possible in the comparison of 1-butene and 1-butene-1,1-d_2, the effects are generally quite small except in the formation of propylene-*t*. The yields of both the abstraction product (HT *vs.* DT) and the labeled parent molecules are quite similar (112 *vs.* 112; 83 *vs.* 81), but would not be expected to show very large differences in any case, since six of the eight positions are C–H in both molecules. The total yield of ethylene-*t* is essentially identical from both 1-butene and 1-butene-1,1-d_2; in each case, the addition occurs at the nonterminal —CH= position and the presence of the two deuterium atoms in the terminal position has a negligible effect on the yield. Although two deuterium atoms in the molecule should reduce the rate of decomposition of *sec*-butyl radicals by about a factor of 1.5 for equivalent excitation energies,[16] this rate difference would have a trivial effect on the total yield under the present circumstances, since most of the radicals are so excited that decomposition always occurs before collisional deexcitation.

One isotope effect is quite marked; the total yield of propylene-*t* is higher from 1-butene than from 1-butene-d_2 at all pressures (39 *vs.* 34 at 70 cm; 54 *vs.* 47 at 7 cm). Two contributions to this total effect seem possibly important, and both operate in the same direction. First, the actual addition of the T atom to $=CD_2$ can be isotopically disfavored relative to addition to $=CH_2$; and second, the excited radical, once formed, would tend to decompose more slowly with increasing deuteration. The first process would reduce the number of excited *sec*-butyl radicals in the deuterated system, while the second could reduce the fraction of these radicals which decompose to the measured product propylene. Isotope effects in which the deuterated molecule in unfavored have been measured for other double-bond additions, largely the result of higher thresholds for the addition process with the deuterated species.[20-22] Probably both processes are contributing to the total effect—in the pressure range between 0.1 and 1.0 atm, the *incremental* increase in propylene-*t* is greater for the all-protonated 1-butene, consistent with an isotopic difference in decomposition rate constants actually competing with collisional deexcitation, *i.e.*, in the $10^9 \sim 10^{10}$ sec^{-1} range. However, in contrast to the yields of ethylene-*t* which are essentially identical from both isotopic 1-butenes, the isotopic difference in propylene-*t* yields *also* exists at 70 cm pressure. If isotope effects on decomposition rate constants were the only controlling factor, the behavior of ethylene-*t* and propylene-*t* yields should be parallel; the presence of an additional factor in the yield of the latter suggests that addition to the terminal $=CD_2$ is also unfavored, and fewer highly excited radicals are formed in this manner in the presence of the deuterated species.

Close comparison of yields between separate pure systems involves the implicit assumption that the tritium atom flux is essentially identical in both of the systems. The tritium atom flux is determined both by the reactive and moderator properties of the molecule involved, and need not be identical over the entire energy range for two such different molecules as *n*-C_4H_{10} and 1-butene. Nevertheless, within the accuracy of measurements, the overall characteristics of these two molecules are quite similar as mea-

(16) B. S. Rabinovitch and D. W. Setser, *Advan. Photochem.*, **3**, 1 (1964).

(17) R. Kushner and F. S. Rowland, *J. Amer. Chem. Soc.*, **91**, 1539 (1969).

(18) E. K. C. Lee, G. Miller, and F. S. Rowland, *ibid.*, **87**, 1190 (1965).

(19) E. K. C. Lee, J. W. Root, and F. S. Rowland, "Chemical Effects of Nuclear Transformations," Vol. I, International Atomic Energy Agency, Vienna, 1965, p 55.

(20) Y.-N. Tang and F. S. Rowland, *J. Amer. Chem. Soc.*, **89**, 6420 (1967).

(21) J. W. Simons and B. S. Rabinovitch, *J. Phys. Chem.*, **68**, 1322 (1964). Rate of the methylene addition to the double bond of *cis*-2-C_4H_8 is 2 $\sim$ 5 % greater than that of *cis*-2-C_4D_8.

(22) Direct measurement indicates that the rates of addition of H to C_2H_4 and C_2D_4 are similar, but with an accuracy thus far of only $\pm 15\%$. W. Braun and M. Lenzi, *Discussions Faraday Soc.*, **44**, 252 (1967).

sured in helium-moderated systems:[4] reactivities ($I_{C_4H_{10}} = 5.9 \pm 0.7$, $I_{C_4H_8} = 4.8 \pm 0.6$); moderating ability ($\alpha_{C_4H_{10}} = 5.0 \pm 0.7$, $\alpha_{C_4H_8} = 4.5 \pm 0.7$) all expressed in units of α_{He}. Measurements have not been made of the moderating characteristics of 1-butene-1,1-d_2, but one can assume that the general processes should be quite close to those of 1-butene. As indicated above, however, the isotope effect observed with propylene-t includes a contribution from the failure to form as many excited *sec*-butyl radicals in the presence of $=CD_2$ groups as with $=CH_2$. These tritium atoms which "fail" to add to $=CD_2$ groups must then do something else—add to $=CD_2$ at a lower energy forming a radical which is later stabilized by collision; thermalize and be scavenged by the O_2 in the system; or react by some competing hot process. When two hot processes are competing and many energetic collisions are possible, an unfavorable effect on one hot process automatically enhances the hot yield of the competing process. In this system, we believe that the competing hot process is abstraction, and that the abstraction yield from 1-butene-1,1-d_2 is 2–4% higher than it would be for 1-butene in Table I in truly equivalent tritium atom fluxes. The apparent absence of an isotopic difference in abstraction between 1-butene and 1-butene-1,1-d_2 is thus obtained by a cancellation of two minor effects, a slightly lower intrinsic yield per collision from the deuterated species, coupled with more collisions because of the inferior reactivity of $=CD_2$ toward atomic tritium. This conclusion is completely in accord with the observed deviations (Table III) from additivity in *n*-butane–1-butene mixtures, as discussed below.

Deviations from Non additivity in Butane–Butene Mixtures. The data of Table III show reasonable additivity in the binary mixture of *n*-butane–1-butene *vs.* the product ratios of the pure compounds. However, the decrease in total HT yield and partially complementary increase in ethylene–propylene yields are indicative of a changing competition between hot reactions in the comparison of pure compounds *vs.* binary mixture. In pure *n*-butane, the low energy competition for tritium atoms is between abstraction, thermalization, and scavenging by oxygen. Under these conditions, the abstraction yield reaches the value 1.97 *vs.* the n-C_4H_9T yield, although this ratio can be reduced as low as 1.29 ± 0.04 for n-C_4H_{10} in excess C_2D_4.[23] If the HT yield from 1-butene is arbitrarily assumed to be unchanged in the 1-butene–*n*-butane mixtures, and the deficit in HT is thus assigned to *n*-butane, the HT/RT yield falls to 1.77. The "missing" tritium atoms, which in n-C_4H_{10} form a chemical bond by abstraction of H, react in the binary mixtures by addition to the double bond. The quantitative implications of Table III are that some of this increase in double bond reaction leads to radicals, both *n*-butyl and *sec*-butyl, sufficiently excited to decompose to the olefins, initiated by tritium atoms possessing 1 or 2 eV kinetic energy from the hot tritium atom in addition to the natural exothermicity of the reaction. However, the increase in olefin yields does not balance the decrease in HT, and one can further postulate that the remainder of the "missing" tritium has gone into addition products with too little energy to undergo secondary decomposition, *i.e.*, <1 eV kinetic energy of tritium. The overall conclusion from both the additivity experiments and the isotope effects on the 1-butenes is that strong competition exists between the hot reactions leading to abstraction and those leading to addition to double bonds over the energy range from a few eV down to below 0.4 eV.

Relative Yields of Substitution Products. The gas-phase binary competition reactions show ratios for the formation of the parent molecules of 0.83 for 1-butene, 0.81 for 1-butene-1,1-d_2, and 1.00 for *n*-butane. These yields fall almost exactly in the ratio of numbers of C–H (and C–D) bonds present in the molecules, and furnish no evidence for any appreciable differences in reactivity of any of the C–H positions toward recoil tritium atoms. This conclusion is consistent with recent measurements showing very little difference between the tertiary and primary positions of isobutane in the gas phase.[24]

Intercomparison of the substitution of T-for-CH_3 in *n*-butane and 1-butene-1,1-d_2 shows in Table I that the yields are 3.2 ± 0.2 for the former and 2.2 ± 0.5 for the latter. After allowing for the two equivalent C–C positions in *n*-butane, the data are suggestive that replacement of CH_3 proceeds in higher yield (2.2 *vs.* 1.6) when the group to which the tritium atom is now bonded is the allyl group rather than the propyl group.[25] The yield of abstraction by energetic tritium atoms is substantially higher from the CH_3 position in $CH_3CD{=}CD_2$ than $CH_3CD_2CH_3$, and has been attributed to the partial weakening of the C–H bond in propylene by allylic resonance.[26] The magnitude of the difference in T-for-CH_3 substitution probabilities is small but the difference is probably also an effect attributable to the effect of the double bond; we surmise that the extra π-bond density of the double bond is partially available for bond formation to the tritium atom, thereby enhancing the yield of the substitution reaction. Such electronic, inductive effects

(23) J. W. Root, W. Breckenridge, and F. S. Rowland, *J. Chem. Phys.*, **43**, 3694 (1965).

(24) The specific activity per bond of the tertiary position of isobutane relative to the primary position has been measured as 0.87 for i-C_4H_{10} and 0.96 for i-C_4D_{10}. T. Smail and F. S. Rowland, *J. Phys. Chem.*, **72**, 1845 (1968); **74**, 456 (1970).

(25) Both products are subject to secondary decomposition in the gas-phase reactions. We are implicitly postulating that $CH_2TCH_2CH_3$* is no less stable toward decomposition than is $CH_2TCH{=}CH_2$*.

(26) E. Tachikawa, Y.-N. Tang, and F. S. Rowland, *J. Amer. Chem. Soc.*, **90**, 3584 (1968).

on the substitution process have been suggested earlier as a contributing factor in the lower yields of T-for-H substitution processes in halocarbons.[8,27] In that case, the electronegativity of the halogen substituents is postulated to withdraw electron density; in the present case, the olefinic substituent furnishes extra electron density; in both cases, the substitution process is more favored if the electron density in the neighborhood of the incipient bond is increased.

(27) F. S. Rowland, E. K. C. Lee, and Y.-N. Tang, *J. Phys. Chem.*, 73, 4024 (1969); see also Y.-N. Tang, Ph. D. Thesis, University of Kansas, 1964.

Recoil Tritium Reactions with 1,3-Dimethylcyclobutane. Estimates of Energy Deposition for the T-for-CH_3 and T-for-H Reactions[1]

by C. T. Ting and F. S. Rowland

Department of Chemistry, University of California, Irvine, California 92664 (*Received July 3, 1969*)

More than 96% of the methylcyclobutane-*t* molecules formed by T-for-CH_3 substitution in 1,3-dimethylcyclobutane undergo secondary decomposition in gas-phase experiments, implying that these substitution reactions usually leave 6–7 eV excitation energy with the product molecule. Secondary decomposition of the labeled parent molecule, formed by T-for-H substitution, is observed both in gas (25%) and liquid (12%) phases. Decomposition occurs after either ring- or alkyl-hydrogen atom replacement, with only small positional differences in fractional decomposition. Substitution in the tertiary C–H position is $\geq 95\%$ stereospecific with retention of configuration. Primary substitution of T-for-H is 0.93 ± 0.04 as likely, per C–H bond, in ring positions as in the alkyl groups.

Introduction

The substitution of an energetic tritium atom for hydrogen in the cyclopropanes,[2-4] cyclobutanes,[5,6] and other molecules, as in (1), has been shown to leave excited products capable of undergoing secondary isomerization or decomposition.[2-8] The study of the

$$T^* + RH \longrightarrow RT^* + H \qquad (1)$$

pressure dependence of the yields of cyclobutane-*t* and its secondary decomposition product, $CH_2{=}CHT$, has served as the basis for an estimate that a median excitation energy of about 5 eV remains following the substitution of T-for-H in cyclobutane.[5] Similar experiments with cyclobutane-d_8 have shown that a comparable amount of energy is deposited during the energetic substitution of T-for-D.[6]

The present experiments were intended primarily to permit corresponding estimates of the excitation energy deposited during the hot substitution of a tritium atom for a methyl group. Experiments involving the more readily available methylcyclobutane or 1,2-dimethylcyclobutane had the disadvantage that the labeled decomposition products of the T-for-CH_3 reaction, shown in (2), can also be formed by one or more modes of decomposition following the T-for-H reaction with the same parent molecule.[9] Consequently, we have synthesized *cis*- and *trans*-1,3-dimethylcyclobutane and used these as the reactant molecules, anticipating that

(1) This research was supported by Atomic Energy Commission Contract No. AT-(11-1)-34, Agreement No. 126, and formed part of the material submitted in the Ph.D. thesis of Cheng Teh Ting, University of California, Irvine, 1969.

(2) J. K. Lee, B. Musgrave, and F. S. Rowland, *Can. J. Chem.*, **38**, 1756 (1960).

(3) Yi-Noo Tang and F. S. Rowland, *J. Phys. Chem.*, **69**, 4297 (1965).

(4) E. K. C. Lee and F. S. Rowland, unpublished experiments.

(5) E. K. C. Lee and F. S. Rowland, *J. Amer. Chem. Soc.*, **85**, 897 (1963).

(6) A. Hosaka and F. S. Rowland, Fourth Informal Conference on Hot Atom Chemistry, Kyoto, Japan, Oct 1967.

(7) F. Schmidt-Bleek and F. S. Rowland, *Angew. Chem.*, **3**, 769 (1964).

(8) R. Wolfgang, *Progr. Reaction Kinetics*, **3**, 97 (1965).

(9) Methylcyclobutane, R=CH_3; R′=R″=H. Labeled T-for-CH_3 product, always $CH_2{=}CHT$; T-for-R″; also always $CH_2{=}CHT$; T-for-R′; approximately equal amounts of $CH_2{=}CHT$ and $CH_3CH{=}CHT$. 1,2-Dimethylcyclobutane, R=R′=CH_3, R″=H. Labeled T-for-CH_3 product, R′CH=CHT and $CH_2{=}CHT$ equally; T-for-R″; R′CH=CHT and $CH_2{=}CHT$ equally, plus RCT=CH_2 and RCT=CHR′ from tertiary T-for-H.

Table I: Distribution of Radioactive Products from Recoil Tritium Reactions with 1,3-Dimethylcyclobutane in the Gas Phase

	Parent 1,3-dimethylcyclobutane											
	trans						*cis*					
Sample composition, cm												
Parent	10.9[a]	6.4	2.6	10.9	8.5	9.5	11.7[a]	6.8	2.7	10.9	8.6	9.9
^{3}He	1.8	2.1	2.0	2.5	1.8	2.5	2.0	1.9	1.1	2.4	1.9	2.1
O_2	6.6	2.1	2.3	7.0	1.1	49.8	5.4	2.2	2.0	6.7	1.2	50.4
Ar	0	0	0	54.4	0	0	0	0	0	54.1	0	0
Important products (Parent-t + propylene-t = 100)												
trans-$C_6H_{11}T$	74.7	71.5	67.1	76.2	67.3	74.1	0.8	0.8	0.6	0.7	0.7	0.8
cis-$C_6H_{11}T$	0.5	0.5	0.6	0.7	0.6	0.5	73.4	70.6	66.0	74.8	72.0	79.9
Propylene-t	25.3	28.5	32.9	23.8	32.7	25.9	26.6	29.4	34.0	25.2	28.0	20.1
Methylcyclobutane-t	0.1	0.1	0.2	0.2	0.2	0.2	0.1	0.1	0.1	0.1	0.1	0.1
Ethylene-t	5.6	6.8	7.4	6.8	6.8	7.6	6.3	5.7	8.1	5.7	6.3	6.7
Other Products[a]												
	HT	CH_3T	HC≡CT	C_2H_3T	*n*-C_4H_9T	1,3-C_6H_8T	Me acetylene-t	1-Pe-t	2-Me-2-Bu-t	4-Me-1-Pe-t		
trans sample	163	7.2	0.6	2.1	0.2	0.4	0.9	0.1	0.8	0.1		
cis sample	162	8.5	0.3	1.4	0.2	0.5	0.8	0.1	n.m.(b)	0.2(c)		

[a] Other products from these samples. [b] Not measured because it is not separated from the parent molecule on a column separating macroscopic amounts of *cis*-1,3-dimethylcyclobutane. [c] Detectable on the tail of the *cis*-1,3-dimethylcyclobutane peak, but difficult to measure quantitatively.

CH_2=CHT should be formed only by decomposition following T-for-CH_3, and possibly in low yield by minor pathways involving substantial molecular rupture.[10] In the course of the experiment, we have also gathered information about the decomposition of the parent molecules following T-for-H substitution in both ring and methyl positions.

$$\begin{array}{l} \mathrm{RCH{-}CHR'} \\ \quad\vert\quad\vert \\ \mathrm{CH_2{-}CHR''} \end{array} \longrightarrow \begin{array}{l} \mathrm{RCH{=}CHR' + R''CH{=}CH_2} \\ \text{or} \\ \mathrm{RCH{=}CH_2 + R'CH{=}CHR''} \end{array} \quad (2)$$

Experimental Section

Preparation of cis- and trans-1,3-Dimethylcyclobutane.[11] A stream of dry HBr (Matheson Co., CP) was added to allene (Matheson Co., > 97% purity) at −80° until equimolar quantities were present. After reaction at −80° for 15 days, a volatile fraction (chiefly 2-bromopropene and 2,2-dibromopropane) was separated by distillation and discarded, leaving a semisolid residue. Repeated crystallization from cold pentane gave white crystalline *trans*-1,3-dibromo-1,3-dimethylcyclobutane (mp 54–55°). This compound was reduced with tri-*n*-butyltin hydride (Orgmet Co.) to a mixture of *cis*- and *trans*-1,3-dimethylcyclobutane. This mixture was purified by distillation, and then separated by preparative gas chromatography on a 20-ft dimethylsulfolane column. The infrared spectra corresponded to those published by Roberts, *et al.*[12] The isomeric purity of each of the 1,3-dimethylcyclobutanes was >99.9%; the chief chemical impurity in each was the opposite isomer. Gas-phase room temperature samples are limited to about 15 cm of parent molecule by their respective vapor pressures.

Sample Preparation, Irradiation, and Analysis. The preparation and neutron irradiation of samples for recoil tritium experiments has been described in detail before.[7,8] The radioactivity distributions in irradiated samples were determined by radio gas chromatography.[13] Most samples were analyzed in a dual-column apparatus[14] which permitted complete separation of all products in a single aliquot.[15] Molecular hydrogen, methane, ethane, and ethylene passed through a 50-ft dimethylsulfolane (DMS) column at 25°, and then into 50-ft propylene carbonate-on-alumina (PCA) column at 0°. The order of columns was then switched[14] and all subsequent hydrocarbons

(10) See E. K. C. Lee and F. S. Rowland, *J. Phys. Chem.*, **74**, 439 (1970); for experimental measurement of CH_2=CHT from T* + CH_3-CH_2CH=CD_2.

(11) This procedure follows that established by K. Griesbaum, *J. Amer. Chem. Soc.*, **86**, 2301 (1964).

(12) M. F. Caserio, S. H. Parker, R. Piccolini, and J. D. Roberts, *ibid.*, **80**, 5507 (1958).

(13) J. K. Lee, E. K. C. Lee, B. Musgrave, Y.-N. Tang, J. W. Root, and F. S. Rowland, *Anal. Chem.*, **34**, 741 (1962).

(14) The dual column is the same as that described in J. W. Root, E. K. C. Lee, and F. S. Rowland, *Science*, **143**, 676 (1964). See also J. W. Root, Ph.D. thesis, University of Kansas, 1964.

(15) C. T. Ting, Ph.D. thesis, University of California, Irvine, 1969

Table II: Distribution of Radioactive Products from Recoil Tritium Reactions with 1,3-Dimethylcyclobutane in the Liquid Phase

	Parent 1,3-dimethylcyclobutane					
	trans			*cis*		
	Scavenger					
	I_2	DPPH	None	I_2	DPPH	None
	Relative Yields of Products (Parent-*t* + propylene-*t* = 100)					
trans-$C_6H_{11}T$	87.9	87.9	87.3	0.8	1.1	6.3
cis-$C_6H_{11}T$	0.2	~1	6.3	89.4	89.4	87.2
Propylene-*t*	(12.1)[a]	12.1	12.7	(10.6)[a]	10.6	12.8
Methylcyclobutane-*t*	2.6	2.7	4.6	2.6	2.7	4.8
Ethylene-*t*	2.0	2.3	2.8	2.1	2.5	2.5

[a] No propylene-*t* is observed in I_2-scavenged samples because of chemical reaction of the original primary product with I_2. The yields have been assumed to be similar to those found in DPPH-scavenged or non scavenged systems.

Table III: Intramolecular Distribution of Tritium in Propylene-*t* and in 1,3-Dimethylcyclobutane-*t* from Recoil Tritium Reactions with 1,3-Dimethylcyclobutane

		Propylene-*t* from sample		Propylene-*t* from pyrolysis of 1,3-dimethylcyclobutane-*t*		Original primary yield
Parent	Phase[a]	% Alkyl	% Yield	% Alkyl	% Yield	% Alkyl
trans	Gas	48.4	25.3	51.0	74.7	51.6
trans	Gas	48.7		54.3		
cis	Gas	48.2	26.6	53.1	73.4	51.4
cis	Gas	47.3		52.6		
trans	Liquid	43.0	12.1	54.6	87.9	53.4
trans	Liquid	44.5		54.8		

[a] Gas samples, approximately 10 cm parent, 6 cm O_2; liquid samples, DPPH-scavenged.

emerged directly from the DMS column into the sequential arrangement of thermal conductivity and proportional counter monitoring devices. The timing of the column switch was chosen such that hydrogen (70.5 min) and methane (76.8 min) emerged from the (DMS + PCA + second pass through DMS) combination in the product gap from one pass through DMS alone between acetylene (62.4 min) and *cis*-2-butene (94 min), while ethylene (116 min) was observed between 3-methyl-1-butene (103 min) and 1,3-butadiene (125 min). The retention times for the 1, 3-dimethylcyclobutanes were *trans*, 183 min; and *cis*, 222 min (without column overload). A 25-ft column packed with glass beads, following the DMS and PCA columns and preceding the monitoring devices, served as a buffer against pressure disturbances during the switching of the order of the working columns. The precision of the percentage values for the labeled parent molecules in Tables I and II is about ±0.5%; for $CHT{=}CH_2$, about 0.2%; for low yield peaks, about 0.1%. The accuracy is estimated to be nearly as good.

Intramolecular Distribution of Tritium in Propylene-t. The distribution of radioactivity between the alkyl and olefinic positions in propylene-*t* was determined by radio gas chromatographic measurements following recycle separation of the isotopic species on two 125-ft $AgNO_3$–ethylene glycol columns.[16] The accuracy of resolution of these two peaks is approximately ±1.0% in each sample, *e.g.*, 48.4 ± 1.0% alkyl in the first line of Table III. The precision is a little better.

Intramolecular Distribution of Tritium in 1,3-Dimethylcyclobutane. For some samples, the tritiated parent 1,3-dimethylcyclobutane (*cis* or *trans*) was separated from other labeled hydrocarbon products by preparative glc on a 50-ft DMS column and collected in a liquid N_2-cooled trap. The compound was then transferred into an evacuated Pyrex ampoule, sealed off, and pyrolyzed at 450° for 2 min. The intramolecular tritium distribution of the propylene-*t* formed by this pyrolytic technique was then determined by radio gas chromatography, as described above. While the tritium-labeled molecules of 1,3-dimethylcyclobutane-*t* will exhibit isotopic rate differences in pyrolysis from the unlabeled parent molecule, position differences in rates among various monotritiated isomers should be negligible. The pyrolyses were carried to about 80% completion.

Results and Discussion

Mechanisms for the Formation of Radioactive Products from Reactions with 1, 3-Dimethylcyclobutane. The substitution of energetic tritium for H in either 1,3-dimethylcyclobutane leads to the labeled parent molecule, as in (3). By analogy with recoil tritium experi-

(16) E. K. C. Lee and F. S. Rowland, *Anal. Chem.*, 36, 2181 (1964).

ments with cyclobutane[5] and with pyrolyses of substituted cyclobutane hydrocarbons in general,[17,18] the more excited of such molecules may undergo decomposition to form two molecules of propylene, one of them carrying a tritium label, as in (4). If no H or T atom migration occurs in the excited molecule, then T should be found in the methyl, secondary-ring, and tertiary-ring positions of the dimethylcyclobutane: decomposition of these labeled molecules will lead to the formation of $CH_2TCH{=}CH_2$, $CH_3CH{=}CHT$, and $CH_3CT{=}CH_2$, respectively.

$$T^* + CH_3\overset{\overset{\frown CH_2 \frown}{|\quad\quad|}}{C}HCH_2CHCH_3 \longrightarrow C_6H_{11}T^* + H \quad (3)$$

$$C_6H_{11}T^* \longrightarrow CH_3CH{=}CH_2 + \text{propylene-}t \quad (4)$$

The substitution of T-for-CH_3, as in (5), forms methylcyclobutane-*t* and its decomposition produces $CH_2{=}CHT$ plus an unlabeled molecule of propylene. Bond formation with the other alkyl fragment produces CH_3T, as in (7).

$$T^* + CH_3\overset{\overset{\frown CH_2 \frown}{|\quad\quad|}}{C}HCH_2CHCH_3 \longrightarrow TCH\overset{\overset{\frown CH_2 \frown}{|\quad\quad|}}{C}HCH_2CHCH_3^* + CH_3 \quad (5)$$

$$TCH\overset{\overset{\frown CH_2 \frown}{|\quad\quad|}}{C}HCH_2CHCH_3^* \longrightarrow CH_2{=}CHT + CH_3CH{=}CH_2 \quad (6)$$

$$T^* + C_6H_{12} \longrightarrow CH_3T + C_5H_9 \quad (7)$$

Among other products expected by analogy with other recoil tritium systems are a large yield of HT by reaction 8 occurring with all three kinds of H atoms[7,8]

$$T^* + C_6H_{12} \longrightarrow HT + C_6H_{11} \quad (8)$$

and small yields of ring-opening products. The latter are formed by the attack in the primary reaction of the tritium atom upon a ring C–C bond, with attachment of the tritium atom to one of the free valencies thereby made available. These excited $C_6H_{12}T$ radicals can then decompose as expected for such branched-chain alkyl radicals, and lead in this system to the following expected products: 1-pentene, 2-methyl-1-pentene, 4-methyl-1-pentene, and 4-methyl-2-pentene (*cis* and *trans*). In addition, if substitution of T-for-H at the tertiary position were accompanied by inversion of configuration about the carbon atom, one should obtain *cis*-1,3-dimethylcyclobutane-*t* as a product from reaction with the *trans* parent, and *vice versa*. Finally, more extensive decomposition accompanying substitution or ring-opening could produce more highly unsaturated C_2–C_4 compounds.

The results obtained in typical O_2-scavenged gas-phase experiments with both parent molecules at several pressures are given in Table I. Much more extensive tables of such data are given in ref 15 for varying O_2, Ar, and parent compositions. Since the interpretation of these experiments is closely concerned with the excitation energies of the labeled product molecules, the results have been expressed relative to the standard: (parent-*t* plus propylene-*t*) = 100. The minor products, insofar as our mechanistic interests are concerned, are listed for two samples. Ring-opening plus decomposition is negligible, as indicated by the low yield of 1-pentene, while extensive decomposition (*e.g.*, butadiene-*t*) is also not very important. The source of C_3H_7T is not clear, but it appears to be a genuine product of reaction of T* with dimethylcyclobutane, and not an artifact of procedure or compound purity.

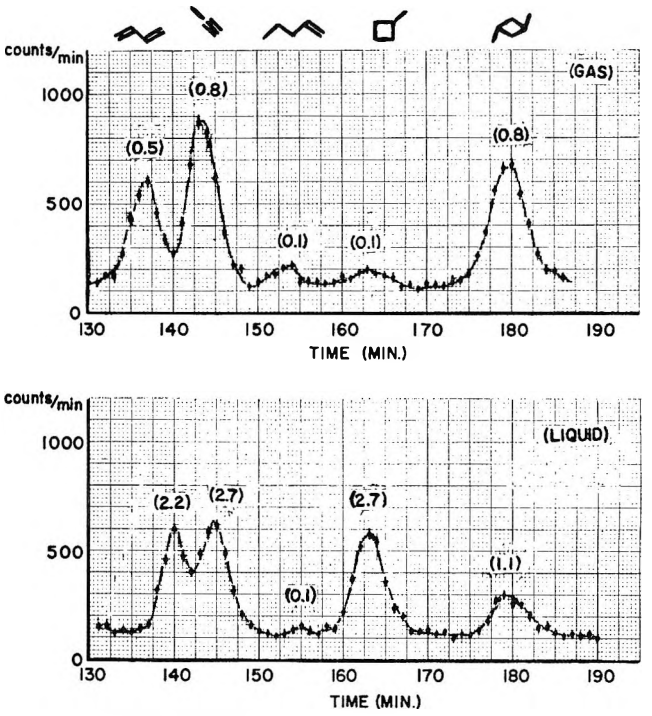

Figure 1. Partial radio gas chromatogram for recoil tritium reactions with *cis*-1,3,-dimethylcyclobutane. Upper diagram, gas phase, 11.7 cm of parent, 5.4 cm of O_2; lower diagram: liquid phase, DPPH scavenger. Relative yields in parentheses *vs.* parent-*t* propylene-*t* as 100.)

Not unexpectedly, the two parent molecules show similar fractions of decomposition—about 27% for 10 cm of parent + 5 cm of O_2. At the same pressure, approximately 50% of cyclobutane-*t* molecules would decompose into ethylene-*t* following the T-for-H reaction in the unsubstituted parent. Over the limited pressure range available, the yields of propylene-*t* and parent-*t* show the pressure dependence expected for competition between collisional stabilization of the labeled parent molecule and its decomposition.

(17) H. R. Gerberich and W. D. Walters, *J. Amer. Chem. Soc.*, **83**, 4884 (1961).

(18) H. M. Frey and R. Walsh, *Chem. Rev.*, **69**, 103 (1969).

The amount of methylcyclobutane-*t* is very low—approximately 2% as large as that of the decomposition product, C_2H_3T. The radio gas chromatogram of the radioactivity through a methylcyclobutane-*t* peak is shown in Figure 1. The yield of the inversion product, the opposite geometric isomer from the parent, is also very low, approximately 1% of the magnitude of the parent yield.

Slight differences are observed between the quantitative radioactivity patterns for the *cis* and *trans* molecules, but the similarities are so strong that we draw the basic conclusion that the substitution reactions are almost completely unaffected by the geometrical differences between the *cis* and *trans* parent molecules.

Typical results from experiments carried out in the liquid phase are given in Table II. The percentage decomposition of the parent dimethylcyclobutane-*t* decreases to about 12% under the conditions of more rapid collisional deexcitation in the liquid phase. Decomposition in cyclobutane, for comparison, is approximately 18% in the liquid phase.

The most noticeable change in the liquid phase experiments is the marked increase in yield of methylcyclobutane-*t*, together with a complementary decrease in the yield of C_2H_3T. The radio gas chromatogram of methylcyclobutane-*t* from the liquid phase is also illustrated in Figure 1.

Excitation Energy Deposition in the T-for-CH_3 Reaction with Dimethylcyclobutane. A striking contrast exists between the gas–liquid comparisons for the T-for-H reaction in cyclobutanes, and for the T-for-CH_3 reaction with the same molecules. While appreciable fractions of labeled parent molecule are stabilized in the gas phase following T-for-H reaction, as shown in Table I and ref 5,[19] almost no methylcyclobutane-*t* molecules are stabilized at 0.2 atm following the T-for-CH_3 reaction.

The liquid phase observations show a yield of methylcyclobutane-*t* about 25 times higher than that found in the gas phase, confirming that the fractional decomposition is very heavy (at least 96%) in the latter. The "missing" methylcyclobutane-*t* in the gas phase is "replaced" by an approximately complementary addition to the yield of C_2H_3T. If the plausible, but unproven, assumption is made that all, or almost all, of the observed C_2H_3T is a secondary production from methylcyclobutane-*t* decomposition, then the data indicate that more than 40% of these excited molecules decompose in the liquid phase (and about 98% in the gas phase) before the excitation energy can be removed by collision. This effective competition between decomposition and collisional deexcitation implies that almost half of the primary T-for-CH_3 products have intrinsic molecular lifetimes, unless collisions intervene, of about 10^{-12} sec or less, and almost all are $<10^{-9}$ sec.

The qualitative conclusion is clear—the substitution of a tritium atom for a CH_3 group in this molecule occurs only by mechanistic paths *requiring* very high internal excitation of the product molecule. Semiquantitative estimates of this excitation energy are discussed in the last section.

Intramolecular Tritium Distribution in Propylene-t and Dimethylcyclobutane-t. If substitution of tritium for hydrogen should occur with equal probability in each H position in 1,3-dimethylcyclobutane, 50% of the tritium atoms would be in CH_2T groups, 33% in –CHT– ring positions, and 17% in $-CTCH_3$ ring positions. Decomposition of these molecules with equal probability would lead to the same 3:2:1 ratio for $CH_2TCH{=}CH_2$, $CH_3CH{=}CHT$, and $CH_3CT{=}CH_2$—or 50% in alkyl-*t* positions and 50% in olefinic-*t* positions. Radio gas chromatographic analysis of the intramolecular distribution in propylene-*t* from gas-phase experiments showed approximately 48% of the tritium present as $CH_2TCH{=}CH_2$, as given in Table III. However, in the liquid phase only 44% of the tritium is found as alkyl-*t*. The tritium distribution in the stabilized parent 1,3-dimethylcyclobutane-*t* has been analyzed after pyrolysis to propylene-*t* by the same technique. In each case, slightly more than half of the tritium in the stabilized parent molecules is bonded in alkyl positions, as shown in Table III.

Summation of the distributions in stabilized parent-*t* + propylene-*t* decomposition product, weighted by the percentage yields of each, indicates that the probability of ring substitution per position is almost as high—about 0.93 ± 0.04—as in the methyl groups. This result is quite consistent with the recent observation that the tertiary positions in $(CH_3)_3CH$ and $(CD_3)_3CD$ are 0.87 and 0.96 times as easily substituted, respectively, as the primary positions in the same molecule.[20]

The per cent alkyl-*t* in propylene-*t* found in the liquid phase is lower than in the corresponding positions of the original parent molecules: 44 *vs.* about 53, indicating slightly preferential decomposition of molecules labeled in ring positions. This observation could be the result of either one or both of (a) different average energy deposition following T-for-H substitution in different positions, such that ring-labeled molecules are slightly more excited than methyl-labeled molecules or (b) nonequilibrium distributions of energy, such that decomposition by ring rupture can occur very early after energy deposition, prior to true equilibration of the excitation energy. In such a situation, initial localization of the excitation energy in the ring C–H positions might make it more readily available for use in decomposition than localization in the methyl groups.

The discrepancy between the original primary alkyl-*t* yield of the *trans* molecule in the gas and liquid phases

(19) Fraction stabilized for c-C_4H_8; 46% at 0.1 atm to 60% at 1.0 atm.

(20) T. Smail and F. S. Rowland, *J. Phys. Chem.*, **72**, 1845 (1968); T. Smail and F. S. Rowland, *ibid.*, **74**, 456 (1970).

is approximately at the limits of error, and a value of 52 ± 1% alkyl-*t* is a satisfactory fit for both phases. One might anticipate an increased alkyl-*t* yield in the liquid phase by "cage"-permitted combinations of CH_2T and methylcyclobutyl radicals; the magnitude of such an effect is certainly very small, and probably negligible.

Substitution for Hydrogen at the Asymmetric Carbon Atoms. The yield of the "opposite" isomer is less than 1% of the yield of the parent isomer for both gas (O_2) and liquid (I_2 or DPPH) well-scavenged experiments. Since only 2 of 12 H atoms are bonded in asymmetric positions (and assuming approximately equal yields at all positions, as indicated by the degradation experiments), ≥ 95% of T-for-H substitutions on the cyclobutane ring must occur with retention of configuration. Even these small yields may arise in part from secondary geometry isomerization of the excited 1,3-dimethylcyclobutane-*t*, and not in the direct primary event itself. One can discount the possibility that appreciable amounts of inversion substitution occur leaving molecules so excited that secondary decomposition always follows because of the general agreement between the O_2- and I_2-scavenged results. A radical mechanism forming the opposite isomer, probably just recombination of methyl and methylcyclobutyl, is also found in unscavenged liquid systems but is suppressed by scavengers. The overwhelming retention of configuration during substitution of T-for-H at an asymmetric carbon atom has been observed in all earlier recoil tritium experiments with straight-chain molecules.[7,8,21]

Quantitative Estimates of Energy Deposition. In principle, the energy deposition following either T-for-H or T-for-CH_3 substitution reactions with 1,3-dimethylcyclobutane can be evaluated just as with cyclobutane, by association of molecular lifetimes (and corresponding rate constants for secondary reaction) with particular excitation energies through a Rice–Ramsperger–Kassel–Marcus calculation of the decomposition rate *vs.* excitation energy.[22] In practice, however, such a quantitative RRKM estimate is both more difficult, and also rather doubtful, in this system. In the T-for-H case, the pyrolysis kinetics have not been measured for either of the 1,3-dimethylcyclobutane molecules, although data for the 1,2-dimethyl isomer are available.[17] In the T-for-CH_3 case, the indicated rate constants for the T-for-CH_3 substitution product are all quite high ($>10^9$ sec^{-1}), and therefore involve extrapolation of the RRKM calculation to energies well above those found in the "calibrating" pyrolytic experiments with methylcyclobutane.[23]

The larger size (and increased number of degrees of freedom) of the dimethylcyclobutane will make its decomposition slower than that of cyclobutane with an equivalent excitation energy. An experimental comparison of dimethylcyclopropane *vs.* cyclopropane has shown that the additional two methyl groups reduce the rate constant for decomposition by 10^3 in the energy range near 4–5 eV.[24] The decomposition of 25% and 12% of the excited molecules in the gas and liquid phases, respectively, requires that at least one quarter of the excited molecules from T-for-H substitution possess excitation energies in the 6–8 eV range, with smaller yields extending even higher in excitation energy.

Since a rate constant of 10^9 sec^{-1} corresponds to an excitation energy of more than 4 eV for cyclobutane itself, the almost total decomposition of the methylcyclobutane-*t* in the gas phase demonstrates that the T-for-CH_3 reaction leaves at least 5 eV on >95% of the product molecules, and implies that the median energy deposition would probably be at least 7 or 8 eV if a full range of high-pressure experiments were feasible and were compared with the decomposition rate constants for methylcyclobutane-*t*. Again, however, the extrapolation of RRKM lifetime–excitation energy relationships to very high energy has not yet been shown to be valid, and more precise estimates of excitation energy do not seem worthwhile at this time. Qualitatively, the conclusion is quite firm that T-for-CH_3 substitution in recoil tritium reactions with the dimethylcyclobutanes leaves 5 eV or more of excitation energy in almost all of the newly formed molecules. Since similar near-zero yields of CH_2TNC have been found for T* reactions with gaseous CH_3NC,[25,26] indicating several eV excitation energy in all T-for-H product molecules, a general rule seems to be operating such that the mechanistic replacement of other groups by hot tritium atoms cannot be accomplished without imparting severe vibrational disturbance to the residual molecular structure.

(21) Y.-N. Tang, C. T. Ting, and F. S. Rowland, *J. Phys. Chem.*, in press.

(22) D. W. Setser and B. S. Rabinovitch, *Advan. Photochem.*, **3**, 1 (1969).

(23) N. N. Das and W. D. Walters, *Z. Phys. Chem.* (Frankfurt am Main), **15**, 22 (1958).

(24) D. W. Setser and B. S. Rabinovitch, *Can. J. Chem.*, **40**, 1425 (1962).

(25) C. T. Ting and F. S. Rowland, *J. Phys. Chem.*, **72**, 763 (1968).

(26) The activation energy for isomerization of CH_3NC to CH_3CN is only 38 kcal/mol. See F. W. Schneider and B. S. Rabinovitch, *J. Amer. Chem. Soc.*, **84**, 4215 (1962); F. W. Schneider and B. S. Rabinovitch, *ibid.*, **85**, 2365 (1963).

Recoil Tritium Reactions in Methane–Hydrogen Mixtures. CD_4–H_2[1]

by John W. Root and F. S. Rowland

Departments of Chemistry, University of California, Davis, California 95616 and University of California, Irvine, California 92664 *(Received June 9, 1969)*

The variations in absolute yield of HT, DT, and CD_3T have been studied over the entire range of mole fractions for CD_4–H_2 mixtures. The specific activity of CD_3T/CD_4 increases at high CD_4 mole fractions, while that of HT/H_2 is almost constant for all composition. These specific activity changes imply that an appreciable amount of HT-forming reaction occurs below the threshold for CD_3T formation. No combination of reactivity integrals and α factors has been found which will simultaneously fit all binary mixtures involving CH_4, CD_4, H_2, H_2, and Ar.

Introduction

Energetic tritium atoms from nuclear recoil react with D_2 to form DT and with CH_4 to form predominantly HT and CH_3T. While the total hot yield of DT in pure D_2 is approximately 93% and that of the hot products from CH_4 totals only 53%, the specific yield ratio $(CH_3T/CH_4)/(DT/D_2)$ is remarkably constant over the entire range of mole fractions in CH_4–D_2 mixtures.[2] This fortuitous circumstance permits relatively simple extensions of the model for such high energy reactions,[3,4] and the data can be quantitatively reproduced with reasonable values of the normal parameters of the kinetic theory of hot atom reactions.[2b,4-6] The success of this parametric treatment encourages additional tests of the theory with suitable systems. As more and more binary systems are satisfactorily fitted in this way, the freedom of choice of parametric values becomes more restricted, since the most important parameters for a particular molecule should remain constant in its binary mixtures with all other molecules.[5]

In light of the earlier CH_4–D_2 data,[2] CD_4–H_2 mixtures should be especially useful for such tests of the invariance of kinetic theory parametric values from system to system, for this combination would then permit cross comparisons with the H_2–D_2 and CH_4–CD_4 pairs.[6,7] The only hot processes occurring with appreciable yield for recoil tritium atoms in the CD_4–H_2 system are the abstraction of D to form DT, the substitution for D to form CD_3T, and the reaction with H_2 to form HT, as indicated in eq 1–3. The use of isotopically different molecules permits direct measurements of the yields of the reaction products from these three reactions.

$$T^* + CD_4 \longrightarrow DT + \cdot CD_3 \quad (1)$$

$$T^* + CD_4 \longrightarrow CD_3T + D \quad (2)$$

$$T^* + H_2 \longrightarrow HT + H \quad (3)$$

Experimental Section

The CD_4–H_2 experiments described here were carried out with the same procedures used for the CH_4–D_2 mixtures, and the two sets of experiments can be directly compared.[2b,8] The only additional information needed for the description of these experiments is that resulting from the isotopic differences in the molecules in the two systems, *e.g.*, the recoil loss calculations are somewhat dependent on the stopping powers assumed for the individual molecules. We have assumed only slight variations between the stopping powers of isotopic molecules: range (in cm at 1 cm pressure and 20°) for CD_4, 16.9 (*vs.* 16.7 for CH_4); range for H_2, 55.0 (*vs.* 55.6 for D_2).[8] The use of identical range values for isotopic molecules would result in trivial changes in the calculated values.

An additional isotopic correction must be applied to the measured yields of HT, DT, and CD_3T associated with the presence of CD_3H as an isotopic impurity in the CD_4. Measurement of the molecular hydrogen radioactivity from CD_4 (containing about 1% CD_3H) shows an (HT/DT) ratio of 0.0158 in systems scavenged with 1–3% O_2.[9] Correction for this reaction with CD_3H is of importance only in the methane-rich samples of the CD_4–H_2 competitions, amounting to approximately 3% at most ($18.7 \times 0.0158 = 0.30$; HT from $H_2 = 11.4 - 0.30 = 11.1$). The measured DT yield has been increased by the multiplicative factor 1.012,

(1) This research has been supported by Atomic Energy Commission Contracts No. AT-(11-1)-407 and AT-(11-1)-34, project agreement 126.

(2) (a) J. W. Root and F. S. Rowland, *J. Chem. Phys.*, **38**, 2030 (1963); (b) J. W. Root and F. S. Rowland, *ibid.*, **46**, 4299 (1967).

(3) P. Estrup and R. Wolfgang, *J. Amer. Chem. Soc.*, **82**, 2661, 2665 (1960).

(4) R. Wolfgang, *J. Chem. Phys.*, **39**, 2983 (1963).

(5) R. Wolfgang, *Progr. Reaction Kinetics*, **3**, 97 (1965).

(6) D. Seewald and R. Wolfgang, *J. Chem. Phys.*, **47**, 143 (1967).

(7) E. K. C. Lee, J. W. Root, and F. S. Rowland, "Chemical Effects of Nuclear Transformations," Vol. 1, International Atomic Energy Agency, Vienna, 1965, p 55.

(8) J. W. Root, Ph.D. Thesis, University of Kansas, Lawrence, Kan., 1964.

(9) The (HT/DT) ratio is substantially larger in I_2-scavenged systems, as shown in ref 8, because of the inability of I_2 to suppress completely the thermal reactions of hydrogen atoms.

Table I: Radioactive Products from Recoil Tritium Reactions in CD_4–H_2 Mixtures

Gas pressures, cm				Radioactive product yields[a], %			Radioactive product specific yields[b] (HT/H₂)	% per bond (CD_3T/CD_4)	Per bond specific yield ratios[b]	
CD_4	H_2	O_2	He^3	Recoil loss, %	DT	CD_3T	HT		$\frac{DT}{(CD_3T)}$	$\frac{HT}{(2H_2)} \times \frac{4CD_4}{(CD_3T)}$
84.2	10.8	3.25	1.13	11.4	18.7	23.7	11.4	48.5	6.68	0.80 ± 0.01	7.26 ± 0.15
64.7	30.6	3.30	1.12	13.5	14.3	18.4	30.4	47.0	6.78	0.79 ± 0.01	6.93
46.0	49.1	3.25	1.13	16.3	10.96	13.5	47.2	45.6	6.98	0.82 ± 0.02	6.53
36.4	58.8	3.30	1.12	18.0	8.88	10.9	57.2	46.2	7.12	0.82 ± 0.02	6.49
25.9	69.1	3.25	1.13	20.0	6.71	7.90	67.9	46.6	7.23	0.86 ± 0.02	6.45
16.5	78.8	3.30	1.12	23.7	4.40	5.20	76.5	46.2	7.52	0.86 ± 0.03	6.14
9.73	85.3	3.25	1.13	26.7	2.76	3.05	84.1	46.8	7.48	0.91 ⊥ 0.03	6.25
5.38	89.9	3.30	1.12	29.0	1.49	1.89	87.4	46.3	8.36	0.80 ± 0.04	5.54

[a] The experimentally observed radioactive product yields are listed, prior to correction for the isotopic impurity CD_3H in CD_4. [b] The specific yields have been corrected for isotopic purity of CD_4 as described in the text.

which allows for both the isotopic impurity and an H/D isotope effect in the abstraction reaction, to obtain the estimated yield for isotopically pure CD_4 in the specific yield calculations.

Results

The radioactivity data obtained from the series of CD_4–H_2 binary mixtures are summarized in Table I, together with the gas pressures of the various components of the mixtures. The number of counts actually observed from the counter for each sample has been corrected for the time of irradiation, the volume of the sample bulb, the pressure of ^3He, and the size of the gas aliquots used for assay. The data listed are thus comparative data for equivalent conditions for the production of total tritium and can be directly compared with the CH_4–D_2 data of ref 2b. After correction for recoil loss, the amounts of radioactivity have been compared with known standards, and the radioactive product yields are listed in Table I in units of per cent total tritium (stopped in the gas phase) for each of the three measured components. The data of Table I are plotted in Figure 1, together with curves which represent the comparable data for the CH_4–D_2 system.[2b]

Our best estimate of the errors involved is that the total activity of our standard was known to ±5%. While this represents reasonable accuracy, the hot yields in H_2-rich samples approach the 90% level, and the estimate of thermalized tritium (100% minus the sum of hot yields) thus has the rather large error of 10 ±5% attached to it. The relative accuracy of intersample comparisons is higher and is apparently ±2% or less, as judged from the consistency of the observations. Comparisons with the CH_4–D_2 data should also be accurate to ±2% or less.

Estimates of the total hot yield from reactions with CD_4 include an estimate of the yield of $\cdot CD_2T$ radicals from the decomposition of excited CD_3T. Evaluation of this number in a bromine-scavenged system shows a factor approaching 0.2 × (CD_3T) for the yield of $\cdot CD_2T$, which is close to the value observed for CH_4.[6] However, we have used 0.1 × (CD_3T) in our calculations for consistency with the published data for CH_4–D_2 mixtures. The results are only slightly affected by this difference in assumptions, and any error would essentially be cancelled in the cross comparisons.

The per bond specific yield ratio $(HT/2H_2)/(CD_3T/4CD_4)$ varies from 5.5 to 7.5 as the mole fraction composition changes, in contrast to the nearly constant value of 4.3 observed for $(DT/2D_2)/(CH_3T/4CH_4)$. These observations indicate (a) isotope effects in recoil tritium reactions with methane and/or hydrogen, and (b) a difference in the average energy at reaction between CD_4 and H_2. The specific yield of CD_3T displays a steady increase with decreasing methane content in CD_4–H_2 mixtures, which is similar to the behavior observed for CH_3T in CH_4–D_2 mixtures. The

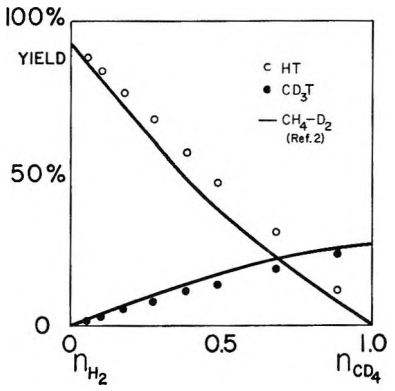

Figure 1. Yields of CD_3T and HT from recoil tritium reactions with CD_4–H_2 mixtures: O, HT; ●, CD_3T; —, corresponding yields of DT and CH_3T from reactions with CH_4–D_2 mixtures.

specific yield of HT is approximately constant over the entire range of mole fractions in the CD_4–H_2 experiments, however. The *sum* of hot yields from reactions 1 to 3 is almost identical over the entire range of CD_4–H_2 mole fractions with the corresponding *sum* of yields from the CH_4–D_2 system.

Discussion

Parameters of the Kinetic Theory of Hot Atom Reactions. The kinetic theory of hot atom reactions describes the reaction probability for a given reaction between an energetic atom and a particular molecule in terms of two parameters, α and I, the average logarithmic energy loss and the reactivity integral, respectively.[2b-6] The ratio (I_A/α_A) for a particular reaction can be directly estimated from the total hot yield observed in a system consisting of pure species A. The experimental approximation to this situation is obtained by ignoring the presence of small quantities of ^3He and O_2, required as hot tritium source and thermal tritium scavenger, respectively. Thus, in the present experiments only CD_4 and H_2 are considered as components. The hot yields for reactions 1 and 3 are then measured individually for pure CD_4 and H_2, or, as in the present case, they are determined by extrapolation to the pure system values from the measured yields in binary mixtures. The total yields for CD_4 and for H_2 are measured using the extrapolation technique as 50 and 92%, respectively. These yield values can be converted into estimates of (I_A/α_A) ratios through the use of eq 4.[3,4,10] The ratios obtained from the present experiments are $(I_{CD_4}/\alpha_{CD_4}) = 0.70$ and $(I_{H_2}/\alpha_{H_2}) = 2.6$. These values are quite similar to those found by extrapolation for the CH_4–D_2 system: $(I_{CH_4}/\alpha_{CH_4}) = 0.76$ and $(I_{D_2}/\alpha_{D_2}) = 2.7$.

$$P_A = 1 - \exp(-I_A/\alpha_A) \qquad (4)$$

Adjustment of Parameters for the Kinetic Theory. One of the most basic assumptions implicit in any use of the formulation given above for a kinetic theory of recoil tritium reactions is the assumption that an energy loss parameter exists which can accurately describe the *fractional* energy losses in collisions over a substantial range in kinetic energies of the hot atoms involved.[11] If this is approximately true, then the absolute energy loss in a collision is not as significant as the fractional energy loss, and the appropriate energy scale is the logarithmic energy scale used in the definition of the reactivity integral.[3,4] If, however, the value of α, the average logarithmic energy loss, does vary appreciably with energy, then the approach followed in the usual kinetic theory treatments has serious limitations.[11]

Virtually no data exist which would permit calculations of α values at different energies, especially for the energy region pertinent for recoil tritium reactions, or roughly 1–20 eV. Accordingly, one can look upon the kinetic theory of hot reactions as a plausible framework within which to attempt a crude description of hot atom chemical systems—a description utilizing two empirical parameters to summarize the data. One can attempt first to determine whether values exist for the empirical parameters, α and I, which will accurately reflect the experimental data. If such values exist, one can then search for additional tests of the plausibility and utility of these values. Computer simulation has shown that the parameters have validity for certain reasonable representations of the probable course of hot atom processes.[10,12,13]

One of the most useful tests for such parameters is a determination of their utility for the description of energetic reactions in systems other than those in which the values were estimated. Application of the pure system values to binary mixtures furnishes one critical test; application of data from one binary system to another binary system furnishes another such test.

Estimates of *total* hot yields in mixed systems require assumptions regarding the combination rules for I and α values in mixed systems. The usual assumption for α values is directly adapted from the theory of neutron moderation

$$\alpha = \sum_i f_i \alpha_i \qquad (5)$$

in which the f_i terms represent the respective fractions of energetic collisions occurring with the ith species in the mixture. The I_i values are also assumed here to follow linear combination rule

$$I = \sum_i f_i I_i \qquad (6)$$

Total Hot Yields and Specific Yield Ratios. The total hot yields of all products in CD_4–H_2 mixtures can readily be fitted over the whole mole fraction range by a simple linear combination of values for the pure components,

(10) P. Coulter and F. S. Rowland, *Radiochim. Acta*, 2, 163 (1964).
(11) P. J. Estrup, *J. Chem. Phys.*, 41, 167 (1964).
(12) R. M. Felder and M. D. Kostin, *ibid.*, 43, 3082 (1965).
(13) R. M. Felder, *ibid.*, 46, 3185 (1967).

and the fit obtained for CD_4–H_2 closely parallels the corresponding results found for CH_4–D_2 mixtures. In the latter case the almost constant ratio of specific yields between CH_4 products (HT and CH_3T) and the D_2 product (DT) permitted the simplifying assumption that the energy ranges of reaction were quite similar for all species, and a good fit was obtained for the individual product yields over the entire mole fraction range.[2,4]

Any suitable calculation of individual hot yields in the CD_4–H_2 system requires a satisfactory explanation for the observed variations in the *ratios* of the specific yields with mole fraction. Although variations in α can easily alter the average number of energetic collisions available at each mole fraction, variation in the *ratio* of specific yields requires different energy dependences for the hot reaction cross sections for the two components. Study of simple models based upon smooth, continuous energy-dependent cross sections quickly demonstrates that the only choices that can account for the constant specific yield of HT, while also permitting a decrease in the (CD_3T/CD_4) ratio with increasing mole fraction of CD_4, involve models in which recoil tritium reactions with H_2 proceed with reasonable probability down to energies substantially below the threshold energy for reactions with CD_4.

Applications to Other Binary Mixtures. Enough data are now avialable for recoil tritium systems involving binary mixtures of Ar with CH_4–CD_4–H_2–D_2 that the relative magnitudes of the parameters of the kinetic theory of hot reactions have been fixed within fairly narrow limits for the pure compounds. Combinations of these parameters can produce information that should be applicable to other binary mixtures.[5] As an example, the formation of CH_3T from CH_4 is favored by a factor of 1.31 ± 0.04 over the formation of CD_3T from CD_4 in direct competition experiments involving CH_4–CD_4 mixtures.[7] Small differences in the energy ranges of hot reaction can be anticipated for CH_4 and CD_4, based upon the observation that the specific yield ratio $(CH_3T/CH_4)/(CD_3T/CD_4)$ rises to a value of about 7 when the tritium atoms are introduced into the system at 2.8 eV through TBr photolysis.[14] On the other hand, the total yields for substitution reactions are very small at 2.8 eV, and the contribution of these reactions to the total hot yield is presumably almost negligible. Unpublished experiments by Chou have shown that nuclear recoil tritium reacts in both neon- and argon-moderated CH_4–CD_4 mixtures to give specific yield ratios in the range of 1.32 ± 0.03. This agreement between moderated and unmoderated values for the nuclear recoil systems implies the absence of any appreciable difference in the average energy at reaction for the two isotopic methanes. Similar conclusions have been reached from comparisons of competitions with cyclobutane[15] and with helium[16] for the isotopic pair CH_3F–CD_3F.

Based on the specific yield ratio 1.31 ± 0.04 as a good approximation for the (I_{CH_4}/I_{CD_4}) ratio, together with values of the (I_{CH_4}/α_{CH_4}) and (I_{CD_4}/α_{CD_4}) ratios obtained from experiments with the pure molecules, the relative α values of the isotopic methanes can be estimated as

$$\left(\frac{\alpha_{CH_4}}{\alpha_{CD_4}}\right) = \left(\frac{I_{CH_4}/0.76}{I_{CD_4}/0.70}\right) = \frac{(0.70)(1.31 \pm 0.04)}{(0.76)} \approx 1.21 \pm 0.05 \quad (7)$$

This calculation shows that energetic tritium atoms lose more energy on the average in collisions with CH_4 than in collisions with CD_4. Furthermore, the calculated $(\alpha_{CH_4}/\alpha_{CD_4})$ ratio is in good agreement with the earlier estimate of $(\alpha_{CH_3F}/\alpha_{CD_3F}) = 1.23 \pm 0.08$.[16] In both cases collisions with the protiated species remove *more* energy on the average than collisions with the deuterated species. This effect is qualitatively in the opposite sense from that anticipated for a quasi-elastic collision model. The latter model is based upon momentum conservation in atom–atom collisions[17] and suggests larger energy transfer between the colliding atoms which are more nearly matching in mass.[18] The rather similar total absolute yields of hot products formed in pure CH_4 and pure CD_4 are thus not inconsistent with the rather large reactive isotope effect between these two molecules, because the greater reactivity in CH_4 is essentially cancelled by the greater collisional energy loss in CH_4, so that fewer collisions are available in the protiated medium.

The I and α parameters have been measured for H_2 and D_2 and have been shown to be quite similar in magnitude—not only are the (I/α) ratios about equal (compare our values of 2.7 and 2.6), but the (I_{H_2}/I_{D_2}) ratio has been estimated as 1.15 ± 0.04 in argon-moderated direct competition experiments.[19] These data can be combined to show that the average energy losses in H_2 and D_2 must be rather similar, but not very accurately known: $(\alpha_{H_2}/\alpha_{D_2}) = 1.1 \pm 0.1$. Such calculations with H_2 and D_2 are particularly subject to large errors because of the very high total hot yields, and the inherent inaccuracy in estimates based upon differences between hot yields of 100 and 90–95%.

Despite the experimentally measured near-equality of I_{H_2} and I_{D_2}, the specific yield ratio $(HT/H_2)/(DT/D_2)$

(14) C. C. Chou, Ph.D. Thesis, University of California, Irvine, Calif., 1968.

(15) E. K. C. Lee and F. S. Rowland, *J. Amer. Chem. Soc.*, **85**, 2907 (1963).

(16) E. K. C. Lee, G. Miller, and F. S. Rowland, *ibid.*, **87**, 190 (1965). See also T. Smail and F. S. Rowland, *J. Phys. Chem.*, **74**, 456 (1970).

(17) H. Jurgeleit and R. Wolfgang, *J. Amer. Chem. Soc.*, **85**, 1057 (1963).

(18) The maximum collisional energy transfer between an energetic recoil atom of mass 3 and a free atom of mass 2 is 96%; between the mass 3 species and a free atom of mass 1 is 75%.

(19) D. Seewald, M. Gersh, and R. Wolfgang, *J. Chem. Phys.*, **45**, 3870 (1966).

has a value of about 1.5 in unmoderated mixtures of H_2 and D_2.[19–21] The reduced value of this ratio in moderated systems implies, by application of the kinetic theory of hot atom reactions, that the reaction with D_2 must occur at a lower average energy than the reaction with H_2. This implication is consistent both with the results of trajectory calculations for the T + H_2 and T + D_2 systems[22] and with the specific yield ratios (about 1.0) found for photochemically produced 2.8-eV tritium atom reactions in H_2–D_2 mixtures.[23]

A qualitative inconsistency can now be seen in the respective requirements that (a) the energy ranges of hot reactions for CH_4 and CD_4 are approximately the same; (b) the ranges for CH_4 and D_2 are about the same; (c) H_2 reacts extensively at energies below the CD_4 threshold; and (d) D_2 reacts at a lower average energy than H_2. We have attempted a variety of simple model calculations for possible choices of reaction energy ranges, with the result that this qualitative inconsistency has been found to persist quite strongly. We have not been able to obtain even an approximately satisfactory set of reactivity integrals capable of reproducing the qualitative features of the experimental observations for all of the various binary pairs. While we do not wish to rule out entirely the possibility that a satisfactory fit might be based on the kinetic theory of hot atom reactions as applied to binary mixtures, we do feel that no fit will be possible involving rather broad, structureless reactivity integrals. The use of detailed hypothetical "fine structure" models seems inappropriate in connection with a theory which has been intended to provide only broad average outlines of reaction excitation functions.

The present failure to obtain a mutually consistent set of reactivity integrals for this group of four molecules does not necessarily eliminate the usefulness of this kind of model for the description of other binary systems. The very high total reactivities, low masses, etc., of the molecular hydrogen species make them rather atypical molecules, so that deviations from simple kinetic theory behavior are perhaps more to be expected in their mixtures with alkanes than, for example, in mixtures of different alkanes with one another. It seems quite plausible to us that the assumption of an energy-independent α for each of the molecules in a closed cycle of binary systems is at best only a rough approximation. Other similarities between the species to be compared may be required in order for the hot atom kinetic theory to be useful for simple descriptions of such binary systems. Such similarities could occur, for example, in the reaction energy ranges, such as might be expected for C–H bonds in species A *vs.* C–H bonds in species B, or in the nature of the energy loss processes involved, as may be true for CH_4 and CD_4 despite the 20% greater average energy loss in CH_4. The present comparison involving CD_4 and H_2 probably fails to mesh with earlier data simply because the nature of both reactive and nonreactive collisions with CD_4 and H_2 are too unlike to permit satisfactory averaging of the kind required. The failure in the CD_4–H_2 system furthermore makes us quite skeptical of the excellent fit found in our CH_4–D_2 mixtures[2]—the near constant ratio of specific yields may well involve some fortuitous "cancellations" of effects involving quite different energy ranges for reaction for CH_4 and D_2.

(20) J. K. Lee, B. Musgrave, and F. S. Rowland, *J. Chem. Phys.*, 32, 1266 (1960).

(21) J. W. Root and F. S. Rowland, unpublished data.

(22) M. Karplus, R. Porter, and R. Sharma, *J. Chem. Phys.*, 45, 3871 (1966).

(23) C. C. Chou and F. S. Rowland, *ibid.*, 46, 812 (1967).

The Primary Replacement Isotope Effect in Recoil Tritium Reactions with Isobutane[1]

by Thomas Smail and F. S. Rowland

Department of Chemistry, University of California, Irvine, California 92664 *(Received April 25, 1969)*

The primary replacement isotope effect for the substitution of T atoms for H or D atoms in hydrocarbons has been measured as 1.25 ± 0.05 through comparison of recoil tritium reactions at the tertiary position in $(CH_3)_3CH$ *vs.* $(CH_3)_3CD$ and $(CD_3)_3CH$ *vs.* $(CD_3)_3CD$. The increased yield for replacement of H *vs.* D is suggested to result from the more rapid response of H atoms to changes in chemical binding during the interactions of the butane molecules with energetic T atoms. The isotope effect in the abstraction of H *vs.* D from the tertiary position in isobutane is 1.65 ± 0.06. Alkyl substituent effects, including steric hindrance, are essentially absent in gas phase experiments with *i*-C_4D_{10} (R = 0.96; R = tertiary T per bond/primary T per bond) and small with *i*-C_4H_{10} (R = 0.87). A gas/liquid phase effect is observed which reduces the liquid phase value of R by 15–25%.

Introduction

The reactions of the energetic tritium atoms from nuclear recoil have been extensively studied in recent years with a variety of hydrocarbons, with considerable emphasis upon the substitution reaction 1 initiated by tritium atoms with greater than thermal energies.[2-4] Isotope effects have been studied for this reaction

$$T^* + RH(D) \longrightarrow RT + H(D) \qquad (1)$$

as well as for hydrogen abstraction and other substitution reactions, through comparison of results obtained with protonated *vs.* partially and fully deuterated target molecules.[5-11] The present paper describes the first measurement of the primary replacement isotope effect[12] for the replacement of H or D by energetic tritium atoms, as in (1), in the absence of other isotope effects.[11]

Isotopic comparisons have been made earlier of the absolute yields of CH_3T and CD_3T from recoil T reactions with pure CH_4 and pure CD_4, respectively.[13] In such a comparison, one must consider three possible sources of isotopic differences: (1) primary replacement isotope effect, the variation in yield caused by the difference in the identity, H *vs.* D, of the replaced atom; (2) secondary isotope effect, the variation in yield attributable to the isotopic difference, CH_3 *vs.* CD_3, in the identity of the group to which the tritium atom becomes bonded during the reaction; and (3) moderator isotope effect, the variation in yield caused by differences in the rates of energy loss in nonreactive collisions with isotopic molecules, CH_4 *vs.* CD_4, which are duly reflected in the number of collisions occurring in the energetic range, and in the yields of hot reactions resulting from those collisions.

Both moderator and secondary isotope effects have been demonstrated to be substantial with each resulting in larger yields for the protonated molecule.[7,8] The secondary isotope effect in the substitution of T-for-F in CH_3F *vs.* CD_3F was shown to favor the former by competition experiments involving mixtures of methyl fluoride with cyclobutane[7] or helium;[8] combination of these results with those found for the pure molecules alone permitted calculation of a moderator effect of 1.23 ± 0.08, favoring more rapid energy loss (and therefore lower yield) for collisions of tritium with CH_3F *vs.* CD_3F.[8] An isotopic preference for the replacement of H in CH_3F *vs.* D in CD_3F was also demonstrated in the same experiments, but involves simultaneously the possibility of both primary replacement and secondary isotope effects, and cannot be unequivocally assigned to either.

The effects of moderator differences can be almost completely cancelled by competition experiments in which both competing molecules are exposed to the

(1) This research has been supported by Atomic Energy Commission Contract No. AT-(11-1-)34, Agreement No. 126.

(2) F. Schmidt-Bleek and F. S. Rowland, *Angew. Chem., Int. Ed.*, **3**, 769 (1964).

(3) R. Wolfgang, *Progr. Reaction Kinetics*, **3**, 97 (1965).

(4) R. Wolfgang, *Ann. Rev. Phys. Chem.*, **16**, 15 (1965).

(5) J. W. Root and F. S. Rowland, *J. Amer. Chem. Soc.*, **85**, 1021 (1963).

(6) H. C. Jurgeleit and R. Wolfgang, *ibid.*, **85**, 1057 (1963).

(7) E. K. C. Lee and F. S. Rowland, *ibid.*, **85**, 2907 (1963).

(8) E. K. C. Lee, G. Miller, and F. S. Rowland, *ibid.*, **87**, 190 (1965).

(9) E. K. C. Lee, J. W. Root, and F. S. Rowland, "Chemical Effects of Nuclear Transformations," Vol. 1, International Atomic Energy Agency, Vienna, 1965, p 55.

(10) C. C. Chou and F. S. Rowland, *J. Amer. Chem. Soc.*, **88**, 2612 (1966).

(11) T. Smail and F. S. Rowland, *J. Phys. Chem.*, **72**, 1845 (1968).

(12) The term "primary replacement isotope effect" has been proposed by us for comparisons of T* + RH *vs.* T* + RD, both leading to RT; the term "primary substitution isotope effect" has similarly been proposed for comparisons of T* + RH *vs.* D* + RH *vs.* H* + RH. No measurement of a primary substitution isotope effect in the absence of other isotopic differences has yet been reported.

(13) J. Cross and R. Wolfgang, *J. Chem. Phys.*, **35**, 2002 (1961).

same tritium atom flux.[7,8,14] Secondary isotope effects can be eliminated by making comparisons of the substitution reaction with molecules which are identical except for one H *vs.* D, as with CHX_3 and CDX_3. Our present measurements have been carried out with a series of isotopic isobutane molecules and involve two sets of comparisons: $(CH_3)_3CH$ *vs.* $(CH_3)_3CD$; and $(CD_3)_3CH$ *vs.* $(CD_3)_3CD$. In the first pair, the great majority of the energetic collisions occur with CH_3 groups, and neither the substitution into the primary position nor the energy loss in nonreactive collisions should be appreciably affected by the presence of H or D in the tertiary position. Consequently, the tertiary H or D atom is exposed to essentially equivalent tritium atom fluxes, and the yield for replacement of each can be directly compared to the substitution for H in the primary position of the same molecule. An equivalent set of comparisons can be made for reactions in which both the substitution in the primary position and energy loss in nonreactive collisions occur with CD_3 groups. The tritium content of the primary and tertiary positions in isobutane can be established by isotopic exchange of the former under conditions permitting retention of the tertiary activity.[15,16]

Experimental Section

Chemicals. Isobutane and 1,3-butadiene were Phillips Research grade. The deuterated isobutanes were supplied by Merck Sharp and Dohme of Canada and were stated to have a minimum isotopic purity of 98%. All gases were used without further purification, other than degassing at −196° just prior to filling of samples. ^3He was degassed from a charcoal trap at −196° and was free of HT impurity.

Sample Preparation. Gas samples were filled according to the usual procedures.[2-9] Liquid samples were prepared by successive condensation of butadiene and then isobutane into an evacuated capillary tube containing about 10 mg of LiF. The composition of the liquid samples was controlled through the use of calibrated volumes on the sample filling vacuum line.

Sample Analysis. The distribution of tritium activity among the various radioactive products was determined by conventional radio gas chromatography.[17] HT/DT, CH_3T, C_2H_3T, and C_2H_5T were separated using a 50-ft, 1/4-in. od column of 30–40 mesh alumina which had been partially deactivated by coating with approximately 10% by wt propylene carbonate. The column was operated at 0° and 0.5 ml/sec He carrier flow rate. HT and DT were resolved with a 7-ft, 1/4-in. od column of γ-alumina (40–50 mesh) coated with approximately 3.5% Fe_2O_3, operated at 0.5 ml/sec He flow rate and 77°K. A "stripper" column of activated charcoal (10-ft, 1/4-in. od) operated at 25° was placed in front of the Fe_2O_3–Al_2O_3 column so that only isotopic hydrogens were allowed into the low-temperature column. Full details of the preparation of these columns has been given.[18] Separation of hydrocarbons through C_4 was obtained with a 50-ft 1/4-in. od column containing 30% by weight of di-*n*-butyl phthalate on 30–60 mesh chromosorb P. The operating conditions were 0° and 0.5 ml/sec He flow rate. This column was also used for the purification of the isobutane fraction from irradiated samples.

Analysis of the Intramolecular Location of Tritium in Isobutane-t. Otvos, *et al.*,[19] demonstrated rapid primary hydrogen atom exchange for isobutane dissolved in concentrated sulfuric acid through a $t\text{-}C_4H_9^+$ intermediate, and this procedure was adapted for intramolecular analysis of the tritium positions in isobutane by Odell, *et al.*[15] The technique used in the present experiments is a modification of that described in detail by Rosenberg.[16]

Isotopic exchange of hydrogen was carried out in sealed glass ampoules, maintaining the relative amounts of isobutane (600 cm-ml) and concentrated sulfuric acid (8 ml) and the gas/liquid volume ratio (1.4) in the ampoule constant to within ±5%. The exchange rate between primary tritium in isobutane and acid protons was determined for these standard experimental conditions, as indicated in Figure 1. In the first set of experiments, isobutene (0.5% x isobutane) was added to accelerate the primary exchange reaction, and exchange was carried out for a total time of 10–12 hr. In the second set of experiments, no isobutene was added, and exchange was carried out for total times of 20–26 hr.

The amounts of isobutane and concentrated sulfuric acid were such that about 1% of the original primary tritium atoms would remain in the isobutane when isotopic equilibrium was reached between hydrocarbon and original acid. About halfway through the exchange period (5–6 hr with isobutene; 10–15 hr without) the isobutane was transferred into a fresh batch of acid and the exchange continued. With two such batches of acid, removal of primary tritium was more than 99.9% complete.

The exchange reaction was followed by measuring the specific radioactivity of the gas chromatographically purified isobutane-*t*, *i.e.*, counts per minute of radioactivity per unit area of mass peak under standard conditions. Typical measurements are given in Table I.

(14) J. W. Root, W. Breckenridge, and F. S. Rowland, *J. Chem. Phys.* **43**, 3694 (1965).

(15) A. Odell, A. Rosenberg, R. Fink, and R. Wolfgang, *ibid.*, **40**, 3730 (1964).

(16) A. Rosenberg, Ph.D. Thesis, Yale University, 1964.

(17) J. K. Lee, E. K. C. Lee, B. Musgrave, Y. N. Tang, J. W. Root, and F. S. Rowland, *Anal. Chem.*, **34**, 741 (1962).

(18) J. W. Root, Ph.D. Thesis, University of Kansas, 1964.

(19) J. W. Otvos, D. P. Stevenson, C. D. Wagner, and O. Beeck, *J. Amer. Chem. Soc.*, **73**, 5741 (1951).

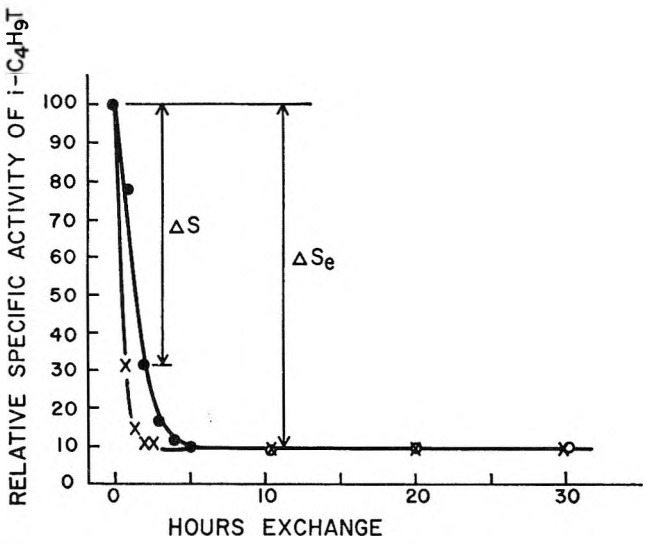

Figure 1. Primary tritium exchange in i-C_4H_9T: ×, 0.5% i-C_4H_8 added; ●, no i-C_4H_8 added.

Table I: Relative Specific Activity of i-C_4H_9T *vs.* Exchange Time in Concentrated H_2SO_4

Time, hr	Relative specific act., = 100 at zero time: i-C_4H_{10} + 0.5%C_4H_8	i-C_4H_{10} Only
2.00	10.8 ± 0.18	31.2 ± 0.27
5.00	9.56 ± 0.18	9.93 ± 0.18
10.3	9.81 ± 0.17	9.43 ± 0.18
20.0	9.37 ± 0.14	9.54 ± 0.18
30.0	8.62 ± 0.14	9.21 ± 0.17

Exchange of Tertiary Hydrogen Atoms. Study of the long term behavior of $(CH_3)_3CT$ in sulfuric acid revealed a slow exchange of the tertiary tritium with the acid. Without added isobutene, the tertiary exchange reaction appeared to have an induction period under our experimental conditions of approximately 20 hr. The addition of 0.5% isobutene removed the induction period, and accelerated the rate of tertiary exchange. The first set of experiments, involving added isobutene in each case, has therefore been corrected for the loss of tertiary tritium activity which occurred during the 10–12 hr necessary for complete removal of the primary tritium atoms. These corrections ranged as large as 10% for the estimate of tritium activity remaining after complete primary exchange. The second set of experiments was conducted after the detailed measurements of the rate of tertiary exchange, and required no correction since the primary exchange was completed while tertiary exchange was still negligible (<1%). The agreement between the two sets of data was satisfactory, although the second set of data is believed by us to be the more accurate.

Isotope Effects on Rate of Tritium Exchange. Possible isotopic differences in the rates of exchange of primary tritium were investigated by comparison of $CH_2TCH(CH_3)_2$ and $CD_2TCD(CD_3)_2$. No significant isotopic difference was observed in the rate of primary exchange in the presence of 0.5% added isobutene (C_4H_8), as shown in Figure 2 for the first-order rates using ΔS and ΔS_e measured as shown in Figure 1. In the absence of isobutene, the primary exchange rate of $CD_2TCD(CD_3)_2$ is indeed slower than that of $CH_2TCH(CH_3)_2$, but exchange is still complete within 20 hr as shown in Table II. The simultaneous removal

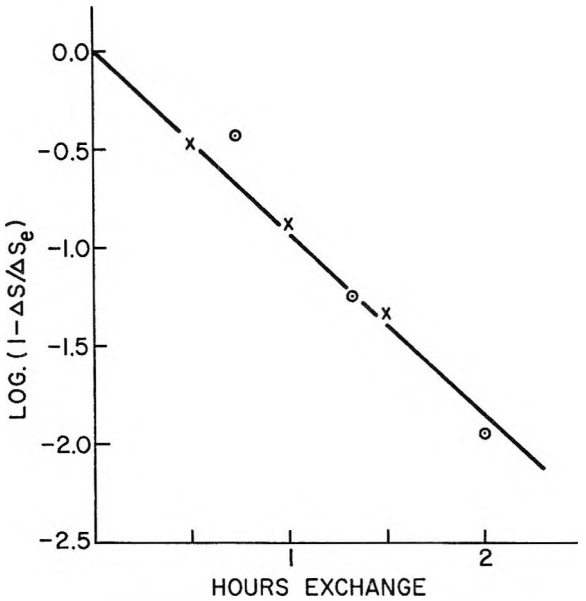

Figure 2. Primary tritium exchange in i-C_4H_9T(⊙) and i-C_4D_9T (×), each with 0.5% i-C_4H_8 present.

Table II: Exchange Rate of Primary Deuterium Atoms in Concentrated Sulfuric Acid, No Added Isobutene

Mass peak areas, total = 100 C_4D_{10}	C_4H_9D	Time of exchange, hr
100	0.0	0
69.7	30.3	1.53
46.5	53.5	3.03
0.04	100.0	20.3

of all nine primary D atoms, as expected for the exchange between $C_4D_9D + C_4H_9^+ \rightleftharpoons C_4D_9^+ + C_4H_9D$, can be readily followed through observation of the mass peaks corresponding to C_4D_{10} and C_4H_9D in the thermal conductivity detector of the usual radio gas chromatographic analysis. A separate experiment showed that the rate of disappearance of the C_4D_{10} mass peak paralleled the rate of removal of primary tritium activity, as would be expected on the basis of the earlier work by Otvos, *et al.*[19]

A typical analysis proceeded as follows. After irradiation, the isobutane was purified by vpc, and a small aliquot was kept for measurement of the initial

Table III: Specific Activity Measurements for Removal of Primary Tritium Activity from C_4D_9T; Specific Activity Ratio, R

Exchange time, mass peak area		Target material: i-C_4D_{10}, gas phase		
hr	Arbitrary units	Observed radioactivity, counts	Specific Activity, counts/unit	Mean value
Unexchanged	64.06	58,530 ± 250	913.7 ± 3.9	
	61.06	56,050 ± 250	917.9 ± 4.0	918.2
	62.65	57,820 ± 250	923.0 ± 4.0	
26.0 Hours	193.26[a]	17,200 ± 150	89.0 ± 0.8	
	179.64	15,570 ± 150	86.7 ± 0.8	87.7
	176.12	15,390 ± 150	87.4 ± 0.8	

[a] After exchange, the mass peak is $(CH_3)_3CD$, and the area has been corrected for the change in thermal response constants.[19]

$$R = \frac{\text{T activity per tertiary C–D bond}}{\text{T activity per primary C–D bond}} = \frac{87.7 \times 9}{918.2 - 87.7} = 0.97$$

Table IV: Distribution of Radioactive Products from Recoil Tritium Reactions with Isotopic Isobutanes

		$(CH_3)_3CH$	$(CH_3)_3CD$	$(CD_3)_3CD$	$(CD_3)_3CH$	$(CH_3)_3CH$	$(CD_3)_3CD$
Pressure, cm	Isobutane	81.2	71.1	75.6	71.2		
	^3He	2.3	2.1	2.2	2.5	liq[a]	liq[a]
	O_2	5.2	6.5	6.2	6.3		
Radioactive Product Yields[b]				(Isobutane-t = 100)			
Hydrogen		191	173	189	206	165	187
Methane		15.8				25.6	
Ethylene		1.0	1.0	0.4	0.8	1.9	1.7
Propane		3.2	3.2	3.5	3.6	4.6	5.4
Acetylene						0.4	
Propylene		7.0	7.2	3.8	4.2	3.4	2.2
Isobutane		100	100	100	100	100	100
Isobutene		1.0	0.9	nd	nd	nd	nd

[a] Contained 11% butadiene as scavenger. [b] Mixed deuterated and protonated species.

Table V: Intersample Comparison of Relative Yields for Abstraction Reactions of Recoil Tritium with Gaseous Isobutanes

Isotopic isobutane	Measured yields[a]		Position yields[b]		$\left(\frac{HT}{DT}\right)_{PRI}$	$\left(\frac{HT}{DT}\right)_{TERT}$
	HT	DT	Primary	Tertiary		
$(CH_3)_3CH$	20700	0	14780	5920	1.15	1.59
$(CH_3)_3CD$	14780	3720	14780	3720		
$(CD_3)_3CH$	7280	12650	12850	7000		1.72
$(CD_3)_3CD$	280	16730	12850	4080		

[a] Counts per minute in counter, normalized for equal irradiation times, ^3He content, and flow rates. [b] Abstraction yields from individual positions.

specific activity. The remainder was frozen onto degassed 98% sulfuric acid and, after thawing, was shaken for the required time (including transfer halfway through to a fresh batch of sulfuric acid). The specific activities of the original and the acid-washed isobutane were then determined under closely parallel chromatographic conditions. Gas chromatographic peak areas were estimated with a Disk integrator, and corrections were made for the variation in thermal response constant with deuteration.[20] All analyses were performed at least in duplicate.

Typical data and calculations are illustrated in Table III. The final experimental goal is the value of R, defined as the ratio of specific activities of the tertiary and primary positions of the molecule. The primary replacement isotope effect is simply the value of the ratio of R_{CHX_3}/R_{CDX_3}.

Results

Intermolecular Distributions of Radioactivity in Iso-

(20) Relative thermal response constants were determined to be i-C_4H_{10}, 1.000; i-C_4D_{10}, 0.960. Response constants for partially deuterated isobutanes were obtained by interpolation.

Table VI: Primary Replacement Isotope Effect for Recoil Tritium Reactions with Isotopic Isobutanes

Compound	R[a] Set 1[b]	R[a] Set 2[c]	Primary replacement isotope effect[d] Set 1	Primary replacement isotope effect[d] Set 2
Gas phase[e]				
$(CH_3)_3CH$	0.85	0.87[g]	1.21	1.26 ± 0.04
$(CH_3)_3CD$	0.70	0.69		
$(CD_3)_3CH$	1.17	1.20	1.30	1.25 ± 0.04
$(CD_3)_3CD$	0.90	0.97		
		0.95		
Liquid phase[f]				
$(CH_3)_3CH$	0.72	0.75	1.18	1.23 ± 0.06
$(CH_3)_3CD$	0.61	0.61		
$(CD_3)_3CH$	0.90	0.99	1.10	1.27 ± 0.06
$(CD_3)_3CD$	0.82	0.78		

[a] R = T activity per tertiary bond/T activity per primary bond; see sample calculation in Table III. [b] 0.5% isobutene added in the exchange. [c] No added isobutene. [d] Primary replacement isotope effect = R_{CHX_3}/R_{CDX_3}. [e] Sample contents: 2 cm of ^3He, 6 cm of O_2, 70 cm of isobutane. [f] Sample contents: LiF, 10 mol % butadiene, isobutane. [g] Error typically ±0.02, taken into account in errors quoted on isotope effects.

butane Systems. The distribution of radioactivity among the various product molecules is shown in Table IV. The observations are in reasonable agreement, both in qualitative identification of product and quantitative yield ratios, with earlier isobutane experiments.[3,16]

The yields of both HT and DT were determined for all of the gas samples, and have been normalized in Table V for equal neutron irradiations, equal ^3He content, and identical chromatographic conditions. The HT from i-C_4D_{10} arises from C_4D_9H impurity. The abstraction from primary and tertiary positions has been estimated by assuming that the tritium atom flux in $(CH_3)_3CH$ and $(CH_3)_3CD$ is the same, and therefore that the HT yield from CH_3 positions is the same for both, with the incremental HT from $(CH_3)_3CH$ assigned to tertiary C–H. An approximate correction (HT:280 = DT:200) has been made for isotopic impurity to both $(CD_3)_3CH$ and $(CD_3)_3CD$ prior to a similar assignment between primary and tertiary positions. The HT/DT abstraction isotope effect at tertiary positions is estimated to be 1.65 ± 0.07 from the data of Table V. The HT/DT ratio in the primary abstraction shows a preference for abstraction from H of only 1.15, but includes both the actual reactive isotope effect and the moderator isotope effect. Since HT/DT reactive isotope effects for CH_3 *vs.* CD_3 groups are usually 1.3–1.4, the isobutane experiments indicate that energy losses are sufficiently greater in $(CH_3)_3CH$ to reduce the tritium atom flux *vs.* $(CD_3)_3CD$ by about 1.15–1.20. Isotopic differences in α[21] of this magnitude [$\alpha(RH)/\alpha(RD) \backsim 1.2$] have been previously noted for CH_4/CD_4, CH_3F/CD_3F, and C_4H_{10}/C_4D_{10}.[7-9,18,22]

A complete summary of the intramolecular tritium distribution in each of the isobutanes is given in Table VI, together with the isotope effect for the replacement of the tertiary hydrogen. Data listed under set 1 refer to the experiments with added isobutene in which corrections for loss of tertiary tritium were required. They are in reasonable agreement with the later results shown in set 2. The latter are believed to be somewhat more dependable since no corrections were needed. No significant phase effect appears in the replacement isotope effect which is constant at about 1.25. However, the intramolecular tritium distribution does show a phase change, with a reduction in the per bond substitution ratio for tertiary/primary hydrogens (R) in the liquid phase.

Discussion

Effects of Isotopic Impurities. While the deuterated isobutanes were stated to have >98% D atom content, the presence of 2% H atoms means that 20% of the molecules in i-C_4D_{10} are i-C_4D_9H. The actual HT measurement from i-C_4D_{10}, corrected for isotope effects in abstraction of $\backsim$1.4, suggests an impurity concentration of about 1.2% H atoms. Since the substitution reaction is practically indiscriminate in position attack (teritary *vs.* primary) and favors H over D by only about 30%, its occurrence in i-C_4D_{10} is only slightly misjudged by experiments involving 88% i-C_4D_{10} and 12% i-C_4D_9H, or in partially-deuterated isobutanes of similar isotopic purity.

Alteration of Isobutane-t Distribution by Secondary Reaction. The substitution of T for H or D in a hydrocarbon usually leaves highly excited T-labeled products, and these molecules frequently are capable of undergoing secondary isomerization and/or decomposition reactions.[2-4,23,24] Since the conclusions summarized in

(21) α = average logarithmic energy loss in nonreactive collisions.

(22) J. W. Root and F. S. Rowland, *J. Phys. Chem.*, 74, 451 (1970).

(23) E. K. C. Lee and F. S. Rowland, *J. Amer. Chem. Soc.*, 85, 897 (1963).

(24) C. T. Ting and F. S. Rowland, *J. Phys. Chem.*, 72, 763 (1968).

Table VI have been reached solely through analysis of the intramolecular location of tritium in various isobutane-*t* molecules, the results are clearly susceptible to error if the isobutane-*t* molecules which actually decompose are not identical in intramolecular T distribution with those that survive.

The products shown in Table IV include those expected from direct abstraction or substitution (hydrogen, methane, propane, isobutane) and some whose source is attributable to secondary reaction (ethylene, propylene, isobutene, acetylene). Electronically excited isobutane is known to decompose to methane + propylene and probably to molecular hydrogen + isobutene.[25] While thermal decomposition of isobutane proceeds by C–C split,[26] the much broader distribution of excitation energies for recoil tritium excited molecules may well result in decomposition of highly vibrationally excited isobutane-*t* by the paths identified for the electronically excited molecules. Some propylene-*t* may also be formed by H_2 loss from excited propane-*t*, while a larger fraction of excited CH_3T should decompose in the gas phase than in liquid experiments.

Both propane-*t* and methane-*t* decrease in yield from liquid to gas, as expected for excited primary products; propylene-*t* increases as expected for a secondary product. Comparison of the gas phase propylene-*t* yields clearly shows isotope effects, with about 75% higher relative yields for the highly protonated molecules than for the two highly deuterated compounds.

Four separate kinds of kinetic effects could perturb the intramolecular distribution of the tritium away from that created during the original primary substitution reaction. We shall discuss each of these briefly, although our final conclusion is that none of these effects would be large enough to account for the observed isotopic differences.

(*a*) *Position Eeffect on Energy Deposition during Substitution.* Replacement at tertiary and primary positions by a tritium atom might leave differing amounts of excitation energy in the resultant molecules. However, experiments with dimethylcyclobutane, for which the decomposition product propylene is readily recovered, have indicated that the energy deposition is quite similar for the replacement of either kind of ring hydrogen or of a methyl group hydrogen.[27]

(*b*) *Isotope Effects on Energy Deposition.* Replacement of H *vs.* D at equivalent positions could leave different excitation energies in the tritium-labeled products. A comparison of the pressure dependence of the parent yield from recoil tritium reactions with cyclobutane and cyclobutane-d_8 has shown that the energy deposition is very nearly equivalent for the replacement of H and D in these two molecules,[28] the effect is presumably unimportant for isobutane-*t* also.

(*c*) *Secondary Isotope Effects on Decomposition Rates.* For any arbitrary excitation energy, the more H atoms in isobutane, the larger the expected rate constant for decomposition.[29] While the magnitude of this effect on k_{decomp} is about a factor of 5 for 8 or 9 H/D pairs, the effect is minimal since the most critical comparisons involve molecules differing only by one H/D pair.

Each of the first three effects can produce measurable but small changes in carefully chosen systems. None, however, will result in substantial changes in the observed tritium atom distribution in this particular system, especially since most of the excited isobutane-*t* molecules survive in both the liquid- and gas-phase irradiations. The fourth possibility is potentially more serious in the isobutane-*t* system.

(*d*) *Primary Isotope Effects on Decomposition Rates.* No primary isotope effect would be associated with those molecules which decompose by C–C split, the pathway followed by thermally excited species.[26] Highly vibrationally excited isobutane may decompose by the molecular elimination of CH_4, and two possible mechanisms may be written

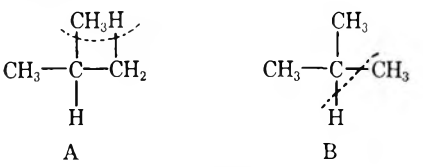

A B

If we assume that transfer of T is very unfavorable relative to transfer of H, then mechanism A will lead to slight enhancement of the primary-*t* in the survivor molecules, since the primary-*t* molecules decompose only $^8/_9$ as fast as the tertiary-*t* molecules. Mechanism B, on the other hand, could lead to considerable depletion of the primary-*t* molecules and little decomposition of the tertiary-*t* species. Mechanisms A and B appeared to be involved to equal extents in the decomposition of electronically excited isobutane.[25] Unless mechanism B predominates strongly over both A and C–C split, a possibility we are inclined to discount, the intramolecular *t*-distribution will not be seriously affected by the decomposition.

Since the fractional decomposition is no more than a few per cent in liquid phase isobutane-*t* samples, the R values for the liquids cannot possibly be more than a few per cent in error in these cases, and the *ratios* of R values would be almost completely insensitive to such errors. Consequently, we conclude that none of the four kinetic factors listed above can have altered the intramolecular isobutane-*t* distribution sufficiently to affect the major qualitative conclusion that the primary replacement isotope effect has a value of about 1.25.

(25) H. Okabe and D. A. Becker, *J. Amer. Chem. Soc.*, **84**, 4004 (1962).

(26) R. S. Konar, J. H. Purnell, and C. P. Quinn, *J. Chem. Soc.*, A1543 (1967).

(27) C. T. Ting and F. S. Rowland, *J. Phys. Chem.*, **74**, 445 (1970).

(28) A. Hosaka and F. S. Rowland, presented at the Fourth Informal Conference on Hot Atom Chemistry, Kyoto, Japan, Oct 1967.

(29) B. S. Rabinovitch and D. W. Setser, *Advan. Photochem.* **3**, 53 (1964).

Mechanism of the Primary Replacement Isotope Effect. The preference for replacement of H *vs.* D by about 25% has been observed here for carbon atoms attached to three relatively heavy methyl goups. Several experiments in which the three heavy substituents are unlike, and the carbon atom is therefore optically asymmetric, have shown that such substitutions occur with >90% retention of configuration,[2-4] and one can therefore conclude that replacement in the tertiary position of isobutane can also be assumed to occur with retention of the original configuration around the carbon atom. Comparison with other molecules also makes it reasonable to assume that most of the molecules of isobutane-*t* are formed with a few eV of excitation energy in the initial primary reaction.[2-4,23,24] A more detailed description of the mechanism of this substitution, in the sense of the knowledge of the trajectories of incoming T and outgoing H or D atoms, or specific modes of excitation of the product molecules, is not available from these experiments.

In simple two-body collisions along the same velocity and angle of approach for a T atom with either H or D, simultaneous conservation of both energy and momentum requires appreciable isotopic differences in the energy distribution after collision. The more nearly equivalent mass of D to that of *T* requires 28% greater energy transfer than with H, corresponding, however, to an exit velocity of the D atom that is only 80% as fast as that of the H atom. The possible importance of such mass–inertia factors in hot atom collisions were first outlined in the "billiard ball" theory for energy transfer from the energetic atom.[30] Such direct collisions of T with H or D have been shown by simple model calculations with methane to predict a higher probability of substitution for the D atom as a direct consequence of greater energy transfer, leaving a less energetic T atom.[13] The prediction of an isotope effect favoring substitution for D in methane is clearly contrary to the experimental observations.[9,13]

A large "rotational inertia" mass effect for substituents other than the replaced group has been investigated with various alkanes and haloalkanes for substitutions of the general form shown in eq 2.[3]

$$T^* + CWXYZ \longrightarrow CTXYZ + W \qquad (2)$$

The effects of the masses of the substituents, X, Y, and Z, have been pictured as a greatly increased moment of inertia of the residual radical when these are heavy (*i.e.*, F, Cl, R, etc.) as compared to the effect of the three H atoms in CH_3, and a correspondingly greatly lowered rate of rotation of the radical into a favorable position for formation of a new C–T bond. The slow departure of the replaced group, W, prohibits the direct physical occupation of the geometric location of the original substituent and prevents the creation of the new bond by the essentially unchanged electronic orbitals of the reactant molecule. The current results exhibit another facet of possible mass–inertial effects, in which the differential changes are involved in the replaced group, W, while X, Y, and Z are maintained as identical substituents.

The primary replacement isotope effect itself undoubtedly reflects the necessity during substitution for substantial adjustment in the magnitude (and probably direction) of interatomic forces; as a minimum, the C–H or C–D force constant must go to zero as the C–T force constant rises to its value at full single-bond strength. As these force fields are changing, the individual substituent groups will respond to them with a velocity dependent upon the instantaneous values of the force constants, and upon the mass of the substituent; the lighter H atoms will adjust more rapidly than the D atoms. The three heavier methyl substituents presumably react less rapidly to such changing forces and the critical factor for successful completion of the substitution reaction may be chiefly the motion *away* of the H or D atom, the 25% increase in substitution with H representing the additional reactions facilitated by the more rapid exit of H. One can speculate that the corresponding reactions, in which the D atom does not move away fast enough for substitution to occur, fall largely into the class of inelastic scattering of T atoms with isobutane molecules. The eventual kinetic energy of the replaced H or D atom presumably is very much less than that calculated from the simple two-body collisions, and may correspond to a negligibly small fraction of the original kinetic energy of the approaching T atom.[28] In this sense, the crucial role of the isotopic mass difference between H and D is not in the possible overall differences in energy transfer, but in the relative facilitation through rapid change in position of the formation of a bonding orbital at a new spatial location in the evolving system.

Estimates of the magnitude of the primary replacement isotope effect when the other substituents are not *all* heavy (*i.e.*, heavy = any substituent except H or D) is still a speculative problem. The secondary isotope effect (CH_3 *vs.* CD_3) in the replacement of F in CH_3F *vs.* CD_3F is about 1.34 ± 0.06,[8] but the cumulative effect in CH_4 *vs.* CD_4 is only 1.31 ± 0.03[9]—about equal to each of the two isotope effects, primary replacement and secondary, when measured individually. Relaxation processes with several light substituents may well involve appreciable motion by several of them, and the overall dynamics of the reaction is not yet clear. Finally, one must also note from the fact that all of the *R* values in Table VI are 1.0 ± 0.3 that the number of heavy substituents (three *vs.* one for tertiary/primary) is no more important a factor in controlling substitution yield than is the H/D competition between the replaced atoms.

Other Mechanistic Considerations. (*a*) *Isotope Ef-*

(30) W. F. Libby, *J. Amer. Chem. Soc.*, 69, 2523 (1947).

fect in Abstraction. An excellent correlation has been found between the HT yield per bond and the bond dissociation energies of the C–H bonds involved for recoil tritium reactions with a series of hydrocarbons under comparable conditions.[14,31,32] This correlation has been explained as the result both of lower thresholds for the abstraction reaction with weaker bonds, and an increase in the probability of reaction per collision above this minimum energy.[31] The differences between C–H and C–D bonds in equivalent positions show isotope effects which increase with the weakness of the bond involved[14,33] and the observation of an HT/DT ratio of 1.65 ± 0.06 for reactions with the tertiary position of isobutane (Bond dissociation energy = 91 ± 1 kcal/mol[34] is in excellent agreement with the trend in HT/RT ratios established with stronger C–H bonds.

(*b*) *Steric Effects in Substitution Reactions.* The possibility of steric interference with T-for-H substitution reaction has been the subject of speculation, hypothesis, and experimental test for a number of years.[2–4,14] The original hypothesis that alkyl substituents might interfere with some substitution pathways was advanced in conjunction with the observation of large variations in HT/RT yield ratios for T* reactions with different RH molecules. Subsequent experiments have shown that these ratio variations result in large part, or entirely, from changes in HT yield with C–H bond type,[14,31] and more direct measurements have been required to ascertain the magnitude of such steric, or other alkyl substituent, effects.

Both intermolecular[35] and intramolecular[15,16] competition experiments in the gas phase have established that these effects are ± 20% at most with alkanes. The intramolecular experiments were also performed with i-C_4H_{10} and resulted in a measured gas-phase R value of 0.80 ± 0.04; the lower specific acitivity of the tertiary position was attributed to 20% more steric hindrance than in the primary positions of this molecule.[15] Our corresponding measurement of 0.87 ± 0.02 is slightly outside the quoted error of the two measurements. We believe that the revised procedures used in our experiments are less subject to error in determination of R than those originally used, particularly in regard to the problem of slow tertiary exchange.[36]

The general question of the origin of any differences in specific activity between primary and tertiary positions in isobutane hinges upon the explanation of the observed phase effect. If gas-phase experiments are still accepted as the most appropriate for testing of intramolecular steric competitions because of the absence of near-neighbor molecules, and if their results are not perturbed by secondary decompositions, then specific activity differences are essentially absent in i-C_4D_{10} (R = 0.96), and not much larger in i-C_4H_{10}(R = 0.87). On this basis, we conclude that the gas-phase evidence supports the conclusion that all alkyl-substituent effects on the substitution reaction, including steric hindrance, are either of minor importance or else essentially cancel the effects of one another in this system.[37]

(*c*) *Phase Effect.* The increases in R of 15–25% for all molecules as the phase is changed from liquid to gas invite explanations of two kinds. The first assumes that the primary substitution reaction occurs in an essentially identical manner in both phases and that the phase difference represents perturbation of the original distribution by secondary decomposition, as described above. Changes of the observed magnitude would require almost complete decomposition by the mechanism shown as structure B and seem to us not to be the probable explanation.

The second kind of explanation assumes that random orientation in collisions is only truly found in gas-phase experiments, while condensed-phase experiments involve some degree of selective orientation of collisions, or of selective caging of products. Such explanations are not particularly satisfying either, since general comparisoms of abstraction to substitution ratios in the two phases (*cf.* Table IV), after adequate correction for secondary decomposition, do not show any substantial overall phase dependence. However, a 20% effect on tertiary positions alone would probably not be experimentally distinguishable as yet, except through measurements such as the present ones. At this time, we have no preferred explanation for the phase effect. Clearly, however, this uncertainty does not affect our main purpose in these experiments—the primary replacement isotope effect is the same in both phases, despite the marked phase difference in tertiary/primary substitution.

(31) E. Tachikawa and F. S. Rowland, *J. Amer. Chem. Soc.*, **90**, 4767 (1968).

(32) E. Tachikawa and F. S. Rowland, *ibid.*, **91**, 559 (1969).

(33) E. Tachikawa, Ph.D. Thesis, University of California, Irvine, 1967.

(34) J. A. Keer, *Chem. Rev.*, **66**, 435 (1966).

(35) J. W. Root and F. S. Rowland, *J. Amer. Chem. Soc.*, **84**, 3027 (1962).

(36) Single experiments with deuterated isobutanes were reported in an appendix in ref 16. Using these data, R values have been calculated as $(CH_3)_3CD$; 0.72 (0.69); $(CD_3)_3CD$, 0.80 (0.96); $(CD_3)_3CH$, 0.73 (1.20); (present data in parentheses). In the two cases where the agreement is poor, the discrepancy is in the direction expected for a loss of tertiary tritium by a slow exchange process as discussed above. No mention of such an exchange process was made in ref 16.

(37) See also the essential absence of steric effects in ref 27.

NOTES

Chemically Activated Pentene-2 from the 4358 and 3660-Å Photolyses of Diazomethane–*cis*-2-Butene–Oxygen Mixtures[1a]

by G. W. Taylor[1b] and J. W. Simons

Chemistry Department, New Mexico State University, Las Cruces, New Mexico 88001 *(Received April 27, 1969)*

Quantitative kinetic studies of the unimolecular primary decomposition step for ground electronic state olefins have been limited to two shock-tube studies[2] and two chemical activation studies.[3,4] Chemical activation studies of unimolecular decompositions having known energetics are of particular interest since comparisons of experimental rate constants to RRKM[5] theory rate calculations give information about activated complex structures for the reactions. This information is similar to that which can be obtained from reliable experimental thermal A factors. Olefins that decompose by either C–H or C–C rupture to give allylic resonance stabilized radicals are expected to decompose with enhanced rates due to lowered critical energies. Recent values of the allylic and methallylic resonance energy[6] along with the appropriate alkane C–C bond dissociation energy[7] can be used to give reliable estimates of the critical energies for these olefin decompositions.

A study of the decomposition kinetics of the chemically activated 2-pentene produced in the photolysis of diazomethane–*cis*-2-butene mixtures at 4358 and 3660 Å is reported here.

Experimental Section

The materials and analytical procedures employed in this study have been described previously.[8]

Results and Discussion

The following reactions[8,9] represent the important steps leading to "hot" 2-pentene decomposition in this system.

$$CH_2N_2 \xrightarrow{4358\ \text{Å};\ 3660\ \text{Å}} CH_2(^1A_1) + N_2 \qquad (I)$$

$$CH_2(^1A_1) + CB2 \xrightarrow{K_2} P2^* \qquad (II)$$

$$\xrightarrow{K_3} DMC^* \qquad (III)$$

$$DMC^* \xrightarrow{K_4} 2MB2^*, 2MB1^* \qquad (IV)$$

$$\xrightarrow{K_5} P2^* \qquad (V)$$

$$\xrightarrow{W} DMC \qquad (VI)$$

$$P2^* \xrightarrow{K_7} CH_3 + CH_3CH = CHCH_2 \qquad (VII)$$

$$\xrightarrow{W} P2 \qquad (VIII)$$

where DMC = *cis* and *trans*-1,2-dimethylcyclopropane, P2 = *cis* and *trans*-2-pentene, W = collisional stabilization rate constant, and (*) = excess vibrational and internal rotational energy. Only the reactions of singlet methylene [CH_2 ($^1A_1$)] are considered here since all photolysis runs were performed in the presence of at least 10% oxygen which scavenges triplet methylene radical products[9d,10] as well as the doublet radicals produced by decomposition in this system. Vibrationally energized *cis*-2-pentene is produced by direct C–H insertion (reaction II) as well as by the structural isomerization of excited *cis*- and *trans*-1,2-dimethylcyclopropane (reaction V).

Experimental Rate Constants. In order to determine experimentally the unimolecular decomposition rate constants for the excited 2-pentene, mixtures of CB2–DM–O_2 in the approximate ratios of 8:1:1 were photo-

(1) (a) The National Science Foundation is gratefully acknowledged for financial support. (b) NDEA Predoctoral Fellow.

(2) (a) W. Tsang, *J. Chem. Phys.*, **46**, 2817 (1967). (b) G. A. Chappell and A. Shaw, *J. Phys. Chem.*, **72**, 4672 (1968).

(3) F. H. Dorer and B. S. Rabinovitch, *ibid.*, **69**, 1952 (1965).

(4) J. W. Simons, B. S. Rabinovitch, and F. H. Dorer, *ibid.*, **70**, 1076 (1966).

(5) R. A. Marcus and O. K. Rice, *J. Phys. Colloid Chem.*, **55**, 894 (1951); R. A. Marcus, *J. Chem. Phys.*, **20**, 359 (1952); B. S. Rabinovitch and D. W. Setser, *Advan. Photochem.*, **3**, 1 (1964).

(6) S. W. Benson, A. N. Bose, and P. Nangia, *J. Amer. Chem. Soc.*, **85**, 1388 (1963); D. M. Golden, K. W. Egger, and S. W. Benson, *ibid.*, **86**, 5416, 5420 (1964); J. A. Kerr, R. Spencer, and A. F. Trotman-Dickenson, *J. Chem. Soc.*, 6652 (1965); R. J. Ellis and H. M. Frey, *ibid.*, Suppl. No. 1, 5578 (1964).

(7) J. A. Kerr, *Chem. Rev.*, **66**, 465 (1966), and references therein.

(8) J. W. Simons and G. W. Taylor, *J. Phys. Chem.*, **73**, 1274 (1969).

(9) (a) H. M. Frey, *Proc. Roy. Soc.*, **A250**, 409 (1959); *ibid.*, **251**, 575 (1954). (b) P. S. Skell and R. C. Woodword, *J. Amer. Chem. Soc.*, **78**, 4486 (1956); *ibid.*, **81**, 3383 (1959), and references therein. (c) D. W. Setser and B. S. Rabinovitch, *Can. J. Chem.*, **40**, 1425 (1962). (d) J. W. Simons and B. S. Rabinovitch, *J. Phys. Chem.*, **68**, 1322 (1964).

(10) (a) F. H. Dorer and B. S. Rabinovitch, *ibid.*, **69**, 1952 (1965). (b) S. Ho, I. Unger, and W. A. Noyes, Jr., *J. Amer. Chem. Soc.*, **87**, 2297 (1965). (c) H. M. Frey, *Chem. Commun.*, **260**, (1965). (d) R. W. Carr, Jr., and G. B. Kistiakowsky, *J. Phys. Chem.*, **70**, 118 (1966). (e) B. S. Rabinovitch, K. W. Watkins, and D. F. Ring, *J. Amer. Chem. Soc.*, **87**, 4960 (1965). (f) R. L. Russell and F. S. Rowland, *ibid.*, **90**, 1671 (1968).

lyzed at 4358 and 3660 Å over a pressure range from 0.05 cm to 150 cm. It was found that the ratio of 2-pentene to the total dimethylcyclopropanes was constant above about 10 cm total pressure; consequently the ratios were averaged for all data above this pressure to obtain the ordinate intercepts of the curves in Figure 1.

Application of the steady-state approximation to the reactions II–VIII leads to eq 1.

$$\frac{[P2]}{[DMC]} = \left(\frac{W}{K_7 + W}\right)\left[\frac{1}{W}\left(K_5 + \frac{K_2K_8}{K_3}\right) + \frac{K_2}{K_3}\right] \quad (1)$$

where $K_8 = K_4 + K_5$.

The collisional deactivation rate constant, W, is assumed to be equal to the collision frequency. The ratio of K_2/K_3 in eq 1 was taken from the ordinate intercepts of the appropriate experimental curves in Figure 1.

Averages over many runs indicate the best value for K_2/K_3 is 0.77 at both wavelengths. The value of K_5 for each wavelength investigated was taken to be half of the value of K_8 the total dimethylcyclopropane structural isomerization rate constant as previously determined.[8] This procedure is supported by RRKM theory calculations and also by the experimental thermal A factors and energies of activation.[9d,11] Using the appropriate values of K_7, where K_7 is the decomposition rate constant for the 2-pentene, for each wavelength eq 1 was fitted to the experimental points as shown in Figure 1 at 4358 and 3660 Å. The values of K_7 that best fit the experimental points at 4358 and 3660 Å in Figure 1 are $(4.05 \pm 0.4) \times 10^7$ sec^{-1} and $(5.5 \pm 0.6) \times 10^7$ sec^{-1}, respectively.

It may be seen from eq 1 that if $W \gg K_7$ *i.e.*, either high total pressures or greater olefin stability, then eq 1 reduces to eq 2.

$$\frac{[P2]}{[DMC]} = \frac{1}{W}\left(K_5 + \frac{K_2K_8}{K_3}\right) + \frac{K_2}{K_3} \quad (2)$$

The dark lines in Figure 1 represent this linear relationship between [P2]/[DMC] and $1/W$. A comparison of these lines with the data in Figure 1 clearly indicates the extent of 2-pentene decomposition in this system.

Theoretical Rate Calculations

The RRKM theory expression for k_E, the unimolecular rate constant at the energy, E, is given by eq 3.

$$k_E = \frac{Q^+}{hQ^*}\frac{\sum P(E^+_{vr})}{N(E^*_{vr})} \quad (3)$$

where Q^+/Q^* is the ratio of the partition functions for adiabatic degrees of freedom including reaction path degeneracy, $\Sigma P(E^+_{vr})$ is the sum of energy eigenstates for the activated complex up to the energy, E^+, and $N(E^*_{vr})$ is the density of energy eigenstates for the active degrees of freedom (vibrations and internal rotations) of the energized molecule at the energy, E^*. The evaluation of the sum and density terms for 2-pentene and the various activated complexes at the appropriate energies were carried out on a CDC-3300 computer using the accurate approximation of Whitten and Rabinovitch.[12]

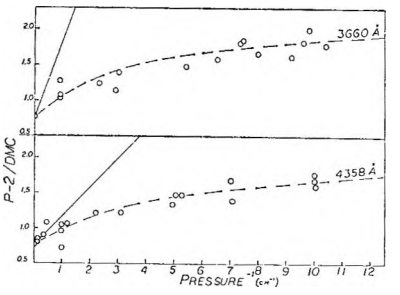

Figure 1. Variation of the ratio of pentene-2 to dimethylcyclopropanes with inverse pressure. Dark lines represent the plot of eq 2 (the upper and lower lines are for 3660 and 4358 Å, respectively). The dashed curves represent the plots of eq 1 at 3660 Å (upper curve) and 4358 Å (lower curve) using the K_7 values giving the best fit to the data.

Energies. The average energy contents, E^*, of the chemically activated dimethylcyclopropanes produced in this system have been previously determined.[8,13] The structural isomerization of *cis*-1,2-dimethylcyclopropane to *cis*-2-pentene is exothermic by 4.9 kcal/mol thus the E^* values for excited *cis*-2-pentene in the 3660 and 4358-Å systems are 124.2 kcal/mol and 120.7 kcal/mol, respectively.[13] It was assumed that these same energies apply for the *cis*-2-pentene and *trans*-2-pentene mixture, called 2-pentene in this work. This assumption introduces a negligible error.

The critical energy for 2-pentene decomposition is determined by the dissociation energy for an equivalent alkane C–C bond, the allylic resonance energy from the formation of a methallyl radical, and the critical energy for recombination of a methyl and methallyl radical. The energy required to break an alkane primary–secondary C–C single bond is 83 kcal/mol at 298.16°K with an uncertainty of about 1 kcal/mol. Recent determinations of the allylic resonance energy are in agreement with a value of 12 ± 1 kcal/mol. The methallylic resonance energy is probably also 12 kcal/mol. The critical energy, E_0, for the decomposition of *cis*-2-pentene is then 70 ± 2 kcal/mol if a 2–3 kcal/mol critical energy for recombination is assumed.

The excess energies, $E^+ = E^* - E_0$, for 2-pentene decomposition are 54.2 kcal/mol at 3660 Å and 50.7 kcal/mol at 4358 Å.

(11) M. C. Flowers and H. M. Frey, *Proc. Roy. Soc.*, A260, 424 (1961).

(12) G. Z. Whitten and B. S. Rabinovitch, *J. Chem. Phys.*, 38, 2466 (1963); 41, 1883 (1964).

(13) Energies derived for $[\Delta H_f°(CH)_2 + E^*(CH_2)]$ in ref 8 have been adjusted downward by 0.4 and 0.7 kcal/mol for 4358 and 3660-Å photolyses, respectively. These adjustments result from more exact RRKM calculations

2-Pentene Molecular Frequencies. The vibrational frequencies for 2-pentene were deduced from the known frequencies for propylene and ethane.[14] The C=C torsional frequency was derived from substituted ethylene torsional frequencies[14] by allowing proportionally for mass changes. Skeletal bending frequencies were estimated from similar alkane vibrations.[14]

Activated Complex Models. The activated complex for 2-pentene decomposition may be schematically represented as

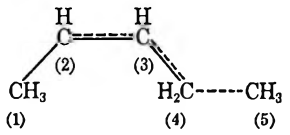

This complex representation is consistent with those previously postulated for 1-olefin decompositions.[3]

Since RRKM theory rate calculations are not very sensitive to the detailed activated complex model employed, the molecular parameters adjusted here were those most reasonably believed to be involved in the reaction coordinate. The C(4)–C(5) stretchingfrequency was taken as the translation along the reaction coordinate in the activated complex. The C(4)–C(5) bond length in the activated complex was set at twice its value in the molecule. 2-Pentene has three internal rotations which were treated as free rotors in the molecule. The tightening in the activated complex due to the allylic resonance will cause a barrier to rotation about the C(3)–C(4) bond and, therefore, one internal free rotor becomes a low-frequency torsional vibration. The magnitude of this torsional frequency was used as the adjustable parameter to best fit theory and experiment (complex II) and to fit our best estimates of the limits (complexes I and III) of the combined uncertainties in the experimental rates and E_0 values used in the theoretical calculations. A 10% uncertainty in the experimental rates was combined with a 2 kcal/mol uncertainty in E_0. The magnitudes of other frequency adjustments were the same in all of the activated complexes and were such as to bring theory and experiment into only approximate agreement in hopefully a reasonable fashion.

Comparison of Theory and Experiment. The theoretical rates of 2-pentene decomposition at 3660 and 4358 Å are presented in Table I for three E_0 values. The experimental rate constants are also given in Table I. It is seen from Table I that E^* = 124.2 kcal/mol and 120.7 kcal/mol gives $k_E = 6.21 \times 10^7$ sec^{-1} and 3.60×10^7 sec^{-1}, respectively, at E_0 = 70 kcal/mol, which are within experimental error of the 3660 and 4358-Å experimental rates, respectively. The experimental rates could be fitted better by independent adjustments of about 1 kcal/mol in the 4358 and 3660-Å E^* values; however, since these energies are based on more reliable results[8] such adjustments seem unjustified.

Table I lists the A factors calculated from absolute rate theory for all three complex models employed. An A factor of $10^{15.8\pm0.3}$ for the decomposition of 4,4-dimethylpentene-1 into *t*-butyl plus allyl radicals has been determined in a shock-tube study by Tsang.[3] This experimental A factor for a similar reaction is similar to the theoretical A factor of $10^{16.15}$ calculated for complex model II. It might be expected that the A factor for 4,4-dimethyl-1-pentene would be slightly larger than the A factor for 2-pentene decomposition because of an increase in the activation entropy for producing a *t*-butyl radical as compared to that for producing a methyl radical; however, the two values are well withing the limits of uncertainty in the two studies as seen from Table I.

Table I: Theoretical k_E, sec^{-1}, for 2-Pentene Decomposition

	Complex Model		
	I	II	III
E_0, kcal/mol	Log A 16.5	16.15	15.8
	E^* = 120.7 kcal/mol		
68	1.56×10^8	7.26×10^7	3.43×10^7
70	7.71×10^7	3.60×10^7	1.70×10^7
72	3.76×10^7	1.76×10^7	8.33×10^6
	$K_7 = (4.05 \pm 0.4) \times 10^7$ sec^{-1} at 4358 Å		
	E^* = 124.2 kcal/mol		
68	2.61×10^8	1.22×10^8	5.73×10^7
70	1.33×10^8	6.21×10^7	2.93×10^7
72	6.67×10^7	3.12×10^7	1.47×10^7
	$K_7 = (5.5 \pm 0.6) \times 10^7$ sec^{-1} at 3660 Å		

Rabinovitch and Dorer[3] have determined the experimental decomposition rate constant for 2-pentene from the photolysis at 4358 Å of diazomethane–1-butene mixtures in the absence of radical scavengers. The average excitation energy is 122.2 kcal/mol using the energetics from our previous work.[8,13] This value is slightly larger than the excitation energy used in the present 4358-Å study because of the difference in the heats of formation at 0°K of *cis*-2-butene and 1-butene. Using a critical energy of 70 kcal/mol, a theoretical decomposition rate constant of 4.57×10^7 sec^{-1} is predicted from complex model II. The experimental value found by Rabinovitch and Dorer is 0.9×10^7 sec^{-1}. Part of this difference may be due to the presence of a significant quantity of ground triplet state methylene radical reaction and part may be due to radical recombination giving extra stabilized 2-pentene at all pressures.

(14) G. Herzberg, "Infrared and Raman Spectra of Polyatomic Molecules," D. Van Nostrand and Co., Princeton, N. J., 1945.

Comment on the Ultrasonic Spectra of $CuSO_4$ and $Cu(en)_2S_2O_3$ in Water at 25°

by P. Hemmes and S. Petrucci

Department of Chemistry, Polytechnic Institute of Brooklyn, Brooklyn, New York *(Received May 13, 1969)*

Ultrasonic relaxation of metal sulfates in water has undergone an intense reinvestigation in recent years.[1-4] In this laboratory the ultrasonic relaxation of solutions of $CuSO_4$ and $Cu(en)_2S_2O_3$ has recently been investigated.[5] The data seemed to follow a single relaxation with the relaxation frequency $f_r = 170 \pm 10$ MHz within the precision of the available data. These results were interpreted by a two-step mechanism, a diffusion-controlled approach between the two

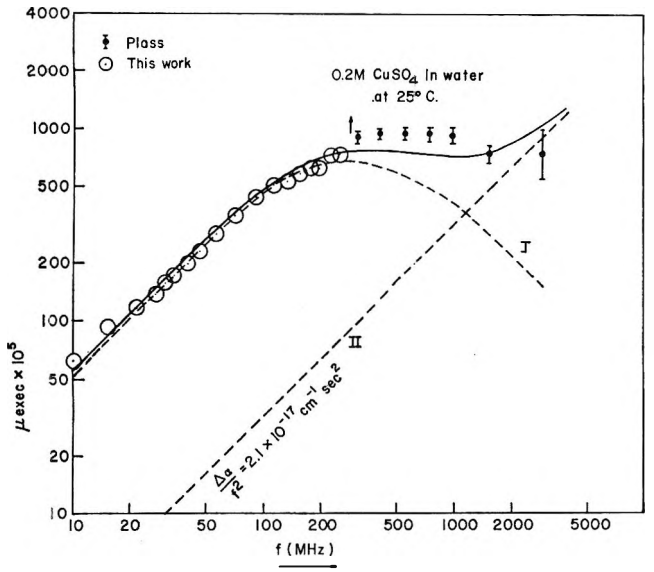

Figure 1. Graph of the excess sound absorption per wavelength μ_{exc} *vs.* the frequency for 0.20 *M* $CuSO_4$ in water at 25°.

ionic partners followed by the slower removal of the axial water from the ions $Cu(H_2O)_6^{2+}$ and $Cu(en)_2(H_2O)_2^{2+}$ by the anions. Because of the claimed existence of a lower relaxation at 5–20 MHz in aqueous $CuSO_4$ at 20° and because of the reported astonishing behavior at high frequency in the same system[2] (the $\mu_{exc}\lambda$ *vs.* f plot showing an almost flat portion in the range of 1000–2000 MHz), it was decided to repeat the ultrasonic measurements of $CuSO_4$ and $Cu(en)_2S_2O_3$ in water at 25°. An ultrasonic interferometric cell of improved mechanical design was used. It has been found that the relaxation frequency for both $CuSO_4$ and $Cu(en)_2S_2O_3$ are rather at 280 MHz (±10%) for the concentration 0.2 *M* and at 270 MHz (±10%) for the concentration 0.05 *M*.

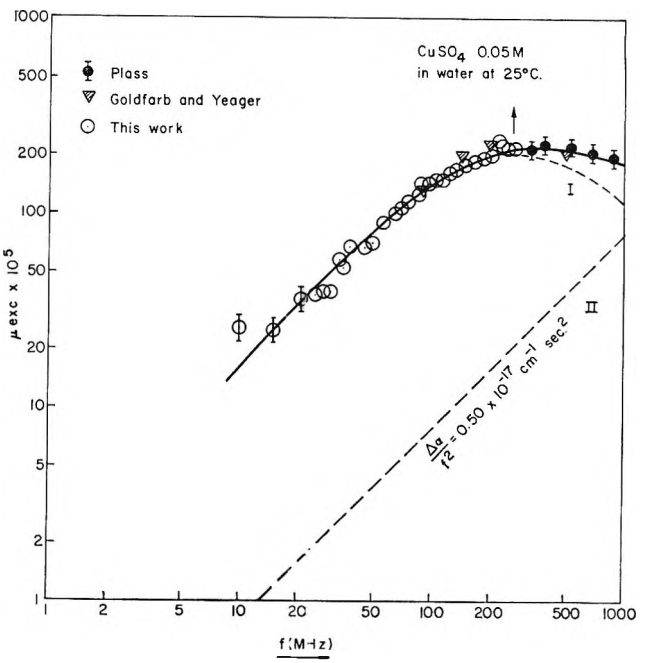

Figure 2. Graph of the excess sound absorption per wavelength μ_{exc} *vs.* the frequency for 0.05 *M* $CuSO_4$ in water at 25°.

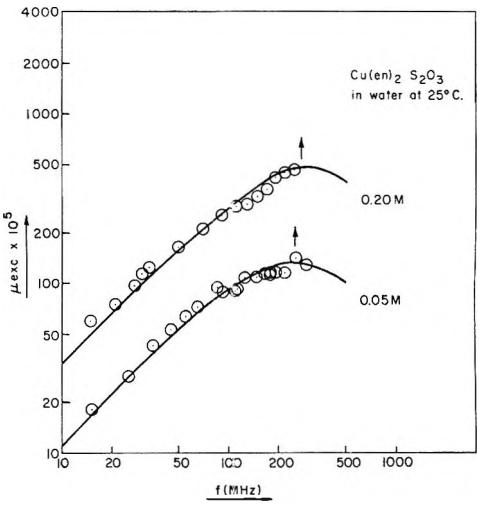

Figure 3. Graph of the excess sound absorption per wavelength μ_{exc} *vs.* the frequency for 0.20 and 0.05 *M* $Cu(en)_2S_2O_3$ in water at 25°.

The new results are shown in Figures 1, 2, and 3.[6] These data are in considerable accord with the ones recently reported by Goldfarb[4] for aqueous $CuSO_4$ as shown in Figure 2. The results of Plass[2] for $CuSO_4$ 0.20

(1) K. Tamm, Reprint from the 6th International Congress on Acoustics, Tokyo, Japan, August 1968, Vol. I, p 25.

(2) K. Plass and A. Kehl, *Acustica*, **20**, 360 (1968).

(3) G. Mass, *Z. Phys. Chem.*, (Frankfurt am Main), **60**, 138 (1968).

(4) L. Goldfarb and E. Yeager, Office of Naval Research, Project No. NR 384-305. Technical Report No. *32*, Jan 1968.

(5) P. Hemmes and S. Petrucci, *J Phys. Chem.*, **72**, 3986 (1968).

(6) The original data can be obtained from the authors upon request.

and 0.05 M at 20° are also shown in Figures 1 and 2, respectively.

For the calculations,[5,7] taking $k_{12}^{\circ} = k_D = 4.2 \times 10^{10}\ M^{-1}\ \text{sec}^{-1}$ from the Debye–Smoluchowski theory,[8] $K_{12}^{-1} = K_F = 95\ M^{-1}$ from the Fuoss theory,[9] $k_{21} = 4.4 \times 10^8\ \text{sec}^{-1}$ from either the ratio k_D/K_{Fuoss} or the Eigen theory,[10] assuming $k_{23} = k_{32} = 7 \times 10^8\ \text{sec}^{-1}$ (k_{23} being reasonably close to the value $= 1.3 \times 10^9\ \text{sec}^{-1}$ found recently by Stuehr[11]) and $K_{23} = k_{32}/k_{32} = 1$, one can calculate for the two electrolytes the overall association constant $K_{\Sigma}^{-1} = 190\ M^{-1}$, $f_{r1} = 282$ MHz at $c = 0.2\ M$ and $f_{r1} = 268$ MHz at $c = 0.05\ M$.

In order to account for the data at high frequencies in Figures 1 and 2, either a spectrum (discrete or continuous) of relaxation times is invoked[2] or the value of the "solvent" used ($\alpha_t/f^2 = 22 \times 10^{-17}\ \text{cm}^{-1}\ \text{sec}^2$) is considered inadequate.[1,2] The second possibility is shown in Figures 1 and 2 where curve II is the assumed contribution to the solution with respect to the solvent $(\Delta\alpha/f^2)_{f>>f_r} = 2.1 \times 10^{-17}$ at $c = 0.2\ M$ and $(\Delta\alpha/f^2)_{f>>f_r} = 0.5 \times 10^{-17}$ at $c = 0.05\ M$. The solid lines in Figures 1 and 2 are obtained by summing curve II to curve I.

(7) M. Eigen and L. DeMaeyer, "Investigation of Rates and Mechanisms of Reaction," A. Weissberger, Ed., John Wiley and Sons, New York, N. Y., 1963, part II.

(8) M. von Smoluchowski, *Z. Phys. Chem.*, (Frankfurt am Main), **92**, 129 (1917); P. Debye, *Trans. Electrochem. Soc.*, **82**, 265 (1942).

(9) R. M. Fuoss, *J. Amer. Chem. Soc.*, **80**, 5059 (1958).

(10) M. Eigen, *Z. Phys. Chem.* (Frankfurt am Main), **1**, 176 (1954).

(11) W. B. Makinen, A. F. Pearlmutter, and J. Stuehr, *J. Amer Chem. Soc.*, **91**, 4083 (1969)